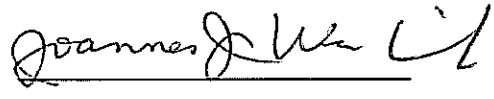
Department of Justice Expert Witness Report:

ADCIRC Storm Surge Simulations

Robinson v. United States

Prepared by

Joannes J. Westerink, Ph.D.



22 December 2008

TABLE OF CONTENTS

	Page
1.0 Introduction	1
1.1 Purpose of Study	1
1.2 Participants	2
2.0 Scope of Study	3
3.0 Physical Description of the Region	9
3.1 Topographic and Bathymetric Data	10
3.1.1 Vertical Datum	10
3.1.2 Topographic Surveys/Data	10
3.1.3 Bathymetric Surveys/Data	14
3.1.4 Vertical Features with Small Horizontal Scales	15
3.2 Influence of Coastal Vegetation	17
4.0 Hydraulic Analysis	21
4.1 Model System Components	21
4.1.1 Wind Models	22
4.1.2 Offshore Wave Model WAM	24
4.1.3 Nearshore Wave Model STWAVE	25
4.1.4 ADCIRC Circulation Model	27
4.1.4.1 ADCIRC Model Description	28
4.1.4.2 SL15 Domain/Grid Definition	29
4.1.4.3 Bathymetric, Topographic and Feature Definition	34
4.1.4.4 Bottom and Lateral Friction Process	34

4.1.4.5 Land, River and Tidal Forcing Functions 36

4.1.4.6 LMSL and Steric Water Level Adjustments 38

4.1.4.7 Atmospheric Forcing Functions 39

4.1.4.8 Wave Radiation Stress Forcing 40

4.1.4.9 Model Operational Parameter Definitions 41

4.2 Solution Procedure (Process Management) 42

5.0 Simulation Results 44

5.1 Scenario H1: *Katrina real run* - Katrina simulation with the 2005 physical system 44

5.1.1 ADCIRC Water Level and Current Computations 44

5.1.2 System Validation 53

5.2 Scenario H2: *No MRGO with 2005 wetlands* 56

5.3 Scenario H3: *No MRGO with 1956 wetlands* 62

5.4 Scenario H4: *No MRGO with 1956 wetlands and a relocated Chalmette levee* 63

5.5 Scenario H5: *MRGO as designed with 2005 wetlands* 64

5.6 Scenario H6: *MRGO as designed with 1956 wetlands* 66

6.0 Discussion and Conclusions 67

6.1 Impact of the MRGO by Region 68

6.1.1 Impact of the MRGO on English Turn and Braithwaite 69

6.1.2 Impact of the MRGO on the Marshes and Waters to the East of the St. Bernard Polder 71

6.1.3 Impact of the MRGO between Paris Road and Seabrook 74

6.2 An Evaluation of the Impact of the MRGO Components on Regional Water Levels 76

6.2.1 The Impact of the MRGO Reach 2 76

6.2.2 The Impact of the MRGO Reach 1/GIWW 77

6.2.3 The Impact of the MRGO Wetland Degradation 78

6.2.4 The Impact of the Constructed Levees in and around the Golden Triangle 78

7.0 References 80

Tables 87

Figures 90

Appendix A: Curriculum Vita 244

Appendix B: Litigation Involvement and Compensation 269

1.0 INTRODUCTION

1.1 PURPOSE OF STUDY

This study (Study) investigates the effects of the Mississippi River Gulf Outlet (MRGO) and the surrounding marsh on storm surge levels during Hurricane Katrina. The Study examines the influence of the MRGO on a region surrounding the MRGO and extending to Lake Pontchartrain through the Inner Harbor Navigation Canal (IHNC), defined as the Study Region shown in Figure 1 and detailed in Figure 2. The Study Region includes the critical areas where failures occurred in the federal levee system protecting what is often referred to as the St. Bernard and New Orleans East Polders. The St. Bernard Polder is defined by the Chalmette Levee that runs on the east bank of the IHNC and then along the south bank of the MRGO to past Bayou Dupre, by the Chalmette Extension Levee which runs from southeast of Bayou Dupre to the east bank Mississippi River levee, and by the east bank Mississippi River levee between Poydras and the IHNC. The New Orleans East Polder is defined by the IHNC East Levee, the Citrus Back Levee and New Orleans East Back Levee, the New Orleans East Levee, and the New Orleans East Lakefront Levee, the Citrus Lakefront Levee, and the New Orleans Lakefront Levee. These levees are part of the Lake Pontchartrain and Vicinity Hurricane Protection Project. A simulation of the surge that occurred during Hurricane Katrina has been made for a case that represents the geometry, topography, bathymetry and surface roughness conditions as they existed in 2005. This simulation will be referred to as the *Katrina Real Run*. In addition, surge simulations have been made for cases in which the physical system description is

perturbed from the *Katrina Real Run* case. The geometric perturbations include reconfigurations of the MRGO, from making it narrower and shallower to its complete removal. Perturbations affecting the topography, bathymetry, and friction were also made in the region that the construction of the MRGO may have influenced. The zone of MRGO wetland influence is shown in Figure 1 (Britsch and Dunbar, 2008). Five perturbed systems are then simulated with the same riverine, tidal and atmospheric forcings as the *Katrina Real Run* simulation and compared in order to quantify how the MRGO may have influenced the Study Region during Hurricane Katrina.

The opinions expressed in this Study are based upon a reasonable degree of scientific and engineering certainty. If additional information or data becomes available, I reserve the right to revise the conclusions and opinions in this Study. I have not had the benefit of Plaintiffs' final expert depositions. Therefore, I reserve the right to amend my opinions for this purpose. Furthermore, I am also prepared to address any additional issues within my areas of expertise which may be raised at trial.

1.2 PARTICIPANTS

The Study was performed by Dr. Joannes J. Westerink as a portion of an investigation commissioned by the Department of Justice. Components of the hydraulic analyses for this study were performed by Dr. John H. Atkinson and Hugh J. Roberts of ARCADIS. Dr. Jane Smith of the U.S. Army Engineer Research and Development Center participated in the STWAVE wind wave simulations.

2.0 SCOPE OF STUDY

State-of-the-art coastal ocean hydrodynamic analysis methods were used to determine the storm surge water levels and near-shore wave characteristics in the Study. An accurate hindcast of Hurricane Katrina and various alternative scenarios were simulated using the Advanced Circulation (ADCIRC) hydrodynamic model and Steady State Spectral Wave (STWAVE) near-shore wave model. Both models, and their associated high resolution computational meshes, have been validated and used during numerous large scale studies, including the Interagency Performance Evaluation Task Force (IPET) (U.S. Army Corps of Engineers, 2007b), the Louisiana Coastal Protection and Restoration (LACPR) initiative (U.S. Army Corps of Engineers, 2008) and the Federal Emergency Management Administration's (FEMA) recent State of Louisiana Digital Flood Insurance Rate Map Study (FEMA DFIRM) (U.S. Army Corps of Engineers, 2007c). The high resolution SL15 ADCIRC mesh developed in the wake of these analyses with local grid resolution improvements in and around the MRGO and IHNC was used as the base numerical mesh for this Study.

Six scenarios were investigated by adjusting pertinent topographic, bathymetric, and frictional descriptors in the SL15 ADCIRC mesh. For each scenario, the stretch of MRGO that joins with the Gulf Intracoastal Waterway (GIWW) east of the IHNC and west of the location where the MRGO and GIWW diverge, east of Paris Road, is described as the MRGO Reach 1/GIWW. Similarly, the portion of the MRGO running southeast from the GIWW from east of Paris Road to the Gulf of Mexico is described as the MRGO Reach 2. Figure 1 and Figure 2 distinguishes both reaches and both

reaches are modified for the defined scenarios. Additionally, in some scenarios, the marshes surrounding the MRGO are configured to approximate 1956 (pre-MRGO) conditions. These marsh areas are outlined in Figure 1 as the zone of MRGO influence. The 1956 conditions were defined by adjusting topographic heights and Manning n frictional parameters based on available land cover data from 1956 (Barras, 2008). The methodology used to adjust marsh parameters for 1956 conditions is the same as that used for 2005 pre-Katrina conditions. Details of the methodology are described in Section 3.

The six scenarios analyzed are summarized in Table 1 and are defined as follows:

Scenario H1: The *Katrina Real Run* is a hindcast that simulates the Katrina storm surge with the best available description of the 2005 physical system. The geometry, topography, bathymetry and frictional characteristics in Southeastern Louisiana are defined to characterize the system as it existed immediately prior to the landfall of Hurricane Katrina. Details of this characterization are provided in Section 3. Scenario H1 topography and bathymetry are shown in the Study Region in Figure 3 through Figure 5 and the Manning n friction parameter which characterizes the roughness of the land and ocean floor is shown in Figure 6 through Figure 8.

Scenario H2: The *No MRGO with 2005 wetlands* scenario defines the physical system in Southeastern Louisiana as it existed immediately prior to the landfall of Hurricane Katrina except that the conveyance of the MRGO Reach1/GIWW channel was substantially reduced and the MRGO Reach 2 channel was eliminated. The MRGO

Reach 1/GIWW channel was narrowed to pre-MRGO 1958 GIWW dimensions per aerial imagery and assumes a naturally scoured depth of 24 feet. The geometry of the 1958 GIWW from the confluence of the IHNC in the east to past the Michoud Canal in the west was obtained from a 1958 aerial photo shown in Figure 9 (Dunbar, 2008). Documents indicated that the existing GIWW channel already had a naturally scoured depth of approximately 24 ft (U.S. Army Corps of Engineers. 1957). Reach 2 of the MRGO was entirely eliminated by raising topography to elevations slightly above that of the adjacent ground and modifying the frictional resistance to that of the adjacent marsh. The H2 scenario also eliminates the dredged spoil mounds southeast of St. Bernard Parish that resulted from the construction of the MRGO but keeps the Chalmette Levee and the associated spoil mounds in place. Scenario H2 topography and bathymetry are shown in the Study Region in Figure 10 through Figure 12 and the Manning n friction parameter spatial distribution is shown in Figure 13 through Figure 15.

Scenario H3: *No MRGO with 1956 wetlands* defines 1956 wetlands and 1958 channels in and around MRGO Reaches 1 and 2. The MRGO Reach 1/GIWW channel was narrowed to pre-MRGO 1958 GIWW dimensions per aerial imagery as shown in Figure 9 and assumes a naturally scoured depth of 24 feet (Dunbar, 2008, U.S. Army Corps of Engineers. 1957). Reach 2 was again eliminated and topography in the MRGO zone of influence defined in Figure 1 was defined to 1956 elevations using 1956 land use information. This included the elimination of the dredged spoil mounds that resulted from the construction of the MRGO but keeps the Chalmette Levee and

Chalmette Extension Levee around the St. Bernard Polder. The marshes in MRGO zone of influence were also frictionally characterized as per 1956 land use information. The characterization of topography, bathymetry and Manning bottom friction values are detailed in Section 3. Scenario H3 topography and bathymetry are shown in the Study Region in Figure 16 through Figure 18 and the Manning n friction parameter spatial distribution is shown in Figure 19 through Figure 21. Scenario H3 differs from Scenario H2 only in marsh topography and frictional characteristics defined in the area hatched in Figure 1. These differences are highlighted in the topographic differences seen in Figure 22 through Figure 24 and the Manning n differences seen in Figure 25 through Figure 27. Topography in the area of influence is generally slightly higher in the H3 case in the MRGO zone of influence except adjacent to the areas where dredged spoils were eliminated in the H2 case both along the Chalmette Levee and along the portion of MRGO Reach 2 southwest of the Chalmette Extension Levee where H2 topography was defined slightly above the adjacent 2005 marsh. The differences in topography away from the dredged spoil mounds are generally less than 1 ft. It is also noted that the Laloutre Ridge was more prominent in the 1956 landscape. Manning n values were generally slightly higher in the H3 scenario but lower in some regions partly due to the fact that the 1956 land use definitions did not distinguish between Brackish and Saline Marsh while the 2000 GAP data did.

Scenario H4: The *No MRGO with 1956 wetlands and relocated Chalmette Levee* case simulates the 1956 conditions in and around MRGO Reaches 1 and 2. The MRGO Reach 1/GIWW channel was narrowed to pre-MRGO 1958 GIWW dimensions per

aerial imagery and assumes a naturally scoured depth of 24 feet as in Scenarios H2 and H3. Reach 2 was again eliminated and topography in the MRGO zone of influence was defined to 1956 elevations using 1956 land use information. This included the elimination of the dredged spoil mounds that resulted from the construction of the MRGO Reach 2. The marshes in the zone of MRGO influence in the Study Region were also frictionally characterized as per 1956 land use information. The Chalmette Levee on the south side of Reaches 1 and 2 of the MRGO was removed. The 40 Arpent levee was modeled with the assumption of a height of 17.5 ft (the design height for the Chalmette Levee along MRGO Reach 2). The Chalmette Extension Levee extending around Poydras to St. Bernard to Verrett was kept in place. Levee alignments can be seen in Figure 28 through Figure 30 which also show topography and bathymetry in the Study Region. Manning n frictional characteristics are shown in Figure 31 through Figure 33. Scenario H4 differs from Scenario H3 only by the removal of the Chalmette Levee from the south side of the MRGO Reach 2 and the raising of the 40 Arpent levee crest to that of the Chalmette Levee along MRGO Reach 2 design specification.

Scenario H5: The *MRGO as designed with 2005 wetlands* scenario defines conditions in Southern Louisiana that existed just prior to the landfall of Hurricane Katrina with the exception that Reaches 1 and 2 are reconfigured to approximate the design dimensions of 36-foot depth, 500-foot bottom width, and side slopes of 1 on 2. The MRGO Reach 2 channel was hydraulically separated from Lake Borgne in the vicinity of Bayou Dupre. The MRGO spoil mounds, topography and frictional characteristics

are all represented as per the 2005 configuration as in Scenario H1. Scenario H5 topography and bathymetry are shown in the Study Region in Figure 34 through Figure 36 and the Manning n friction parameter spatial distribution is shown in Figure 37 through Figure 39. Scenario H5 differs from Scenario H1 in that Reach 1 and 2 now are characterized by the design dimensions and not the observed 2005 geometry.

Scenario H6: The *MRGO as designed with 1956 wetlands* scenario defines the MRGO Reaches 1 and 2 as they were designed and uses 1956 conditions in the marshes surrounding Reach 1 and Reach 2. Reaches 1 and 2 were reconfigured to approximate the design dimensions of a 36-foot depth, a 500-foot bottom width, and 1 on 2 side slope channel. The MRGO Reach 2 channel was again hydraulically separated from Lake Borgne in the vicinity of Bayou Dupre. Most of the MRGO spoil mounds were kept in place reflecting that the digging of the MRGO would still have produced these spoils. However, some of the spoil mounds southeast of the Laloutre Ridge were eliminated to understand the sensitivity of the reduced spoil volumes associated with the smaller channel. Scenario H6 topography and bathymetry are shown in the Study Region in Figure 40 through Figure 42 and the Manning n friction parameter spatial distribution is shown in Figure 43 through Figure 45. Scenario H6 differs from Scenario H5 only in marsh topography and frictional characteristics defined in the area to 1956 conditions as highlighted in the H6 to H5 difference plots presented in Figure 46 through Figure 51.

3.0 PHYSICAL DESCRIPTION OF THE REGION

The computational modeling of surge and waves requires that the physical system be accurately described and characterized and that the bathymetry, topography, and surface roughness characteristics of the region must be accurately represented. All topographic features, *e.g.*, levees, river banks, and roads, must be incorporated into the model. These features must be included because they can impede flow and focus the storm surge. Topographical mappings and surveys, including high-resolution light detection and ranging (Lidar)-based surveys, can neglect these features because of their relatively small horizontal scale. They therefore require special handling in order to ensure that they are faithfully represented in the models. In addition, the wind, wave, and circulation models all require an accurate description of the roughness of the terrain over which the wind blows, the waves propagate, and the surge flows.

The following sections summarize descriptions of the map-based information used in the study models, including the datum, the bathymetry, the topography, and land use. More detailed information is provided in the FEMA DFIRM report (U.S. Army Corps of Engineers, 2007c). The ADCIRC and STWAVE models were applied to the physical system described by these data in order to assess the storm surge and wave environments during the Hurricane *Katrina Real Run* and in the previously described H2 through H6 hypothetical scenarios.

3.1 TOPOGRAPHIC AND BATHYMETRIC DATA

3.1.1 Vertical Datum

The vertical datum for the computational meshes utilized in this study is the NAVD88 (2004.65) datum. NAVD88 (2004.65) is a geodetic equipotential surface and therefore provides a sound reference for our computations when adjusted for the offset to local mean sea level (LMSL). Further data can be found in the FEMA DFIRM report (U.S. Army Corps of Engineers, 2007c) and the IPET Geodetic Vertical and Water Level Datums report (U.S. Army Corps of Engineers, 2007a).

3.1.2 Topographic Surveys/Data

Accurate topographical mapping is essential if the flow physics of a region are to be accurately modeled. Topography influences wind-wave and surge propagation speed and direction, as well as frictional dissipation. In addition, topography can amplify or attenuate storm surge. Topographic data sources are summarized in Figure 52 and Figure 53. The most recent and best topographic values came from the Louisiana State University (LSU) Atlas Lidar data set (Louisiana State University, 2004). Unfortunately, this data set does not encompass the entire region and also may have inconsistencies in wetlands. Consequently, gaps in the LSU Atlas Lidar data set were filled with values from the 30-meter National Elevation Dataset (NED) (USGS, 2004). All data

sets were converted to Geographic North American Datum of 1983 (NAD83) and elevations adjusted to the NAVD88 (2004.65) datum.

Atlas Lidar does not generally extend into many of the marshes and wetlands within Southeastern Louisiana as is detailed in Figure 52. Additionally, the questionable ability of Lidar to identify accurate elevations for features in wetlands such floating marshes, led us to not use Lidar as a topographic source in low lying wetlands. In these regions, estimates of topographic and bathymetric depths have been applied based on USGS GAP land cover maps which clearly define the coastal marshes (Hartley et al., 2000). The GAP land cover data for Louisiana is presented in Figure 54. Similarly, 1956 conditions were approximated using a 1956 land cover dataset for Louisiana shown in Figure 55 (Barras, 2008). The land use maps were coupled with controlled marsh elevation approximations and adjacent water depth estimates relative to NAVD88 (2004.65). The USGS provided guidance on approximating the topographic elevation based upon vegetative species (Couvillion, 2008). Land cover classes in both the 2000 GAP and 1956 land use data sets were organized into the broader categories of “water,” “fresh water marsh,” “non-fresh water marsh,” and “swamp,” depending upon the specific vegetative species included in the various classes. The specific heights corresponding to these categories are listed below. Nodal elevations were then set by tallying the number of marsh pixels and water pixels within the elements surrounding each node and finding an average value based on the elevation assumptions. Any errors created by assuming marsh elevations should not greatly affect the results due

to the fact that the marshes have small elevation gradients; thus, small inaccuracies in elevation data should not affect surge results considerably when the surge is large. Grid scale averaging was applied as follows:

$$z = (h_{water} \cdot n_{water} + h_{fresh} \cdot n_{fresh} + h_{nonfresh} \cdot n_{nonfresh} + h_{swamp} \cdot n_{swamp}) / n_{total}$$

where:

z is the grid scale averaged elevation referenced to the NAVD88 (2004.65) datum;

h_{water} is an approximated water elevation of 1.3 ft below the NAVD88 (2005.65) geoid.

n_{water} is the total number of land cover pixels defined as water within a nodal control volume;

h_{fresh} is an approximated fresh marsh elevation of 1.5 ft above the NAVD88 (2004.65) geoid;

n_{fresh} is the total number of land cover pixels defined as fresh marsh within a nodal control volume;

$h_{nonfresh}$ is an approximated nonfresh marsh elevation of 1.1 ft above the NAVD88 (2004.65) geoid;

$n_{nonfresh}$ is the total number of land cover pixels defined as nonfresh marsh within a nodal control volume;

h_{swamp} is an approximated swamp elevation of 2.5 ft above the NAVD88 (2004.65) geoid;

n_{swamp} is the total number of swamp land cover pixels defined as marsh within a nodal control volume; and

n_{total} is the total number of land cover pixels within a nodal control volume.

Finally, barrier island topographic elevations were incorporated from a variety of sources as summarized in Figure 53. The Chandeleur Islands topographic elevations were obtained from post-Katrina Lidar surveys performed by the USGS (Salinger, 2006). The Mississippi Sound Islands were obtained from post-Katrina Lidar surveys performed by the USACE (Lillicrop, 2006). Half Moon Island, which is at the entrance of Lake Borgne; Deer Island, which protects Biloxi Bay; and Singing River Island, which lies southwest of Pascagoula, all had topography extracted from the Mississippi Automated Resource Information System (MARIS) 10-meter by 10-meter DEM database (Mississippi Automated Resource Information System, 2006).

It is noted that bathymetry and topography were predominantly defined for the condition that existed prior to August 2005 and Hurricane Katrina as defined with the available data. Many of the bathymetric surveys were collected over decades prior to 2005 while the topographic Lidar data for Louisiana was collected beginning in 2002. The other notable exception to incorporating pre-Katrina topographic data was for the Lidar-based surveys of the Chandeleur

and Mississippi Sound islands. Because these barrier islands represent critical controls to flow and induce significant wave radiation stress setup during the peak of the storm and our modeling does not include active degradation of these offshore sediment features, these are included in their post-Katrina configuration. The significant wave action would have degraded these barrier islands early in the Katrina event and their configuration during Hurricane Katrina will be closer to the post-Katrina configuration than to the pre-Katrina configuration.

3.1.3 Bathymetric Surveys/Data

Accurate bathymetric data is also crucial to flow modeling. Bathymetry controls long wave and short wind-wave propagation, speed, direction, structure, and dissipation. Bathymetry in the Western North Atlantic, the Gulf of Mexico, and the Caribbean Sea are included in the models. These data were drawn from a number of sources, including the raw bathymetric sounding database from the National Ocean Service (NOS), the Digital Nautical Charts (DNC) bathymetric database, and ETOPO5 (Mukai et al., 2001a; Mukai et al., 2001b). The NOS raw sounding database provides the most comprehensive coverage over U.S. continental shelf waters. This database includes more than 13 million sounding values and is the basis of NOS/NOAA bathymetric charts. Although not as comprehensive as the NOS raw soundings, DNC values are available within the Gulf of Mexico and much of the western North Atlantic and Caribbean Sea. ETOPO5 coverage is worldwide. Data accuracy and

preferences are in this descending order: NOS, DNC, ETOPO5 (Mukai et al., 2001a; Mukai et al., 2001b). Bathymetry for inland waterways in Southern Louisiana is provided by regional bathymetric surveys and dredging surveys, typically from the USACE New Orleans District (MVN). Detailed information on bathymetric data sources can be found in the FEMA DFIRM report (U.S. Army Corps of Engineers, 2007c).

3.1.4 Vertical Features with Small Horizontal Scales

In addition to describing bathymetry and topography, the model must account for pronounced vertical features with small horizontal scales relative to the grid scale. While features such as barrier islands, river banks, and salt domes as well as the associated flows are generally well resolved in grids with resolutions down to about 100 feet, features such as levees, floodwalls, railroads, and raised highways will not be sufficiently well resolved with 100-foot grid resolution. These small-scale features can, of course, be significant horizontal obstructions to flow causing water to rise or be diverted elsewhere. These obstructions must therefore be incorporated into the model as sub-grid scale features. These features were included as sub- and super-critical weirs.

Figure 56 shows all the federal levees. Federal levee centerline alignments and elevations were defined using the USACE GIS database with pre-Hurricane Katrina conditions in 2005. The configuration and position of these levees were checked against 1-foot by 1-foot Lidar data available prior to Hurricane

Katrina (U.S. Army Corps of Engineers, 2000; Army Corps of Engineers, 2007a, Ebersole, 2008).

Federal, state, and local roads as well as railroads were positioned in the horizontal using the USACE GIS database and had vertical positions defined from the Louisiana and Mississippi Lidar datasets (Louisiana State University, 2004; URS, 2006a). The crown height was obtained automatically by searching a defined region around the raised feature's point of interest. Limited detailed comparisons between Lidar data and ground surveys were done by URS and show elevation differences of up to approximately 1 foot for raised features in this region (Suhayda, 2007). These differences are related to local subsidence and datum errors in the Atlas Lidar data. Lidar information was still utilized due to the fact that the data set was the most comprehensive set available, outside of the survey sources used for the federal levees. Features were only included as sub-grid scale features if the crown height was more than 3 feet above the adjacent topography. Features lower than 3 ft were incorporated in the gridded topography.

In select areas, railroad crown heights were modified from the Lidar defined height data. The CSX railroad between Chef Menteur Pass and the Pearl River Basin between Lake Pontchartrain and Lake Borgne where the railroad is exposed to open water or low-lying non-forested marsh was lowered by about 5 feet from the Lidar-defined heights. Much of this railroad was degraded during Hurricane Katrina due to severe wave action and the high overtopping rates in

this region. CSX engineers on site involved in the post-Katrina railroad reconstruction indicated to the IPET team (Ebersole and Westerink, 2006; U.S. Army Corps of Engineers, 2007b) the level of degradation that occurred during the storm. Essentially, the top layer of gravel ballast was washed off together with the railroad tracks while the more solid clay core of the railroad bed remained intact. Farther into Mississippi, where the railroad is well protected by forests, the railroad appears to have suffered much less and the Lidar-based crown heights in these regions are not degraded. Raised road beds were typically defined using the Lidar-based crown height and assumed not to be degraded during a storm event. The exception to this was U.S. Highway 90 (US 90) between the Chef Menteur Pass and the Rigolets, which was degraded, because it was washed out in sections (based on a site visit by Ebersole and Westerink, 2006). Note that US 90 in Mississippi was not included as a sub-grid scale feature because this road is very limited in its vertical definition and can be well represented using standard grid meshing.

3.2 INFLUENCE OF COASTAL VEGETATION

Surface roughness significantly influences the flow of the overlying fluid, whether it is water or air. In the case of water flowing or waves propagating over a surface, the bottom friction force that is developed is an important resistance mechanism that must be accurately quantified. The Manning n bottom friction resistance formulation is applied in this study. This formulation is a widely used standard applied in hydraulic computations. In the case of air

flowing over a rough surface, the wind boundary layer is modified and the resulting 10 meters above ground level wind speed that is used to compute the surface drag is computed using the surface roughness and standard boundary layer theory. The wind boundary layer does not adjust instantaneously to the local roughness but adjusts slowly based on the upwind roughness (U.S. Army Corps of Engineers, 2007b; Westerink et al, 2008). Finally, it can be shown that very little wind momentum transfers through heavily forested canopies (Reid and Whitaker, 1976).

Land roughness in overland regions is characterized by land use conditions such as urban, forested, agricultural, or marsh as described by the USGS National Land Cover Dataset (NLCD) Classification raster map based upon Landsat imagery (Vogelmann et al., 2001) and the USGS GAP data (Hartley et al., 2000). Note that the aerial coverage of GAP data is not as widespread as NLCD. There are further differences between the NLCD and GAP with the NLCD being a "national" data set and being most reliable at large regional averages and not as good for capturing local details. The GAP data sets better characterize the small-scale variation of vegetation types near the coastal margin. GAP has been field checked by biologists and botanists and is considered to be more reliable. For example, NLCD only includes two classifications for wetlands: woody wetland and emergent herbaceous wetland. Most of Louisiana wetlands are classified as emergent herbaceous wetland. However, ground verification of these data through on-site visits, as well as by examining both satellite imagery and raw Lidar images (i.e., no bare earth),

indicates that this land classification is applied to grassy marshland as well as to thickly covered cypress forest covered marshes. On the other hand, the GAP database for Louisiana defines 11 classifications of wetland including Fresh Marsh, Intermediate Marsh, Brackish Marsh, Saline Marsh, Wetland Forest – Deciduous, Wetland Forest – Evergreen, Wetland Forest – Mixed, Wetland Scrub/Shrub – Deciduous, Wetland Scrub/Shrub – Evergreen, Wetland Scrub/Shrub – Mixed, and Wetland Barren. The Wetland Forest – Evergreen, for example, concisely defines the ubiquitous cypress forests in Louisiana. The Louisiana GAP map is shown in Figure 54.

The combined Louisiana and Mississippi GAP data and classifications, supplemented with NLCD over areas where GAP data were not available (Texas and Alabama), have been used to define the hydraulic bottom roughness. The Manning n associated with these land classifications was selected or interpolated/extrapolated from standard hydraulic literature (Chow, 1959; Henderson, 1966; Arcement and Schneider, 1989; Barnes, 1967). The LA-GAP classifications associated with Manning n that were selected and applied in Louisiana are given in Table 2. These values were used for all six scenarios in Southern Louisiana except for Scenarios H3, H4 and H6 within the MRGO zone of influence defined in Figure 1. For these cases within the zone of MRGO influence the 1956 land cover map in Figure 55 is used to define the land cover and Table 3 is used to define the Manning n.

The roughness lengths or more specifically "nominal" roughness lengths $z_{0_{land}}$ used to adjust the wind boundary layer are defined by the FEMA HAZUS program (Federal Emergency Management Agency, 2005). Because the FEMA HAZUS definitions were specifically defined for the NLCD, a modified form of the NLCD was used in order to define the roughness lengths. As was noted earlier, the NLCD classification was missing cypress forests. Therefore, any areas in the NLCD where GAP coverage indicated Wetland Forest – Evergreen have been overwritten in Louisiana. In effect, an additional cypress forest classification was created for the NLCD in Louisiana. This combined classification was used to define the roughness lengths as detailed in the FEMA DFIRM report (U.S. Army Corps of Engineers, 2007c).

Canopied areas can be identified with regions where the modified NLCD defines Deciduous Forest, Evergreen Forest, Mixed Forest, Woody Wetland, or Cypress Forest. Canopies are assumed to be so high that no water overtops them and that they are thick enough for wind not to penetrate them. Away from canopies, inundation of the physical roughness scales is allowed because as the areas are flooded, a reduction in the wind roughness length scale occurs as is described in Westerink et al. (2008) and the FEMA DFIRM report (U.S. Army Corps of Engineers, 2007c).

4.0 HYDRAULIC ANALYSIS

4.1 MODEL SYSTEM COMPONENTS

This Study utilizes a systems-based, integrated atmospheric-hydrodynamic modeling approach. The first components in the modeling sequence are the wind and atmospheric pressure field models. Kinematic models that use data assimilation methods are used to define the wind fields and pressure decay relationships in conjunction with observational data are applied to define the atmospheric pressure fields (Cox et al., 1995; Cox and Cardone, 2000; Powell and Houston, 1996; Powell et al., 1996; Powell et al., 1998). Due to the amount of wind data available for Hurricane Katrina, very accurate hindcast winds were generated.

Once the winds were generated, the global ocean model WAM was run in order to generate deep water waves in a Gulf of Mexico wide domain (Komen et al., 1994). These results were then applied as boundary conditions in three regional finer scale near-shore wave STWAVE models that provide comprehensive coverage in Southeastern Louisiana. These boundary conditions were applied using morphic interpolation to prevent peaks from being split due to refraction at adjoining points (Smith and Vincent, 2002). The STWAVE computations also include preliminary water levels obtained via linear interpolation of ADCIRC wind and atmospheric pressure, riverine flows, and tides. The last component to be run was the ADCIRC hydrodynamic model,

which is run with wind and atmospheric pressure, wind-wave radiation stresses from STWAVE, riverine flows, and tides.

There is significant interaction between the various component models. The wind models produce marine winds that are reduced for overland areas depending on the upwind roughness length scales and the existence of canopies. Once an area is inundated, the physical roughness elements are subject to immersion, and the nominal roughness length scales are subsequently reduced. Upon full immersion of the physical roughness elements, marine winds are again applied. The ADCIRC computations are forced with wave radiation stresses linearly interpolated from the three localized STWAVE computations for meshes located southeast of the Mississippi River, south of the Mississippi River and along the Mississippi/Alabama coast. The STWAVE computations themselves were run with boundary forcing information from the Gulf of Mexico WAM grid and surface water elevation information from preliminary ADCIRC simulations which included all forcing functions with the exception of the wave radiation stresses. Finally, we note that in order to consider the full nonlinear interaction of all flow components, the ADCIRC computations simultaneously include wind, atmospheric pressure, riverine flows, and wave radiation stresses, as well as tides.

4.1.1 Wind Models

The most significant forcing term in the storm surge computations is the wind stress and pressure field. Katrina winds used in this Study were developed for

the previous LACPR and FEMA DFIRM studies by Cardone (2007), Cardone et al. (2007), Cox (2007), and Powell et al. (2008). These winds are data assimilated winds using NOAA's Hurricane Research Division (HRD) H*WIND system (Powell and Houston, 1996; Powell et al., 1996; Powell et al., 1998) which are blended with Gulf-scale winds using the IOKA System (Cox et al., 1995; Cox and Cardone, 2000) developed by Oceanweather Inc. (OWI). Observational data comes from anemometers, airborne and land-based Doppler radar, airborne stepped-frequency microwave radiometer, buoys, ships, aircraft, coastal stations, and satellite measurements. For Katrina, the measured winds in the inner core are assimilated using NOAA's Hurricane Research Division Wind Analysis System (H*WIND) (Powell et al., 1996, 1998) and are then blended with Gulf-scale winds using an Interactive Objective Kinematic Analysis (IOKA) System (Cox et al., 1995; Cardone et al., 2007). H*WIND composites observations of wind velocity relative to the storm's center and transforms them to a common reference condition of 10-meter height, peak 1-minute averaged "sustained" wind speed, and marine exposure. A special set of H*WIND reanalyzed snapshots are available for Katrina (Powell et al., 2008). Peripheral winds are derived from the NOAA National Centers for Environmental Prediction/National Center for Atmospheric Research Reanalysis Project (Kalnay et al., 1996). Before inner-core and peripheral wind fields are blended, the inner core peak "sustained" winds are transformed to 30-minute average wind speeds using a gust model consistent with the H*WIND system. A final step is to inject local marine data,

adjusted to a consistent 10-meter elevation and neutral stability using the IOKA System. Lagrangian based interpolation is used to produce the final wind fields on a regular 500m x 500m grid with snapshots every 15 minutes.

4.1.2 Offshore Wave Model WAM

The WAM model is run to generate deepwater wave fields and directional spectra in a Gulf of Mexico domain. WAM is a third-generation discrete spectral wave model that solves the wave action balance equation and includes source-sink terms, atmospheric input, nonlinear wave-wave interactions, white-capping, bottom friction, and depth-limited wave breaking. The spatial and temporal variation of wave-action in frequency and direction is solved over a fixed spatial grid (Komen et al., 1994). WAM has recently undergone major revisions to source term specification, multi-grid nesting, and depth-limited breaking (Gunther, 2005, Jensen, 2006). The model computes directional wave spectra for 28 discrete frequency bands, and 24 directional bands centered every 15 degrees.

The WAM model domain, shown in Figure 57 extends over the entire Gulf of Mexico with a grid at 0.05° resolution. It is assumed that the wind waves are generated in the Gulf and that wave energy entering the Gulf and reaching the area of interest through the Florida and Yucatan Straits is minimal. The water depth is derived from the General Bathymetric Chart of the Oceans (GEBCO, 2003). The H*WIND/IOKA 30-minute averaged wind fields are linearly interpolated in time and space onto the WAM grid. WAM was extensively

validated for a variety of hurricanes as detailed in the FEMA DFIRM report (U.S. Army Corps of Engineers, 2007c).

4.1.3 Nearshore Wave Model STWAVE

The numerical model STWAVE (Smith, 2000; Smith et al., 2001; Smith and Smith, 2001; Thompson et al., 2004; Smith and Zundel, 2006, Smith, 2007) was used to generate and transform waves to the shore for Hurricane Katrina. The source terms include wind input, nonlinear wave-wave interactions, dissipation within the wave field, and surf-zone breaking. The assumptions made in STWAVE are as follows: Mild bottom slope and negligible wave reflection; Steady waves, currents, and winds; Linear refraction and shoaling; Depth-uniform current. STWAVE can be implemented as either a half-plane model, meaning that only waves propagating toward the coast are represented, or a full-plane model, allowing generation and propagation in all directions. Wave breaking in the surf zone limits the maximum wave height based on the local water depth and wave steepness.

STWAVE is a finite-difference model and calculates wave spectra on a rectangular grid. The model outputs zero-moment wave height, peak wave period (T_p), and mean wave direction (α_m) at all grid points and two-dimensional spectra at selected grid points. Recent upgrades to STWAVE include an option to input spatially variable wind and surge fields. The surge significantly alters the wave transformation and generation for the hurricane

simulations in shallow areas (such as Lake Borgne) and where low-lying areas are flooded.

STWAVE is applied on three grids for the Southern Louisiana area: Louisiana Southeast, Louisiana South, and Mississippi/Alabama (Figure 58). The STWAVE grids cover the coastal areas east, southeast, and south of New Orleans at a resolution of 656 feet (200 meters). The domain for the Louisiana Southeast grid is approximately 84.9 by 92.4 miles (136.6 by 148.8 km) and extends from the Mississippi Sound in the northeast to the Mississippi River in the southwest. The domain for the Louisiana South grid is approximately 102.5 by 104.2 miles (165.0 by 167.8 km) and extends from the Mississippi River in the east to the Atchafalaya River in the west. The domain for the Mississippi and Alabama coasts was added to simulate the wave momentum fluxes that increase the surge in the Mississippi Sound and Lake Pontchartrain. The Mississippi/Alabama domain is approximately 70.0 by 75.2 miles (112.6 by 121.0 km) and extends from east of Mobile Bay to Biloxi, Mississippi. All bathymetry and bottom friction parameters for these grids were interpolated from the ADCIRC grid. These three grids are run with the half-plane STWAVE for computational efficiency.

The simulations are forced with both the wave spectra interpolated on the offshore boundary from the WAM model. The input for each grid also includes surge fields (interpolated from ADCIRC surge fields), and wind (interpolated from the ADCIRC wind fields, which apply land effects to the OWI wind

fields). The wind applied in STWAVE is spatially and temporally variable for all domains. STWAVE was run at 30-minute intervals for 96 quasi-steady state time steps (U.S. Army Corps of Engineers, 2007c).

The importance of time dependence in the solution was investigated on a Lake Pontchartrain grid by comparing results from the SWAN near-shore wave model run in stationary and non-stationary mode. These results were nearly identical, indicating that a stationary solution is sufficient (U.S. Army Corps of Engineers, 2007c).

STWAVE validation is provided in a number of references (e.g., Smith et al., 1998; Smith et al., 2000; Smith, 2000; Smith and Smith, 2001; Ris et al., 2002; Thompson et al., 2004; U.S. Army Corps of Engineers, 2007c). STWAVE also shows reasonable agreement with the limited measurements in Lake Pontchartrain for Hurricane Katrina (U.S. Army Corps of Engineers, 2007c).

STWAVE passes radiation stresses to the circulation model to calculate wave setup and provides wave parameters for the calculation of wave run-up and overtopping on structures.

4.1.4 ADCIRC Circulation Model

ADCIRC was selected as the basis for the surge modeling effort. This model is the standard coastal surge model utilized by the USACE. The domain and geometric/topographic description and resulting computational grids developed

for the Study used the LACPR and FEMA DFIRM SL15 domain/grid with resolution improvements in the Study Region as the base. The SL15 domain and grid extend across the floodplains of Southern Louisiana and Mississippi and span the entire Gulf of Mexico to the deep Atlantic Ocean, as shown in Figure 59 and Figure 60. The SL15 domain boundaries were selected to ensure the correct development, propagation, and attenuation of storm surge without necessitating nesting solutions or specifying ad hoc boundary conditions for tides or storm surge.

4.1.4.1 ***ADCIRC Model Description***

ADCIRC-2DDI, the two-dimensional, depth-integrated implementation of the ADCIRC coastal ocean model, is used to perform the hydrodynamic computations on unstructured meshes (Luettich et al., 1992; Westerink et al., 1992; Westerink, 1993; Luettich and Westerink, 2004). The model uses the depth-integrated barotropic equations of mass and momentum conservation subject to the incompressibility, Boussinesq, and hydrostatic pressure approximations. Additionally, the equations of motion are solved for an unstructured finite element mesh, permitting shallow water equation solutions that can localize resolution leading to globally and locally more accurate solutions within the realm of feasible computational expense. Details of the ADCIRC model can be found in Luettich and Westerink (2004), Atkinson et al. (2004), Dawson et al. (2006), Westerink et al., 2008.

4.1.4.2 ***SL15 Domain/Grid Definition***

The SL15 model domain and grid, shown in Figure 59 and Figure 60, was developed for the LACPR and FEMA DFIRM studies and has been further refined in and around the IHNC and MRGO for this study (U.S. Army Corps of Engineers, 2007b, U.S. Army Corps of Engineers, 2007c). The SL15 domain has an eastern open ocean boundary that lies along the 60 degree west meridian, extending south from the vicinity of Glace Bay in Nova Scotia, Canada, to the vicinity of Coracora Island in eastern Venezuela (Westerink et al., 1994; Blain et al., 1994; Mukai et al., 2002; Westerink et al., 2008; Ebersole et al., 2007, U.S. Army Corps of Engineers, 2007b; U.S. Army Corps of Engineers, 2007c). This domain has a superior open ocean boundary that is primarily located in the deep ocean and lies outside of any resonant basin. There is little geometric complexity along this boundary. Tidal response is dominated by the astronomical constituents, nonlinear energy is limited due to the depth, and the boundary is not located near tidal amphidromes. Hurricane storm surge response along this boundary is essentially an inverted barometric pressure effect directly correlated to the atmospheric pressure deficit in the meteorological forcing; it can therefore be easily specified. This boundary allows the model to accurately capture basin-to-basin and shelf-to-basin physics.

Much of the domain is bordered by a land boundary made up of the eastern coastlines of North, Central, and South America. The highly detailed/resolved

region extends to the west of Beaumont, Texas, and to the east of Mobile Bay. These areas in Texas and Alabama were included in order to allow storm surge that affects Louisiana and Mississippi to realistically attenuate and laterally spread into the adjacent states. In Southern Louisiana and Mississippi, the domain includes a large overland region that is at risk for storm surge induced flooding. Details of the domain with bathymetry and topography as well as levees and raised roadways across Southeastern Louisiana can be seen in Figure 61, Figure 63, Figure 3, Figure 4 and Figure 5. The northern land boundary extends inland and runs along high topography or major hydraulic controls. From Texas, the land boundary runs along the 30ft to 75ft land contour to Simmesport, Louisiana. The boundary was positioned such that lower lying valleys and the adjacent highlands were included. From the vicinity of Simmesport at the Old River flood control, the domain boundary is defined along the west bank Mississippi River levee up to Baton Rouge. At Baton Rouge, the domain boundary runs along Interstate 12 to east of Hammond, Louisiana. Then the boundary heads straight east through Covington, Louisiana, and Abita Springs, Louisiana, until State Highway 41 is reached which runs along the Pearl River Basin. From here, the northern boundary encompasses the 30ft to 75ft contours incorporating valleys that penetrate north all the way to the eastern highlands of Mobile Bay. It is critical that boundary location and boundary condition specification do not hinder physically realistic model response.

We have incorporated critical hydraulic features and controls that both enhance and attenuate storm surge. Rivers and channels can be conduits for storm surge propagation far inland. Topographical features such as levee systems stop flow and can focus storm surge energy into local areas, resulting in the amplification of storm surge. Floodplains and wetlands cause attenuation of flood wave propagation. In Louisiana, there are many interconnected features including deep naturally scoured channels, wetlands, and an extremely extensive and intricate system of river banks, levees, and raised roadways. We have incorporated the Mississippi and Atchafalaya rivers, numerous major dredged navigation canals including the GIWW, the IHNC, the MRGO, Chef Menteur Pass, the Rigolets, and lakes and bays including Lake Pontchartrain, Lake Maurepas, Lake Borgne, Barataria Bay, Timbalier Bay, Terrebonne Bay, Lake Salvador, Lac des Allemands, Atchafalaya Bay, Vermilion Bay, White Lake, Grand Lake, Calcasieu Lake, and Sabine Lake. In Mississippi, we have incorporated St. Louis Bay, Biloxi Bay, Pascagoula Bay, and Mobile Bay as well as the connected channels. All significant levee systems, elevated roads, and railways have been specifically incorporated into the domain as barrier boundaries. These raised features are represented either as internal barrier boundaries or as external barrier boundaries when they are at the edge of the domain and compute overtopping using weir formulae. The levee and raised topographic systems are very extensive in Southern Louisiana and surround many rivers, lakes, and cities including the Mississippi River, the western shore of Lake Pontchartrain, the city of New Orleans, and the channels that intersect

it, between Thibodaux and Larose, at Morgan City, and around the Atchafalaya flood basin. Thus, all the federal levee systems have been incorporated as have numerous state, local, and private levee systems. There are numerous highways and state roads that are elevated and act as hydraulic controls: Interstates 12 and 10, US 61, US 90, and US 11 and many of the state routes. In Mississippi, we have incorporated the CSX railroad as well as Interstate 10 and a limited number of north-south raised roads.

The computational grid, shown in Figure 60, Figure 62, and Figure 64, has been constructed to provide sufficient resolution for the tidal, wind, wind-wave, atmospheric pressure, and riverine flow forcing functions from the ocean basins to the coastal floodplain. Efficient and effective resolution of tidal response within the basins and on the shelf is determined by tidal wavelength criteria (Westerink et al., 1994; Luettich and Westerink, 1995). The grid also has increased resolution at the shelf break guided by a topographic length scale criteria in order to capture the higher localized wave number content (Hagen et al., 2000; Hagen et al., 2001). Hurricane forcing and response are also examined to determine the level of resolution required in order to accurately model hurricane effects. In deep water, under-resolution of the inverted barometer forcing function results in under-prediction of the peak inverted barometer effect. This phenomenon, which involves smearing of the inverted barometric pressure effect, results from insufficient resolution for the interpolation of the input atmospheric pressure field onto the hydrodynamic mesh. Enhanced resolution in shelf waters adjacent to hurricane landfall

locations is critical because under-resolution can lead to over-prediction of peak storm surge (Blain et al., 1998).

The grid design provides localized refinement of the coastal floodplains of Southern Louisiana and Mississippi and of the important hydraulic features. The SL15 grid is refined locally to resolve features such as inlets, rivers, navigation channels, levee systems, and local topography/bathymetry. An unprecedented level of detail in Southern Louisiana and Mississippi is incorporated, with nodal spacing reaching as low as 65 feet in the most highly refined areas. This high level of resolution includes the MRGO, GIWW and the IHNC.

In addition, wave breaking zones have been identified based on local bathymetric gradients, and a swath of 150- to 700-foot grid resolution has been placed along the coast, over barrier islands, and around Lake Pontchartrain to ensure that the grid scale of the flow model is consistent with that of the STWAVE model. We accommodated the STWAVE forcing function by adding a high level of resolution where there were significant gradients in the wave radiation stresses and forcing of surge through wave transformation and breaking are the largest. We accommodated the three STWAVE grids shown earlier in this report and added resolution in these transformation/breaking zones along the coast from west of Atchafalaya Bay, Terrebonne Bay, Timbalier Bay, Barataria Bay, Breton Sound, Chandeleur Sound, and the Mississippi Sound. These high-resolution zones allow for the strong wave

radiation stress gradients to fully force the water body in these important regions and ensure that the resulting wave radiation stress induced setup is sufficiently accurate. Barrier islands were in particular very highly resolved to 150 to 250 feet due to the significant wave breaking and the resulting important wave radiation stresses as well as the very high currents that develop over the features.

4.1.4.3 ***Bathymetric, Topographic and Feature Definition***

As described in Section 3, geometry, topography, and bathymetry in the SL15 model were all defined to replicate the prevailing conditions in August 2005 prior to Hurricane Katrina with the exception of some of the barrier islands and area between Lake Pontchartrain and Lake Borgne that were included as post-Katrina September 2005 configurations.

4.1.4.4 ***Bottom and Lateral Friction Process***

The standard quadratic parameterization of bottom stress is applied. In order to model the spatially variable frictional losses, we apply a Manning n formulation in order to compute the bottom friction coefficient. Nodal Manning n coefficients are spatially assigned using the LA-GAP, MS-GAP, and NLCD land type definition and the associated Manning n value defined in Section 3 and the FEMA DFIRM report (U.S. Army Corps of Engineers, 2007c). Figure 65, Figure 6, Figure 7, and Figure 8 show the applied Manning n values in Southeastern Louisiana for case H1. The Manning n values for the

water and land regions were selected by consulting standard Manning values given in the hydraulic literature. The Manning n values were based on “Open Channel Hydraulics” (Chow, 1959) and the "Guide for Selecting Manning’s Roughness Coefficients for Natural Channels and Flood Plains" (Arcement and Schneider, 1989). For the open ocean, large inland lakes, sheltered estuaries, inland lakes, deep straight inlets channels, deep meandering rivers, and shallow meandering channels, n is assigned to equal 0.02, 0.02, 0.025, 0.025, 0.02, 0.025, and 0.045, respectively. We apply a grid scale rectangle surrounding the node of interest and again select all GAP or NLCD based land use values and average their associated Manning n. This effectively implements grid scale averaging for the Manning n selection process. The LA-GAP, map and classifications associated with Manning n that were selected and applied in Louisiana are presented in Figure 54 and Table 2. NLCD and MS-GAP values are described in the FEMA DFIRM report (U.S. Army Corps of Engineers, 2007c). These values were used for all six scenarios in Southern Louisiana except for Scenarios H3, H4 and H6 within the MRGO zone of influence defined in Figure 1. For these cases within the zone of MRGO influence, the 1956 land cover map in Figure 55 is used to define the land cover and Table 3 is used to define the Manning n.

4.1.4.5 ***Land, River and Tidal Forcing Functions***

At land boundary nodes outside of Southern Louisiana and Mississippi, a no-normal flow condition is applied. At land boundaries in Southern Louisiana and Mississippi, no normal flow and external barrier boundaries are specified.

At river boundaries, a simple elevation or flux boundary condition would reflect tides and surge waves that are propagating upriver back into the domain. In order to prevent this non-physical reflection from occurring, a wave radiation boundary condition was developed that specifies flux into the domain while allowing surface waves to propagate out (Luettich and Westerink, 2003; Westerink et al., 2008).

River inflow to the Mississippi River at Baton Rouge and to the Atchafalaya River at Simmesport is specified as a flux per unit width as defined by the wave radiation boundary condition. Historical hindcasts are simulated with discharge values averaged over the time of the storm available from stream gauge data from the hurricane event. A 2-day spin-up period with a 0.5-day hyperbolic ramping function is applied to the river boundary forcing prior to any additional model forcing. This allows for a dynamic steady state in the rivers to be established prior to interaction with any other forcing terms to properly define pre-tide and pre-storm river stage on the boundaries, ζ_{river}.

For the Hurricane Katrina simulation in this report, the Mississippi and Atchafalaya rivers are forced with steady flows of 167,000 ft^3/s and 70,000 ft^3/s

respectively. Actual flow rates in the Mississippi river ranged from 167,000 ft^3/s to 172,000 ft^3/s between August 27 and August 31. Actual flow rates in the Atchafalaya River ranged from 70,000 ft^3/s to 75,000 ft^3/s between August 27 and August 31. Steady flows are applied to work with the river radiation boundary conditions used in these rivers. The river flows were ramped up from zero flow to the full specified flow between 08/07/0000 UTC-08/07/1200 UTC and were allowed to establish equilibrium between 08/07/1200 UTC-08/09/0000 UTC. After 08/09/0000 UTC the radiation boundary conditions are applied.

Water level fluctuations in the ocean's surface due to low frequency phenomena are specified through several forcing functions. First, the open ocean boundary is forced with the K_1, O_1, M_2, S_2, and N_2 tidal constituents, interpolating tidal amplitude and phase from Le Provost's global tidal model based upon satellite altimetry (Le Provost et al., 1998) onto the open ocean boundary nodes. Second, tidal potential forcing that incorporates an appropriate effective earth elasticity factor for each constituent was applied on the interior of the domain for these same constituents (Westerink et al., 1994; Mukai et al., 2002). The nodal factor and equilibrium argument for boundary and interior domain forcing tidal constituents were determined based on the starting time of the simulation (Luettich and Westerink, 2004).

The resonant characteristics of the Gulf of Mexico require a period of model simulation in order for the start-up transients to physically dissipate and

dynamically correct tidal response to be generated. The model is run with tidal forcing for a minimum of 16 days before hurricane forcing so that the tidal signal can become effectively established; this spin-up time was determined through testing of model sensitivity to the generation of resonant modes using separate single semi-diurnal and diurnal tidal constituents. A hyperbolic tangent ramp function is applied to the first 10 days of the tidal forcing to minimize the generation of start-up transients. For Hurricane Katrina, tidal forcing with ramping was initiated at 08/09/0000 UTC with hyperbolic ramp completing at 08/19/0000 UTC. Tides are then allowed to establish a dynamic equilibrium between 08/19/0000 UTC-08/25/0000 UTC.

4.1.4.6 ***LMSL and Steric Water Level Adjustments***

The computations are referenced to NAVD88 (2004.65), which is a geodetic equipotential surface. The average offset between LMSL and NAVD88 (2004.65) examined by IPET within Southern Louisiana is 0.44 foot (U.S. Army Corps of Engineers, 2007c).

In order to make the seasonal sea surface adjustment for hindcast storms, NOAA's long-term sea level station data is investigated at the time of landfall of the storm. Thus for Katrina, which occurred in late August, sea surface level increase above the annual average is regionally estimated as 0.34 foot above LMSL.

Initial water levels in all regions are therefore raised at the start of the computation with the combined average regional difference between LMSL and NAVD88 (2004.65) in addition to the steric increase in water. For Katrina, this adjustment equals 0.44 foot + 0.34 foot = 0.78 foot. This adjustment is specified in both the initial conditions as well as in surface elevation-specified boundary conditions. Thus, the initial water levels are raised by this amount in areas where this water surface is such that it lies above the defined bathymetry/topography by more than the minimum wetting depth, H_0, and where the computational points do not lie within a specially defined dry ring levee region. In addition, the defined offset is added to the open ocean boundary conditions, which are located in the deep Atlantic Ocean. Further details can be found in the FEMA DFIRM report (U.S. Army Corps of Engineers, 2007b).

4.1.4.7 ***Atmospheric Forcing Functions***

As is typical in ADCIRC version 46.58, the wind surface stress is computed by a standard quadratic drag law, with the drag coefficient defined by Garratt's drag formula (Garratt, 1977). The drag coefficient is limited to 0.0035 to represent sheeting processes. Powell et al. (2003) found upper limit values based on GPS dropwindsondes as low as 0.0025 although there appears to be strong quadrantal variation, the limit may be higher in outer portions of the storm and values in shallow shelf waters are only now being obtained.

Upwind wind roughness values are computed in 12 directions to account for the gradual modification in the wind boundary layer with example directional roughness values given in Figure 66 through Figure 69. Canopied areas identified with regions defined by dense forest in the LA-GAP, MS-GAP, and NLCD land type datasets are shown in Figure 70 and are implemented so that no wind forcing penetrates them. Further details of atmospheric forcing functions can be found in Westerink et al. (2008) and U.S. Army Corps of Engineers (2007c).

The Katrina simulations in this report were forced with wind and atmospheric pressure fields used for the FEMA DFIRM study and provided by Oceanweather Inc. and the NOAA Hurricane Research Division (HRD) for the period of 8/25/2005 00:00 UTC through 8/31/2005 00:00 UTC every 15 minutes. The 30 minute averaged winds obtained from OWI were converted to 10 minute averaged winds by multiplying by a factor of 1.09 as recommended by Cardone (2007) to be consistent with the averaging period used in the air-sea drag law. The wind and pressure fields at a fractional time are computed by a linear interpolation in time (U.S. Army Corps of Engineers, 2007c).

4.1.4.8 ***Wave Radiation Stress Forcing***

In our modeling system, we consider the interaction between the wind waves and the surge by applying wave radiation stress forcing. We force the ADCIRC computations with wave radiation stresses from the three localized STWAVE computations from eastern Louisiana, west of the Mississippi River, east of the

Mississippi River, and south of the Mississippi-Alabama coasts. Although the WAM model is used to force the open water boundary for the STWAVE computations, no forcing information is directly applied from the WAM model to the ADCIRC circulation computation. We note that a preliminary ADCIRC simulation is performed without wave radiation stress forcing and that this provides preliminary water level and current information for the STWAVE computations. Thus, the water levels provided to STWAVE do not include the effect of wave setup. This establishes a good level of two-way coupling between the two models. The resulting STWAVE radiation stress gradients computed every half-hour were then interpolated to the unstructured ADCIRC grid using bi-quadratic interpolation within the structured wave grid. Further details can be found U.S. Army Corps of Engineers (2007c).

The STWAVE computed wave radiation stress fields are read every 30 minutes during the period 08/28/1200 UTC-08/30/1200 UTC and are linearly interpolated in time and space.

4.1.4.9 ***Model Operational Parameter Definitions***

For hurricane storm surge inundation, wet/dry parameters that are relatively unrestrictive have been found to work well: the minimum wetting depth H_0 = 0.10 m and the minimum forward current to initiate wetting U_{min} = 0.01 m s^{-1}. The applied computational time step in the simulations is 0.5 second.

4.2 SOLUTION PROCEDURE (PROCESS MANAGEMENT)

Each simulation is performed in five computational parts or *Production Steps*. The boundary conditions (river and tide), tidal potential functions, wind and pressure fields, and the wave energy spectra boundary conditions (as computed by the deep water wave model WAM) are all required inputs to the system.

ADCIRC0: Each simulation is started or spun up from a cold or no motion condition at 8/7/0000 UTC, first for the river forcings in the Atchafalaya and Mississippi rivers, followed by the tidal forcings. The rivers are spun up first using flow specified boundary conditions at Simmesport LA and at Baton Rouge LA to reach a dynamic steady state after 2 days (8/7/0000 UTC – 8/9/0000 UTC). The river boundary conditions are then switched to radiation type so that the downriver flow is maintained but tides and surges are allowed to propagate upriver instead of being reflected back into the domain at the boundaries (Westerink et al,, 2008). Then ADCIRC tidal forcing at the Atlantic open ocean boundary (obtained from a global tidal model) as well as deterministic lateral internal tidal forcing functions specified throughout the domain are added to the computation. The tides are allowed to reach a dynamic equilibrium during the 16 days of tide simulation (8/9/0000 UTC – 8/25/0000 UTC). The model state is output to disk to provide initial conditions for continuation of the simulation (step ADCIRC1), and for the subsequent rerun of step ADCIRC2 that includes wave radiation stresses from STWAVE (step ADCIRC3).

ADCIRC1: Each simulation is started from the river and tide spin up (ADCIRC0). ADCIRC is run from the start of the PBL wind field to about 24 hours prior to landfall of the storm (ADCIRC1, River+Tides+Winds) (8/25/0000 UTC – 8/28/1200 UTC). The model state is output to disk to provide initial conditions for continuation of the simulation (step ADCIRC2), and for the subsequent rerun of step ADCIRC2 that includes wave radiation stresses from STWAVE (step ADCIRC3).

ADCIRC2: The ADCIRC1 solution (River+Tides+Winds) is then continued to the termination of the PBL wind/pressure fields (8/28/1200 UTC – 8/30/1200 UTC). The ADCIRC2 global water level (fort.63) and wind field (fort.74) are output to provide to STWAVE as input.

STWAVE: The ADCIRC2 solution in the previous step is interpolated to the STWAVE domains, and each STWAVE domain is executed to generate wave radiation stress gradients for input back to ADCIRC in step ADCIRC 3 (8/28/1200 UTC – 8/30/1200 UTC).

ADCIRC3: ADCIRC2 is re-run over the same time period as in step ADCIRC2, but including the wave radiation stress gradient computed by STWAVE and interpolated onto the ADCIRC grid. This is the River+Winds+Tides+RadStress solution and is also referred to as the ADCIRC+STWAVE step and is run past the end of the wind fields in order to allow the recession process to be computed (8/28/1200 UTC – 9/1/0000 UTC).

5.0 SIMULATION RESULTS

5.1 SCENARIO H1: *KATRINA REAL RUN* - KATRINA SIMULATION WITH THE 2005 PHYSICAL SYSTEM

5.1.1 ADCIRC Water Level and Current Computations

The evolution of the storm surge produced by Hurricane Katrina in southeastern Louisiana and southwestern Mississippi is shown in a sequence of contour maps representing a time period between 29 August at 7:00 UTC and 29 August at 23:00 UTC. The contour maps show a sequence of the winds, the surge levels, and the water currents during the Katrina event at various levels of detail. Two areas of detail are shown: southeastern Louisiana and southwestern Mississippi; and Lake Pontchartrain and metropolitan New Orleans.

For the area of southeastern Louisiana and southwestern Mississippi, Figures Figure 71 to Figure 81 show the contour maps of the wind speeds with wind vectors superimposed. Figure 82 to Figure 92 show the surface water elevation contour maps with superimposed wind vectors. Figure 93 to Figure 103 show the currents with superimposed current vectors. These figures show water elevations in feet, water currents in ft/sec, and wind speeds in knots.

The next sequence, Figure 104 through Figure 136, show the same information as Figure 71 through Figure 103, but with a more detailed view of Lake Pontchartrain and metropolitan New Orleans.

In general, the contour maps clearly show that storm response over Southeastern Louisiana is highly localized and varies rapidly over even a few miles. Surge heights are controlled in part by physical features such as the protruding delta, the shelf, barrier islands, levees, river berms, raised roads, inlets, channels and rivers. Breaks, discontinuities, and bridge openings in the raised features are also important. The importance of raised features is enhanced by the presence of shallow water adjacent to the raised feature. The shallower the water, the more effective is wind stress for increasing surface water gradients and in piling up water against obstructions. The geometry of the Study Region, the broad shelf, the ubiquitous shallow waterbodies, the low lying wetlands and the large size of the Katrina storm combined with the extreme waves generated during its most intense phase, enabled this storm to produce very large storm surges in Southeastern Louisiana.

On 29 August at 7:00 UTC (shown in Figure 71, Figure 82, Figure 93, Figure 104, Figure 115, Figure 126), Hurricane Katrina had degraded to a Category 4 storm with the eye approximately 80 miles south of the initial landfall location. The predominantly easterly wind is blowing water into Breton and Chandeleur Sounds as well as into Lake Borgne. In particular, water is pushed westward until it is stopped by the Mississippi River levees and by the St. Bernard/Chalmette protection levee where surge is building up to 10 ft. The water level is also increased on the southwest end of Lake Pontchartrain where the railroad berm holds the water. Simultaneously, water levels are suppressed in eastern Lake Pontchartrain. The combined water level rise in Lake Borgne

and the drawdown of water in eastern Lake Pontchartrain causes a strong surface water gradient across the inlets that connect these two water bodies, Chef Menteur Pass and the Rigolets Strait. This gradient moves a current that drives water into Lake Pontchartrain which is further reinforced by the easterly winds. The velocities in the Rigolets and Chef Menteur channels between these two water bodies are already 4-7 ft/s. The flow through these passes initiates the critical rise of the mean water level within Lake Pontchartrain. Finally, note that the predominantly easterly and northerly winds to the west of the Mississippi River force a drawdown of water away from the west-facing levees in these regions.

On 29 August at 10:00 UTC (shown in Figure 72, Figure 83, Figure 94, Figure 105, Figure 116, Figure 127), Hurricane Katrina is located 30 miles south of its initial landfall location and the winds over the critical regions are still predominantly from the east. Figure 72 shows very clearly the position of the eye and the highest wind velocities in the right front quarter of the storm. The wind speeds over the region mostly exceed 64 knots, which means the winds are mostly at Hurricane strength. The highest wind speeds, up to 90-95 knots, are located south of the Mississippi delta and have a southeasterly to easterly direction. Lake Borgne is due north of the storm center and directly in the storm's path where the winds are east-northeasterly at speeds of 55 to 65 knots. Lake Pontchartrain is in the left-front quadrant of the storm, a little more distant from the eye of the storm, and winds there are from the north-northeast at 40 to 55 knots.

Surge is building up to about 18 feet along the Mississippi levees between Buras and Pointe a la Hache. The easterly wind direction over Breton Sound pushes the water to the west against the levees in this region. The water level in the Inner Harbor Navigation Canal (IHNC) is already 11 feet. The difference in water level between Lake Borgne and the eastern part of Lake Pontchartrain is already about 6 feet and the currents in Chef Menteur Pass and the Rigolets Strait are increasing to 5 to 8 ft/s. We also note the high velocities (up to 9 ft/s) over the Chandeleur Islands and around the Mississippi River delta.

On 29 August at 11:00 UTC (shown in Figure 73, Figure 84, Figure 95, Figure 106, Figure 117, Figure 128), Hurricane Katrina is nearing landfall. The eye is located westward from the southern Plaquemines Parish levees, and the highest wind velocities are located just east of the delta. The surge continues to build up against the levees of lower Plaquemines Parish reaching elevations up to 19 ft. The surge in this region has started to propagate up the Mississippi River and also extends broadly into Breton Sound. Further north, surge continues to build up against the St. Bernard/Chalmette protection levee, due to the now north-easterly winds, up to 13 feet. The difference in water level between Lake Pontchartrain and Lake Borgne continues to increase up to 7-8 feet.

On 29 August at 12:00 UTC (shown in Figure 74, Figure 85, Figure 96, Figure 107, Figure 118, Figure 129), the eye location has caused a significant shift in the wind patterns in the coastal region. The storm has just made landfall and most of the waters surrounding southeastern Louisiana are exposed to wind

speeds greater than 80 knots. Because the center of the storm is moving through the region, the different water bodies in the area are being exposed to different and rapidly changing wind conditions. Winds in Breton Sound continue to blow from the south and southeast at speeds between 80 and 100 knots. Winds over Lake Borgne are now blowing from the northeast at speeds of approximately 90 knots. In Lake Pontchartrain, winds are shifting rapidly and are now from the north-northeast at speeds ranging from 55 to 80 knots depending on location within the Lake (higher wind speeds on the east side of the Lake).

Surge has started to be blown off the southern-most east-facing levees of Plaquemines Parish, although surge continues to build up further north along the river levees. Surge has now reached 16 ft along the St. Bernard/Chalmette protection levee and is being driven through the GIWW into the IHNC and Lake Pontchartrain. In addition, the northeasterly winds over Lake Pontchartrain are building up surge against the lake levees of Jefferson Parish and Orleans Parish. In addition, the strong surface water gradient aided by the winds between Lake Borgne and Lake Pontchartrain continue to drive water from Lake Borgne into Lake Pontchartrain. This process is enhanced by the drawdown in the northeast corner of Lake Pontchartrain. The currents in Chef Menteur Pass and the Rigolets Strait are increasing to 7 to 10 ft/s. Note the higher velocities in Lake Pontchartrain around eastern New Orleans. The current vectors in Figure 96 and Figure 129 show that large amounts of water are pushed inside Breton Sounds, Chandeleur Sounds and Mississippi Sounds.

On 29 August at 13:00 UTC (shown in Figure 75, Figure 86, Figure 97, Figure 108, Figure 119, Figure 130), the storm continues to move in a northern direction over Lake Borgne. The wind patterns over the area are quickly changing. The wind directions in Lake Pontchartrain are starting to move from northeast to north-northwestern winds. The surge that built up against the lower Mississippi River levees is propagating rapidly in a northeasterly direction towards Chandeleur Sound. The component of the surge propagating up the Mississippi River reaches 16 ft. Surge is also being driven from the west in southern Plaquemines Parish near the city of Venice. Surge is peaking along the St. Bernard Parish/ Chalmette protection levee and in the triangular region defined by levees along the GIWW and the MRGO. Within Lake Pontchartrain, surge is now strongly focused on the south side of the lake and a well defined drawdown exists along the north shore. It is noted that surge has not built up along the concavity in the Mississippi River along English Turn, due to the change in the direction of the winds. In this region water is now pushed away from English Turn.

On 29 August at 14:00 UTC (shown in Figure 76, Figure 87, Figure 98, Figure 109, Figure 120, Figure 131), Hurricane Katrina is now located over Lake Borgne. Compared to a few hours earlier, the wind field pattern has completely changed. In Lake Pontchartrain, the wind now blows from a north-northwestern direction. Due to the western wind direction, the water is pushed away from the lower Plaquemines Parish and Mississippi River delta levees. The surge originating along these levees continues to propagate across Chandeleur Sound

towards the Mississippi Sound in a northeasterly direction. Surge is attenuating along lower Plaquemines on the east side of the river, as is the surge that is propagating up the Mississippi River itself, due to winds from the west and north. Water continues to pile up from the west along the levees near Venice. Surge along the St. Bernard/Chalmette protection levee and in the Golden Triangle confluence is attenuating. Water is being blown from the north of Lake Pontchartrain and continues to build up along the southern shores of Lake Pontchartrain to around 9 ft. Water is accumulating from the east and overtopping the CSX railroad between Lake Borgne and Lake Pontchartrain. The gradient in water level between the northern and southern side of Lake Pontchartrain increases to about 7 feet. Nevertheless, the difference in water level in Lake Borgne and Lake Pontchartrain is also still increasing and still causing high volumes of water to flow into Lake Pontchartrain.

On 29 August at 15:00 UTC (shown in Figure 77, Figure 88, Figure 99, Figure 110, Figure 121, Figure 132), Hurricane Katrina is near its second landfall at the Louisiana-Mississippi border. The surge that propagated from Southern Plaquemines Parish has now combined with the local surge being generated by the strong southerly winds and is dramatically increasing water levels between Bay St. Louis and Biloxi with peaks reaching 24 ft. Water is blown from the west to the east in Lake Pontchartrain. In addition, water is overtopping the CSX railroad west of Lake Borgne and the Mississippi Sound. Water is also driven in a westerly direction across Mobile Bay.

On 29 August at 16:00 UTC (shown in Figure 78, Figure 89, Figure 100, Figure 111, Figure 122, Figure 133), Hurricane Katrina continues to move north. Surge along the State of Mississippi shoreline is spreading inland and continues to build up driven by the winds from the south to levels reaching 29 ft. Water is being blown from west to east across Lake Pontchartrain and water continues to move from Lake Borgne into Lake Pontchartrain from the east, overtopping the CSX railroad and U.S. 90. Note the sustained difference between the surge level in Lake Borgne (up to 18-20 ft.) and Lake Pontchartrain (12 ft.). The currents in the Rigolets Strait are still up to 6 to 9 ft/s. Now the hurricane has made landfall for the second time, water has started flowing back from Chandeleur Sound into the Gulf of Mexico. Note the increase in velocity at the Chandeleur Islands.

On 29 August at 17:00 UTC (shown in Figure 79, Figure 90, Figure 101, Figure 112, Figure 123, Figure 134), surge continues to propagate inland along the State of Mississippi shore. Winds are still blowing from the west across Lake Pontchartrain causing a drawdown in the west and a surge in the east while simultaneously water very forcefully penetrates from Lake Borgne flowing in from the east due to the water level differentials. The wind velocities are decreasing. The current vectors in Chandeleur Sound and Mississippi Sound have started to turn towards the Gulf, causing high velocities over the Chandeleur Islands and the Mississippi Sound Islands. Note the difference between the surge level at the Gulf-side of the Chandeleur Islands and the

Sound-side. These islands act like a barrier, resisting the high waters flowing from the sound back to the open Gulf.

On 29 August at 20:00 UTC (shown in Figure 80, Figure 91, Figure 102, Figure 113, Figure 124, Figure 135), Hurricane Katrina has moved well inland. Surge along the State of Mississippi coast is subsiding. However, high water remains in Lake Pontchartrain as well as Lake Maurepas. The gradient in water levels between the western and eastern side of Lake Pontchartrain is reducing. In addition, water is withdrawing from Lake Borgne. Note that water is still flowing into Lake Pontchartrain. The water level in the Gulf is back to its normal level. The barrier islands still capture the surge within Breton Sound, Chandeleur Sound and Mississippi Sound. Most of the water gets out through the area between the Chandeleur islands and the Ship Islands.

On 29 August at 23:00 UTC (shown in Figure 81, Figure 92, Figure 103, Figure 114, Figure 125, Figure 136), these processes continue. Note that water in Lake Pontchartrain is at 7 ft and is only slowly leveling due to the lack of strong water surface elevation gradients. Water continues to flow from Lake Borgne into Lake Pontchartrain at a slowing rate due to the decreasing surface water gradients between these lakes. The outflow of surge is heavily resisted by the barrier islands, which causes the surge levels in Mississippi Sound to be about 8 feet.

Figure 137 to Figure 141 show the maximum surge levels and that occurred during Hurricane Katrina for the various scales of interest. The maximum surge

level is close to 30 feet along the Mississippi shoreline. Peak water levels in southeastern Louisiana were computed to be about 18-19 ft along the east-facing Mississippi River and back levees that protect communities along the river in south Plaquemines Parish. The maximum water level occurs midway along the levee system and decreases to the north to a minimum peak value of less than 14 ft near English Turn. Adjacent to the levees along the MRGO, maximum computed water levels are 16 to 17 ft. The model predicts a low gradient in water level within the MRGO Reach 1/GIWW, decreasing water levels from east to west, with a peak water level of about 14 ft at the confluence of the MRGO Reach 1/GIWW and the IHNC. From this point south to the IHNC Lock, water levels are fairly constant, approximately 14 ft. From the confluence to the northern extent of the IHNC, a high water level gradient is computed, decreasing from a value of 14 ft at the confluence to approximately 9 ft in Lake Pontchartrain at Lakefront Airport. In Lake Pontchartrain, the maximum surge level is about 8 to 9 feet along the total south and eastern shoreline. This maximum level occurred between 14:00 to 17:00 UTC, shifting from the southern shoreline to the eastern shoreline. At 23:00 UTC, the water level in the lake was still about 7 feet, which indicates that water once captured inside the lake cannot move out again because the surge levels in Lake Borgne are not reduced.

5.1.2 System Validation

The computed high water levels are compared to both USACE and URS/FEMA high water marks (HWM) that were collected immediately after

the storm. The USACE collected 206 reliable HWMs and URS/FEMA collected 193 reliable HWMs during post-storm surveys with the locations and model to measurement differences shown in Figure 142 and Figure 143, respectively (U.S. Army Corps of Engineers, 2007c; URS 2006b; URS 2006c). The HWMs were collected as indicators of the *still-water levels* and thus did not include the active motion of wind waves but did include the effects of wave setup. The two sets of HWMs offer wide coverage of the impacted region. The overall match is good, with 73% of the USACE HWMs and 76% of the URS/FEMA HWMs matching the model results to within 1.64 ft. Missing features, processes, and/or poor grid resolution are associated with the larger differences between the model and measured HWMs. For example at Socola, LA, in Plaquemines Parish, a HWM location within the levee system is substantially under-predicted. The ADCIRC SL15 simulations are not intended to model interior polder inundation. Inadequate resolution in the circulation and wave models leads to the under-prediction of wave induced setup on the south shore of Lake Pontchartrain. Further inland, the model over or under-predicts surge unless the area is connected to well-defined inland waterways, which allow surge to flow past or to the HWM locations. For far inland locations adjacent to steep topography, such as up the Pearl River basin, rainfall runoff may have significantly added to the surge levels.

Scatter plots of measured versus predicted HWM's are presented in Figure 144 and Figure 145. For the USACE marks, the slope of the best-fit line is 0.99 and the correlation coefficient, R^2, is 0.93. For the URS marks, the slope of the

best-fit line is 1.02 and R^2 equals 0.94. Error statistics for Katrina are summarized in Table 4. For both data sets, the average absolute difference between modeled and measured HWMs is 1.21-1.33 ft, and the standard deviation is 1.49-1.60 ft. A portion of these differences can be attributed to uncertainties in the measured HWMs themselves. If two or more measured HWMs are hydraulically connected (defined as being within 500m horizontally, having no barrier in between them and, having computed water levels within 0.33 ft), then HWM uncertainties are estimated by examining the differences in these adjacent HWMs. Table 4 indicates that the estimated uncertainties in the measured HWMs are 20-30% of the differences between the modeled and measured HWMs. When the HWM uncertainties are removed from the predicted to measured differences, then the estimated average absolute model error range is between 0.91-0.96 ft, and the standard deviation is 1.40 - 1.50 ft. The "model to data" error can be attributed to a wide range of modest uncertainties in the description of the forcing functions, the processes represented in the model, the physical system, and the parameterization that are used to describe the sub-grid scale processes.

The wind fields are the best that have ever been developed to characterize a hurricane. However, when compared to the NDBC buoy wind data the match between the buoy anemometer winds and the H*WIND/IOKA wind correlates to a correlation coefficient squared of 0.93. This is related to the fact that there is not perfectly measured wind data at every point in space and time. We note that it is wind speed cubed for low wind speeds and the wind speed squared for

high wind speeds that drive the surge. Thus a 5% error in wind speed can readily lead to a 10% to 16% error in the computed surge.

We assume that the flow is two-dimensional, while in reality there may be some variability over the vertical which could enhance or reduce surge levels (Resio and Westerink, 2008). In addition, the model computes pure coastal surge, while for inland channels such as the Pearl River, there may be a significant rainfall runoff input into the channel which is of course reflected in the measurements but not in the simulation.

Topography from Lidar and estimated marsh values or bathymetric values in and around Southern Louisiana are also not perfect. In fact, the Lidar can be as much as 1 ft off, while some of the NOAA bathymetric soundings were taken in the early part of the 20th century.

Air-sea momentum transfer coefficients and Manning n bottom friction coefficients may not perfectly capture the momentum transfer processes or dissipation processes. All of these uncertainties are actively being addressed in the scientific community through micro- and macro-scale measurements, as well as through high resolution modeling studies.

5.2 SCENARIO H2: *NO MRGO WITH 2005 WETLANDS*

In the H2 *No MRGO with 2005 wetlands* scenario, the MRGO Reach 2 channel was removed and the MRGO Reach 1/GIWW channel was reduced to

the approximate dimensions of the GIWW in 1958, prior to the construction of the MRGO. These changes were implemented in order to understand the effects on storm surge resulting from the complete removal of the MRGO. Maximum water surface elevations generated during the H2 simulation can be seen in Figure 146 through Figure 148. These figures indicate that Scenario H2 is very similar to Scenario H1. Again as the storm's eye approaches from the south, storm surge is driven by northeasterly, easterly and southeasterly winds that push water against these levees, building to heights of approximately 18 feet along Plaquemines Parish and to 15 feet along the Chalmette Levee from Paris Road to Bayou Dupre. Also similar to Scenario H1, the maximum storm surge elevation is 14 feet in the vicinity of the Golden Triangle at the confluence of the MRGO and GIWW and 9 feet in southern Lake Pontchartrain.

Differences in maximum water levels between Scenarios H2 and H1 are presented in Figure 149 through Figure 151. Differences greater than 0.25 ft occur in the vicinity of English Turn and Braithwaite, to the east of the St. Bernard Polder along the northeast facing section of the Chalmette Levee between Paris Road and Bayou Dupre, and along MRGO Reach 1/GIWW and the IHNC.

Maximum storm surge levels at English Turn/Braithwaite are between 0.5 ft and 1 ft lower in simulation H2 compared to simulation H1. The regional differences between the H2 and H1 grids are that MRGO Reach 2 has been eliminated and that the spoil mounds adjacent to the MRGO have been

removed. The influence of the MRGO Reach 2 in conveying flow towards English Turn is minimal in that the flow is pushed broadly across the entire region from the northeast, east and southeast. This is illustrated in Figure 93 through Figure 103 and Figure 126 through Figure 136. Water levels of more than 15 ft across Lake Borgne and Breton and Chandeleur Sounds with winds from the northeast, east, and southeast allow for relatively efficient and very broad flows to occur from these directions across the region, minimizing the relative influence of MRGO Reach 2 in the vicinity of English Turn.

The increase water elevation in H2 near English Turn can however be attributed to the removal of the dredge spoil mounds that run along the west bank of the MRGO Reach 2, to the southwest of the St. Bernard Polder. The removal of the dredged spoil mound allows more water to move towards English Turn during early stages of the H2 scenario, creating the differences in maximum storm surge. Figure 4 and Figure 11 show the topography of the H1 and H2 scenarios. Note the dredge spoils mounds ranging from 2 to 10 feet in elevation on the west side of the MRGO in the H1 scenario. These spoil mounds would not have existed if MRGO Reach 2 had not been constructed and were therefore removed in Scenario H2 to create a realistic landscape in the model. In the H1 case, as the storm approaches from the south, the dredge spoil mounds block or slow early flow coming from the east and southeast from making its way to the English Turn area. Conversely, the removal of the dredge spoil mounds in the H2 case allows flow to cross the Caernarvon marsh more easily from east to west. Note that both the Caernarvon Marsh as well as

the dredged spoils only slow down high water from getting to English Turn and Braithwaite. For Katrina this in fact helped reduce the maximum water level that occurred there since as the storm passed, the winds turned and blew out of the north and then west and thus away from the Chalmette Extension Levee and English Turn.

Small differences also occur to the east of the St. Bernard Polder between Paris Road and Bayou Dupre. The surge levels in this area are slightly lower in H2 as compared to the base case H1. As seen in Figure 150 and Figure 151, differences of less than 0.5 ft occur in this area. This small differential is most likely mostly related to the elimination of the MRGO Reach 2 dredged spoil mounds that allowed more water to flow to English Turn, lowering water levels to the east of the St. Bernard Polder but raising them along English Turn.

The largest differences between Scenarios H2 and H1 occur along MRGO Reach 1/GIWW and the IHNC. A significant reduction of conveyance in MRGO Reach 1/GIWW was implemented for Scenario H2, due to returning the MRGO Reach 1/GIWW to pre-MRGO width and corresponding increased frictional resistance in the channel. This leads to a change in the distribution of the water surface elevation gradient between Paris Road and Seabrook. Note that both Paris Road and Seabrook represent hydraulic controls in this system. This means that there is simply not enough hydraulic conveyance given the size of the MRGO Reach 1/GIWW channel to affect the water levels at Paris Road or those on the south side of Lake Pontchartrain at Seabrook during a

hurricane. Thus, the IHNC and MRGO Reach 1/GIWW connection between these two points can not move enough water compared to the amount of water being delivered across the marshes and/or lakes during a large storm.

The distribution of the surface water elevation between Paris Road and Seabrook is dramatically affected by the H1 to H2 modifications. The water surface has to find its way from the higher elevations at Paris Road to the lower elevation at Seabrook. In case H1, the relatively low drop in sea surface between Paris Road to the confluence of the MRGO Reach 1/GIWW and the IHNC is a result of the proportionally larger conveyance and reduced friction as compared to the much larger drop in sea surface elevation between the confluence of the MRGO Reach 1/GIWW and IHNC to Seabrook. This latter stretch of the channel is narrower and contains numerous significant flow constrictions at narrow bridges that are highly dissipative.

In simulation H2, upon the removal of the MRGO Reach 1/GIWW and its replacement with the original much narrower GIWW, the drop in surface elevation between Paris Road and Seabrook tends to occur much more from Paris Road to the confluence of the MRGO Reach 1/GIWW and the IHNC. In fact, a reduction of up to 3.5 ft in maximum water surface elevation occurs at the confluence of the MRGO Reach1/GIWW and the IHNC for Scenario H2 as compared to Scenario H1. Thus, the reduction in width and simultaneous increase in friction that occurred along the MRGO Reach 1/GIWW leads to the increase in the proportion of the total dissipation and therefore total surface

elevation drop occurring between Paris Road to the confluence of MRGO Reach 1/GIWW and IHNC as compared to the confluence of the MRGO Reach 1/GIWW and IHNC to Seabrook.

Figure 183 through Figure 210 show storm surge hydrographs for all six scenarios along the IHNC, MRGO Reach 1/GIWW, MRGO Reach 2 and in Lake Borgne at locations defined in Figure 182. These time series depict the timing and duration differences of storm surge levels for all six scenarios. It is noted that within the IHNC and MRGO Reach 1/GIWW, the pre-storm astronomical tides are significantly more damped in case H2 in comparison to case H1. This is related to the fact that in the H1 simulation, the low energy astronomical tides are substantially enhanced by the efficient hydraulic connection between MRGO Reach 2 and Lake Borgne to the east of Bayou Dupre. Inspection of the storm portion of the hydrographs reveals that the storm surge time series are nearly the same for Scenarios H1 and H2 outside of the southern reaches of the IHNC and western extents of Reach 1 where the greatest differences in maximum storm surge elevations are seen in Figure 151. The southern reach of the IHNC and western portion of Reach 1 demonstrate not only lessened stormed surge levels, but a shorter duration of peak surge. This trend is expected due to the decrease in conveyance across MRGO Reach 1/GIWW.

5.3 SCENARIO H3: *NO MRGO WITH 1956 WETLANDS*

Scenario H3 again simulates the complete removal of the MRGO as case H2 but now modifies the marshes that were possibly influenced by the MRGO to a 1956 configuration. Figure 152 through Figure 154 depict storm surge levels for simulation H3 and indicates that the results are very similar to those of simulation H2. Areas of notable storm surge build up caused by natural and manmade topography remain nearly the same as the H2 scenario. Additionally, the gradient of maximum water surface elevation across MRGO Reach 1/GIWW and the IHNC is analogous to that of H2. Differences in maximum water surface elevation between H1 and H3 can be seen in Figure 155 through Figure 157, while differences between H2 and H3 can been seen in Figure 158 through Figure 160.

Water level differences in the vicinity of English Turn between H3 and H1 are somewhat less than those between H2 and H1 indicating that more water gets to English Turn than in case H1 but that less water gets there than in case H2. While H3 also eliminated the dredged spoil mounds adjacent to MRGO Reach 2, it has a more substantial Laloutre Ridge and slightly raised marshes in the area of MRGO influence.

The H3 simulation response in the region to the east of the St. Bernard Polder to the IHNC is similar to that of simulation H2 with differences of less than 0.25 ft. Minimal difference in the maximum storm surge between H2 and H3 demonstrates the limited affect of marshes on storm surge in the area during

Hurricane Katrina. The increased marsh elevation and frictional resistance in the H3 scenario are easily overwhelmed by the large scale inundation during the storm. The impact of bottom friction influences inundation less as water depth increases. Thus, when the region to the east of the St. Bernard Polder, including the Golden Triangle, broadly fill with storm surge of more than 15 ft, the effects of small increases in marsh friction only marginally affect the flow velocity and direction.

Hydrographs in Figure 183 through Figure 210 show that the timing and duration of peak storm surge during the H2 and H3 scenarios are consistent.

5.4 SCENARIO H4: *NO MRGO WITH 1956 WETLANDS AND A RELOCATED CHALMETTE LEVEE*

Scenario H4 was constructed by removing the Chalmette Levee on the south side of MRGO Reaches 1 and 2. Figure 161 through Figure 163 display the maximum water surface elevation for simulation H4, while Figure 164 through Figure 166 present the differences between H1 and H4. Note that the tan color in the difference figures denotes areas that were wetted during the H4 simulation, but not the H1 simulation.

Maximum water surface elevations decrease by up to 1.5 ft to the east of the location of the Chalmette Levee between Paris Road and Bayou Dupree in simulation H4 as compared to H1. However, the maximum water levels against the 40 Arpent Levee in Scenario H4 are similar if not higher than those that are

driven up against the Chalmette Levee in Scenario H1. The higher surges appear in the local concavity created by tying in the 40 Arpent Levee with the new sub-polder defined to the south by the Chalmette Extension Levee. As water moves to the west, the raised ground in and around Bayou Bienvenue to the east of the IHNC as well as a sewage treatment plant, a waste disposal site, Paris Road and the substantial dredged spoil mounds along the MRGO Reach 1/GIWW that were all left in the H4 model, appear to slow the flow and lower water levels as water moves to the west. As a result, water moving west into the IHNC is forced to flow adjacent to the New Orleans East levees. The surface elevation drop in the conveyance to the north is more than in Scenario H1 but less than in the better constricted Scenarios H2 and H3. Overall though, the reduction of water levels in the Golden Triangle region leads to water levels in the IHNC that are similar to cases H2 and H3. However, this may be due in part to all of the raised features that were left behind in the H4 model when the Chalmette Levee was moved back to the 40 Arpent Levee.

Hydrographs in Figure 183 through Figure 210 show that the storm surge time series for Scenarios H2, H3 and H4 parallel one another. In all cases along the IHNC, the peak surge duration is nearly the same, but the peak surge elevation is slightly higher in the H4 case.

5.5 SCENARIO H5: *MRGO AS DESIGNED WITH 2005 WETLANDS*

Scenario H5 differs from Scenario H1 in that Reach 1 and 2 are characterized by their approximate design dimensions rather than the observed 2004

geometry. Figure 167 through Figure 169 present the maximum water surface elevations reported in the H5 scenario, while Figure 170 through Figure 172 display the difference in water surface elevations compared to the H1 Scenario. Differences of less than 0.5 foot are seen throughout the entire domain. No differences are reported at English Turn, due to similar implementation of dredge spoil mounds. In addition, no differences occur to the east of the St. Bernard Polder. The maximum difference is seen in the southern extent of the IHNC, where the H5 results are on the order of 0.25 foot less than those of the H1 scenario.

Similar to previous comparisons, the effects of Reach 2 on the storm surge in the Study Region are limited. The reason for the limited differences is twofold. First, narrowing the MRGO Reach 2 to approximate design dimensions minimally affects the flow into St. Bernard or the Golden Triangle area because water flows in from the east. Second, the MRGO Reach 2 in any configuration simply does not modify the conveyance once the region is inundated. Thus, when the marsh around the MRGO and Lake Borgne is inundated by storm surge up to 15 feet, the overall response in the system is not affected by any change in the MRGO channel dimensions.

The reduction in the conveyance and the increase in friction along the banks of the MRGO Reach 1/GIWW essentially redistributes and increases the friction along the MRGO Reach 1/GIWW and the IHNC. This leads to a very small redistribution of how the water surface elevation drops between the two major

hydraulic controls, Paris Road to Seabrook. Thus the gradient in water surface elevation between Paris Road and Seabrook in the H5 case is very similar to the H1 case.

Hydrographs are presented in Figure 183 through Figure 210. It is noted that within the IHNC and MRGO Reaches 1 and 2, the pre-storm astronomical tides are still significantly more damped in case H5 in comparison to case H1. This is again related to the fact that the efficient hydraulic connection between MRGO Reach 2 and Lake Borgne to the east of Bayou Dupre has been closed in the H5 scenario. This lowers the amplitude of the relatively low energy astronomical tides within the channels. The hydrographs demonstrate that high energy storm surge is very similar in both peak values and also similar in the duration of peak surges when comparing cases H5 and H1.

5.6 SCENARIO H6: *MRGO AS DESIGNED WITH 1956 WETLANDS*

Scenario H6 differs from Scenario H1 in that MRGO Reach 1 and 2 are characterized by the approximate design dimensions rather than the observed 2004 geometry and that the wetlands have been restored to their 1956 configuration in the zone of MRGO influence. Note that the MRGO dredged mounds have been predominantly kept in place. Figure 173 through Figure 175 present the maximum water surface elevations reported in the H6 scenario, while Figure 176 through Figure 178 display the difference in water surface elevations compared to the H1 scenario. Finally, Figure 179 through Figure 181 display the difference in water surface elevations compared to the H5

scenario. The differences between cases H6 and H1 are very minimal and are in fact almost the same as between those between cases H5 and H1. Thus very minimal differences between cases H6 and H5 reflecting the very limited effect on storm surge in the region is caused by a variance in marsh parameters.

Hydrographs in Figure 183 through Figure 210 reveal that the time series for storm surge inundation are nearly identical for the H5 and H6 cases. The primary difference seen between Scenarios H5 and H6 is seen in English Turn. A slightly higher maximum water surface elevation in H6 than H1 at English Turn can be seen in Figure 178. This is due to dredge spoil mounds at the very southern extents of the MRGO for H6 being removed when implementing historical marsh elevations for the scenario. Note that most of the dredged spoil mounds were included. H5 and H1 however incorporated dredge spoil mounds extending south of Laloutre Ridge further into the Gulf as can be seen in Figure 3, Figure 34, and Figure 40.

6.0 DISCUSSION AND CONCLUSIONS

The Study has examined the effect on water level of a number of perturbations of the MRGO and the surrounding marshes on Hurricane Katrina's storm surge. The channel reconfigurations examine the following features: reducing the MRGO Reach 1/GIWW to the 1958 GIWW; reducing MRGO Reach 1/GIWW to the design width and depth; eliminating MRGO Reach 2 entirely; and reducing the width and depth of MRGO Reach 2 to its design width. The

wetland reconfigurations include restoring the wetlands in the zone of MRGO influence, defined in Figure 1, to their 1956 configuration and eliminating some or most of the dredged spoils mounds that were associated with the construction of the MRGO. Finally the levee system reconfiguration consisted of removing the Chalmette Levee and raising the 40 Arpent Levee.

6.1 IMPACT OF THE MRGO BY REGION

In most of the Study Region, the influence of any of these perturbations resulted in less than 0.25 ft in maximum water surface elevation difference between the various scenarios. This is related to the fact that the physics that drives a major storm surge are not significantly influenced by the presence of the MRGO or by the marshes. The conveyance of the MRGO is minimal compared to the conveyance of the surrounding marshes when they are covered with a minimum of 15 ft of water as they were during Hurricane Katrina. In addition, as long as the winds blow long enough from the direction of the open water, the dominant balance in the governing equations (derived from Newton's second law) will develop to be between the wind stress and water surface gradients. The effect of bottom friction is minimized by the large depth of water and, when a steady state is reached, often entirely eliminated since bottom friction only develops if there is a current.

The main areas that the construction of the MRGO and/or the possible degradation of the surrounding marshes impacted in terms of water levels during Katrina are the areas: (1) in the vicinity of English Turn/Braithwaite;

(2) the marshes and waters extending to the east of the St. Bernard Polder and; (3) the MRGO Reach 1/GIWW and IHNC connection between Paris Road and Seabrook.

6.1.1 Impact of the MRGO on English Turn and Braithwaite

The area in and around English Turn/Braithwaite shows a small sensitivity to the configuration of the wetlands but more importantly shows a sensitivity to any barrier to the flow in the vicinity such as the MRGO dredged spoil mounds. The flow in and around this area is very complex both due to the geometric configuration and due to Hurricane Katrina's eye tracking right through the area causing rapidly shifting winds both in space and in time. Regionally the winds affecting English Turn/Braithwaite are from the east and northeast prior to the passage of the storm (Figure 71 through Figure 75, Figure 104 through Figure 108) and then shift from the west and northwest as the storm passes and moves north (Figure 76 through Figure 81 and Figure 109 through Figure 114). Locally right near English Turn/Braithwaite and the adjacent Chalmette Extension Levee, the winds are pushing water away from the area both prior to the passage of the storm (Figure 82 through Figure 86 and Figure 115 through Figure 119) and after the passage of the storm (Figure 87 through Figure 92 and Figure 120 through Figure 125). The water surface elevation response in the local area is an interplay between the regional winds pushing water into the area, the local winds pushing water away from the immediate vicinity of English Turn/Braithwaite and the Chalmette Extension Levee resulting in the very high water surface elevation gradients seen in the figures. In addition,

there is a complex interplay between the forces in the governing equations between the highly variable in space and time wind forcing field, the atmospheric pressure field, the very significant water surface elevation gradients, fictional forces that depend on current speeds, local acceleration, and advective acceleration which must all together remain in balance.

The sensitivity of the maximum high water at English Turn/Braithwaite is the greatest when the dredged spoil mounds are eliminated since the flow comes in from the east and northeast and the presence of the dredged spoil mounds slow the volume of the flow towards English Turn/Braithwaite. Examining the currents in the H1 *Katrina Real Run* base scenario prior to the passage of the storm (Figure 126 through Figure 130) indicates that the regional flow towards the English Turn/Braithwaite area was from the east and from the northeast and that this flow was driven across both the Laloutre Ridge and the MRGO dredged spoil mounds. Therefore eliminating the substantial dredged spoil mounds along the MRGO would increase the flow and the rise of water in the English Turn/Braithwaite area as was the case for the H2 scenario. Scenario H2 high water at English Turn/Braithwaite was up to 1 ft higher than the base *Katrina Real Run* scenario. Once the storm passes, the dominant regional currents are towards the east. Scenarios H5 and H6 which did not remove the dredged spoil mounds show almost no change in water surface elevations at English Turn/Braithwaite. The H3 to H2 and H6 to H5 scenario comparisons indicate that the slowing of the flow of water towards the English Turn/Braithwaite area due to the condition of the wetlands, even in this

complex region with rapidly shifting winds during Katrina, is not nearly as important as the influence of the MRGO spoil mounds. The largest difference due to wetland conditions in the area is between 0.25 and 0.5 ft.

6.1.2 Impact of the MRGO on the Marshes and Waters to the East of the St. Bernard Polder

The second area impacted by the system configuration modifications is just to the east of the St. Bernard Polder where water levels decrease by up to 0.5 ft in some of the scenarios. The winds that affect water levels here are better organized than those affecting English Turn/Braithwaite. In this area, both the local and regional winds prior to the passage of the storm are from the northeast and east (Figure 71 through Figure 75, Figure 104 through Figure 108) and shift consistently towards the east after the storm (Figure 76 through Figure 81 and Figure 109 through Figure 114). This uniform organization in space and time prior to the passage of the storm drives the water up against the Chalmette Levee as well into the Golden Triangle prior to the passage of the storm (Figure 82 through Figure 86 and Figure 115 through Figure 119). The currents prior to the passage of the storm that are responsible for the high water in the area, shown in Figure 126 through Figure 130 for the base H1 scenario, are predominantly from the northeast and east.

The up to 0.5 ft perturbations in maximum water surface elevations that are seen to the east of the St. Bernard Polder stem primarily from the removal of the MRGO dredged spoil mounds. Scenarios H2 and H3 indicate that there is up to 0.5 ft less water there when the MRGO spoil mounds are eliminated. The

larger volume of water that is able to push its way through to English Turn/Braithwaite reduces water levels to the east of the St. Bernard Polder but increases water levels at English Turn/Braithwaite. In Scenarios H5 and H6 where the spoil mounds were not eliminated, water surface elevations to the east of the St. Bernard Polder were not significantly affected since the MRGO spoil mounds were in place. Also the H2 to H3 and H5 to H6 comparisons indicate that high water in the area is essentially not affected by the health of the marshes in the region.

The direction, duration, spatial extent, and organization of the winds relative to the geometric configuration is critical in understanding how high the water will rise in a region and how the marshes impact the region. Resio and Westerink (2008) point out that for a storm on a southwesterly track that runs further to the west, like Hurricane Rita, there is a tendency for much more uniform easterly winds to blow for a much longer period and therefore for a steady state balance to develop between surface water elevation gradients and wind stress. This means that local acceleration, advective acceleration and friction, which is dependent on currents, are no longer a part of or are a much smaller part of the momentum conservation balance (i.e. Newton's second law). Resio and Westerink (2008) present simulations that show that up to 10 ft of water was pushed across 25 mi of Caernarvon Marsh during Hurricane Rita.

Forecasts of Hurricane Gustav performed with the SL15 model by the University of North Carolina at Chapel Hill, Louisiana State University, and

the University of Notre Dame, show the evolution of storm surge in Figure 211 through Figure 251. These simulations indicate that even a borderline Category 3 or Category 2 storm that was never closer than approximately 75 mi from the Study Region developed surge of approximately 11 ft at the IHNC Lock and 11 ft across nearly 25 mi of Caernarvon Marsh at English Turn/Braithwaite. The forecasted high water elevation value in the IHNC is confirmed by the measured value of approximately 10.6 ft at the IHNC lock (http://www2.mvr.usace.army.mil/WaterControl/stationinfo2.cfm?sid=76160&fid=&dt=S). The forecasted high water at English Turn/Braithwaite is confirmed in photos (U.S. Army Corps of Engineers, New Orleans District, 2008), shown in Figure 252 through Figure 256, taken during Gustav showing the back levees at Braithwaite overtopping. These levees range from 11 to 13 ft in elevation

Another example of extensive overland inland surge propagation is highlighted in the case of Hurricane Ike in Texas. The inland penetration that occurred during Hurricane Ike extended north of the Bolivar Peninsula to the east of Galveston where sea water inundation reached more than 17 mi inland over gradually sloping land that rises from the Gulf of Mexico to about 25 ft to 30 ft. A NASA post storm satellite photo can be found at http://www.nasa.gov/images/content/280677main_ike_flooding_HI.jpg with a description of the image posted at http://www.nasa.gov/mission_pages/hurricanes/archives/2008/h2008_ike.html showing the brown vegetation as indicators of saltwater inundation. Based on

preliminary high water marks collected by FEMA, the coastal high water was between 15 ft and 19 ft in the vicinity of the Bolivar Peninsula and high water marks about 11.5 mi north of there were about 17 ft. The NASA inundation image indicates that water was driven all the way to the vicinity of Winnie, TX. This implies that high water at the northern extent of inundation reached at least 25 ft with a strong positive gradient of water levels in the inland direction. The English Turn/Braithwaite areas during Hurricane Gustav and the Bolivar Peninsula to Winnie TX area during Hurricane Ike indicate that the simple rule of thumb widely thought to control surge attenuation in wetlands is a huge oversimplification of a very complex set of dynamics and geometries. It is clear that as Resio and Westerink (2008) point out, wetlands do not necessarily reduce high water in an area. It depends on the duration and consistency of the winds as well as the geometry of the system. Thus wetlands may slow the progress of water, but if the winds blow long enough and strongly enough, water will penetrate through wetlands.

6.1.3 Impact of the MRGO between Paris Road and Seabrook

The third area impacted by the system configuration modifications is along the MRGO Reach 1/GIWW and IHNC channels between Paris Road and Seabrook. It is noted that the volume of water driven through these channels is insubstantial regardless of the channel configuration relative to the storm driven water levels at Paris Road and Seabrook. Thus the peak storm water levels in the Golden Triangle area and along the south shore of Lake Pontchartrain are not affected by the channel connecting them since this channel simply cannot

move enough water. Paris Road and Seabrook act as hydraulic controls for the distribution of water levels between these two points with the water levels at Paris Road and Seabrook being determined by the larger scale processes.

The water level distribution between the two controls is substantially affected by the channel configuration and the distribution of conveyance and friction in the channels. A substantial narrowing of the MRGO Reach 1/GIWW configuration to the approximate 1958 geometry in Scenarios H2 and H3 increases the friction along the MRGO Reach 1/GIWW and causes much more of the total drop in water levels between Paris Rd and Seabrook to occur along the MRGO Reach 1/GIWW. This effectively lowers water levels at the confluence of the IHNC and MRGO Reach 1/GIWW by as much as 3.5 ft. A more modest reduction in the MRGO Reach 1/GIWW geometry to its approximate design geometry only reduces water levels at the confluence of the IHNC and MRGO Reach 1/GIWW by less than 0.5 ft. Wetlands do not significantly influence the water levels or water level distribution in the MRGO Reach 1/GIWW and the IHNC, as is shown by comparing cases H2 to H3 and H5 to H6, since the water levels at the controls (Paris Road/Golden Triangle and Seabrook/south shore of Lake Pontchartrain) are not affected.

We note that the surface water elevation distribution between Paris Road and Seabrook can be readily affected by changes in friction and conveyance in the northern segment of the IHNC between the confluence of the IHNC and Reach 1 of the MRGO/GIWW to Seabrook. This sensitivity was not examined in this

Study but it is logical that building flow constrictions within the northern section of the IHNC would cause more of the drop in water elevation to occur there and therefore higher water during a storm event to occur within the southern section of the IHNC. This concept is illustrated in the high water distribution in the base *Katrina Real Run* where most of the drop in elevation between Paris Road and Seabrook occurs within the northern segment of the IHNC where the conveyance is smallest and the frictional resistance is the highest. Thus the more the northern section of the IHNC is constrained, the higher the water levels will be at the confluence of the IHNC and MRGO Reach 1/GIWW.

6.2 AN EVALUATION OF THE IMPACT OF THE MRGO COMPONENTS ON REGIONAL WATER LEVELS

The impact of the individual components of the MRGO is summarized in the following sub-sections.

6.2.1 The Impact of the MRGO Reach 2

The six scenarios examined demonstrate the influence of the channel, dredged spoil mound, levee, and wetland changes that have occurred since the construction of the MRGO. The existence of the MRGO Reach 2 has minimal impact on maximum Hurricane Katrina storm water levels in the Study Region either in its present state or as designed. This lack of influence of the MRGO Reach 2 is related to the fact that the dominant winds that caused the high water

in the region came from the east as did the currents that were driven by these winds.

The spoil mounds that were created when MRGO Reach 2 was constructed do appear to reduce water levels at English Turn/Braithwaite by about 1 ft for the Katrina event. However for more westerly storms like Rita and Gustav, these spoil mounds do not affect the surge there since the mounds only increase the time needed for the water to get there. Thus when the winds blow longer and are spatially more uniform, the influence of the dredged mounds is eliminated. The same MRGO spoil mounds that reduce water levels at English Turn/Braithwaite, increase water levels modestly (by less than 0.5 ft) to the east of the St. Bernard Polder. This is a simple mass balance effect: if you stop the water flowing from the east of the St. Bernard Polder from going to English Turn/Braithwaite, it keeps water levels higher in the vicinity of the St. Bernard Polder.

6.2.2 The Impact of the MRGO Reach 1/GIWW

The construction of MRGO Reach 1/GIWW does impact maximum Hurricane Katrina water levels in MRGO Reach 1/GIWW and the IHNC. Although water levels at Paris Road and Seabrook are not impacted, the distribution of water level along the MRGO Reach 1/GIWW and IHNC has changed with water levels dropping more quickly as they flow towards Lake Pontchartrain. This results in lower water levels at the confluence of the MRGO Reach 1/GIWW and the IHNC by up to 3.5 ft. The difference in water levels between the

MRGO Reach 1/GIWW as designed and as it exists today, however, is minimal.

6.2.3 The Impact of the MRGO Wetland Degradation

The impact on water levels during Katrina that could be attributed to wetland degradation or subsidence in the zone of influence of the MRGO is minimal. This is in part due to the fact that Katrina drove more than 15 ft of water on the entire Mississippi-Alabama shelf and the entire region was massively inundated. In addition, the broad scale regional winds were consistently from the east until the storm passed. This allowed enough time for the water to flow into the area and to pile up against the banks and levees of the system. Examples of inland penetration during Gustav and Ike clearly demonstrate that wetlands do not necessarily provide protection against inland flood propagation. This is particularly true in a region like the Study Region in which the protruding Mississippi delta allows the easterly winds to pile up water for a long time as compared to a straight east-west coast, in which case the early and more sustained easterly winds predominantly drive shore parallel currents and only the southerly winds produce storm surge.

6.2.4 The Impact of the Constructed Levees in and around the Golden Triangle

Finally, the Golden Triangle formed by the St. Bernard Polder and New Orleans East Polder does act as to amplify water levels as does any concavity

in the geometry when water is propagated into it. This is certainly the case for English Turn. Eliminating the Chalmette Levee and raising the 40 Arpent Levee does lower water levels to the east of the current position of the Chalmette Levee during a Hurricane Katrina simulation. However water levels against the raised 40 Arpent levee are similar if not higher as compared to what they were against the Chalmette levee. Furthermore due to partial blocking of the flow by the higher grounds of Bayou Bienvenue as well as various high areas and the dredged spoils along the MRGO Reach 1/GIWW that have been left in the H4 model, water levels in the IHNC are very similar to Scenarios H2 and H3. Eliminating the various high grounds and the MRGO Reach 1/GIWW dredged spoils would likely lead to more water penetrating the IHNC.

7.0 REFERENCES

Arcement, G.J., and V.R. Schneider. 1989. "Guide for Selecting Manning's Roughness Coefficients for Natural Channels and Flood Plains", *U.S. Geological Survey Water-Supply Paper 2339*, U.S. Geological Survey, Denver, Colorado.

Atkinson, J.H., J.J. Westerink, and J.M. Hervouet. 2004. "Similarities between the Quasi-Bubble and the Generalized Wave Continuity Equation Solutions to the Shallow Water Equations," *International Journal for Numerical Methods in Fluids*, 45, 689-714.

Barnes, H.H. 1967. "Roughness Characteristics of Natural Channels," *U.S. Geological Survey Water-Supply Paper 1849*, U.S. Geological Survey, Washington D.C.

Barras, J.A. 2008. Expert Report for the U.S. Department of Justice.

Blain, C.A., J.J. Westerink, and R.A. Luettich. 1994. "The influence of domain size on the response characteristics of a hurricane storm surge model." *J. Geophys. Res., [Oceans]*, 99 (C9), 18467-18479.

Blain, C.A., J.J. Westerink, and R.A. Luettich. 1998. "Grid convergence studies for the prediction of hurricane storm surge." *Int. J. Num. Meth. Fluids*, 26, 369-401.

Britsch, D and J. Dunbar. 2008. USACE-MVN and ERDC-GSL, Personal Communication.

Cardone, V. 2007. Oceanweather, Inc. Personal communication.

Cardone, V.J., A.T. Cox, and G.Z. Forristall. 2007. OTC 18652: Hindcast of Winds, Waves and Currents in Northern Gulf of Mexico in Hurricanes Katrina (2005) and Rita (2005). *2007 Offshore Technology Conference*, Houston, TX.

Chow, S. 1971. "A study of the wind field in the planetary boundary layer of a moving tropical cyclone". M.S. Thesis, New York University.

Chow, V.T. 1959. "Open Channel Hydraulics," McGraw-Hill Book Company, New York.

Couvillion, Brady. 2008. Personal communication; USGS.

Cox, A. 2007. Oceanweather, Inc. Personal communication.

Cox, A.T., and V.J. Cardone. 2000. "Operational system for the prediction of tropical cyclone generated winds and waves." *6th International Workshop on Wave Hindcasting and Forecasting*, November 6-10, 2000, Monterey, California.

Cox, A.T., J.A. Greenwood, V.J. Cardone, and V.R. Swail. 1995. "An interactive objective kinematic analysis system." *Fourth International Workshop on Wave Hindcasting and Forecasting*, Banff, Alberta, Canada, Atmospheric Environment Service, 109-118.

Dawson, C., J.J. Westerink, J.C. Feyen, and D. Pothina. 2006. "Continuous, Discontinuous and Coupled Discontinuous-Continuous Galerkin Finite Element Methods for the Shallow Water Equations," *Int. J. for Num. Meth. Fluids*, 52, 63-88.

Dunbar, Joseph B. 2008. Personal communication, U.S. Army Research and Development Center.

Ebersole, B.A., and J.J. Westerink. 2006. On-site visit. March.

Ebersole, B.A. 2008. Personal communication, U.S. Army Research and Development Center.

Federal Emergency Management Agency. 2005. "HAZUS: Hazard loss estimation methodology." http://www.fema. gov/hazus/index.shtm.

Garratt, J.R. 1977. "Review of drag coefficients over oceans and continents." *Mon. Wea. Rev.*, 105, 915-929.

General Bathymetric Chart of the Oceans, *British Oceanographic Data Centre Centenary Edition-2003*, http://www.bodc.ac.uk.

Gunther, H. 2005. *WAM Cycle 4.5 Version 2.0*, Institute for Coastal Research, GKSS Research Centre Geesthacht, 38pp.

Hagen, S.C., J.J. Westerink, and R.L. Kolar. 2000. "Finite element grids based on a localized truncation error analysis." *Int. J. Num. Meth. Fluids*, 32, 241-261.

Hagen, S.C., J.J. Westerink, R.L. Kolar, and O. Horstmann. 2001. "Two dimensional unstructured mesh generation for tidal models." *Int. J. Num. Meth. Fluids*, 35, 669-686.

Hartley, S., R. Pace, III, J.B. Johnston, M. Swann, C. O'Neil, L. Handley, and L. Smith. 2000. A GAP analysis of Louisiana: Final report and data: Lafayette, Louisiana, U.S. Department of the Interior, U.S. Geological Survey.

Henderson, F.M. 1966. "Open Channel Flow," Macmillan Publishing Company, New York.

Jensen, R.E., V.J. Cardone, and A.T. Cox. 2006. "Performance of third generation wave models in extreme hurricanes", *Ninth International Workshop on Wave Hindcasting and Forecasting,* Banff, Alberta, Canada, Atmospheric Environment Service.

Kalnay, E., M. Kanamitsu, R. Kistler, W. Collins, D. Deaven, L. Gandin, M. Iredell, S. Saha, G. White, J. Woollen, Y. Zhu, M. Chelliah, W. Ebisuzaki, W. Higgins, J. Janowiak, K.C. Mo, C. Ropelewski, J. Wang, A. Leetmaa, R. Reynolds, R. Jenne, and D. Joseph. 1996. "The NCEP/NCAR 40-year reanalysis project." *Bulletin of the American Meteorological Society.* American Meteorological Society, Boston, Massachusetts. Vol. 77, no. 3, pp. 437-471 (1 p.3/4).

Komen, G., L. Cavaleri, M. Donelan, K. Hasselmann, S. Hasselmann, and P.A.E.M. Janssen. 1994. *Dynamics and Modelling of Ocean Waves*. Cambridge University Press, Cambridge, UK, 560 pages.

Le Provost, C., F. Lyard, J. Molines, M. Genco, and F. Rabilloud. 1998. "A hydrodynamic ocean tide model improved by assimilating a satellite altimeter-derived data set." *J. Geophys. Res. [Oceans]*, 103, 5513-5529.

Lillicrop, J. 2006. Coastal Engineering Research Center, U.S. Army Corps of Engineers, USACE Waterways Experiment Station, Vicksburg, Mississippi. Personal communication.

Louisiana State University. 2004. Louisiana Lidar. http://atlas.lsu.edu/lidar/.

Luettich, R.A., and J.J. Westerink. 1995. "Continental shelf scale convergence studies with a barotropic model." *Quantitative Skill Assessment for Coastal Ocean Models, Coastal and Estuarine Studies Series No. 47,* D.R. Lynch and A.M. Davies, Eds., Amer. Geophys. Union, 349-371.

Luettich, R.A., and J.J. Westerink. 2003. "Combined discharge and radiation boundary condition in the ADCIRC hydrodynamic model: theory and documentation." *Contractors' Report*, U.S. Army Corps of Engineers New Orleans District. Available at: U.S. Army Engineer Corps of Engineers, New Orleans, ATTN: CEMVN-IM-SM Library, P.O. Box 60267, New Orleans, Louisiana, 70160-0267.

Luettich, R.A., and J.J. Westerink. 2004. "Formulation and Numerical Implementation of the 2D/3D ADCIRC Finite Element Model Version 44.XX". Available at: http://adcirc.org/adcirc_theory_2004_12_08.pdf.

Luettich, R.A., J.J. Westerink, and N.W. Scheffner. 1992. "ADCIRC: an advanced three-dimensional circulation model for shelves, coasts and estuaries, report 1: theory and methodology of ADCIRC-2DDI and ADCIRC-3DL." *Tech. Rep. DRP-92-6*, U.S. Army Corps of Engineers. Available at: ERDC Vicksburg (WES), U.S. Army Engineer Waterways Experiment Station (WES), ATTN: ERDC-ITL-K, 3909 Halls Ferry Road, Vicksburg, Mississippi, 39180-6199.

Mississippi Automated Resource Information System. 2006. Mississippi island 10 meter by 10 meter DEM. http://www.maris.state.ms.us/HTM/DownloadData/DEM.html.

Mukai, A., J.J. Westerink, and R.A. Luettich. 2001a. "Guidelines for Using the Eastcoast 2001 Database of Tidal Constituents within the Western North Atlantic Ocean, Gulf of Mexico and Caribbean Sea," *Coastal and Hydraulic Engineering Technical Note*, U.S. Army Engineer Research and Development Center.

Mukai, A., J.J. Westerink, R.A. Luettich, and D. Mark. 2001b. "A Tidal Constituent Database for the Western North Atlantic Ocean, Gulf of Mexico and Caribbean Sea," *Technical Report*, U.S. Army Engineer Research and Development Center.

Mukai, A., J.J. Westerink, R.A. Luettich, and D. Mark. 2002. "Eastcoast 2001: a tidal constituent database for the Western North Atlantic, Gulf of Mexico and Caribbean Sea," U.S. Army Corps of Engineers Research and Development Center, Coastal and Hydraulics Laboratory, *Technical Report, ERDC/CHL TR-02-24*. 201p. September.

Powell, M., and S. Houston. 1996. "Hurricane Andrew's landfall in South Florida. Part II: Surface wind fields and potential real-time applications." *Wea. Forecasting*, 11, 329-349.

Powell, M., S. Houston, and T. Reinhold. 1996. "Hurricane Andrew's landfall in South Florida. Part I: Standardizing measurements for documentation of surface windfields." *Wea. Forecasting*, 11, 304-328.

Powell, M., S. Houston, L. Amat, and N. Morrisseau-Leroy. 1998. "The HRD real-time hurricane wind analysis system." *J. Wind Engr. Indust. Aero.*, 77-78: 53-64.

Powell, M.D., P.J. Vickery, and T.A. Reinhold. 2003. "Reduced drag coefficient for high wind speeds in tropical cyclones." *Nature*, 422 (6929): 279-283 March 20, 2003.

Powell, M. D., S. Murillo, P. Dodge, E. Uhlhorn, J. Gamache, V. Cardone, A. Cox, S. Otero, N. Carrasco, B. Annane and R. St. Fleur. 2008. "Reconstruction of Hurricane Katrina's Wind field for Storm Surge and Wave Hindcasting." Submitted to *Ocean Engineering.*

Reid, R.O. 1990. "Water Level Changes - Tides and Storm Surges, Handbook of Coastal and Ocean Engineering," Gulf Publishing Co.

Reid, R.O., and R. Whitaker. 1976. "Wind-driven flow of water influenced by a canopy." *J. Waterw., Harbors, Coastal Engr. Div.- Am. Soc. Civ. Eng.*, 102, WW1, 61-77.

Resio, D.T. and J.J. Westerink. 2008. "Hurricanes and the Physics of Surges," *Physics Today*, **61**, 9, 33-38, 2008.

Ris, R., L. Holthuijsen, J.M. Smith, N. Booij, and A. van Dongeren. 2002. "The ONR Test Bed for Coastal and Oceanic Wave Models", Proceedings, ICCE 2002, World Scientific, 380-391.

Salinger, A. 2006. Personal communication.

Smith, J.M. 2000. "Benchmark Tests of STWAVE," *Proceedings, 6th International Workshop on Wave Hindcasting and Forecasting*, Environment Canada, 369-379.

Smith, J.M., and A.K. Zundel. 2006. "Full-Plane STWAVE: I. SMS Graphical Interface," *ERDC/CHL CHETN I-71*. U.S. Army Engineer Research and Development Center, Vicksburg, MS. http://chl.wes.army.lmil/library/publications/ chetn/.

Smith, J.M. 2007. "Full-Plane STWAVE: II. Model Overview," *ERDC TN-SWWRP-07-5*, U.S. Army Engineer Research and Development Center, Vicksburg, MS.

Smith, J.M., H.E. Bermudez, and B.A. Ebersole. 2000. "Modeling Waves at Willapa Bay, Washington," *Proceedings, 27th International Conference on Coastal Engineering, ASCE*, 826-839.

Smith, J.M., A.R. Sherlock, and D.T. Resio. 2001. "STWAVE: Steady-State Spectral Wave Model User's Manual for STWAVE, Version 3.0." USACE, Engineer Research and Development Center, *Technical Report ERDC/CHL SR-01-1*, Vicksburg, MS 80 pp. http://chl.erdc.usace.army.mil/Media/2/4/4/erdc-chl-sr-01-11.pdf.

Smith, J.M., A. Militello, and S.J. Smith. 1998. "Modeling Waves at Ponce de Leon Inlet, Florida," *Proceedings, 5th International Workshop on Wave Hindcasting and Forecasting, Environment Canada*, pp. 201-214.

Smith, S.J., and J.M. Smith. 2001. "Numerical Modeling of Waves at Ponce de Leon Inlet, Florida." *J. Waterway, Port, Coastal and Ocean Engineering,* 127(3), 176-184.

Smith, J.M., and C.L. Vincent. 2002. "Application of Spectral Equilibrium Ranges in the Surf Zone." 28th International Conference on Coastal Engineering, July 2002, Cardiff, Wales.

Suhayda, J. 2007. Taylor Engineering, Baton Rouge, Louisiana. Personal communication.

Thompson, E.F., J.M. Smith, and H.C. Miller. 2004. "Wave Transformation Modeling at Cape Fear River Entrance, North Carolina." *J. Coastal Research,* 20 (4), 1135-1154.

URS. 2006a. HMTAP Task Order 18, Mississippi Coastal Analysis Project, *Geospatial Technology Task Repor*t (Task 3).

URS. 2006b. "Final coastal and riverine high-water marks collection for Hurricane Katrina in Louisiana," Final Report for the Federal Emergency Management Agency.

URS. 2006c. "Final coastal and riverine high-water marks collection for Hurricane Katrina in Mississippi," Final Report for the Federal Emergency Management Agency.

U.S. Army Corps of Engineers. 1957. Mississippi River - Gulf Outlet Design Memorandum 1-A, Plate 2.

U.S. Army Corps of Engineers, New Orleans District. 2000. Aerial Survey of Lake Pontchartrain Vicinity and Chalmette Loop Levee Systems. May.

U.S. Army Corps of Engineers, Mobile District. 2005. "Lidar Report Mississippi and Alabama Coastal Mapping".

U.S. Army Corps of Engineers. 2007a. "Performance Evaluation of the New Orleans and Southeast Louisiana Hurricane Protection System. Final Report of the Interagency Performance Evaluation Task Form, Volume II – Geodetic Vertical and Water Level Datums," 26 March.

U.S. Army Corps of Engineers. 2007b. "Performance Evaluation of the New Orleans and Southeast Louisiana Hurricane Protection System. Final Report of the Interagency Performance Evaluation Task Force; Volume IV – The Storm." 26 March.

U.S. Army Corps of Engineers. 2007c. "FEMA Flood Insurance Study: Southeastern Parishes, Louisiana - Intermediate Submission 2." U.S. Army Corps of Engineers, New Orleans District, New Orleans LA.

U.S. Army Corps of Engineers. 2008. "Louisiana Coastal Protection and Restoration Technical Report - Draft." New Orleans District, Mississippi Valley Division, February.

U.S. Army Corps of Engineers, New Orleans District. 2008. September 1, 2008

USGS. 2000. "A GAP Analysis of Louisiana," Final Report. June.

Vogelmann, J.E., S.M. Howard, L. Yang, C.R. Larson, B.K. Wylie, and N. Van Driel. 2001. "Completion of the 1990s National Land Cover Data Set for the Conterminous United States from Landsat Thematic Mapper Data and Ancillary Data Sources", *Photogrammetric Engineering and Remote Sensing*, 67:650-652.

Westerink, J.J. 1993. "Tidal prediction in the Gulf of Mexico/Galveston Bay using model ADCIRC-2DDI," Contractors Report to the U.S. Army Engineer Waterways Experiment Station, Vicksburg, Mississippi. January.

Westerink, J.J., and W.G. Gray. 1991. "Progress in Surface Water Modeling," Reviews of Geophysics, Supplement, 29, 210-217.

Westerink, J.J., R.A. Luettich, A.M. Baptista, N.W. Scheffner, and P. Farrar. 1992. "Tide and storm surge predictions using a finite element model," *J. Hydraul. Eng.*, 118, 1373-1390.

Westerink, J.J., R.A. Luettich, and J.C. Muccino. 1994. "Modeling Tides in the Western North Atlantic Using Unstructured Graded Grids," *Tellus*, 46A, 178-199.

Westerink, J.J., R.A. Luettich , J.C. Feyen, J.H. Atkinson, C. Dawson, H.J. Roberts, M.D. Powell, J.P. Dunion, E.J. Kubatko, H. Pourtaheri. 2008. "A Basin to Channel Scale Unstructured Grid Hurricane Storm Surge Model Applied to Southern Louisiana," *Monthly Weather Review*, **136**, 3, 833-864.

Table 1: Description of the six scenarios simulated in this report.

United States' Scenario	Plaintiffs' Scenario	MRGO Reach 1/GIWW	MRGO Reach 2	Chalmette Levee	Marsh	Description
H1 *Katrina Real Run*	1	2005 pre-Katrina dimensions	2005 pre-Katrina dimensions	2005 pre-Katrina dimensions	2005 pre-Katrina conditions	Conditions at Hurricane Katrina landfall.
H2 *No MRGO with 2005 wetlands*		1958 pre-MRGO (existing GIWW dimensions)	None (channel eliminated and topography raised to surrounding area)	2005 pre-Katrina dimensions	2005 pre-Katrina conditions	Conditions at Katrina landfall, if MRGO had not been constructed.
H3 *No MRGO with 1956 wetlands*	2C	1958 pre-MRGO (existing GIWW dimensions)	None (channel eliminated and topography raised to surrounding area	2005 pre-Katrina dimensions	1956 pre-MRGO conditions	Conditions at Katrina landfall, if MRGO had not been constructed and marsh had remained in pre-MRGO condition.
H4 *No MRGO with 1956 wetlands and a relocated Chalmette Levee*	2A	1958 pre-MRGO (existing GIWW dimensions)	None (channel eliminated and topography raised to surrounding area)	Idealized levee (17.5 ft) at 40 Arpent location	1956 Pre-MRGO conditions	Conditions at Katrina landfall, if MRGO had not been constructed, marsh had been in 1956 pre-MRGO condition, and Chalmette levee had been constructed at 40 Arpent location.
H5 *MRGO as designed with 2005 wetlands*		Ideal MRGO (approximate design dimensions)	Ideal MRGO (approximate design dimensions)	2005 pre-Katrina dimensions	2005 Pre-Katrina conditions	Conditions at Katrina landfall, if MRGO had been at design dimensions.
H6 *MRGO as designed with 1956 wetlands*	3	Ideal MRGO (approximate design dimensions)	Ideal MRGO (approximate design dimensions)	2005 Pre-Katrina dimensions	1956 Pre-MRGO conditions	Conditions at Katrina landfall, if MRGO had been at design dimensions and marsh had been in 1956 pre-MRGO condition.

Table 2: Manning n values for Louisiana Gap (LA-GAP) classification.

LA-GAP Class	Description	Manning-n
1	Fresh Marsh	0.055
2	Intermediate Marsh	0.050
3	Brackish Marsh	0.045
4	Saline Marsh	0.035
5	Wetland Forest – Deciduous	0.140
6	Wetland Forest – Evergreen	0.160
7	Wetland Forest – Mixed	0.150
8	Upland Forest – Deciduous	0.160
9	Upland Forest – Evergreen	0.180
10	Upland Forest – Mixed	0.170
11	Dense Pine Thicket	0.180
12	Wetland Scrub/Shrub – Deciduous	0.060
13	Wetland Scrub/Shrub – Evergreen	0.080
14	Wetland Scrub/Shrub – Mixed	0.070
15	Upland Scrub/Shrub – Deciduous	0.070
16	Upland Scrub/Shrub – Evergreen	0.090
17	Upland Scrub/Shrub – Mixed	0.080
18	Agriculture – Crops – Grass	0.040
19	Vegetated Urban	0.120
20	Non-Vegetated Urban	0.120
21	Wetland Barren	0.030
22	Upland Barren	0.030
23	Water	0.02-0.045

Table 3: Manning n values for 1956 Louisiana land use classification.

Type	**Description**	**Equivalent GAP**	**Manning-n**
3	Fresh Marsh	Type 1 – Fresh Marsh	0.055
4	Non Fresh Marsh	Type 3 /4 – Brackish and Saline Marsh	0.050
7	Forest	Type 5 – Wetland Forest	0.045
8	Swamp	Type 5 – Wetland Forest	0.035
11	Agriculture/Pasture	Type 18 - Agriculture	0.140
12	Developed	Type 19 - Urban	0.160
23	Water	Type 23 - Water	0.02-0.045

Table 4: Summary of difference/error statistics for the H1 *Katrina Real Run* and the measured Katrina HWM data sets. Average absolute differences/errors and standard deviations are given in ft.

Data Set	ADCIRC to Measured HWMs		Measured HWMs		Estimated ADCIRC Errors	
	Average Absolute Difference	Standard Deviation	Average Absolute Difference	Standard Deviation	Average Absolute Error	Standard Deviation
USACE	1.33	1.60	0.37	0.56	0.96	1.50
URS	1.21	1.49	0.30	0.50	0.91	1.40

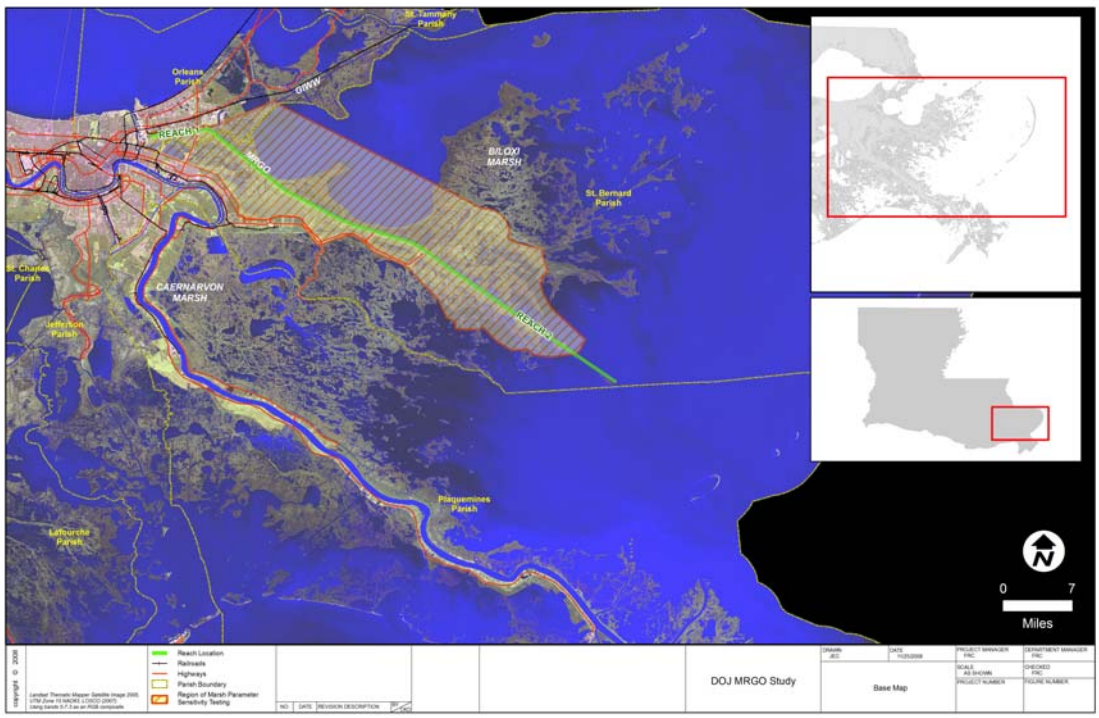


Figure 1: Study Region includes the east bank of the IHNC, the GIWW between the IHNC and Chef Menteur Pass, the Golden Triangle, the Biloxi Marsh, the Caernarvon Marsh and the eastern portion of Plaquemines Parish. Zone within the Study Region where the wetlands may have been influenced by the construction of the MRGO is shown as hatched (Britsch and Dunbar, 2008).



Figure 2: Detail of Study Region showing the region from the IHNC, the St. Bernard Polder and the New Orleans East Polder.

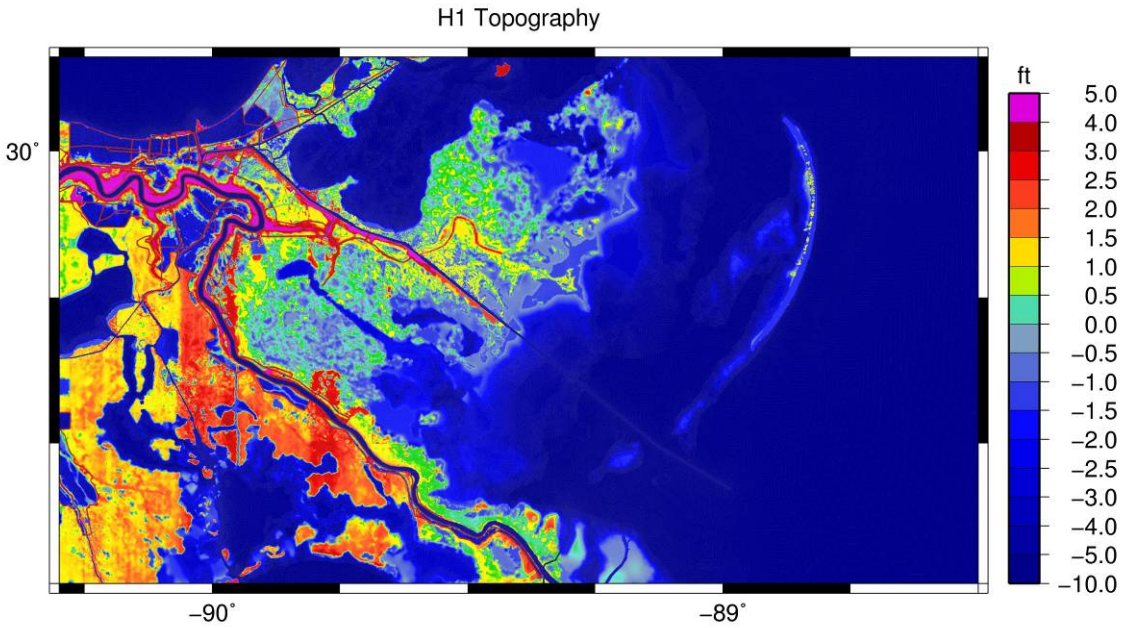


Figure 3: H1 model topography and bathymetry (ft relative to NAVD88 2004.65) in Southeastern Louisiana used in the *Katrina Real Run* simulation.

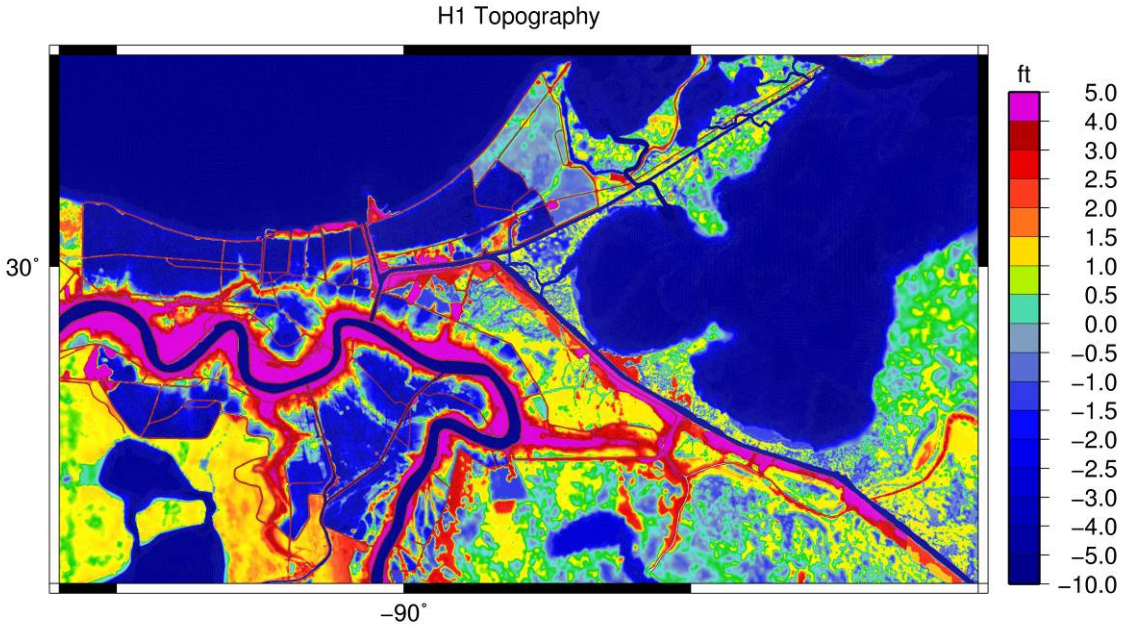


Figure 4: H1 model topography and bathymetry (ft relative to NAVD88 2004.65) in and around metropolitan New Orleans used in the *Katrina Real Run* simulation.

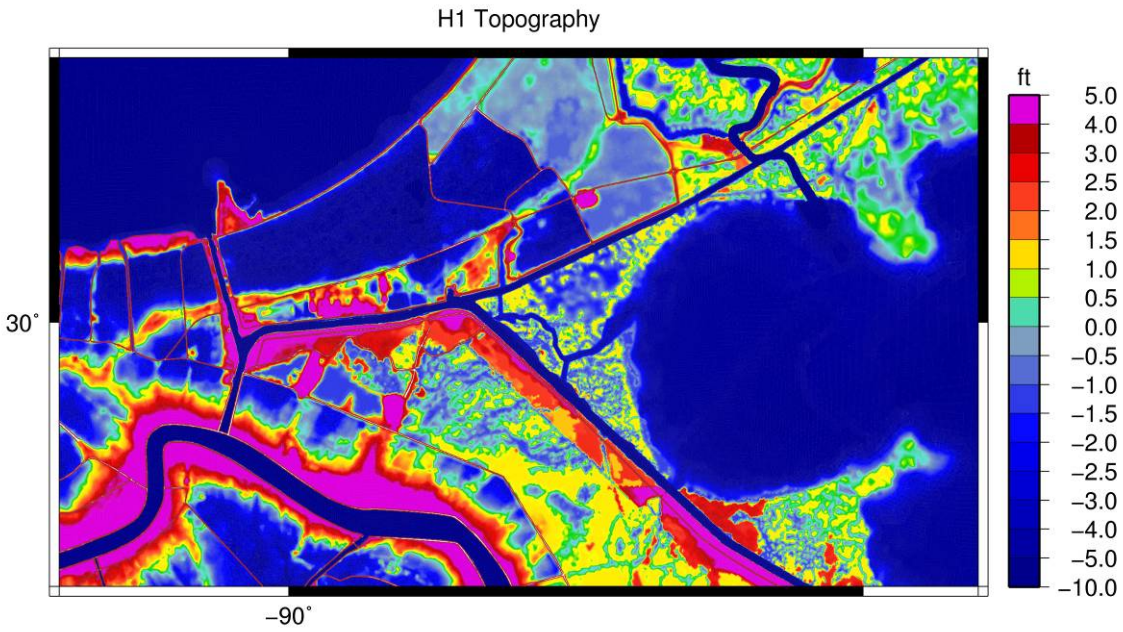


Figure 5: H1 model topography and bathymetry (ft relative to NAVD88 2004.65) in the vicinity of the IHNC to the Golden Triangle used in the *Katrina Real Run* simulation.

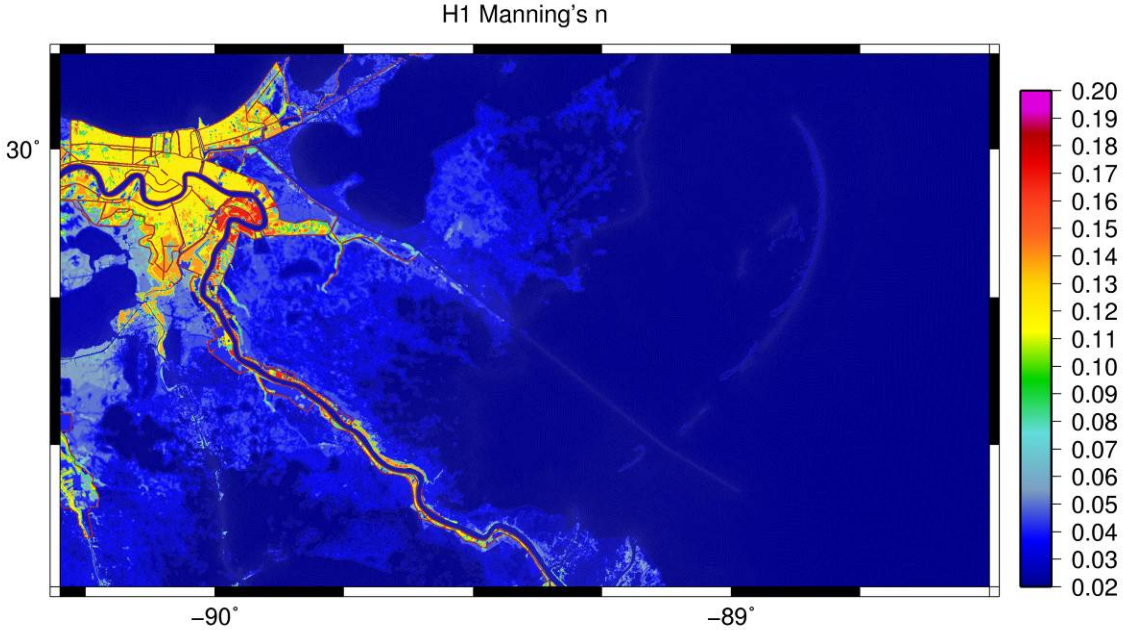


Figure 6: H1 model Manning n bottom friction values Southeastern Louisiana used in the *Katrina Real Run* simulation.

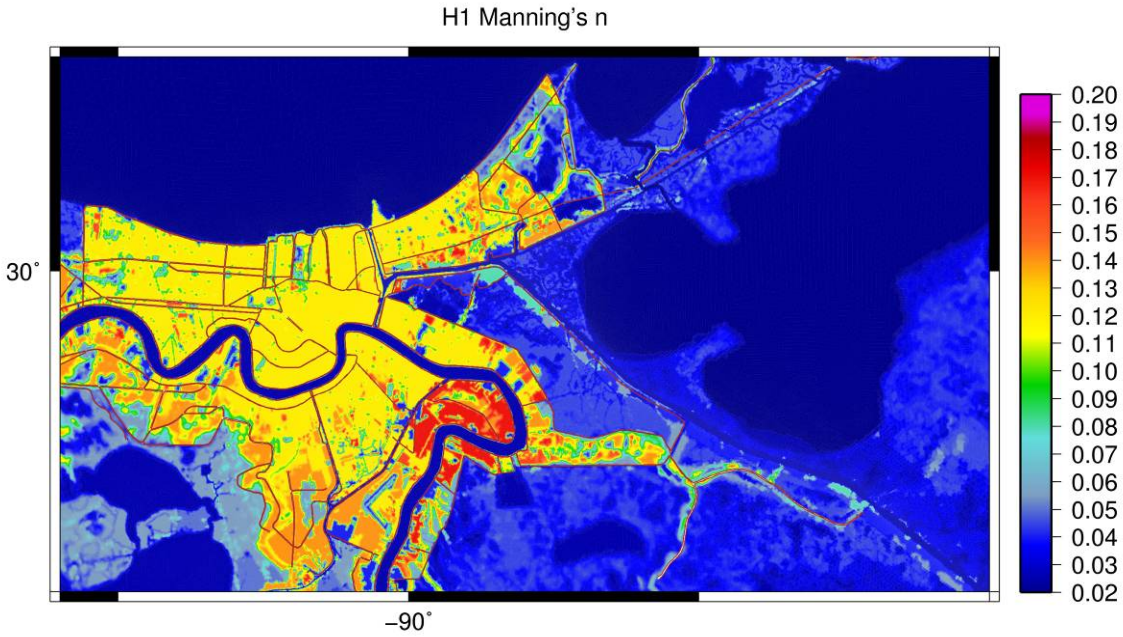


Figure 7: H1 model Manning n bottom friction values in and around metropolitan New Orleans used in the *Katrina Real Run* simulation.

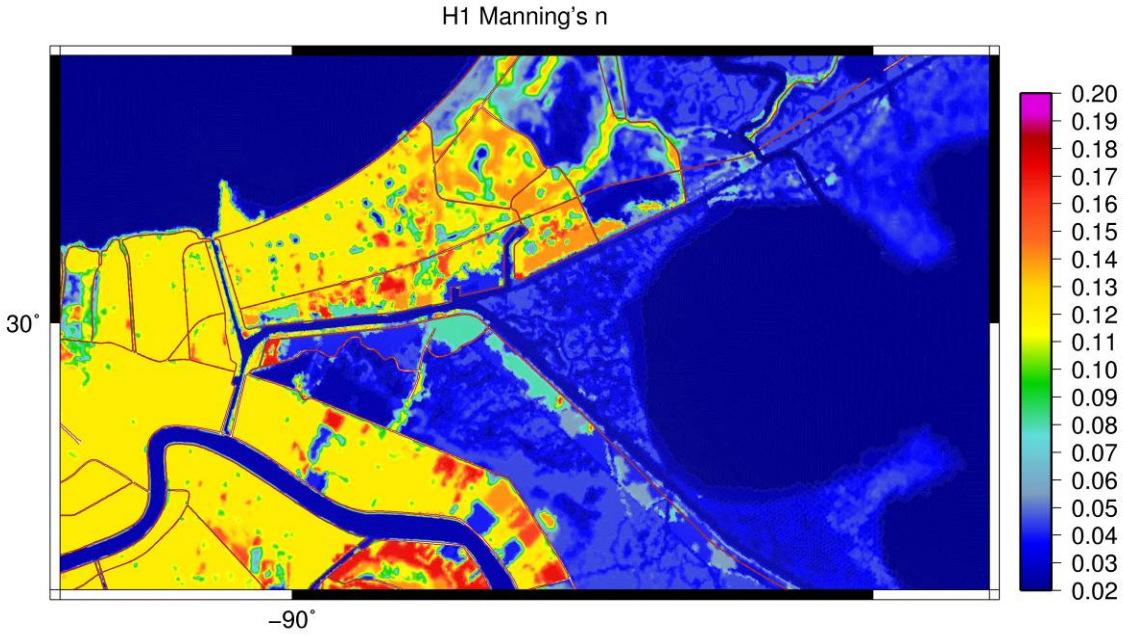


Figure 8: H1 model Manning n bottom friction values in the vicinity of the IHNC to the Golden Triangle used in the *Katrina Real Run* simulation.



Figure 9: 1958 aerial photo of the GIWW from its confluence with the IHNC in the east, past the Michoud Canal in the west (Dunbar, 2008).

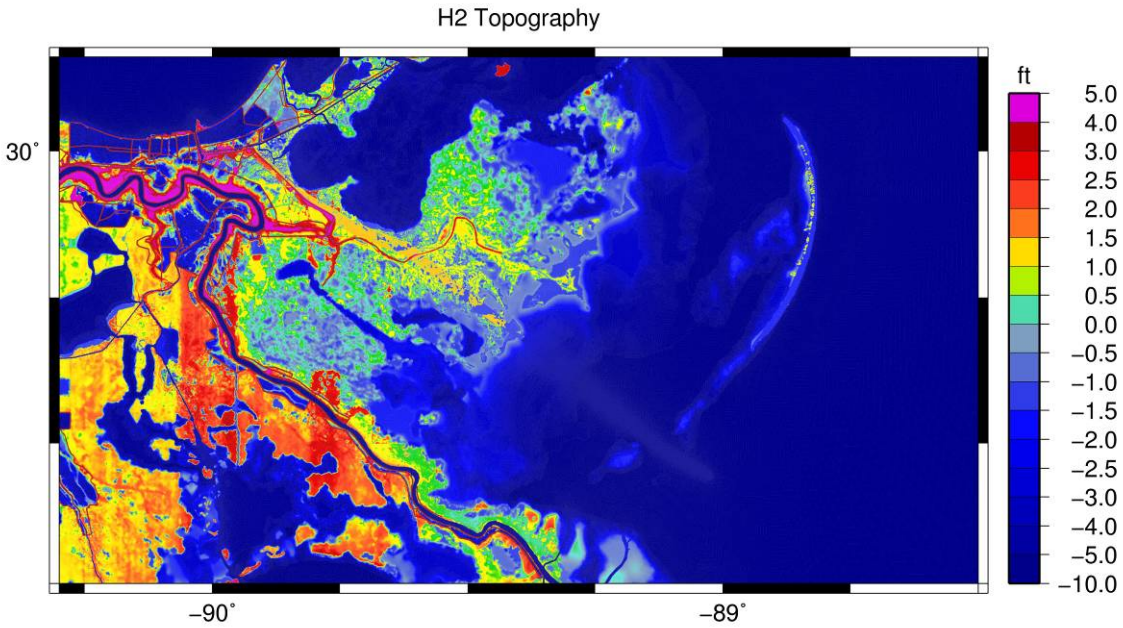


Figure 10: H2 model topography and bathymetry (ft relative to NAVD88 2004.65) in Southeastern Louisiana used in the *No MRGO with 2005 wetlands* simulation.

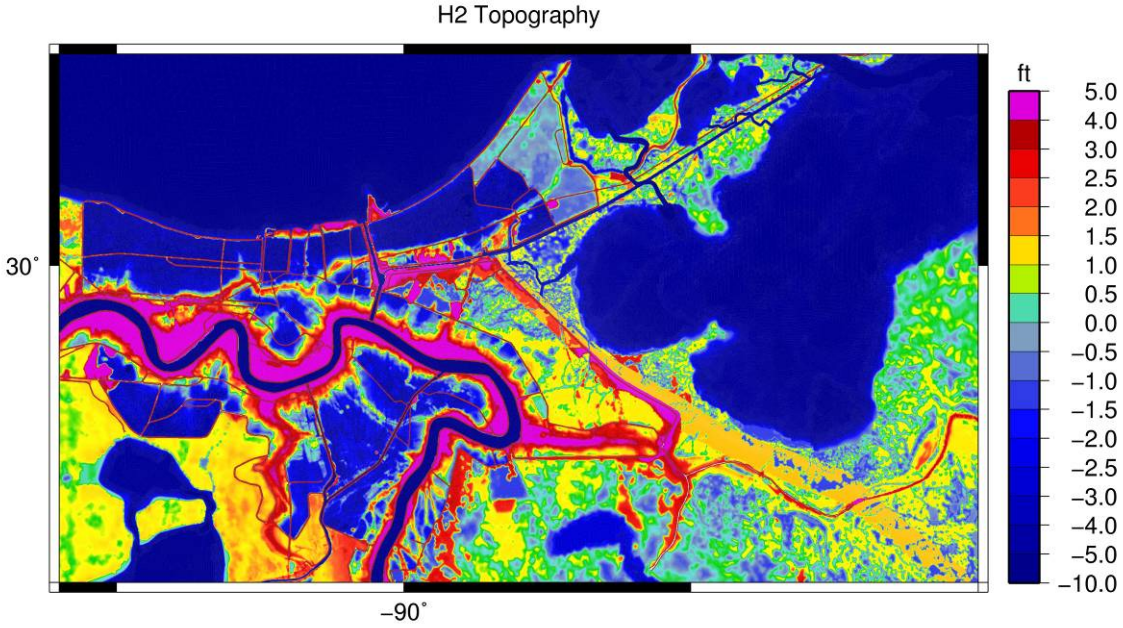


Figure 11: H2 model topography and bathymetry (ft relative to NAVD88 2004.65) in and around metropolitan New Orleans used in the *No MRGO with 2005 wetlands* simulation.

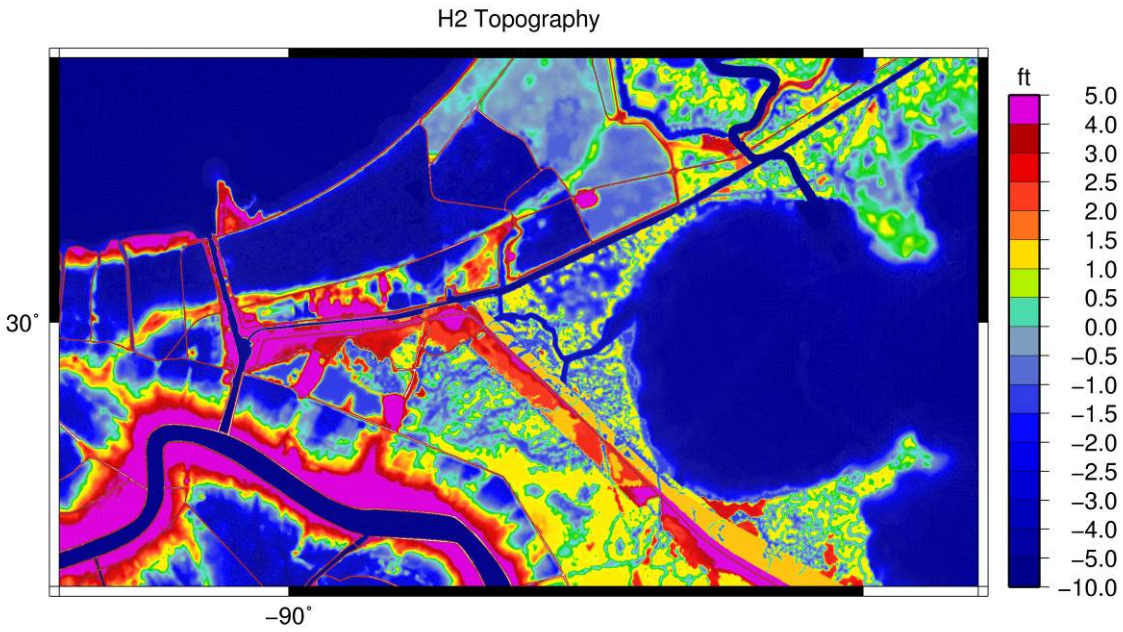


Figure 12: H2 model topography and bathymetry (ft relative to NAVD88 2004.65) in the vicinity of the IHNC to the Golden Triangle used in the *No MRGO with 2005 wetlands* simulation.

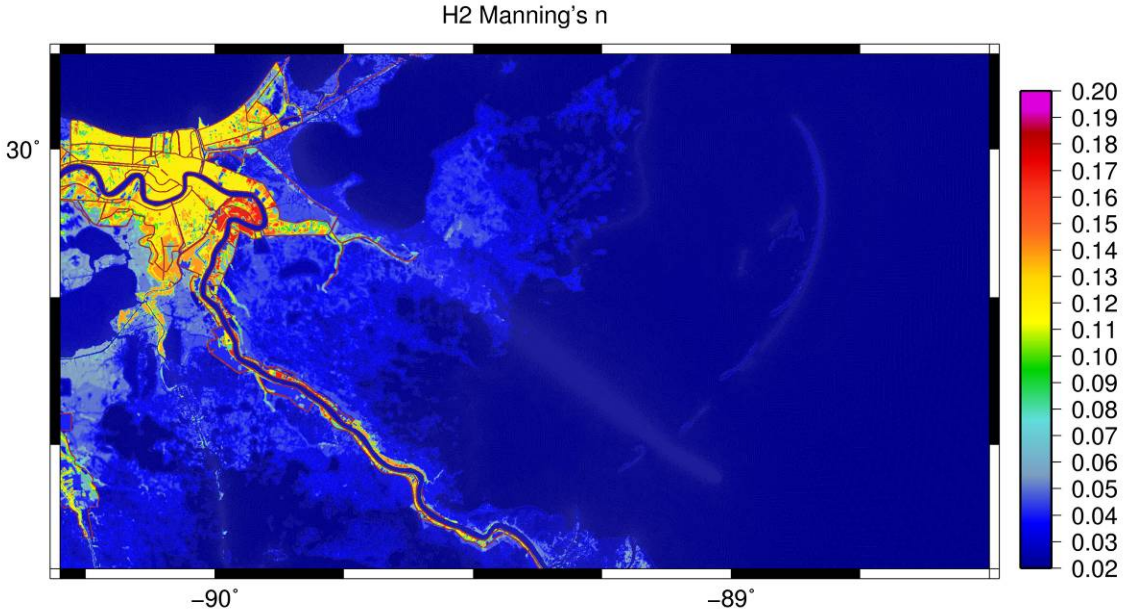


Figure 13: H2 model Manning n bottom friction values Southeastern Louisiana used in the *No MRGO with 2005 wetlands* simulation.

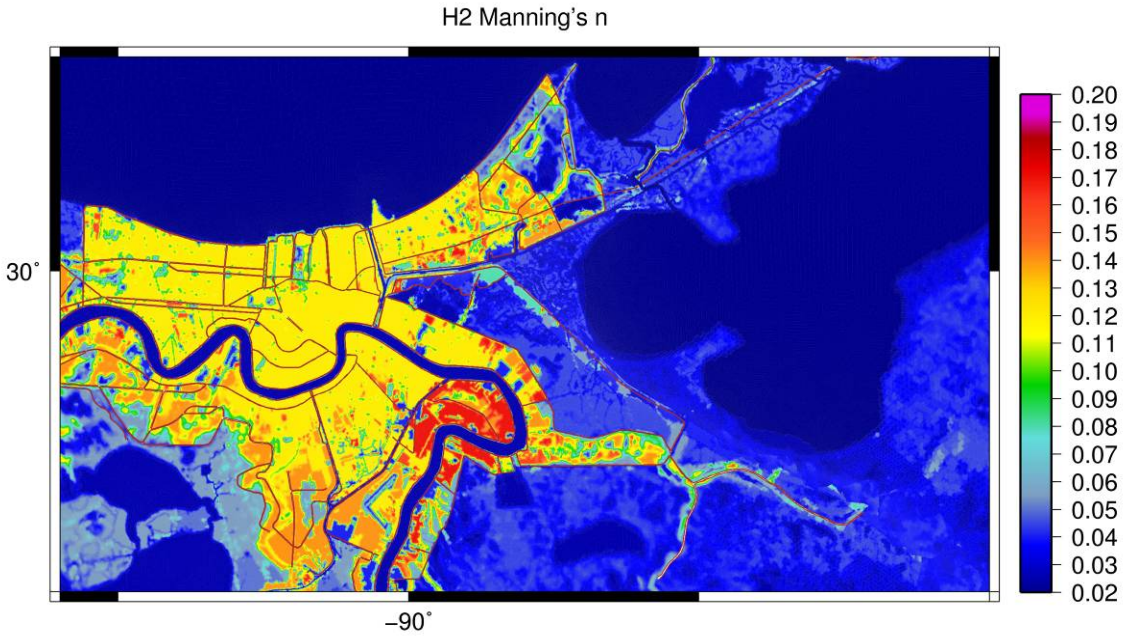


Figure 14: H2 model Manning n bottom friction values in and around metropolitan New Orleans used in the *No MRGO with 2005 wetlands* simulation.

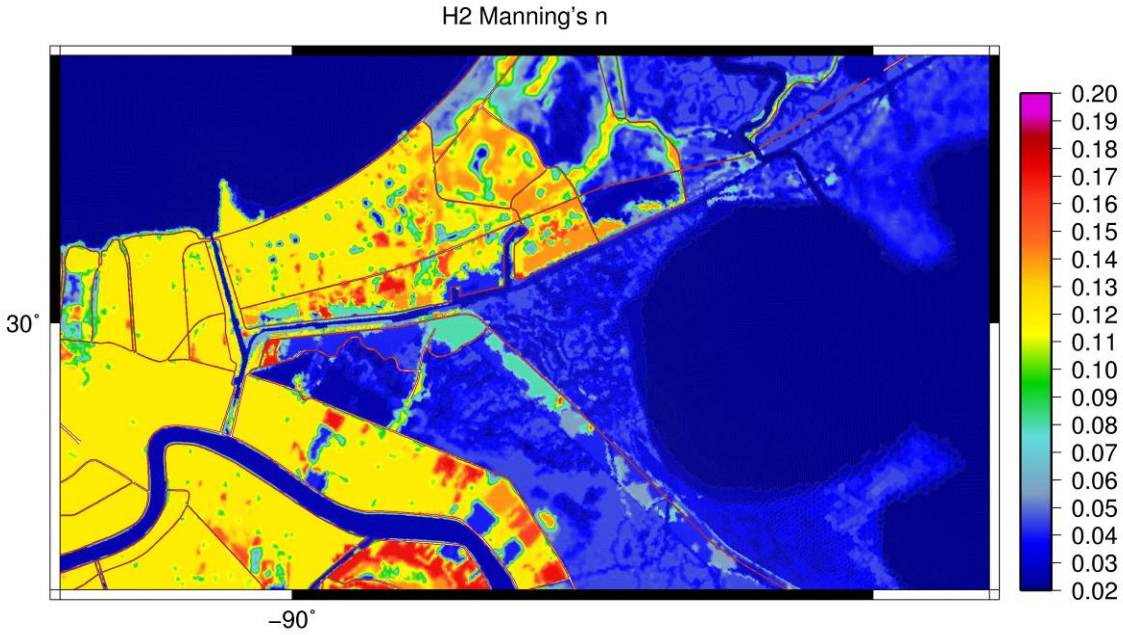


Figure 15: H2 model Manning n bottom friction values in the vicinity of the IHNC to the Golden Triangle used in the *No MRGO with 2005 wetlands* simulation.

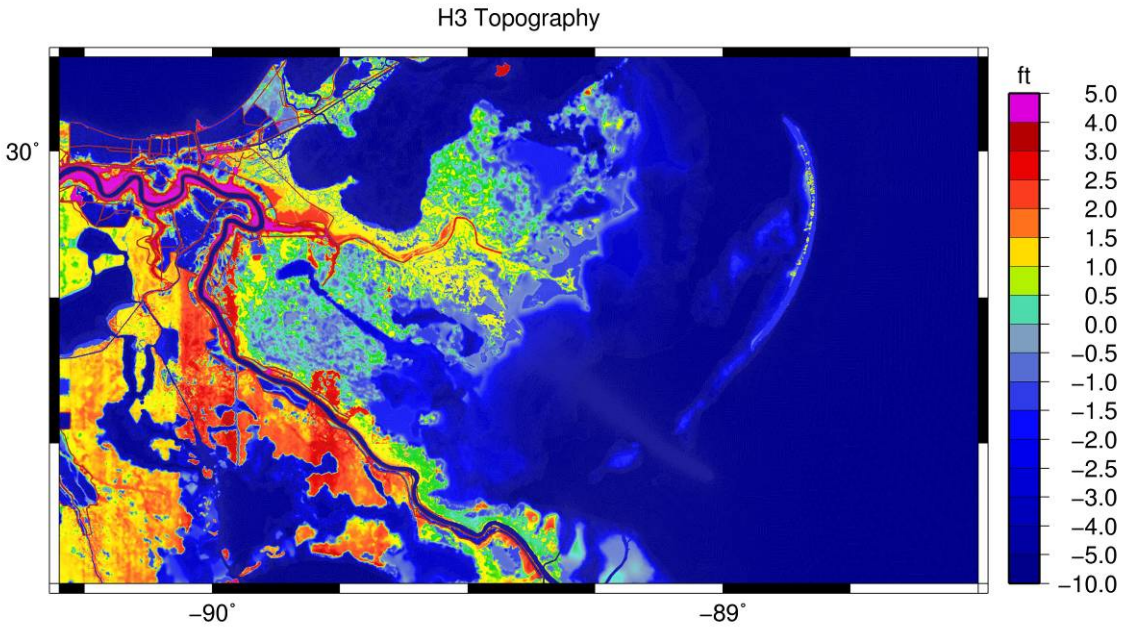


Figure 16: H3 model topography and bathymetry (ft relative to NAVD88 2004.65) in Southeastern Louisiana used in the *No MRGO with 1956 wetlands* simulation.

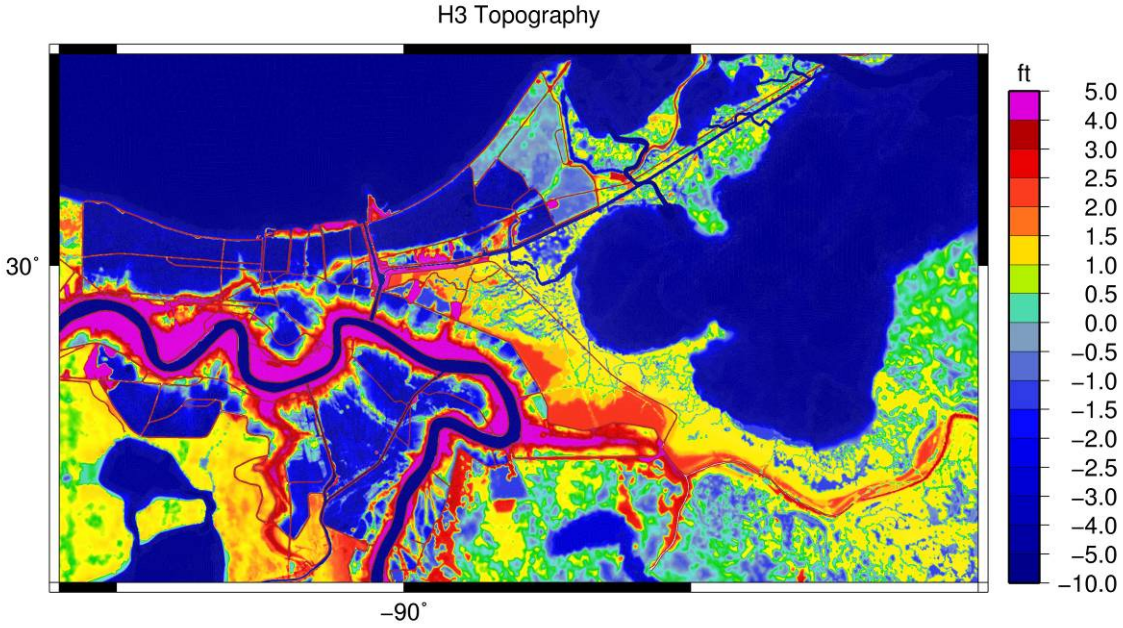


Figure 17: H3 model topography and bathymetry (ft relative to NAVD88 2004.65) in and around metropolitan New Orleans used in the *No MRGO with 1956 wetlands* simulation.

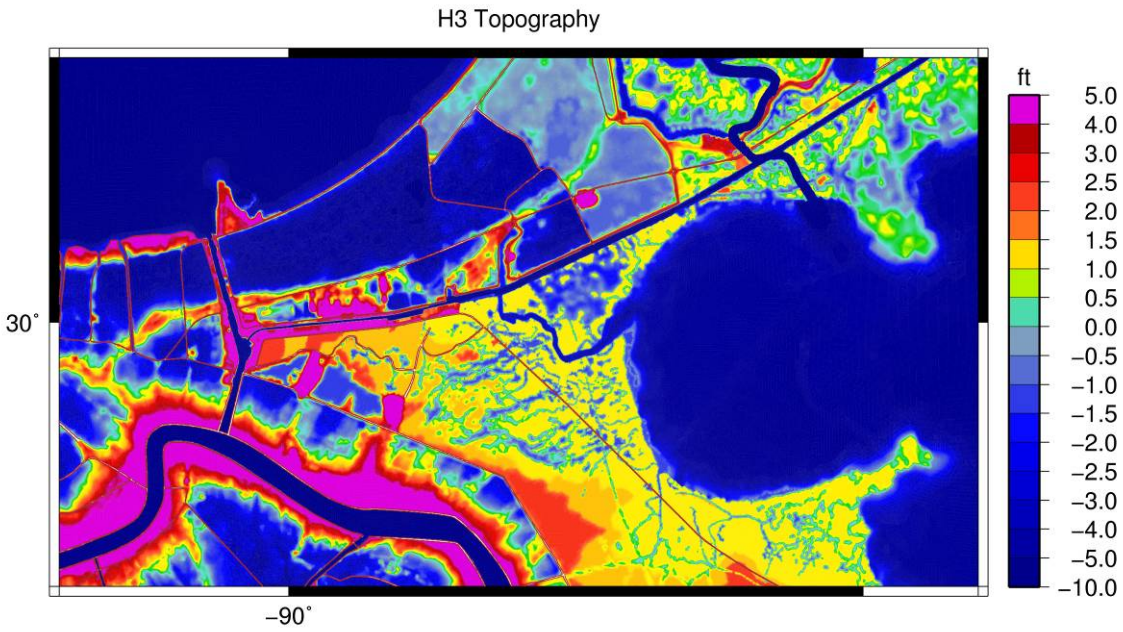


Figure 18: H3 model topography and bathymetry (ft relative to NAVD88 2004.65) in the vicinity of the IHNC to the Golden Triangle used in the *No MRGO with 1956 wetlands* simulation.

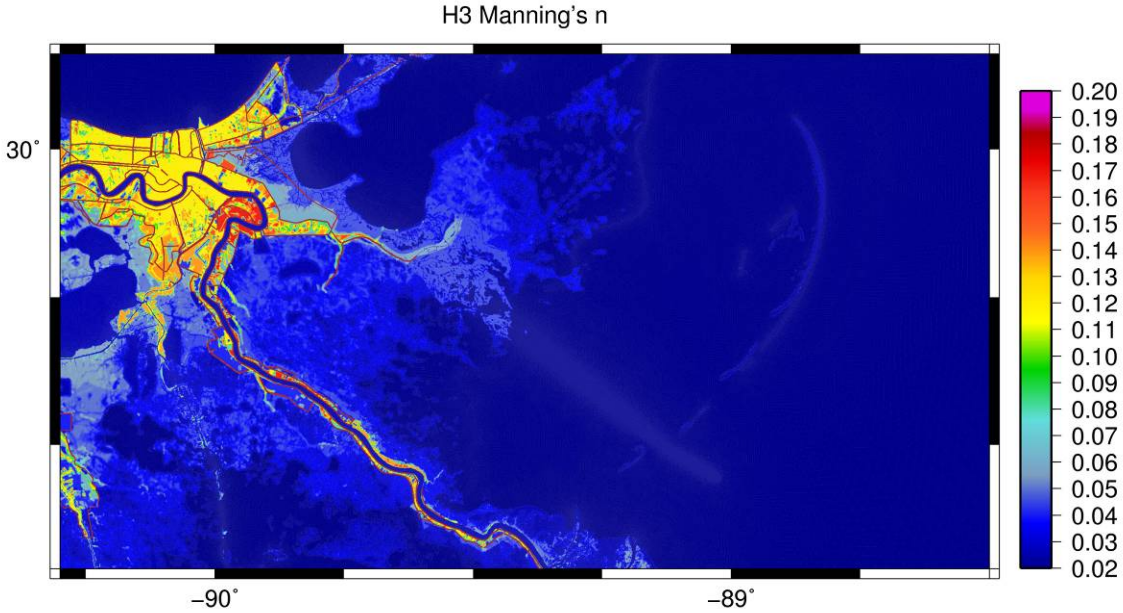


Figure 19: H3 model Manning n bottom friction values Southeastern Louisiana used in the *No MRGO with 1956 wetlands* simulation.

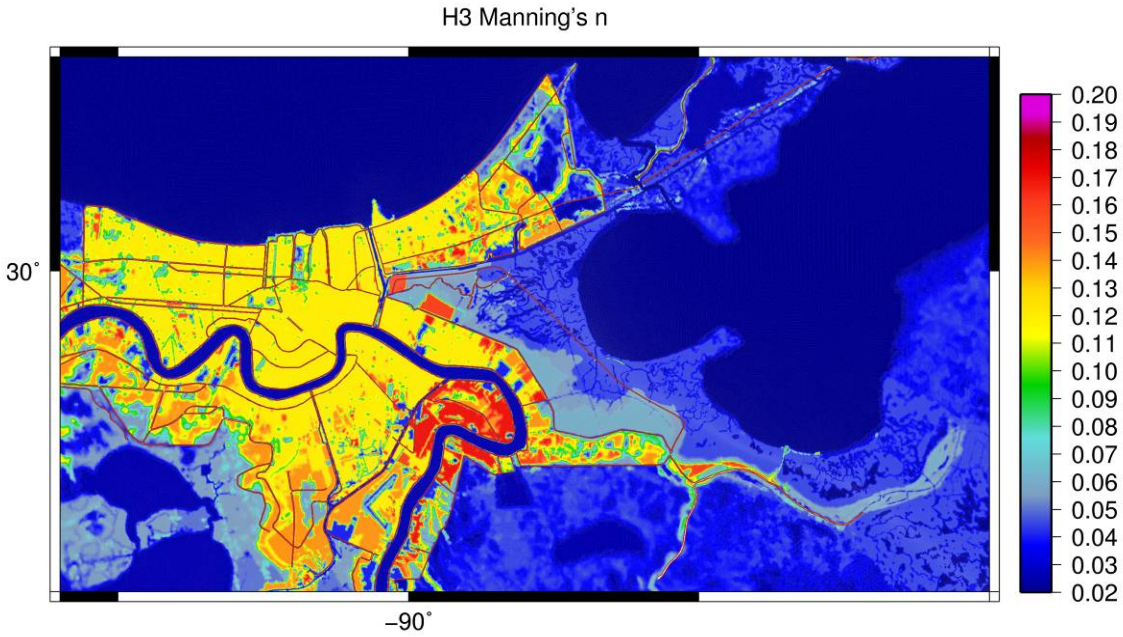


Figure 20: H3 model Manning n bottom friction values in and around metropolitan New Orleans used in the *No MRGO with 1956 wetlands* simulation.

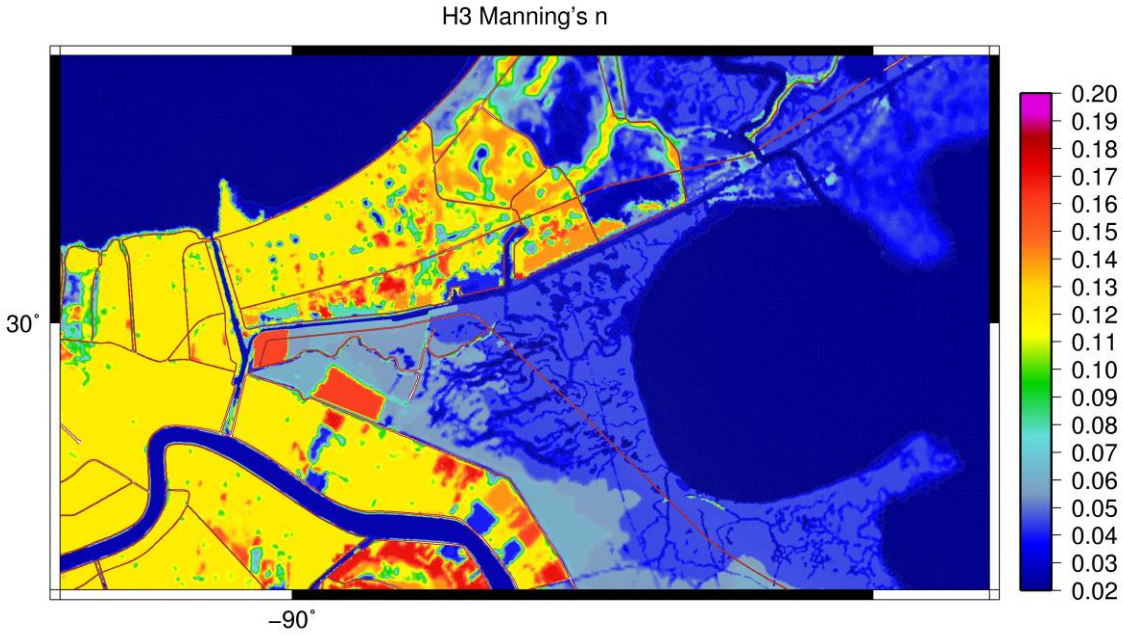


Figure 21: H3 model Manning n bottom friction values in the vicinity of the IHNC to the Golden Triangle used in the *No MRGO with 1956 wetlands* simulation.

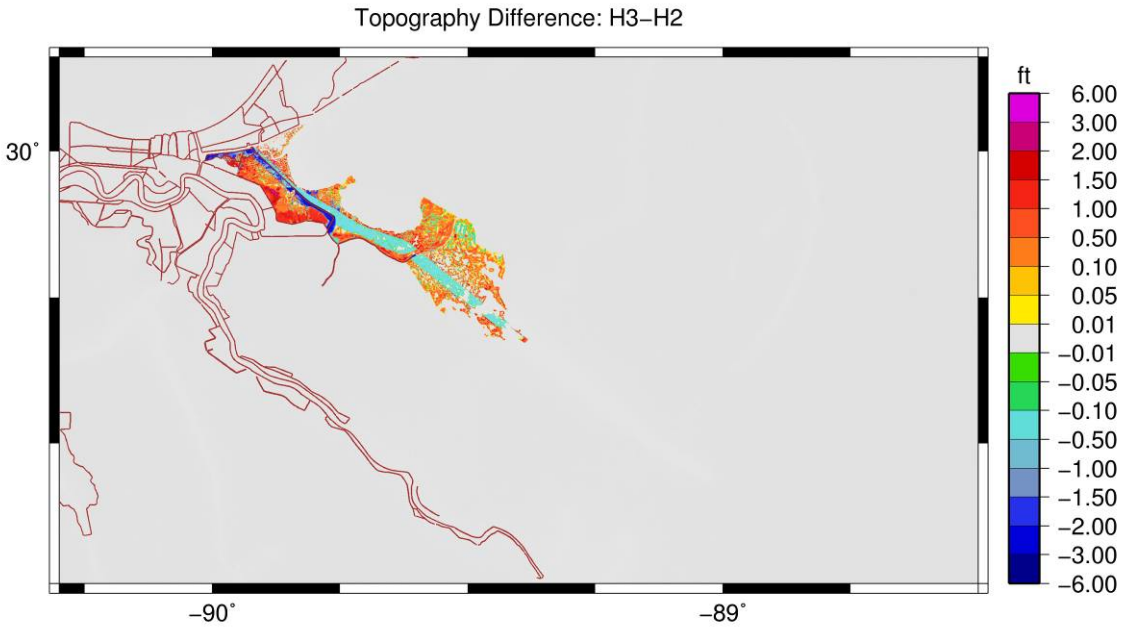


Figure 22: H3 to H2 model differences in topography and bathymetry (ft) in Southeastern Louisiana. Warm colors indicate that H3 is higher while cool colors indicate that H2 is higher.

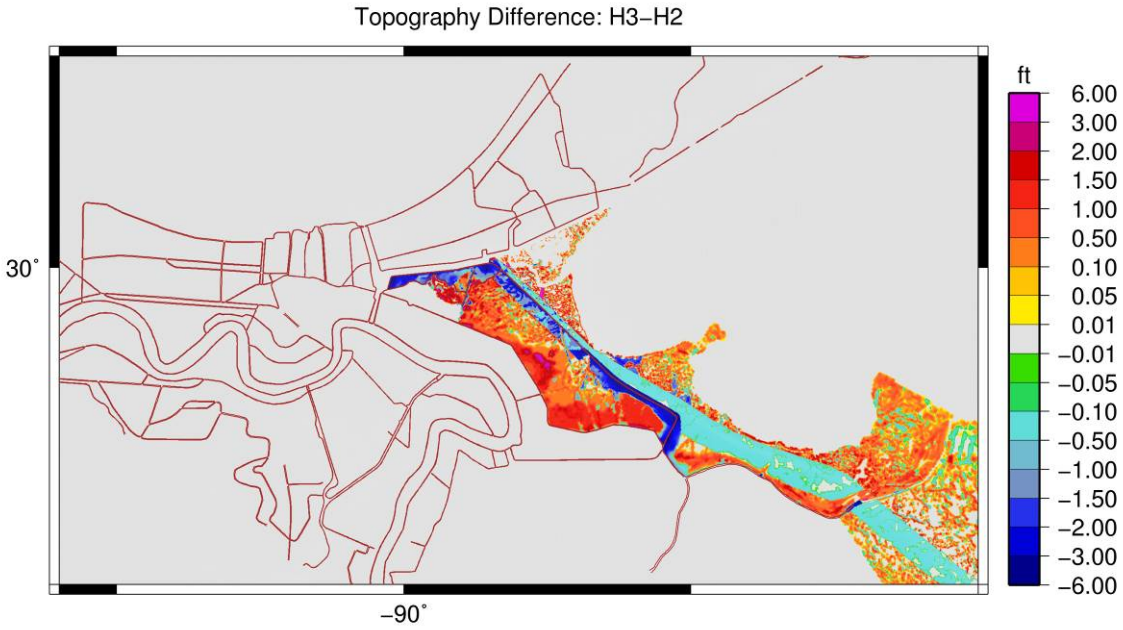


Figure 23: H3 to H2 model differences in topography (ft) in and around metropolitan New Orleans. Warm colors indicate that H3 is higher while cool colors indicate that H2 is higher.

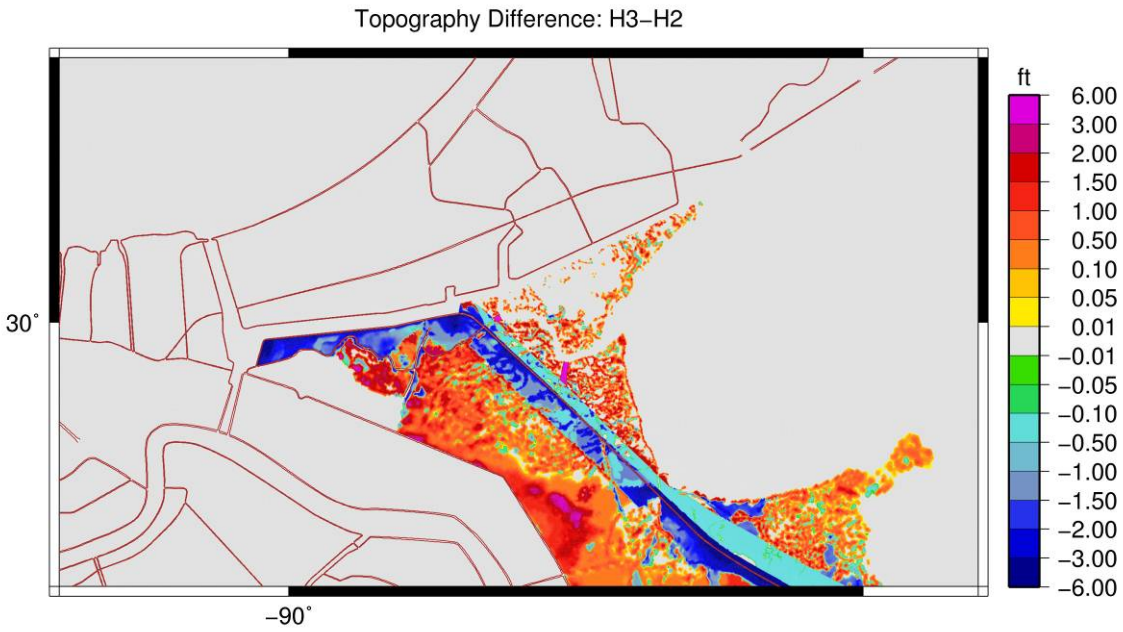


Figure 24: H3 to H2 model differences in topography (ft) relative in the vicinity of the IHNC to the Golden Triangle. Warm colors indicate that H3 is higher while cool colors indicate that H2 is higher.

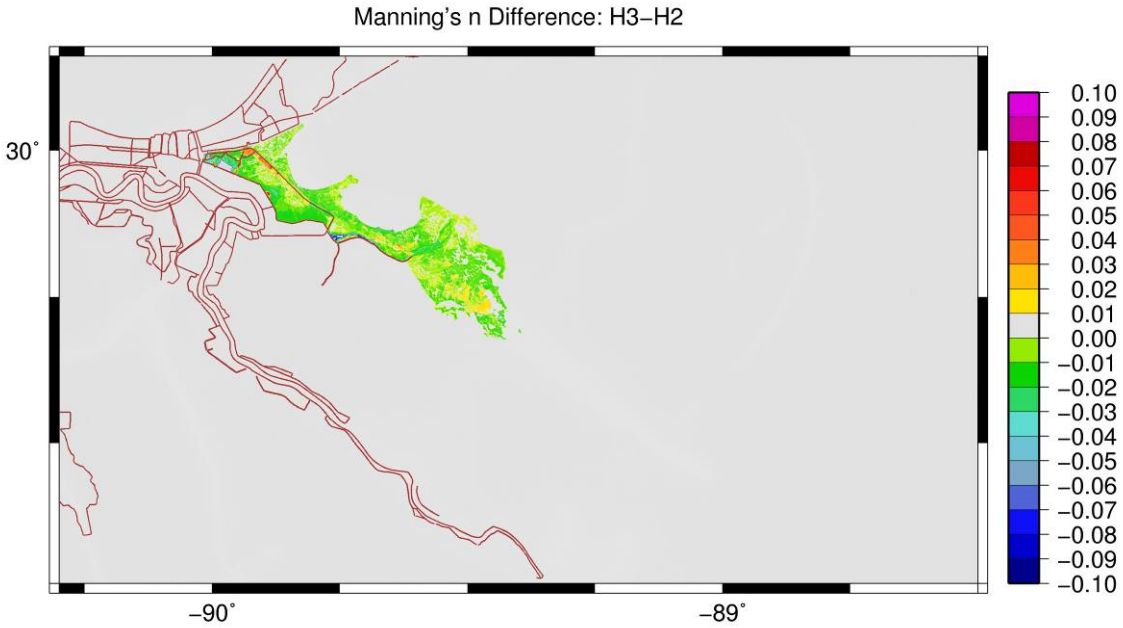


Figure 25: H3 to H2 model differences in Manning n bottom friction values in Southeastern Louisiana. Warm colors indicate that H2 has higher assigned Manning n values while cool colors indicate that H3 has higher assigned Manning n values.

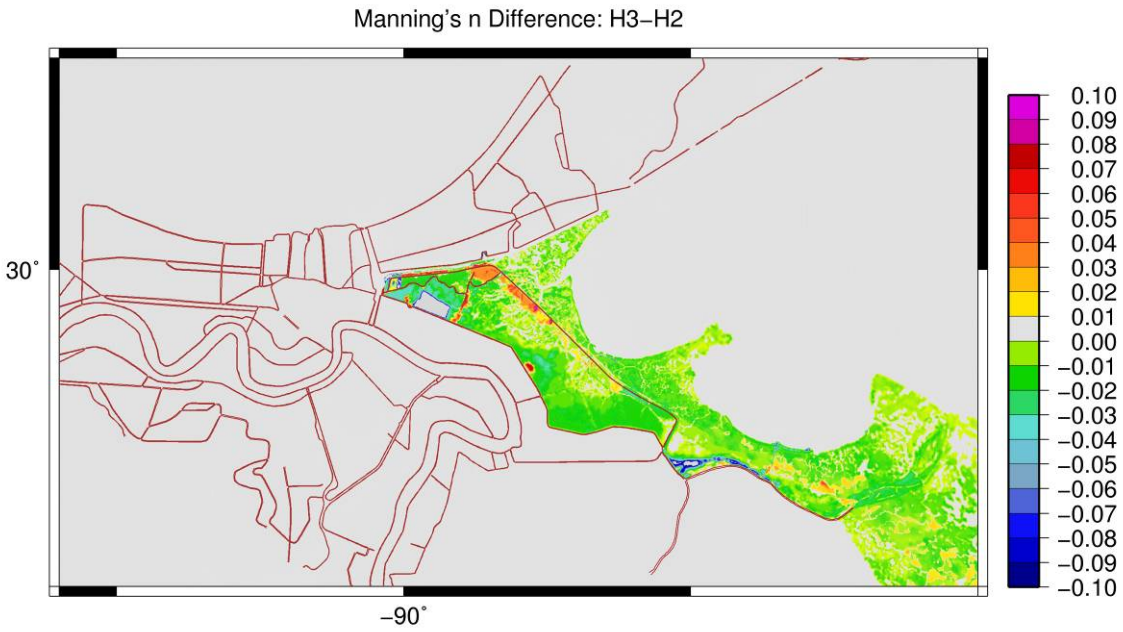


Figure 26: H3 to H2 model differences in Manning n bottom friction values in and around metropolitan New Orleans. Warm colors indicate that H2 has higher assigned Manning n values while cool colors indicate that H3 has higher assigned Manning n values.

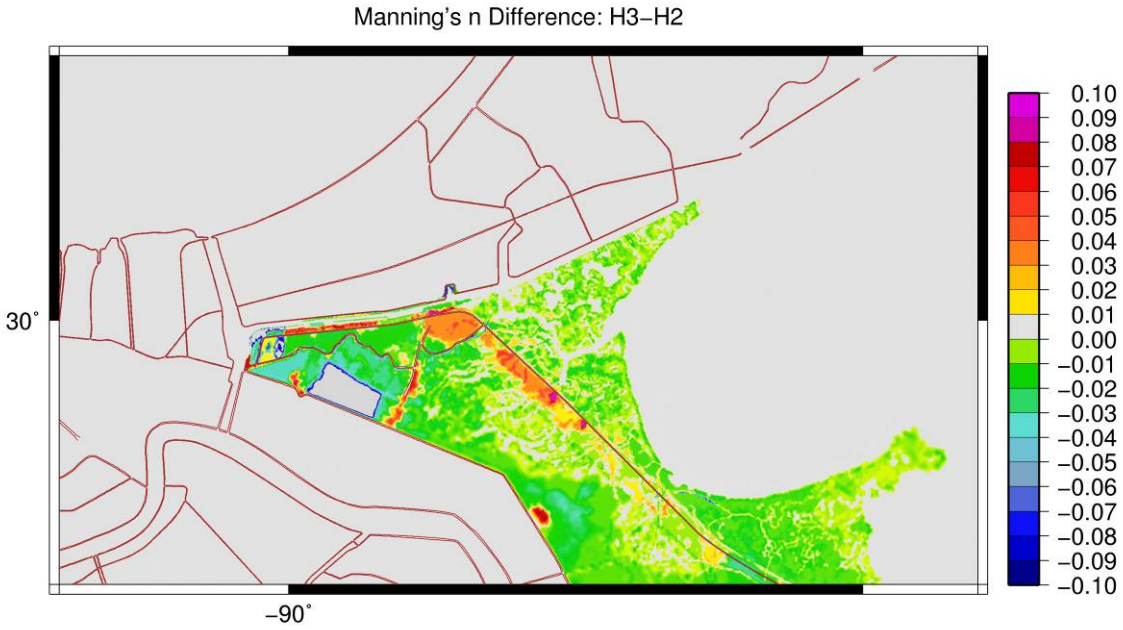


Figure 27: H3 to H2 model differences in Manning n bottom friction values in the vicinity of the IHNC to the Golden Triangle. Warm colors indicate that H2 has higher assigned Manning n values while cool colors indicate that H3 has higher assigned Manning n values.

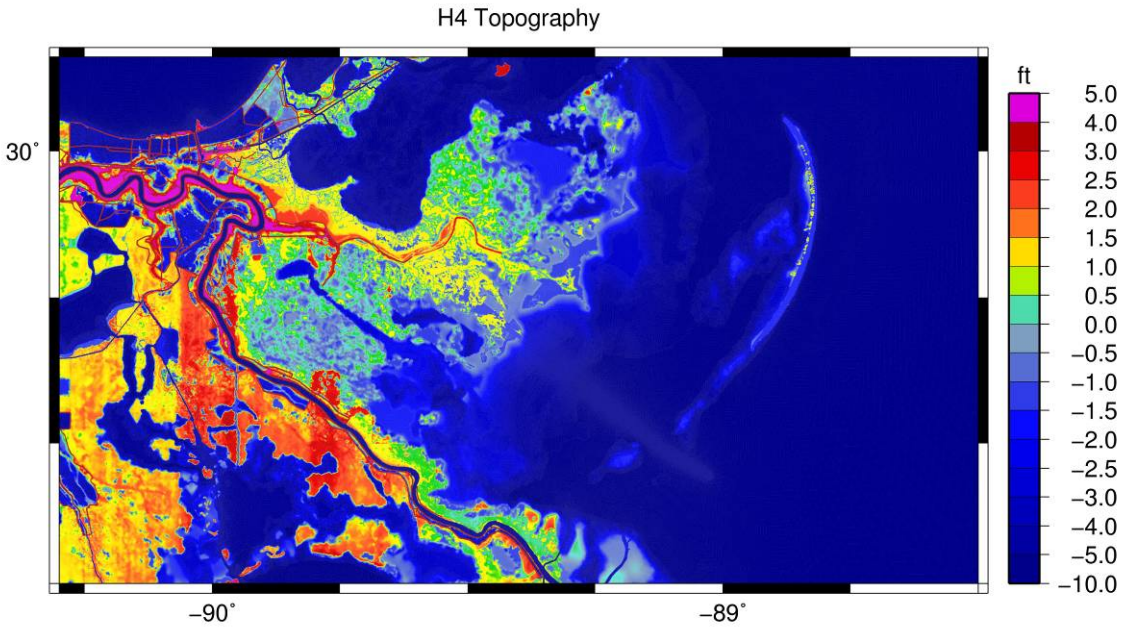


Figure 28: H4 model topography and bathymetry (ft relative to NAVD88 2004.65) in Southeastern Louisiana used in the *No MRGO with 1956 wetlands with relocated Chalmette Levee* simulation.

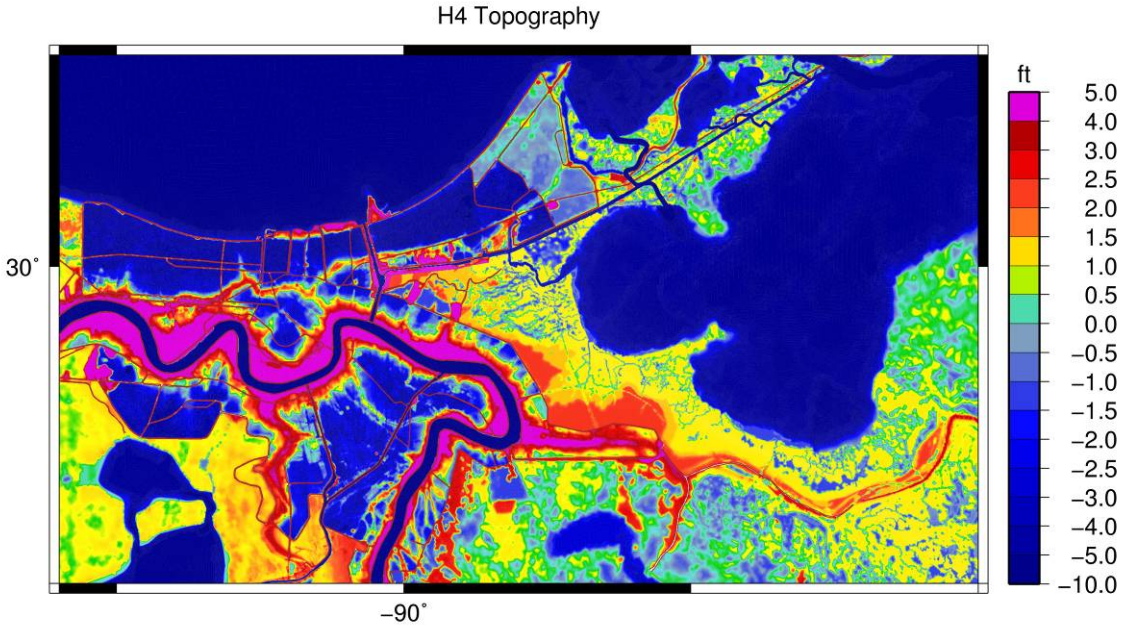


Figure 29: H4 model topography and bathymetry (ft relative to NAVD88 2004.65) in and around metropolitan New Orleans used in the *No MRGO with 1956 wetlands with relocated Chalmette Levee* simulation.

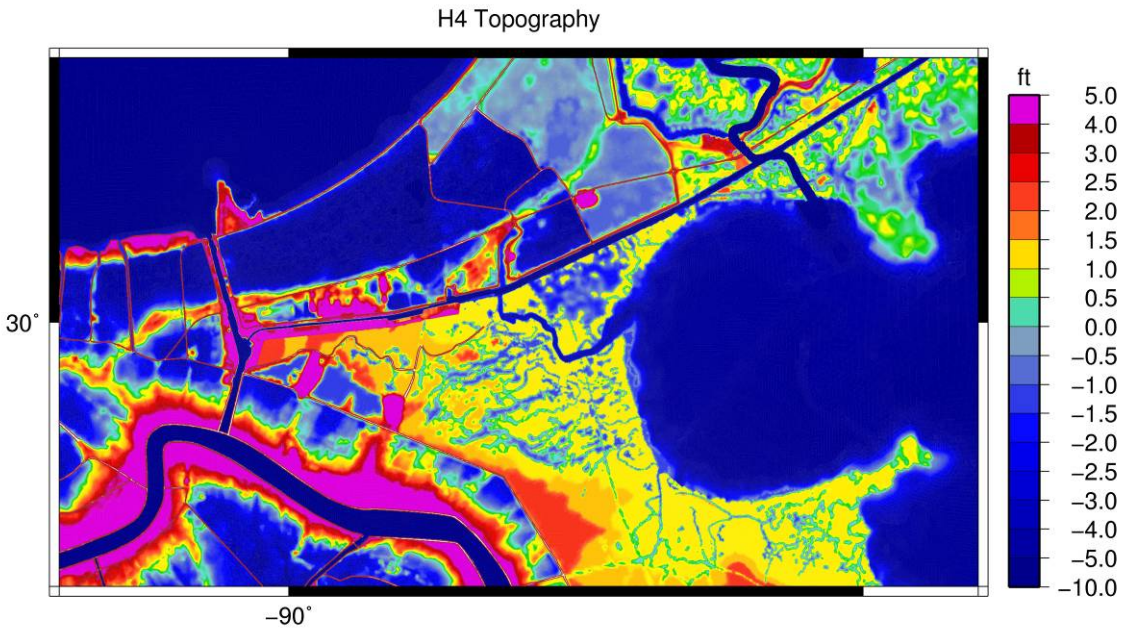


Figure 30: H4 model topography and bathymetry (ft relative to NAVD88 2004.65) in the vicinity of the IHNC to the Golden Triangle used in the *No MRGO with 1956 wetlands with relocated Chalmette Levee* simulation.

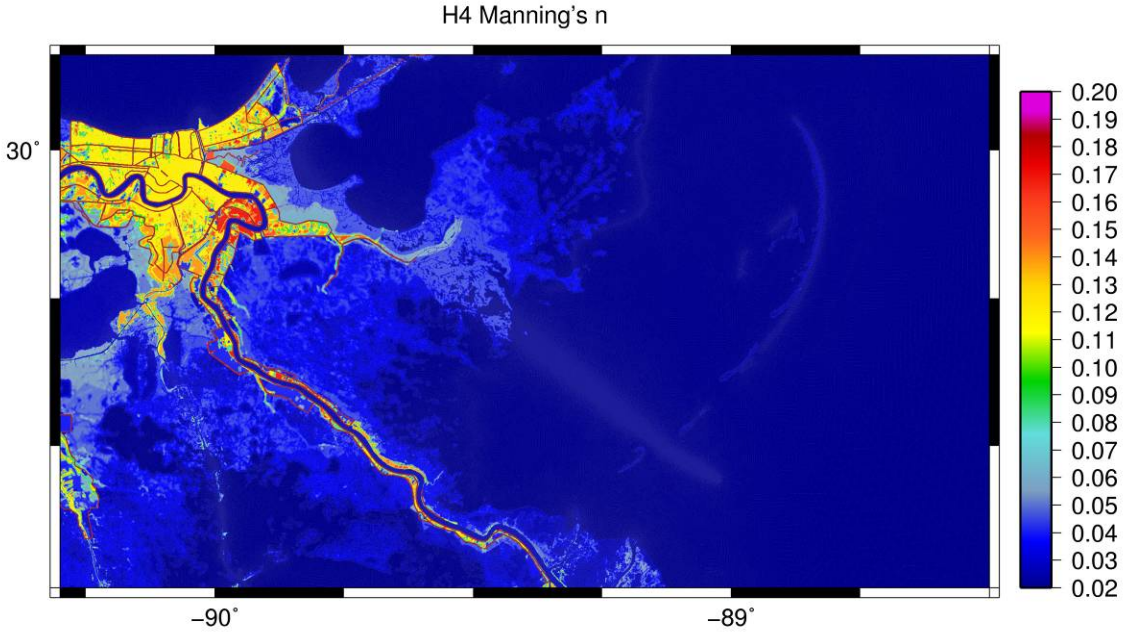


Figure 31: H4 model Manning n bottom friction values Southeastern Louisiana used in the *No MRGO with 1956 wetlands with relocated Chalmette Levee* simulation.

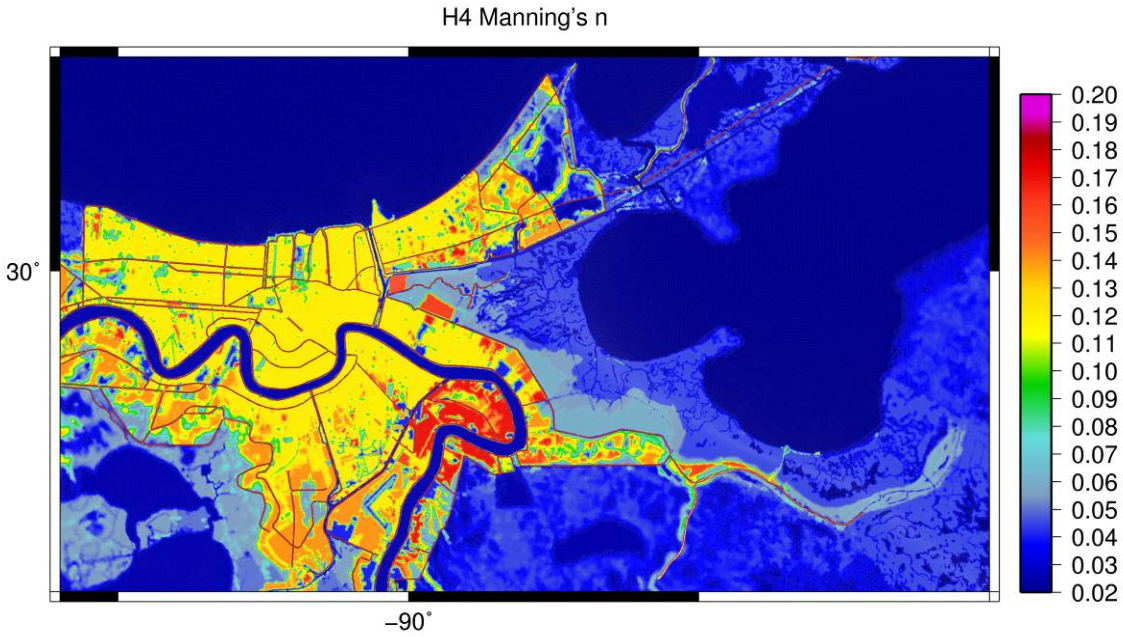


Figure 32: H4 model Manning n bottom friction values in and around metropolitan New Orleans used in the *No MRGO with 1956 wetlands with relocated Chalmette Levee* simulation.

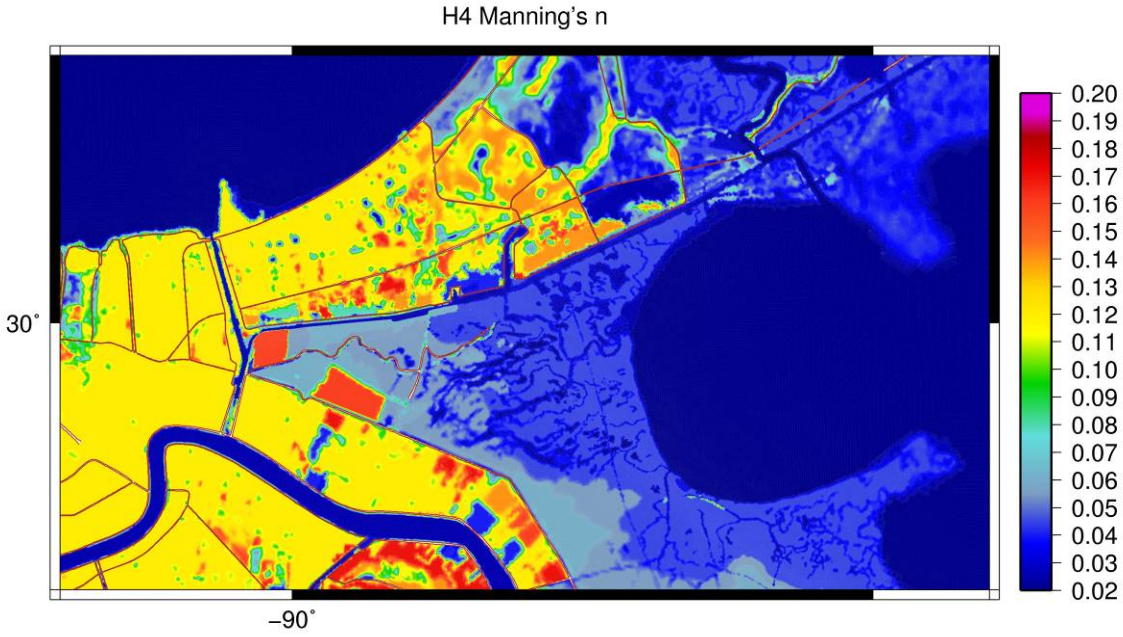


Figure 33: H4 model Manning n bottom friction values in the vicinity of the IHNC to the Golden Triangle used in the *No MRGO with 1956 wetlands with relocated Chalmette Levee* simulation.

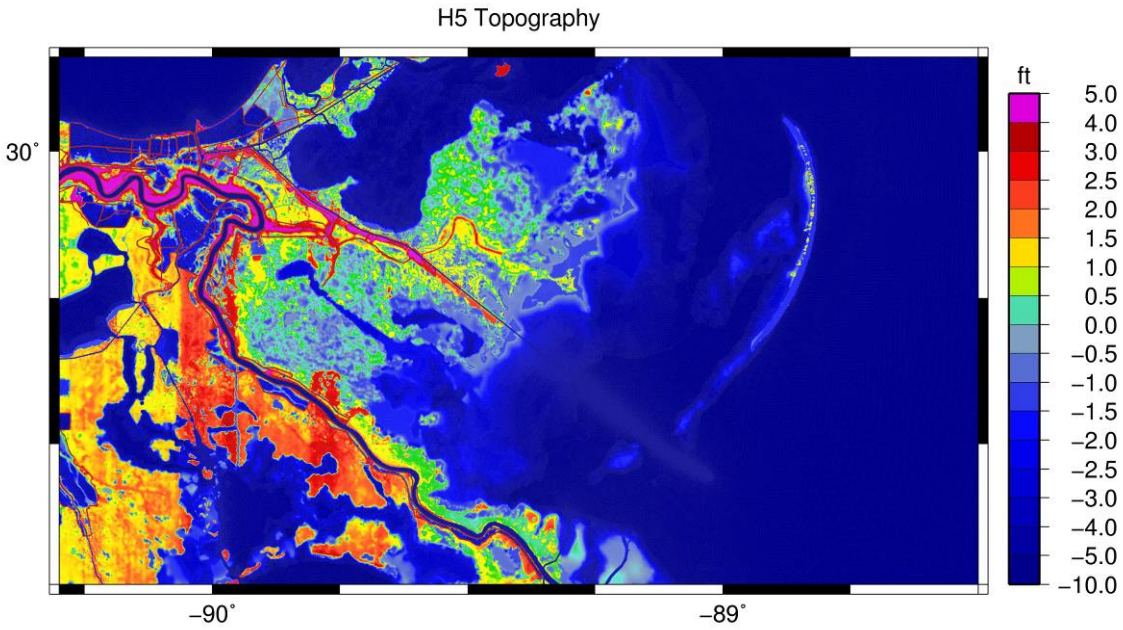


Figure 34: H5 model topography and bathymetry (ft relative to NAVD88 2004.65) in Southeastern Louisiana used in the MRGO as designed with 2005 wetlands simulation.

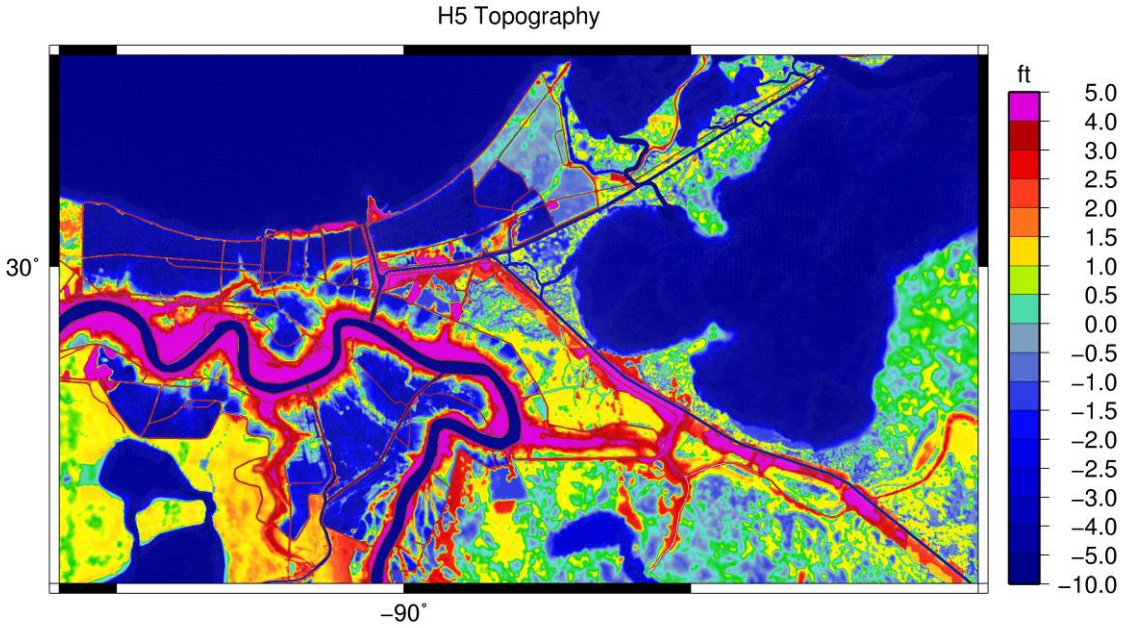


Figure 35: H5 model topography and bathymetry (ft relative to NAVD88 2004.65) in and around metropolitan New Orleans used in the *MRGO as designed with 2005 wetlands* simulation.

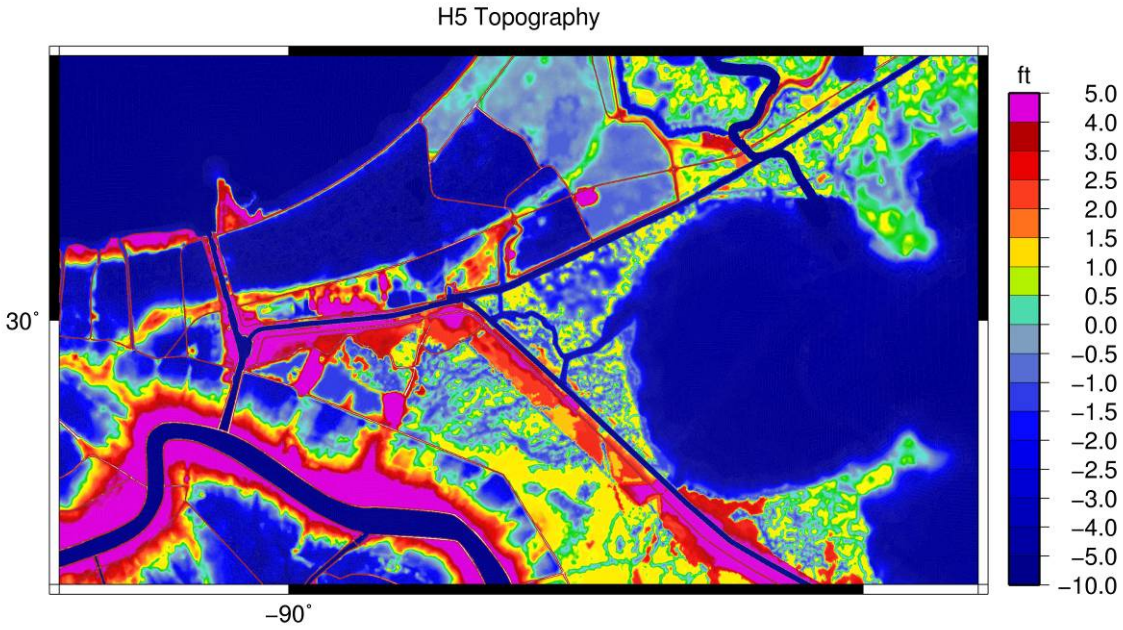


Figure 36: H5 model topography and bathymetry (ft relative to NAVD88 2004.65) in the vicinity of the IHNC to the Golden Triangle used in the *MRGO as designed with 2005 wetlands* simulation.

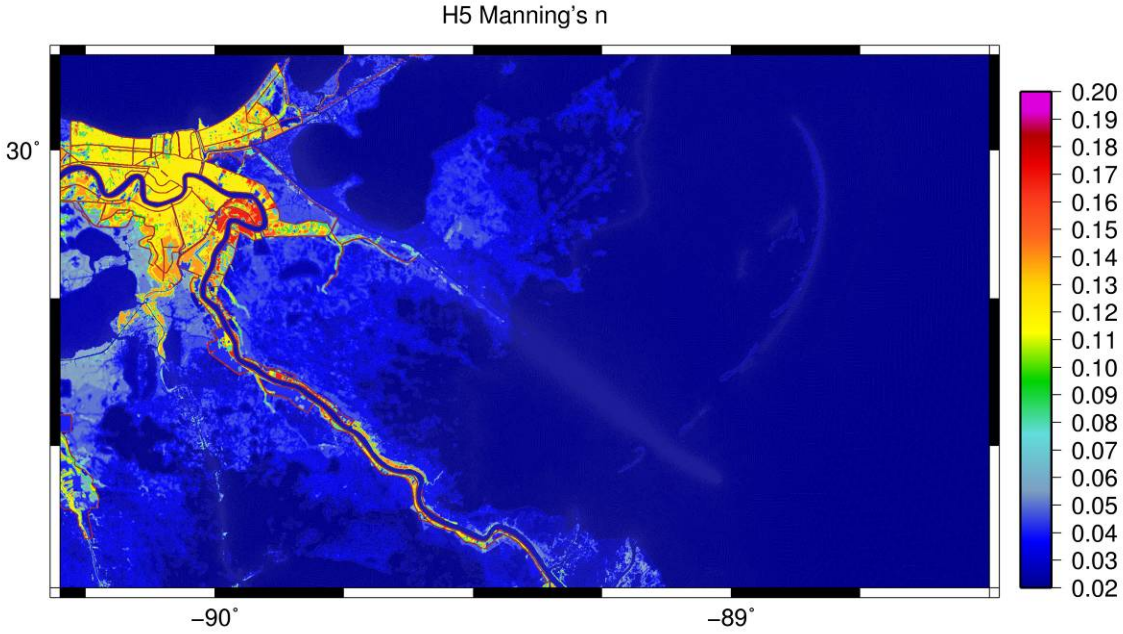


Figure 37: H5 model Manning n bottom friction values Southeastern Louisiana used in the *MRGO as designed with 2005 wetlands* simulation.

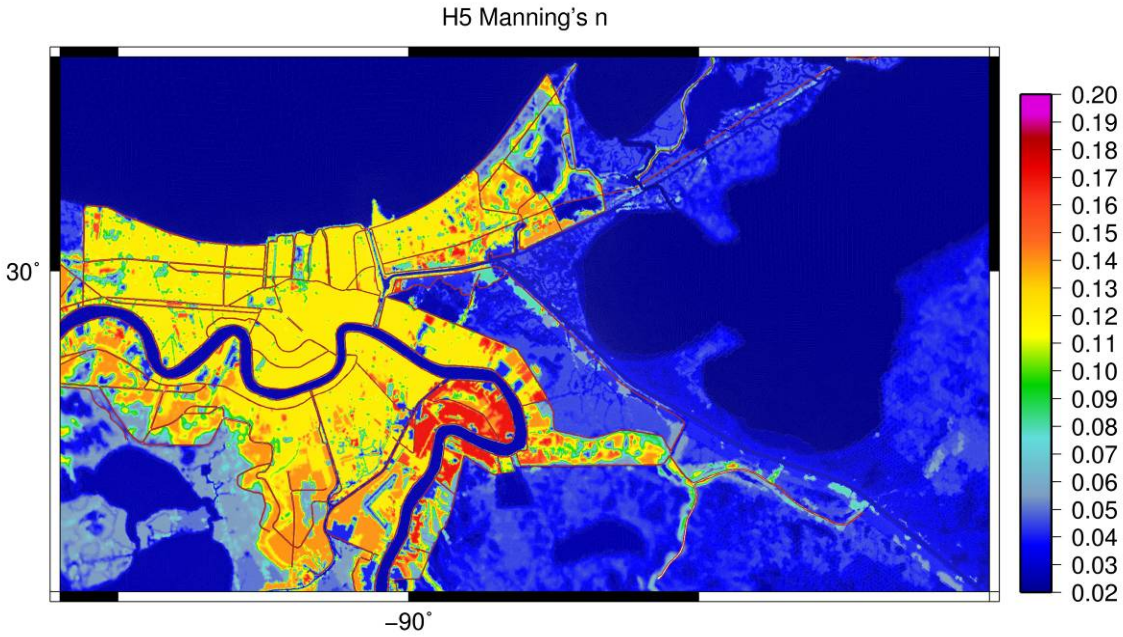


Figure 38: H5 model Manning n bottom friction values in and around metropolitan New Orleans used in the *MRGO as designed with 2005 wetlands* simulation.

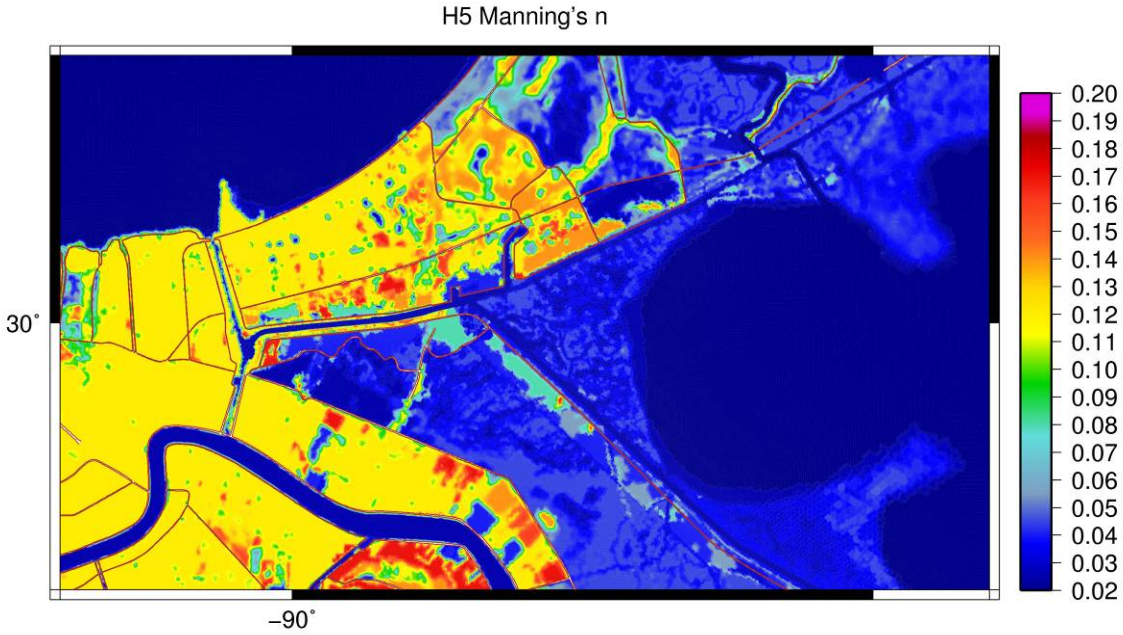


Figure 39: H5 model Manning n bottom friction values in the vicinity of the IHNC to the Golden Triangle used in the *MRGO as designed with 2005 wetlands* simulation.

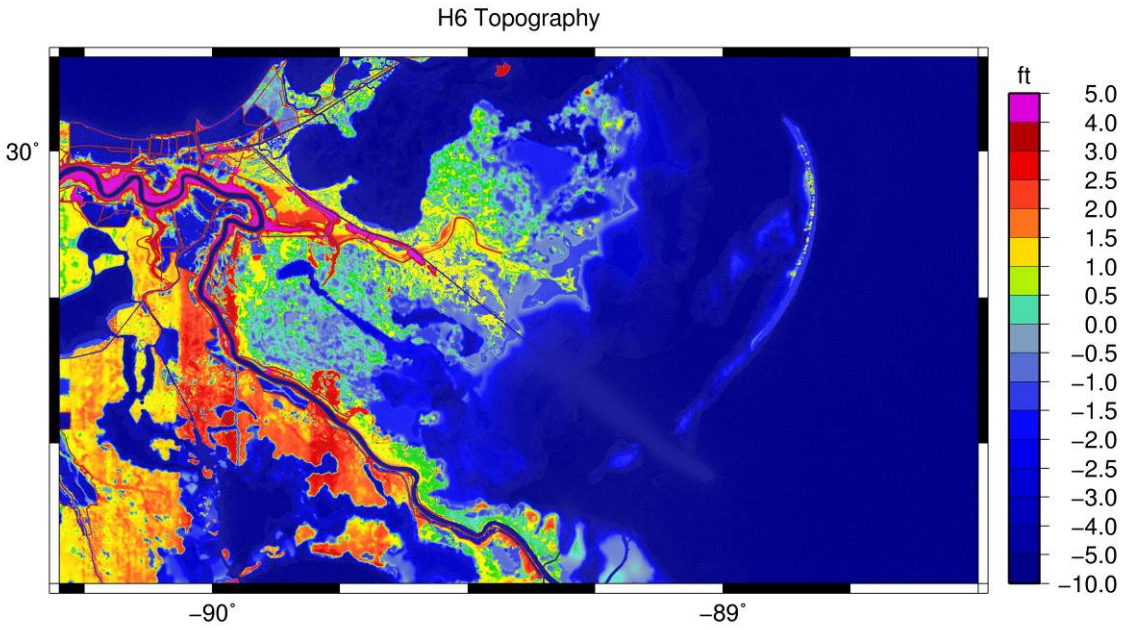


Figure 40: H6 model topography and bathymetry (ft relative to NAVD88 2004.65) in Southeastern Louisiana used in the *MRGO as designed with 1956 wetlands* simulation.

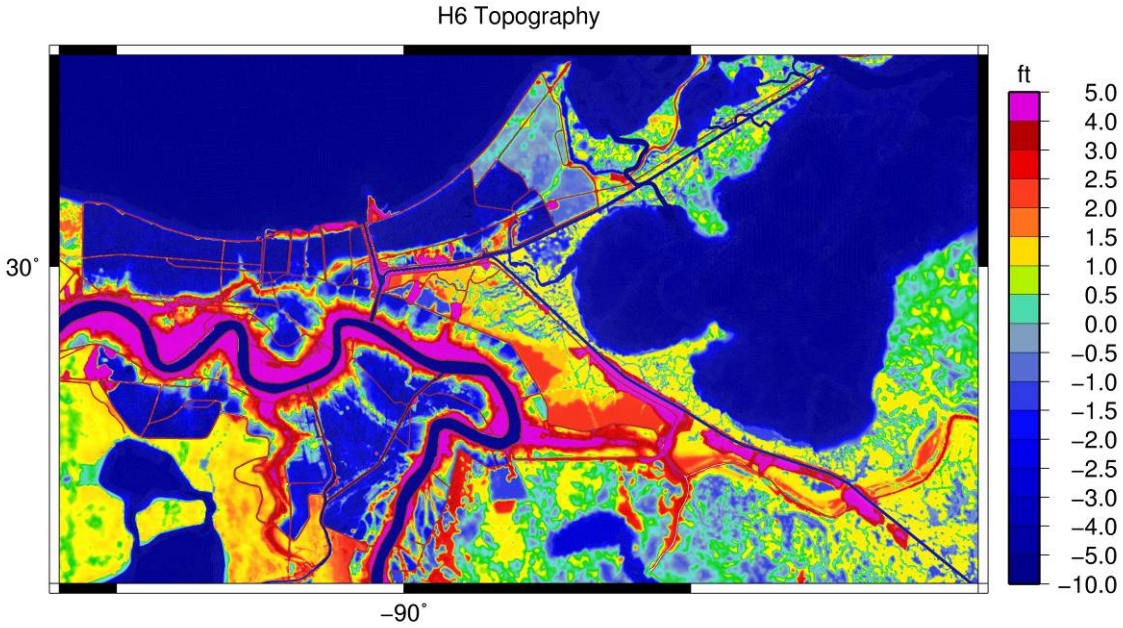


Figure 41: H6 model topography and bathymetry (ft relative to NAVD88 2004.65) in and around metropolitan New Orleans used in the *MRGO as designed with 1956 wetlands* simulation.

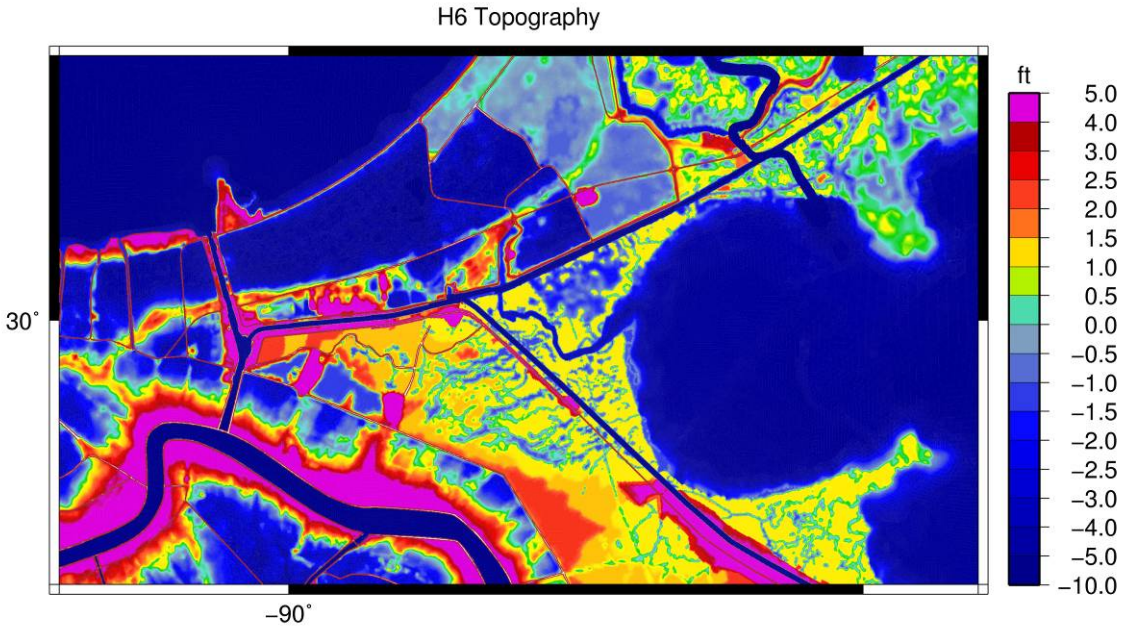


Figure 42: H6 model topography and bathymetry (ft relative to NAVD88 2004.65) in the vicinity of the IHNC to the Golden Triangle used in the *MRGO as designed with 1956 wetlands* simulation.

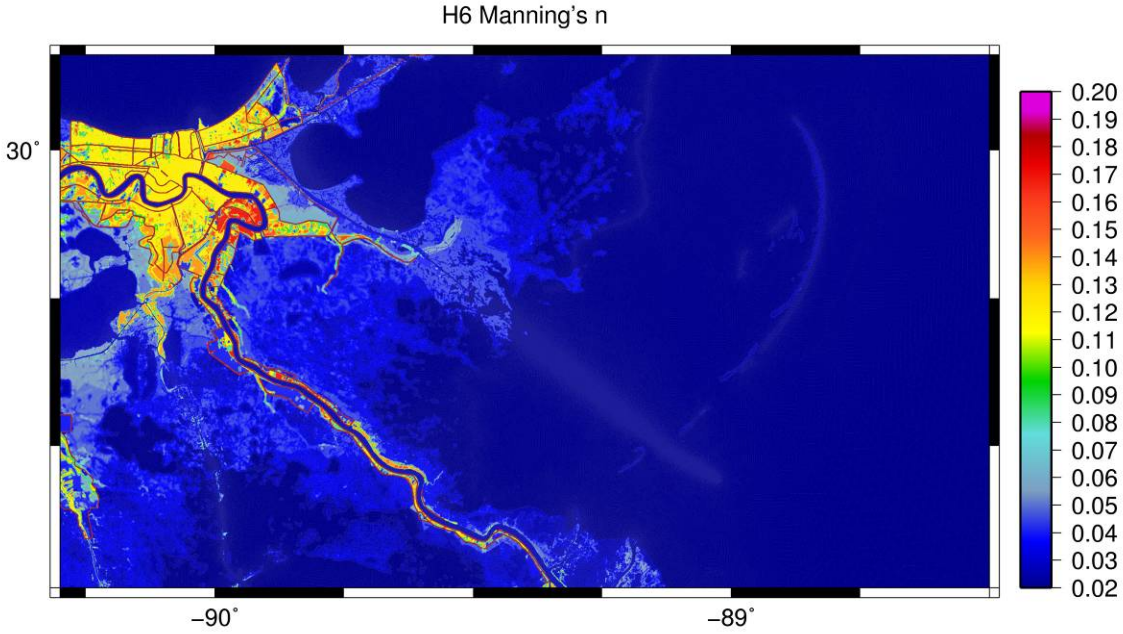


Figure 43: H6 model Manning n bottom friction values Southeastern Louisiana used in the *MRGO as designed with 1956 wetlands* simulation.

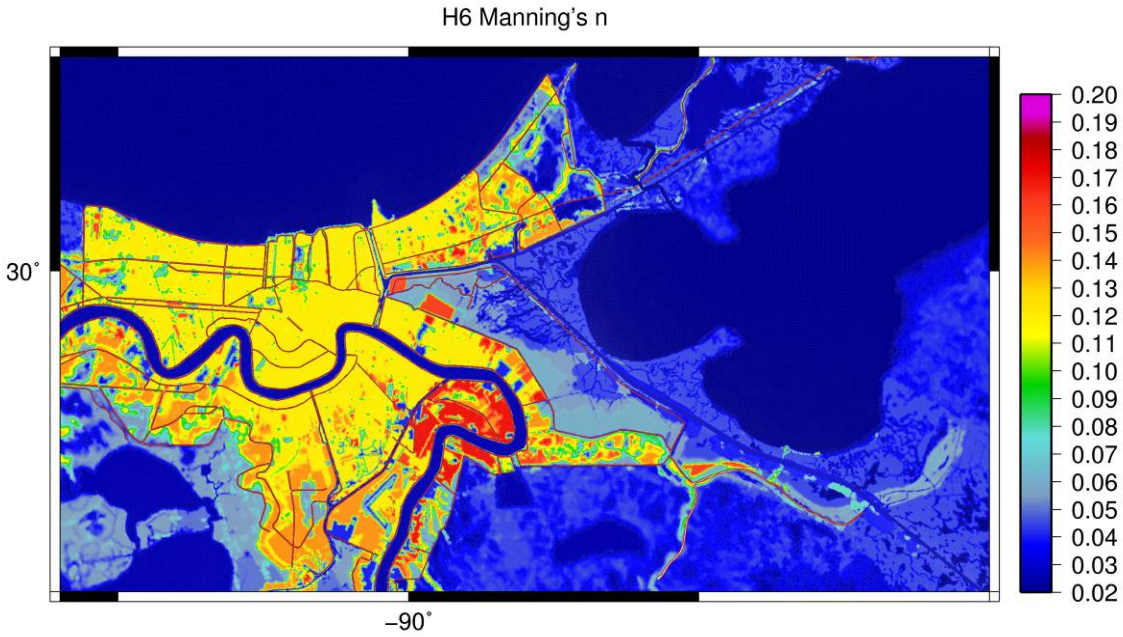


Figure 44: H6 model Manning n bottom friction values in and around metropolitan New Orleans used in the *MRGO as designed with 1956 wetlands* simulation.

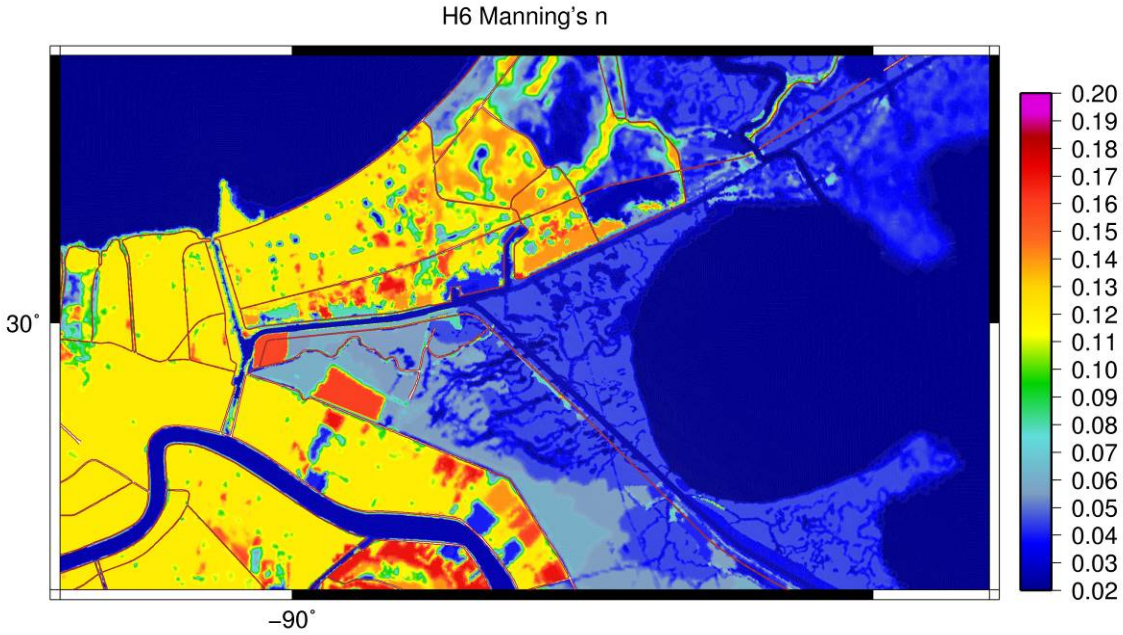


Figure 45: H6 model Manning n bottom friction values in the vicinity of the IHNC to the Golden Triangle used in the *MRGO as designed with 1956 wetlands* simulation.

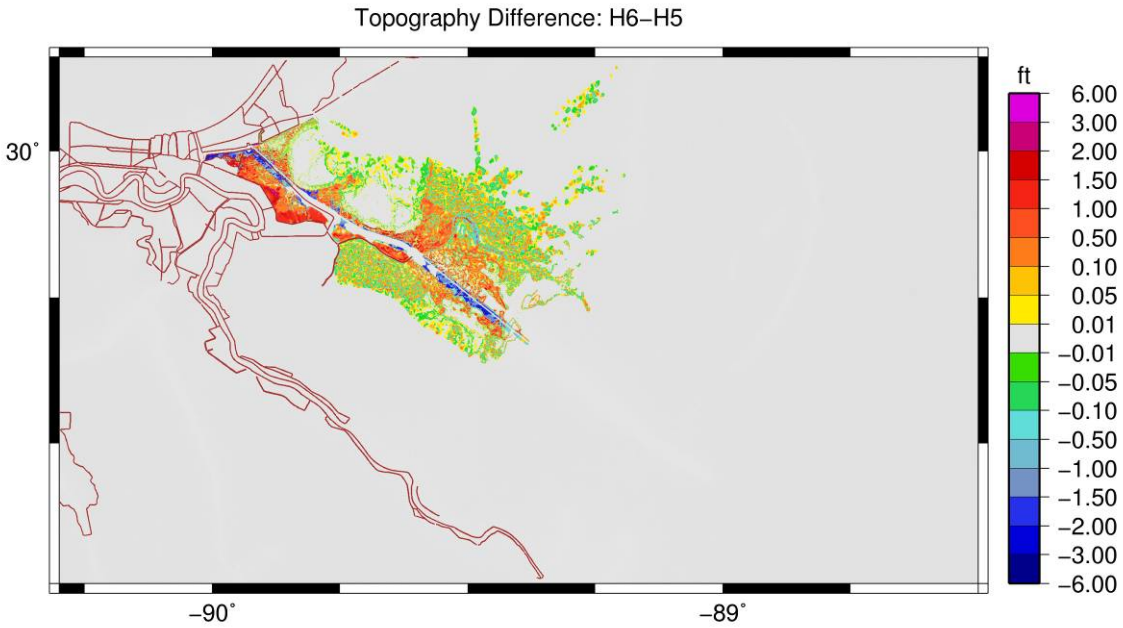


Figure 46: H6 to H5 model differences in topography and bathymetry (ft) in Southeastern Louisiana. Warm colors indicate that H3 is higher while cool colors indicate that H2 is higher.

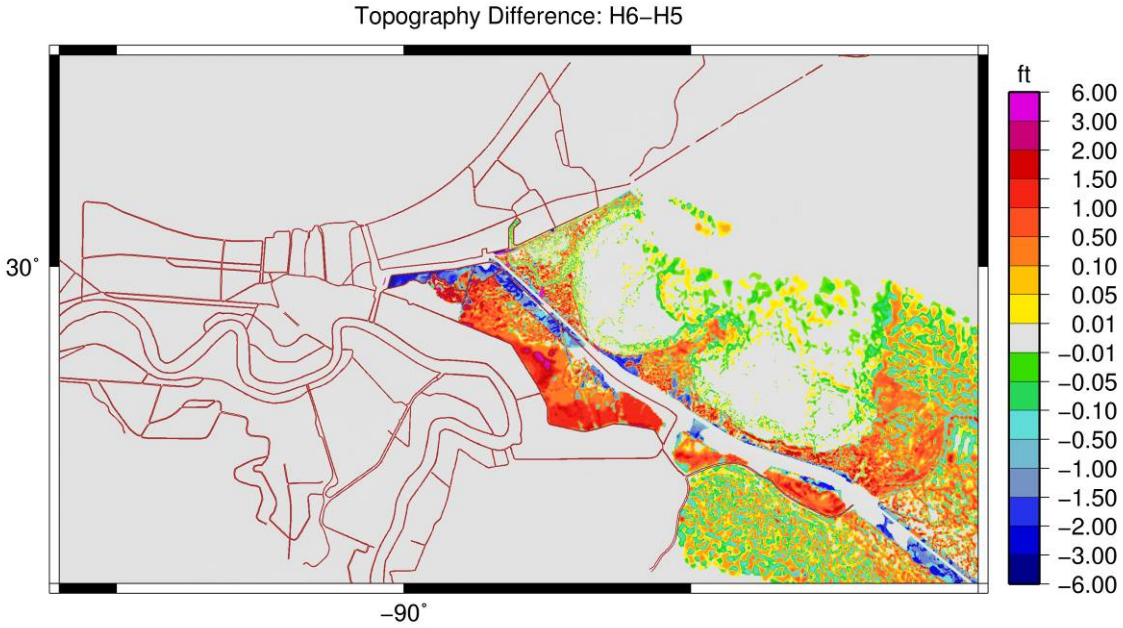


Figure 47: H6 to H5 model differences in topography (ft) in and around metropolitan New Orleans. Warm colors indicate that H3 is higher while cool colors indicate that H2 is higher.

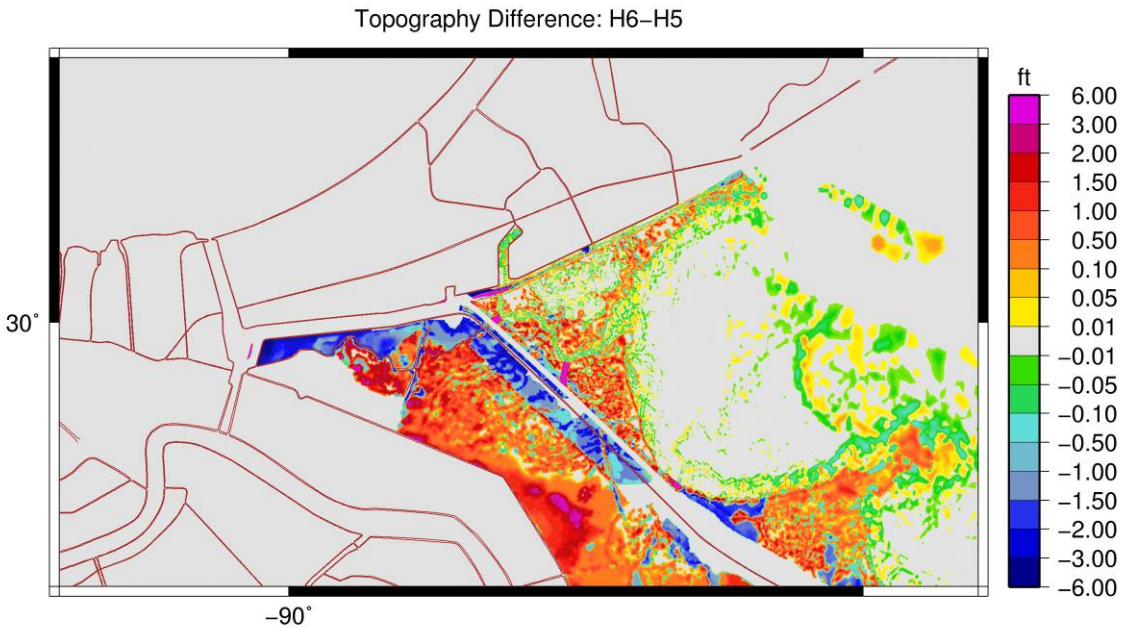


Figure 48: H6 to H5 model differences in topography (ft) relative in the vicinity of the IHNC to the Golden Triangle. Warm colors indicate that H3 is higher while cool colors indicate that H2 is higher.

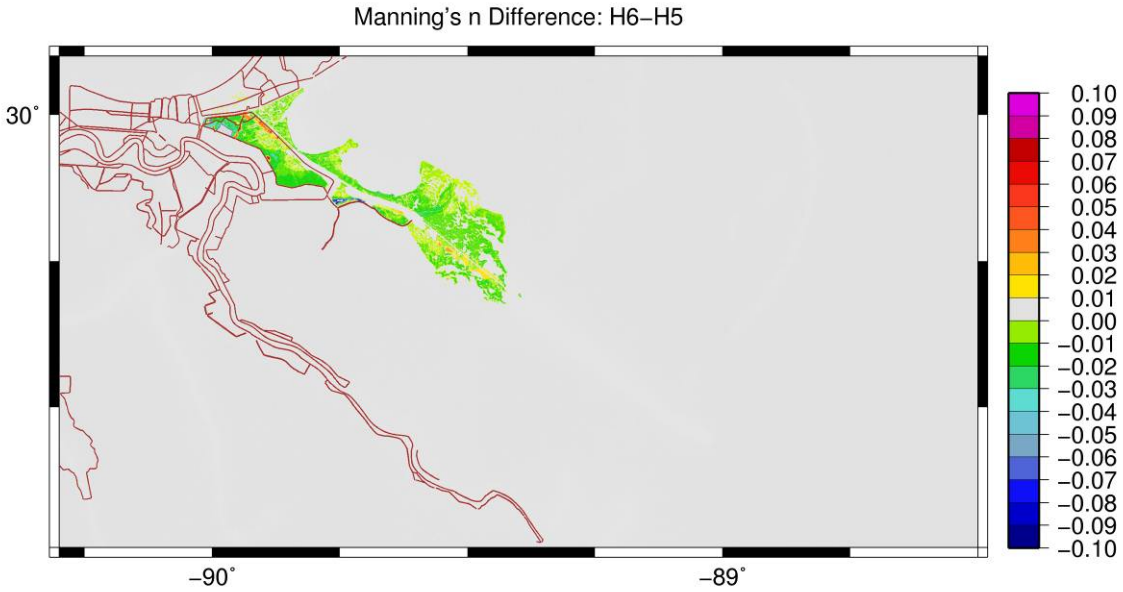


Figure 49: H6 to H5 model differences in Manning n bottom friction values in Southeastern Louisiana. Warm colors indicate that H2 has higher assigned Manning n values while cool colors indicate that H3 has higher assigned Manning n values.

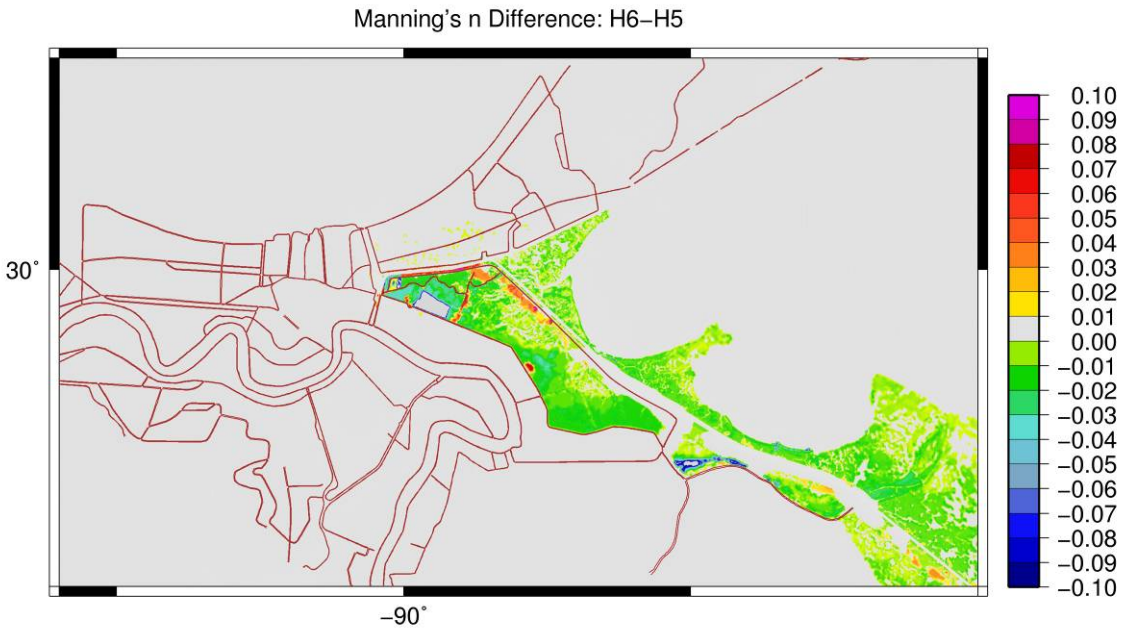


Figure 50: H6 to H5 model differences in Manning n bottom friction values in and around metropolitan New Orleans. Warm colors indicate that H2 has higher assigned Manning n values while cool colors indicate that H3 has higher assigned Manning n values.

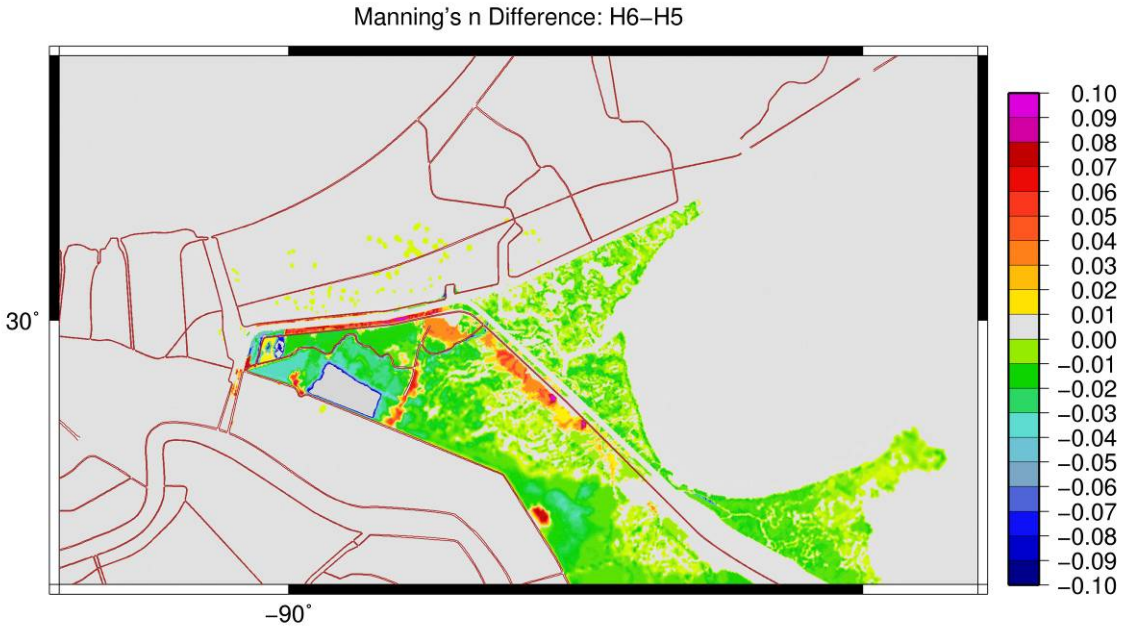


Figure 51: H6 to H5 model differences in Manning n bottom friction values in the vicinity of the IHNC to the Golden Triangle. Warm colors indicate that H2 has higher assigned Manning n values while cool colors indicate that H3 has higher assigned Manning n values.

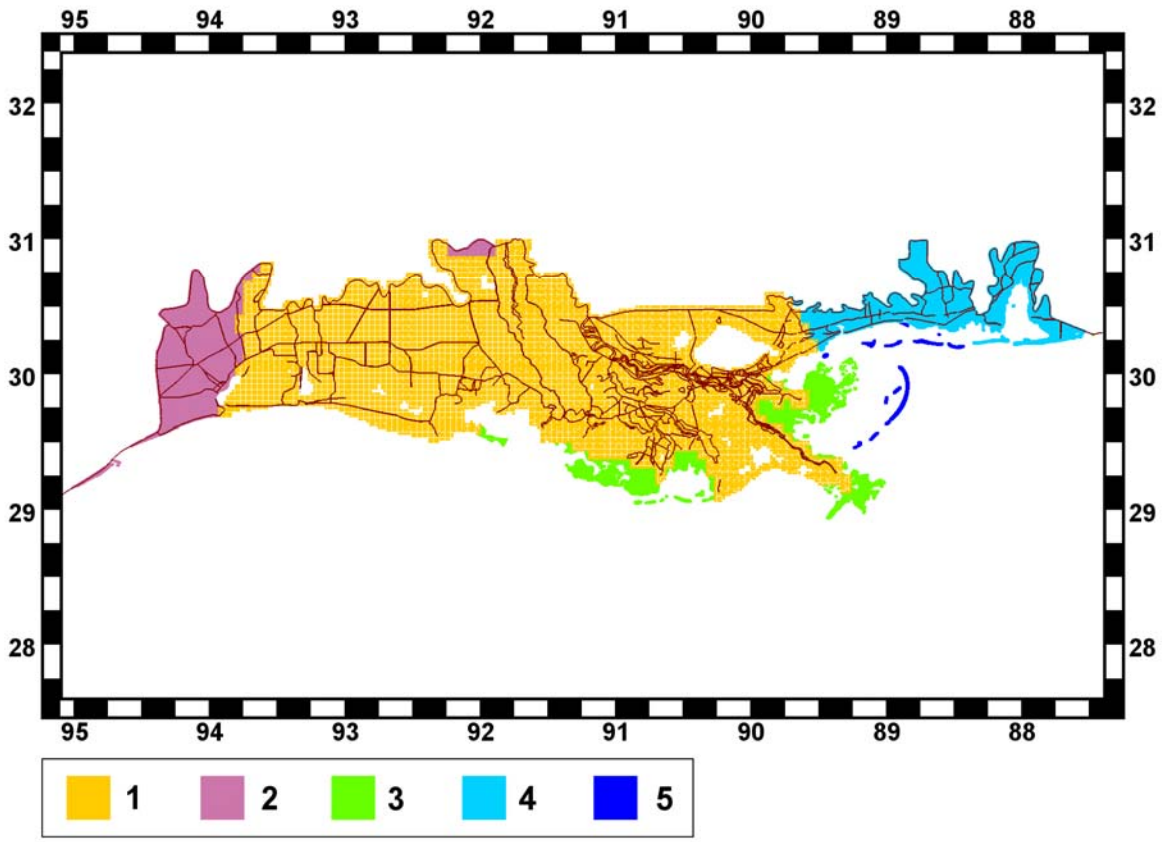


Figure 52: Topographic data source distribution. Different colors indicate different sources. **Color 1** = Atlas LIDAR DEM's, 5 m resolution (http://atlus.lsu.edu/LIDAR). **Color 2** = USGS National Elevation Dataset, 30 m resolution (http://gisdata.usgs.net/ned/). **Color 3** = USGS GAP data (http://gapanalysis.nbii.gov/). **Color 4** = Topography received from "HMTAP TASK ORDER 18, MISSISSIPPI COASTAL ANALYSIS PROJECT, GEOSPATIAL TECHNOLOGY TASK PROJECT (TASK 3)," December 5, 2006. **Color 5** = Various topographic sources (see Figure 53).

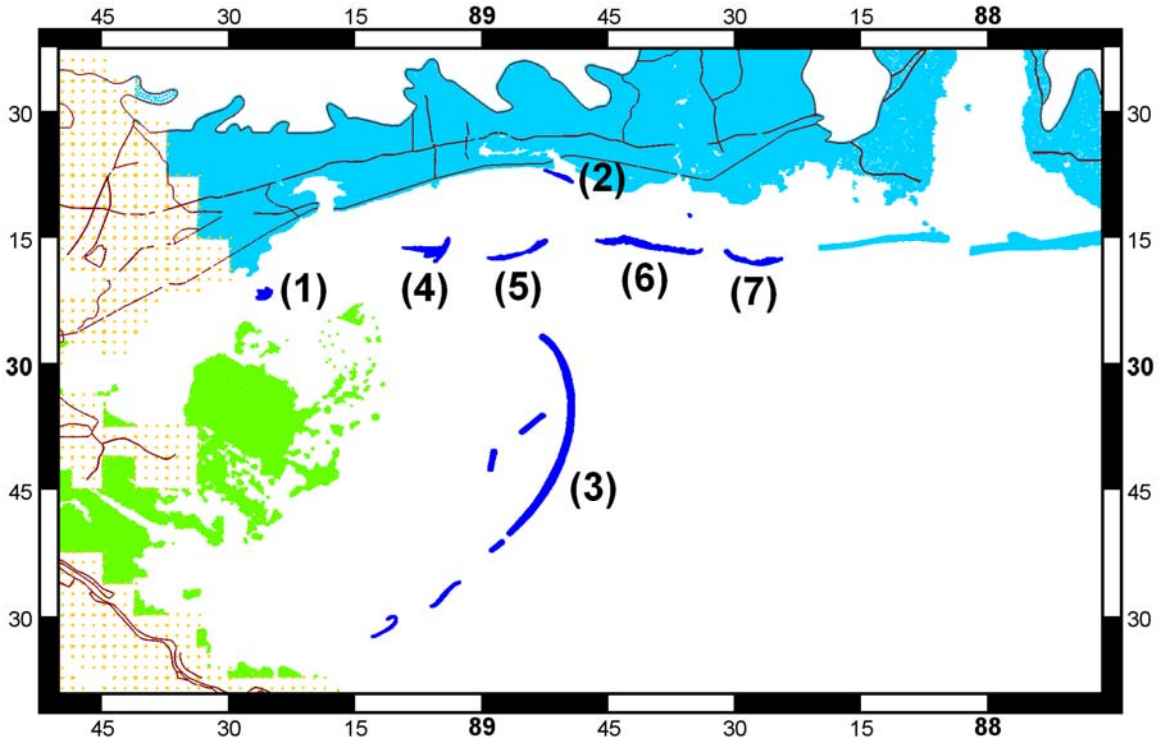


Figure 53: Topographic data sources for barrier islands on LA/MS coasts. **(1)** Half Moon Island and **(2)** Deer Island – MARIS DEM's, 10 m resolution (http://www.maris.state.ms.us/HTM/DownloadData/DEM.html). **(3)** Chandeleur Islands – USGS Post-Katrina survey. **(4)** Cat Island, **(5)** Ship Island, **(6)** Horn Island, and **(7)** Petit Bois Island – Pre-Katrina USGS National Elevation Dataset, 30 m resolution (http://gisdata.usgs.net/ned/).

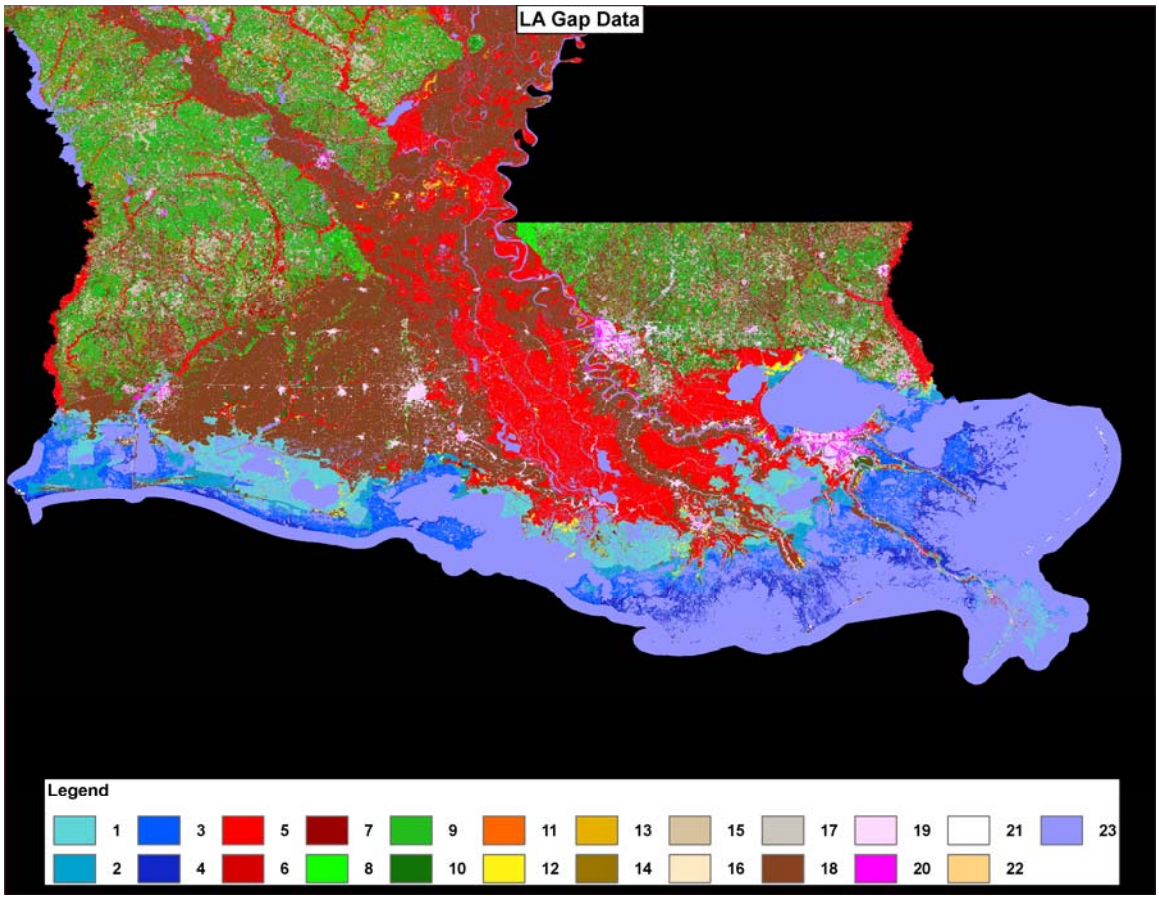


Figure 54: Louisiana Gap Analysis Program (LA-GAP) data (Hartley et al., 2000).

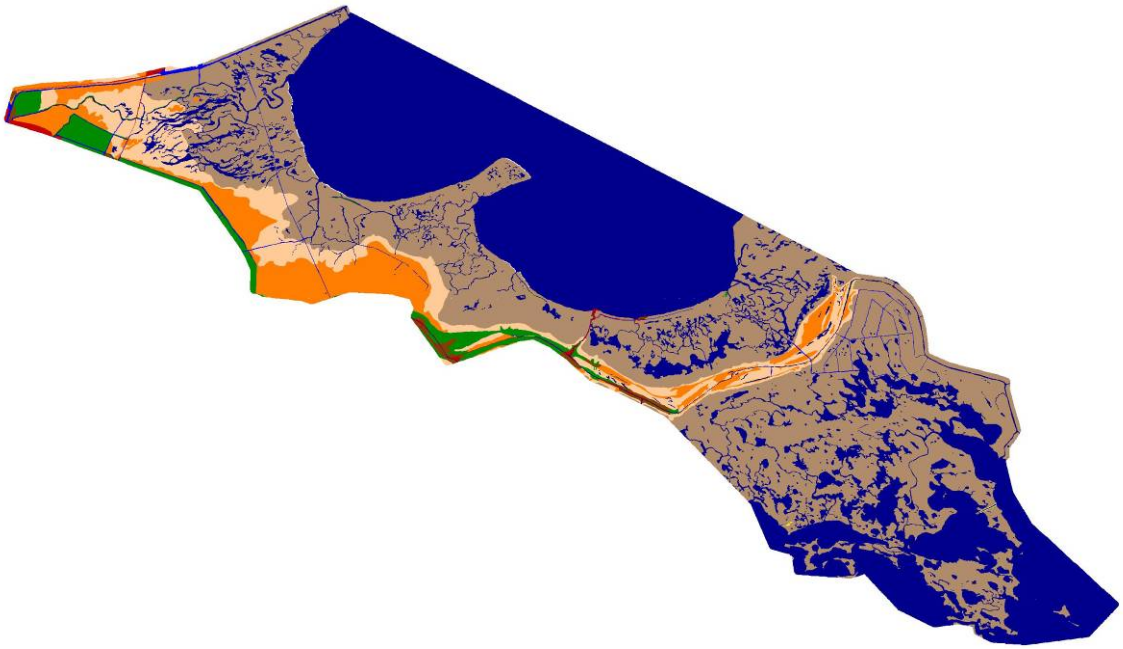


Figure 55: Land use within the MRGO region of influence in 1956 (Barras, 2008). Brown represents non-fresh marsh; tan represents fresh marsh; orange represents swamp; dark brown represents agricultural/pasture; red represents developed areas.

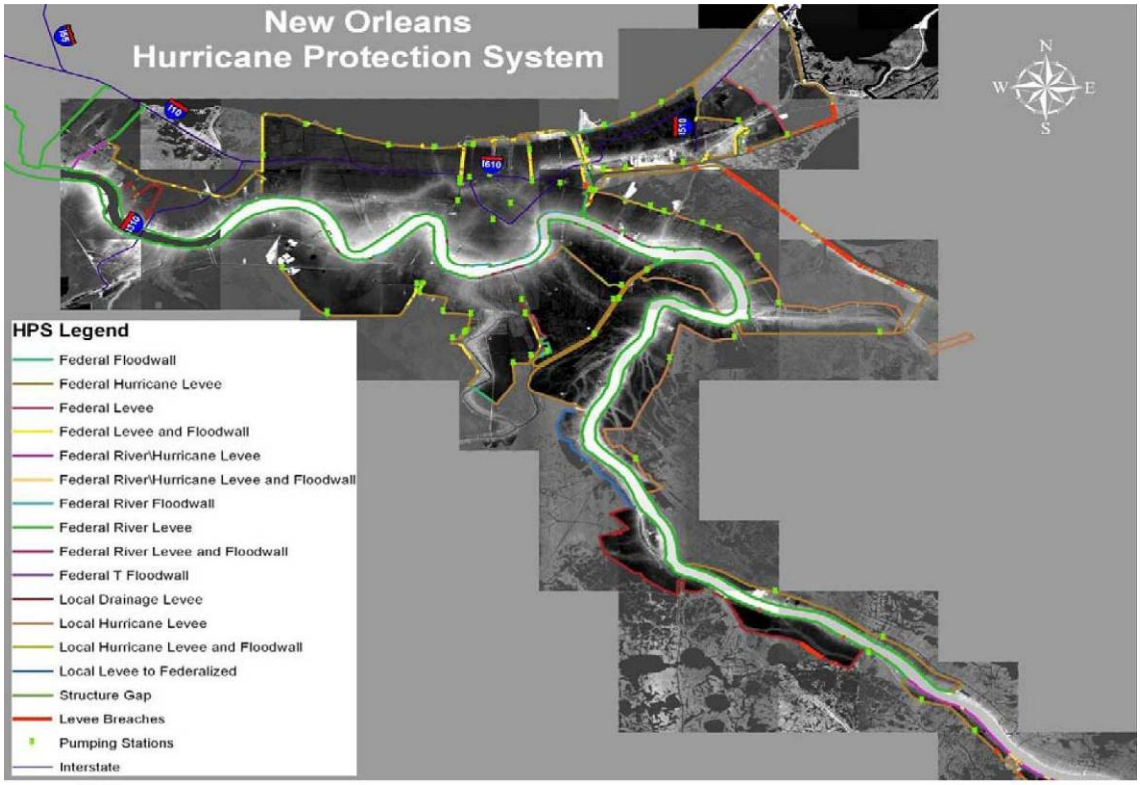


Figure 56: Inventory of existing levees (U.S. Army Corps of Engineers, 2007c).

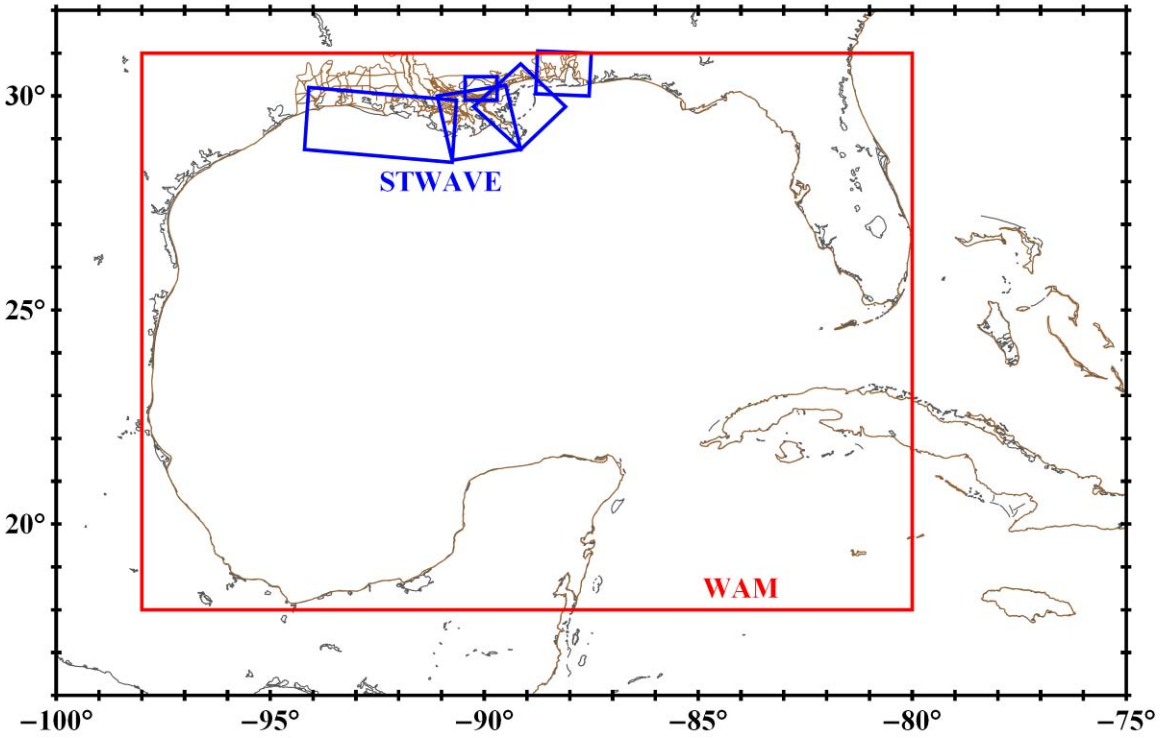


Figure 57: WAM model domain shown in red and nested STWAVE model domains shown in blue.

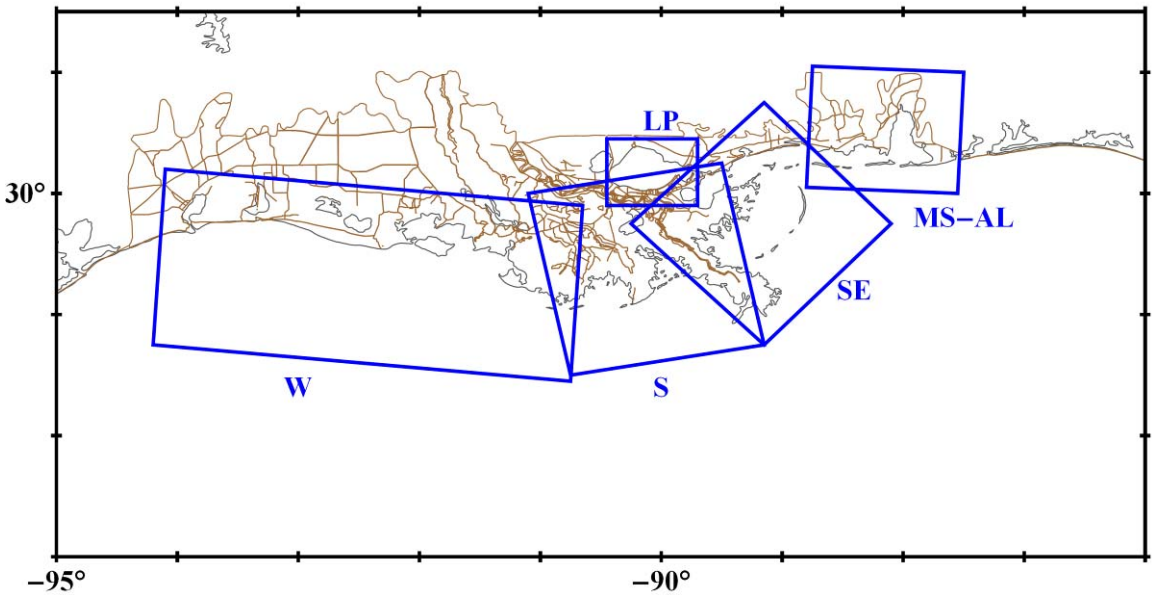


Figure 58: STWAVE model domains across Southern Louisiana and Mississippi. This Study applied the S, SE and MS-AL STWAVE domains.

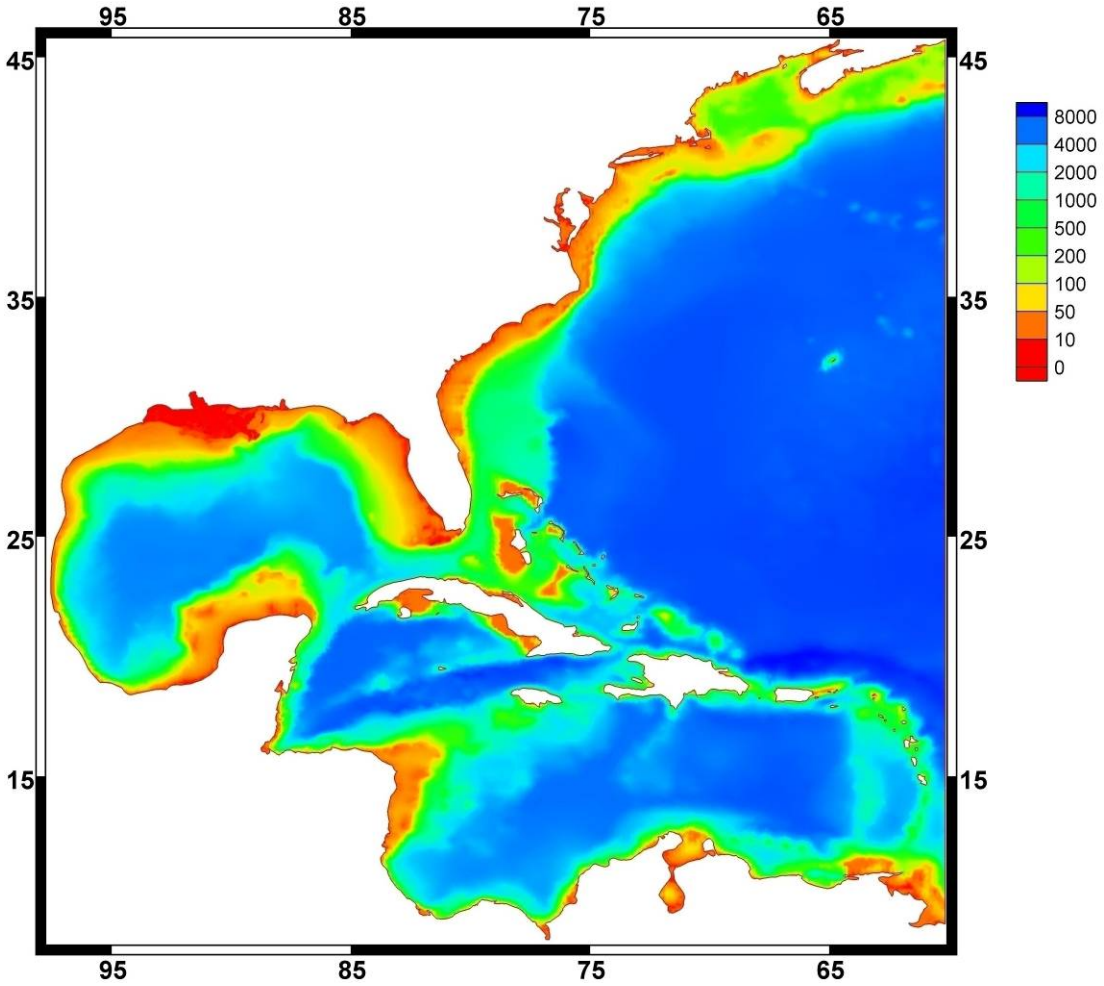


Figure 59: ADCIRC SL15 with bathymetry (m) for the total domain.

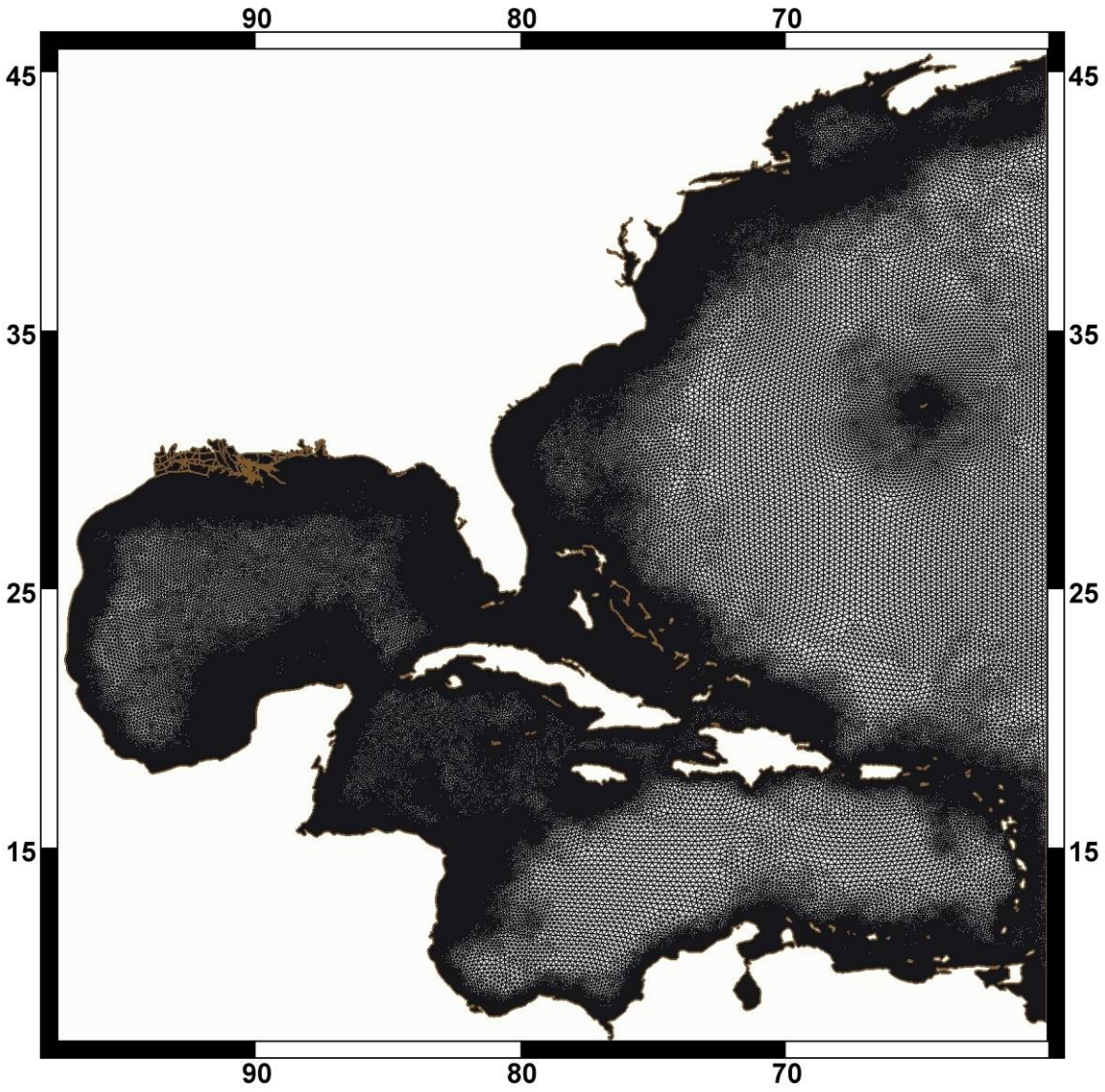


Figure 60: The unstructured ADCIRC SL15 grid.

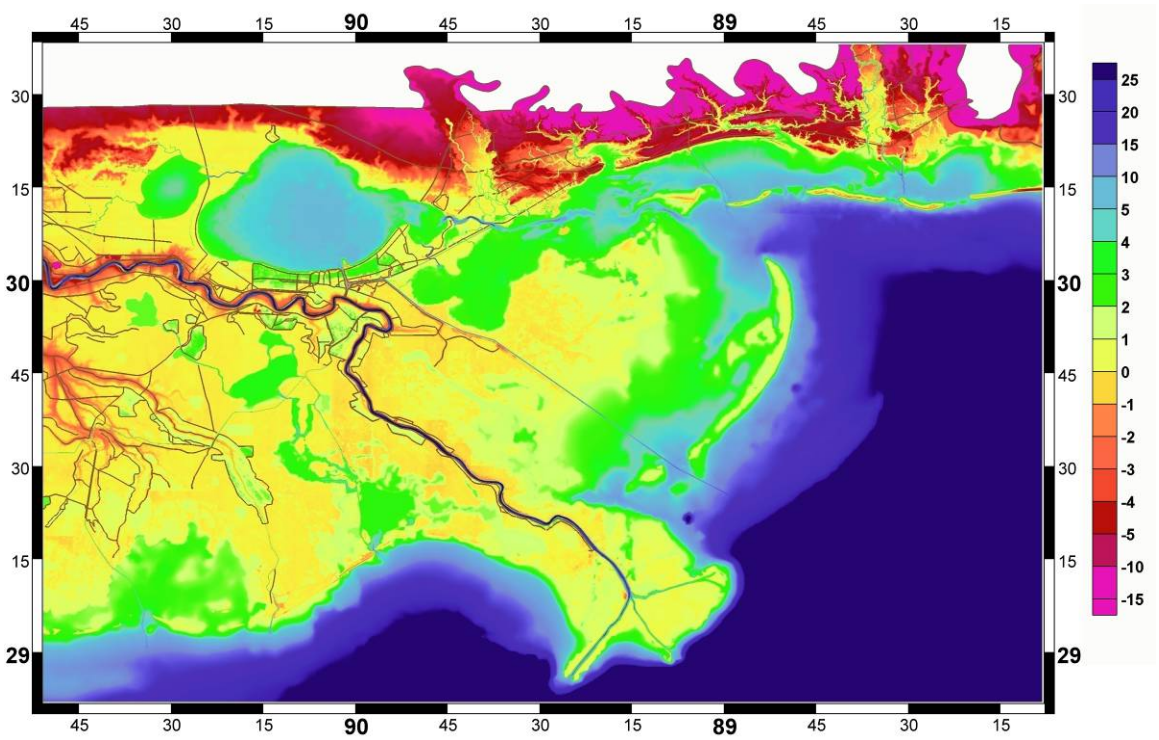


Figure 61: A detail of the SL15 domain with bathymetry and topography (m) across Southeastern Louisiana with raised features, as levees, railroads, highways in brown.

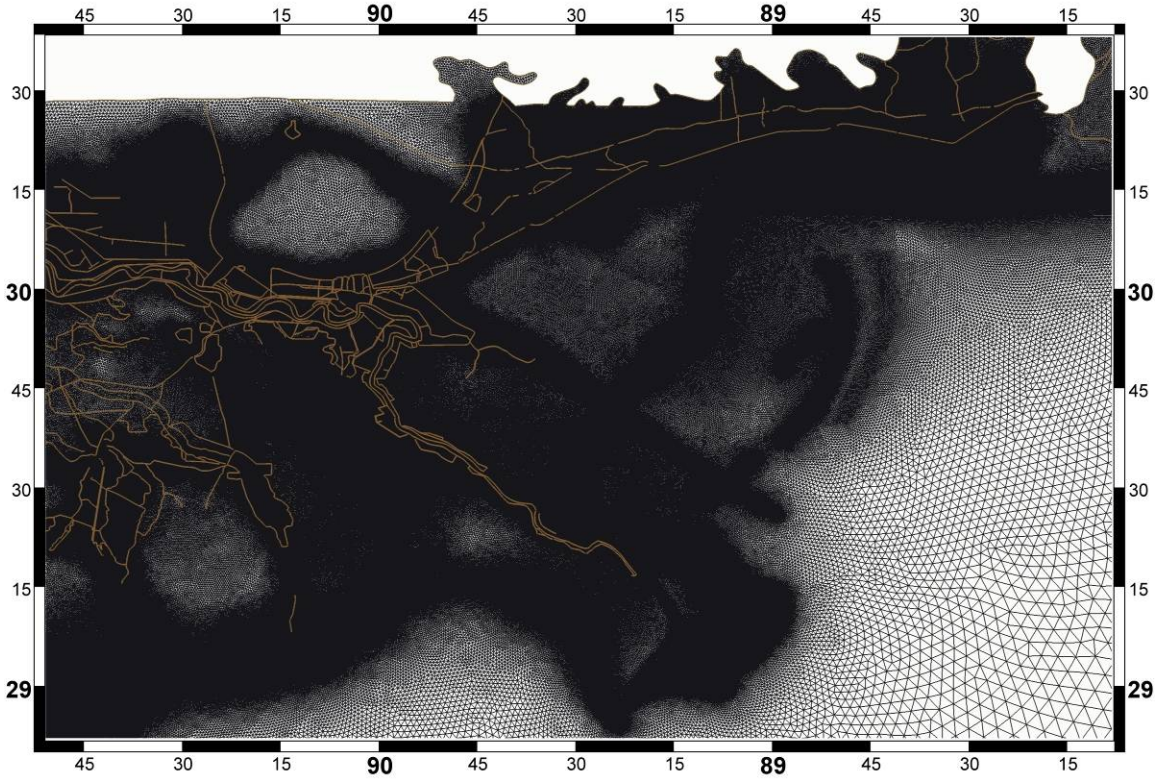


Figure 62: A detail of the unstructured ADCIRC SL15 grid in Southeastern Louisiana with raised features, as levees, railroads, highways shown in brown.

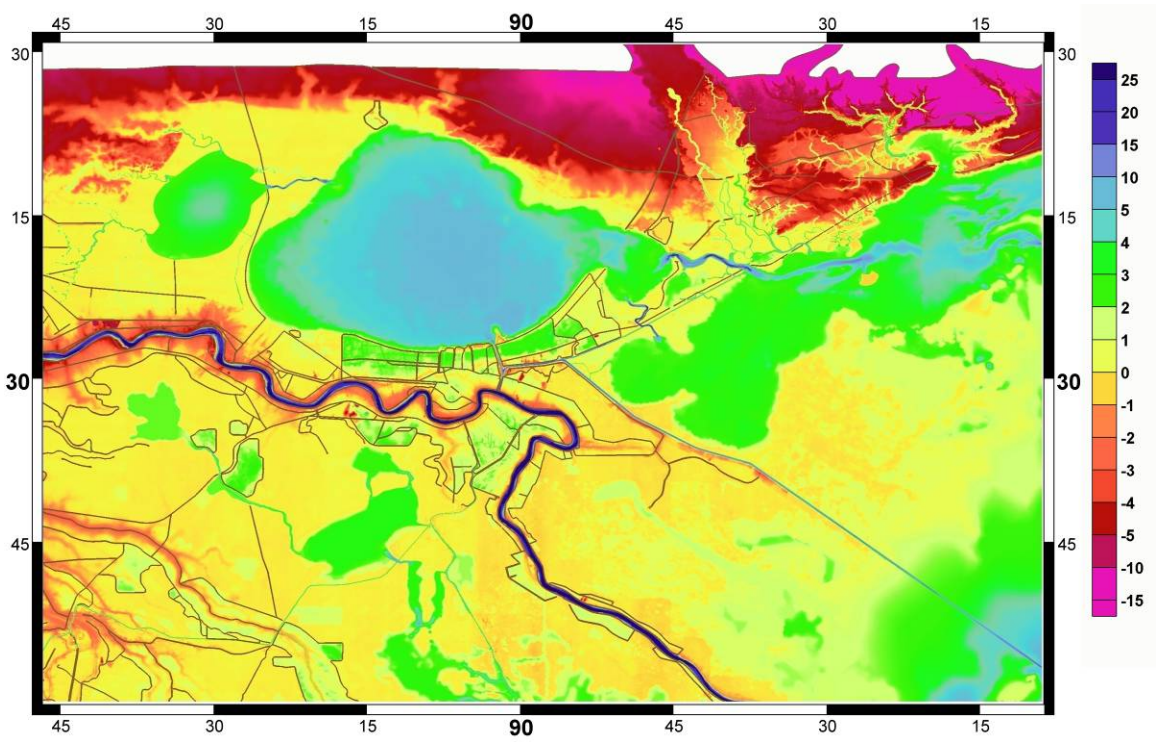


Figure 63: A detail of the SL15 domain with bathymetry and topography (m) across the area around New Orleans and Lake Pontchartrain with raised features shown in brown.

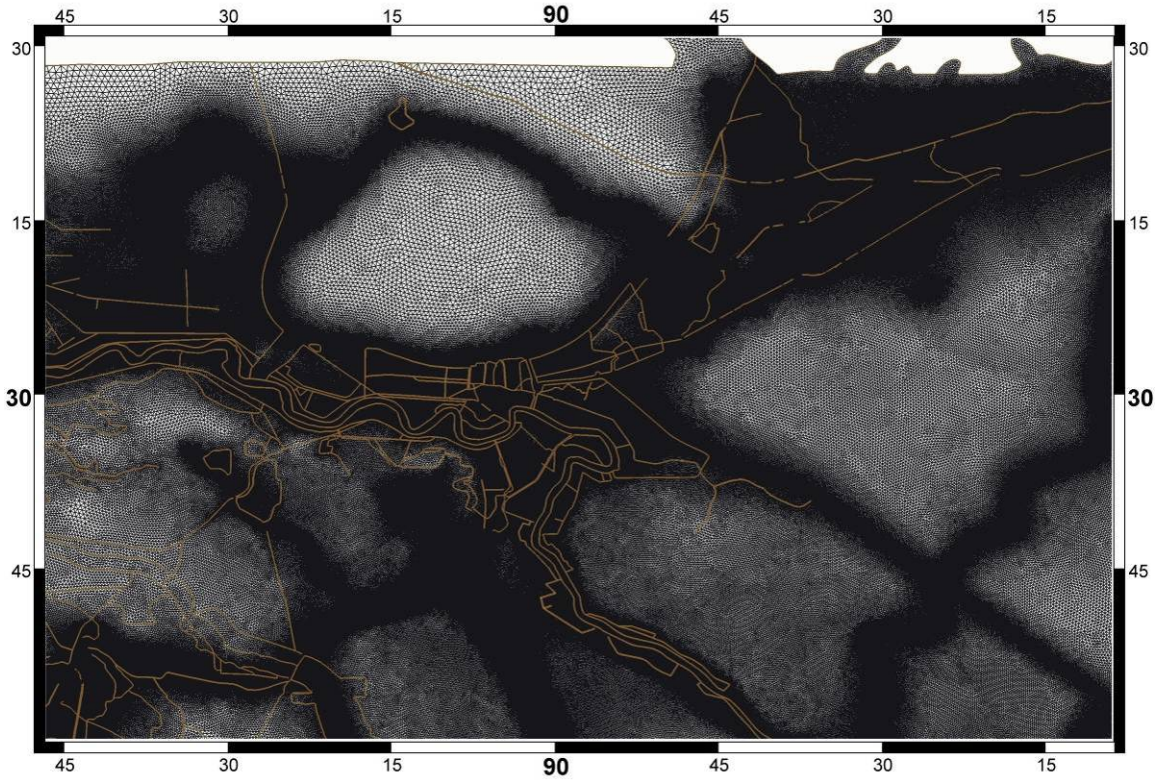


Figure 64: A detail of the unstructured ADCIRC SL15 grid the area around New Orleans and Lake Pontchartrain with raised features (as levees, railroads, highways) in brown.

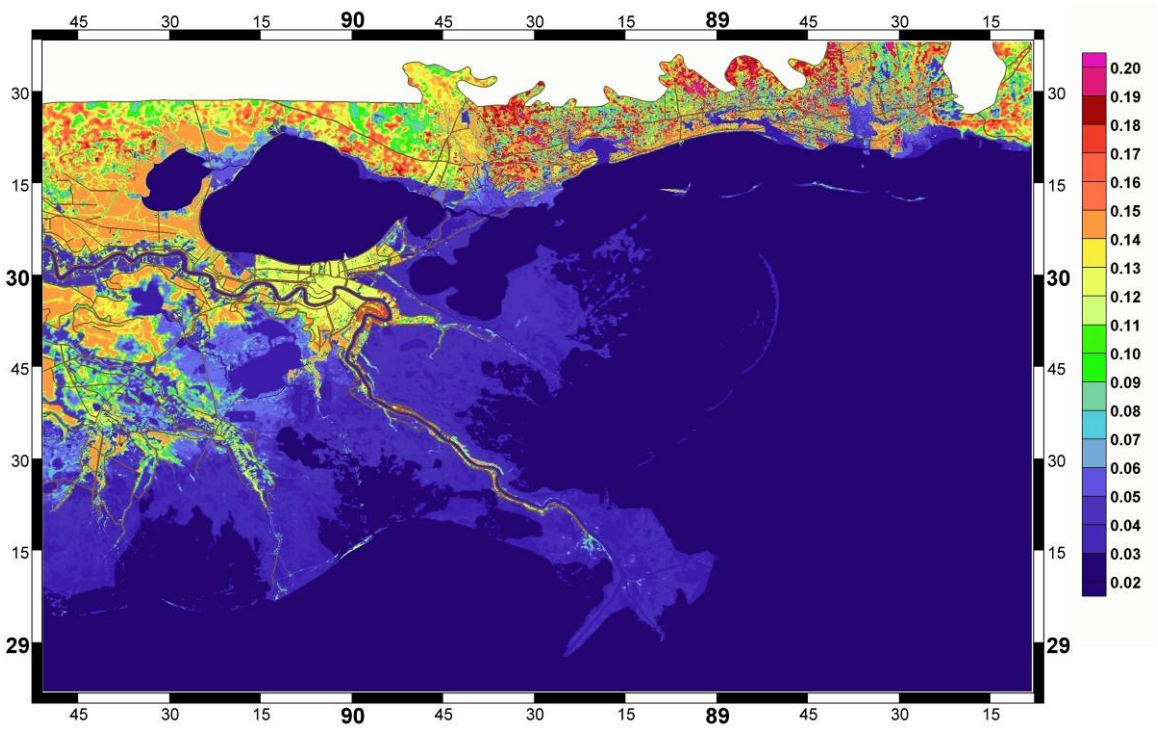


Figure 65: A detail of the bottom friction (Manning friction coefficients) for Southeastern Louisiana.

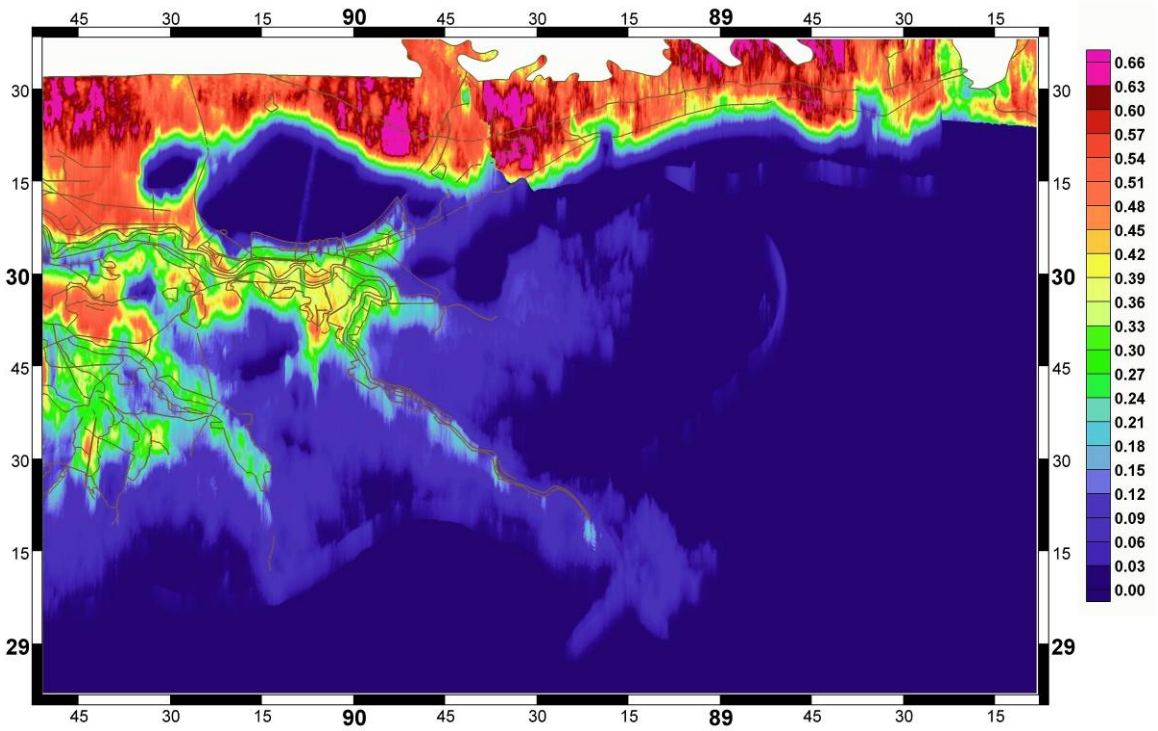


Figure 66: A detail of the applied directional wind reduction factor for northerly winds for Southeastern Louisiana.

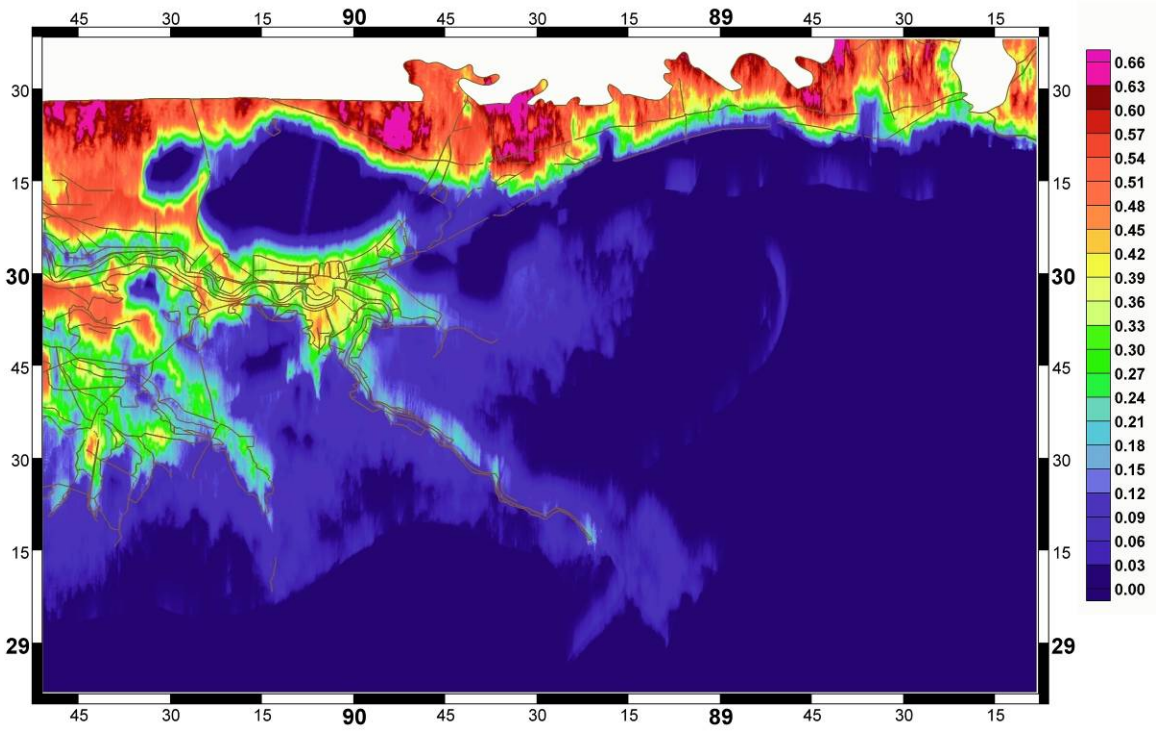


Figure 67: A detail of the applied directional wind reduction factor for southerly winds for Southeastern Louisiana

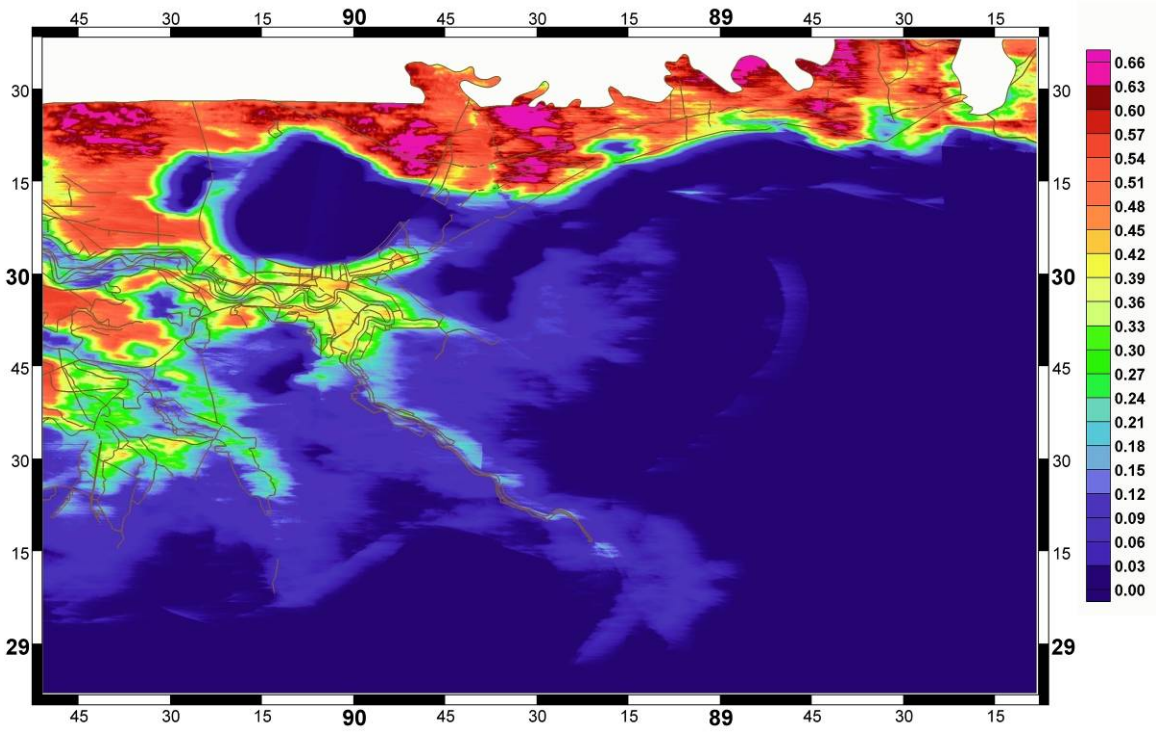


Figure 68: A detail of the applied directional wind reduction factor for westerly winds for Southeastern Louisiana.

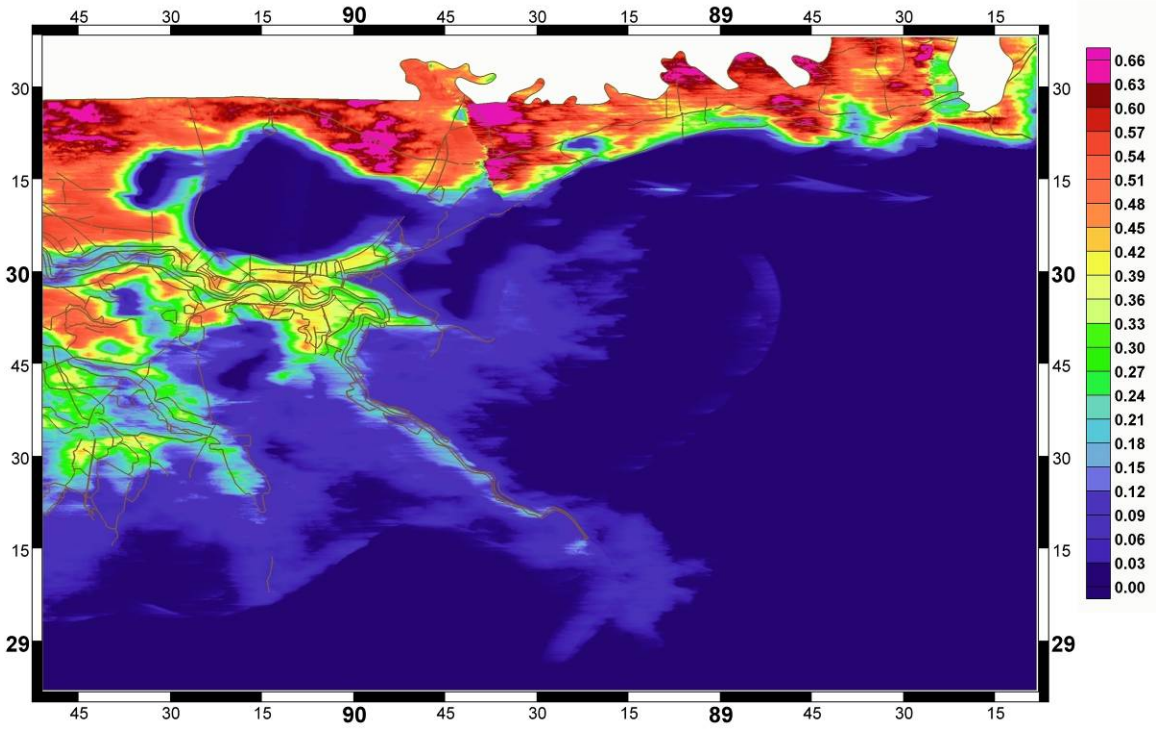


Figure 69: A detail of the applied directional wind reduction factor for easterly winds for Southeastern Louisiana.

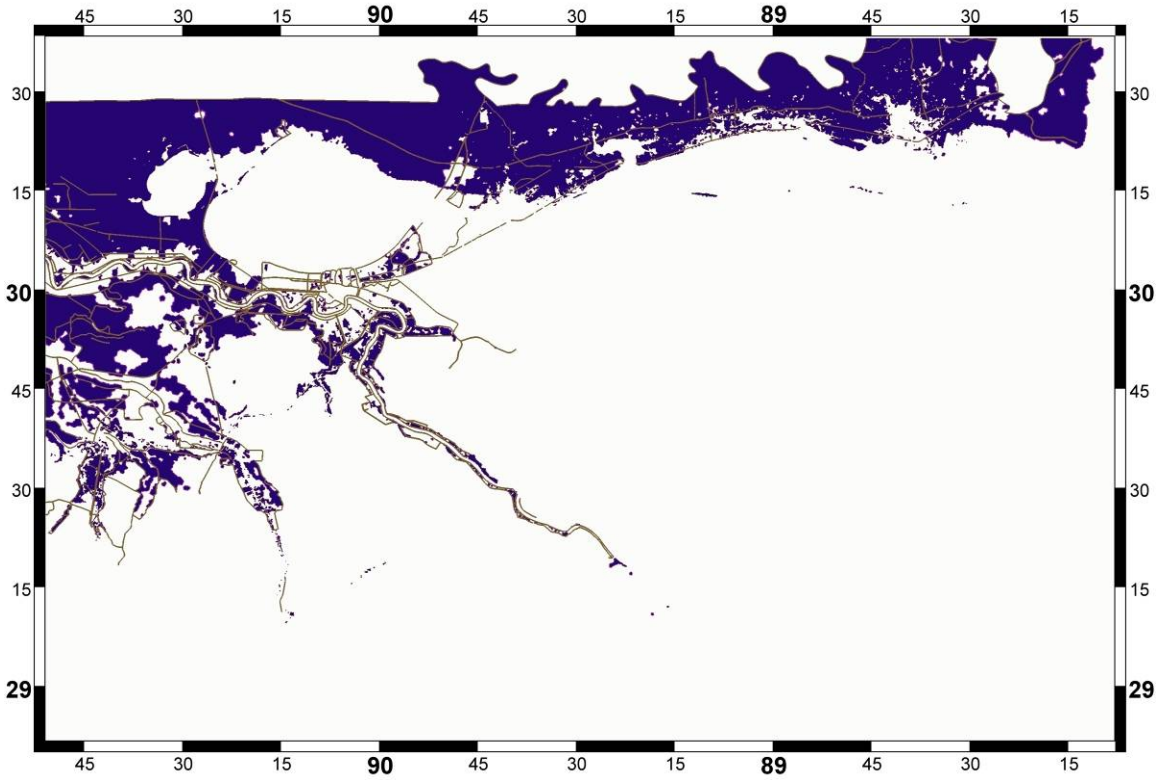


Figure 70: A detail of the heavily forested areas (blue area) in Southeastern Louisiana where a canopy factor has been applied.

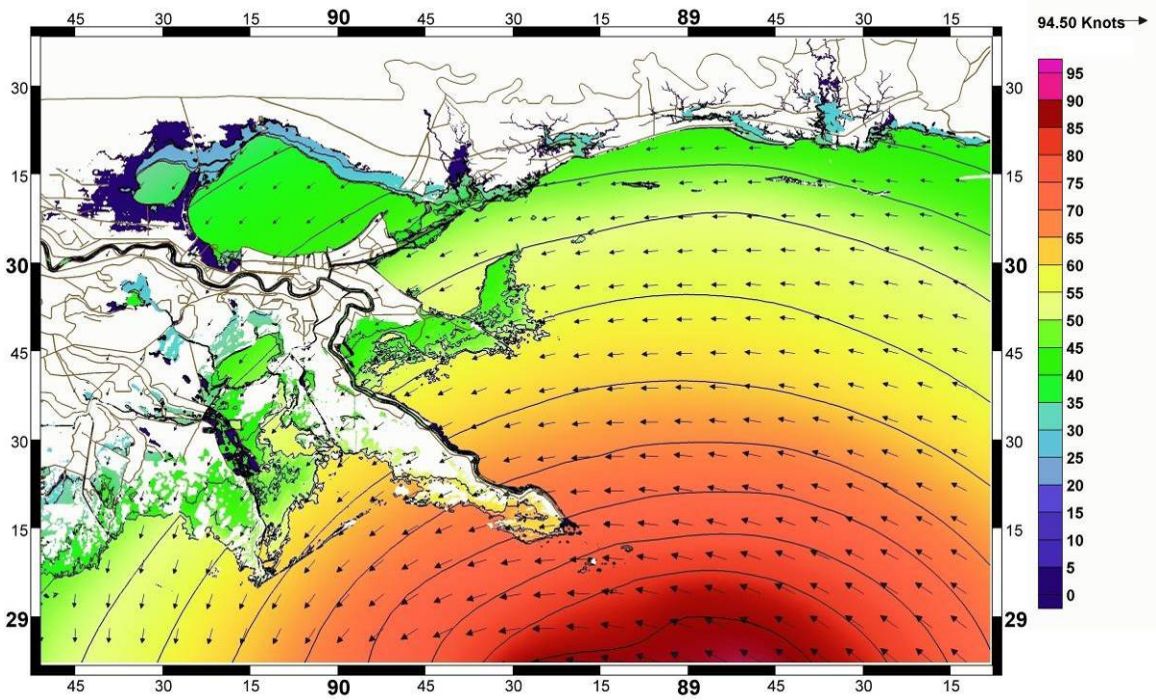


Figure 71: ADCIRC contour map of the wind speed (knots) and wind vectors (knots) for Hurricane Katrina at 7:00 UTC on August 29, 2005 for Southeastern Louisiana.

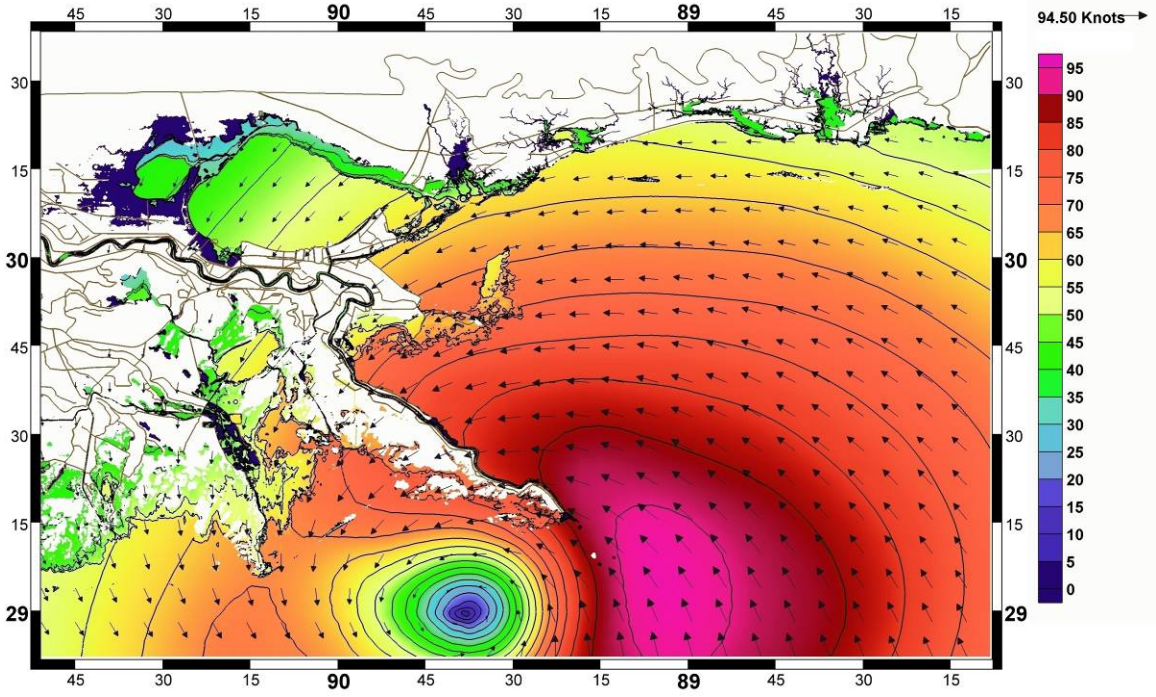


Figure 72: ADCIRC contour map of the wind speed (knots) and wind vectors (knots) for Hurricane Katrina at 10:00 UTC on August 29, 2005 for Southeastern Louisiana.

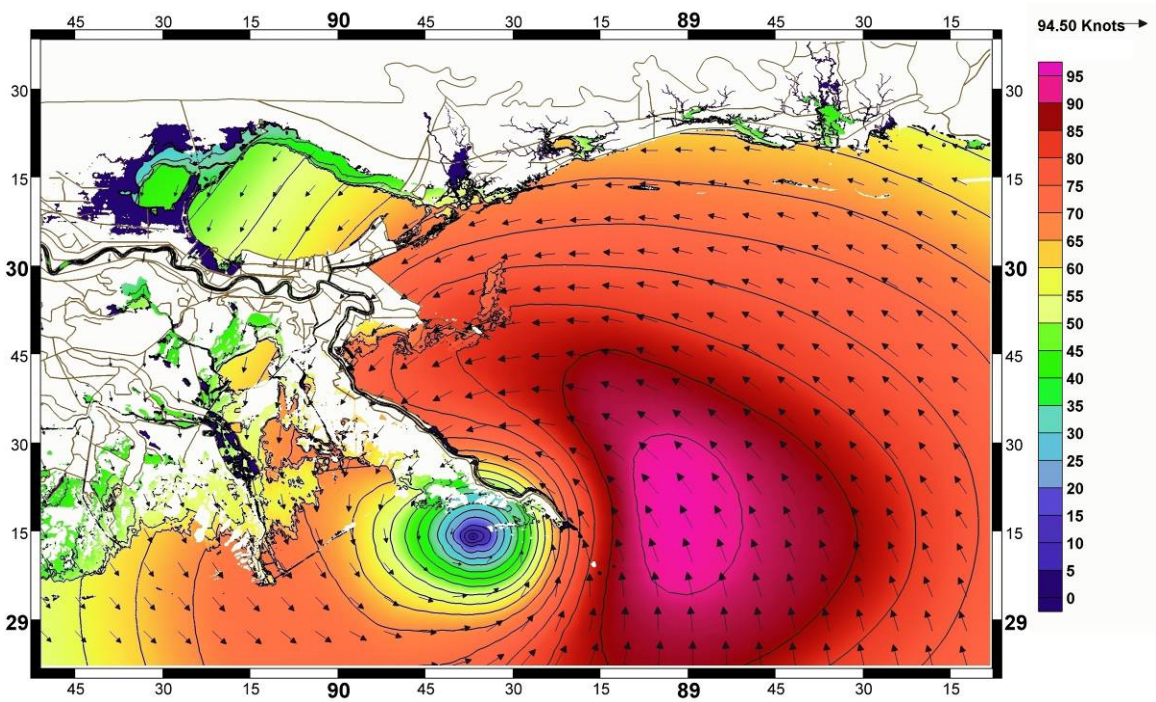


Figure 73: ADCIRC contour map of the wind speed (knots) and wind vectors (knots) for Hurricane Katrina at 11:00 UTC on August 29, 2005 for Southeastern Louisiana.

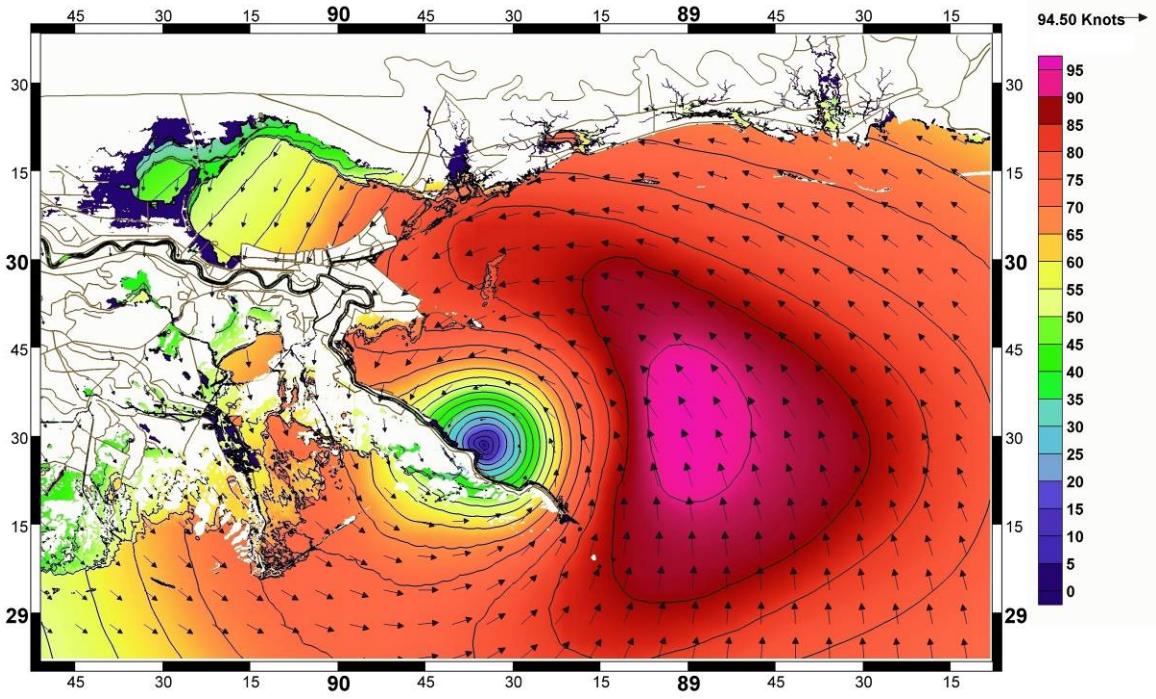


Figure 74: ADCIRC contour map of the wind speed (knots) and wind vectors (knots) for Hurricane Katrina at 12:00 UTC on August 29, 2005 for Southeastern Louisiana.

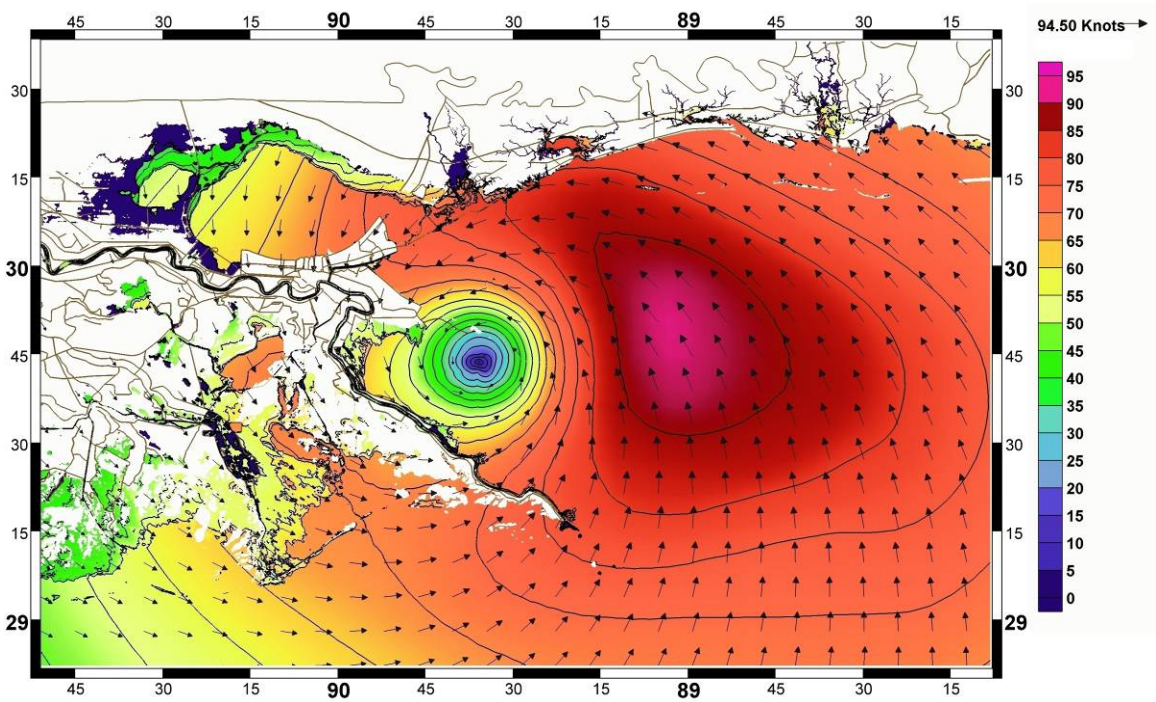


Figure 75: ADCIRC contour map of the wind speed (knots) and wind vectors (knots) for Hurricane Katrina at 13:00 UTC on August 29, 2005 for Southeastern Louisiana.

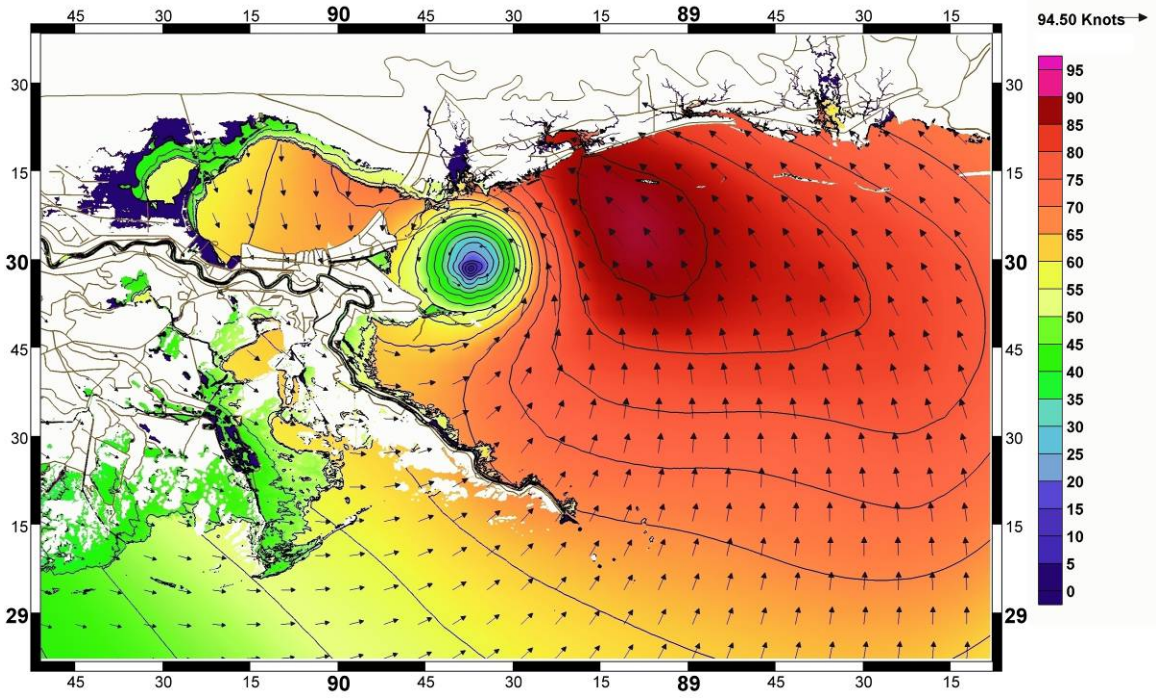


Figure 76: ADCIRC contour map of the wind speed (knots) and wind vectors (knots) for Hurricane Katrina at 14:00 UTC on August 29, 2005 for Southeastern Louisiana.

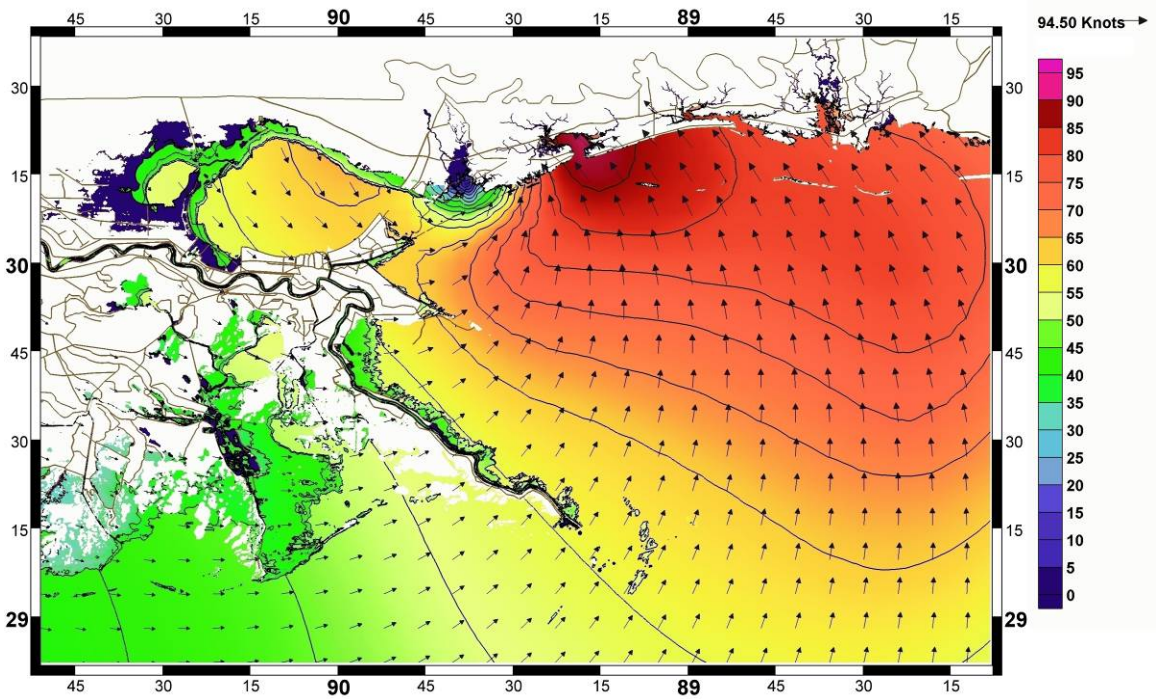


Figure 77: ADCIRC contour map of the wind speed (knots) and wind vectors (knots) for Hurricane Katrina at 15:00 UTC on August 29, 2005 for Southeastern Louisiana.

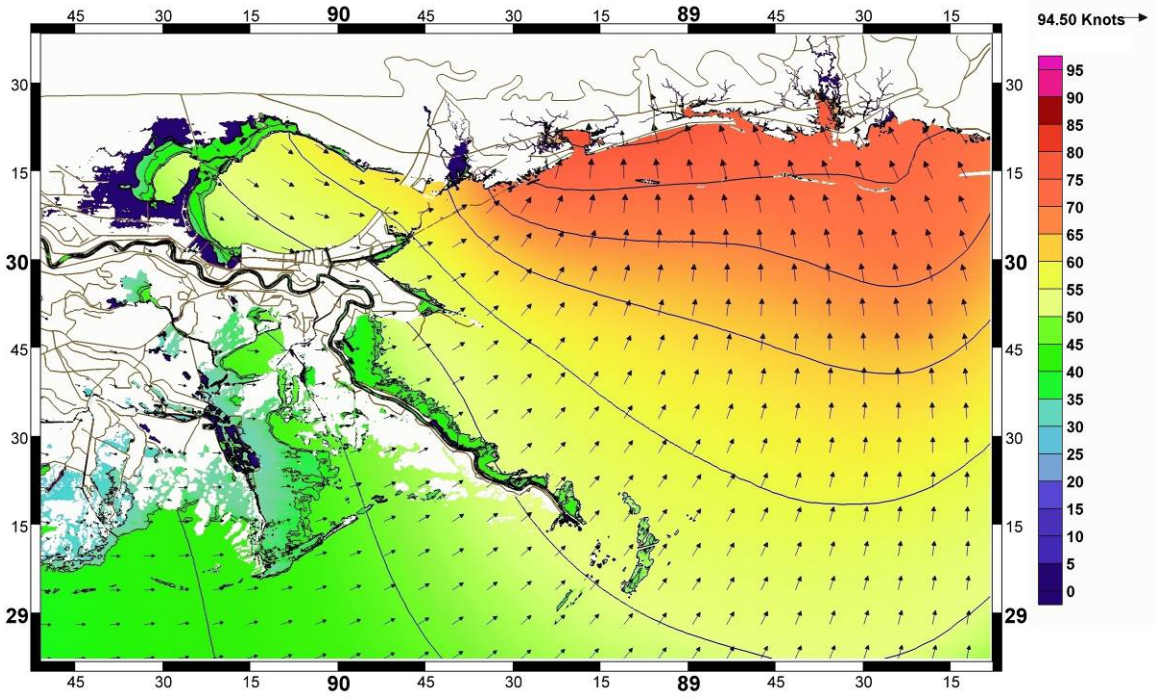


Figure 78: ADCIRC contour map of the wind speed (knots) and wind vectors (knots) for Hurricane Katrina at 16:00 UTC on August 29, 2005 for Southeastern Louisiana.

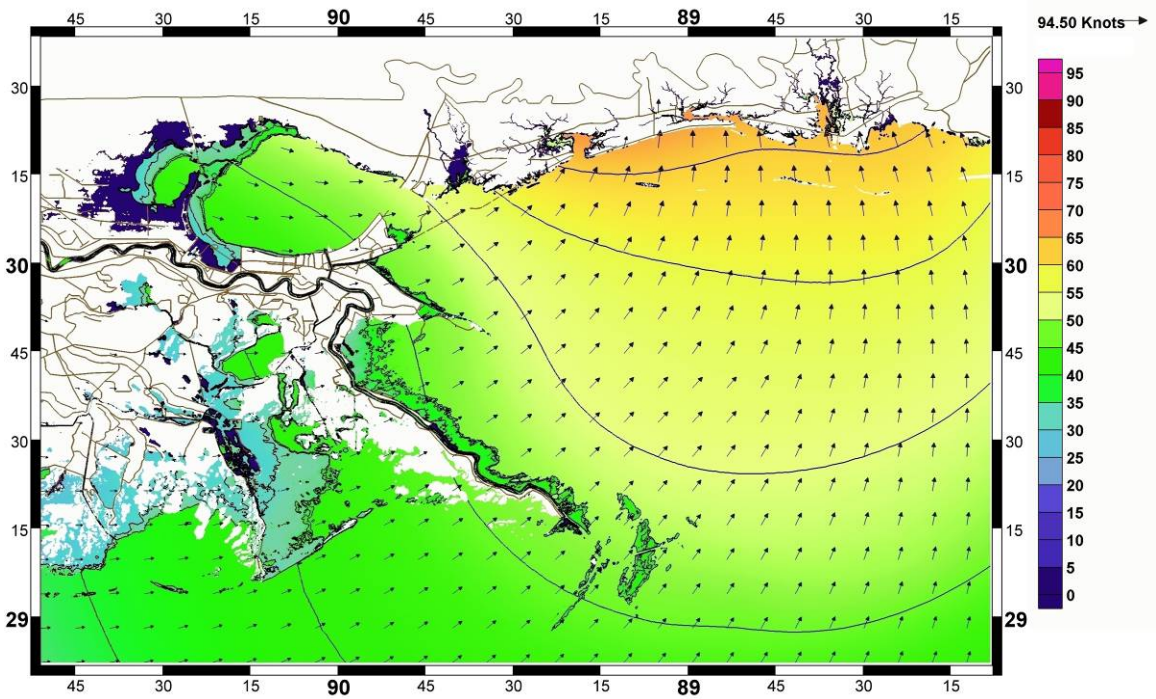


Figure 79: ADCIRC contour map of the wind speed (knots) and wind vectors (knots) for Hurricane Katrina at 17:00 UTC on August 29, 2005 for Southeastern Louisiana.

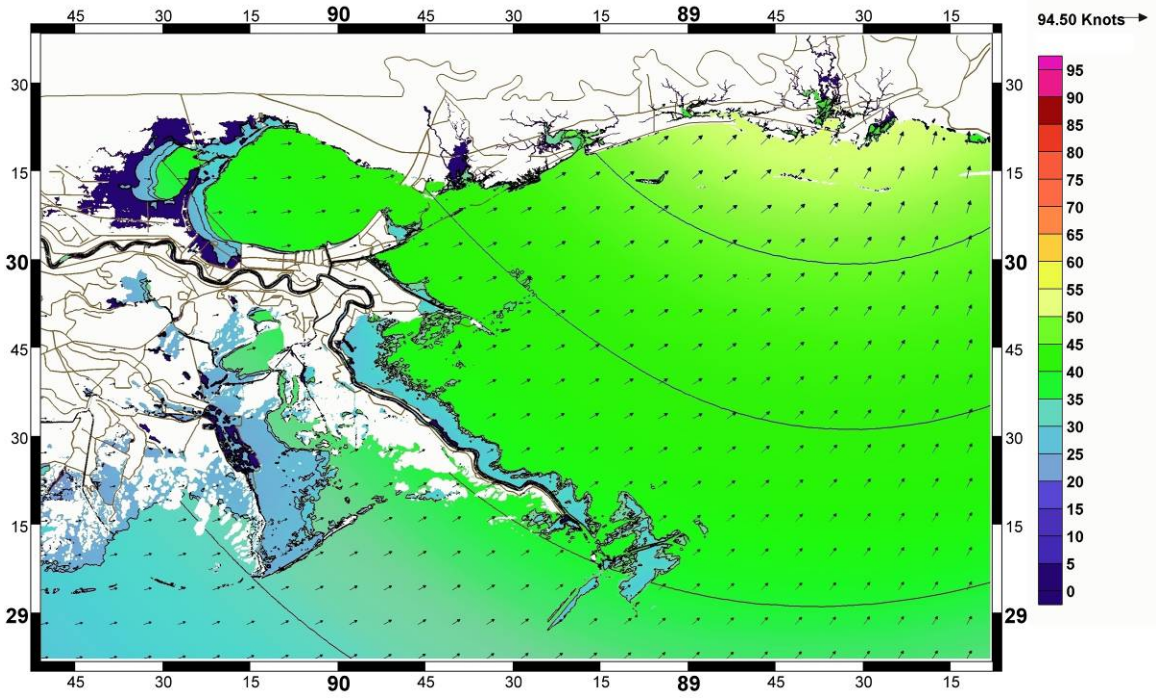


Figure 80: ADCIRC contour map of the wind speed (knots) and wind vectors (knots) for Hurricane Katrina at 20:00 UTC on August 29, 2005 for Southeastern Louisiana.

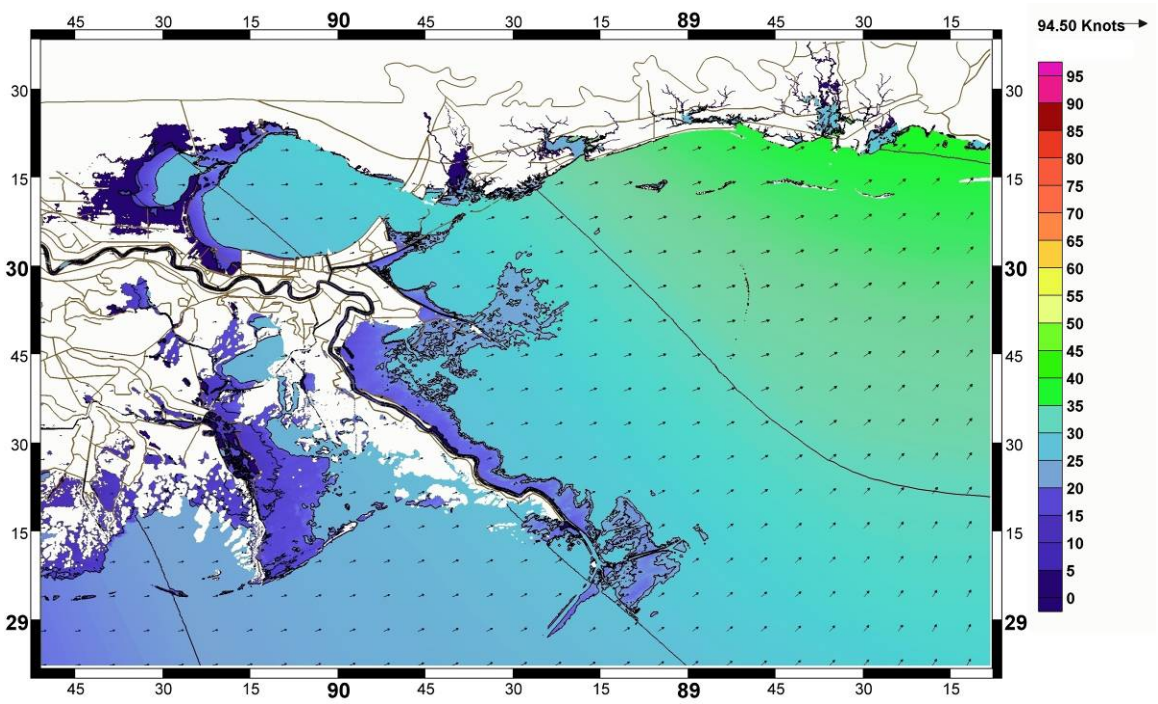


Figure 81: ADCIRC contour map of the wind speed (knots) and wind vectors (knots) for Hurricane Katrina at 23:00 UTC on August 29, 2005 for Southeastern Louisiana.

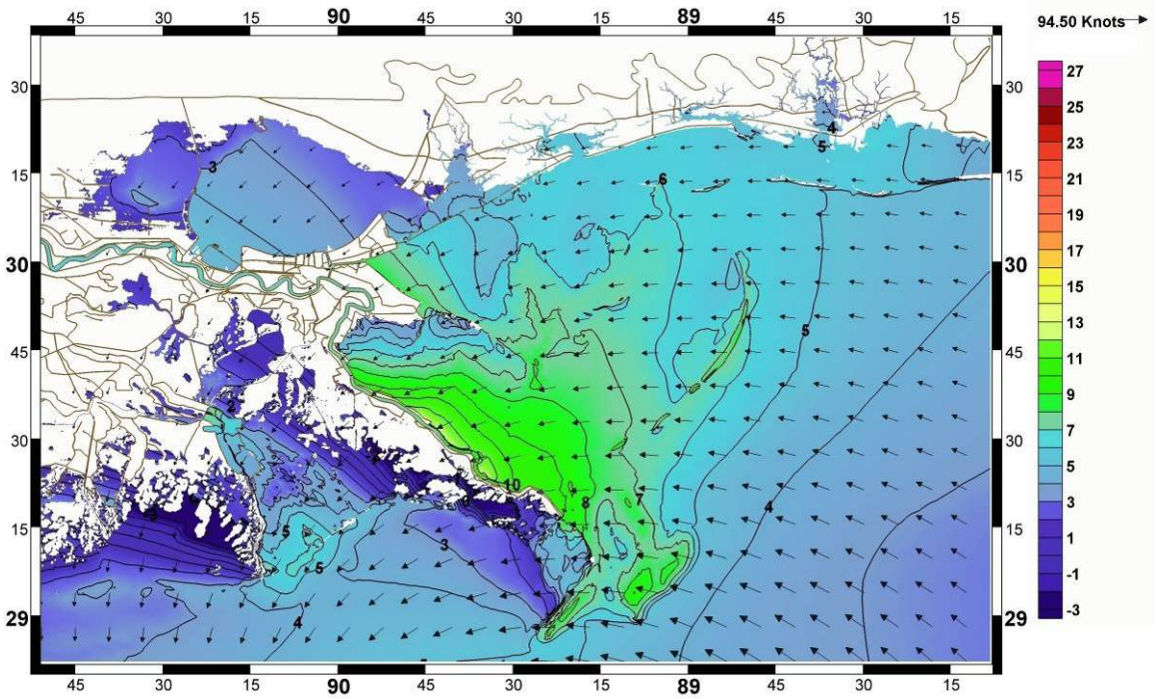


Figure 82: ADCIRC elevation contours (ft) and wind vectors (knots) for Hurricane Katrina at 7:00 UTC on August 29, 2005 for Southeastern Louisiana.

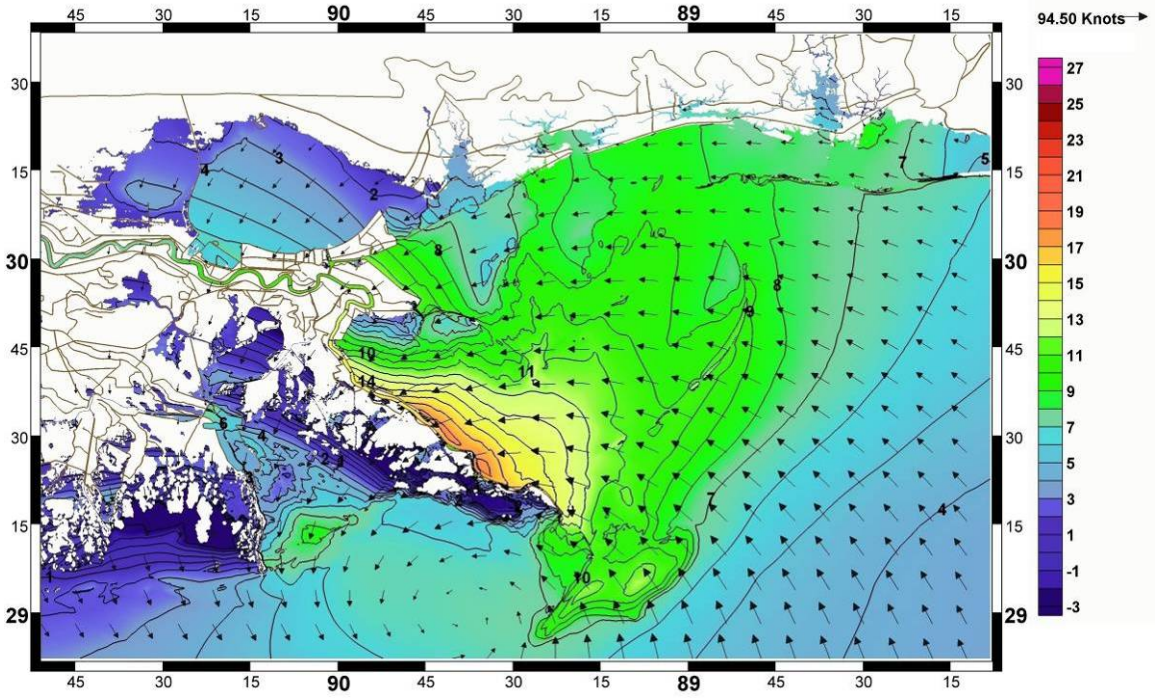


Figure 83: ADCIRC elevation contours (ft) and wind vectors (knots) for Hurricane Katrina at 10:00 UTC on August 29, 2005 for Southeastern Louisiana.

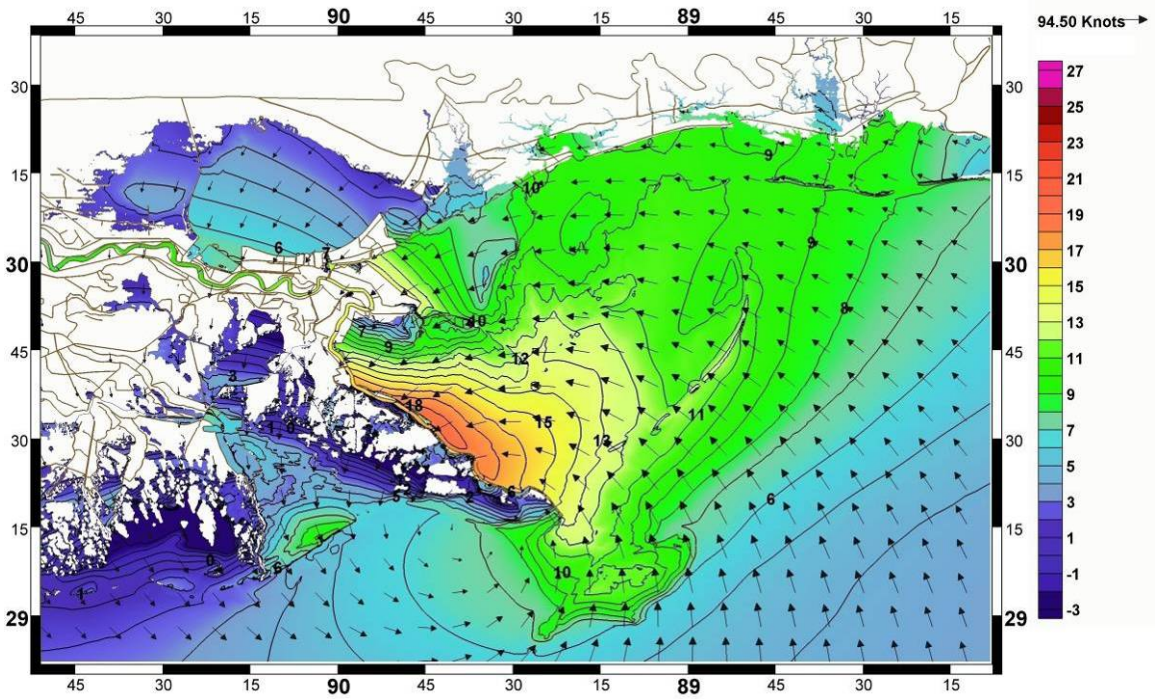


Figure 84: ADCIRC elevation contours (ft) and wind vectors (knots) for Hurricane Katrina at 11:00 UTC on August 29, 2005 for Southeastern Louisiana.

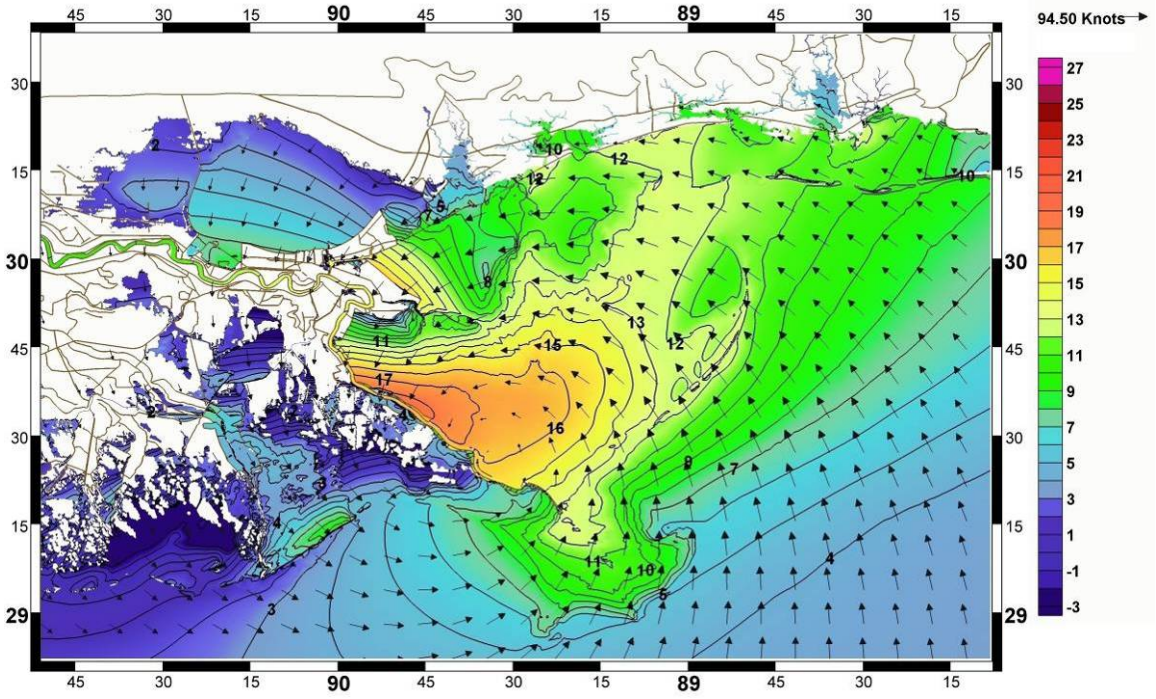


Figure 85: ADCIRC elevation contours (ft) and wind vectors (in knots) for Hurricane Katrina at 12:00 UTC on August 29, 2005 for Southeastern Louisiana.

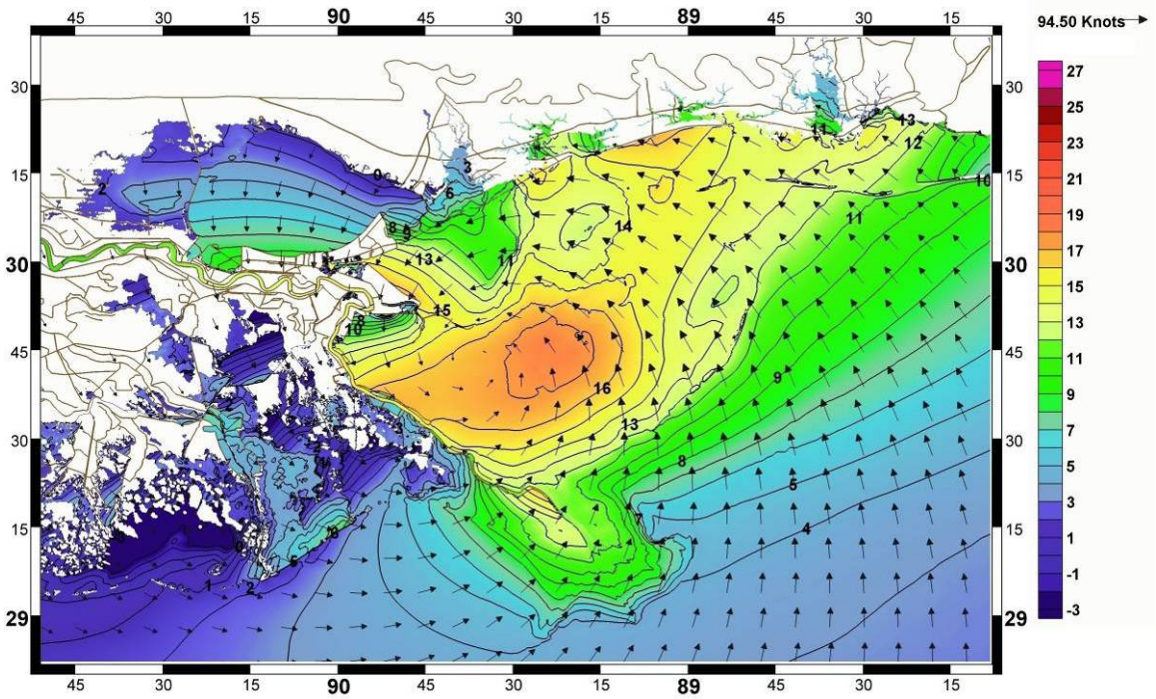


Figure 86: ADCIRC elevation contours (ft) and wind vectors (knots) for Hurricane Katrina at 13:00 UTC on August 29, 2005 for Southeastern Louisiana.

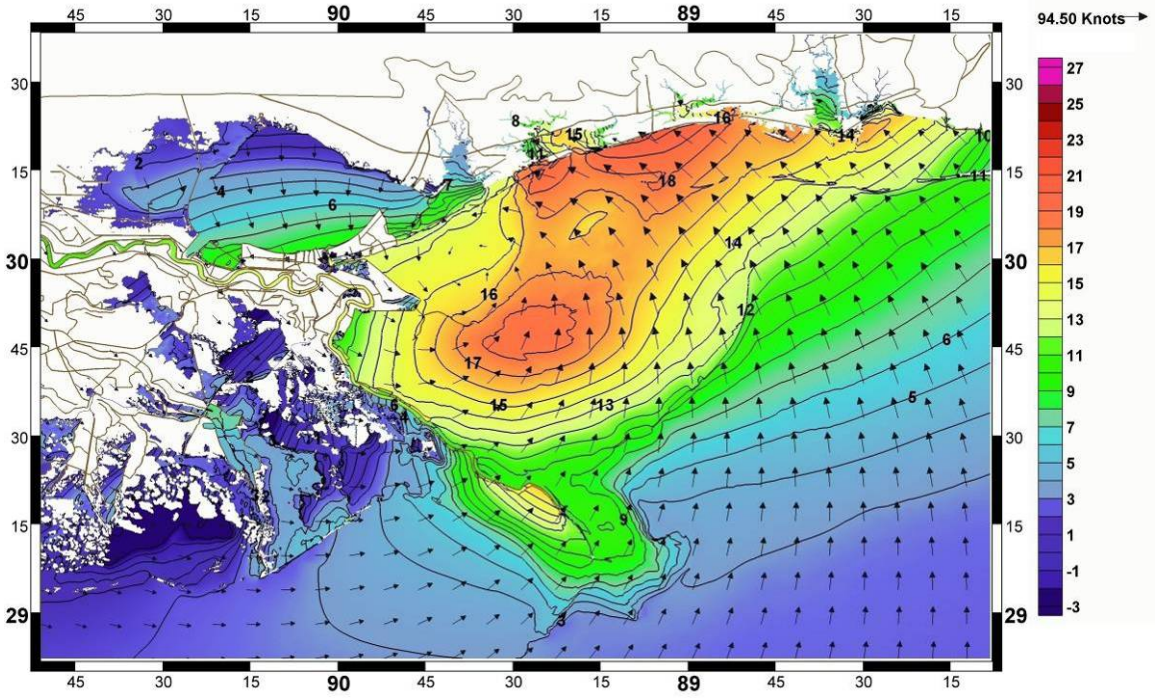


Figure 87: ADCIRC elevation contours (ft) and wind vectors (in knots) for Hurricane Katrina at 14:00 UTC on August 29, 2005 for Southeastern Louisiana.

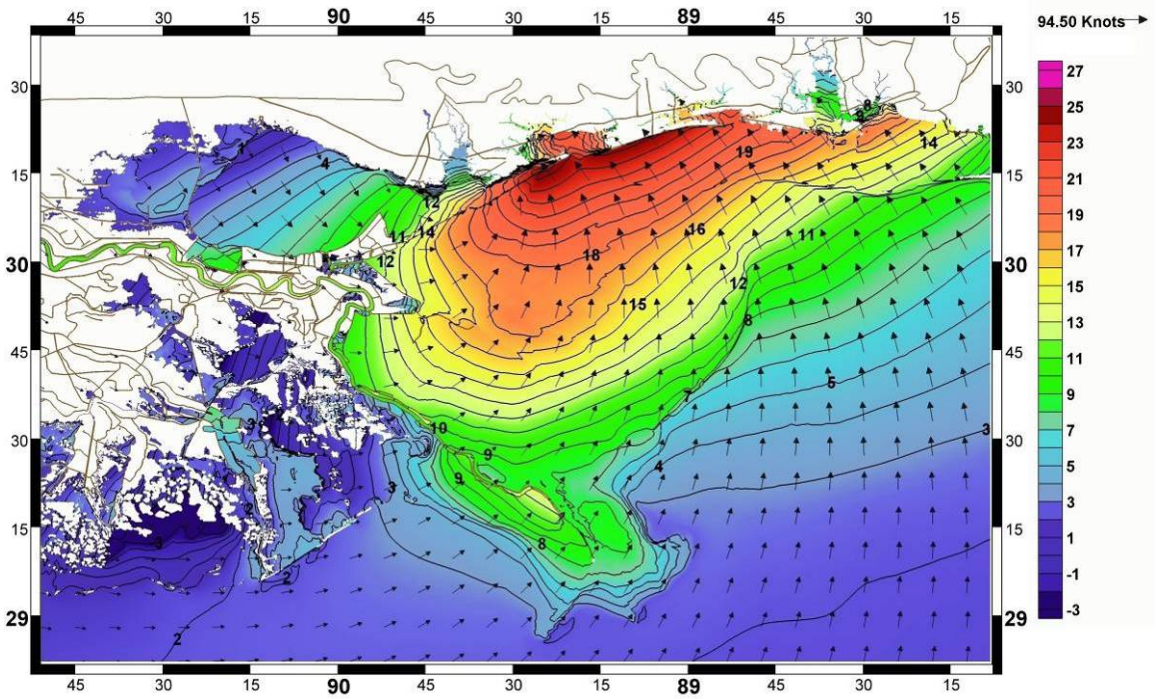


Figure 88: ADCIRC elevation contours (ft) and wind vectors (knots) for Hurricane Katrina at 15:00 UTC on August 29, 2005 for Southeastern Louisiana.

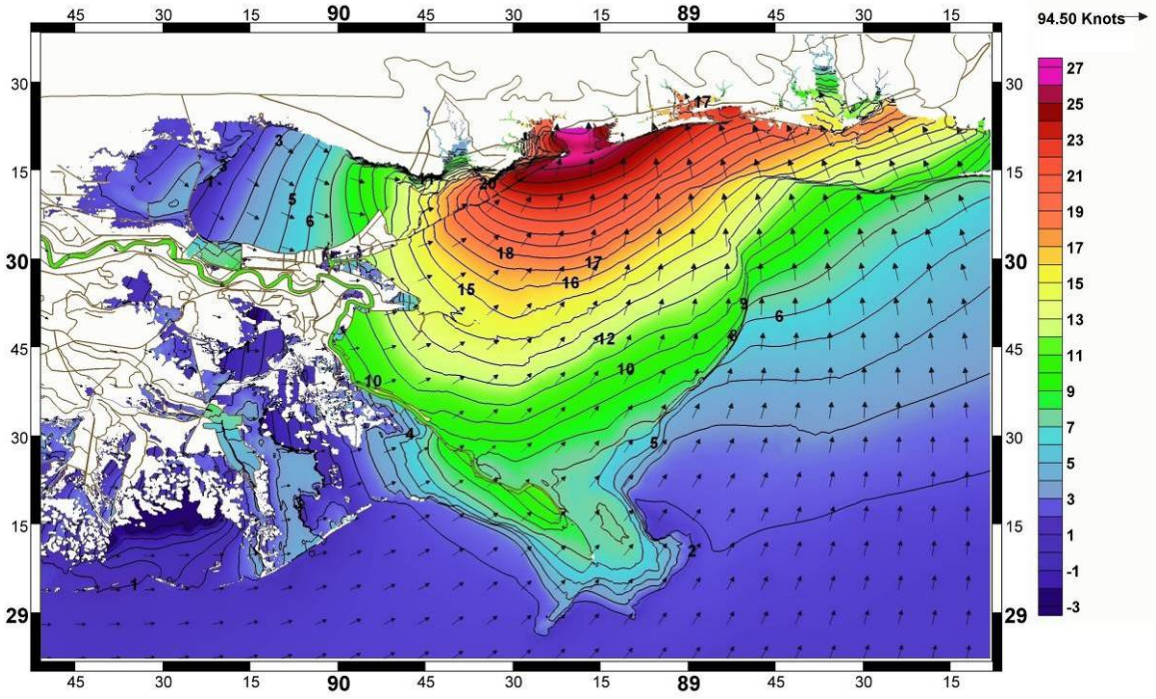


Figure 89: ADCIRC elevation contours (ft) and wind vectors (knots) for Hurricane Katrina at 16:00 UTC on August 29, 2005 for Southeastern Louisiana.

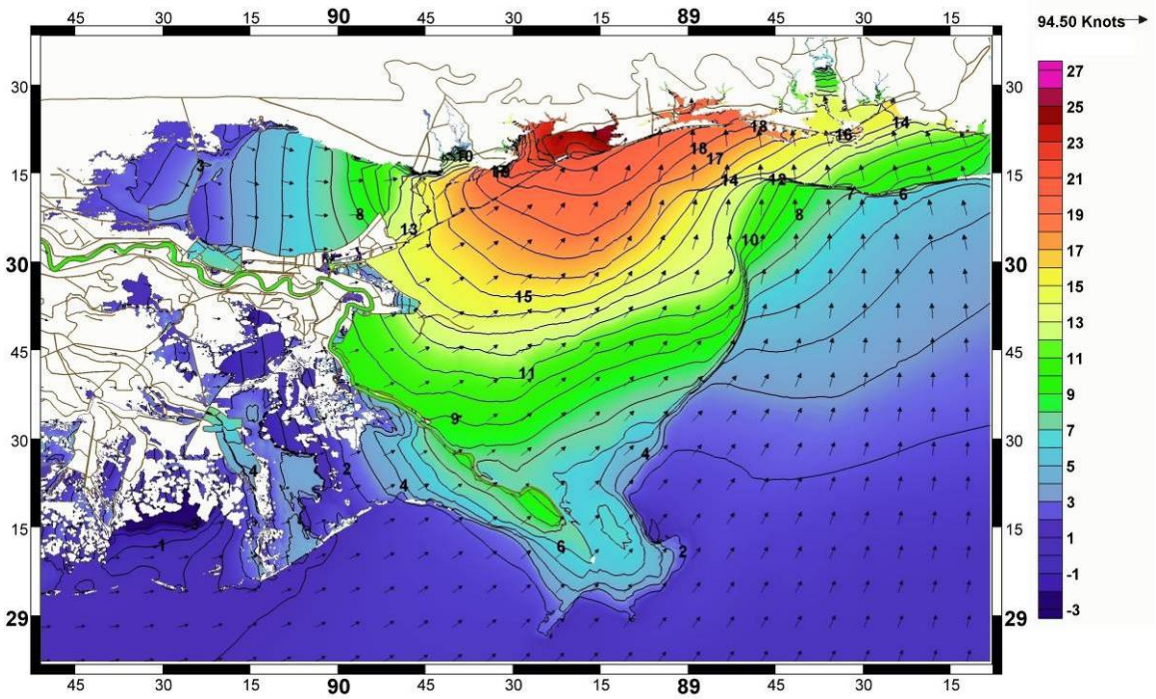


Figure 90: ADCIRC elevation contours (ft) and wind vectors (in knots) for Hurricane Katrina at 17:00 UTC on August 29, 2005 for Southeastern Louisiana.

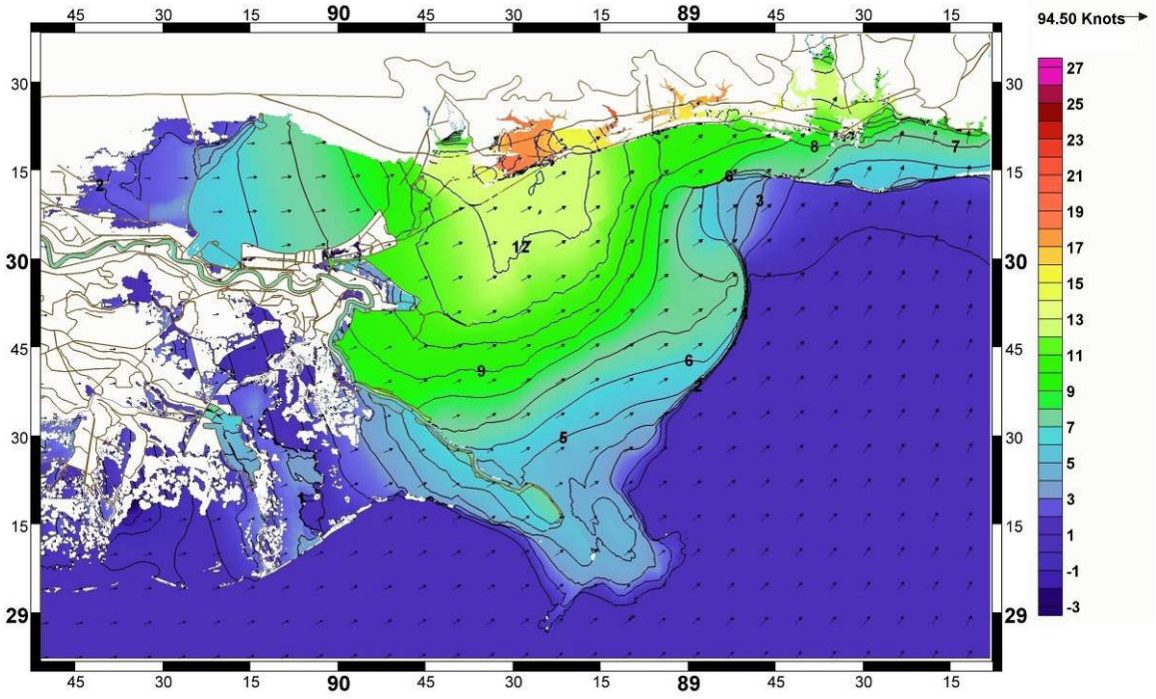


Figure 91: ADCIRC elevation contours (ft) and wind vectors (knots) for Hurricane Katrina at 20:00 UTC on August 29, 2005 for Southeastern Louisiana.

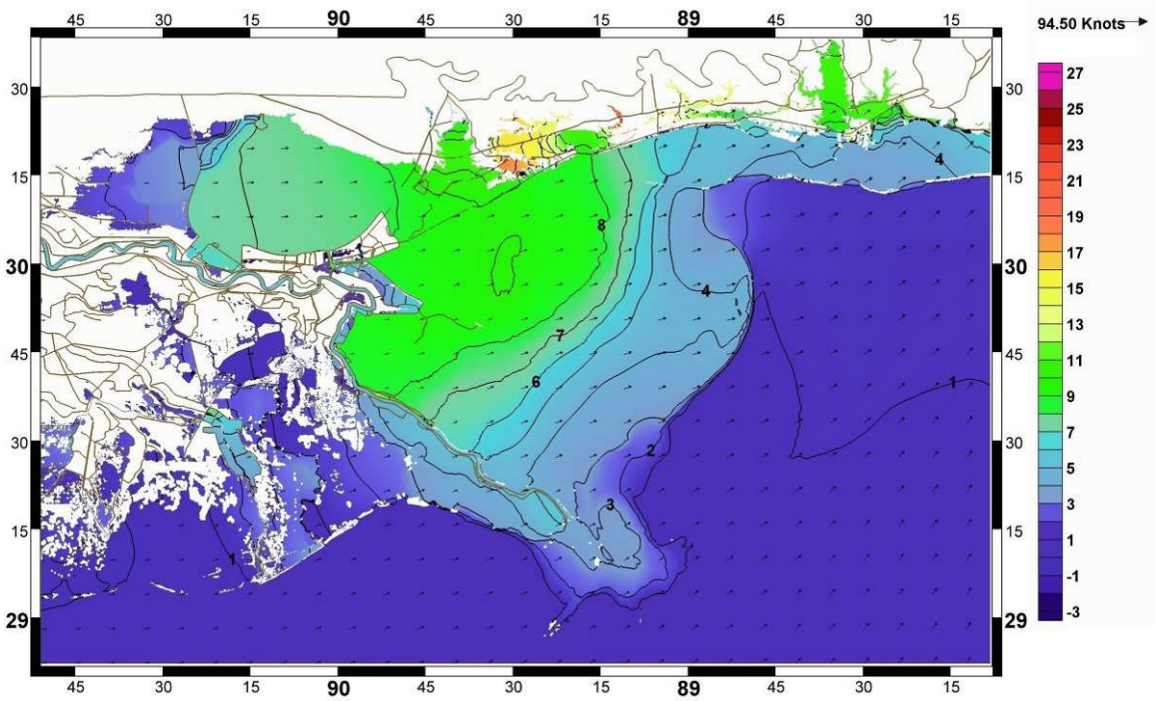


Figure 92: ADCIRC elevation contours (ft) and wind vectors (knots) for Hurricane Katrina at 23:00 UTC on August 29, 2005 for Southeastern Louisiana.

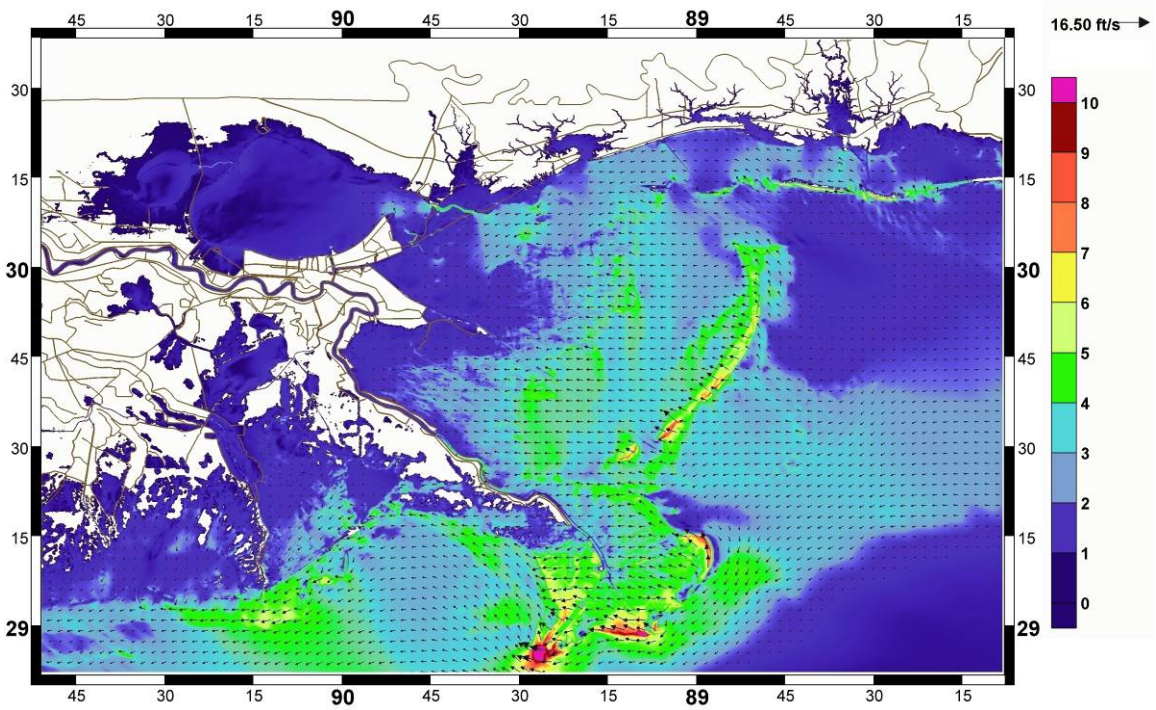


Figure 93: ADCIRC current contours (ft/sec) and current vectors (ft/sec) for Hurricane Katrina at 7:00 UTC on August 29, 2005 for Southeastern Louisiana.

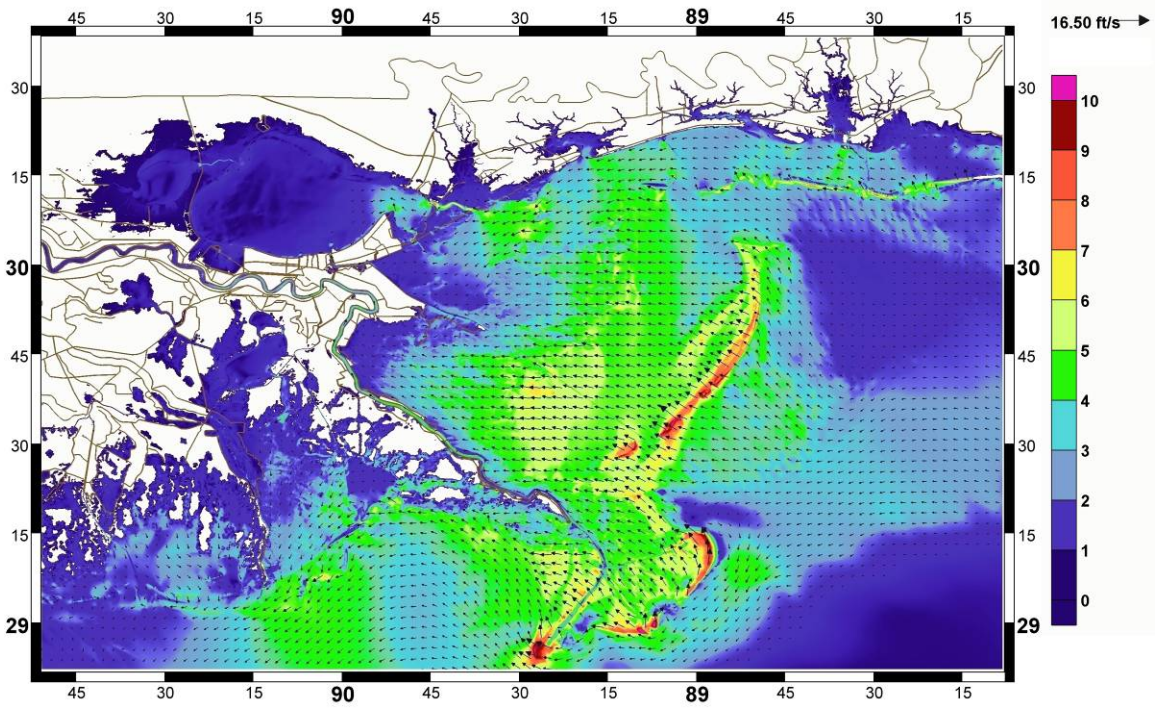


Figure 94: ADCIRC current contours (ft/sec) and current vectors (ft/sec) for Hurricane Katrina at 10:00 UTC on August 29, 2005 for Southeastern Louisiana.

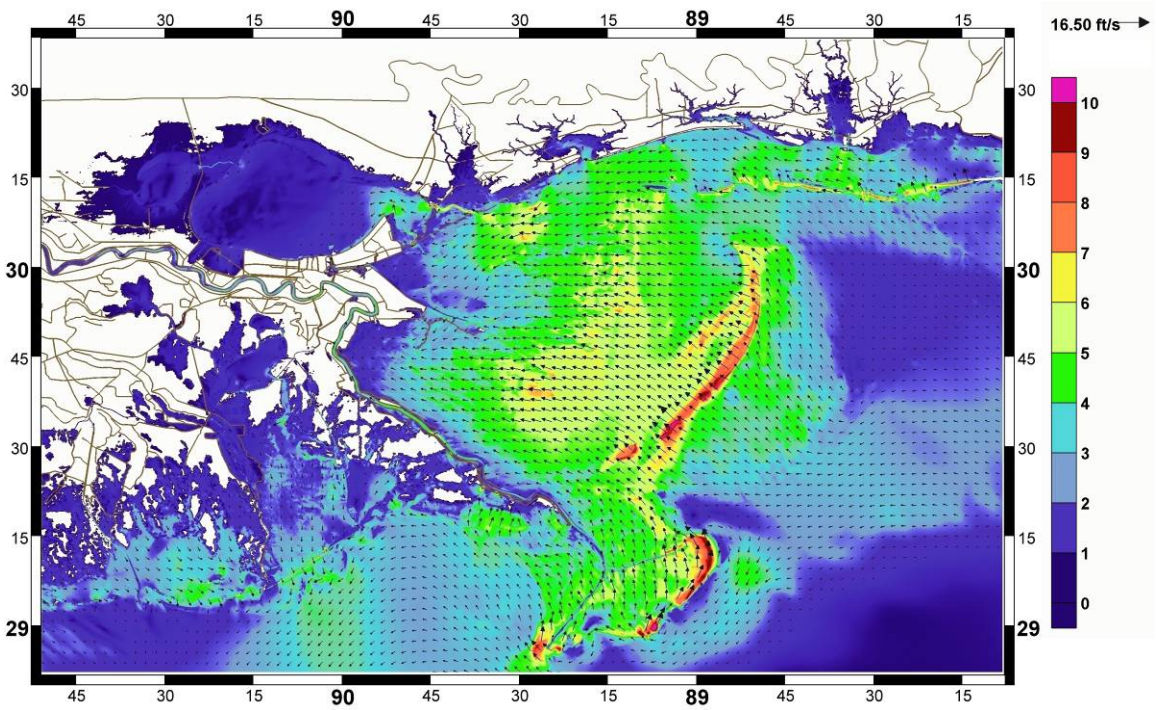


Figure 95: ADCIRC current contours (ft/sec) and current vectors (ft/sec) for Hurricane Katrina at 11:00 UTC on August 29, 2005 for Southeastern Louisiana.

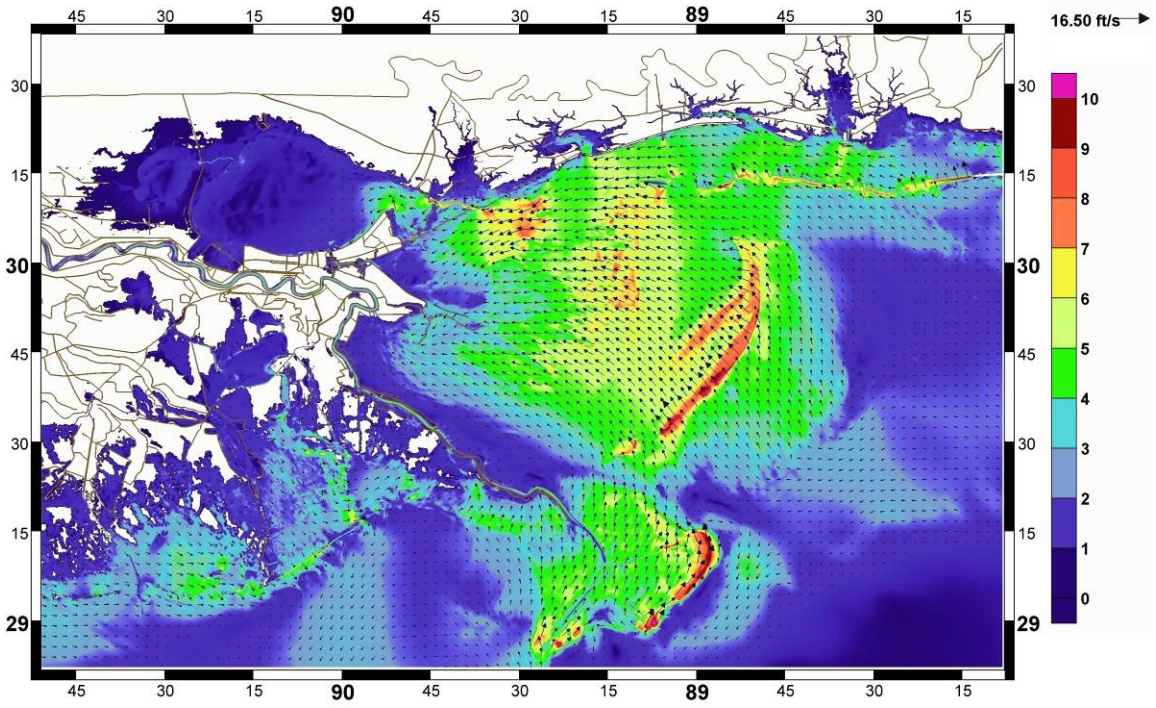


Figure 96: ADCIRC current contours (ft/sec) and current wind vectors (ft/sec) for Hurricane Katrina at 12:00 UTC on August 29, 2005 for Southeastern Louisiana.

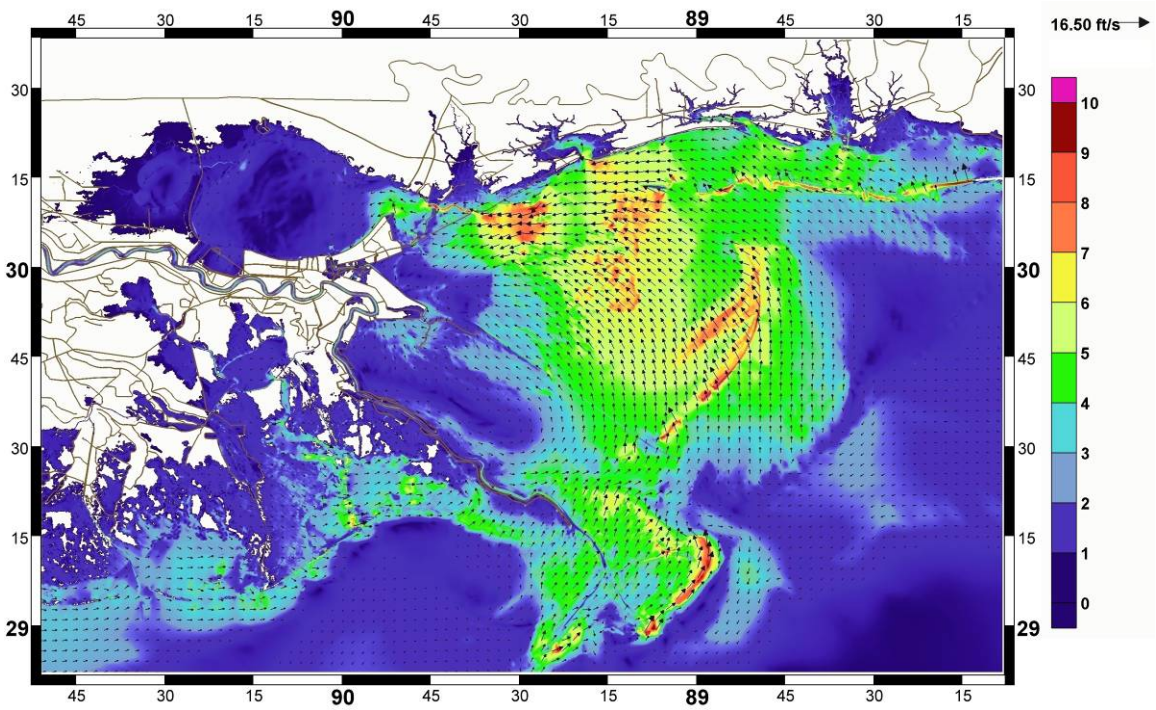


Figure 97: ADCIRC current contours (ft/sec) and current vectors (ft/sec) for Hurricane Katrina at 13:00 UTC on August 29, 2005 for Southeastern Louisiana.

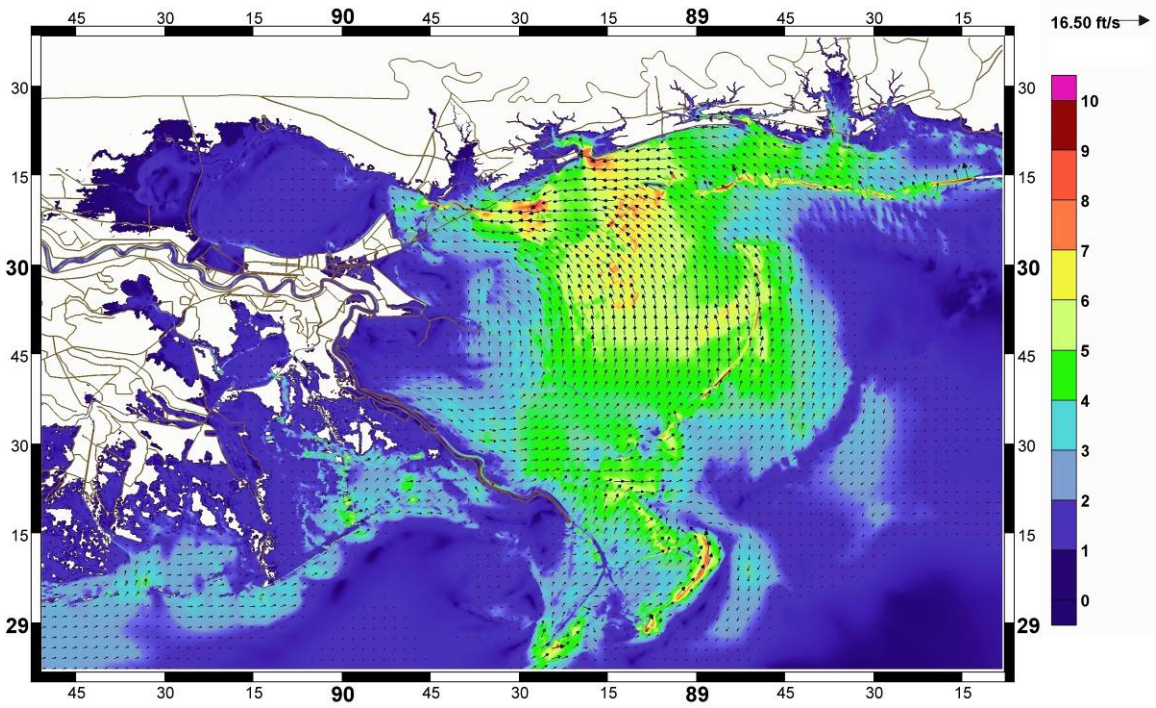


Figure 98: ADCIRC current contours (ft/sec) and current vectors (ft/sec) for Hurricane Katrina at 14:00 UTC on August 29, 2005 for Southeastern Louisiana.

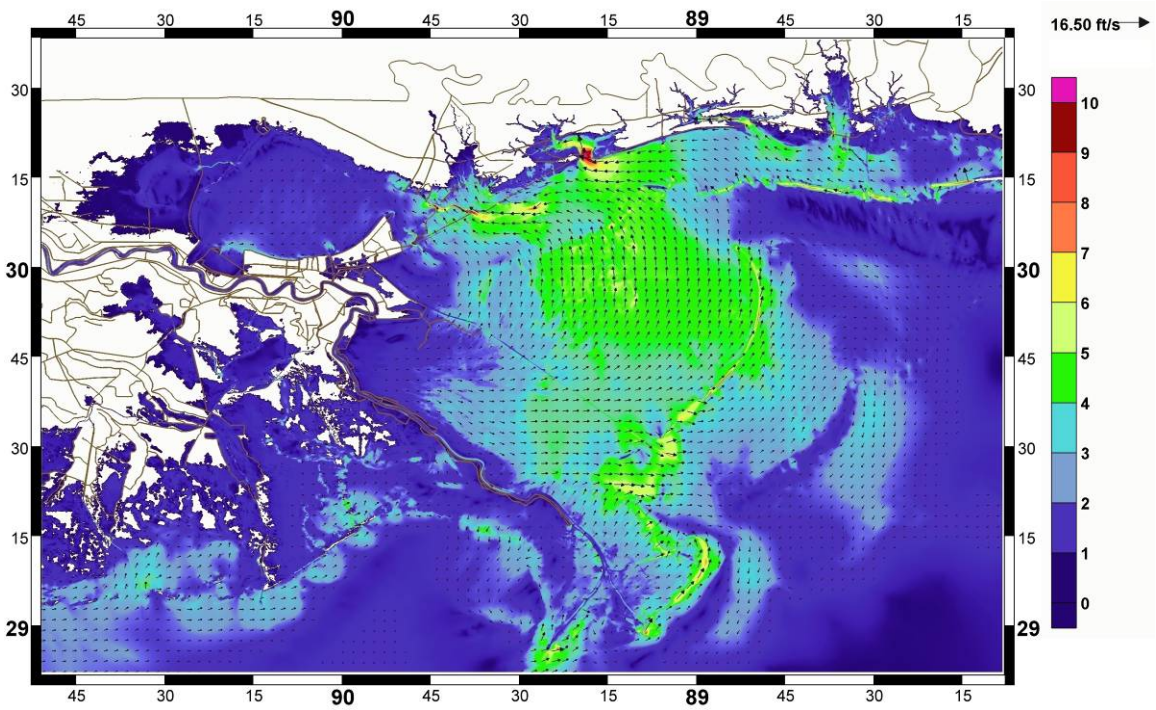


Figure 99: ADCIRC current contours (ft/sec) and current vectors (ft/sec) for Hurricane Katrina at 15:00 UTC on August 29, 2005 for Southeastern Louisiana.

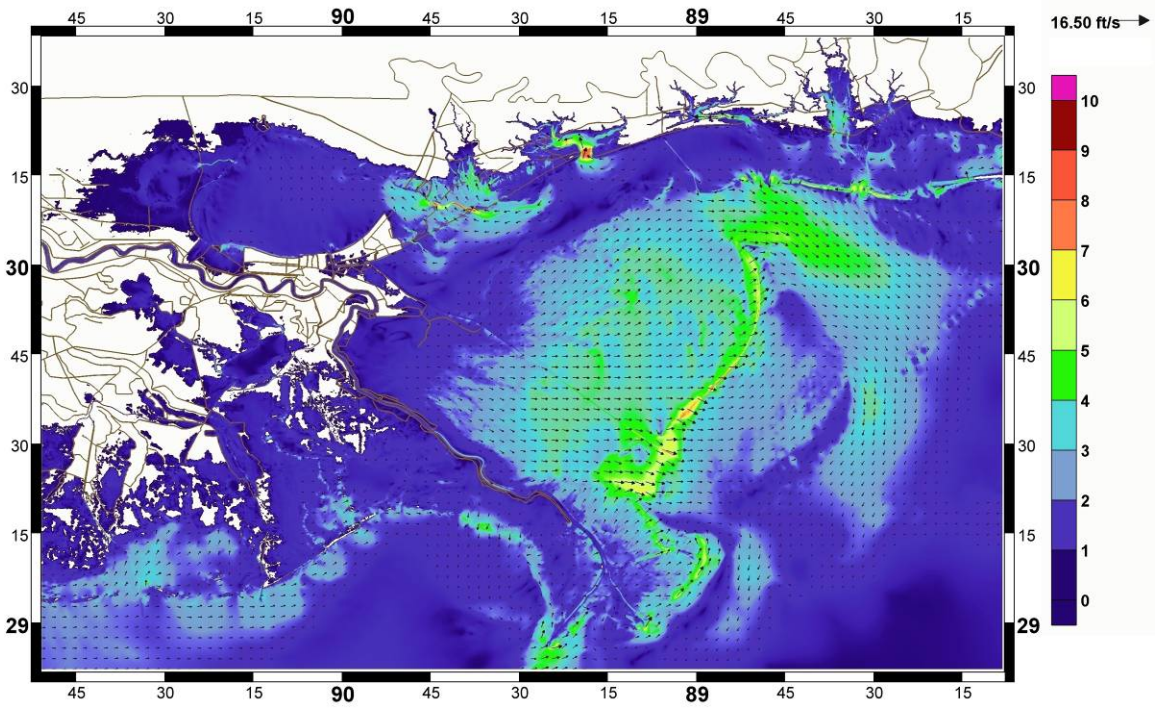


Figure 100: ADCIRC current contours (ft/sec) and current vectors (ft/sec) for Hurricane Katrina at 16:00 UTC on August 29, 2005 for Southeastern Louisiana.

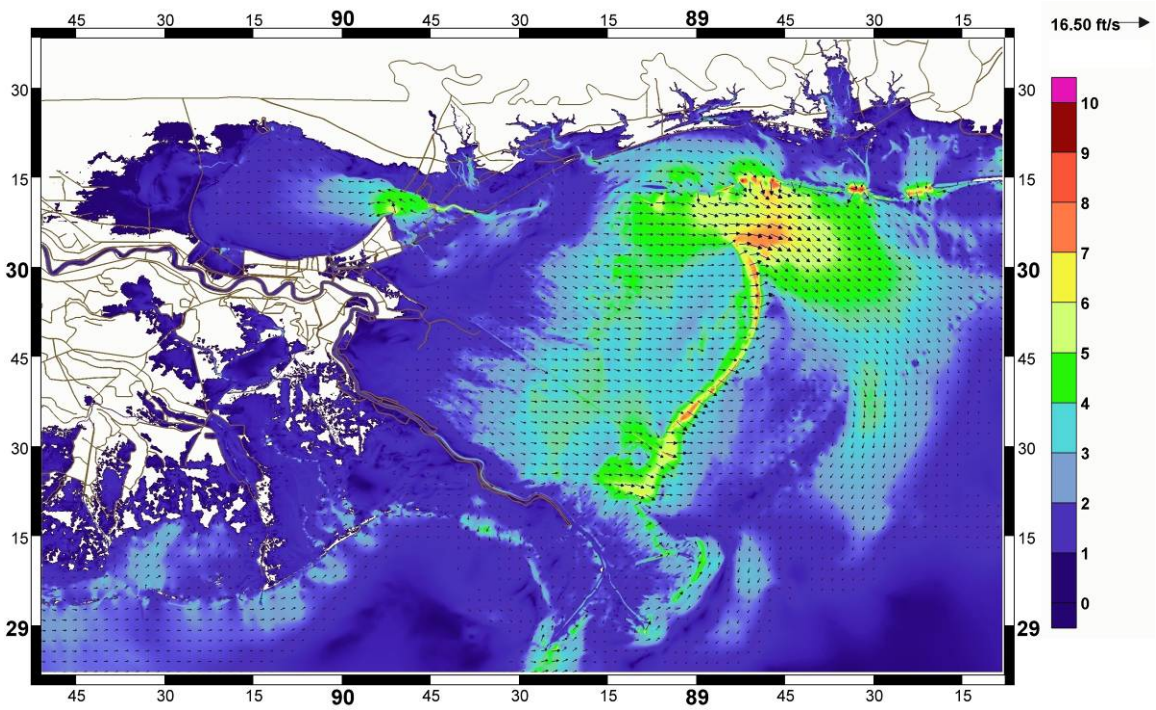


Figure 101: ADCIRC current contours (ft/sec) and current vectors (ft/sec) for Hurricane Katrina at 17:00 UTC on August 29, 2005 for Southeastern Louisiana.

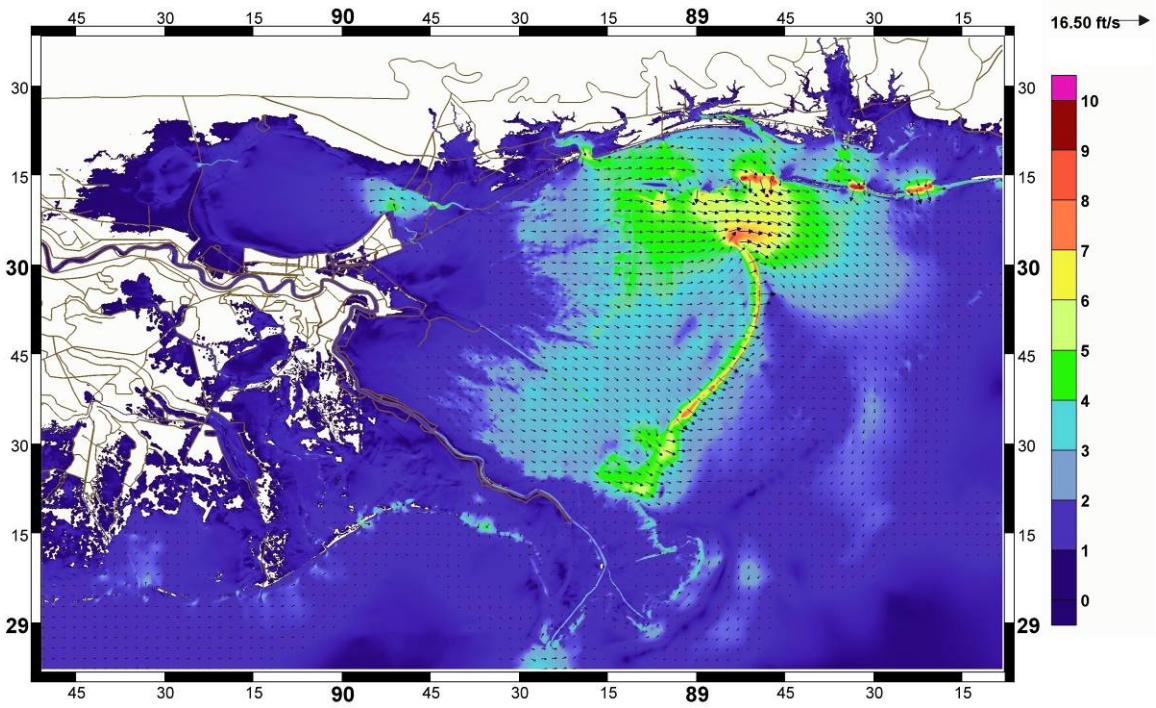


Figure 102: ADCIRC current contours (ft/sec) and current vectors (ft/sec) for Hurricane Katrina at 20:00 UTC on August 29, 2005 for Southeastern Louisiana.

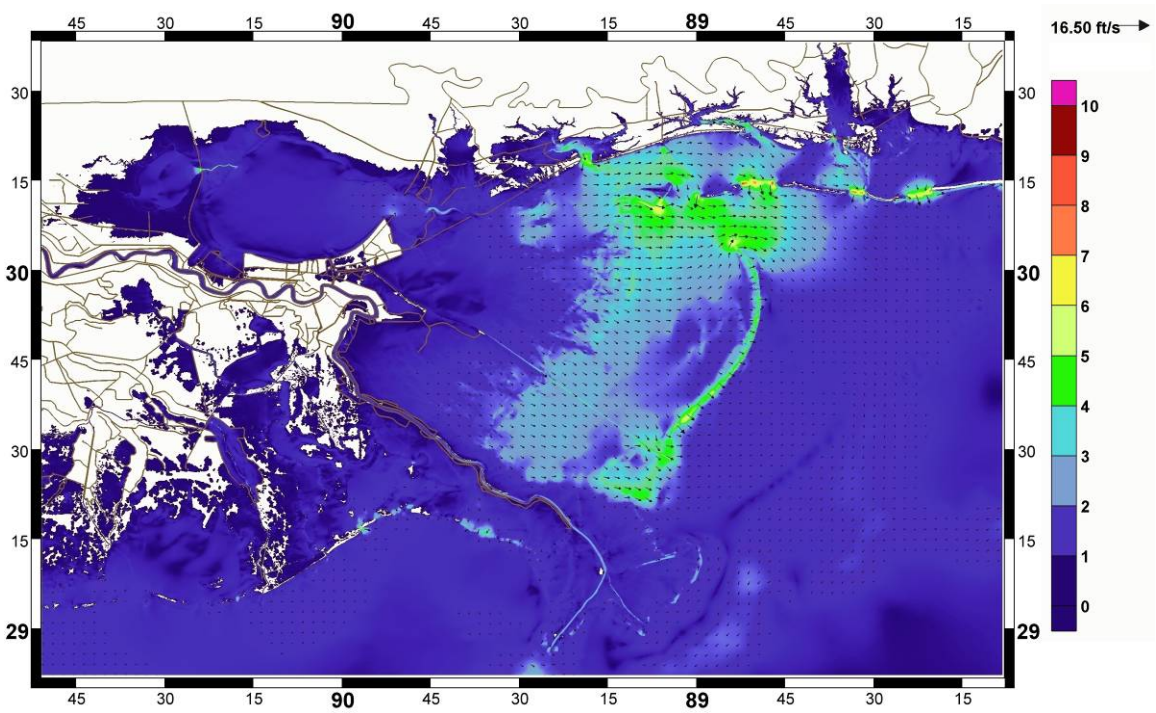


Figure 103: ADCIRC current contours (ft/sec) and current vectors (ft/sec) for Hurricane Katrina at 23:00 UTC on August 29, 2005 for Southeastern Louisiana.

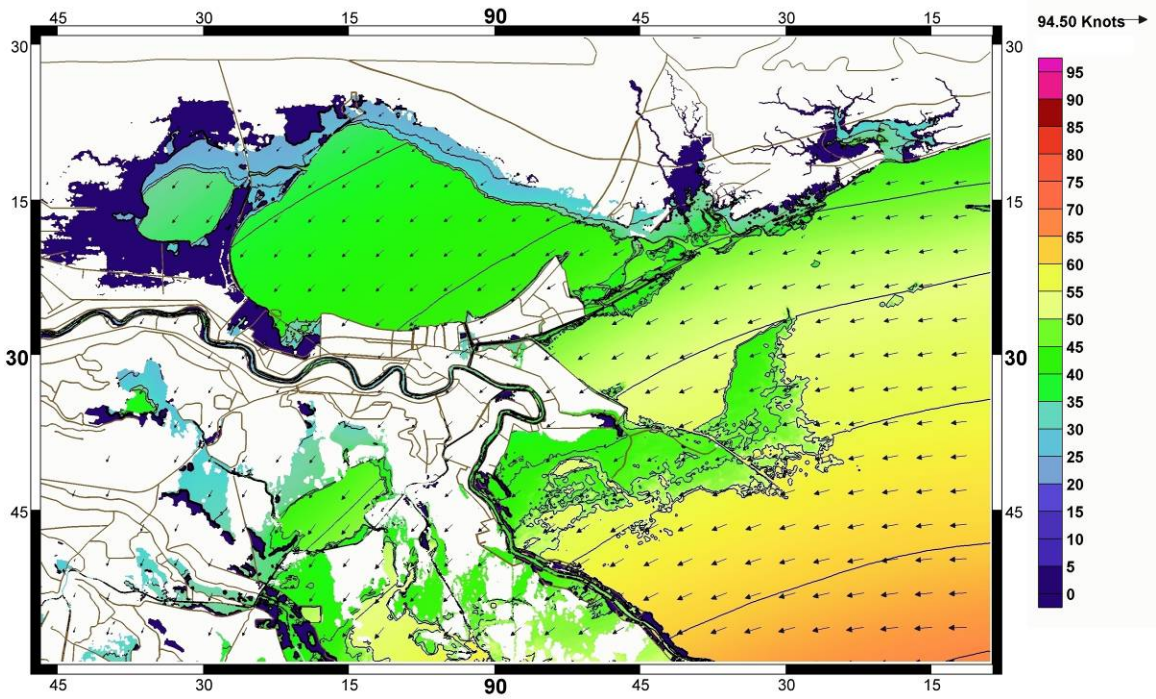


Figure 104: ADCIRC contour map of the wind speed (knots) and wind vectors (knots) for Hurricane Katrina at 7:00 UTC on August 29, 2005 for the area around New Orleans and Lake Pontchartrain.

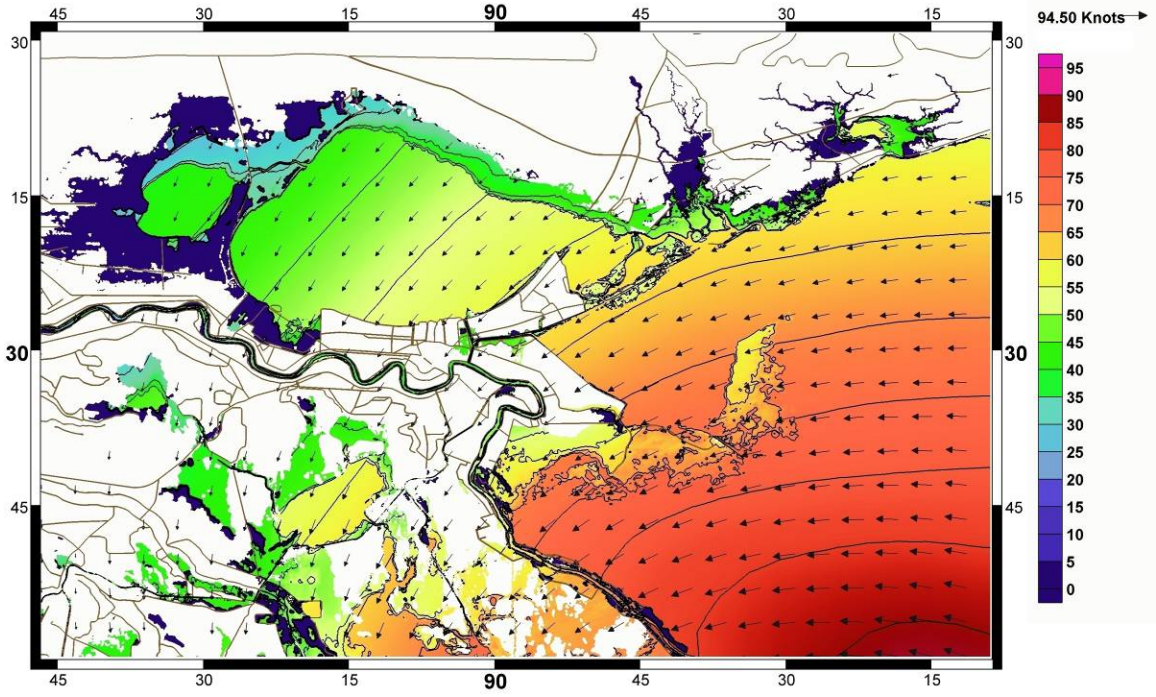


Figure 105: ADCIRC contour map of the wind speed (knots) and wind vectors (knots) for Hurricane Katrina at 10:00 UTC on August 29, 2005 for the area around New Orleans and Lake Pontchartrain.

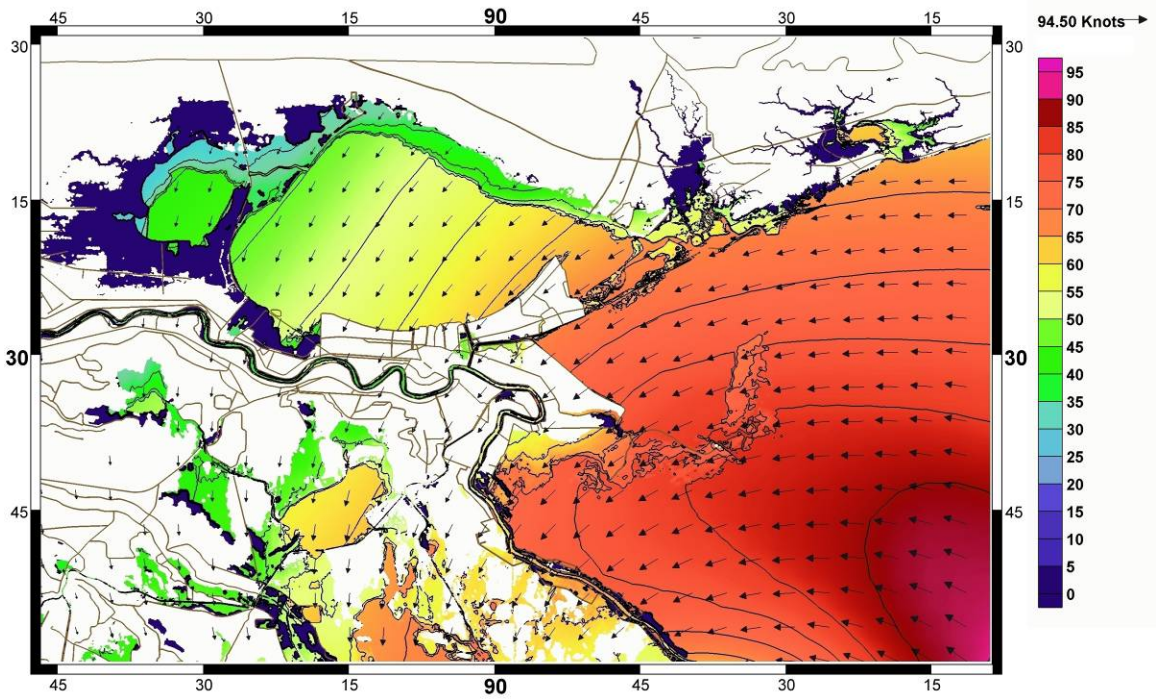


Figure 106: ADCIRC contour map of the wind speed (knots) and wind vectors (knots) for Hurricane Katrina at 11:00 UTC on August 29, 2005 for the area around New Orleans and Lake Pontchartrain.

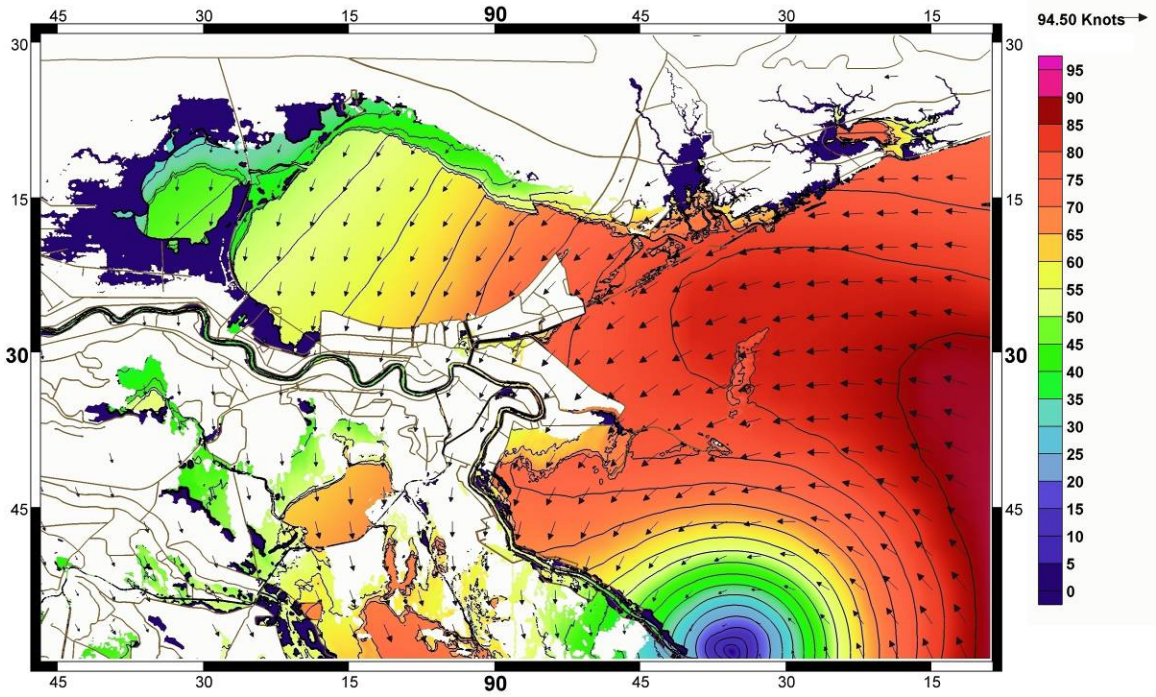


Figure 107: ADCIRC contour map of the wind speed (knots) and wind vectors (knots) for Hurricane Katrina at 12:00 UTC on August 29, 2005 for the area around New Orleans and Lake Pontchartrain.

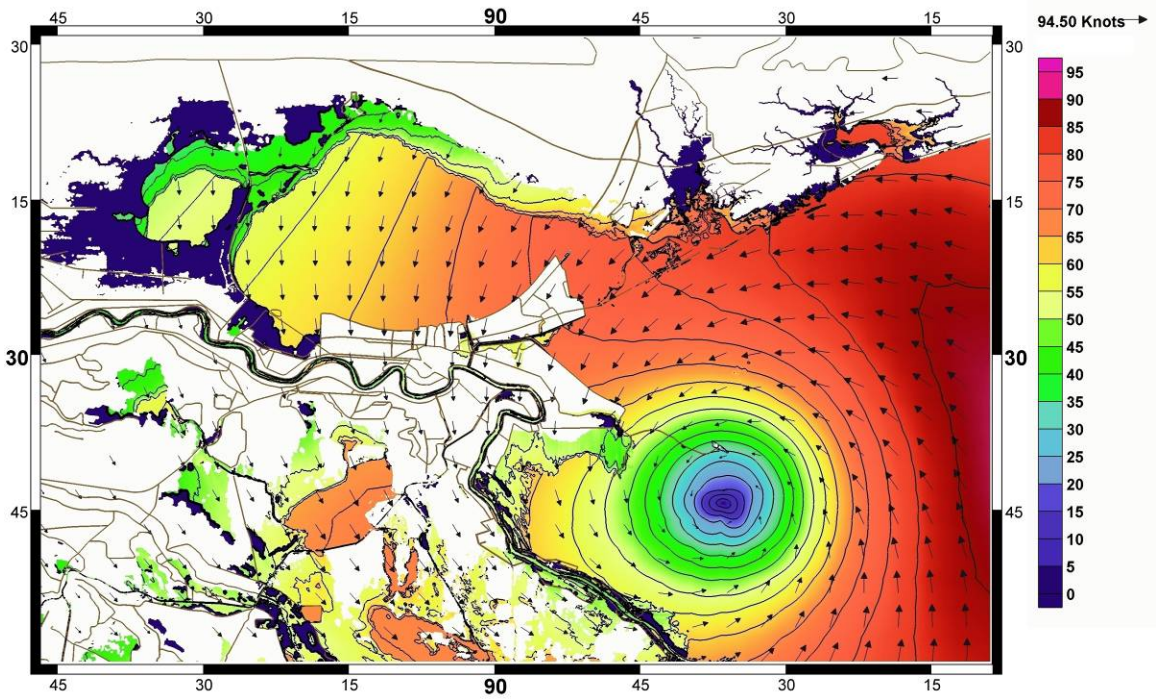


Figure 108: ADCIRC contour map of the wind speed (knots) and wind vectors (knots) for Hurricane Katrina at 13:00 UTC on August 29, 2005 for the area around New Orleans and Lake Pontchartrain.

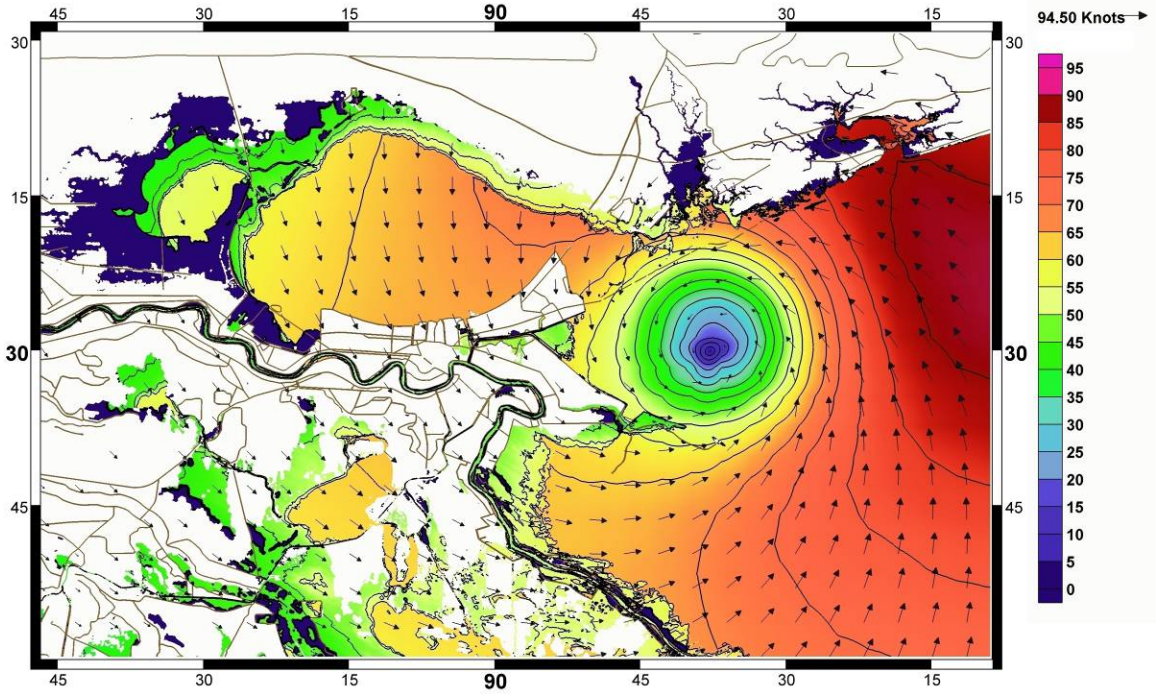


Figure 109: ADCIRC contour map of the wind speed (knots) and wind vectors (knots) for Hurricane Katrina at 14:00 UTC on August 29, 2005 for the area around New Orleans and Lake Pontchartrain.

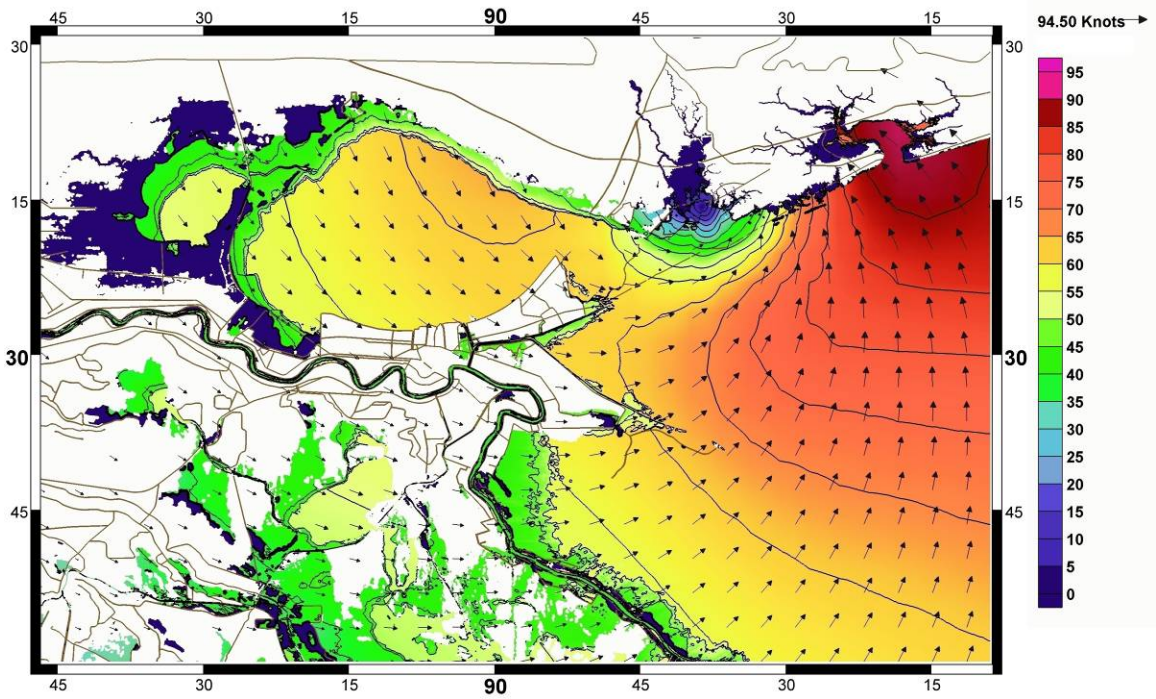


Figure 110: ADCIRC contour map of the wind speed (knots) and wind vectors (knots) for Hurricane Katrina at 15:00 UTC on August 29, 2005 for the area around New Orleans and Lake Pontchartrain.

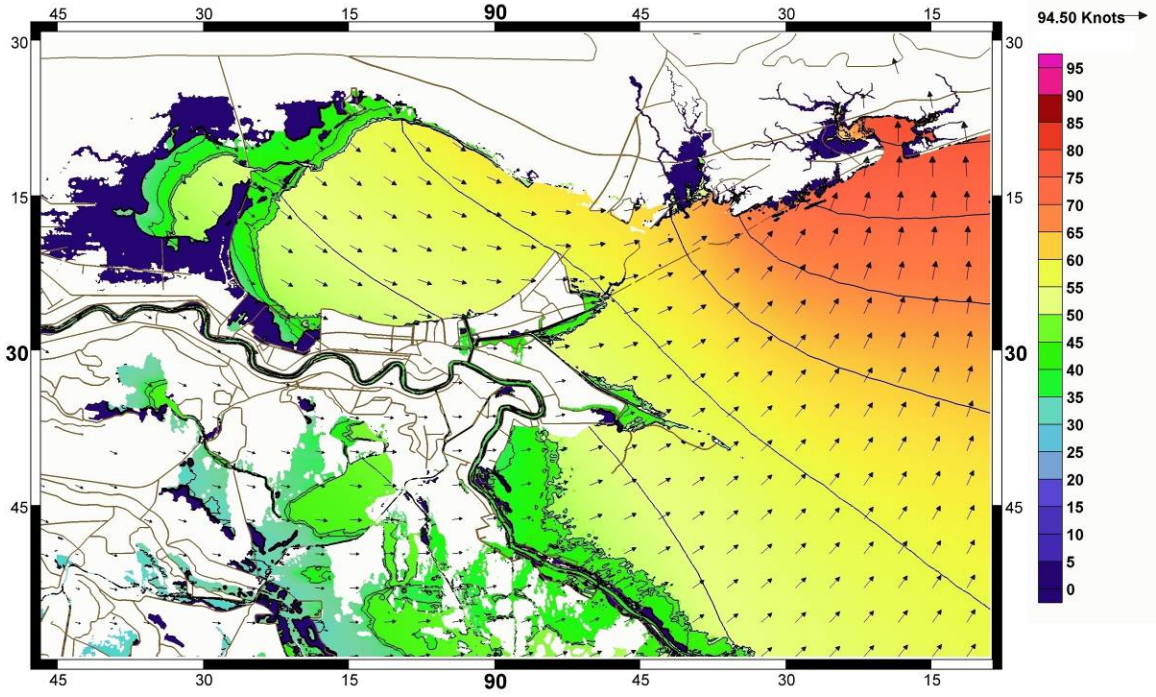


Figure 111: ADCIRC contour map of the wind speed (knots) and wind vectors (knots) for Hurricane Katrina at 16:00 UTC on August 29, 2005 for the area around New Orleans and Lake Pontchartrain.

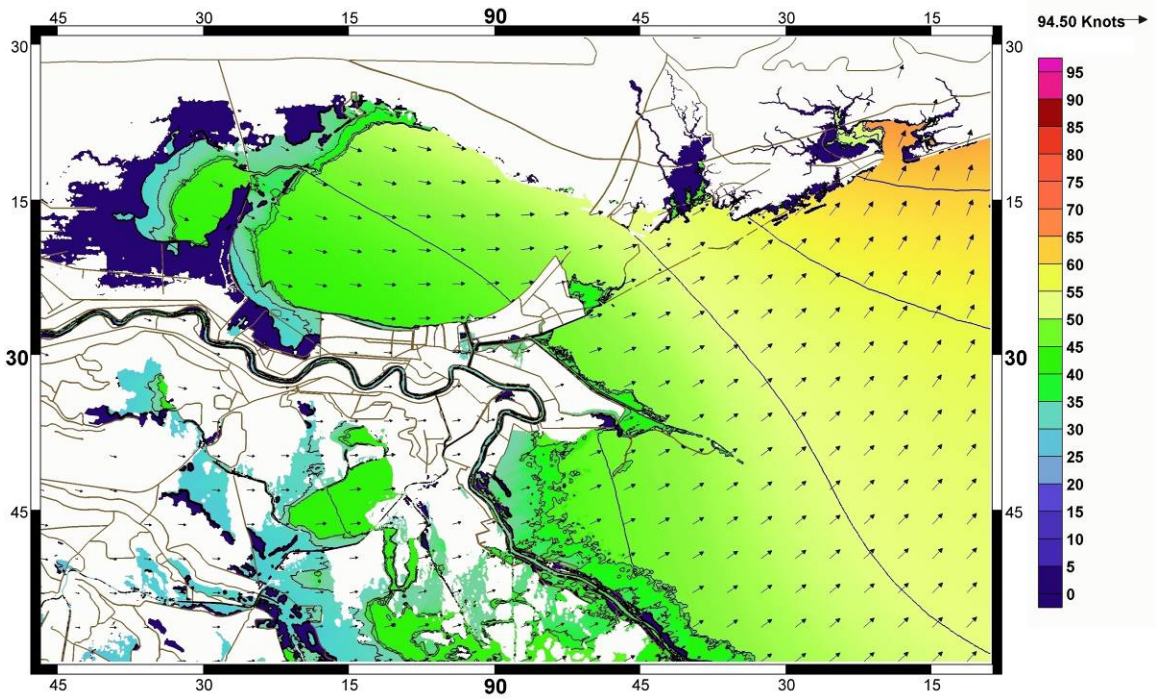


Figure 112: ADCIRC contour map of the wind speed (knots) and wind vectors (knots) for Hurricane Katrina at 17:00 UTC on August 29, 2005 for the area around New Orleans and Lake Pontchartrain.

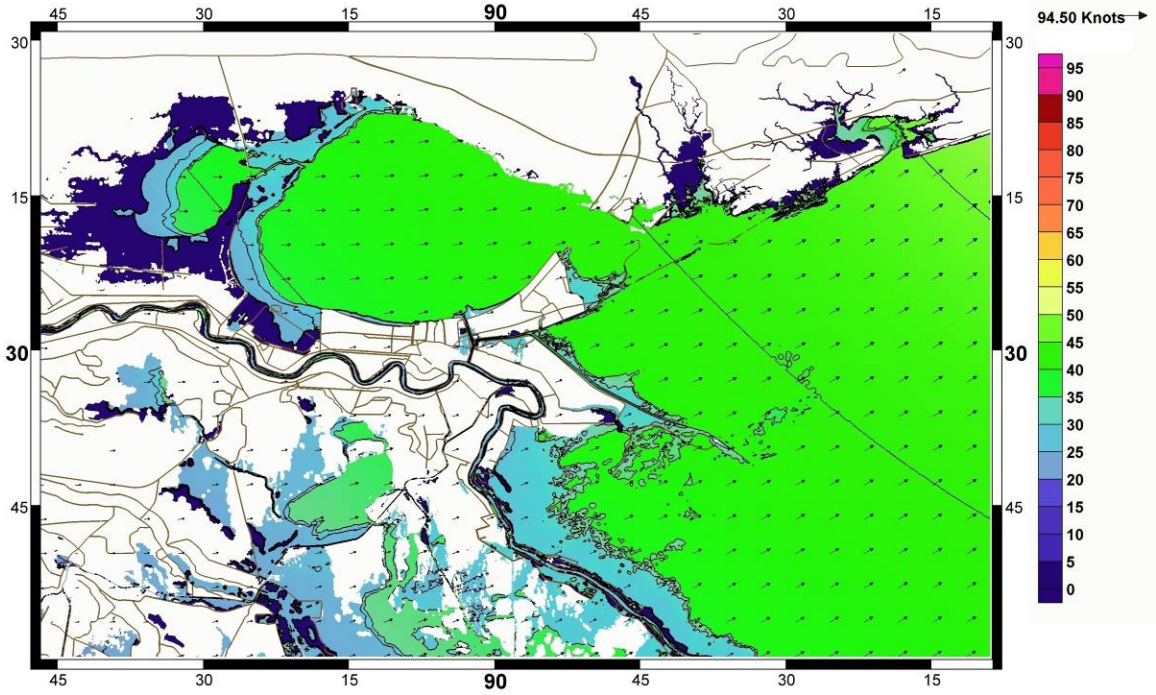


Figure 113: ADCIRC contour map of the wind speed (knots) and wind vectors (knots) for Hurricane Katrina at 20:00 UTC on August 29, 2005 for the area around New Orleans and Lake Pontchartrain.

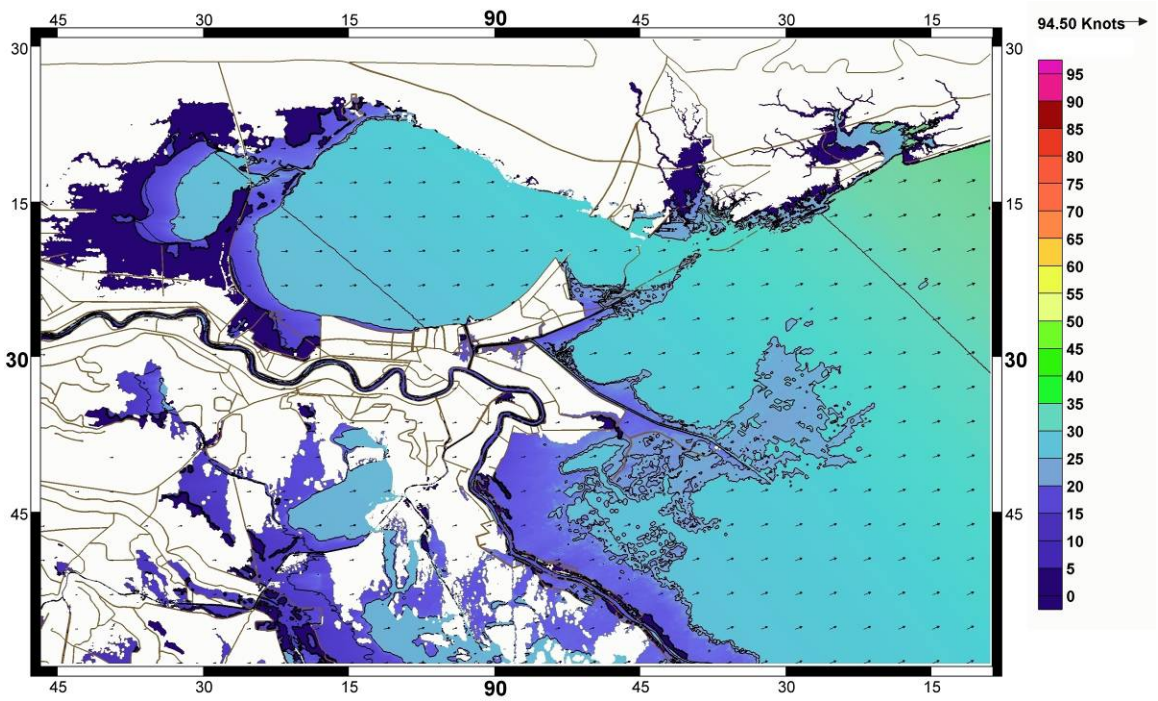


Figure 114: ADCIRC contour map of the wind speed (knots) and wind vectors (knots) for Hurricane Katrina at 23:00 UTC on August 29, 2005 for the area around New Orleans and Lake Pontchartrain

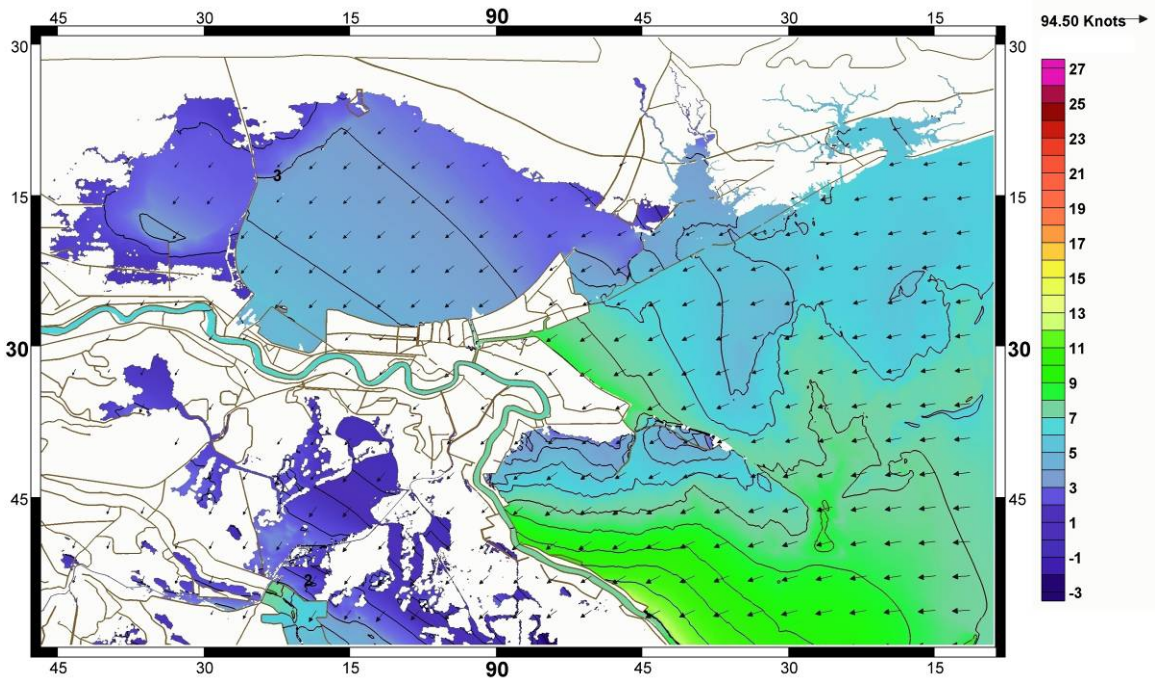


Figure 115: ADCIRC elevation contours (ft) and wind vectors (knots) for Hurricane Katrina at 7:00 UTC on August 29, 2005 for the area around New Orleans and Lake Pontchartrain.

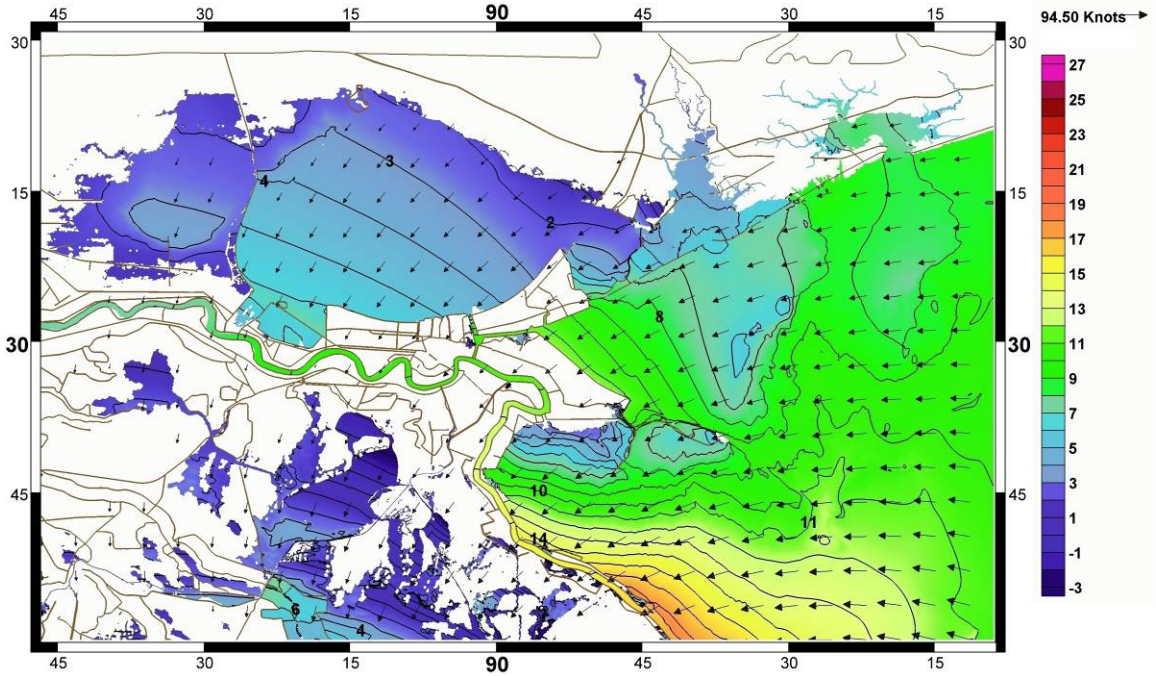


Figure 116: ADCIRC elevation contours (ft) and wind vectors (knots) for Hurricane Katrina at 10:00 UTC on August 29, 2005 for the area around New Orleans and Lake Pontchartrain.

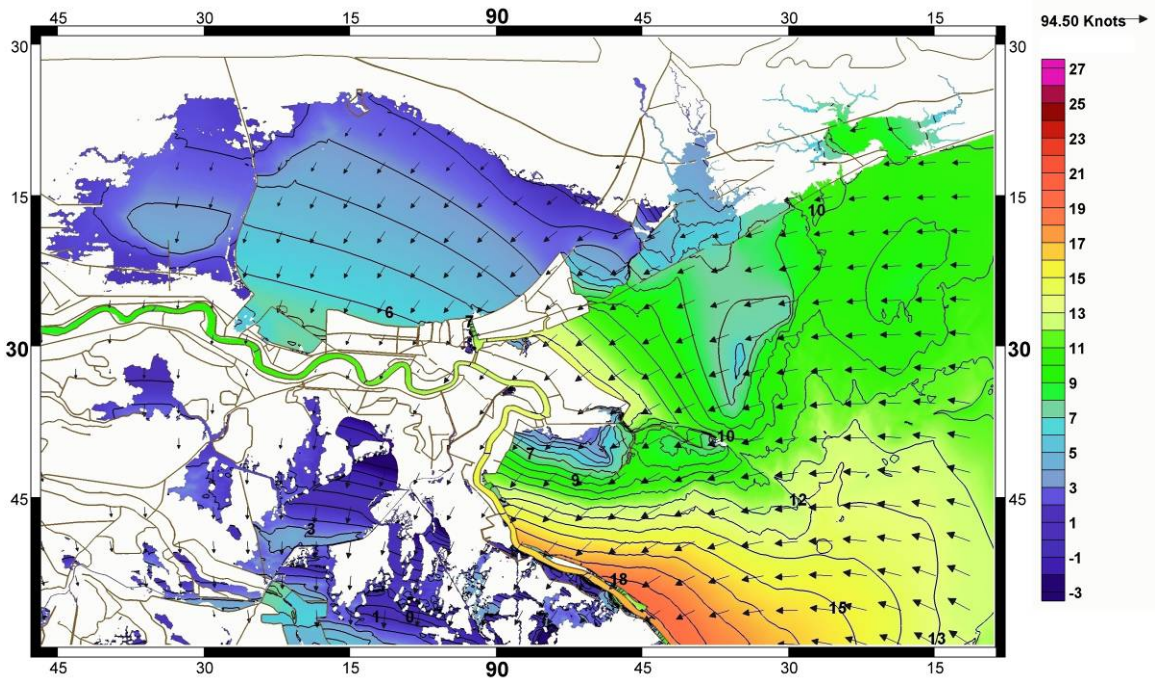


Figure 117: ADCIRC elevation contours (ft) and wind vectors (knots) for Hurricane Katrina at 11:00 UTC on August 29, 2005 for the area around New Orleans and Lake Pontchartrain.

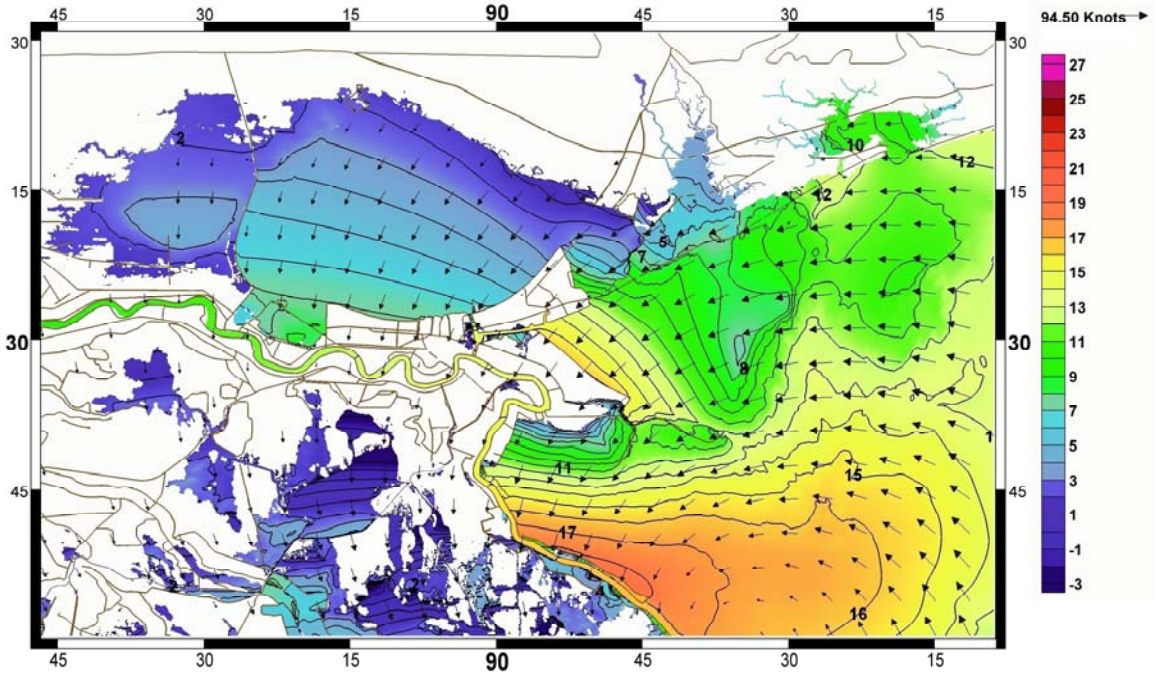


Figure 118: ADCIRC elevation contours (ft) and wind vectors (knots) for Hurricane Katrina at 12:00 UTC on August 29, 2005 for the area around New Orleans and Lake Pontchartrain.

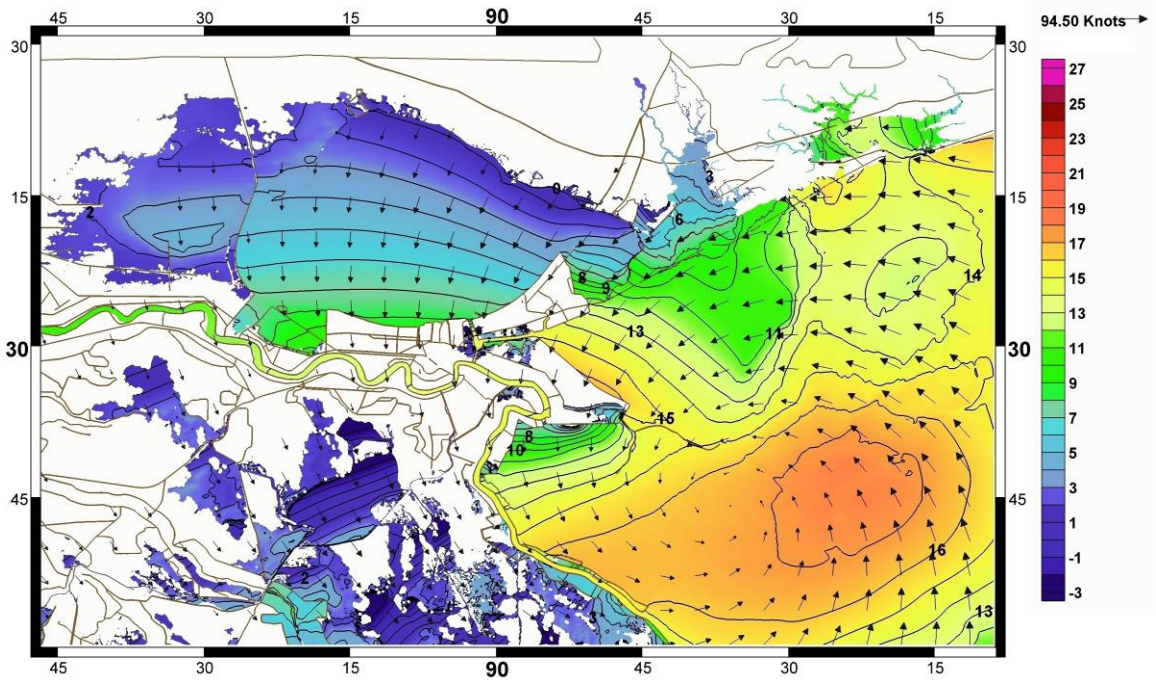


Figure 119: ADCIRC elevation contours (ft) and wind vectors (knots) for Hurricane Katrina at 13:00 UTC on August 29, 2005 for the area around New Orleans and Lake Pontchartrain.

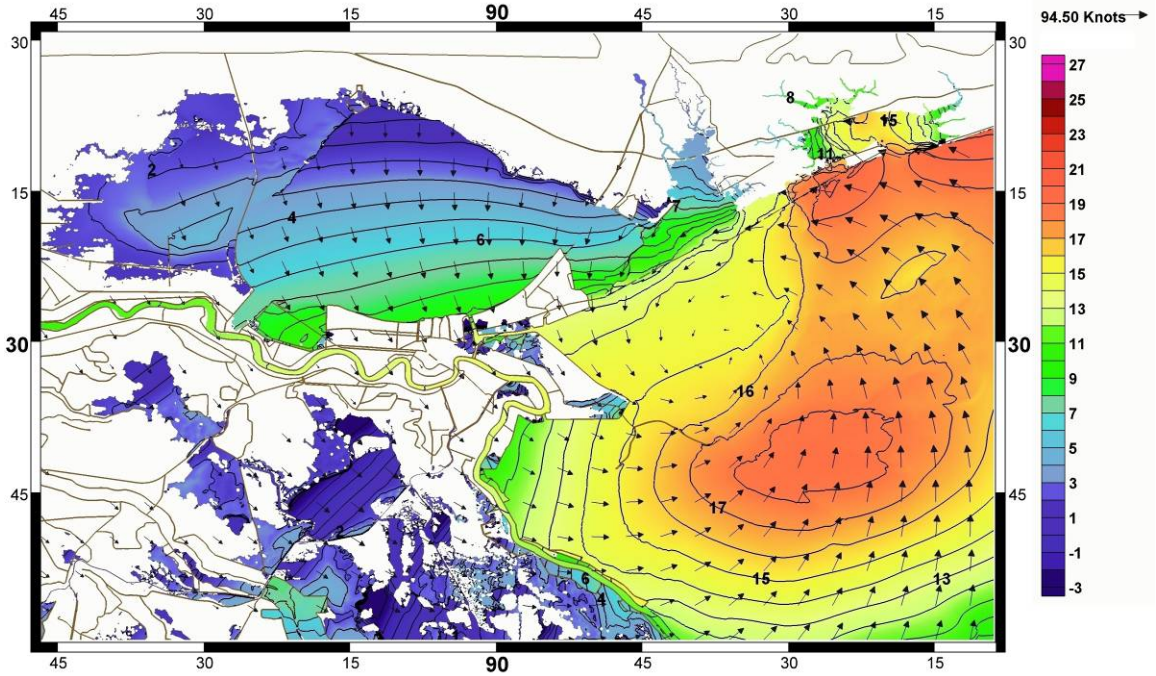


Figure 120: ADCIRC elevation contours (ft) and wind vectors (knots) for Hurricane Katrina at 14:00 UTC on August 29, 2005 for the area around New Orleans and Lake Pontchartrain.

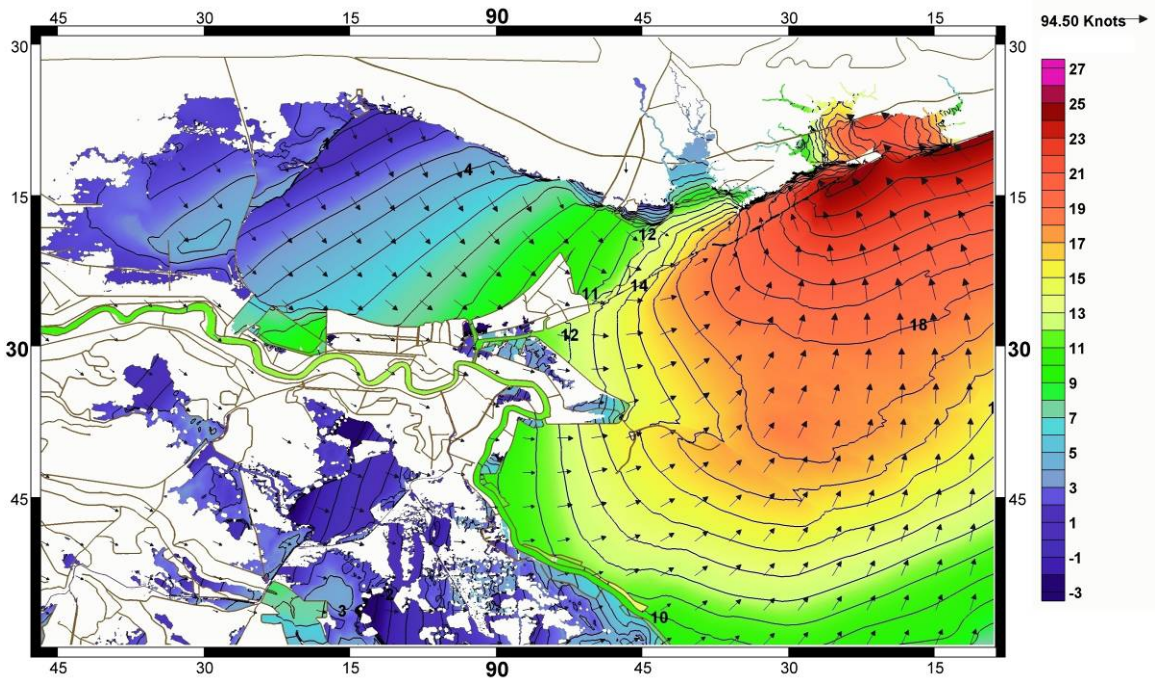


Figure 121: ADCIRC elevation contours (ft) and wind vectors (knots) for Hurricane Katrina at 15:00 UTC on August 29, 2005 for the area around New Orleans and Lake Pontchartrain.

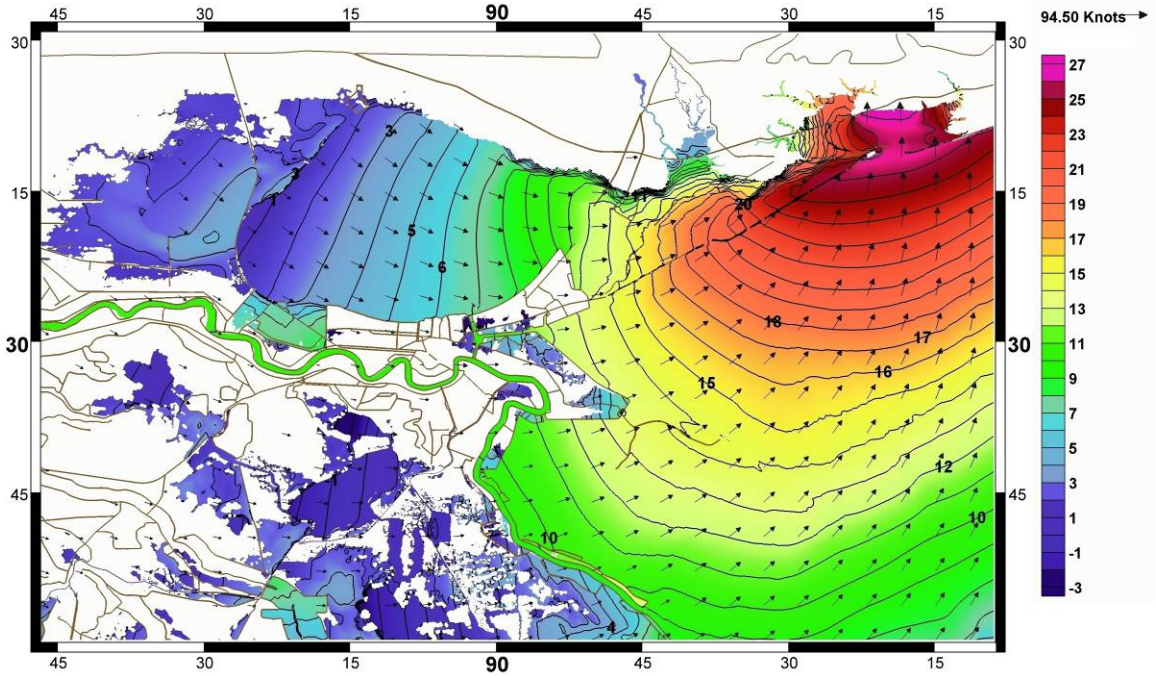


Figure 122: ADCIRC elevation contours (ft) and wind vectors (knots) for Hurricane Katrina at 16:00 UTC on August 29, 2005 for the area around New Orleans and Lake Pontchartrain.

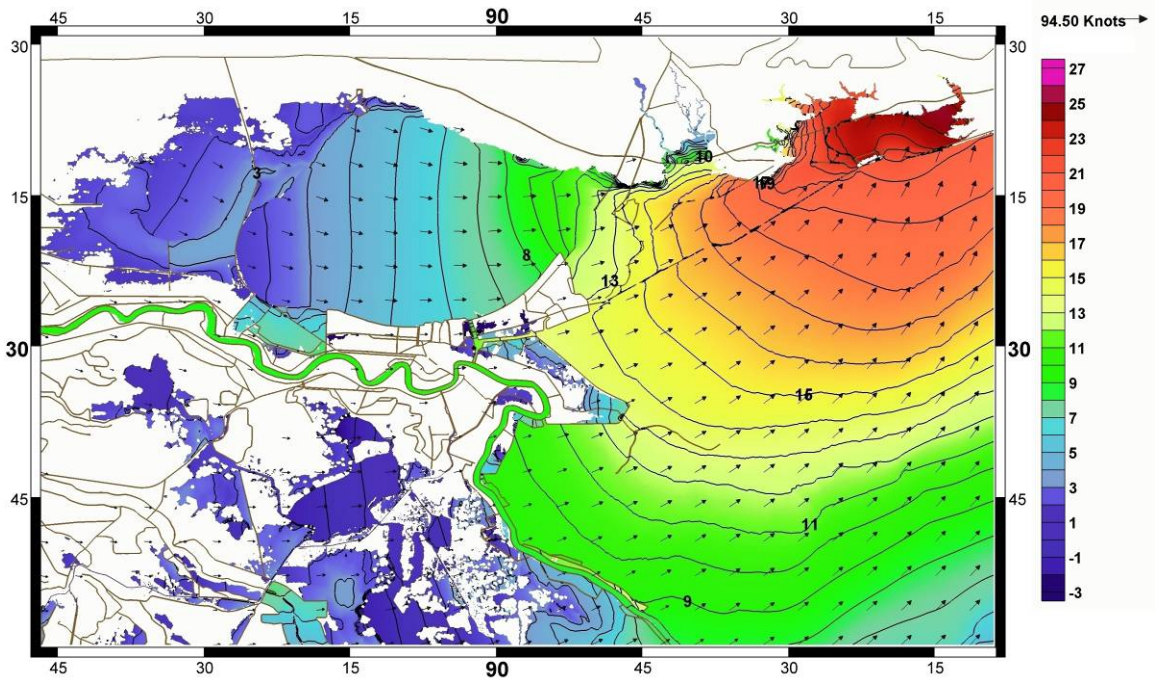


Figure 123: ADCIRC elevation contours (ft) and wind vectors (knots) for Hurricane Katrina at 17:00 UTC on August 29, 2005 for the area around New Orleans and Lake Pontchartrain.

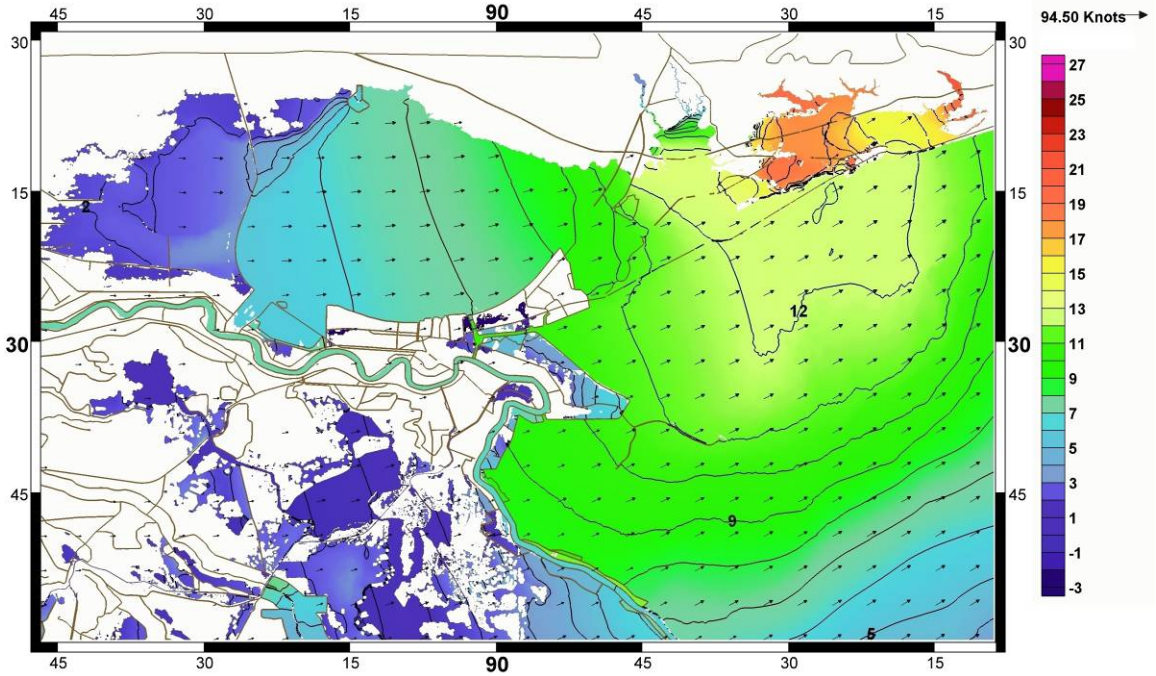


Figure 124: ADCIRC elevation contours (ft) and wind vectors (knots) for Hurricane Katrina at 20:00 UTC on August 29, 2005 for the area around New Orleans and Lake Pontchartrain.

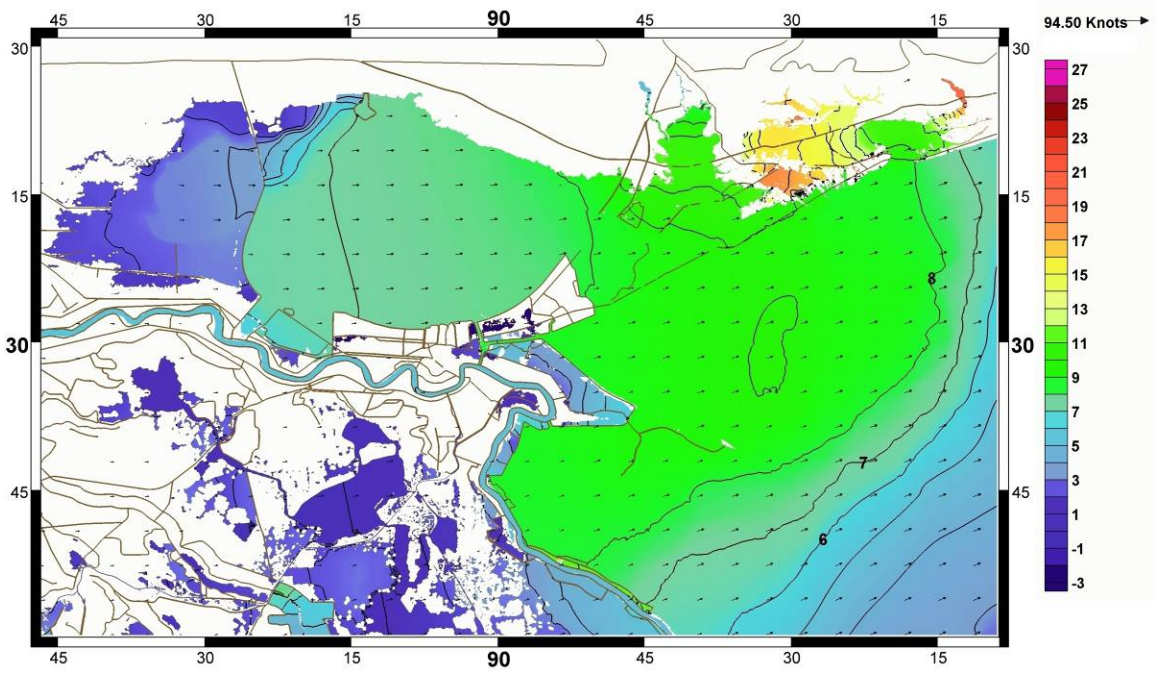


Figure 125: ADCIRC elevation contours (ft) and wind vectors (knots) for Hurricane Katrina at 23:00 UTC on August 29, 2005 for the area around New Orleans and Lake Pontchartrain.

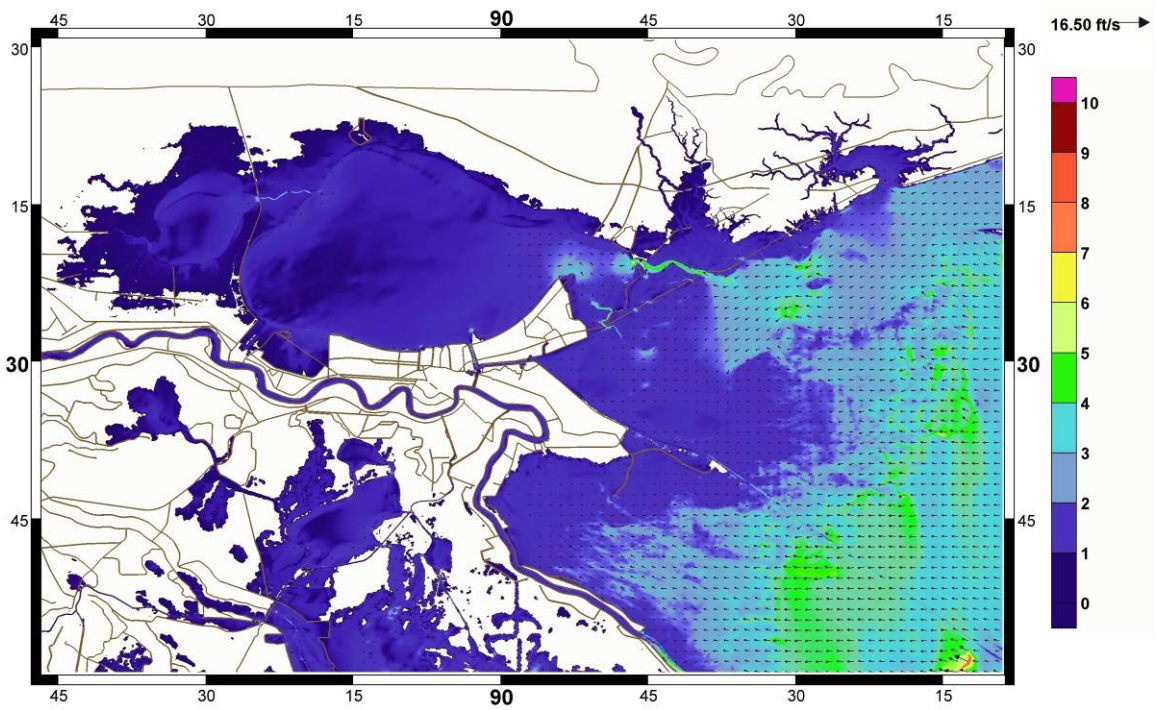


Figure 126: ADCIRC current contours (ft/sec) and current vectors (ft/sec) for Hurricane Katrina at 7:00 UTC on August 29, 2005 for the area around New Orleans and Lake Pontchartrain.

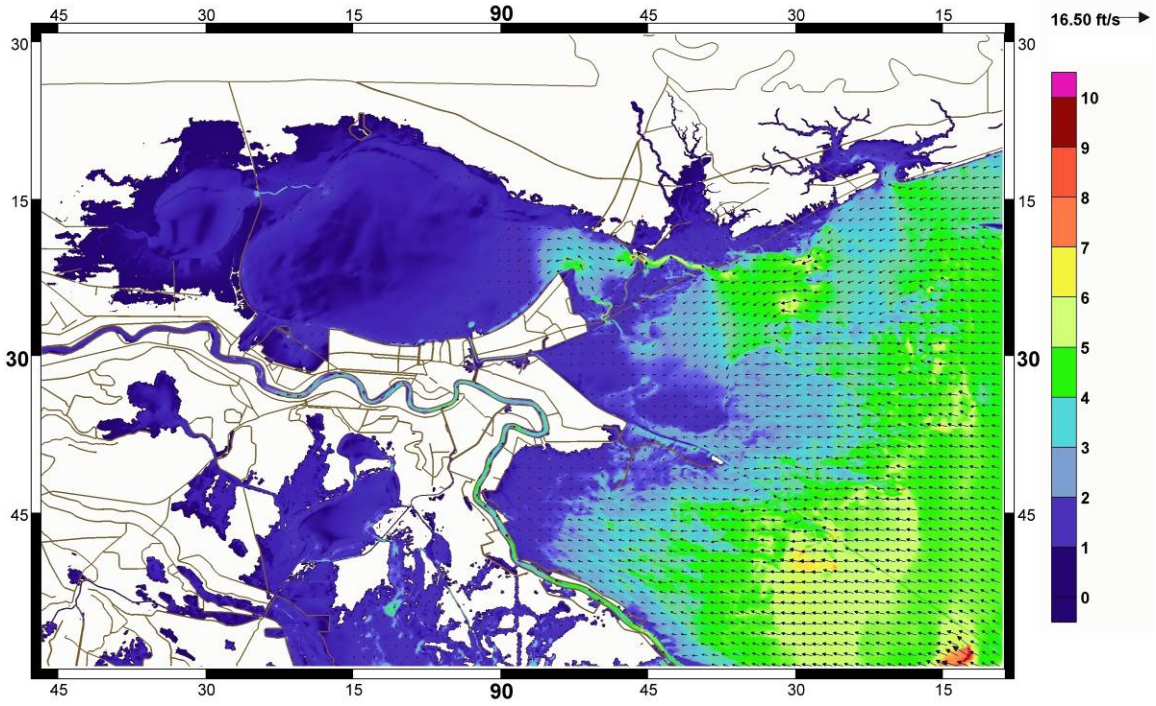


Figure 127: ADCIRC current contours (ft/sec) and current vectors (ft/sec) for Hurricane Katrina at 10:00 UTC on August 29, 2005 for the area around New Orleans and Lake Pontchartrain.

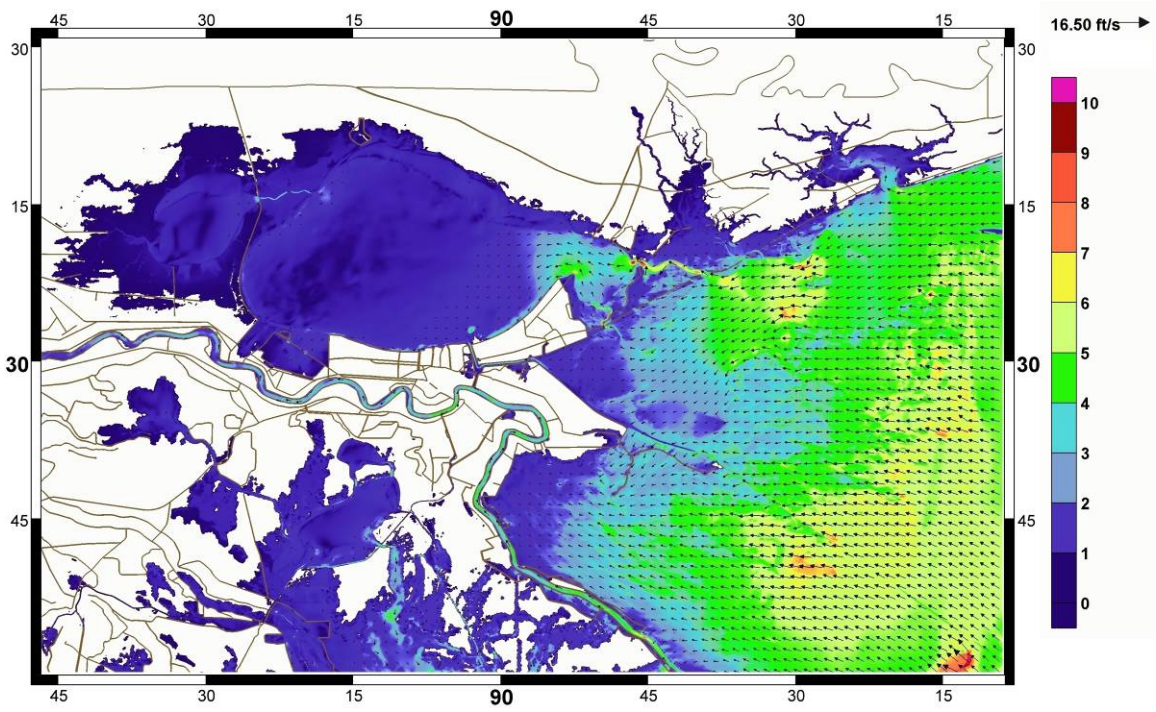


Figure 128: ADCIRC current contours (ft/sec) and current vectors (ft/sec) for Hurricane Katrina at 11:00 UTC on August 29, 2005 for the area around New Orleans and Lake Pontchartrain.

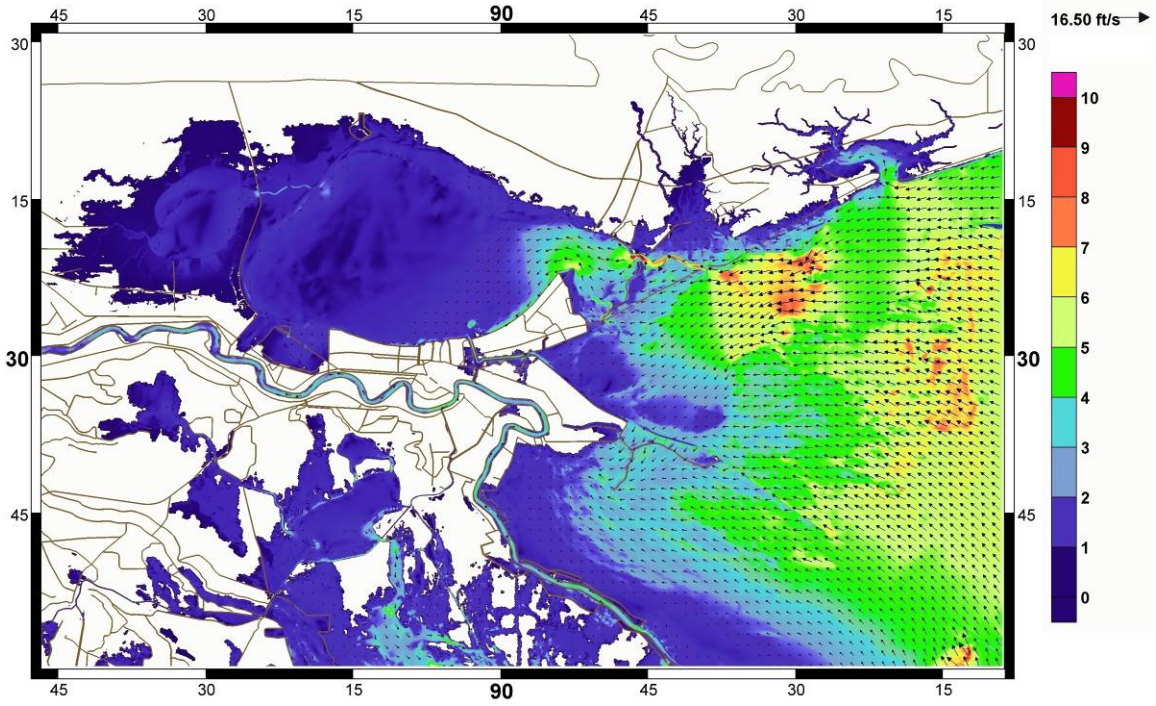


Figure 129: ADCIRC current contours (ft/sec) and current vectors (ft/sec) for Hurricane Katrina at 12:00 UTC on August 29, 2005 for the area around New Orleans and Lake Pontchartrain.

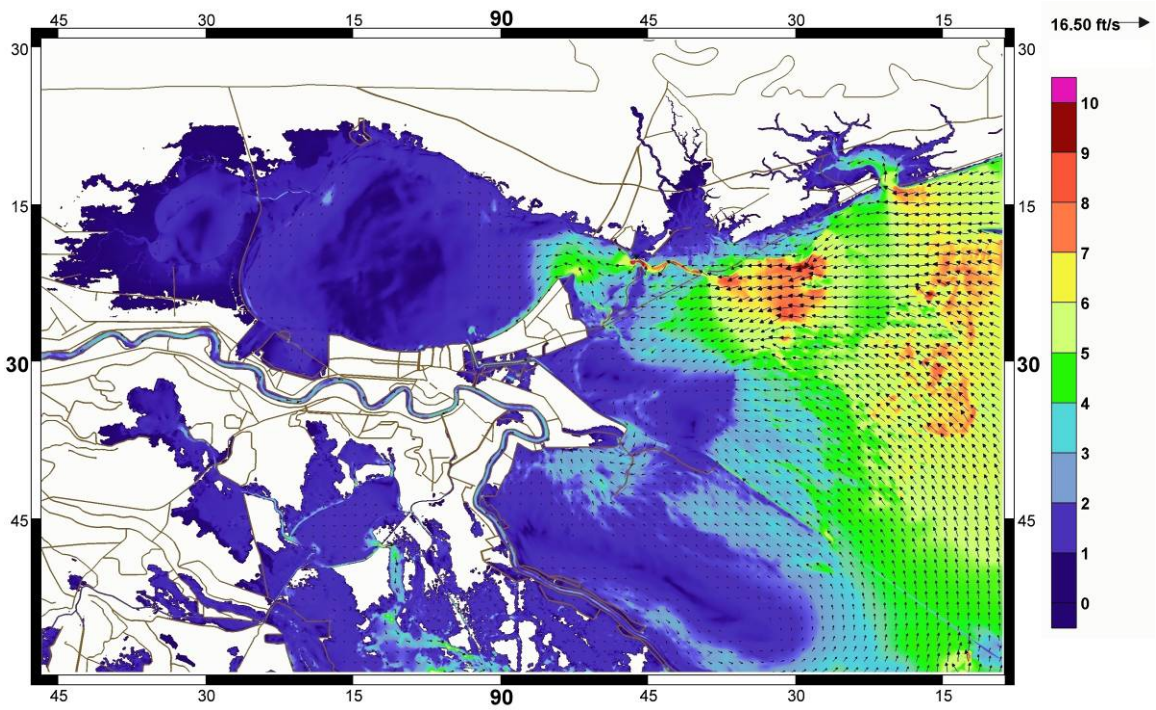


Figure 130: ADCIRC current contours (ft/sec) and current vectors (ft/sec) for Hurricane Katrina at 13:00 UTC on August 29, 2005 for the area around New Orleans and Lake Pontchartrain.

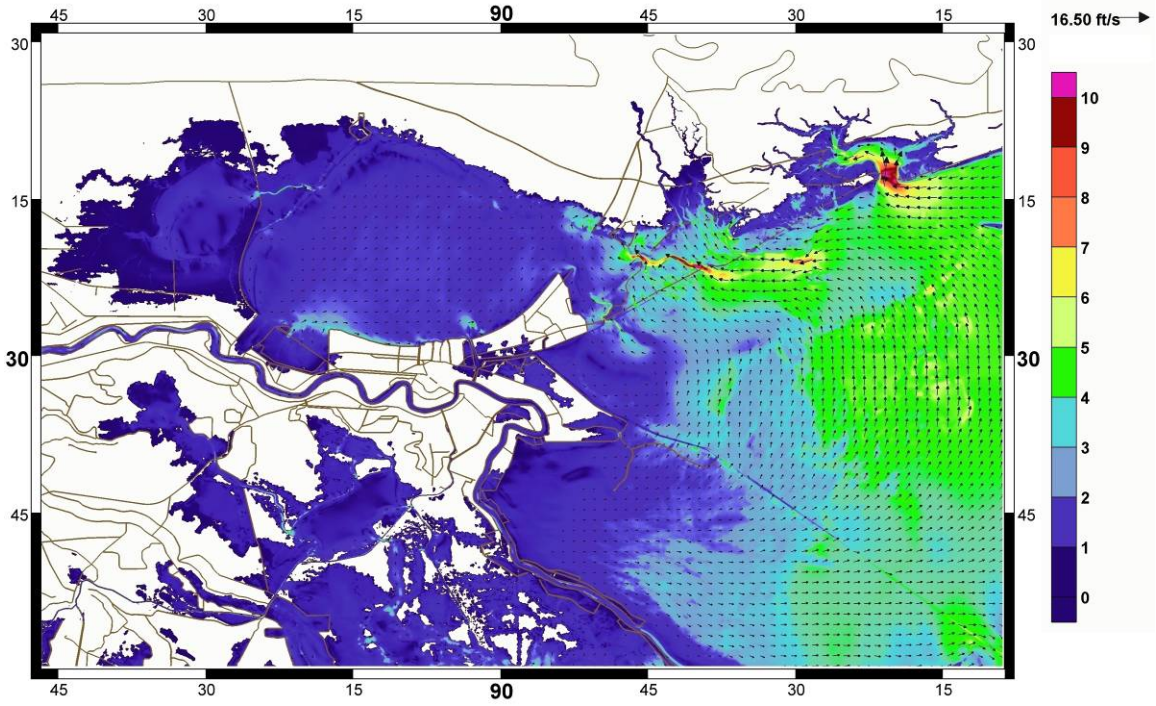


Figure 131: ADCIRC current contours (ft/sec) and current vectors (ft/sec) for Hurricane Katrina at 14:00 UTC on August 29, 2005 for the area around New Orleans and Lake Pontchartrain.

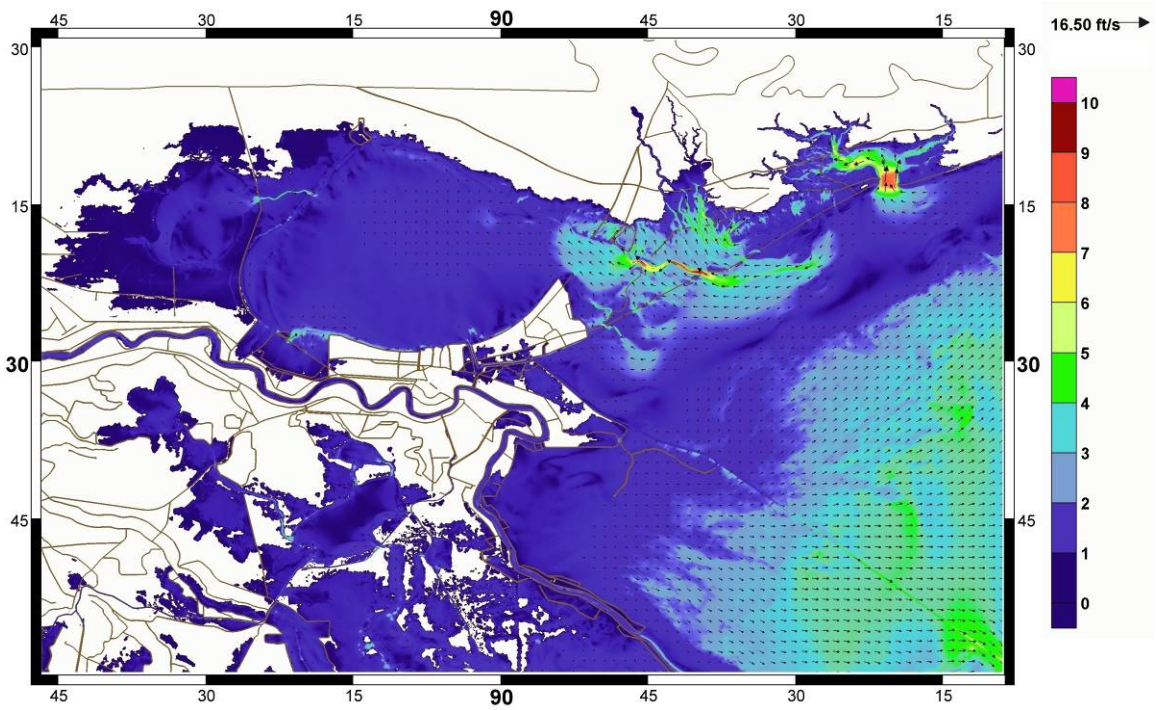


Figure 132: ADCIRC current contours (ft/sec) and current vectors (ft/sec) for Hurricane Katrina at 15:00 UTC on August 29, 2005 for the area around New Orleans and Lake Pontchartrain.

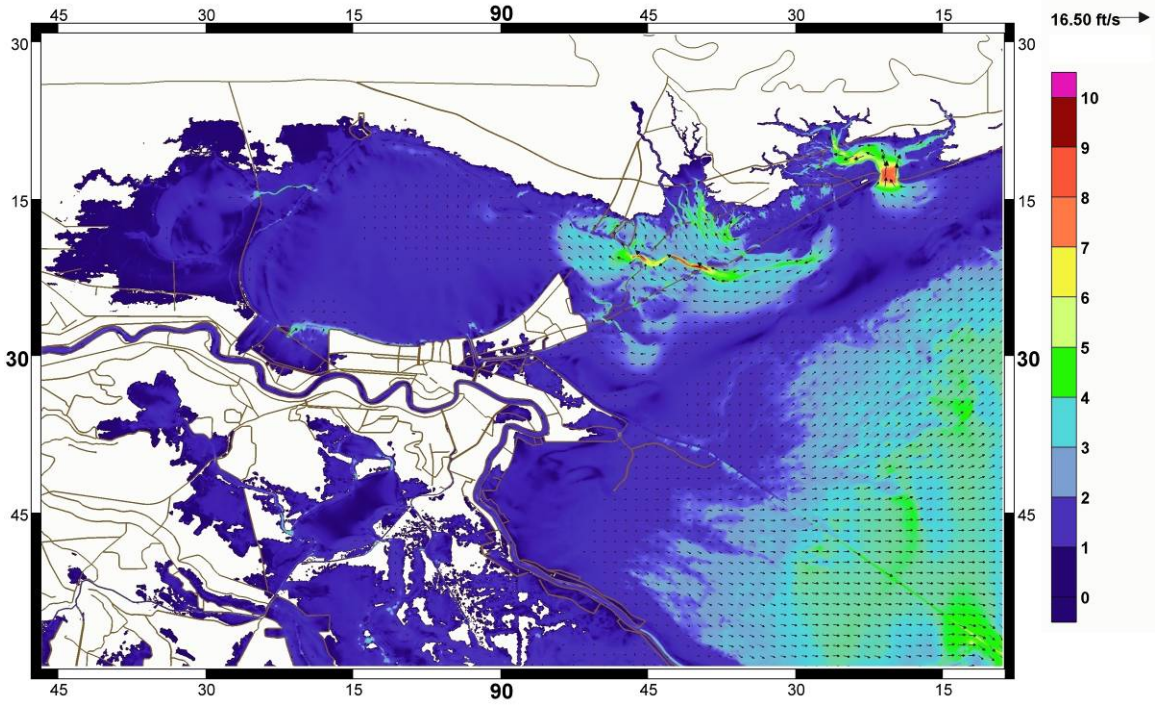


Figure 133: ADCIRC current contours (ft/sec) and current vectors (ft/sec) for Hurricane Katrina at 16:00 UTC on August 29, 2005 for the area around New Orleans and Lake Pontchartrain.

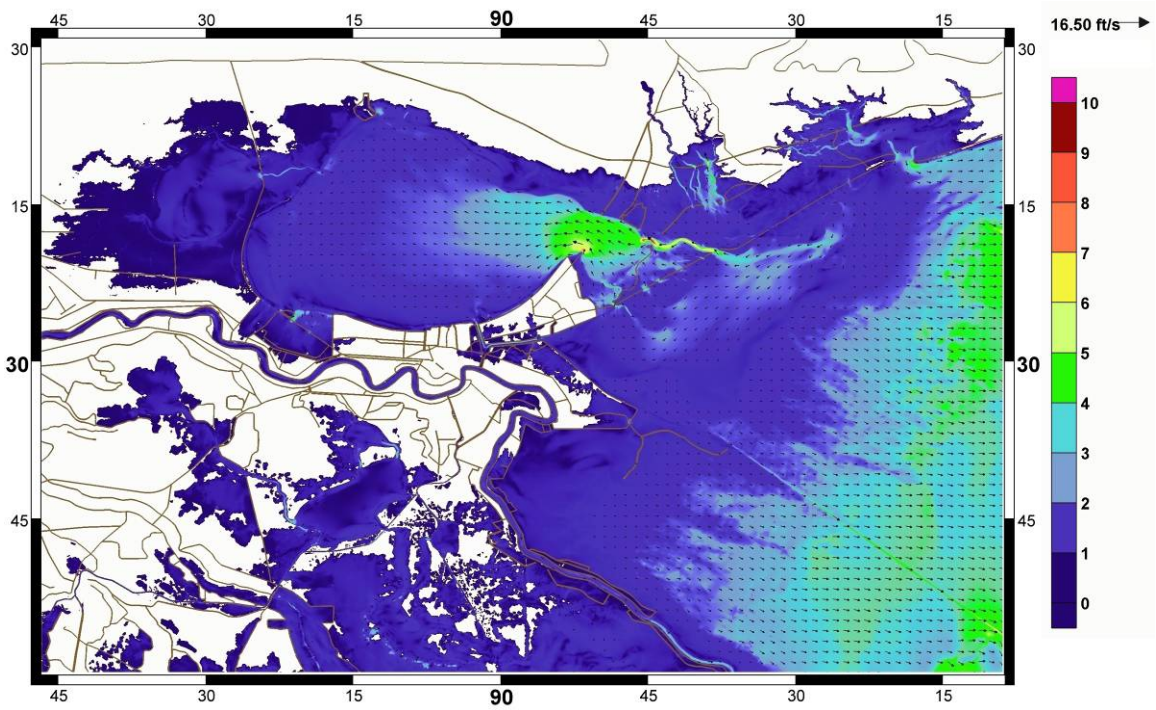


Figure 134: ADCIRC current contours (ft/sec) and current vectors (ft/sec) for Hurricane Katrina at 17:00 UTC on August 29, 2005 for the area around New Orleans and Lake Pontchartrain.

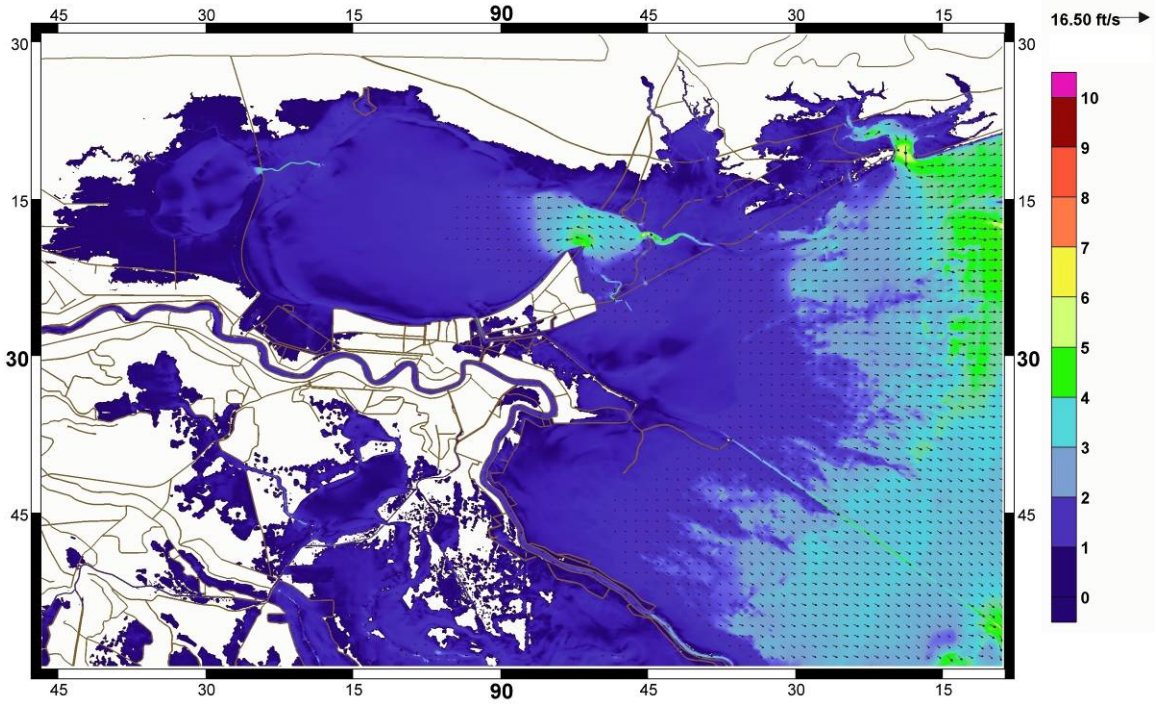


Figure 135: ADCIRC current contours (ft/sec) and current vectors (ft/sec) for Hurricane Katrina at 20:00 UTC on August 29, 2005 for the area around New Orleans and Lake Pontchartrain.

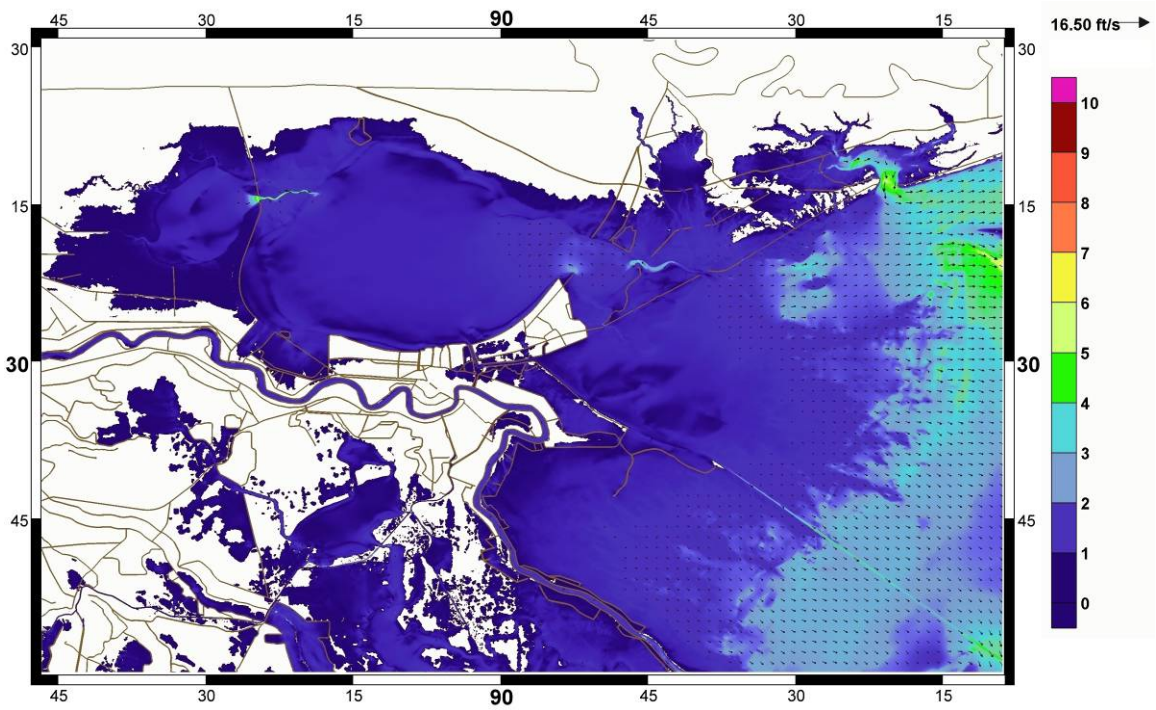


Figure 136: ADCIRC current contours (ft/sec) and current vectors (ft/sec) for Hurricane Katrina at 23:00 UTC on August 29, 2005 for the area around New Orleans and Lake Pontchartrain.

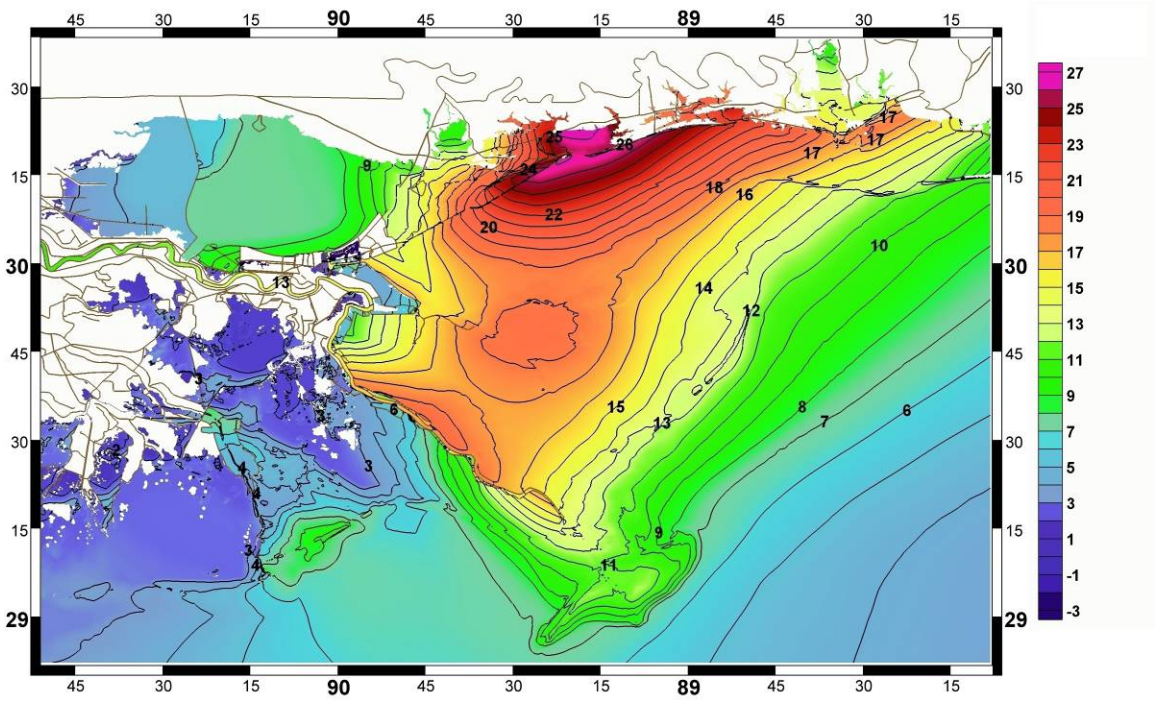


Figure 137: ADCIRC maximum elevation contours (ft) during Hurricane Katrina for Southeastern Louisiana.

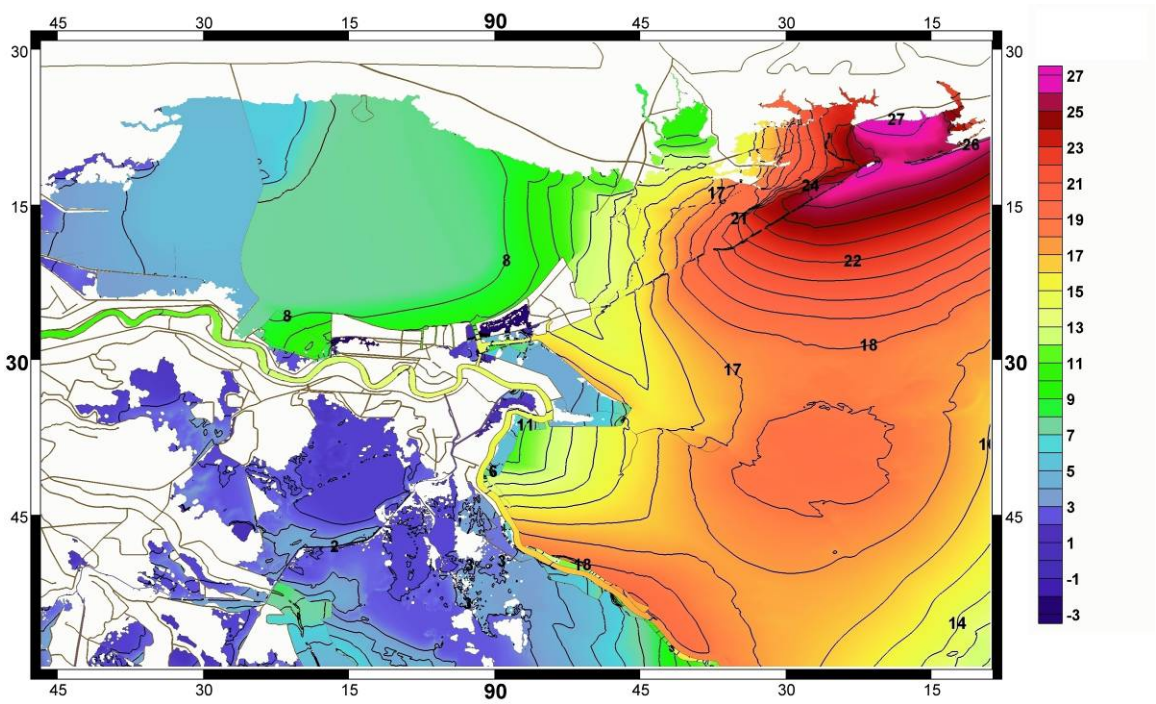


Figure 138: ADCIRC maximum elevation contours (ft) during Hurricane Katrina for the area around New Orleans and Lake Pontchartrain.

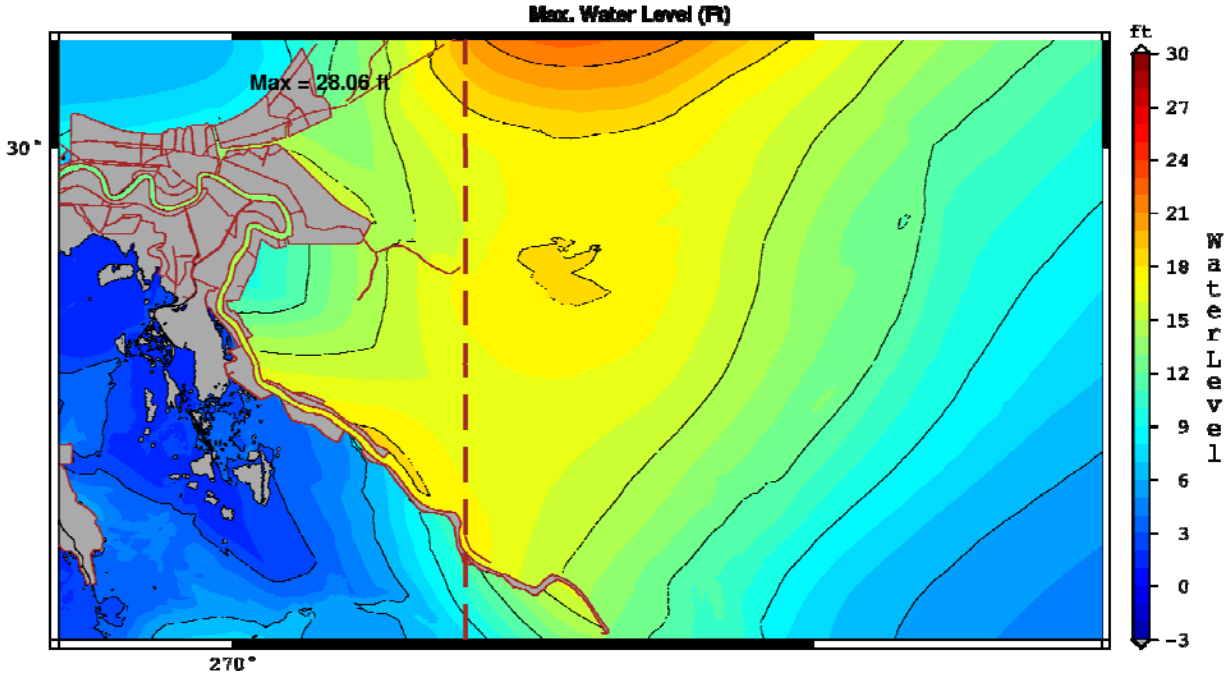


Figure 139: Maximum water surface elevation (ft) in Southeastern Louisiana for the H1 scenario. Brown lines denote raised features. Black lines designate 3 foot contours. The thick brown dashed line represents the storm track.

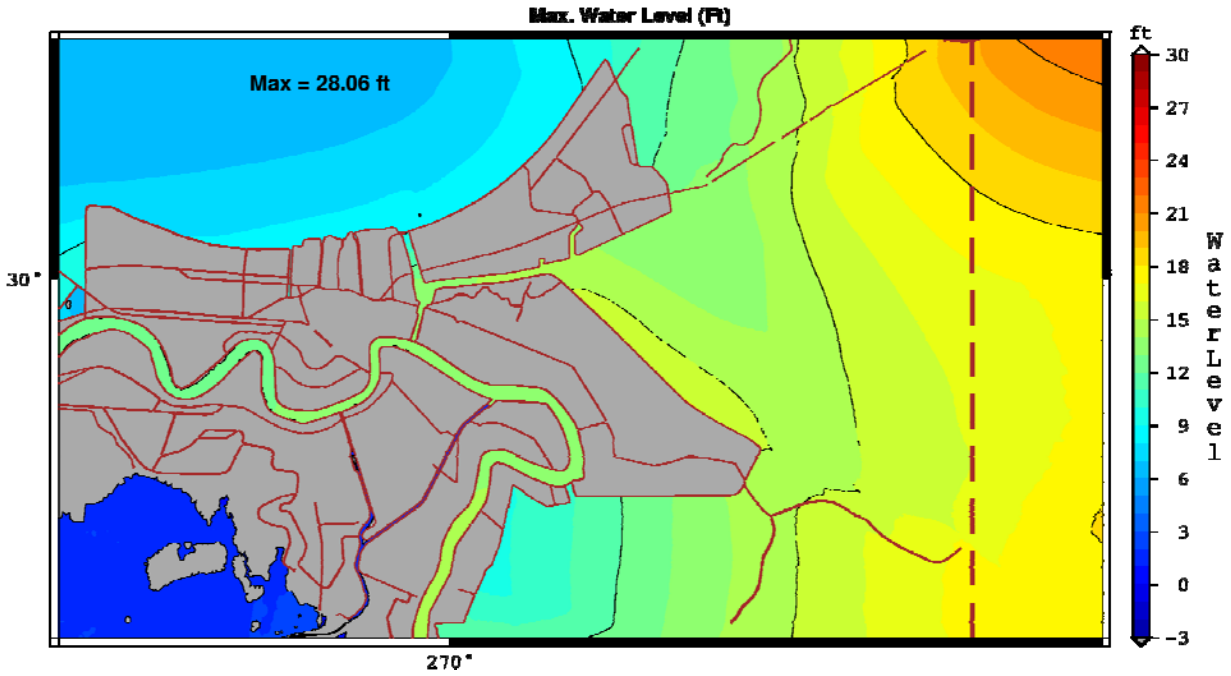


Figure 140: Maximum water surface elevation (ft) in the New Orleans area for the H1 scenario. Brown lines denote raised features. Black lines designate 3 foot contours. The thick brown dashed line represents the storm track.

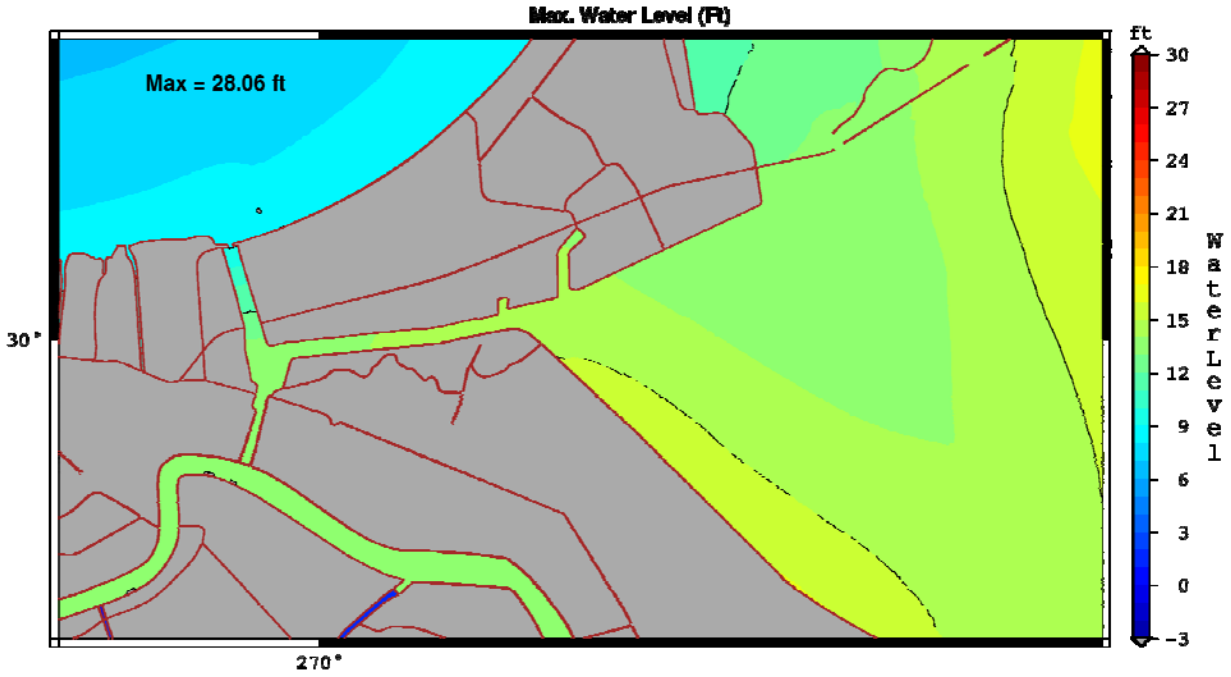


Figure 141: Maximum water surface elevation (ft) in the vicinity of the IHNC for the H1 scenario. Brown lines denote raised features. Black lines designate 3 foot contours.

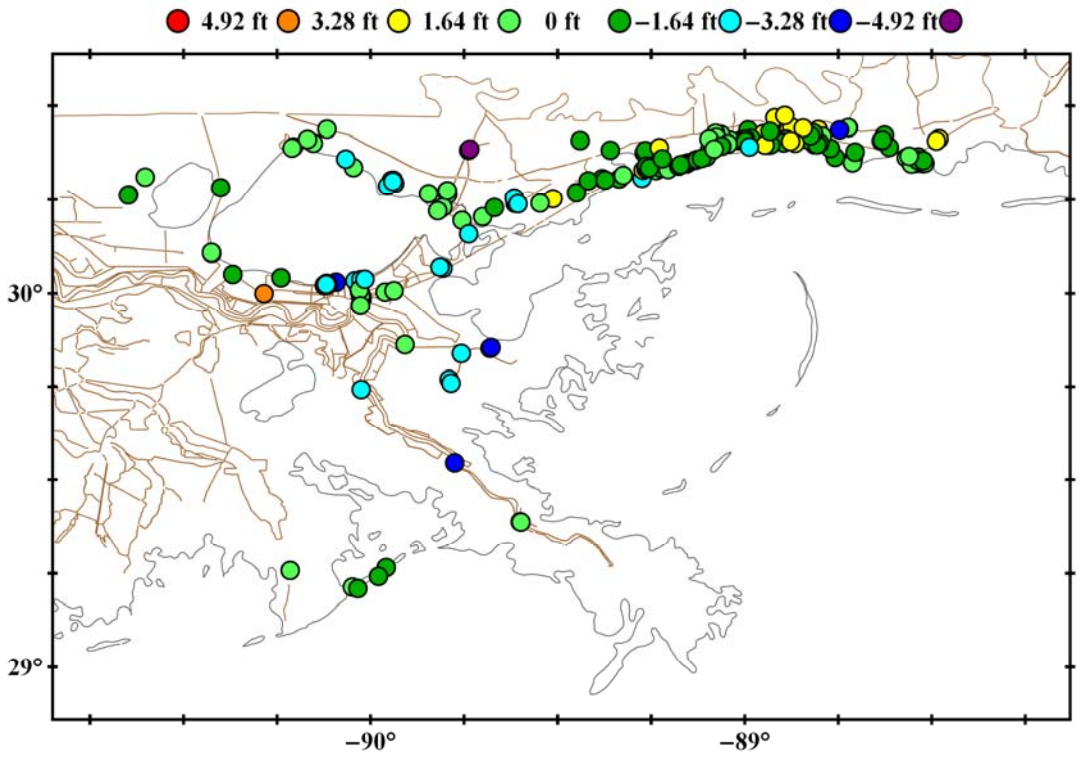


Figure 142: Locations of USACE HWMs for Hurricane Katrina. Colors indicate the difference between the maximum computed water elevation from the ADCIRC SL15 H1 hindcast and the measured HWM. Green and light green points indicate a match within 1.64 ft. Red, orange and light green circles indicate over-predictions by the model; green, blue and dark blue circles indicate under-predictions.

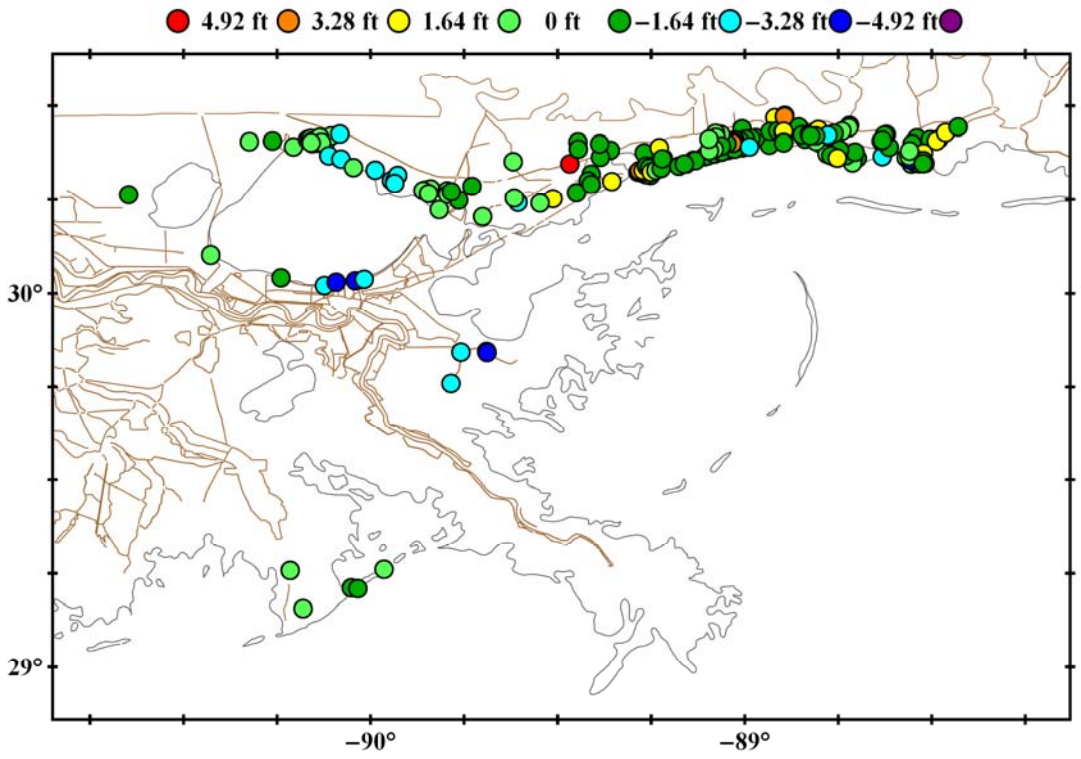


Figure 143: Locations of URS HWMs for Hurricane Katrina. Colors indicate the difference between the maximum computed water elevation from the ADCIRC SL15 Hh1 hindcast and the measured HWM. Green and light green points indicate a match within 1.64 ft. Red, orange and light green circles indicate over-predictions by the model; green, blue and dark blue circles indicate under-predictions.

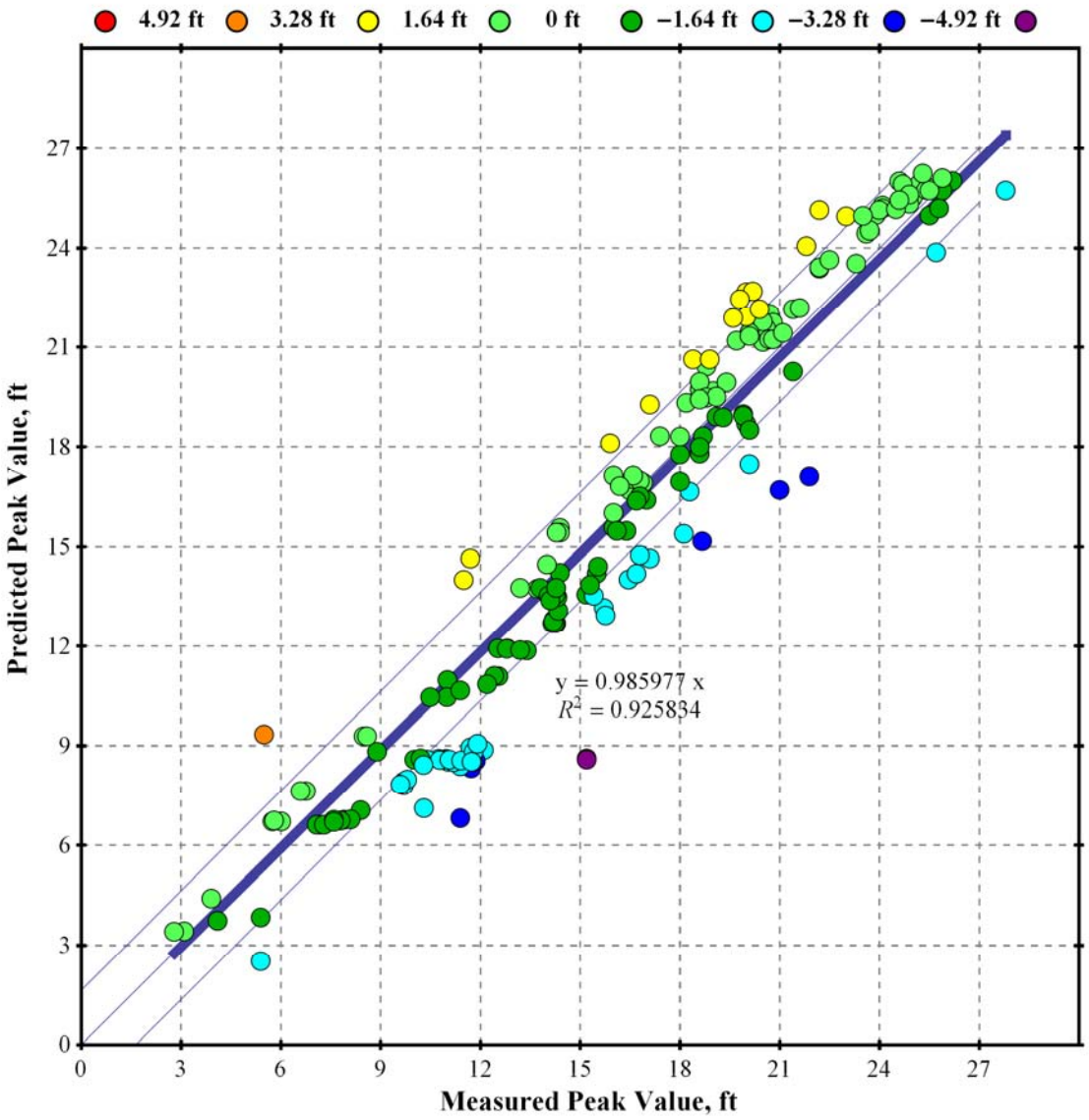


Figure 144: Comparisons between observed USACE high water marks and ADCIRC maximum surges at 206 locations shown in Figure 142. Green and light green points indicate a match within 1.64 ft. Red, orange and light green circles indicate over-predictions by the model; green, blue and dark blue circles indicate under-predictions. The slope of the best-fit line through all points is 0.99 and R^2 value is 0.93.

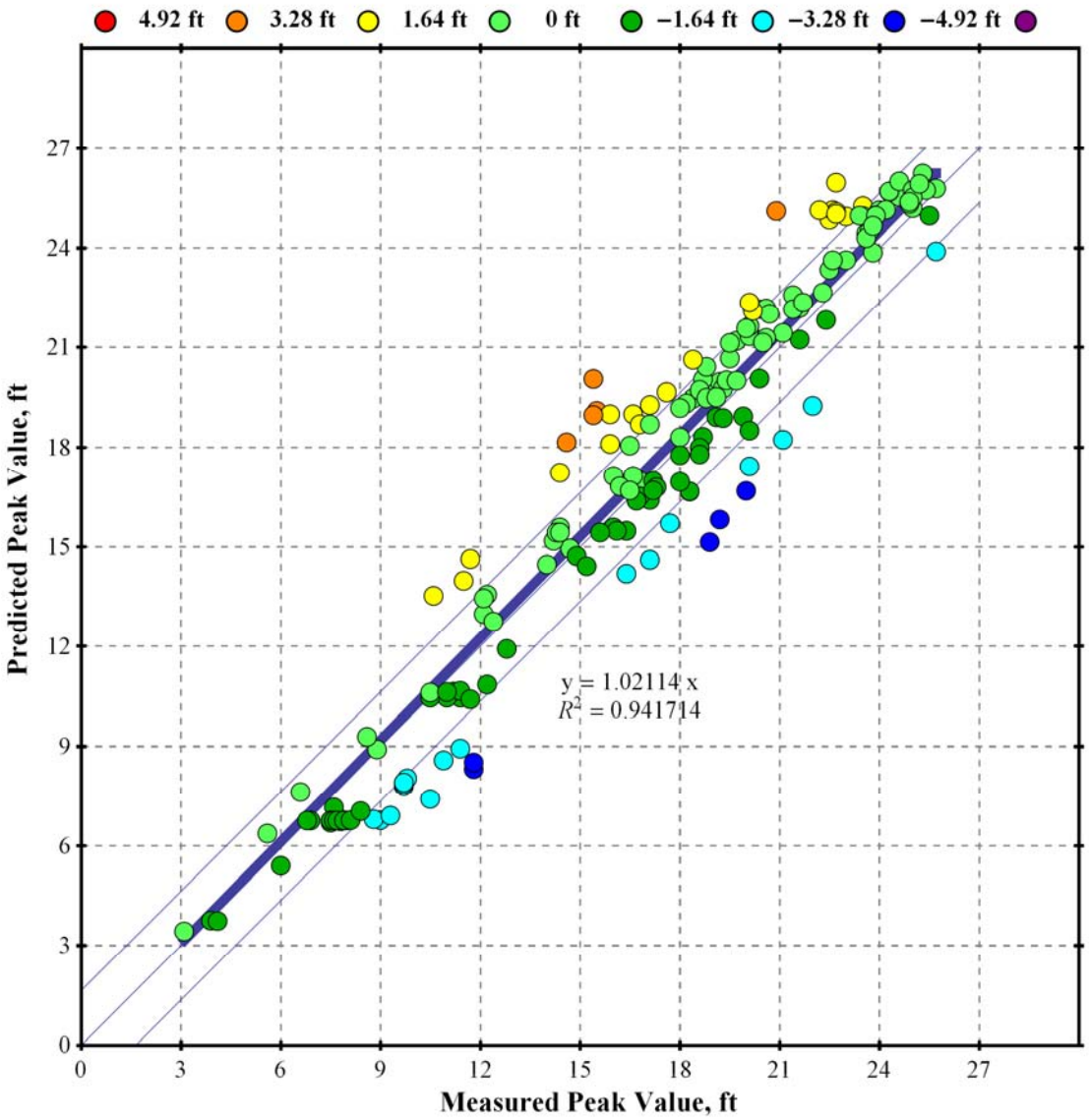


Figure 145: Comparisons between observed URS high water marks and ADCIRC maximum surges at 193 locations shown in Figure 143. Green and light green points indicate a match within 1.64 ft. Red, orange and light green circles indicate over-predictions by the model; green, blue and dark blue circles indicate under-predictions. The slope of the best-fit line through all points is 1.02 and R^2 value is 0.94.

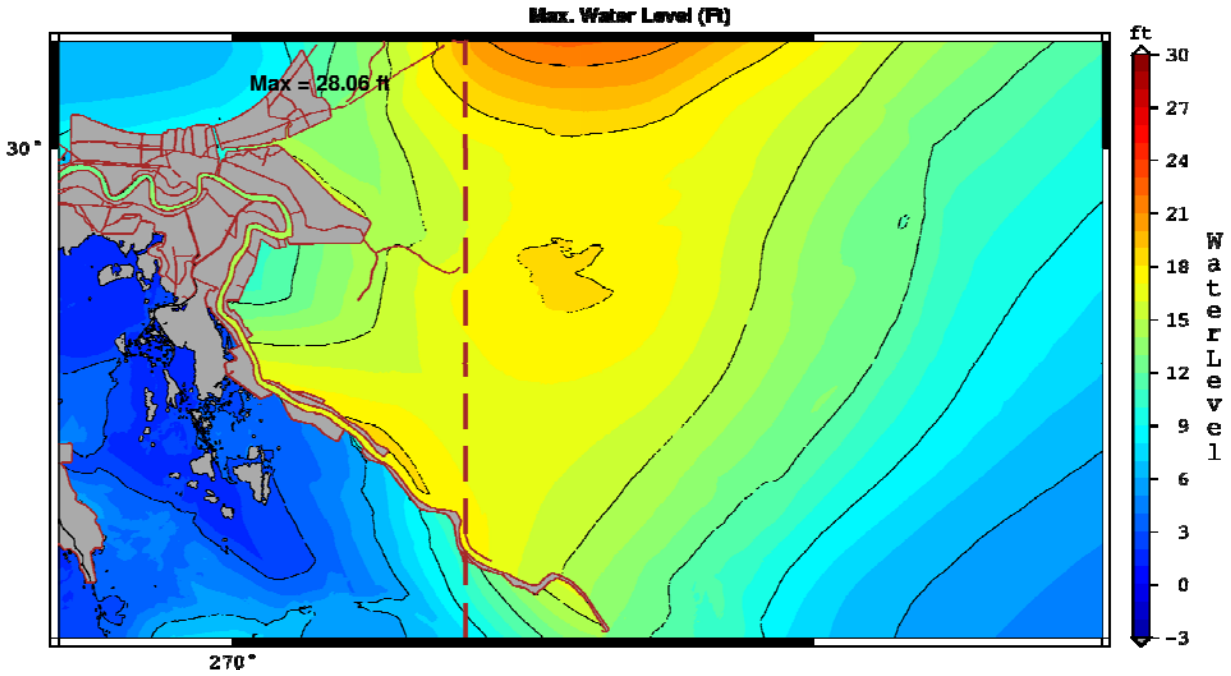


Figure 146: Maximum water surface elevation (ft) in Southeastern Louisiana for the H2 scenario. Brown lines denote raised features. Black lines designate 3 foot contours. The thick brown dashed line represents the storm track.

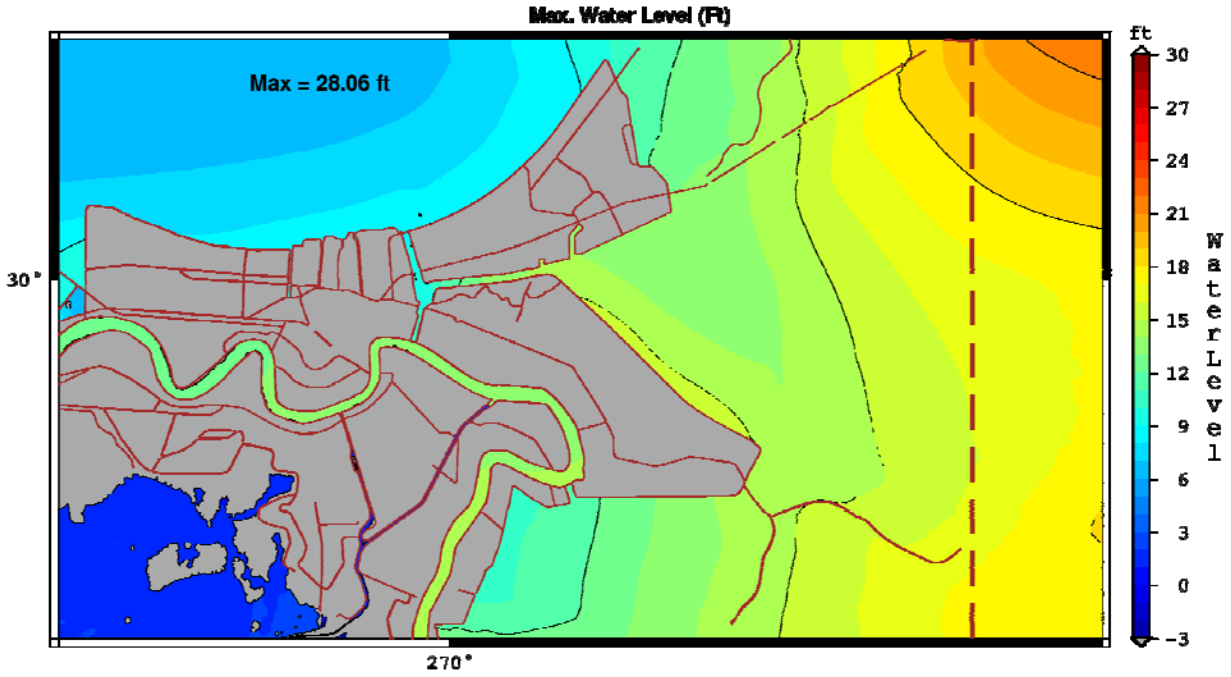


Figure 147: Maximum water surface elevation (ft) in the New Orleans area for the H2 scenario. Brown lines denote raised features. Black lines designate 3 foot contours. The thick brown dashed line represents the storm track.

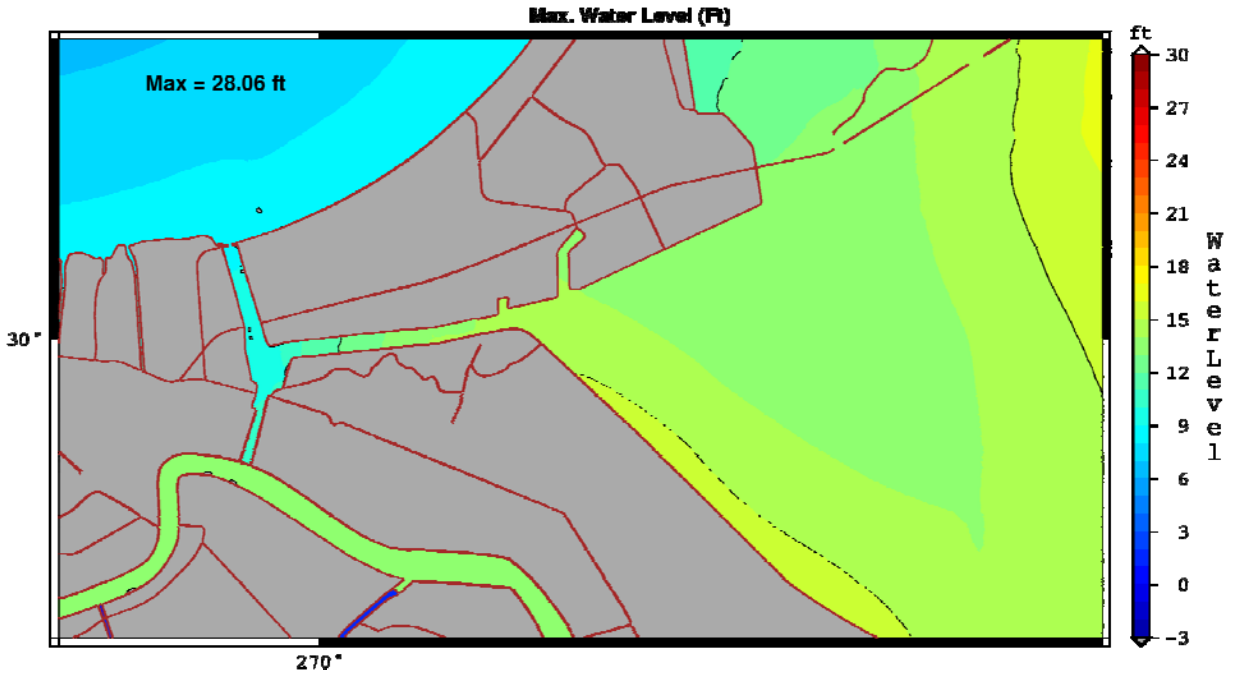


Figure 148: Maximum water surface elevation (ft) in the vicinity of the IHNC for the H2 scenario. Brown lines denote raised features. Black lines designate 3 foot contours.

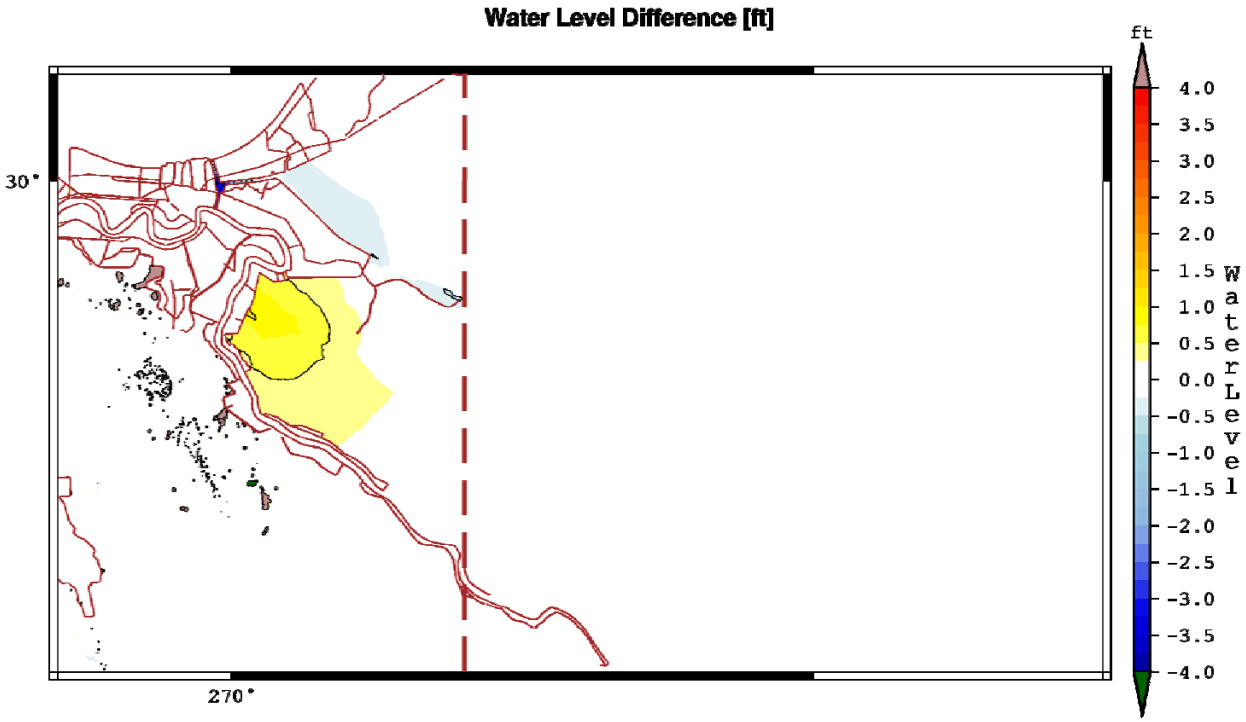


Figure 149: Difference between H1 and H2 maximum water surface elevations (ft) in Southeastern Louisiana. Regions that H2 reports higher maximum water surface elevations are represented by warm colors; cool colors report higher H1 elevations.

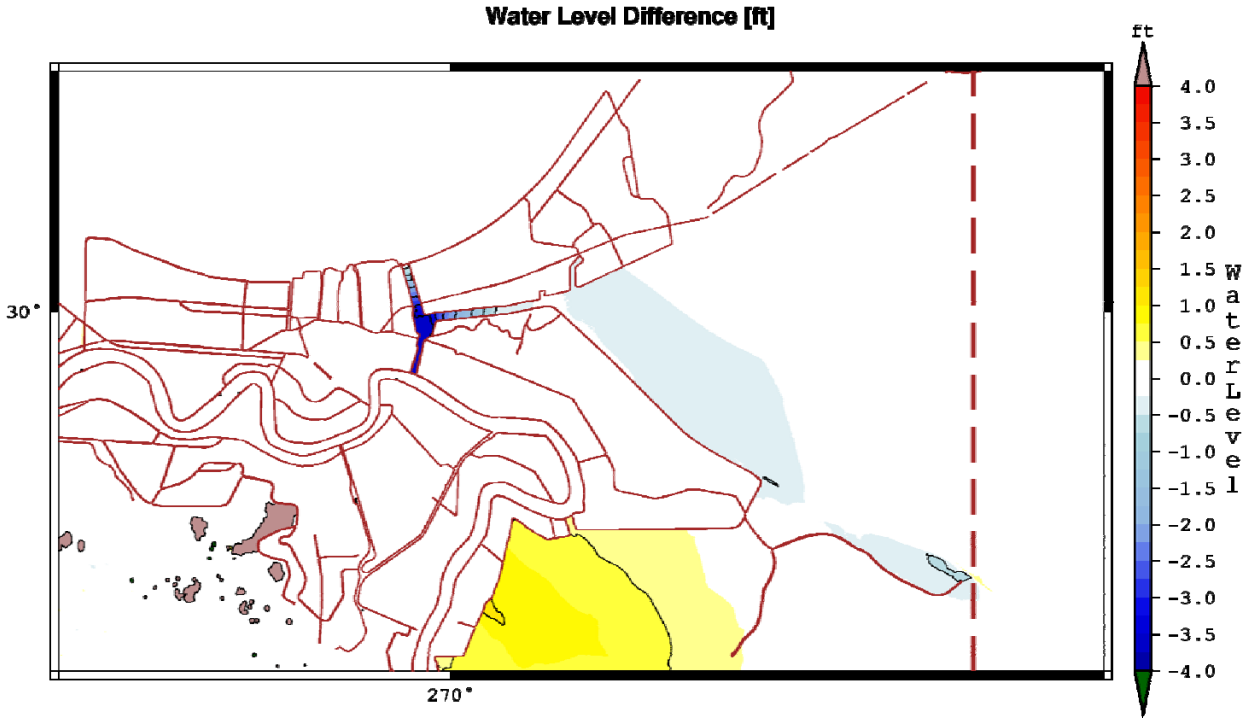


Figure 150: Difference between H1 and H2 maximum water surface elevations (ft) in the New Orleans area. Regions that H2 reports higher maximum water surface elevations are represented by warm colors; cool colors report higher H1 elevations.

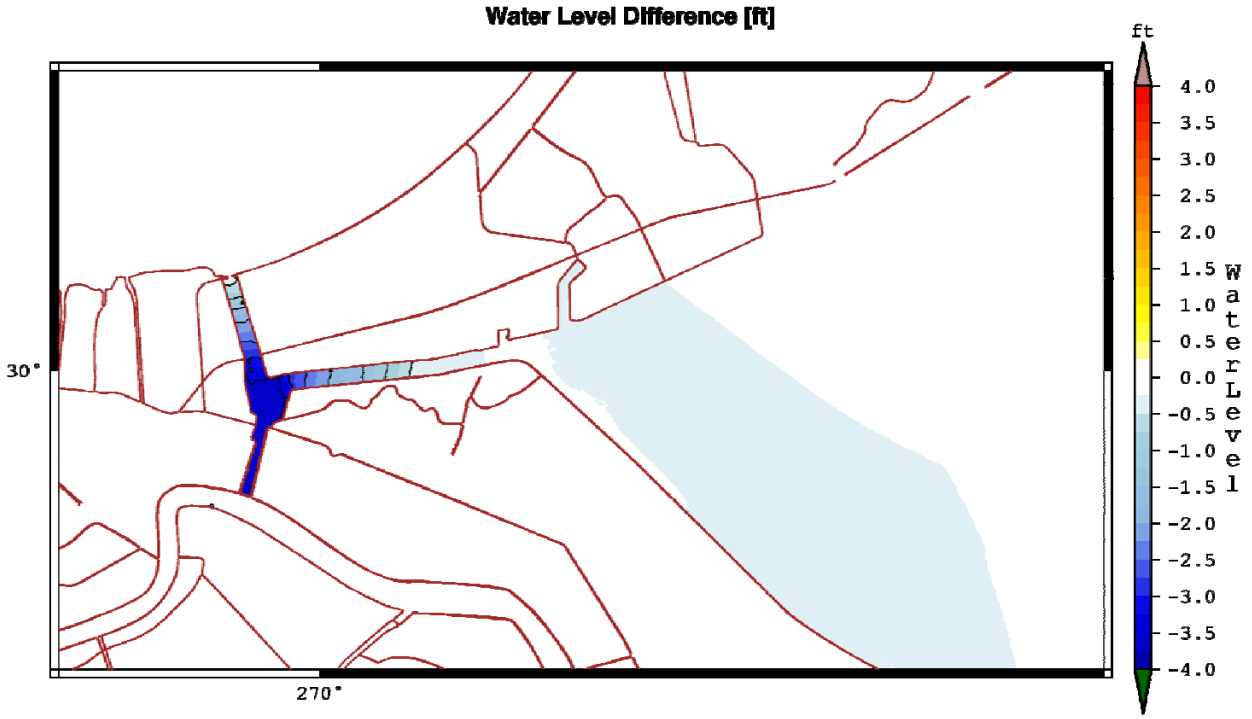


Figure 151: Difference between H1 and H2 maximum water surface elevations (ft) in the vicinity of the IHNC. Regions that H2 reports higher maximum water surface elevations are represented by warm colors; cool colors report higher H1 elevations.

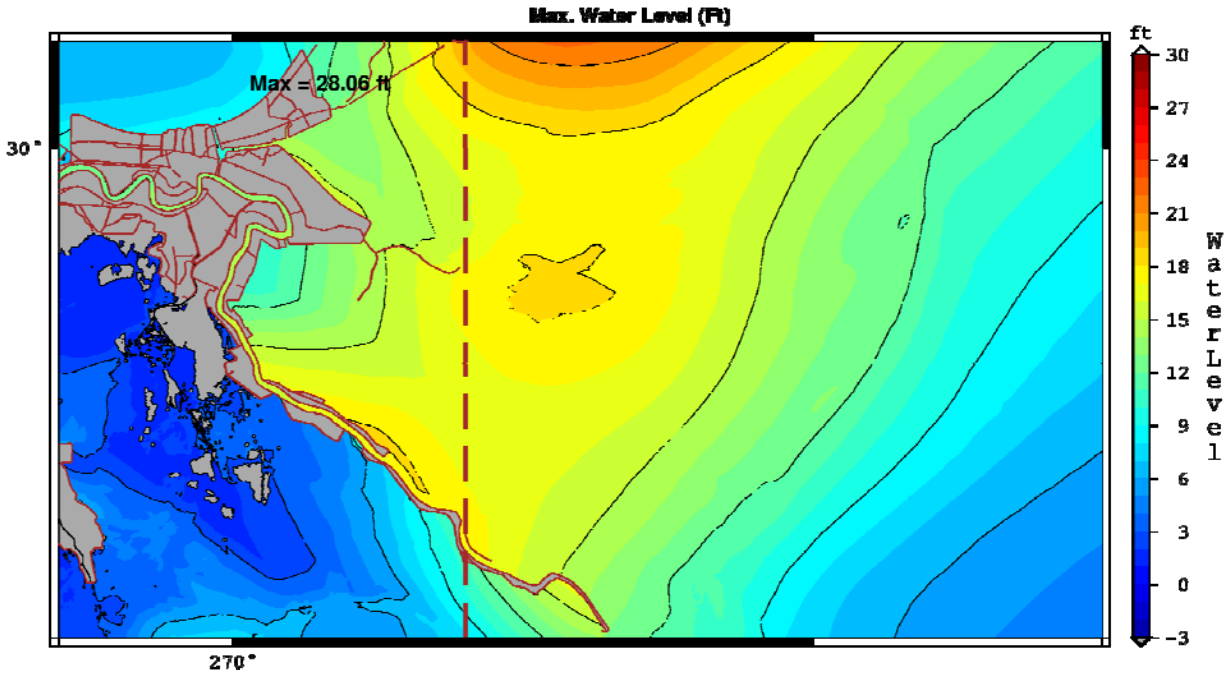


Figure 152: Maximum water surface elevation (ft) in Southeastern Louisiana for the H3 scenario. Brown lines denote raised features. Black lines designate 3 foot contours. The thick brown dashed line represents the storm track.

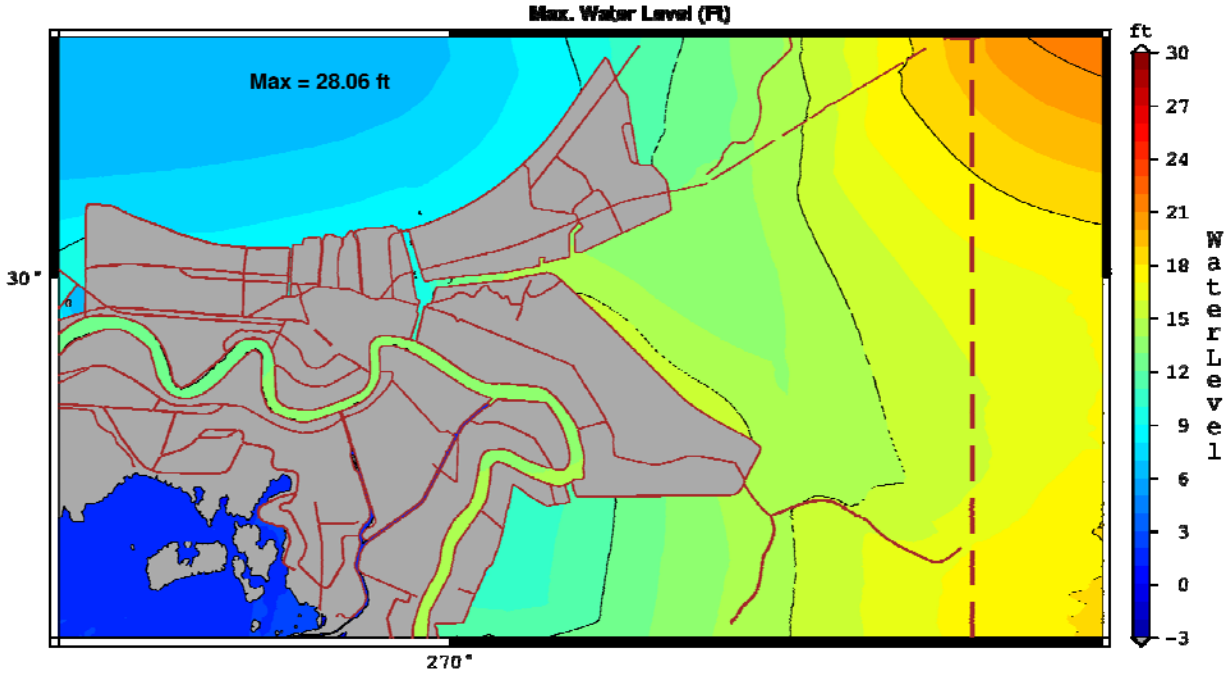


Figure 153: Maximum water surface elevation (ft) in the New Orleans area for the H3 scenario. Brown lines denote raised features. Black lines designate 3 foot contours. The thick brown dashed line represents the storm track.

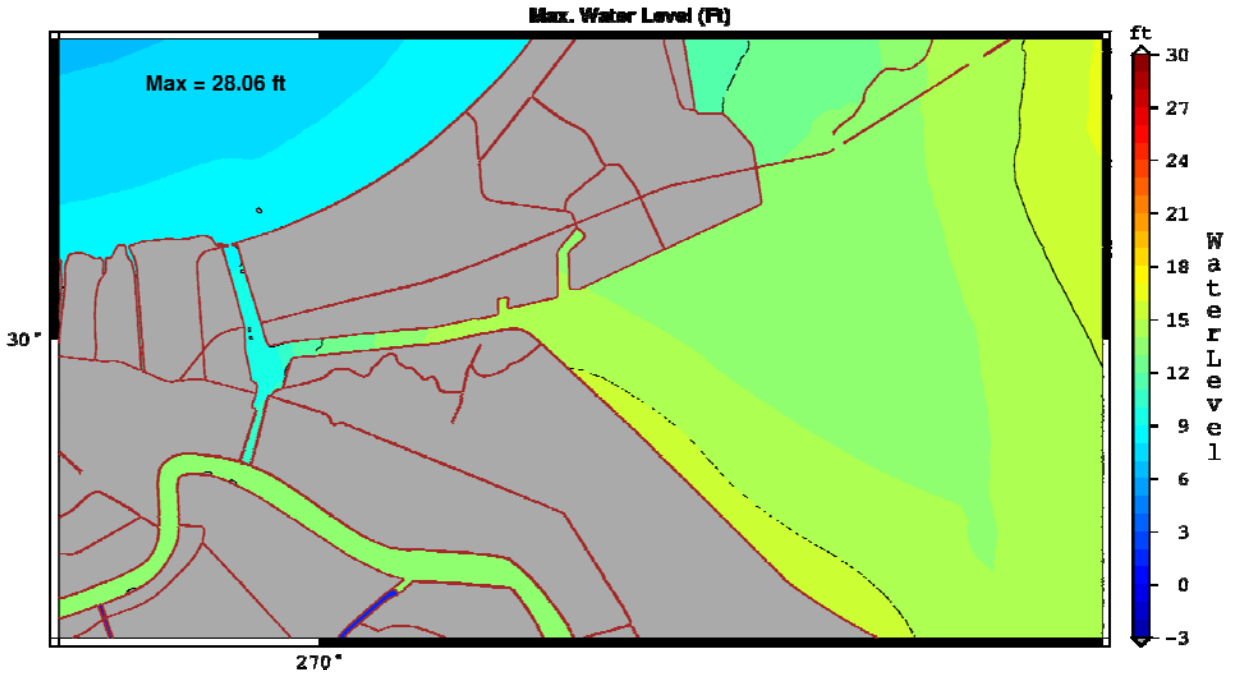


Figure 154: Maximum water surface elevation (ft) in the vicinity of the IHNC for the H3 scenario. Brown lines denote raised features. Black lines designate 3 foot contours.

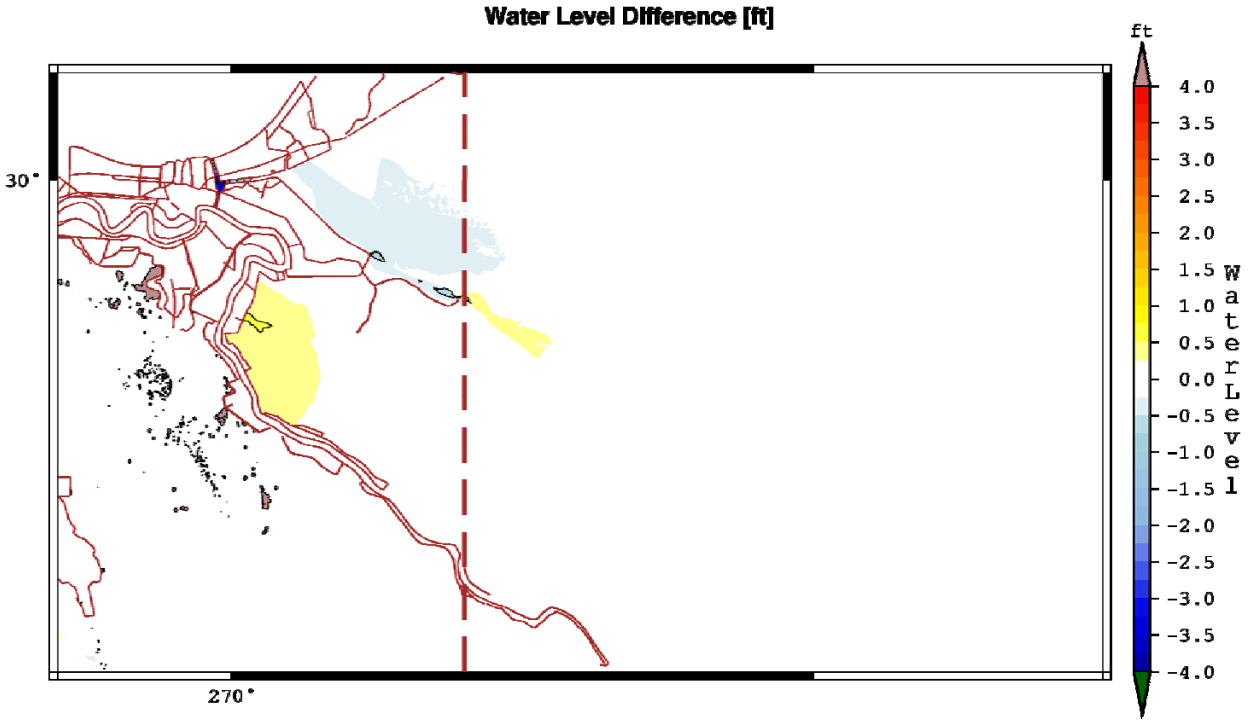


Figure 155: Difference between H1 and H3 maximum water surface elevations (ft) in Southeastern Louisiana. Regions that H3 reports higher maximum water surface elevations are represented by warm colors; cool colors report higher H1 elevations.

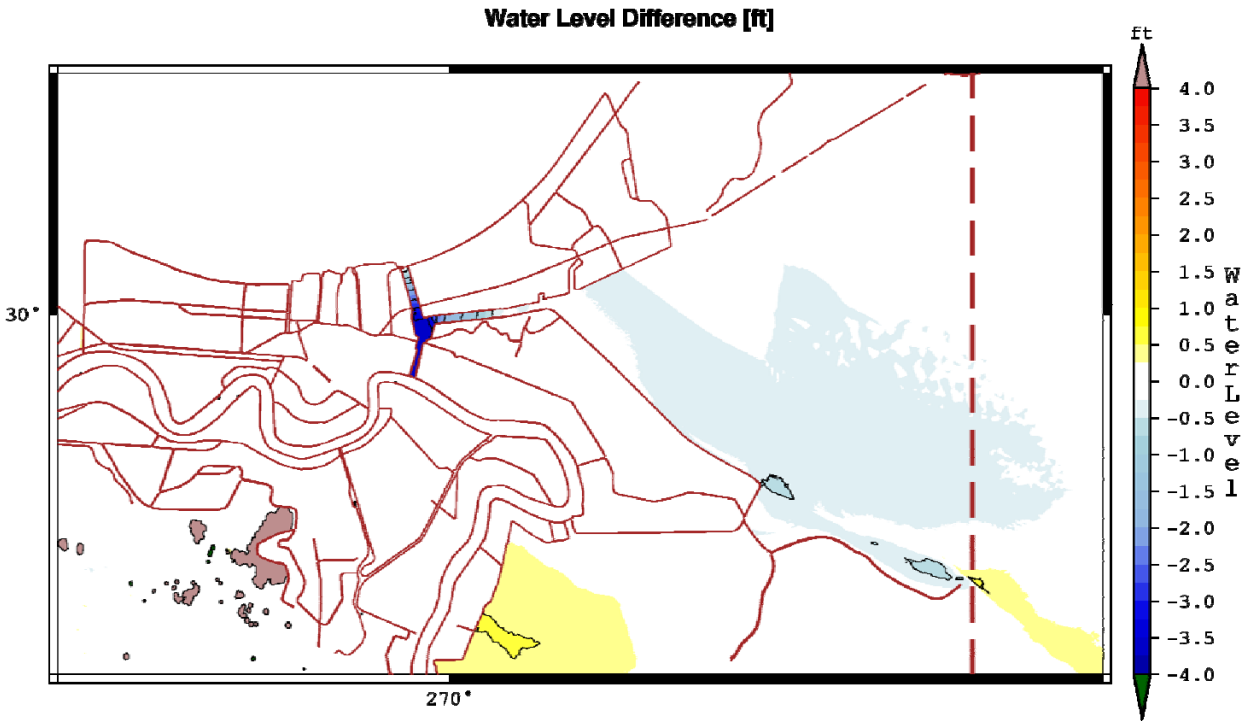


Figure 156: Difference between H1 and H3 maximum water surface elevations (ft) in the vicinity of the IHNC. Regions that H3 reports higher maximum water surface elevations are represented by warm colors; cool colors report higher H1 elevations.

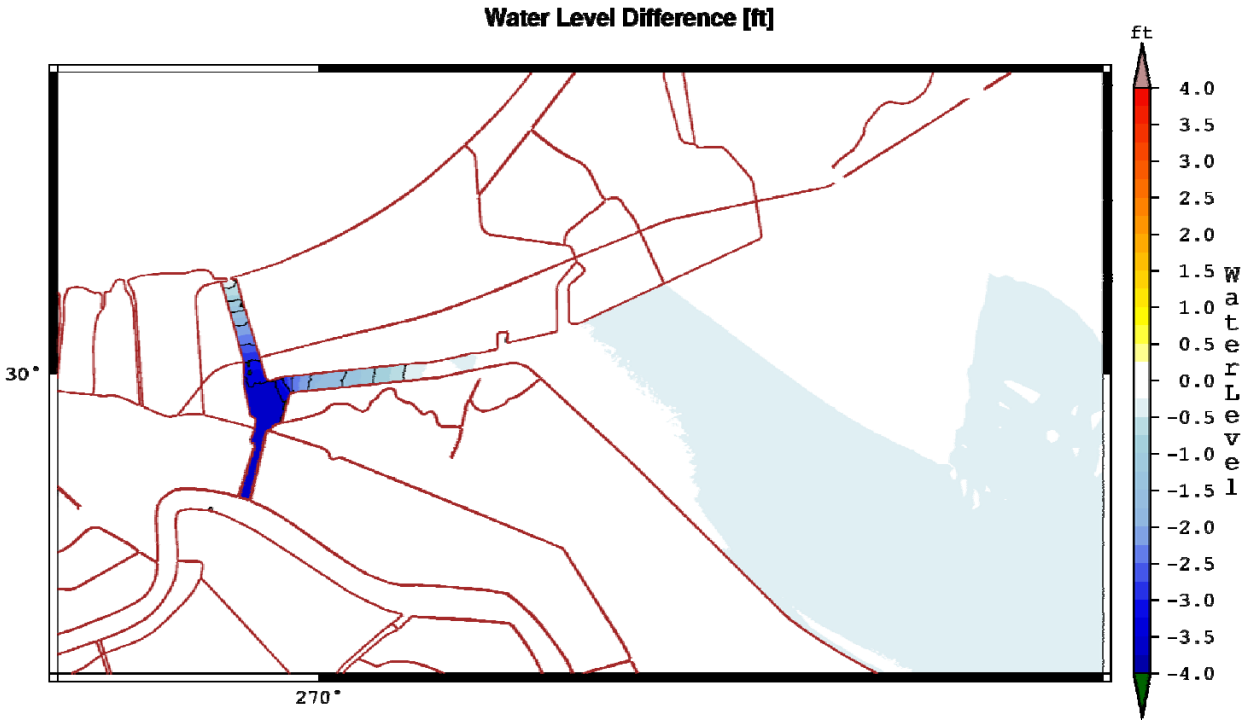


Figure 157: Difference between H1 and H3 maximum water surface elevations (ft) in the vicinity of the IHNC. Regions that H3 reports higher maximum water surface elevations are represented by warm colors; cool colors report higher H1 elevations.

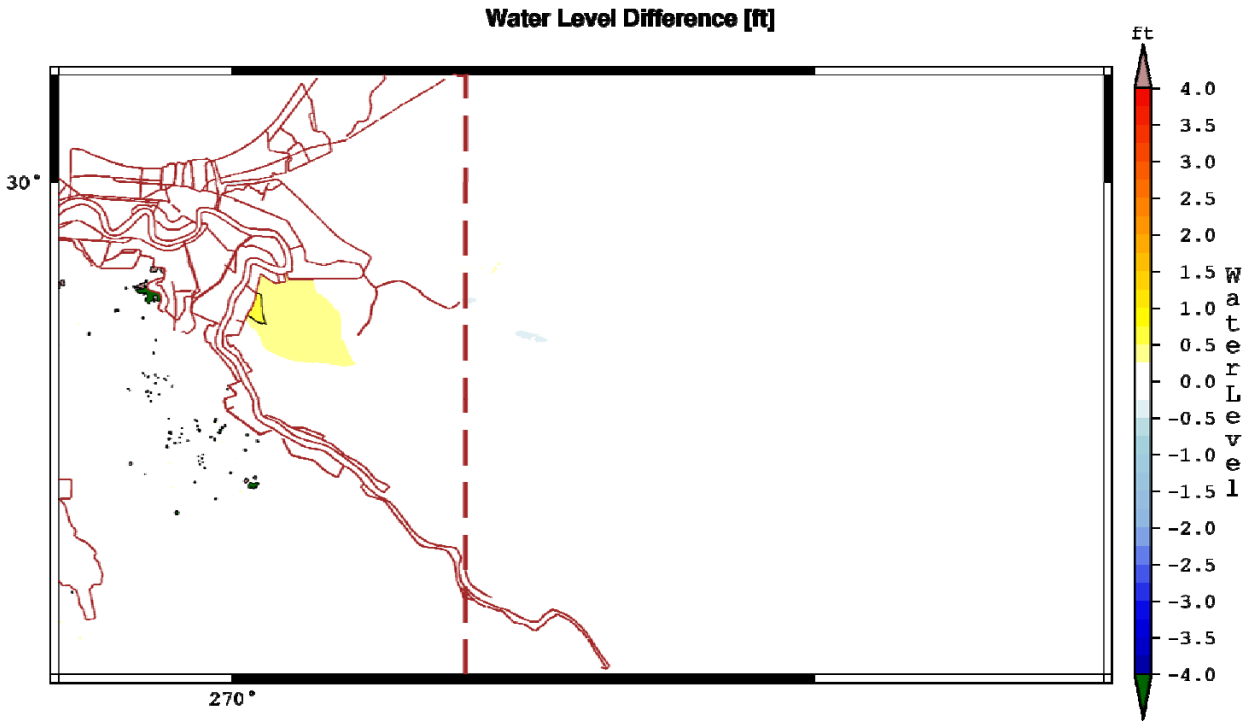


Figure 158: Difference between H2 and H3 maximum water surface elevations (ft) in Southeastern Louisiana. Regions that H2 reports higher maximum water surface elevations are represented by warm colors; cool colors report higher H3 elevations.

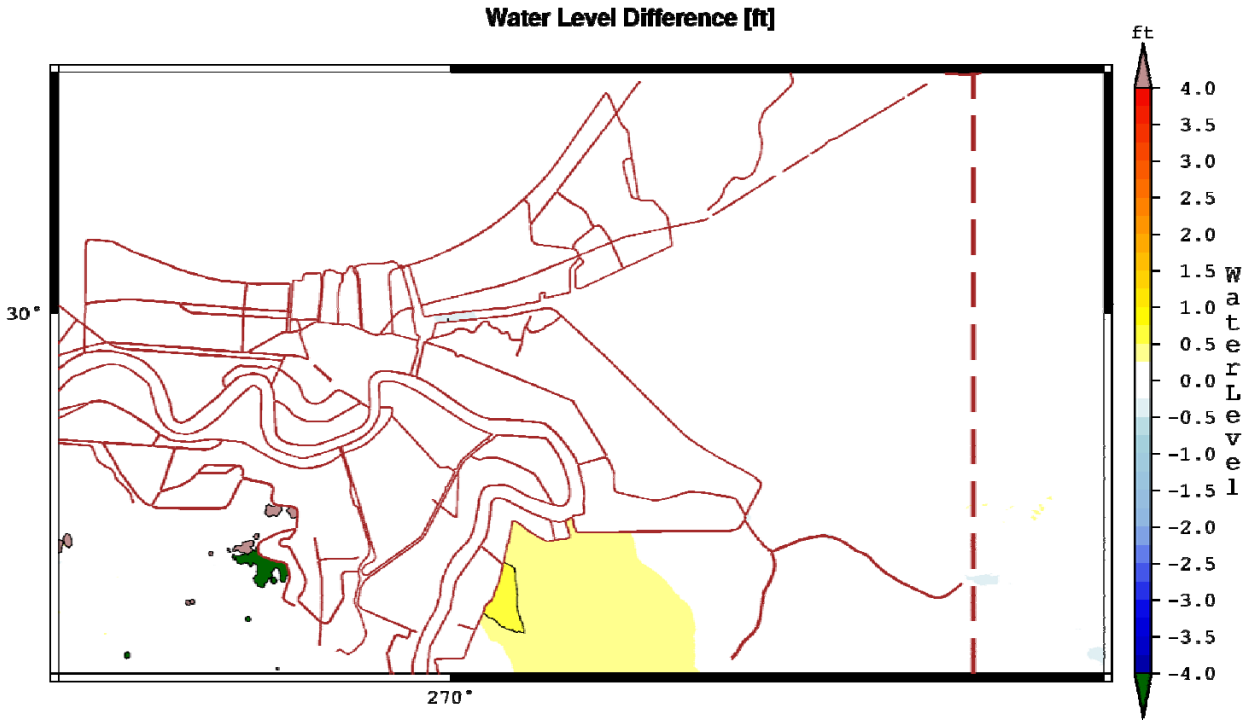


Figure 159: Difference between H2 and H3 maximum water surface elevations (ft) in the vicinity of the IHNC. Regions that H2 reports higher maximum water surface elevations are represented by warm colors; cool colors report higher H3 elevations.

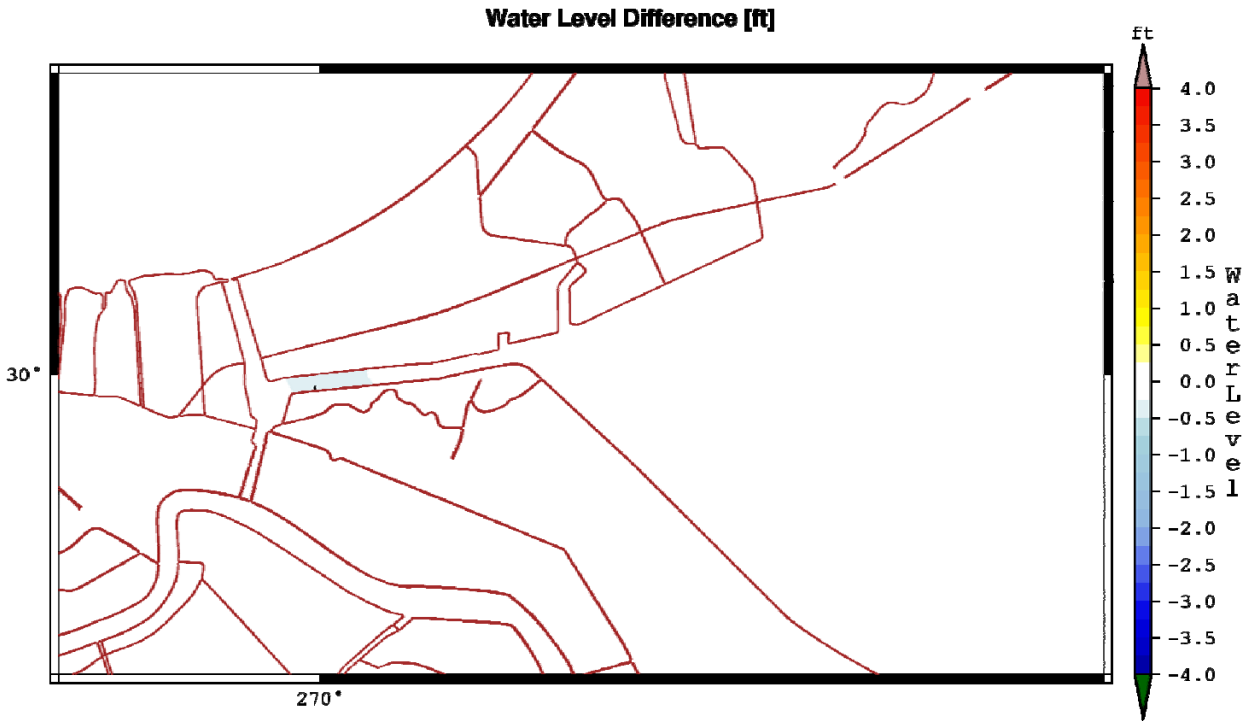


Figure 160: Difference between H2 and H3 maximum water surface elevations (ft) in the vicinity of the IHNC. Regions that H2 reports higher maximum water surface elevations are represented by warm colors; cool colors report higher H3 elevations.

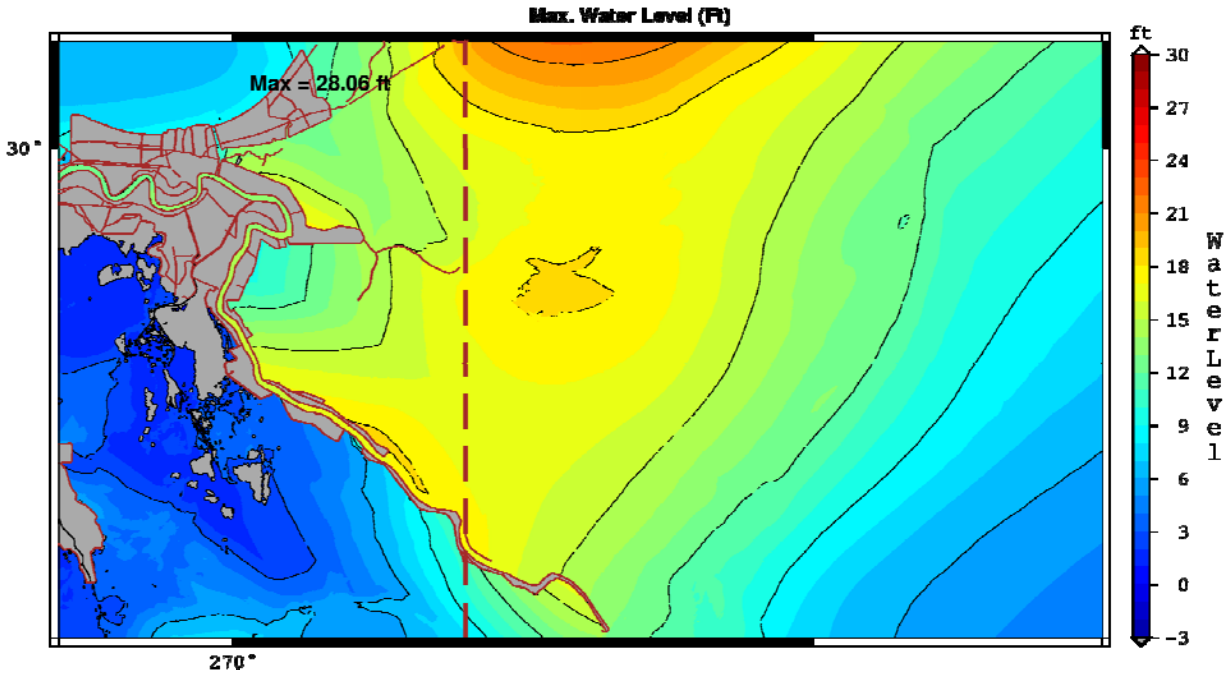


Figure 161: Maximum water surface elevation (ft) in Southeastern Louisiana for the H4 scenario. Brown lines denote raised features. Black lines designate 3 foot contours. The thick brown dashed line represents the storm track.

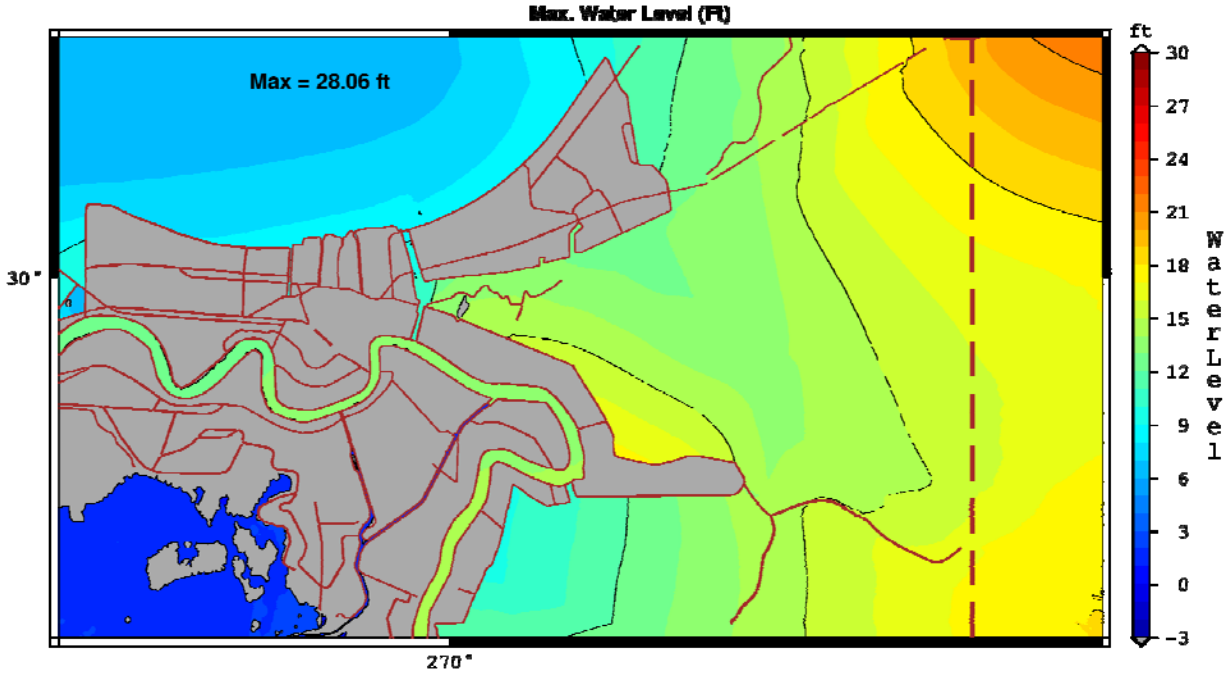


Figure 162: Maximum water surface elevation (ft) in the New Orleans area for the H4 scenario. Brown lines denote raised features. Black lines designate 3 foot contours. The thick brown dashed line represents the storm track.

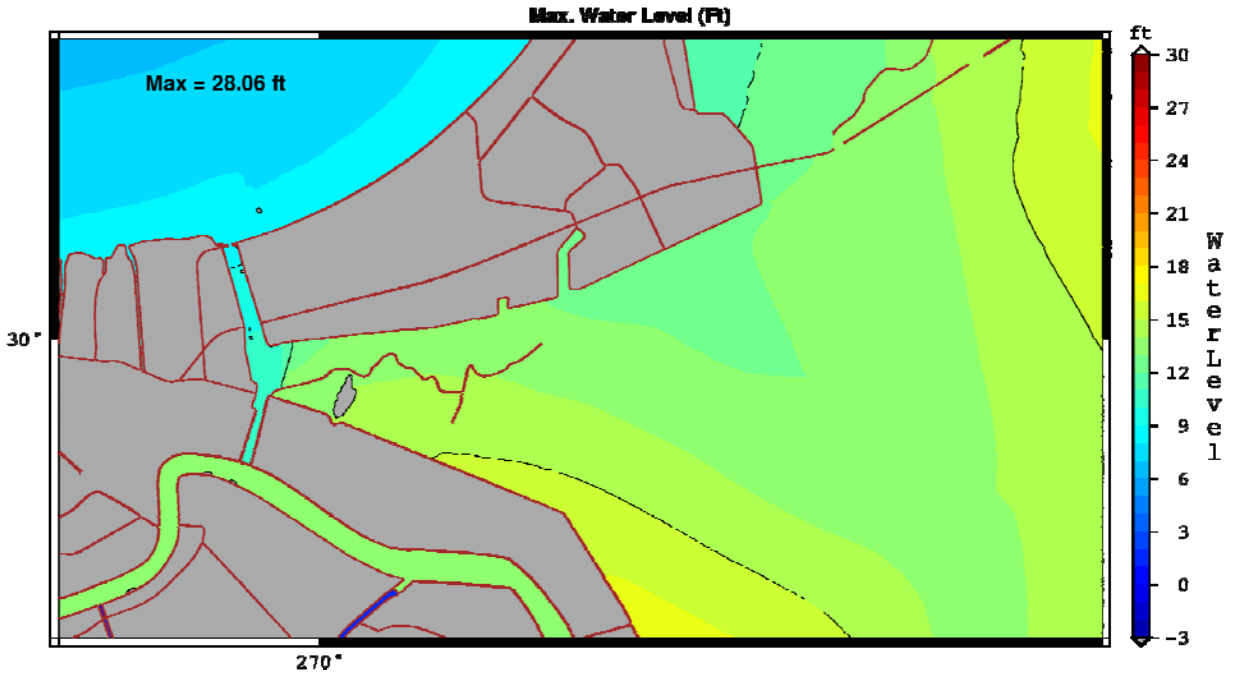


Figure 163: Maximum water surface elevation (ft) in the vicinity of the IHNC for the H4 scenario. Brown lines denote raised features. Black lines designate 3 foot contours.

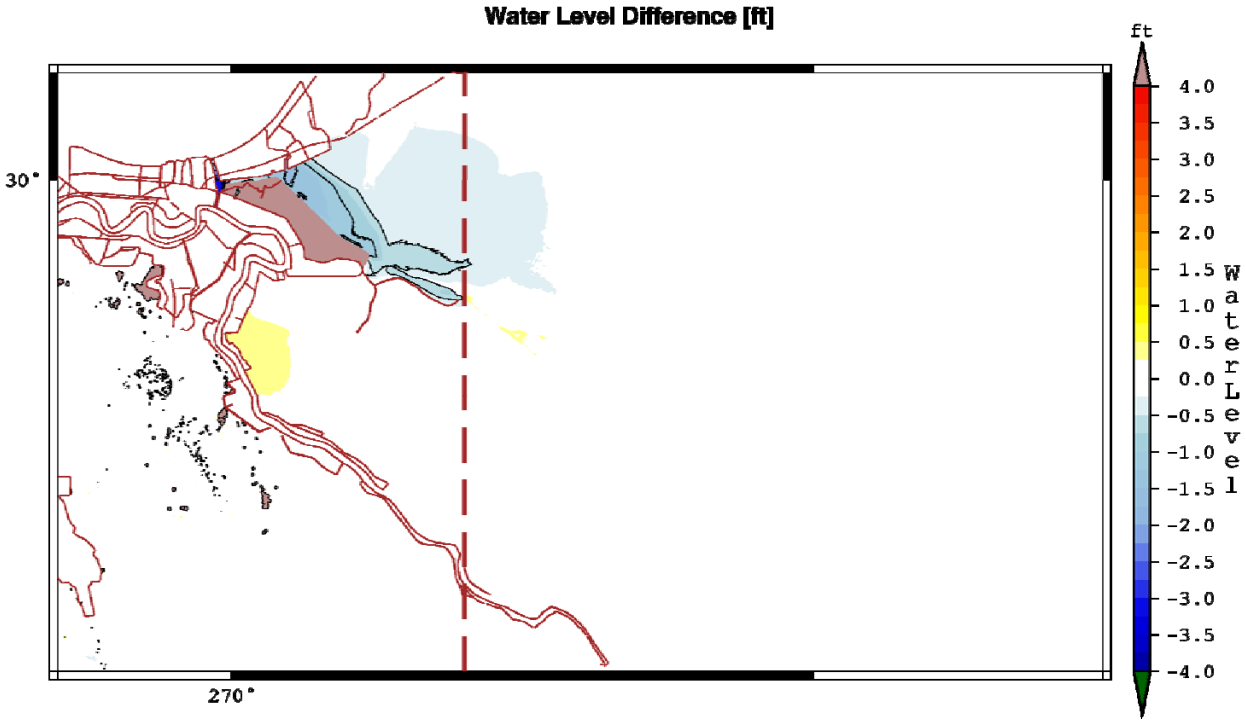


Figure 164: Difference between H1 and H4 maximum water surface elevations (ft) in Southeastern Louisiana. Regions that H4 reports higher maximum water surface elevations are represented by warm colors; cool colors report higher H1 elevations.

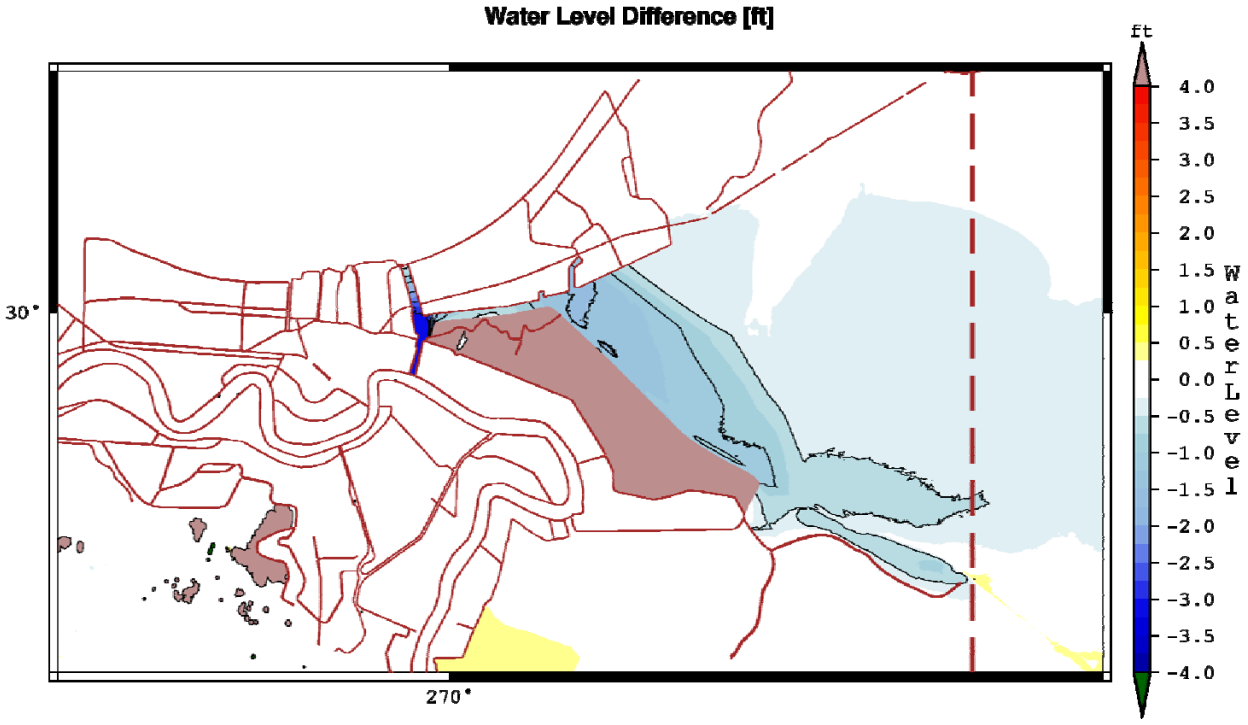


Figure 165: Difference between H1 and H4 maximum water surface elevations (ft) in the vicinity of the IHNC. Regions that H4 reports higher maximum water surface elevations are represented by warm colors; cool colors report higher H1 elevations.

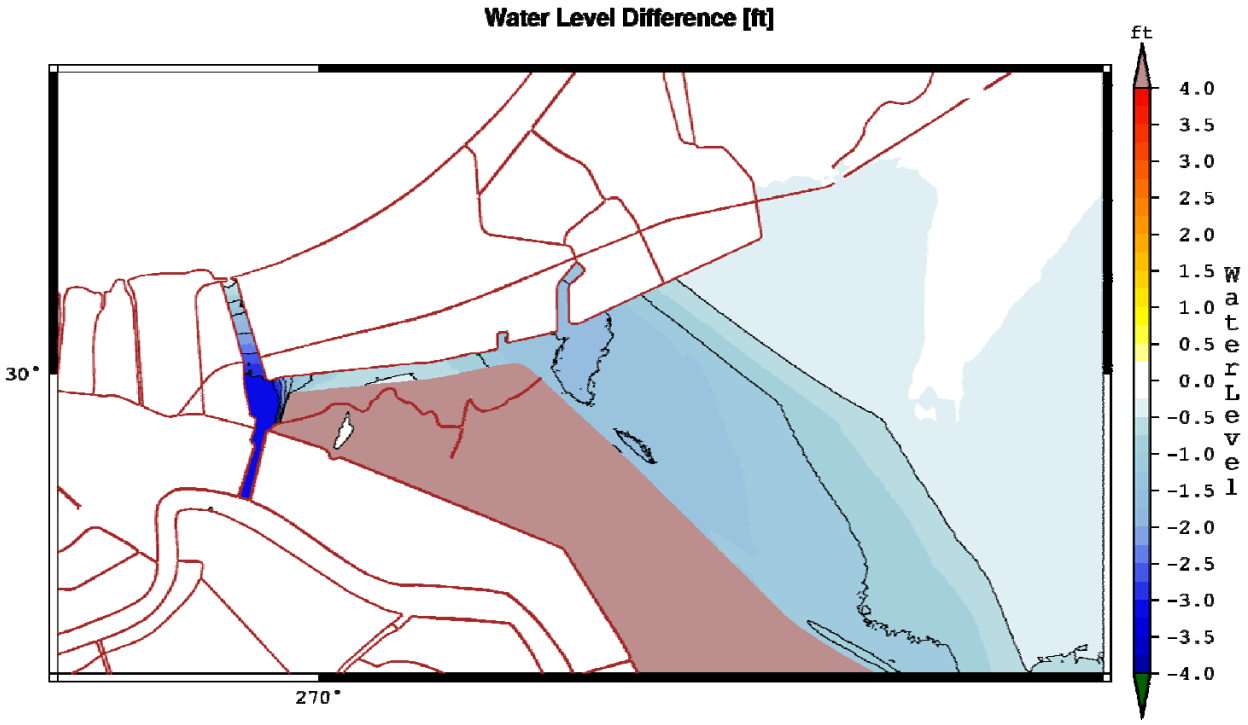


Figure 166: Difference between H1 and H4 maximum water surface elevations (ft) in the vicinity of the IHNC. Regions that H4 reports higher maximum water surface elevations are represented by warm colors; cool colors report higher H1 elevations.

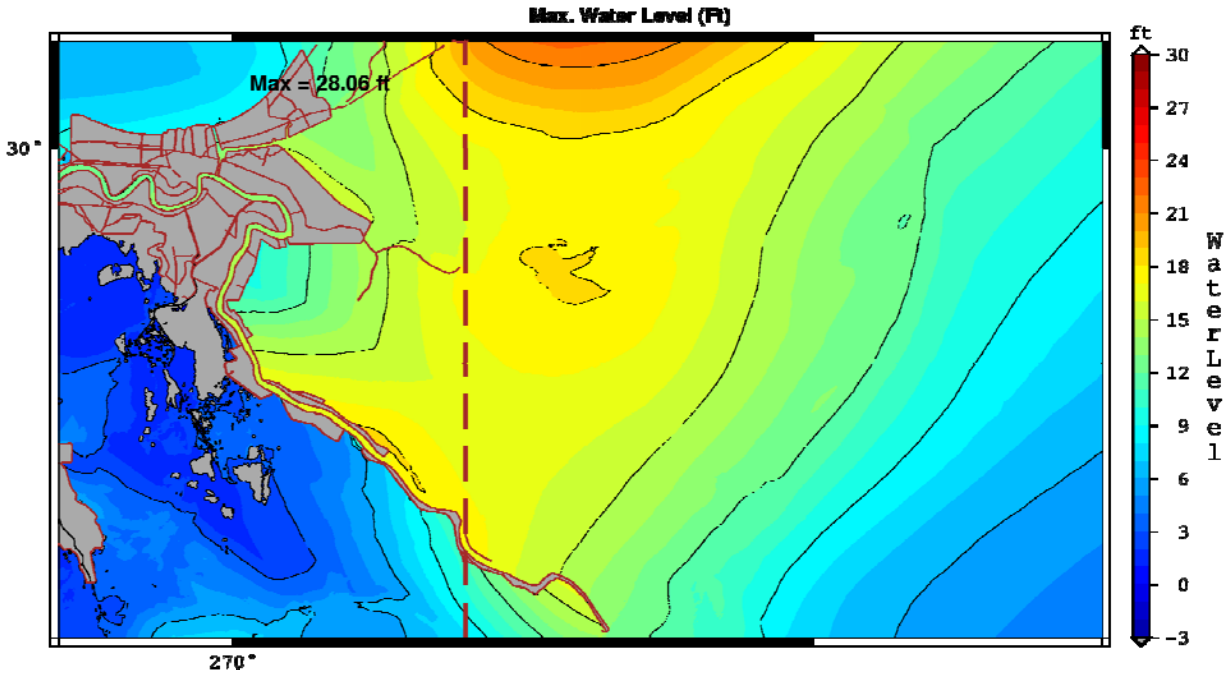


Figure 167: Maximum water surface elevation (ft) in Southeastern Louisiana for the H5 scenario. Brown lines denote raised features. Black lines designate 3 foot contours. The thick brown dashed line represents the storm track.

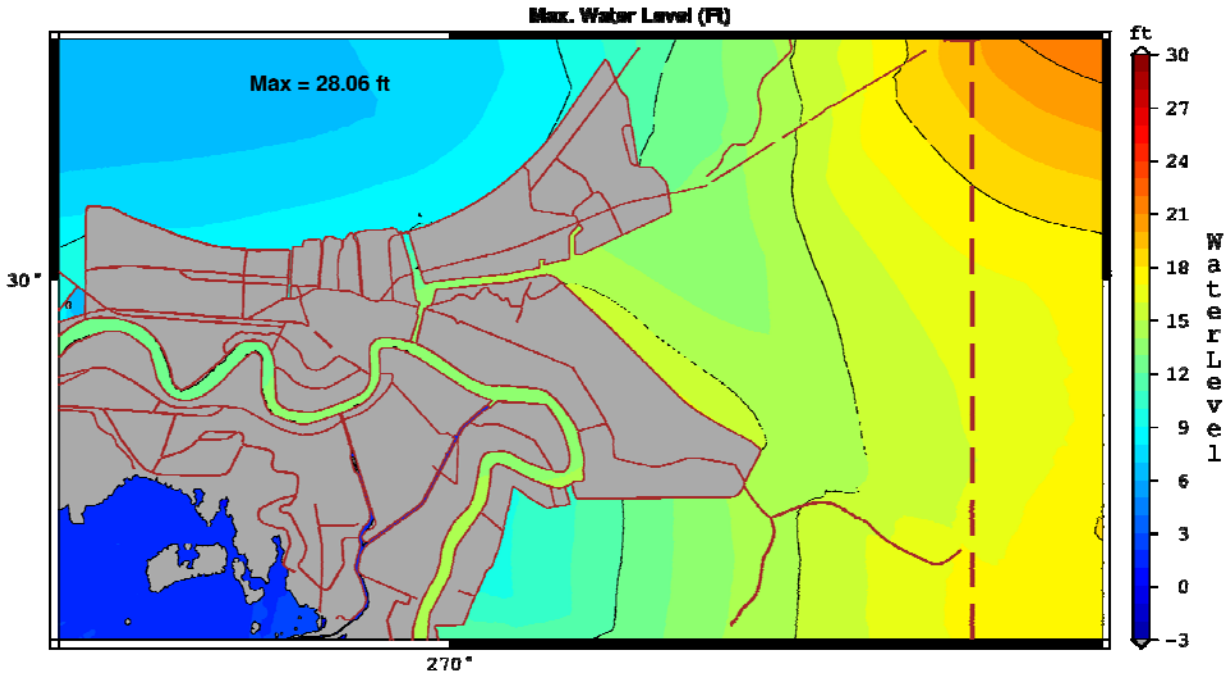


Figure 168: Maximum water surface elevation (ft) in the New Orleans area for the H5 scenario. Brown lines denote raised features. Black lines designate 3 foot contours. The thick brown dashed line represents the storm track.

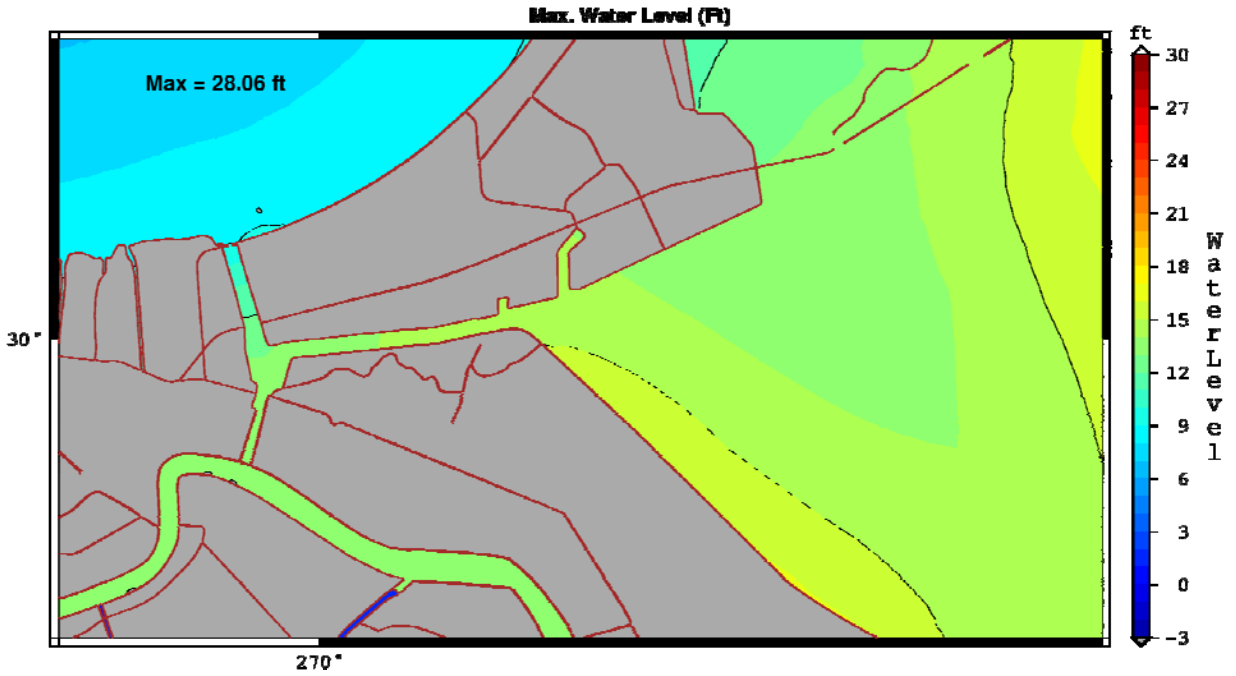


Figure 169: Maximum water surface elevation (ft) in the vicinity of the IHNC for the H5 scenario. Brown lines denote raised features. Black lines designate 3 foot contours.

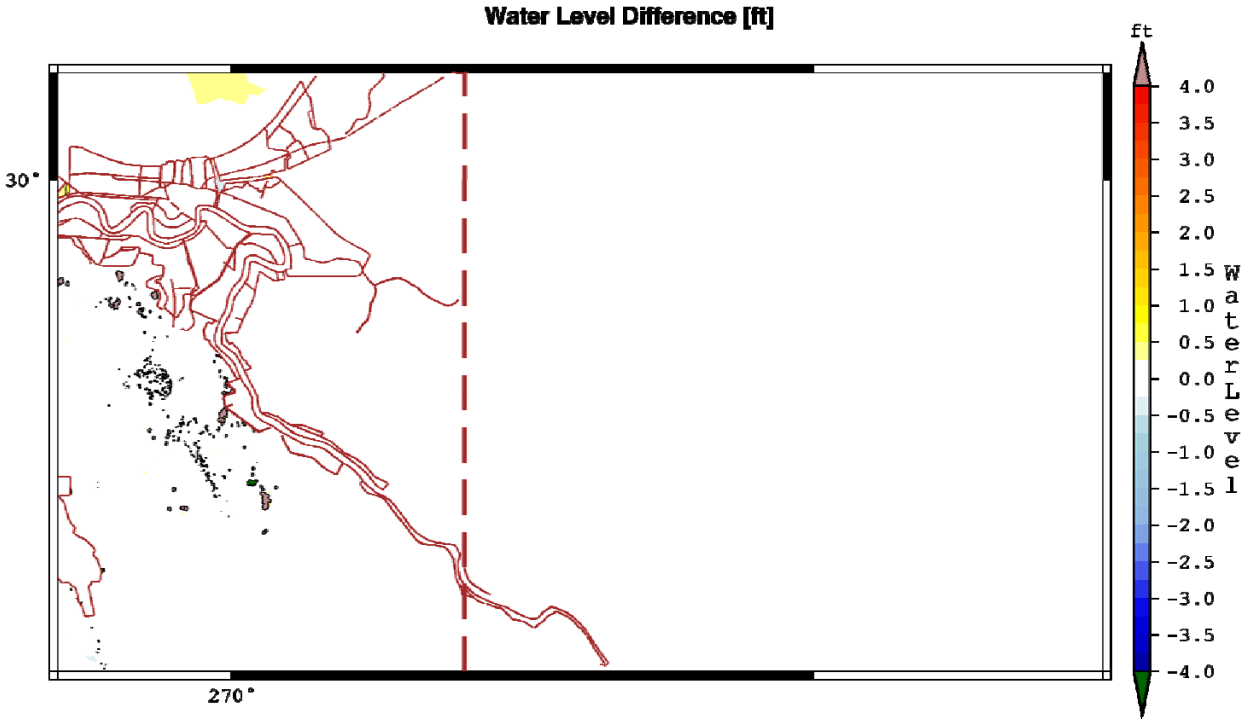


Figure 170: Difference between H1 and H5 maximum water surface elevations (ft) in Southeastern Louisiana. Regions that H5 reports higher maximum water surface elevations are represented by warm colors; cool colors report higher H1 elevations.

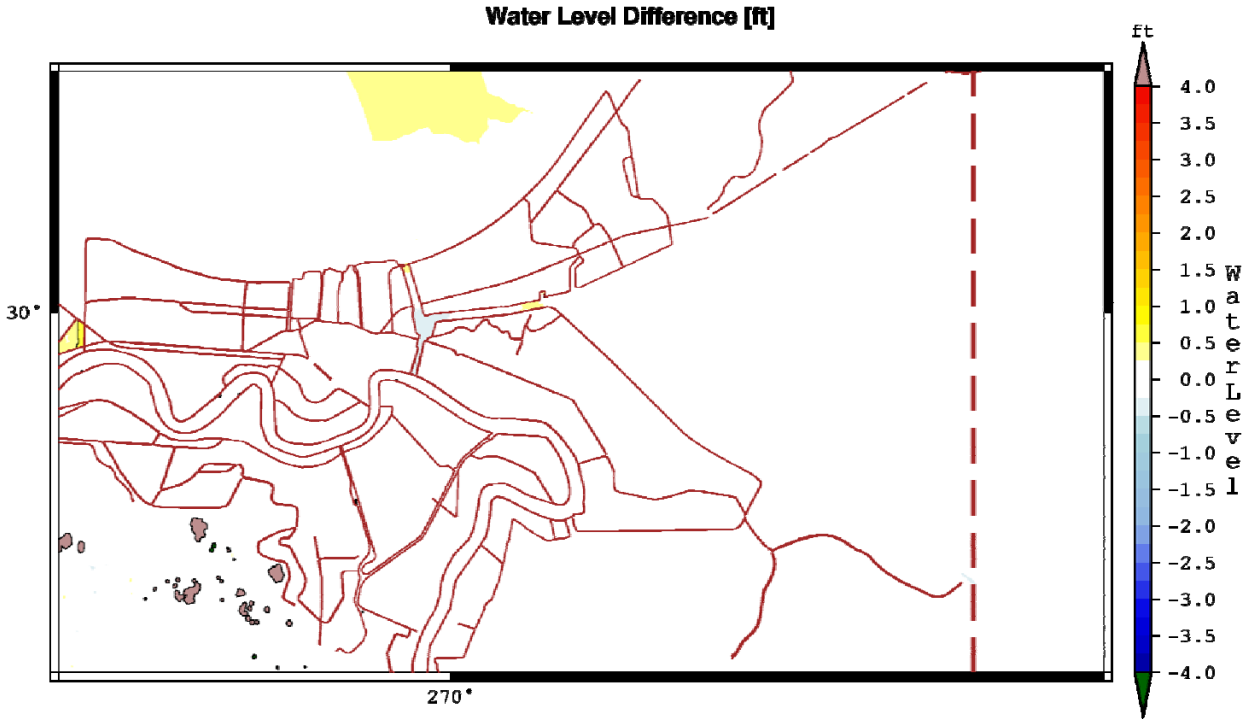


Figure 171: Difference between H1 and H5 maximum water surface elevations (ft) in the vicinity of the IHNC. Regions that H5 reports higher maximum water surface elevations are represented by warm colors; cool colors report higher H1 elevations.

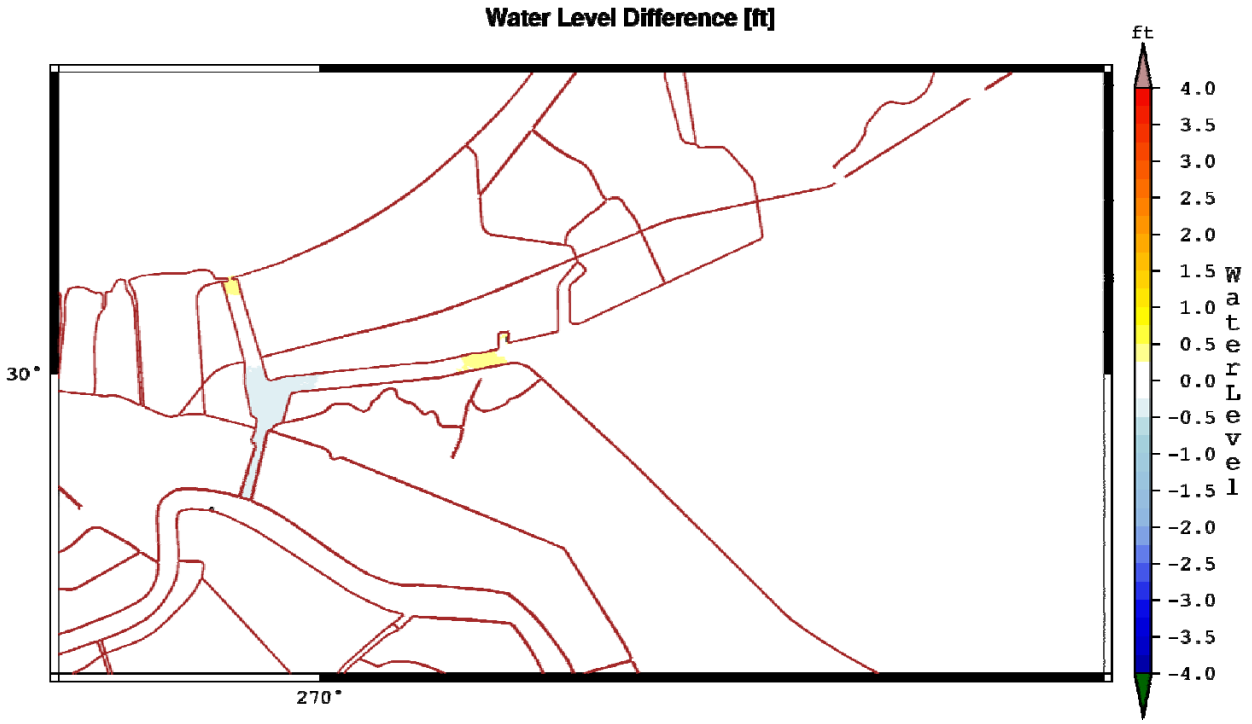


Figure 172: Difference between H1 and H5 maximum water surface elevations (ft) in the vicinity of the IHNC. Regions that H5 reports higher maximum water surface elevations are represented by warm colors; cool colors report higher H1 elevations.

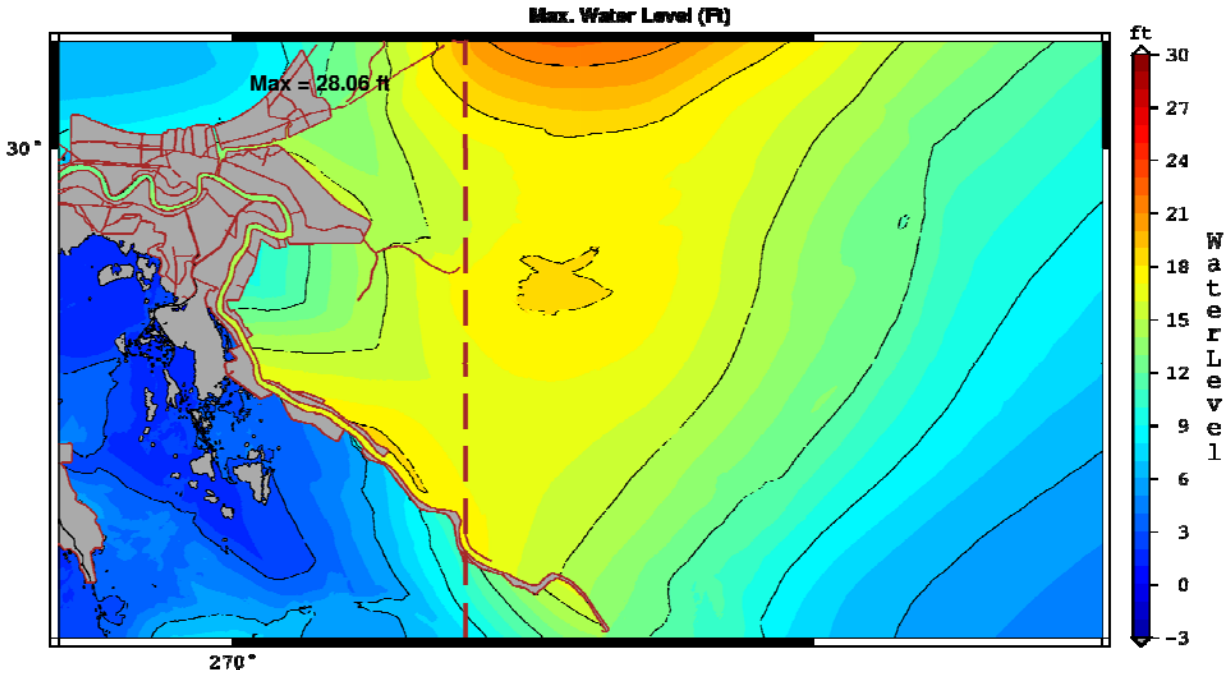


Figure 173: Maximum water surface elevation (ft) in Southeastern Louisiana for the H6 scenario. Brown lines denote raised features. Black lines designate 3 foot contours. The thick brown dashed line represents the storm track.

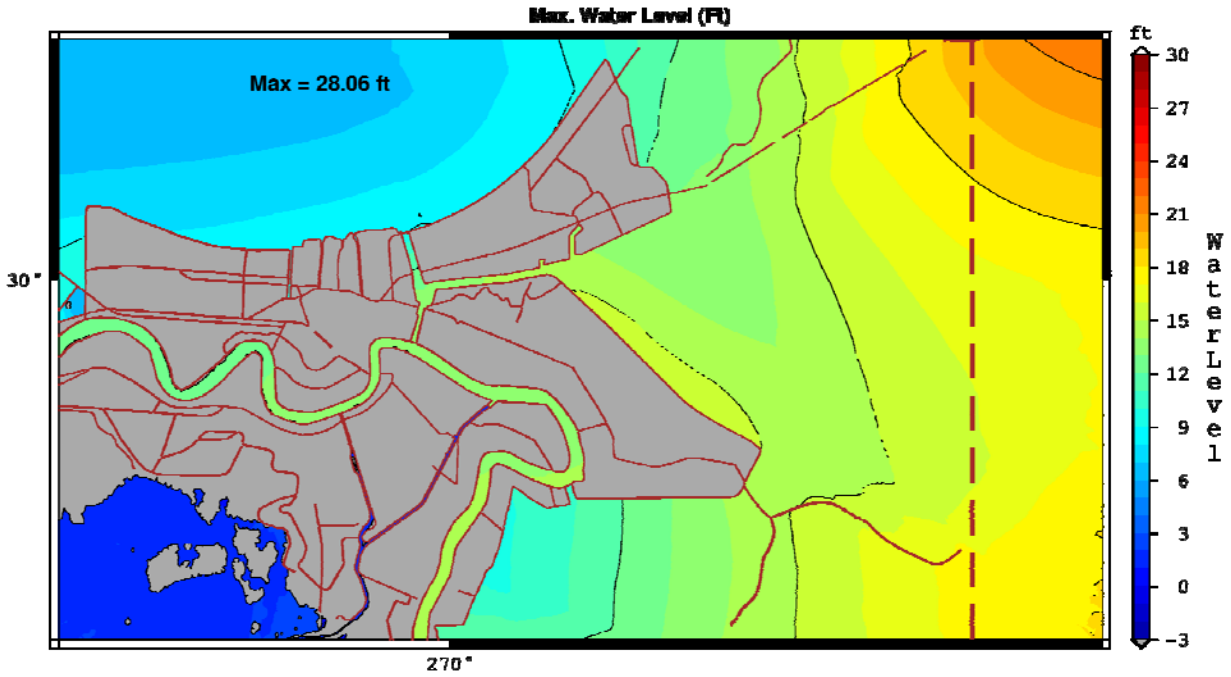


Figure 174: Maximum water surface elevation (ft) in the New Orleans area for the H6 scenario. Brown lines denote raised features. Black lines designate 3 foot contours. The thick brown dashed line represents the storm track.

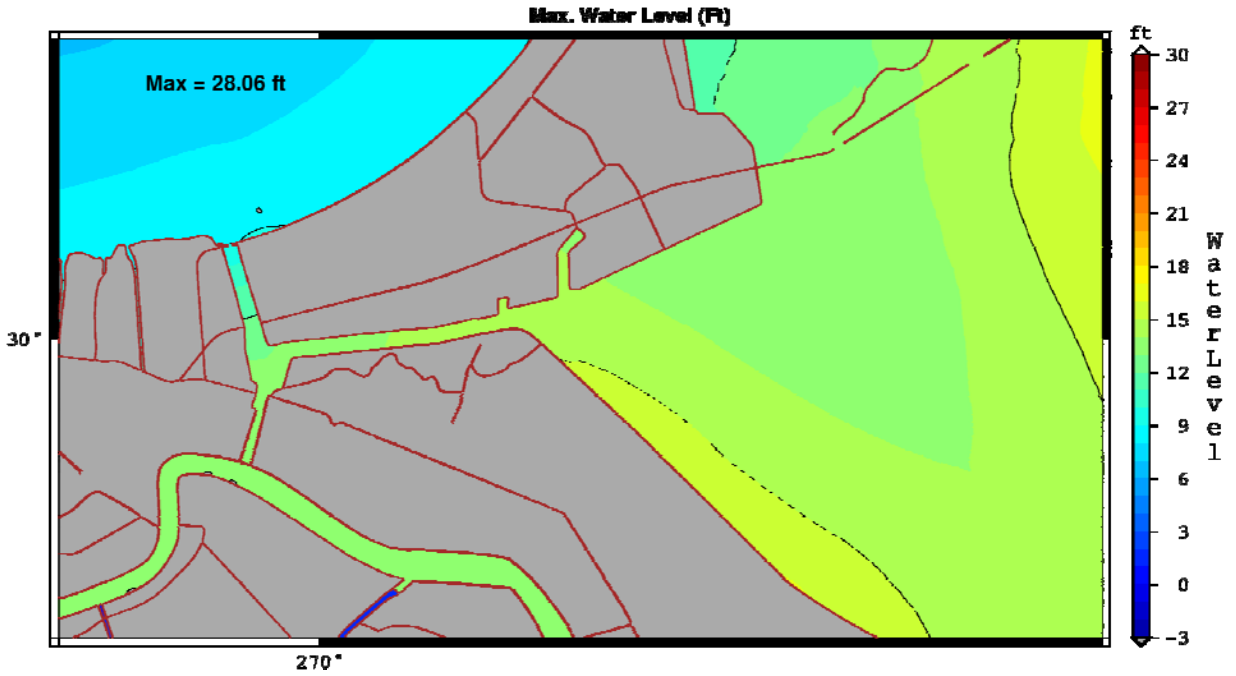


Figure 175: Maximum water surface elevation (ft) in the vicinity of the IHNC for the H6 scenario. Brown lines denote raised features. Black lines designate 3 foot contours.

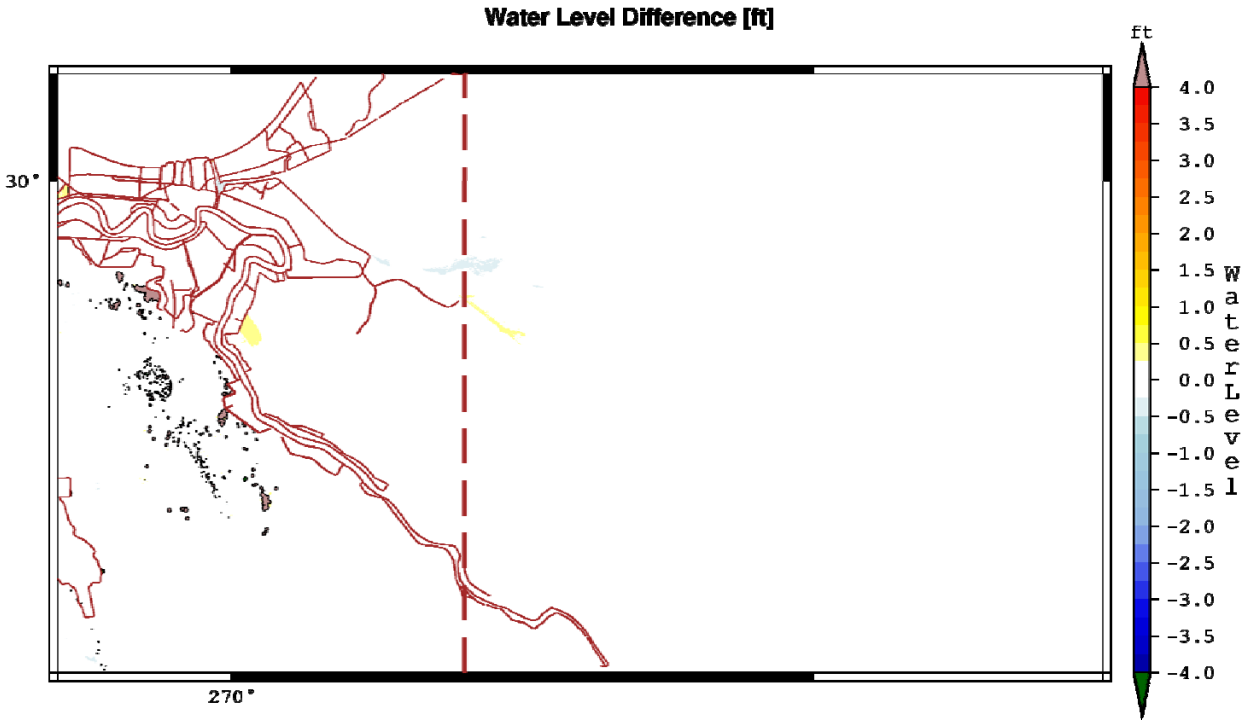


Figure 176: Difference between H1 and H6 maximum water surface elevations (ft) in Southeastern Louisiana. Regions that H6 reports higher maximum water surface elevations are represented by warm colors; cool colors report higher H1 elevations.

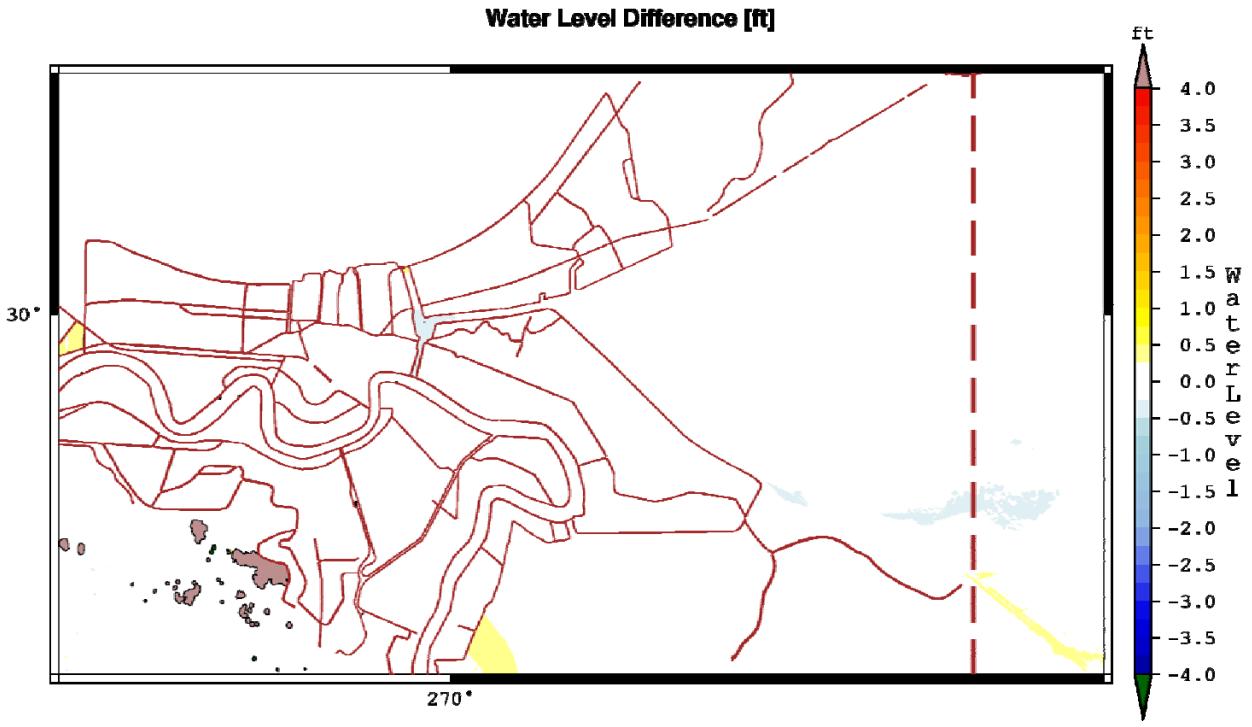


Figure 177: Difference between H1 and H6 maximum water surface elevations (ft) in the vicinity of the IHNC. Regions that H6 reports higher maximum water surface elevations are represented by warm colors; cool colors report higher H1 elevations.

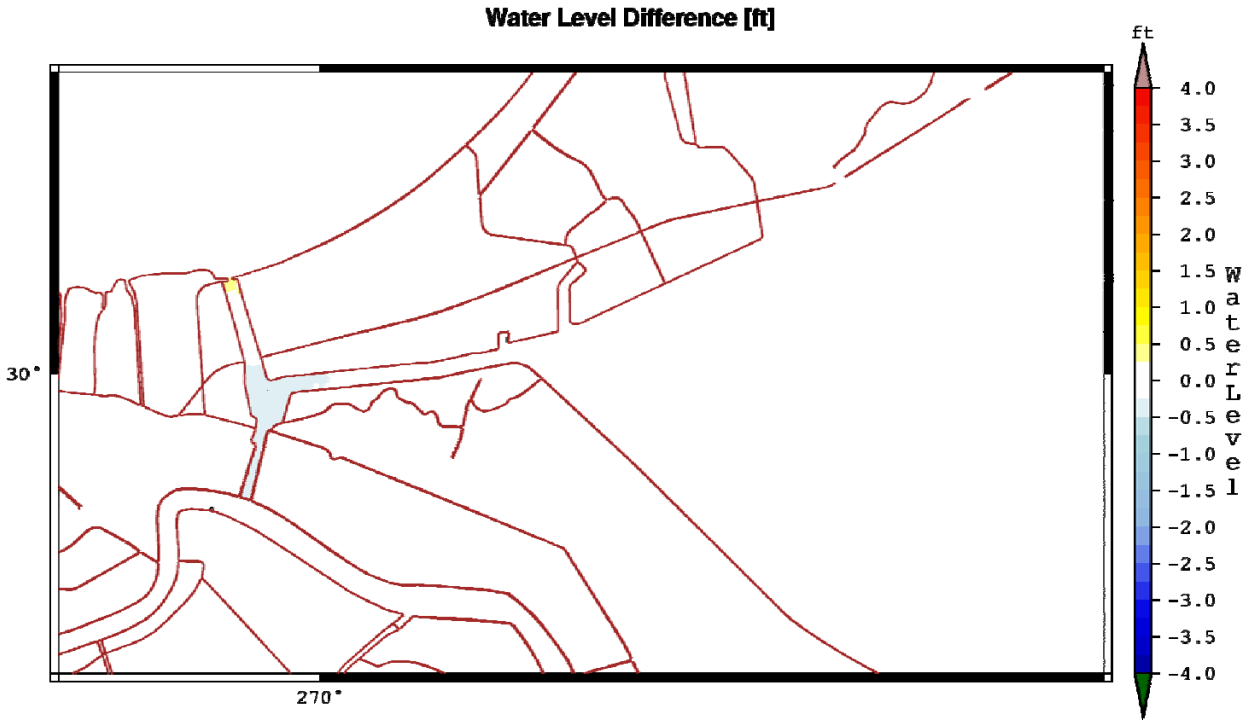


Figure 178: Difference between H1 and H6 maximum water surface elevations (ft) in the vicinity of the IHNC. Regions that H6 reports higher maximum water surface elevations are represented by warm colors; cool colors report higher H1 elevations.

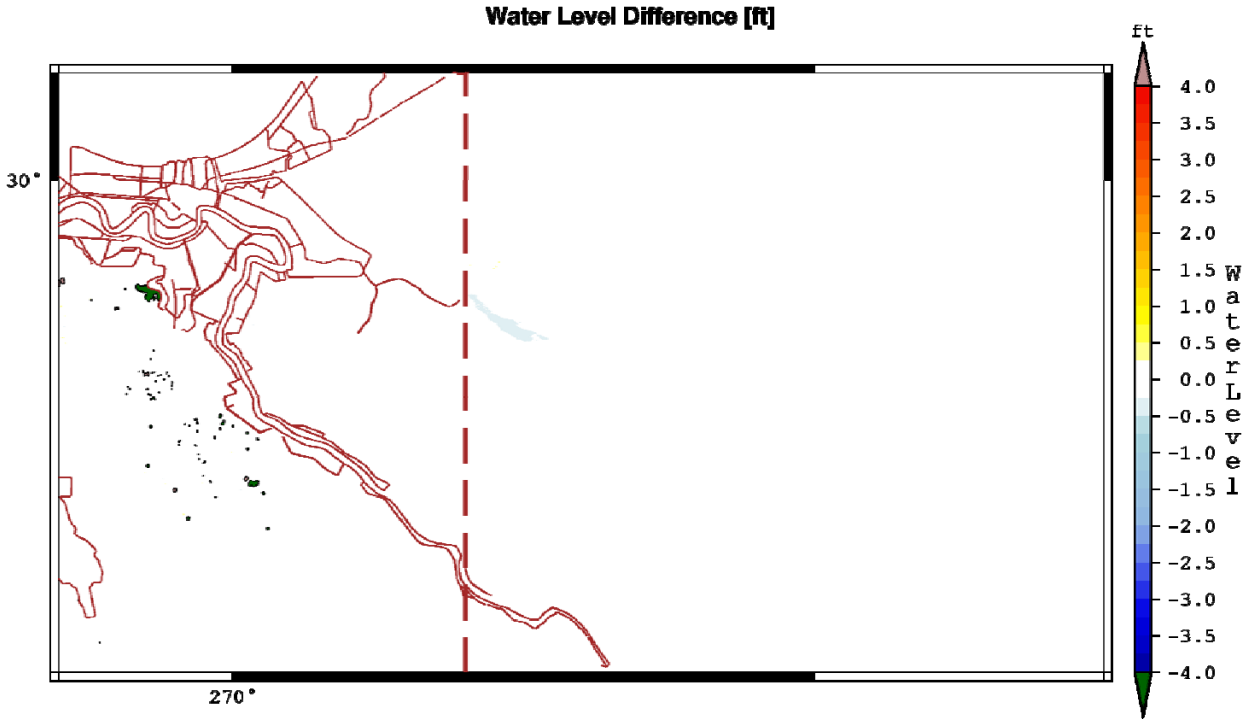


Figure 179: Difference between H5 and H6 maximum water surface elevations (ft) in Southeastern Louisiana. Regions that H5 reports higher maximum water surface elevations are represented by warm colors; cool colors report higher H6 elevations.

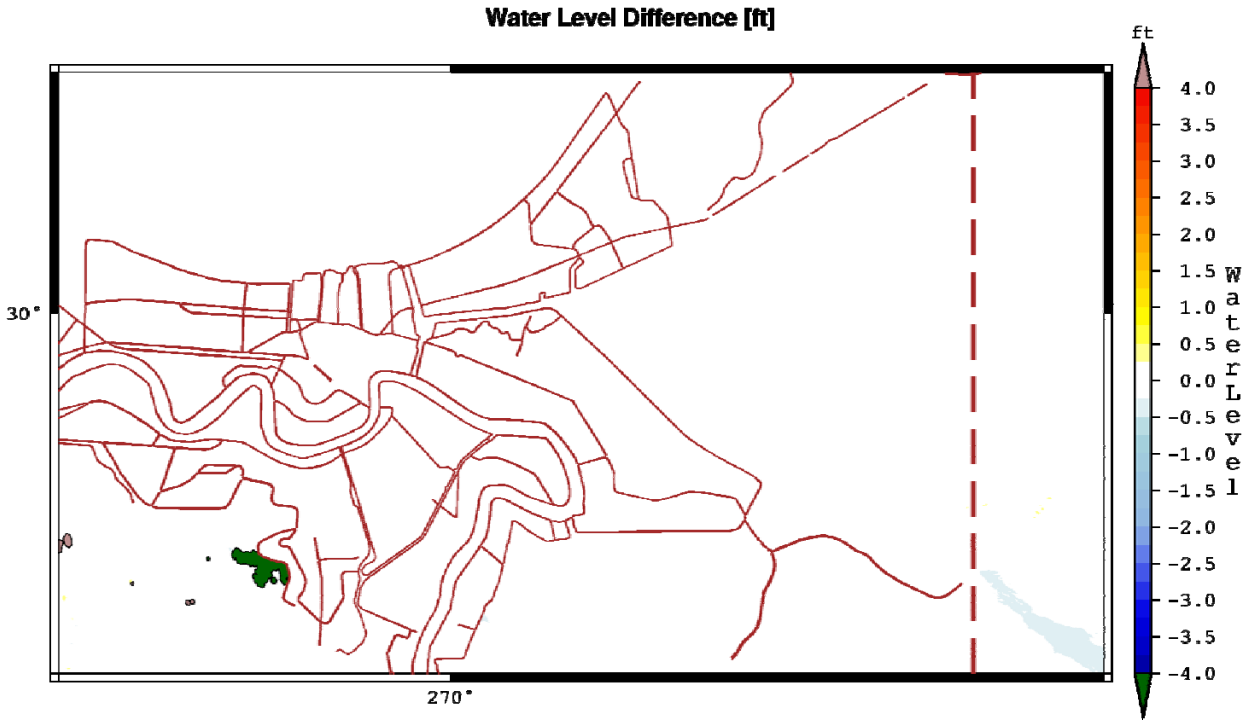


Figure 180: Difference between H5 and H6 maximum water surface elevations (ft) in the vicinity of the IHNC. Regions that H5 reports higher maximum water surface elevations are represented by warm colors; cool colors report higher H6 elevations.

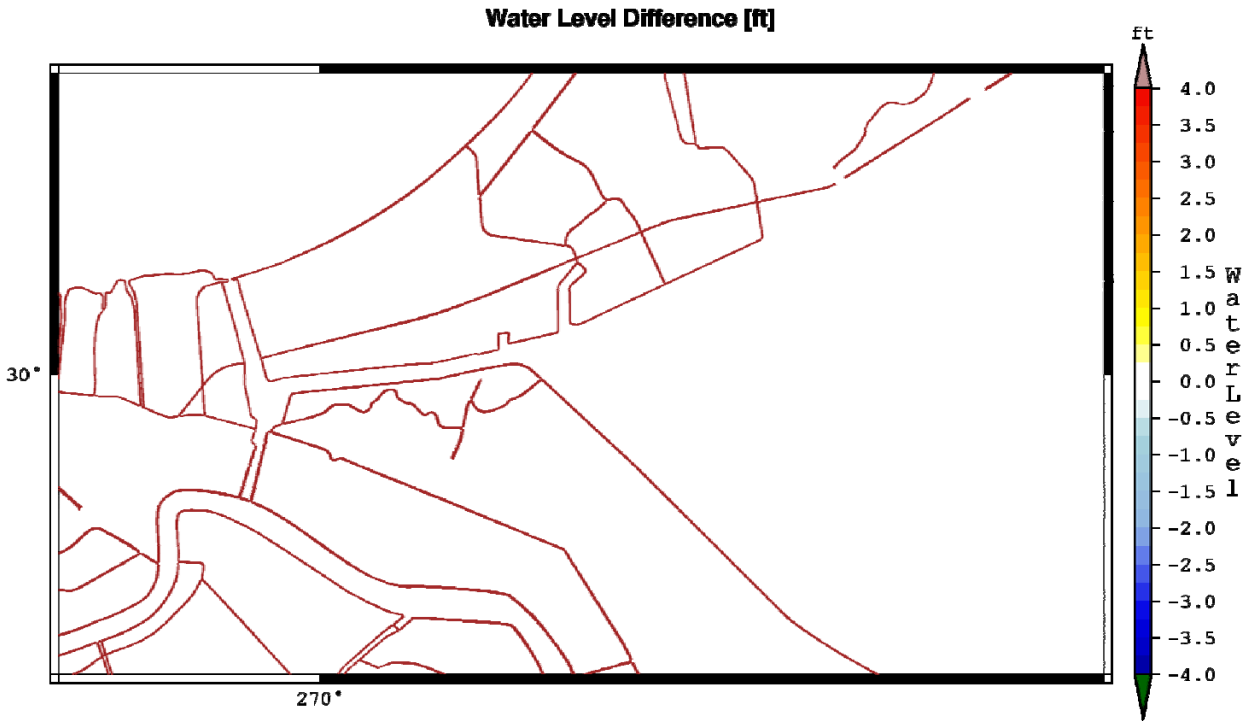


Figure 181: Difference between H5 and H6 maximum water surface elevations (ft) in the vicinity of the IHNC. Regions that H5 reports higher maximum water surface elevations are represented by warm colors; cool colors report higher H6 elevations.

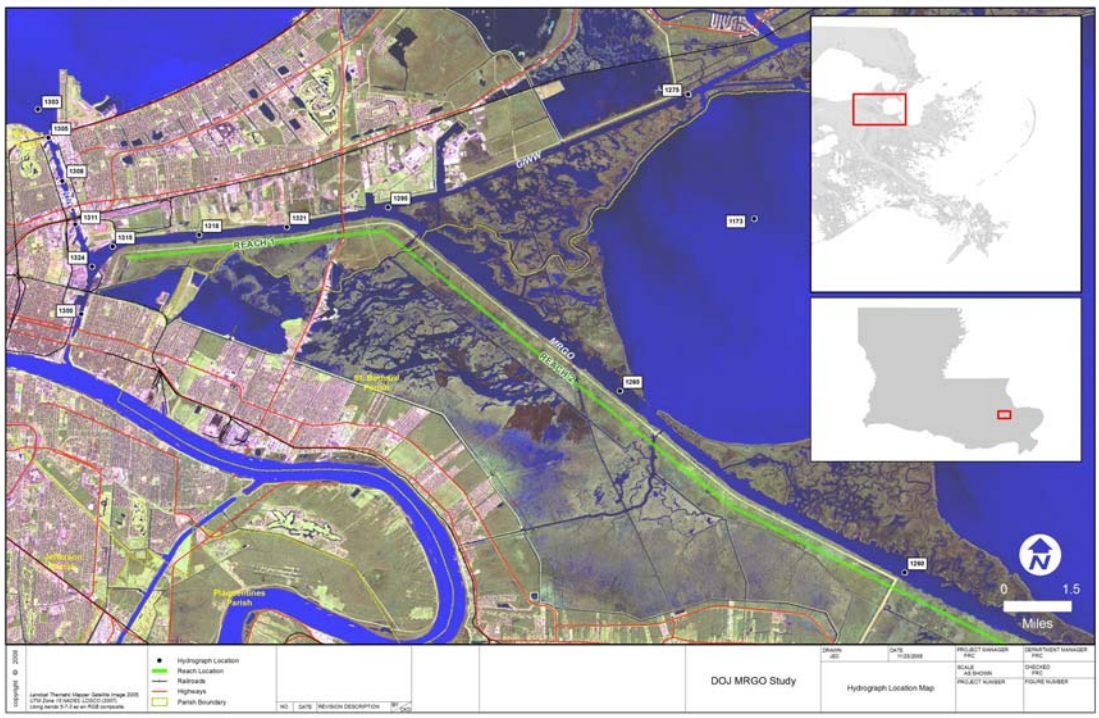


Figure 182: Water surface elevation hydrograph locations used for time series comparison of the six scenarios.

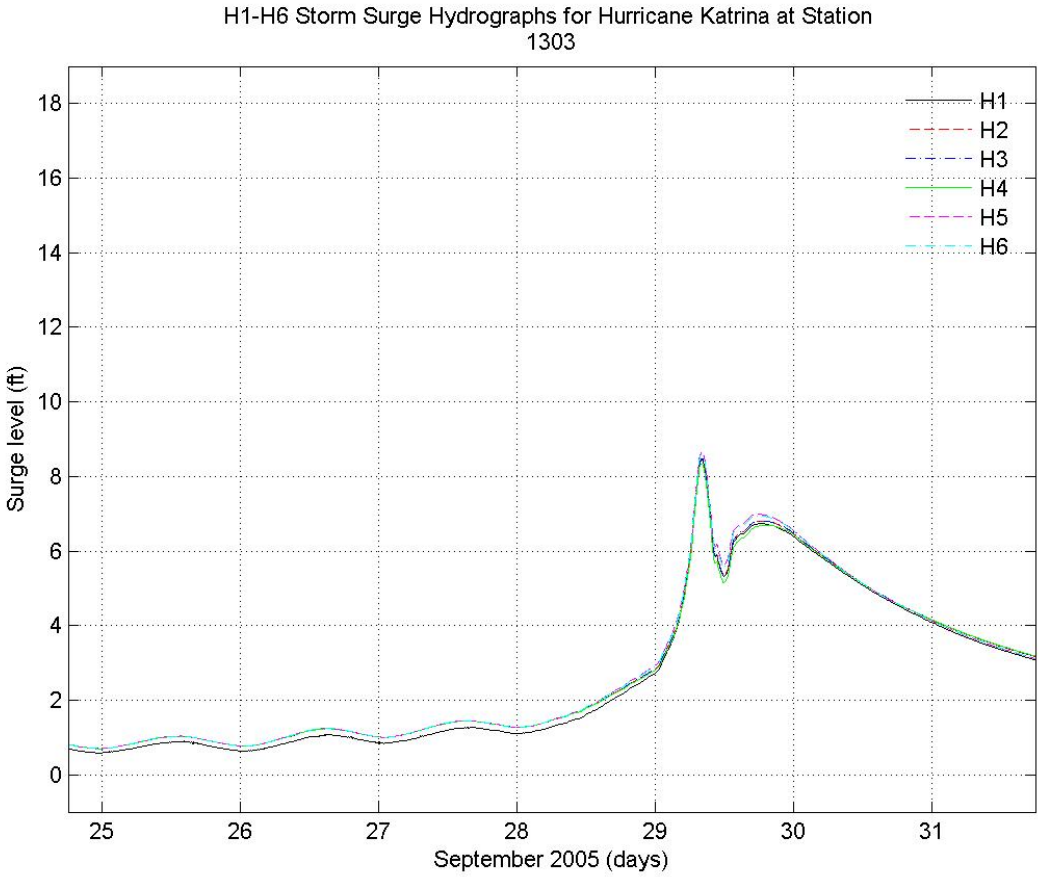


Figure 183: Time series of water surface elevation (ft) over 7 days in late September, 2005 for Scenarios H1-H6 north of Seabrook.

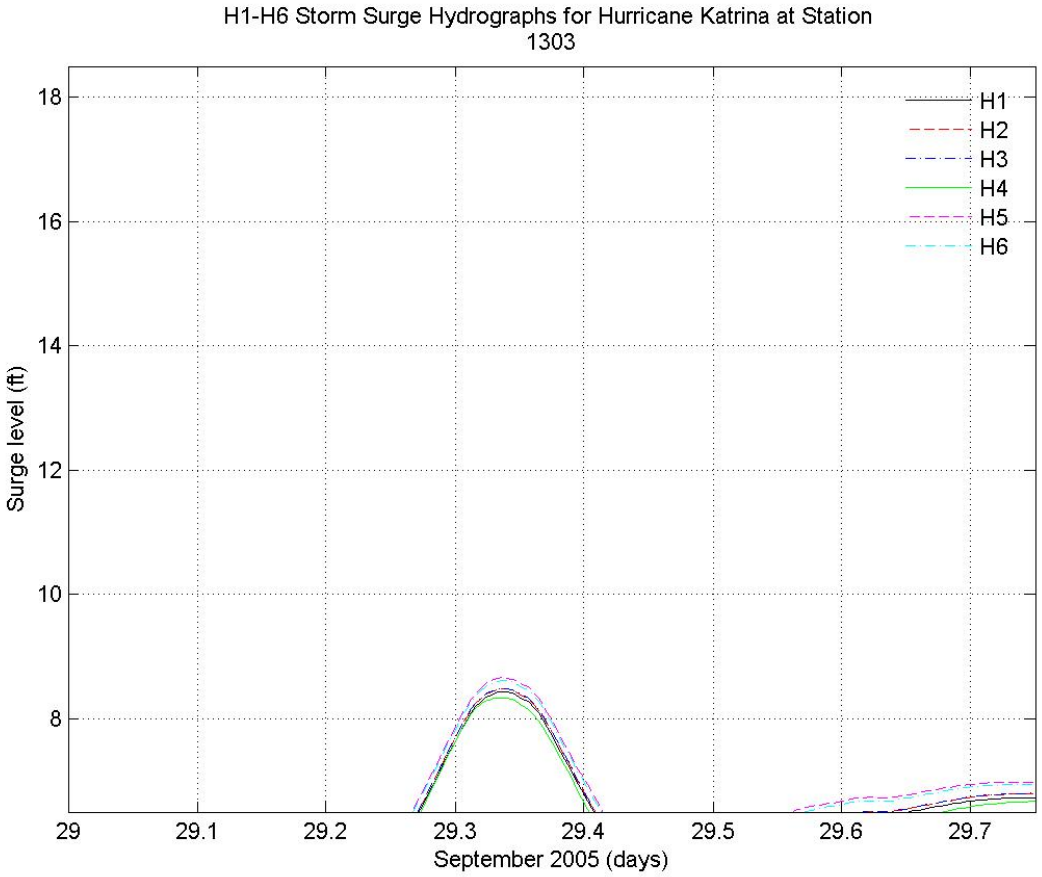


Figure 184: Time series of water surface elevation (ft) during the peak surge for Scenarios H1-H6 north of Seabrook.

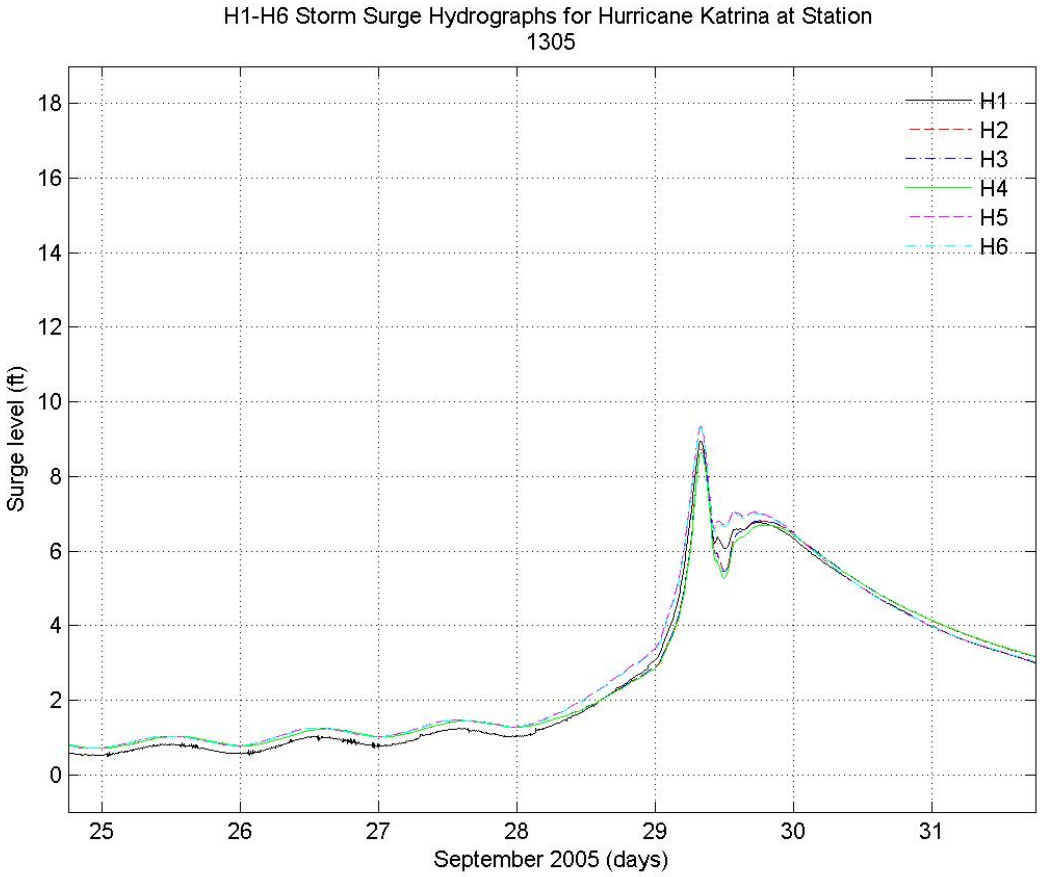


Figure 185: Time series of water surface elevation (ft) over 7 days in late September, 2005 for Scenarios H1-H6 near Seabrook.

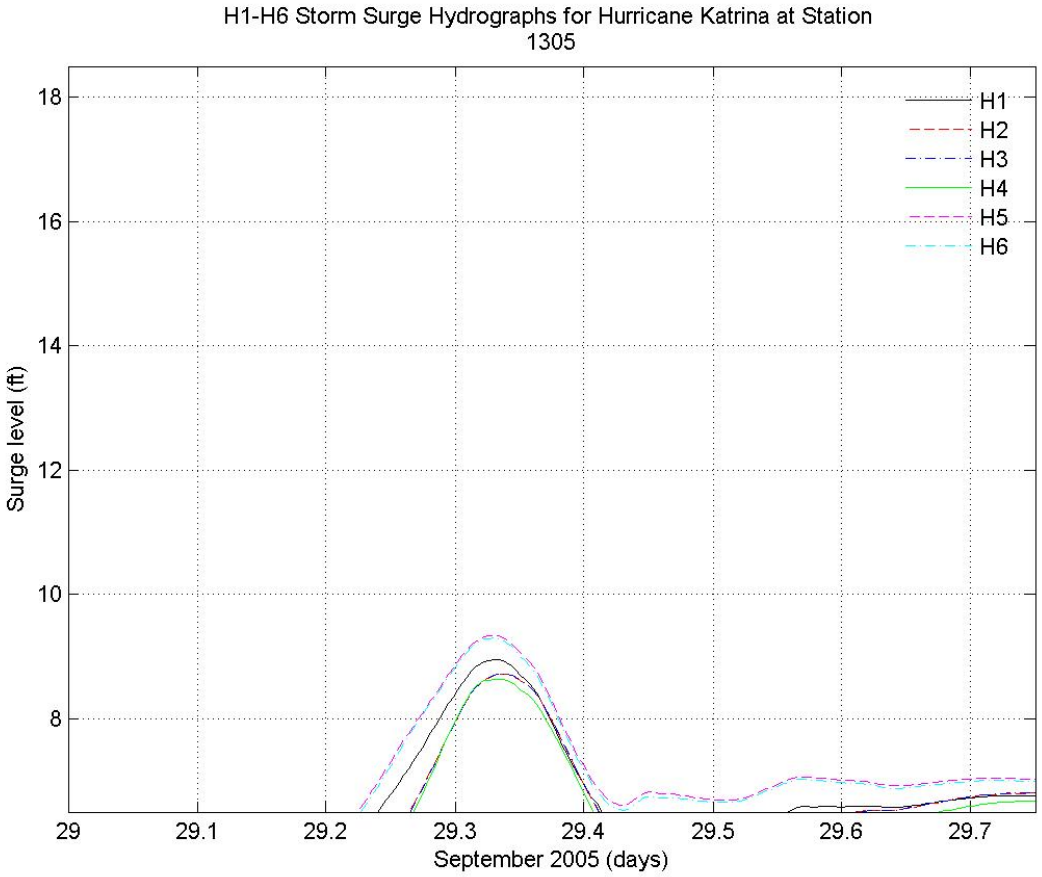


Figure 186: Time series of water surface elevation (ft) during the peak surge for Scenarios H1-H6 near Seabrook.

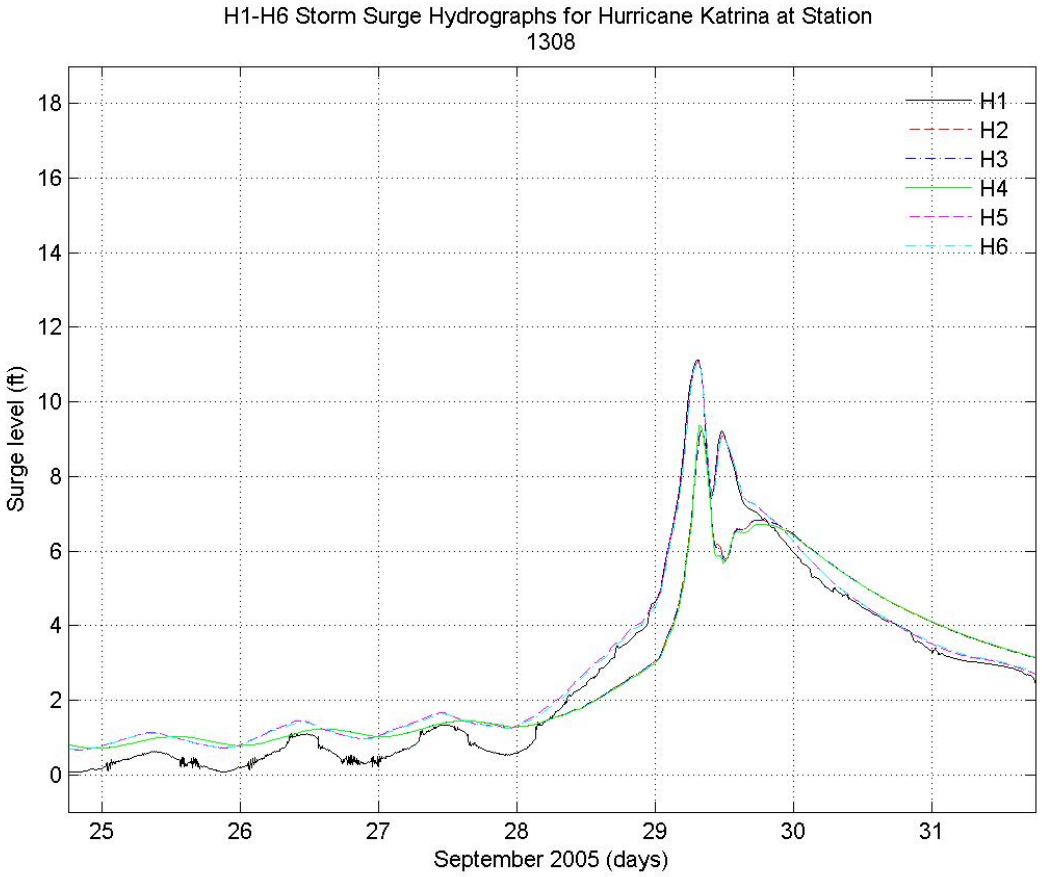


Figure 187: Time series of water surface elevation (ft) over 7 days in late September, 2005 for Scenarios H1-H6 between Seabrook and I-10.

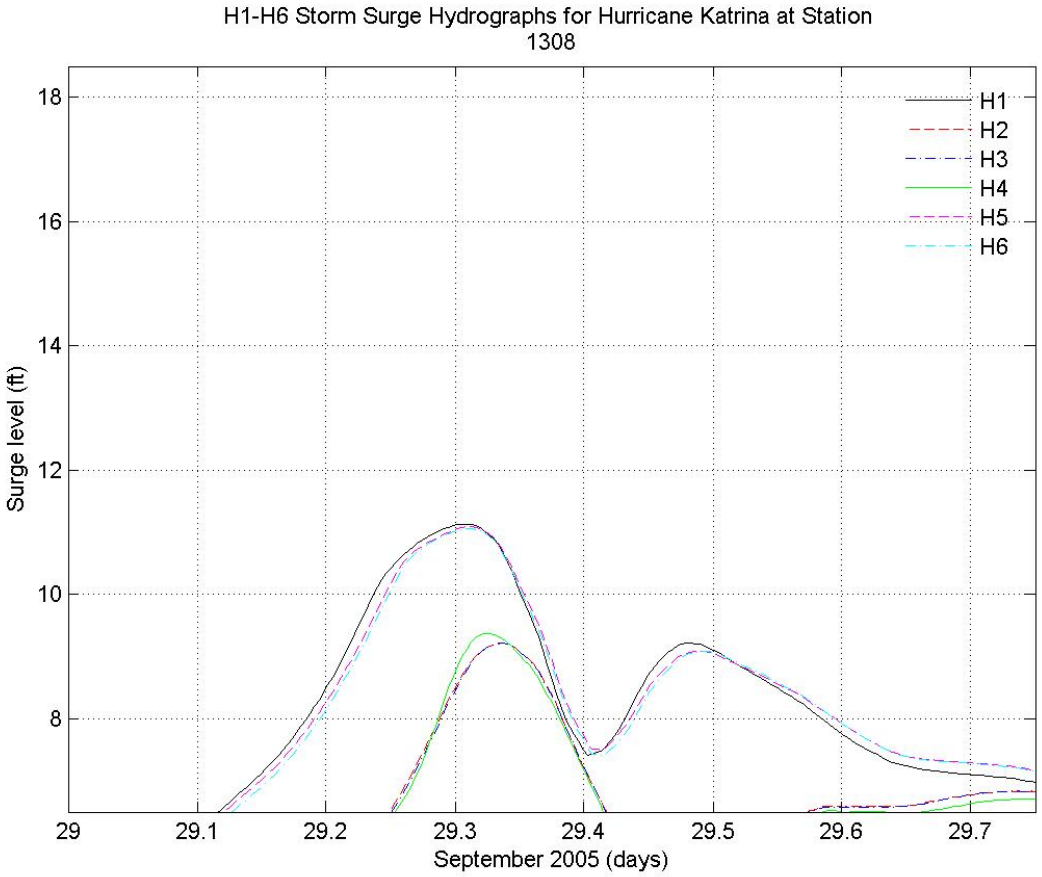


Figure 188: Time series of water surface elevation (ft) during the peak surge for Scenarios H1-H6 between Seabrook and I-10.

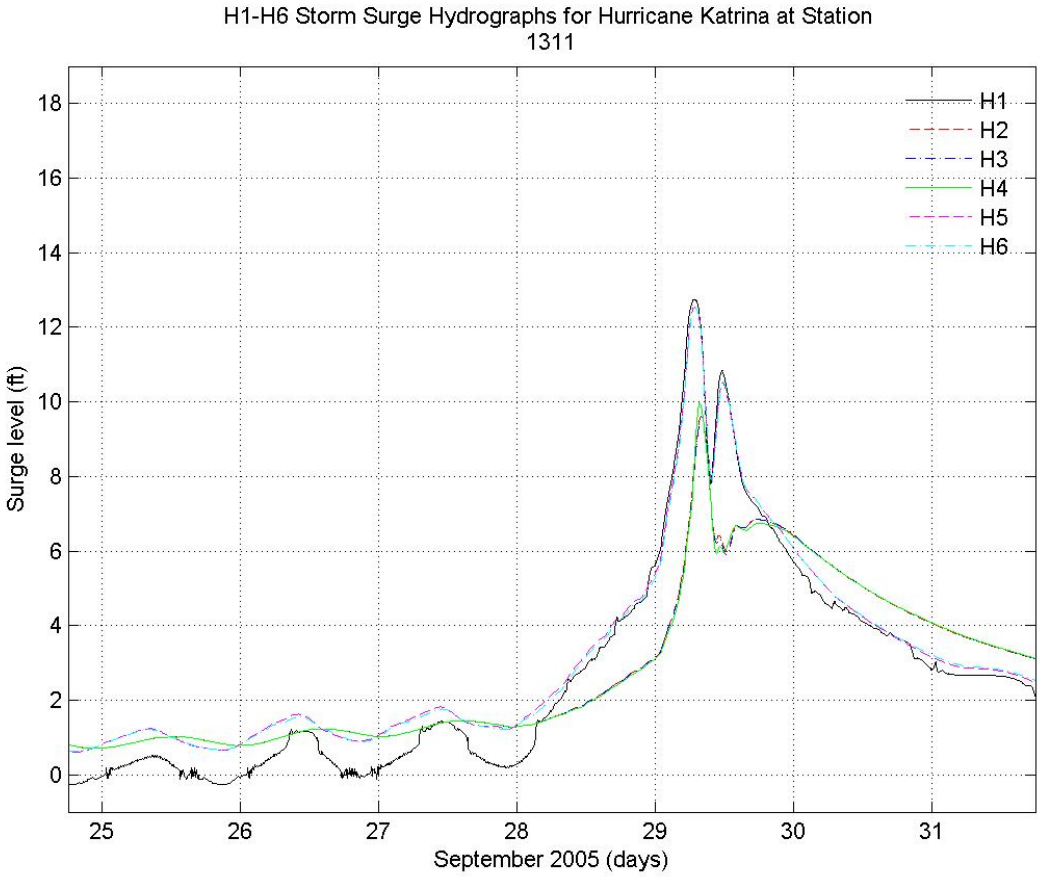


Figure 189: Time series of water surface elevation (ft) over 7 days in late September, 2005 for Scenarios H1-H6 near I-10.

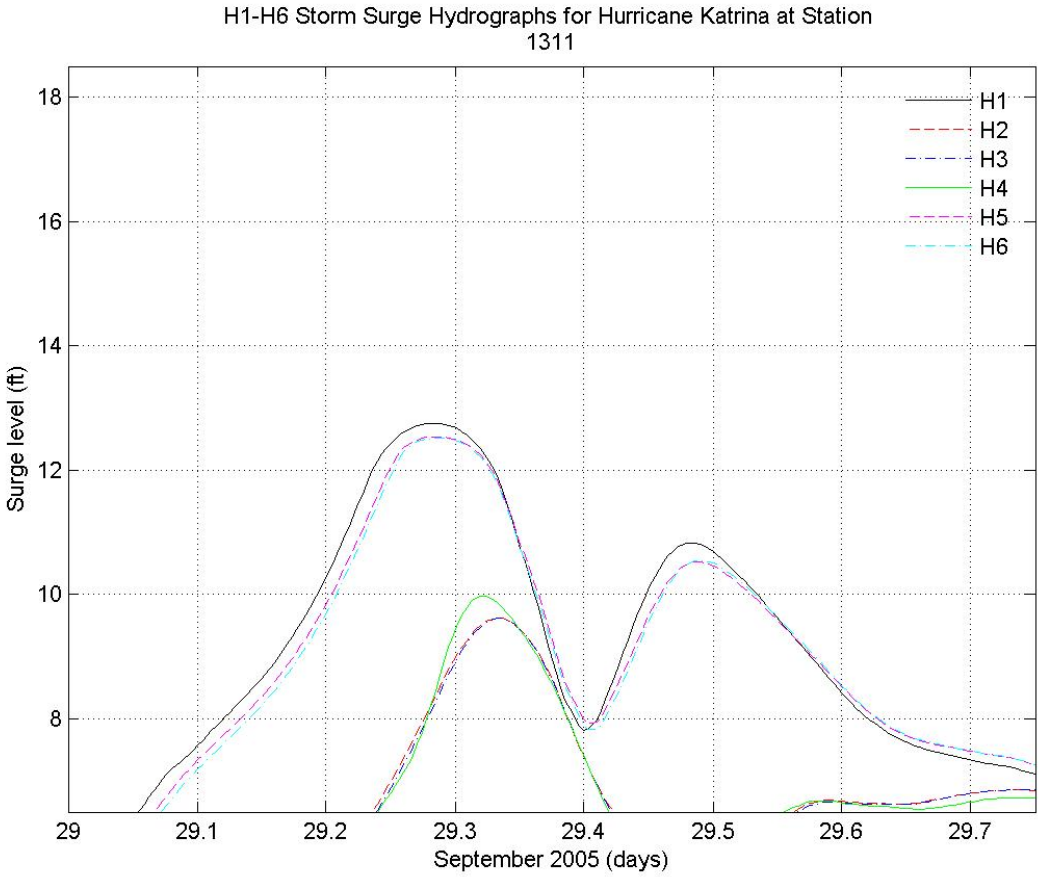


Figure 190: Time series of water surface elevation (ft) during the peak surge for Scenarios H1-H6 near I-10.

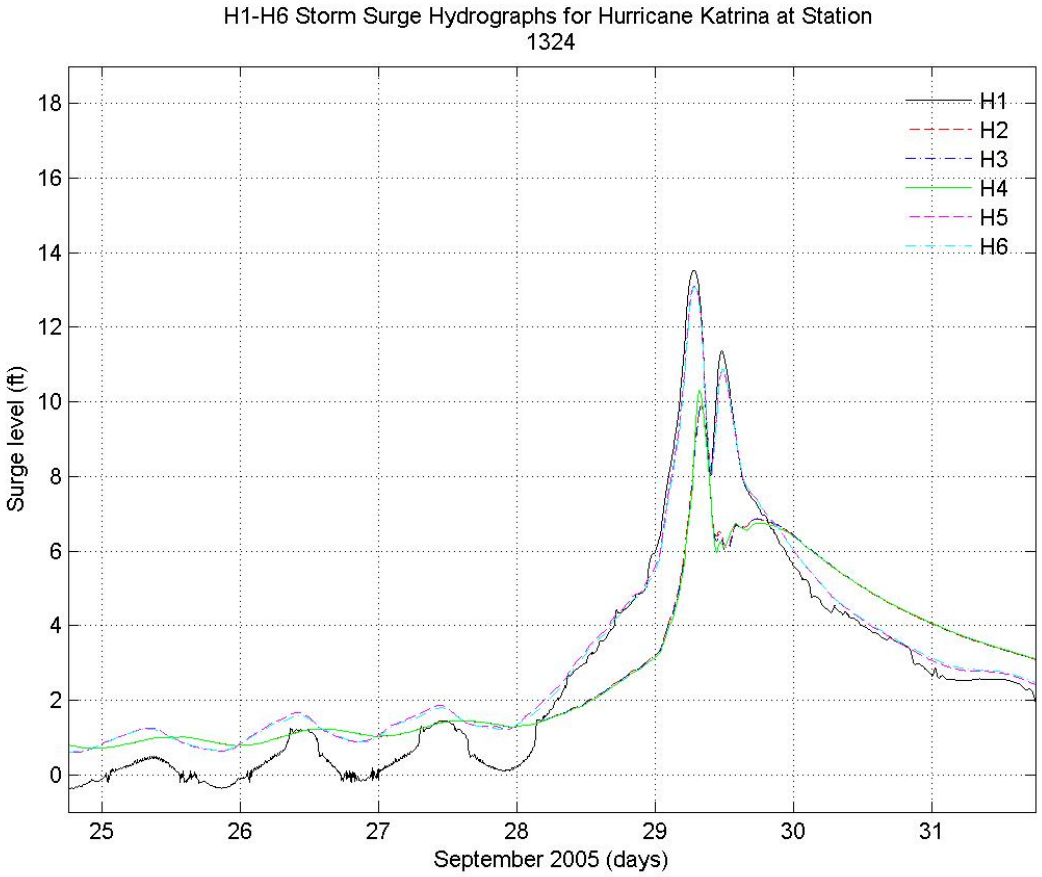


Figure 191: Time series of water surface elevation (ft) over 7 days in late September, 2005 for Scenarios H1-H6 at the confluence of the GIWW and IHNC.

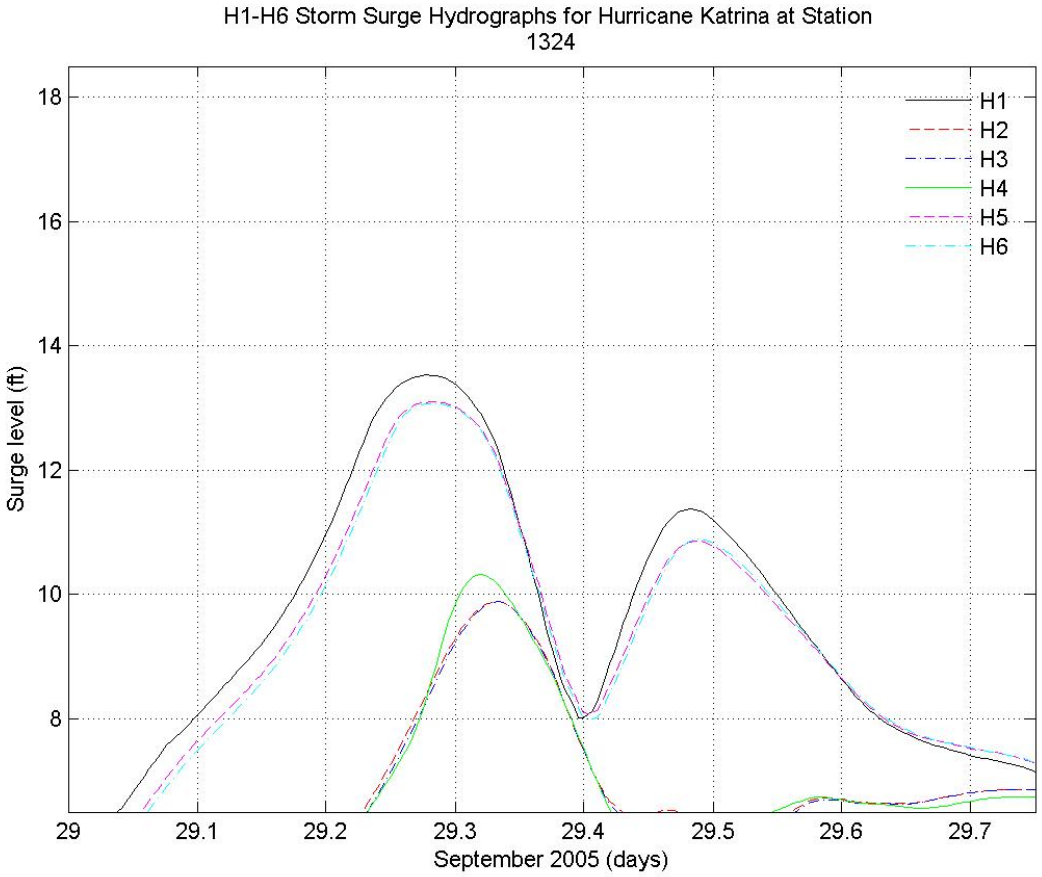


Figure 192: Time series of water surface elevation (ft) during the peak surge for Scenarios H1-H6 at the confluence of the GIWW and IHNC.

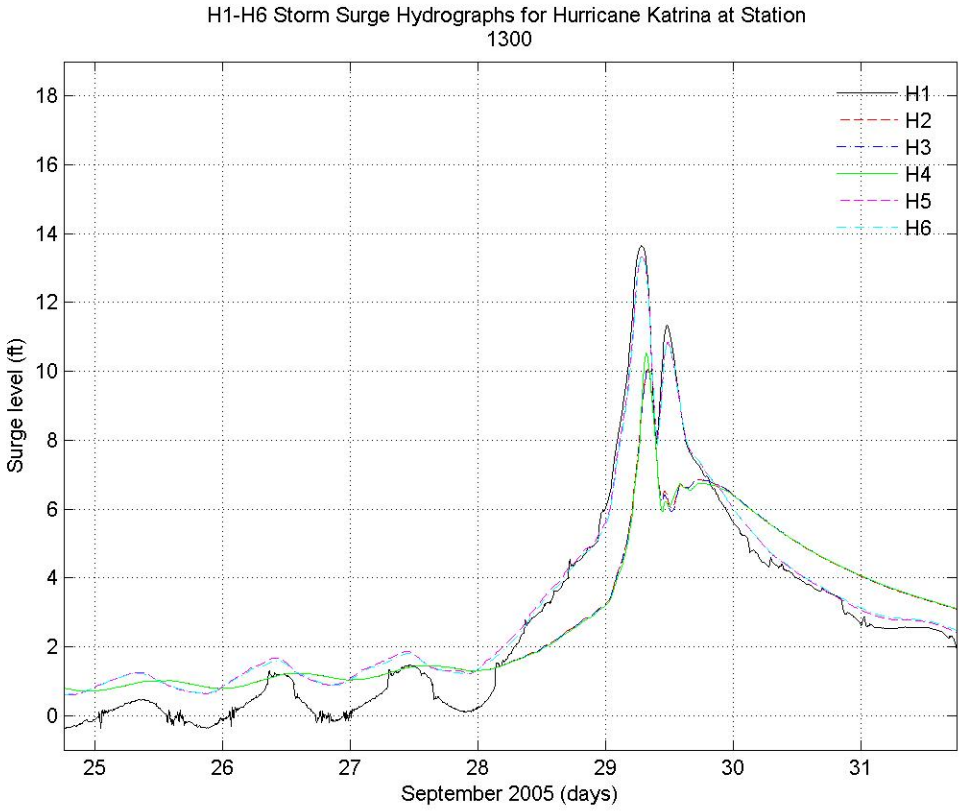


Figure 193: Time series of water surface elevation (ft) over 7 days in late September, 2005 for Scenarios H1-H6 north of the IHNC/Mississippi River locks.

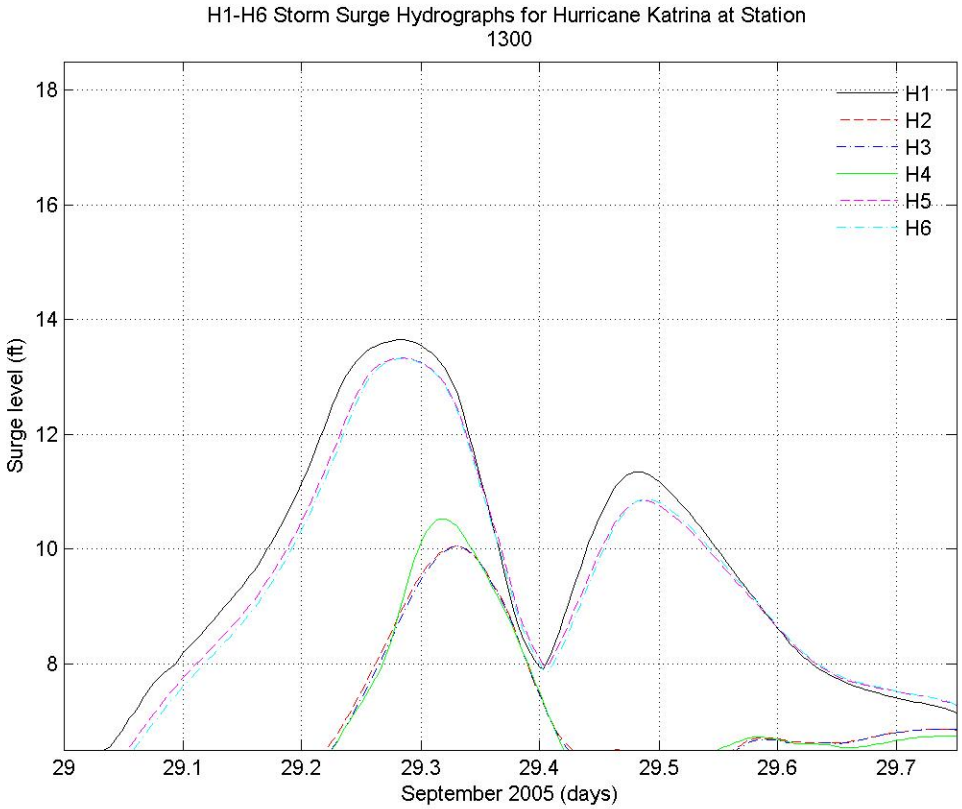


Figure 194: Time series of water surface elevation (ft) during the peak surge for Scenarios H1-H6 north of the IHNC/Mississippi River locks.

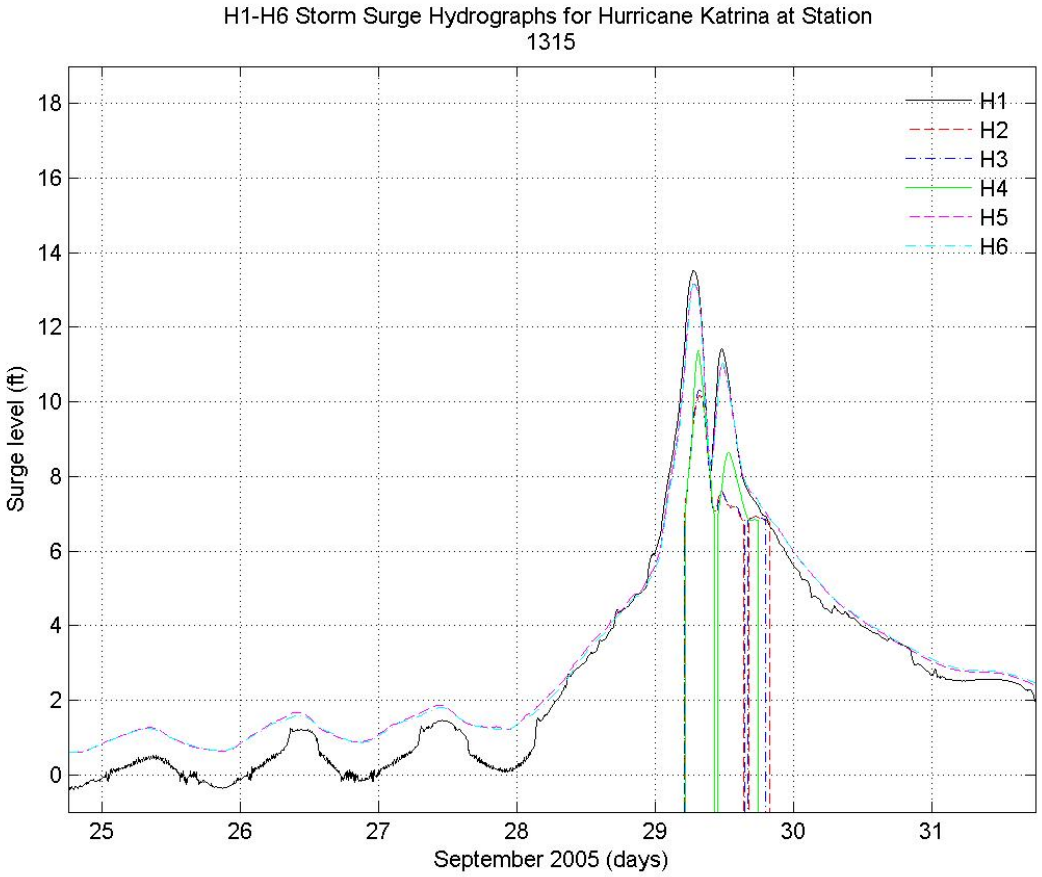


Figure 195: Time series of water surface elevation (ft) over 7 days in late September, 2005 for Scenarios H1-H6 east of the confluence of the GIWW and IHNC.

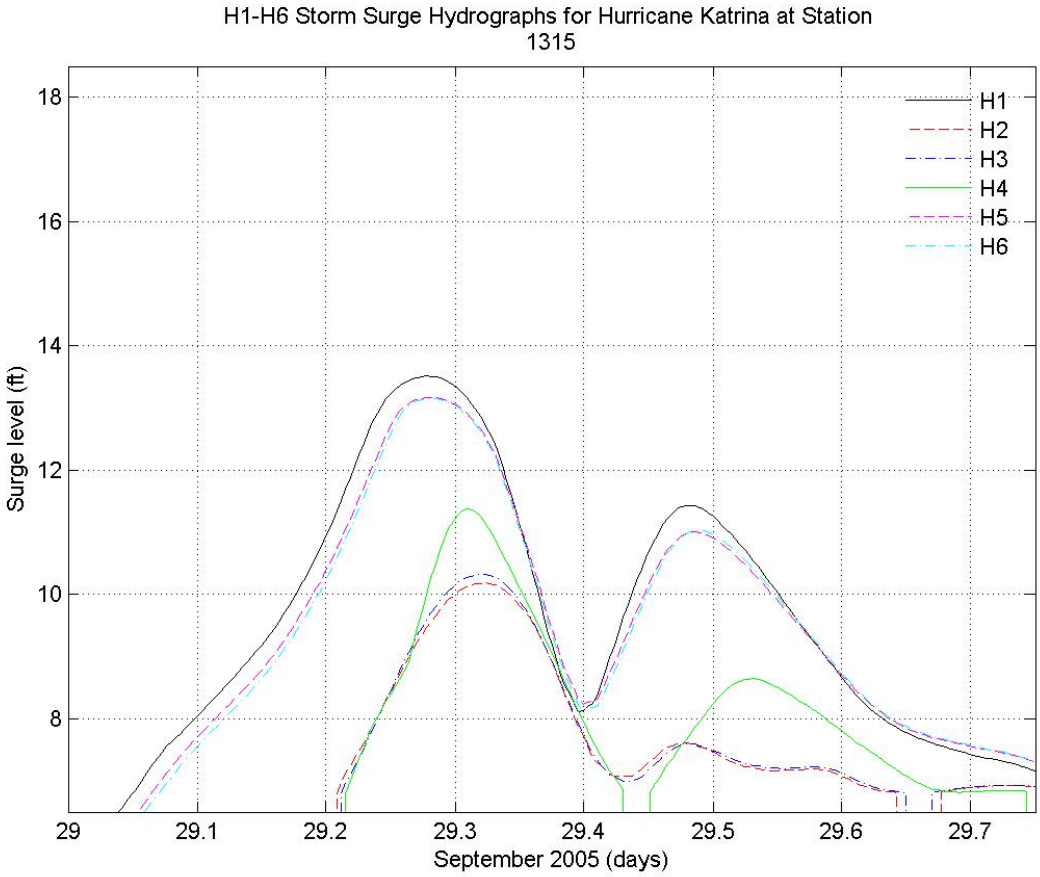


Figure 196: Time series of water surface elevation (ft) during the peak surge for Scenarios H1-H6 east of the confluence of the GIWW and IHNC.

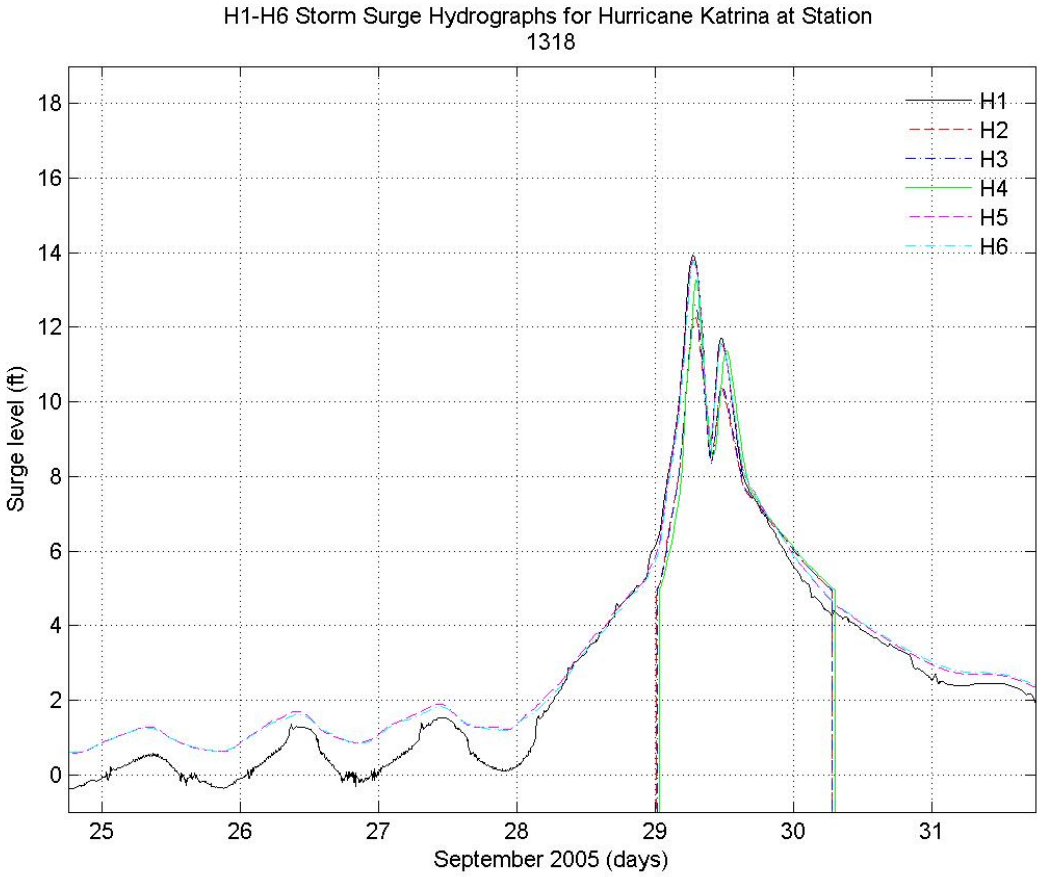


Figure 197: Time series of water surface elevation (ft) over 7 days in late September, 2005 for Scenarios H1-H6 between Paris Road and the IHNC.

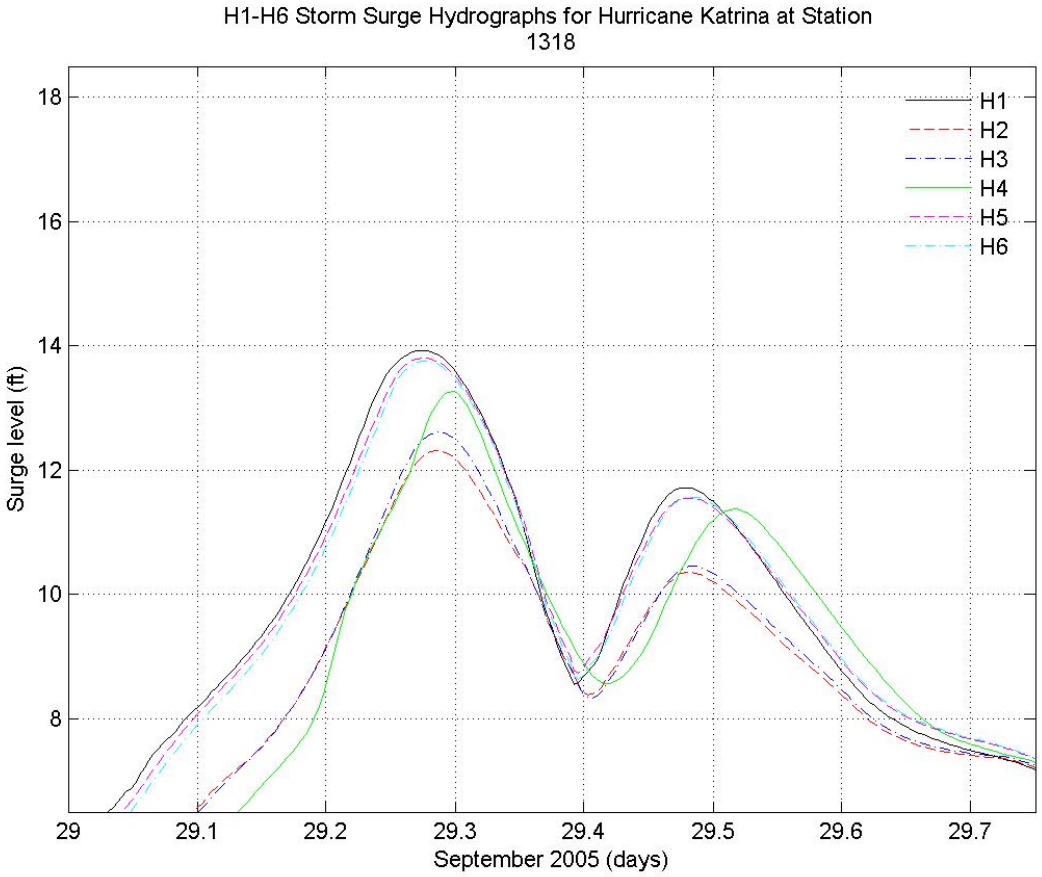


Figure 198: Time series of water surface elevation (ft) during the peak surge for Scenarios H1-H6 between Paris Road and the IHNC.

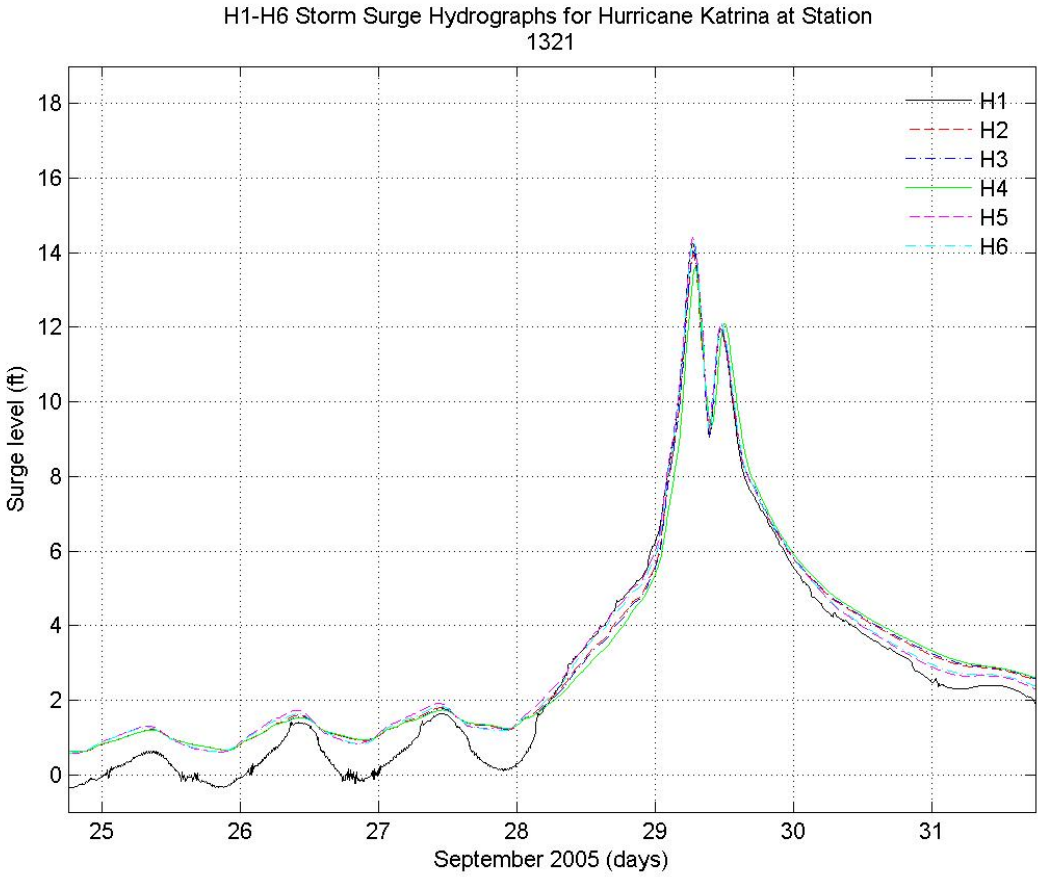


Figure 199: Time series of water surface elevation (ft) over 7 days in late September, 2005 for Scenarios H1-H6 west of Paris Road.

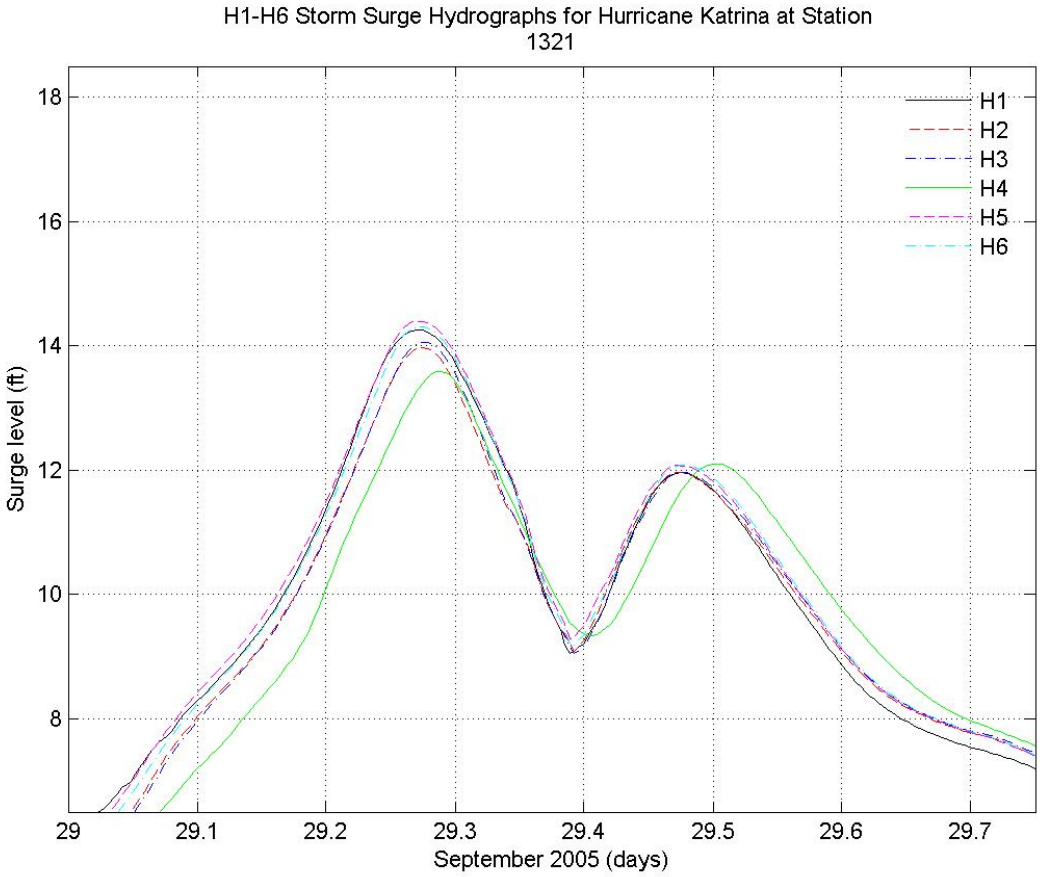


Figure 200: Time series of water surface elevation (ft) during the peak surge for Scenarios H1-H6 west of Paris Road.

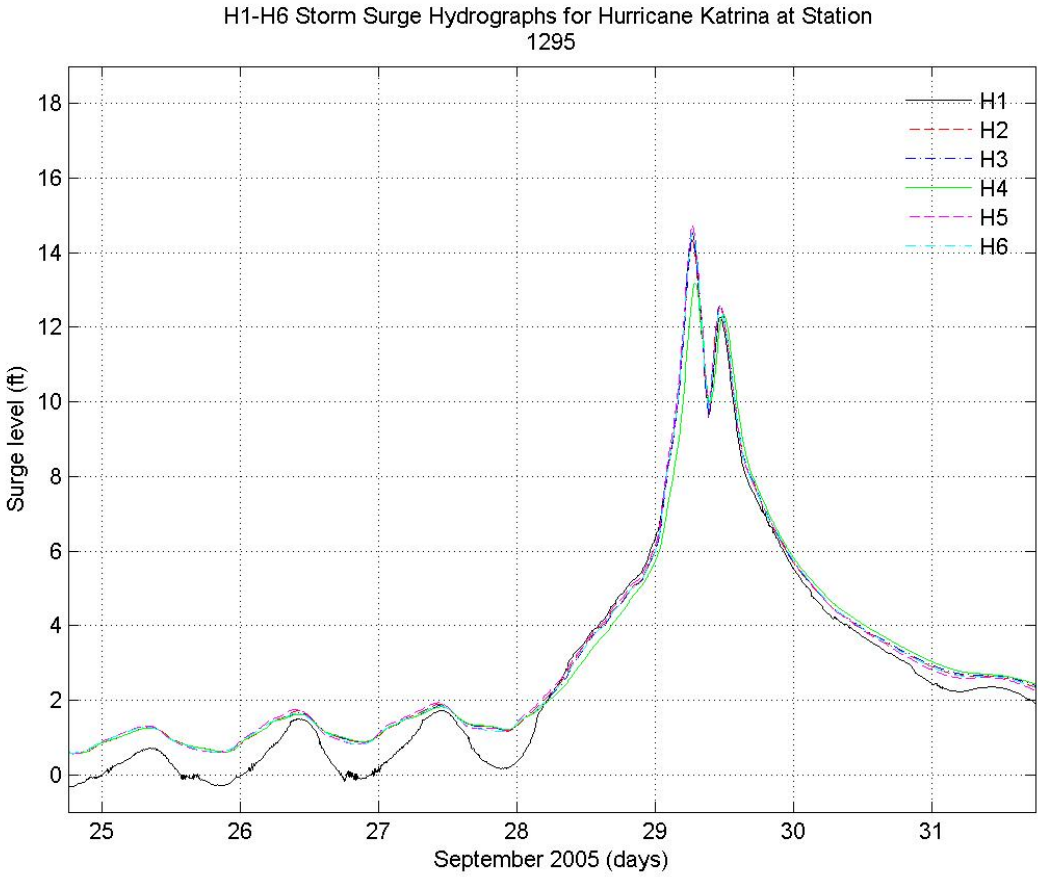


Figure 201: Time series of water surface elevation (ft) over 7 days in late September, 2005 for Scenarios H1-H6 east of the confluence of the GIWW and MRGO.

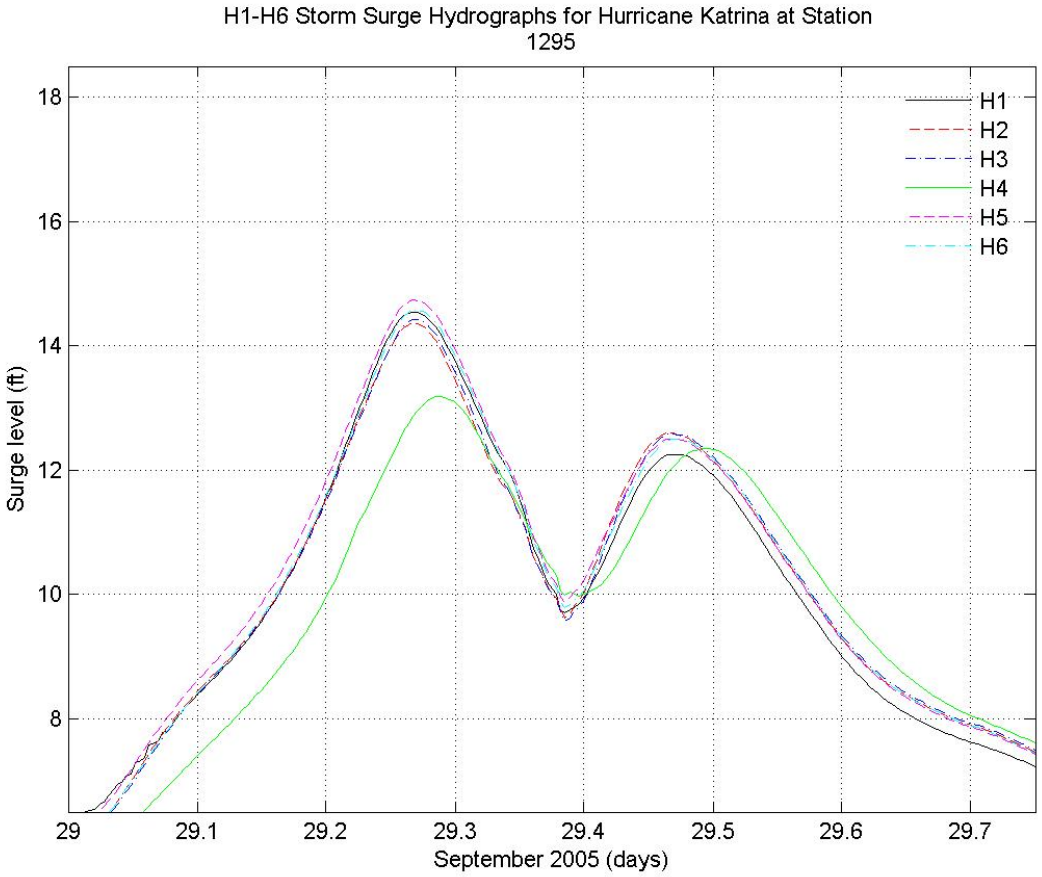


Figure 202: Time series of water surface elevation (ft) during the peak surge for Scenarios H1-H6 east of the confluence of the GIWW and MRGO.

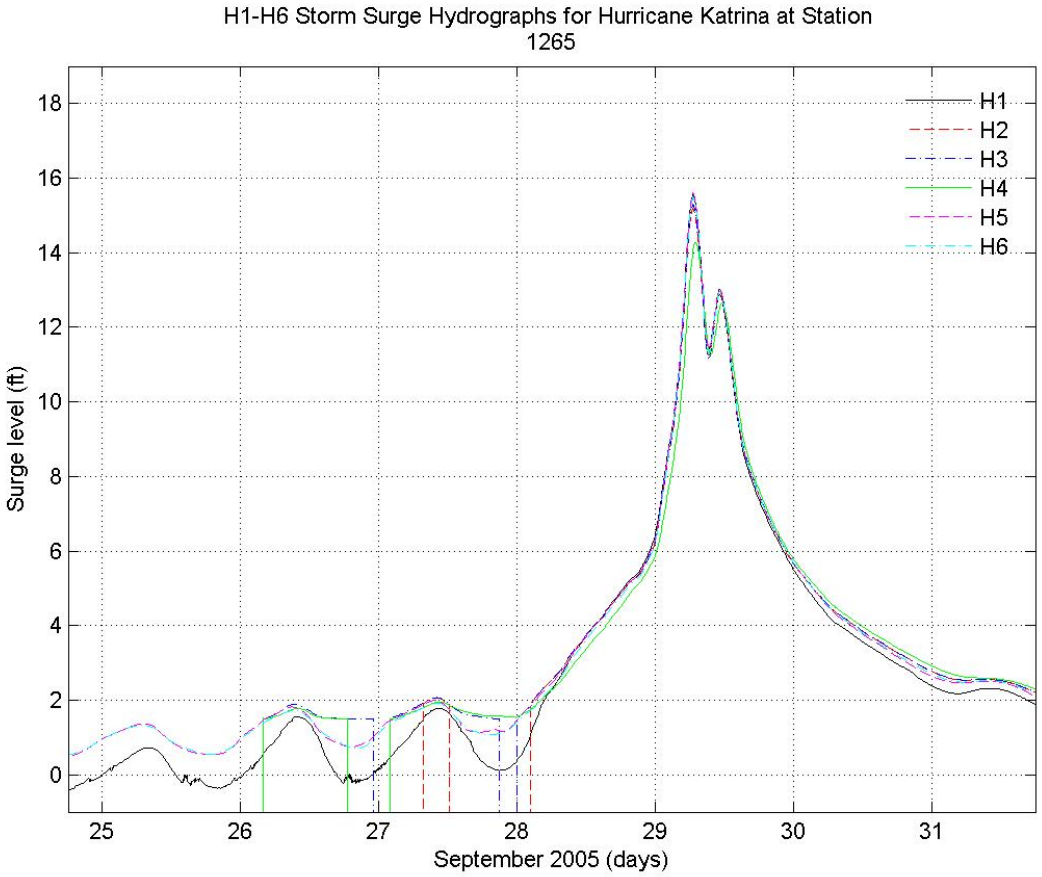


Figure 203: Time series of water surface elevation (ft) over 7 days in late September, 2005 for Scenarios H1-H6 in the MRGO near Bayou Pollett.

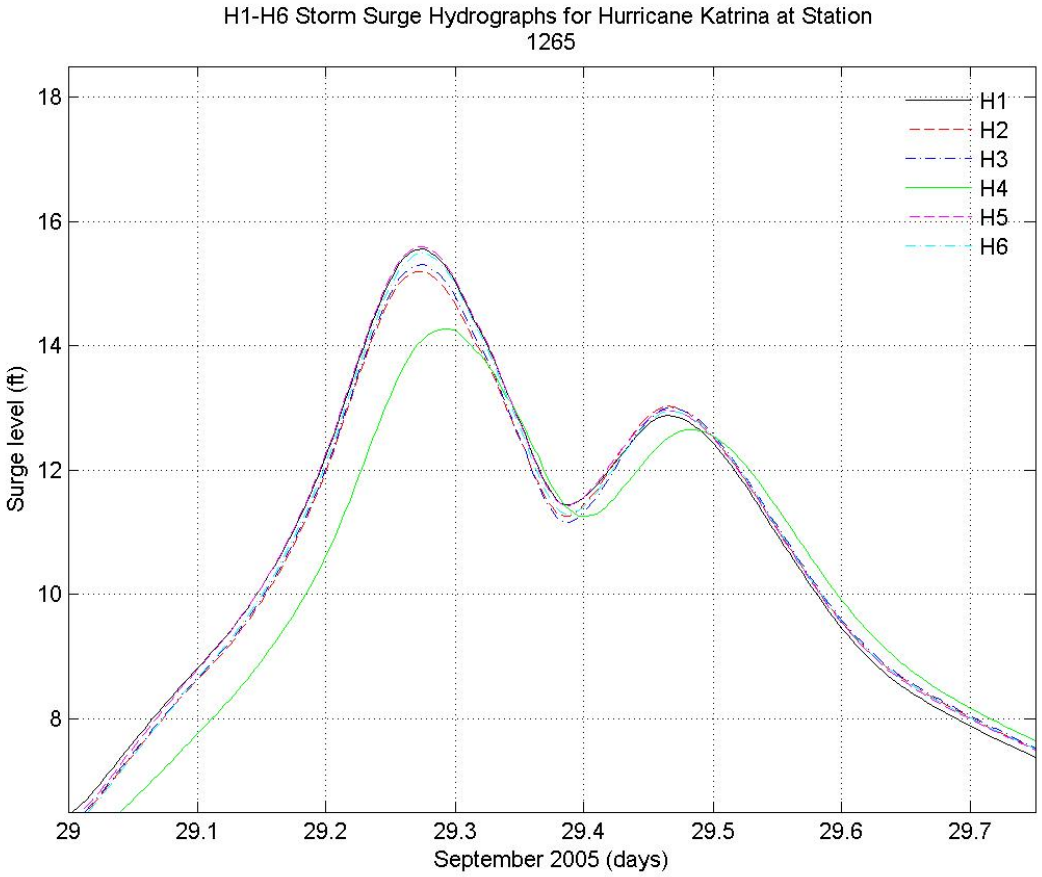


Figure 204: Time series of water surface elevation (ft) during the peak surge for Scenarios H1-H6 in the MRGO near Bayou Pollett.

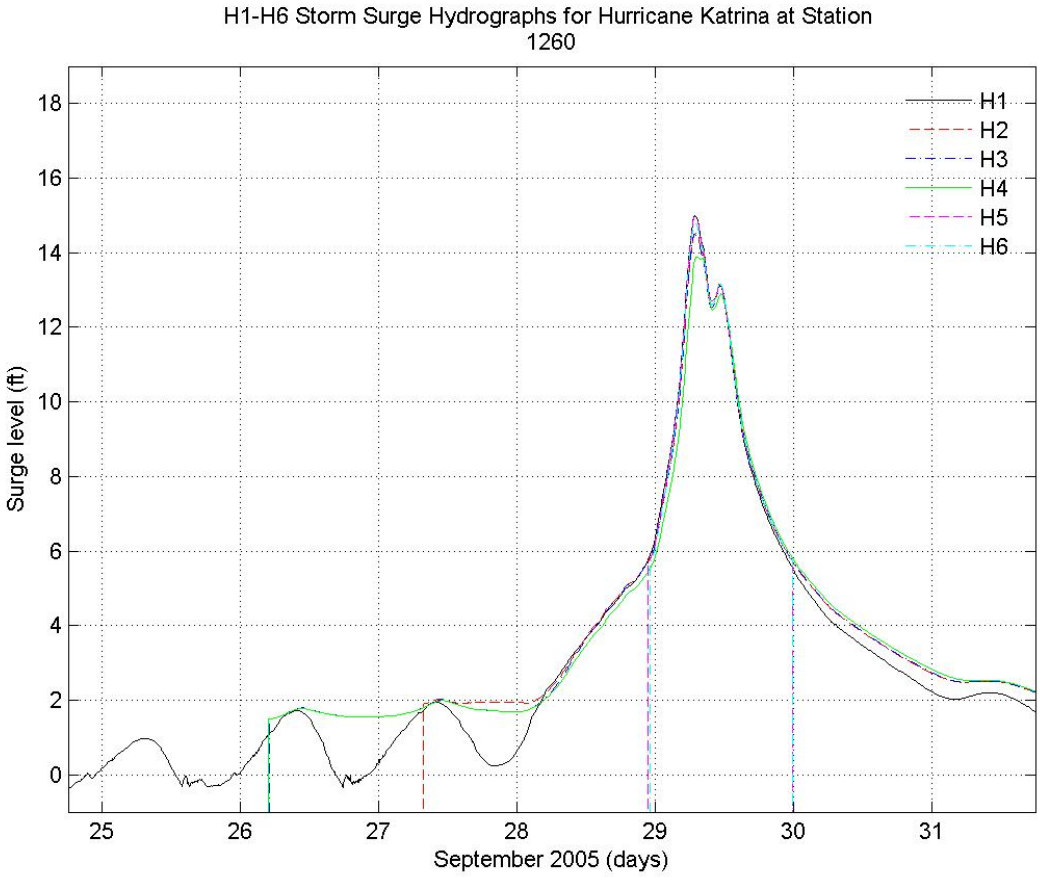


Figure 205: Time series of water surface elevation (ft) over 7 days in late September, 2005 for Scenarios H1-H6 in the MRGO near the southern extents of St. Bernard Parish.

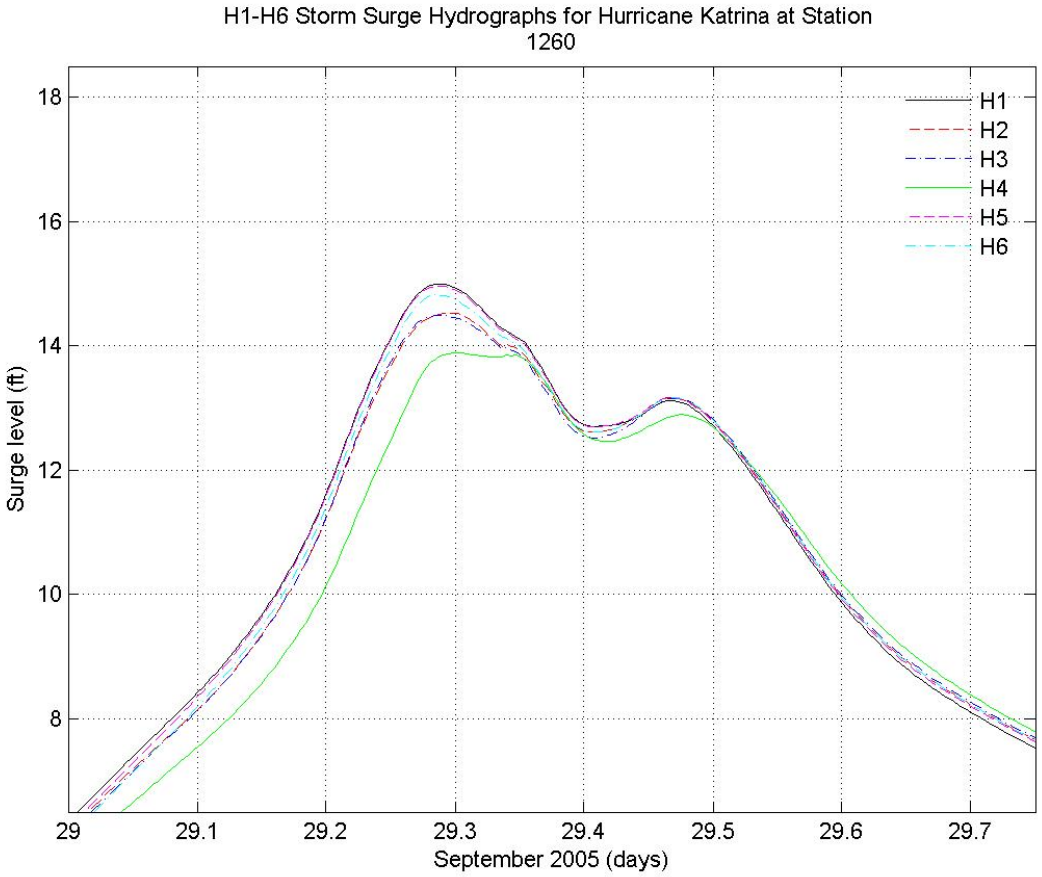


Figure 206: Time series of water surface elevation (ft) during the peak surge for Scenarios H1-H6 in the MRGO near the southern extents of St. Bernard Parish.

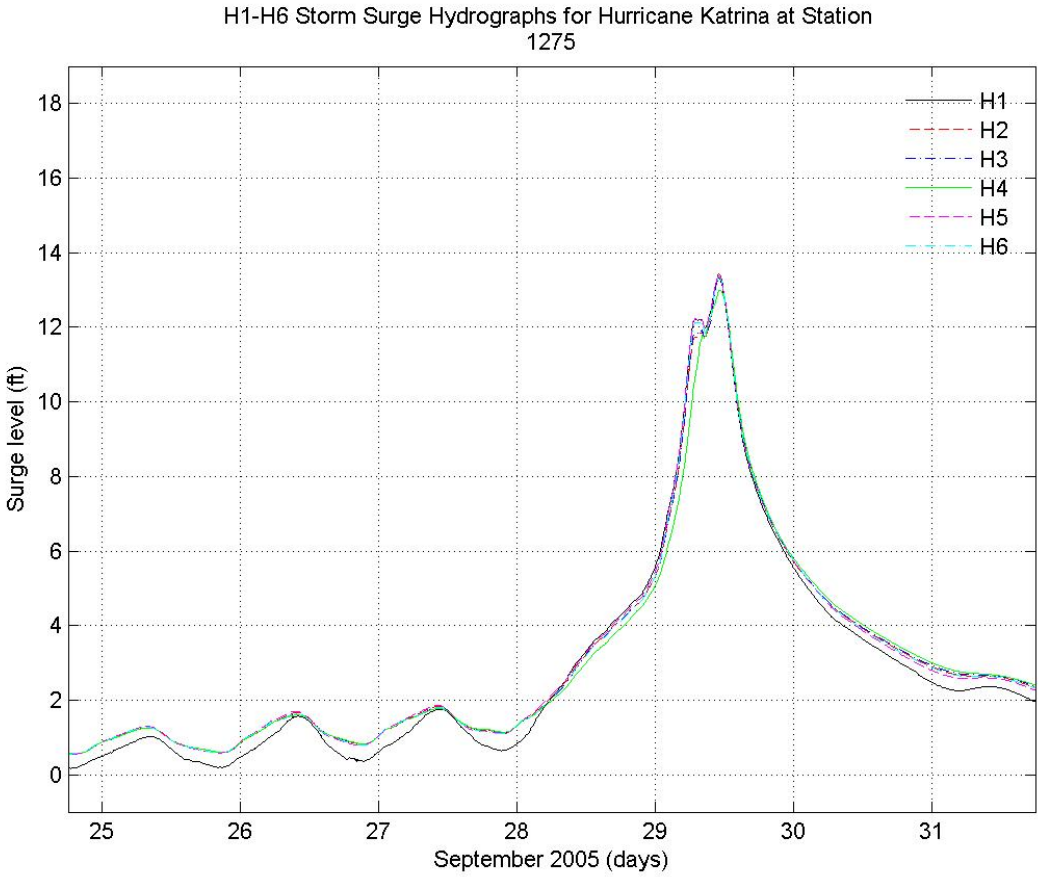


Figure 207: Time series of water surface elevation (ft) over 7 days in late September, 2005 for Scenarios H1-H6 in the GIWW near Bayou Thomas.

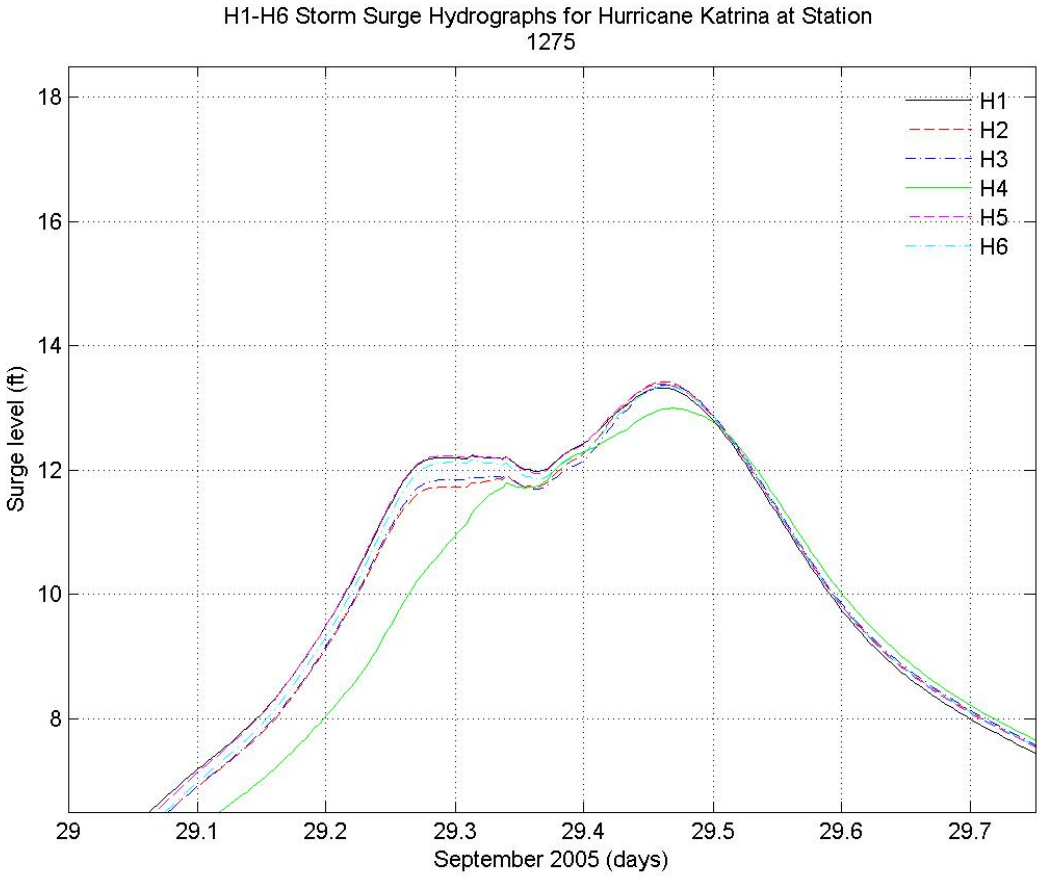


Figure 208: Time series of water surface elevation (ft) during the peak surge for Scenarios H1-H6 in the GIWW near Bayou Thomas.

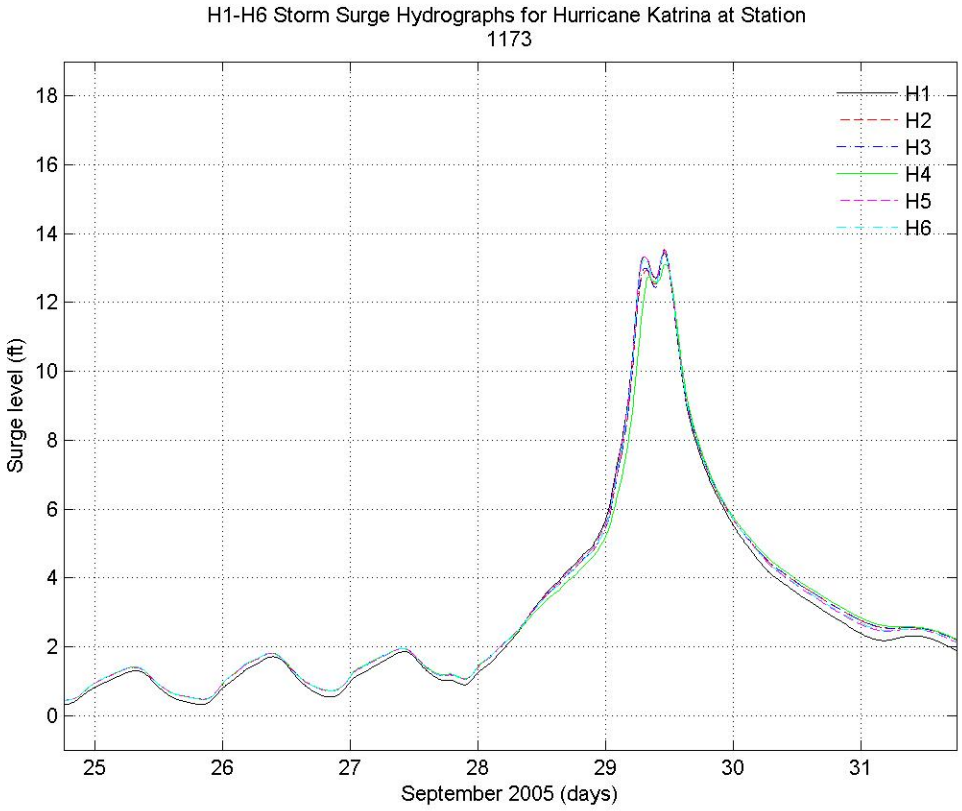


Figure 209: Time series of water surface elevation (ft) over 7 days in late September, 2005 for Scenarios H1-H6 in Lake Borgne.

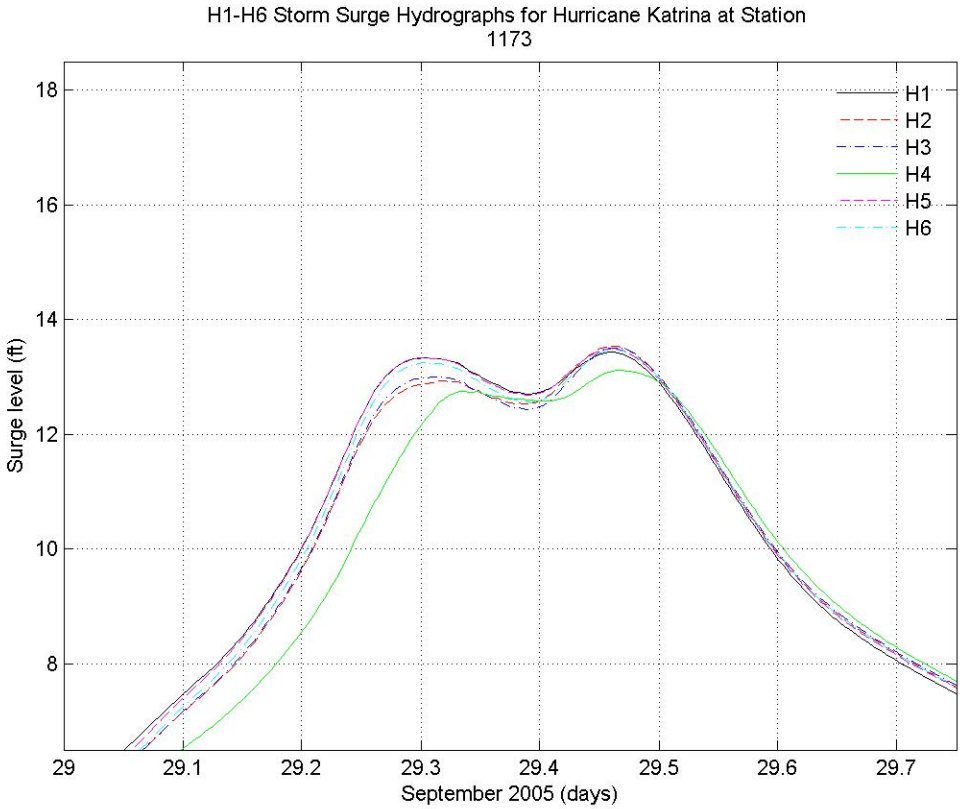


Figure 210: Time series of water surface elevation (ft) during the peak surge for Scenarios H1-H6 in Lake Borgne.

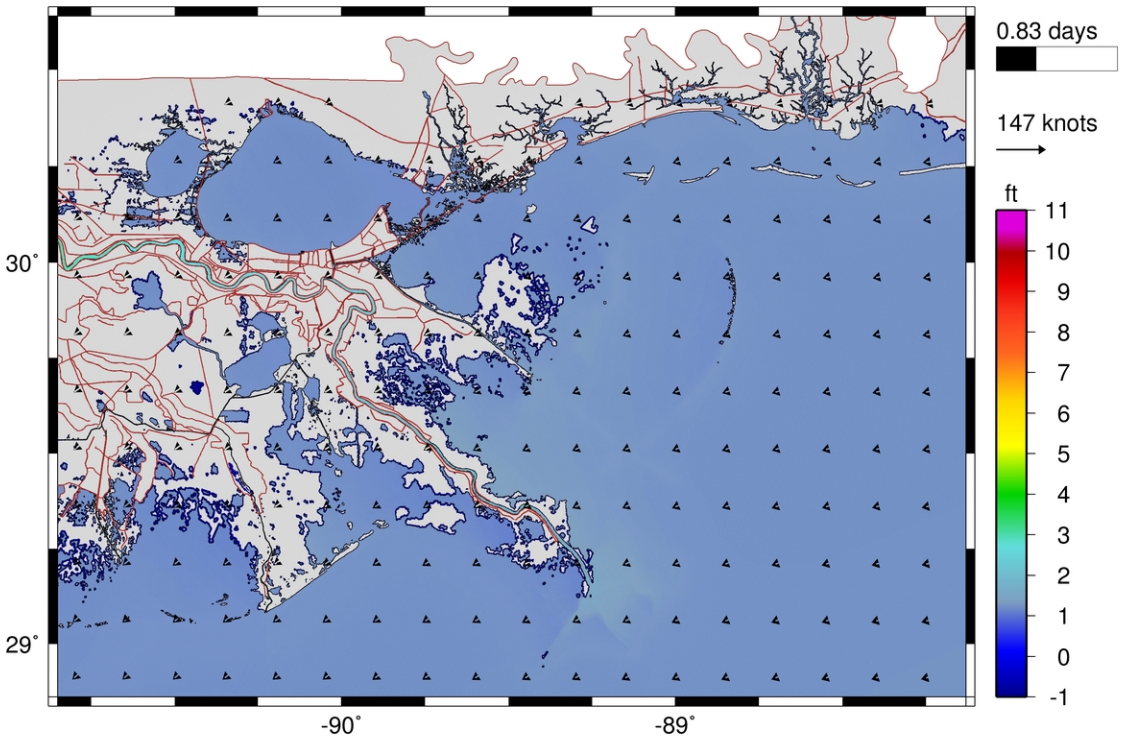


Figure 211: ADCIRC surface elevations (ft) and wind vectors (knots) for a Hurricane Gustav forecast using Advisory 32 at time equals 0.83 days.

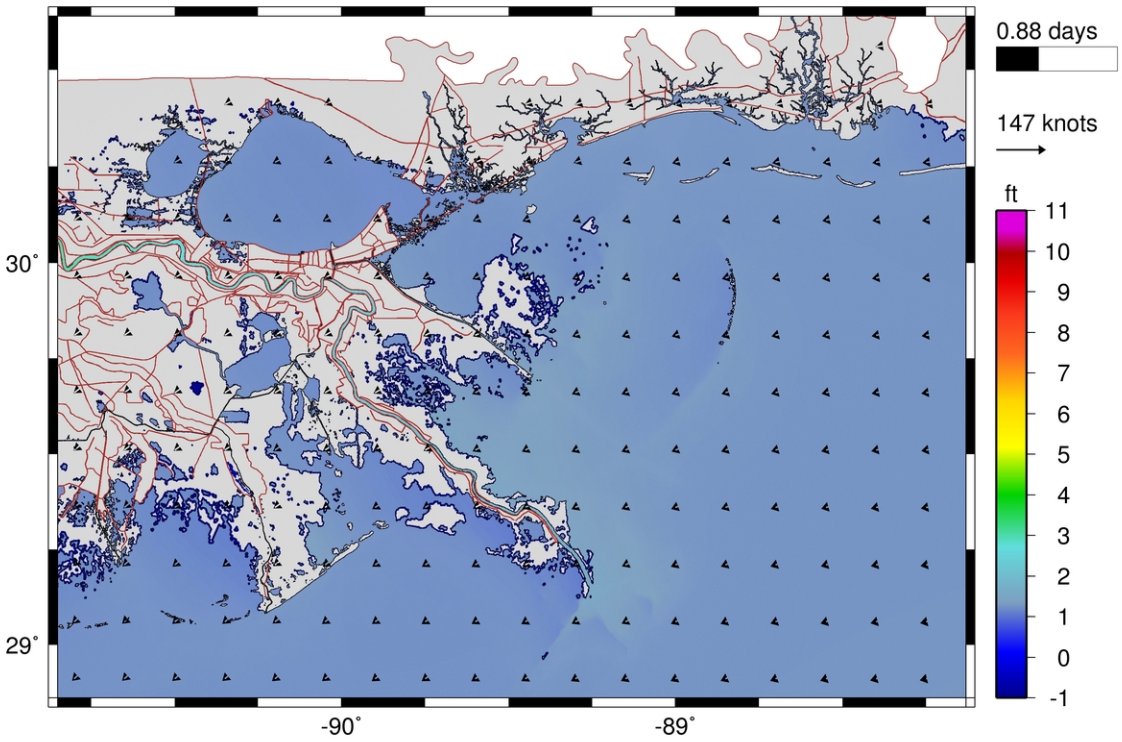


Figure 212: ADCIRC surface elevations (ft) and wind vectors (knots) for a Hurricane Gustav forecast using Advisory 32 at time equals 0.88 days.

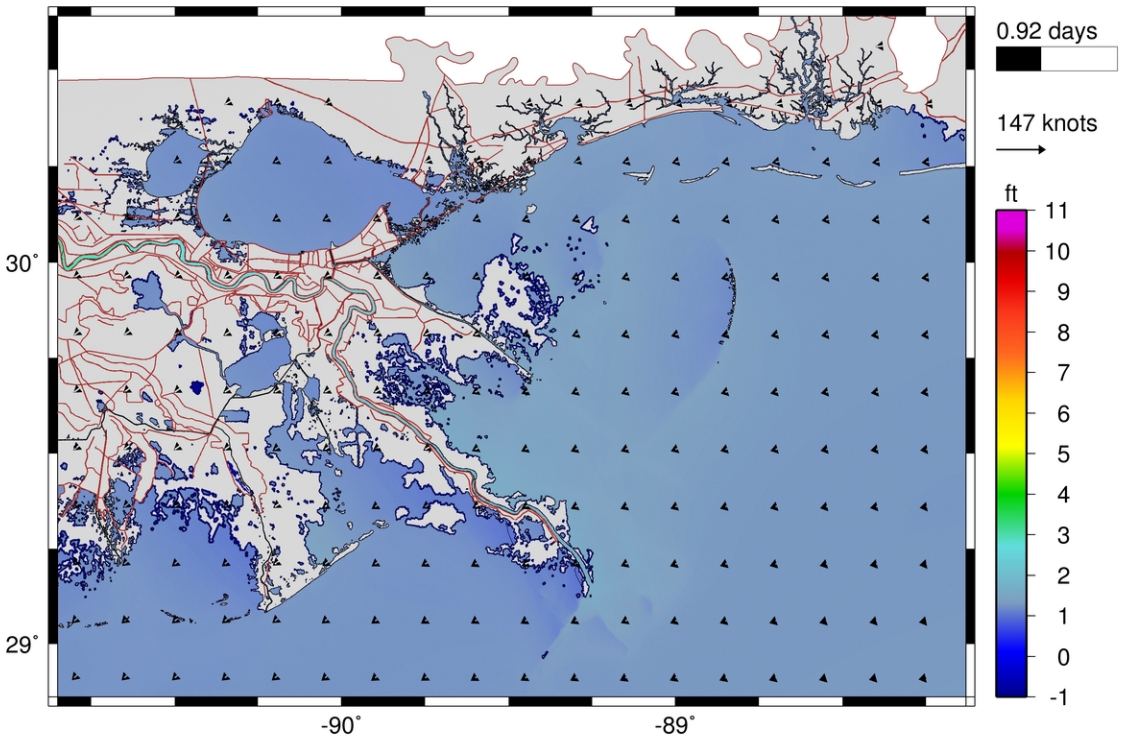


Figure 213: ADCIRC surface elevations (ft) and wind vectors (knots) for a Hurricane Gustav forecast using Advisory 32 at time equals 0.92 days.

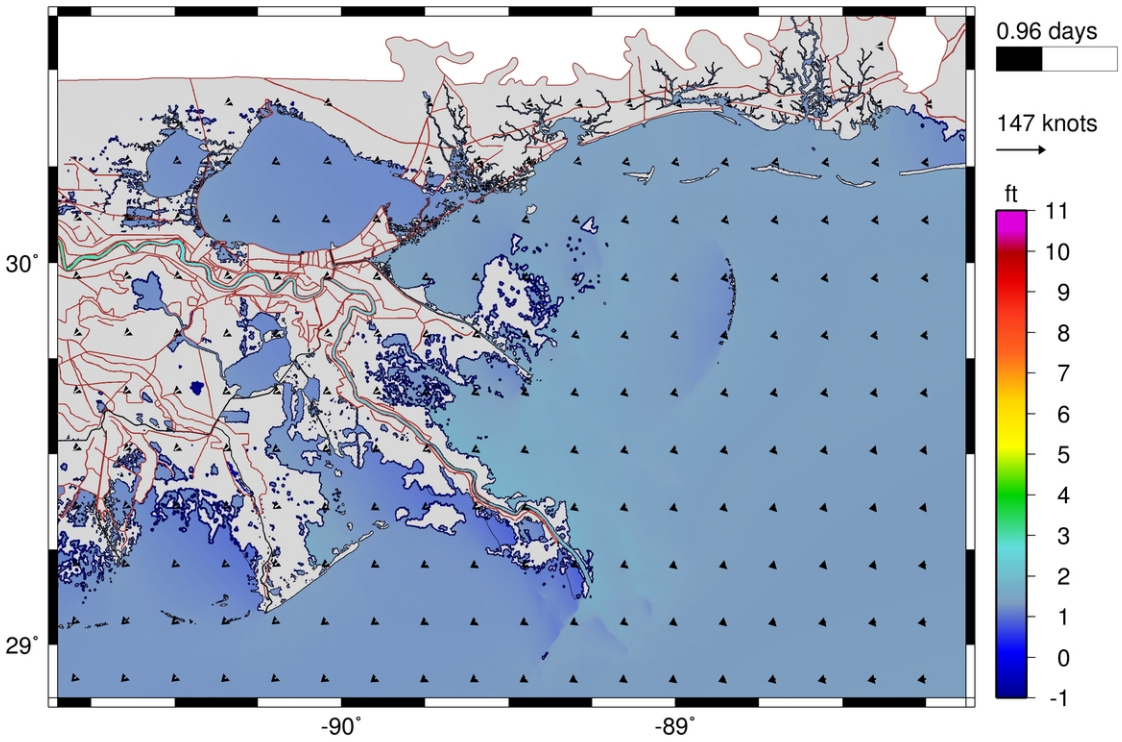


Figure 214: ADCIRC surface elevations (ft) and wind vectors (knots) for a Hurricane Gustav forecast using Advisory 32 at time equals 0.96 days.

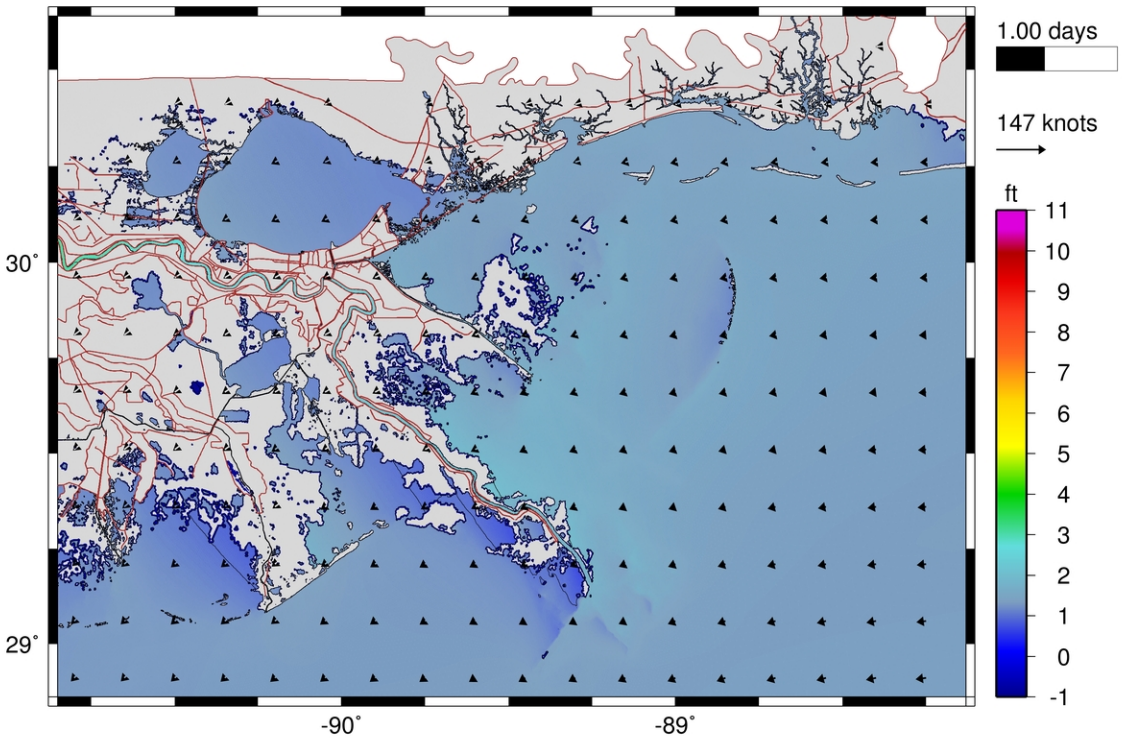


Figure 215: ADCIRC surface elevations (ft) and wind vectors (knots) for a Hurricane Gustav forecast using Advisory 32 at time equals 1.00 days.

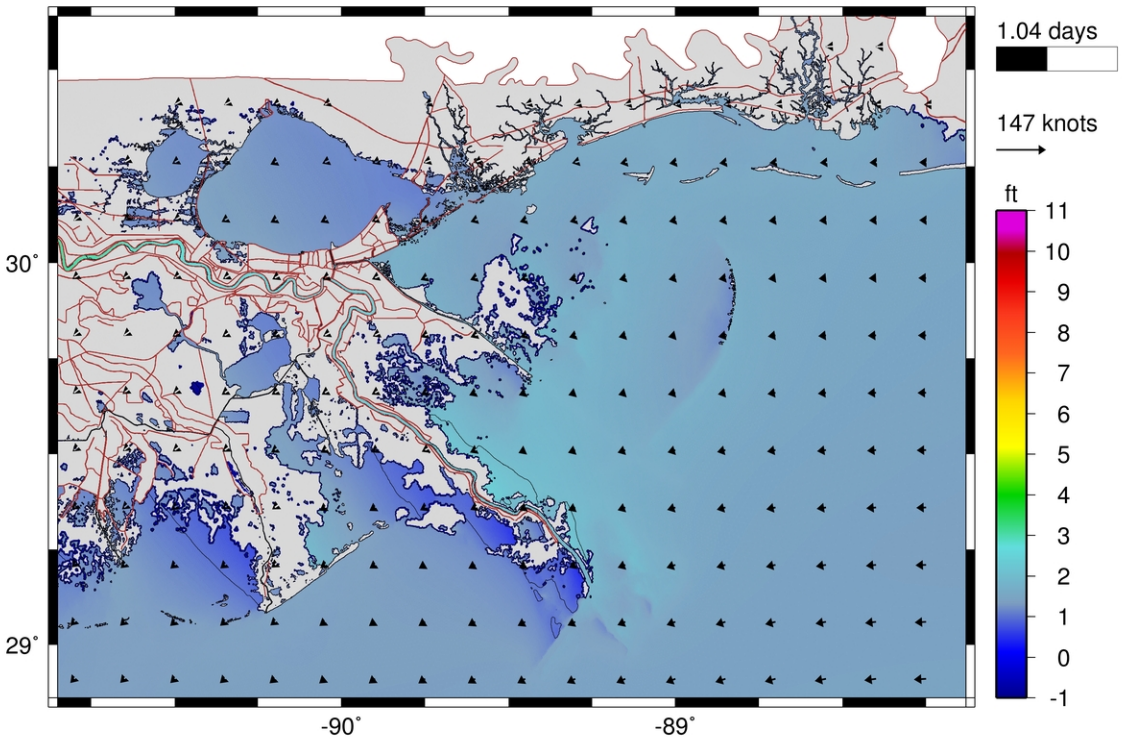


Figure 216: ADCIRC surface elevations (ft) and wind vectors (knots) for a Hurricane Gustav forecast using Advisory 32 at time equals 1.04 days.

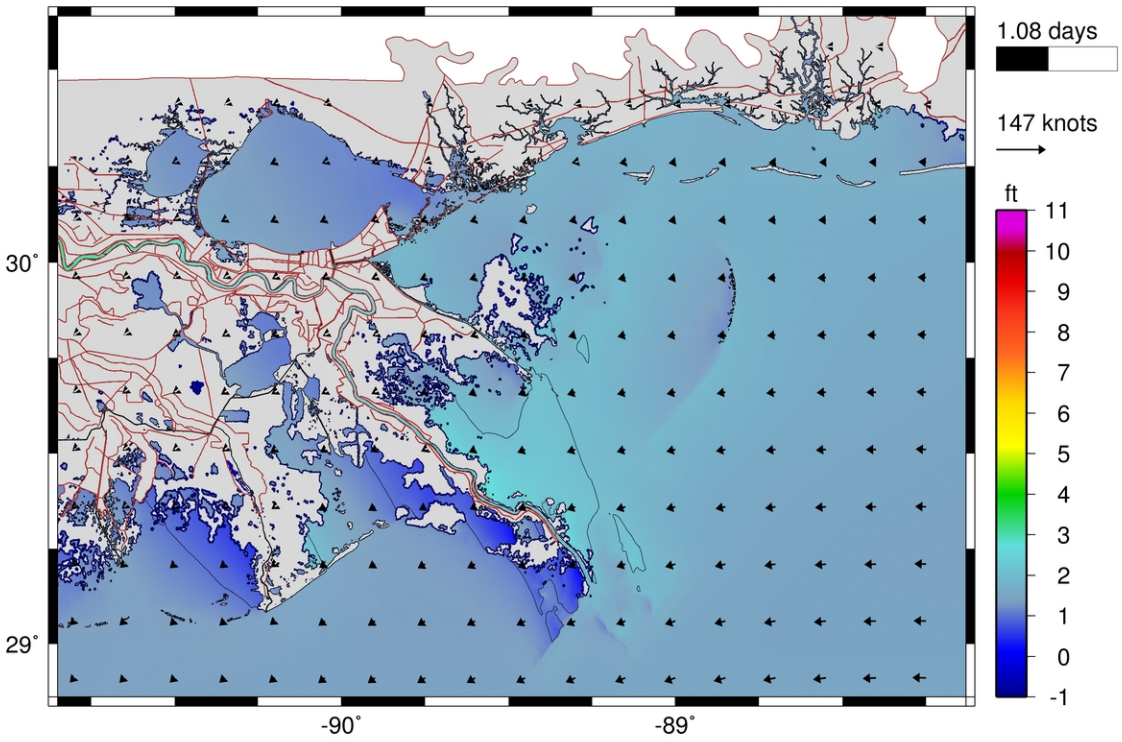


Figure 217: ADCIRC surface elevations (ft) and wind vectors (knots) for a Hurricane Gustav forecast using Advisory 32 at time equals 1.08 days.

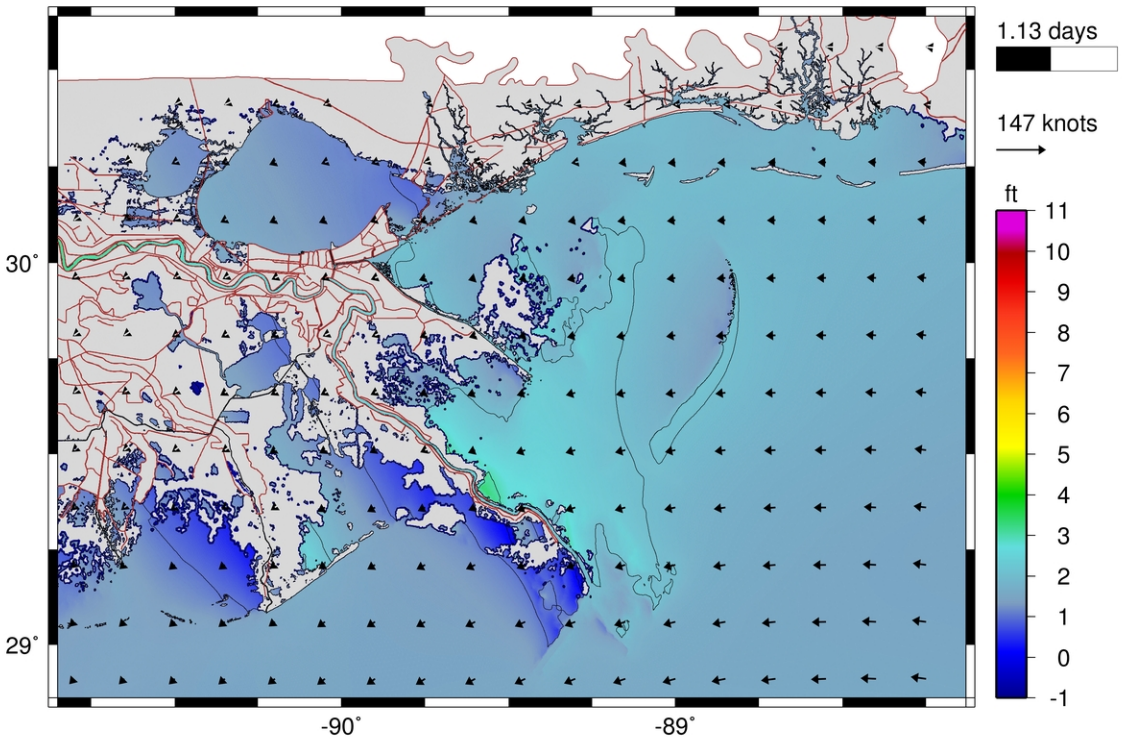


Figure 218: ADCIRC surface elevations (ft) and wind vectors (knots) for a Hurricane Gustav forecast using Advisory 32 at time equals 1.13 days.

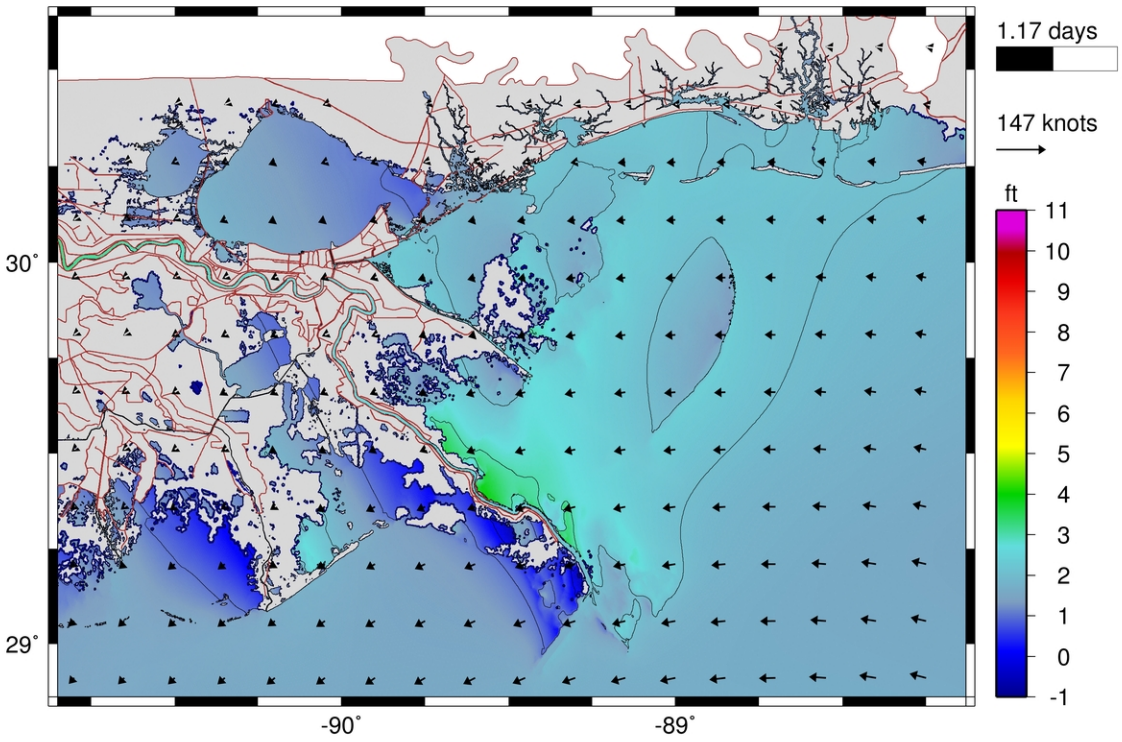


Figure 219: ADCIRC surface elevations (ft) and wind vectors (knots) for a Hurricane Gustav forecast using Advisory 32 at time equals 1.17 days.

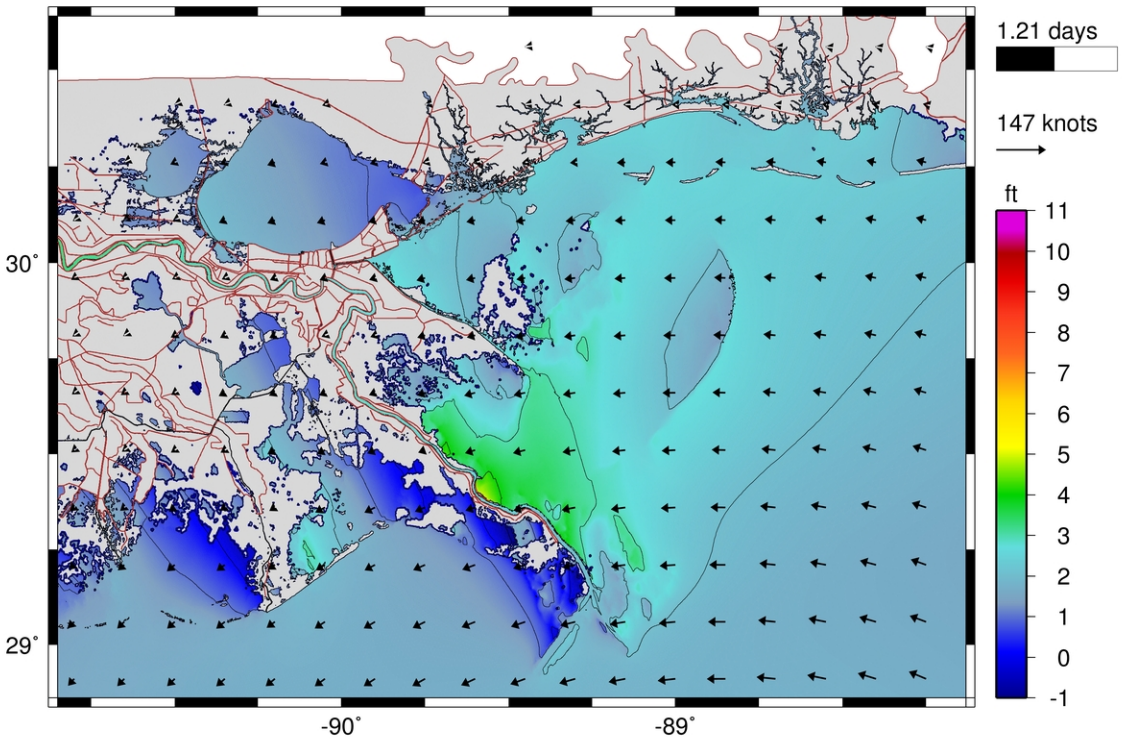


Figure 220: ADCIRC surface elevations (ft) and wind vectors (knots) for a Hurricane Gustav forecast using Advisory 32 at time equals 1.21 days.

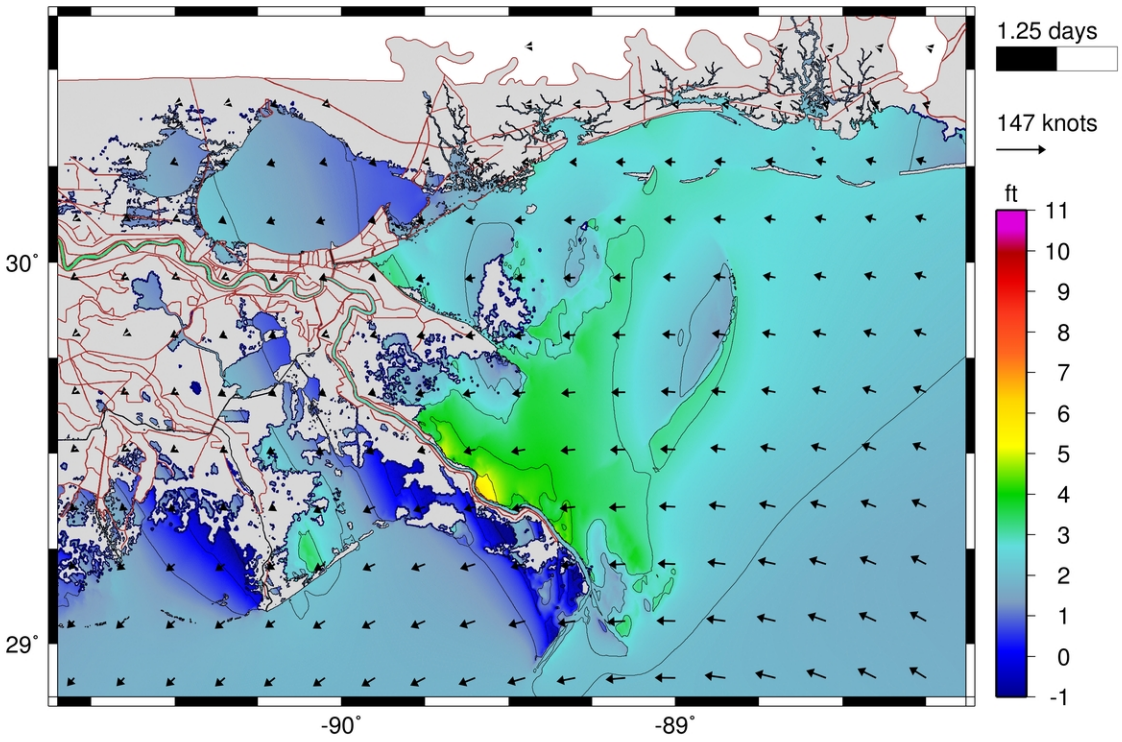


Figure 221: ADCIRC surface elevations (ft) and wind vectors (knots) for a Hurricane Gustav forecast using Advisory 32 at time equals 1.25 days.

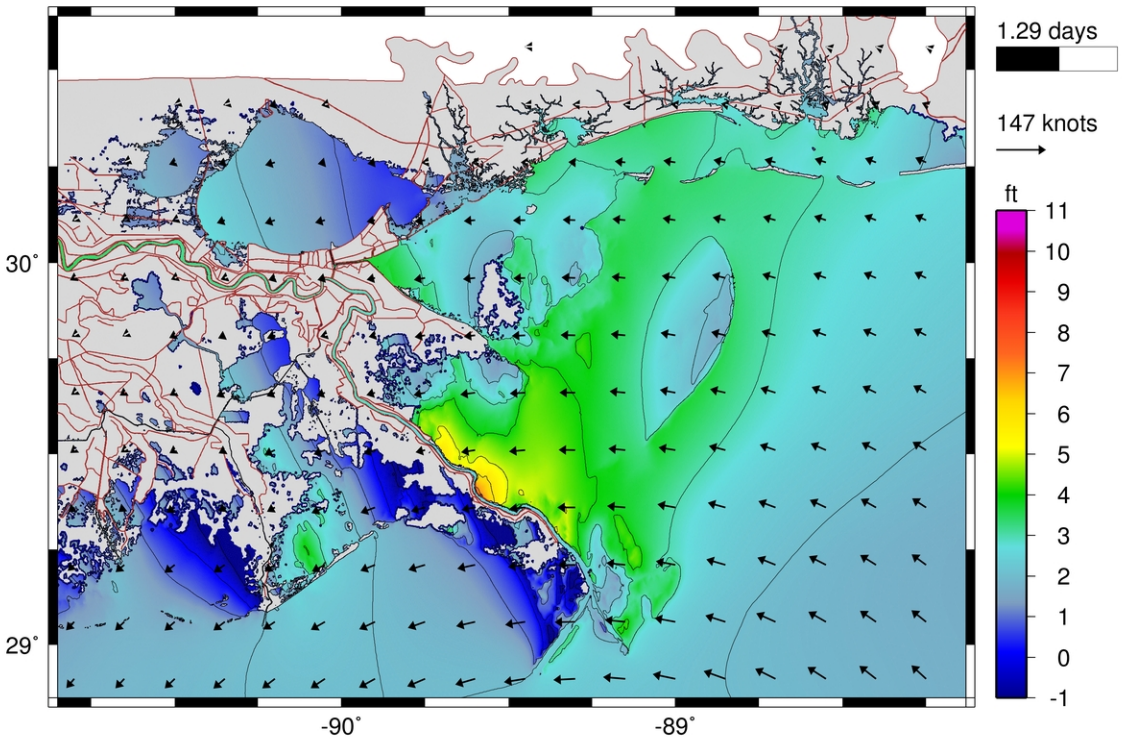


Figure 222: ADCIRC surface elevations (ft) and wind vectors (knots) for a Hurricane Gustav forecast using Advisory 32 at time equals 1.29 days.

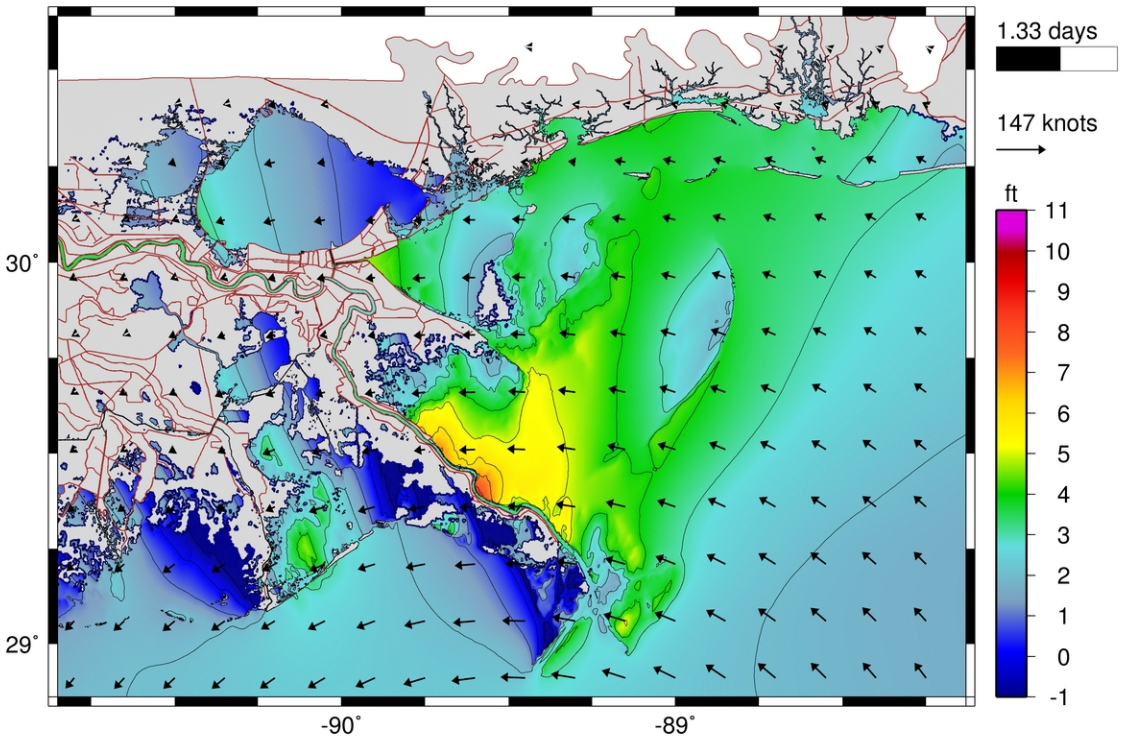


Figure 223: ADCIRC surface elevations (ft) and wind vectors (knots) for a Hurricane Gustav forecast using Advisory 32 at time equals 1.33 days.

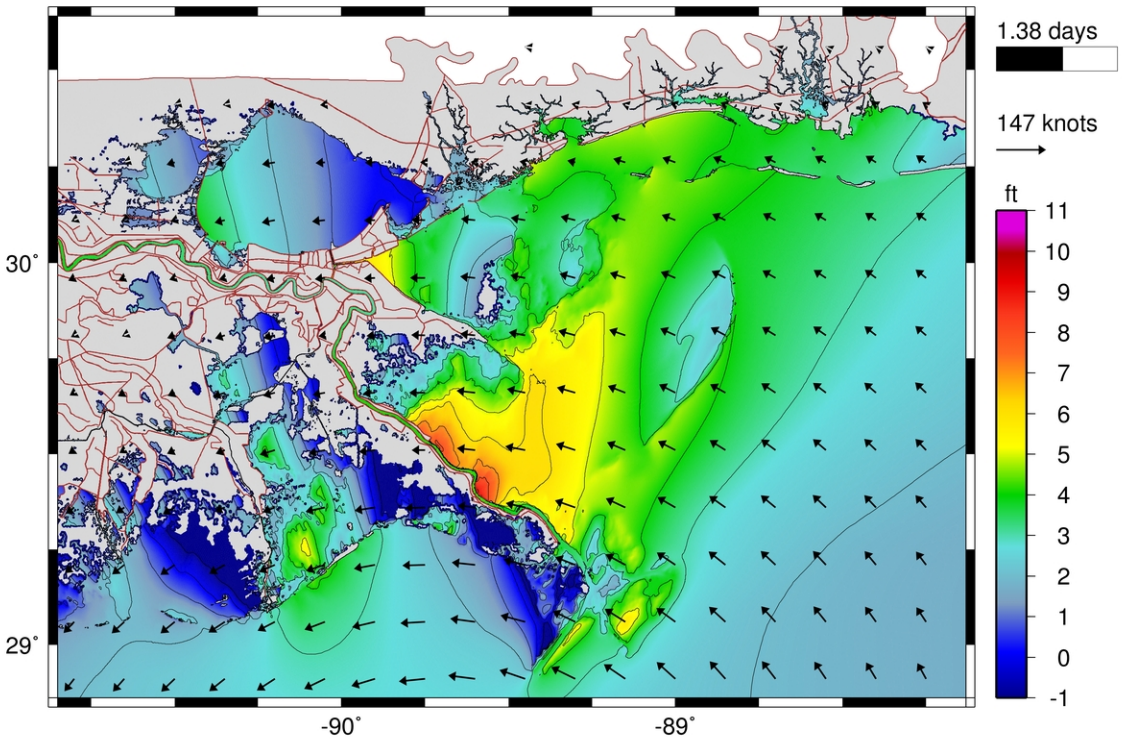


Figure 224: ADCIRC surface elevations (ft) and wind vectors (knots) for a Hurricane Gustav forecast using Advisory 32 at time equals 1.38 days.

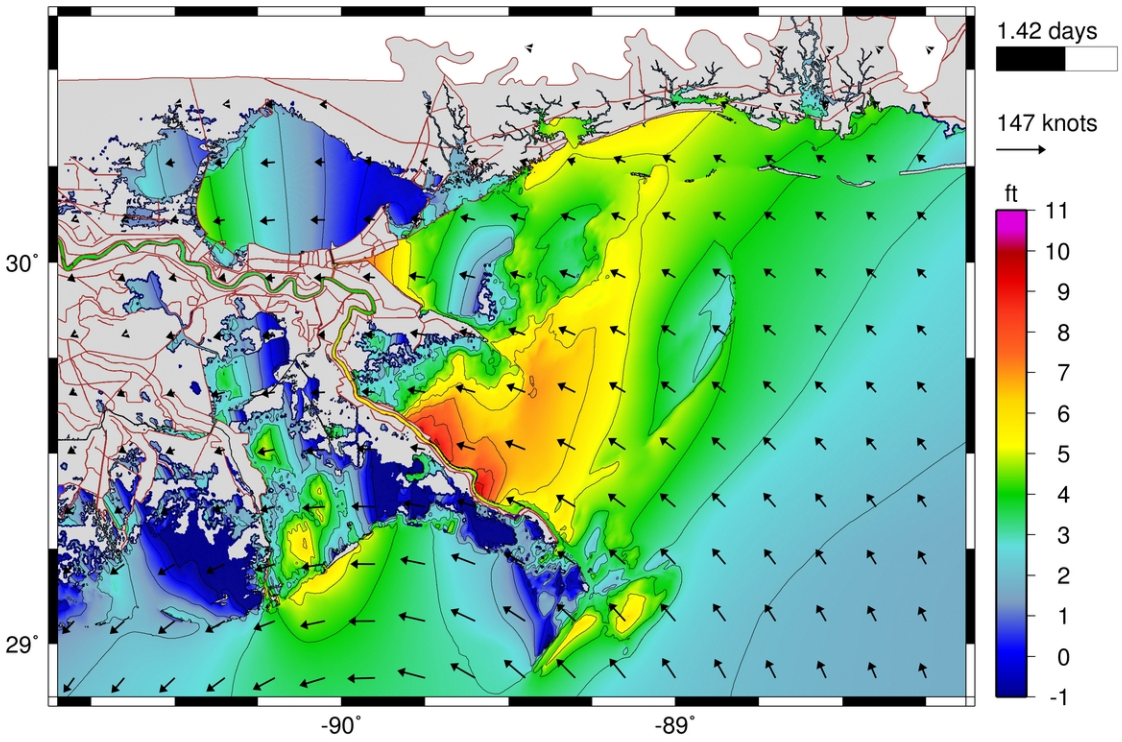


Figure 225: ADCIRC surface elevations (ft) and wind vectors (knots) for a Hurricane Gustav forecast using Advisory 32 at time equals 1.42 days.

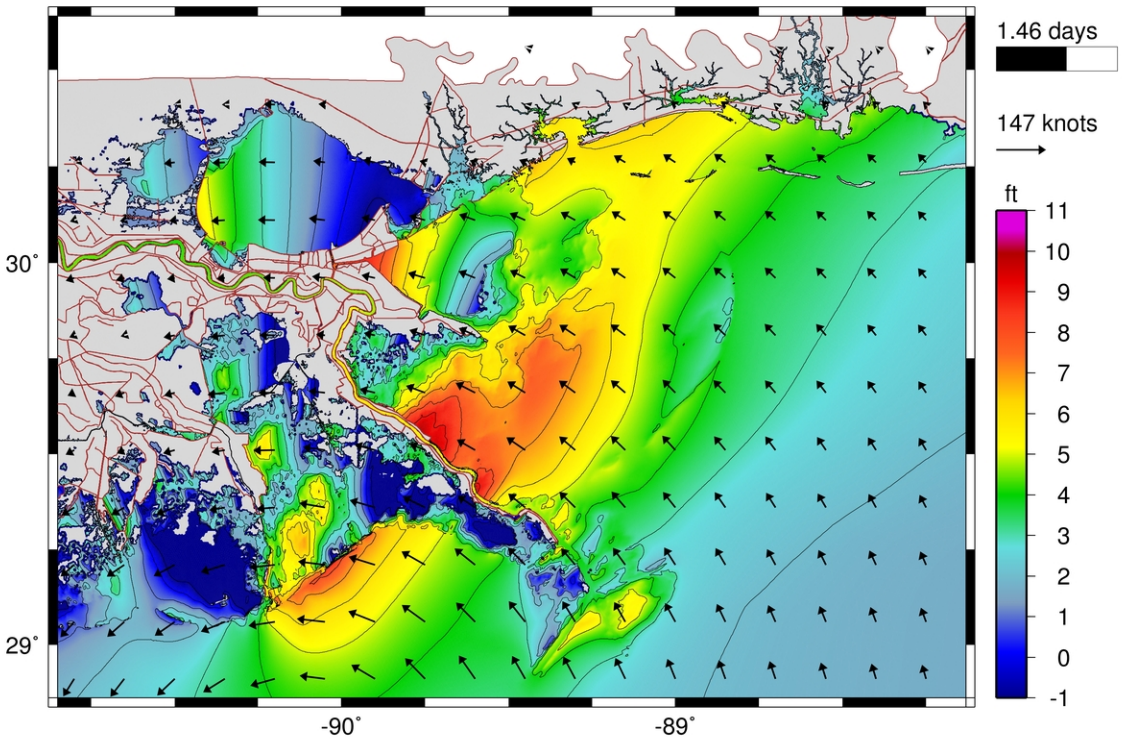


Figure 226: ADCIRC surface elevations (ft) and wind vectors (knots) for a Hurricane Gustav forecast using Advisory 32 at time equals 1.46 days.

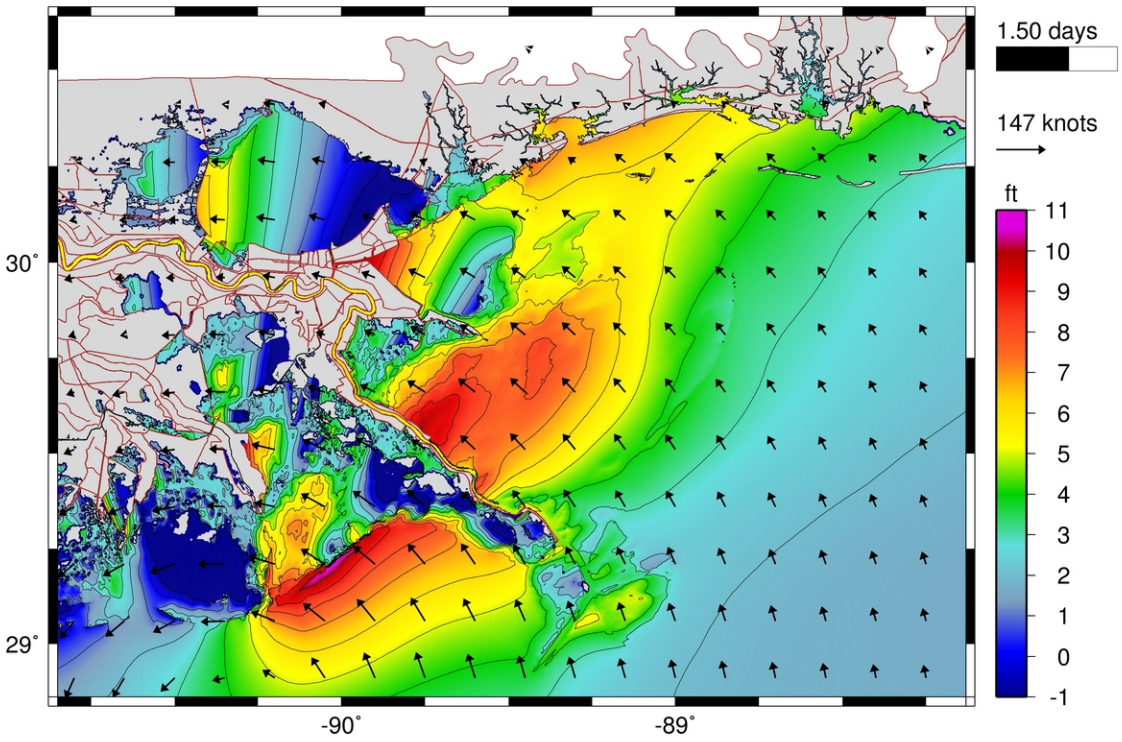


Figure 227: ADCIRC surface elevations (ft) and wind vectors (knots) for a Hurricane Gustav forecast using Advisory 32 at time equals 1.50 days.

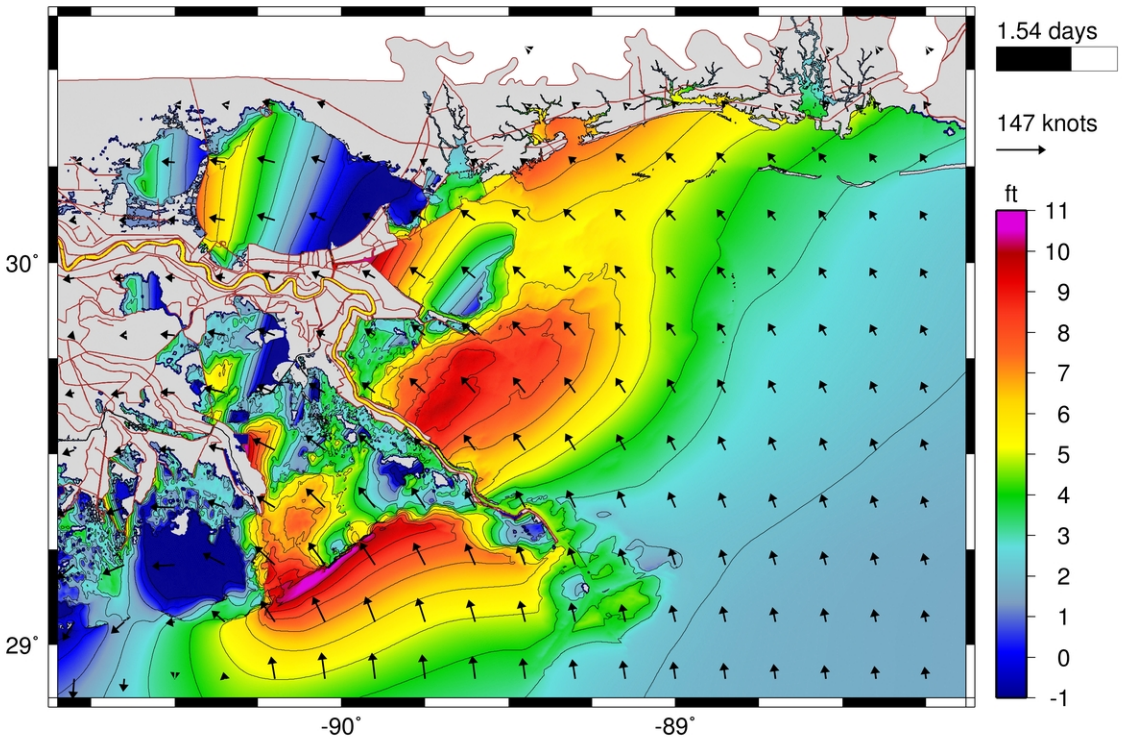


Figure 228: ADCIRC surface elevations (ft) and wind vectors (knots) for a Hurricane Gustav forecast using Advisory 32 at time equals 1.54 days.

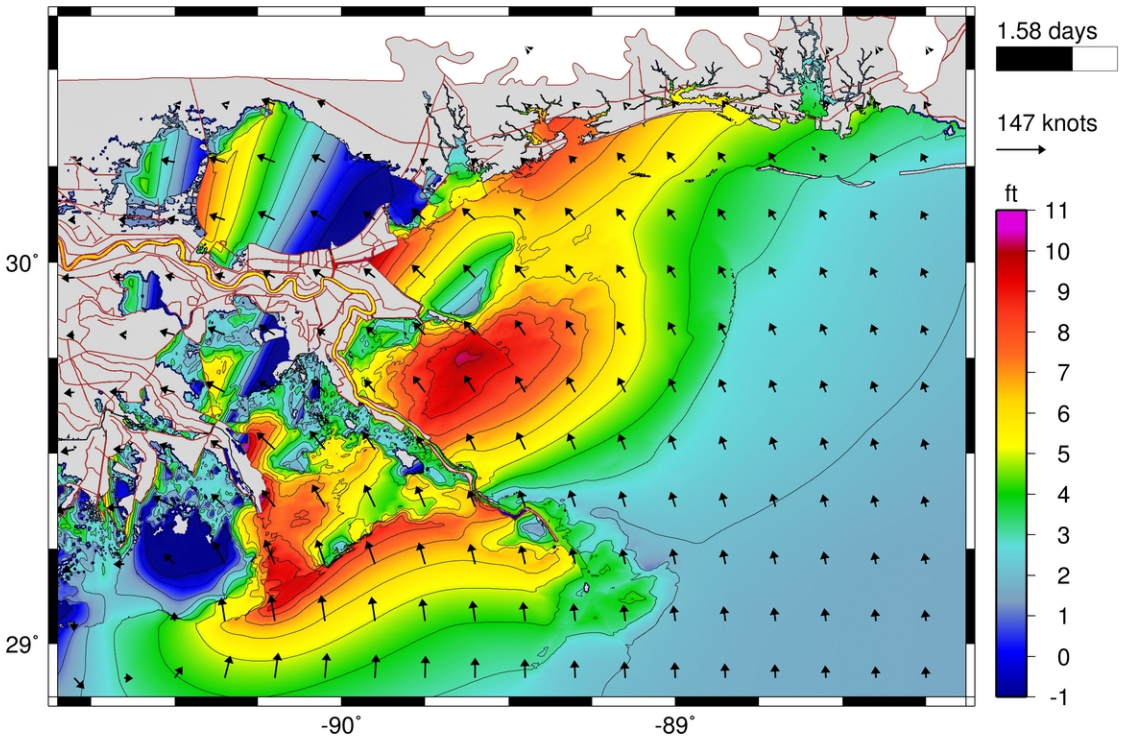


Figure 229: ADCIRC surface elevations (ft) and wind vectors (knots) for a Hurricane Gustav forecast using Advisory 32 at time equals 1.58 days.

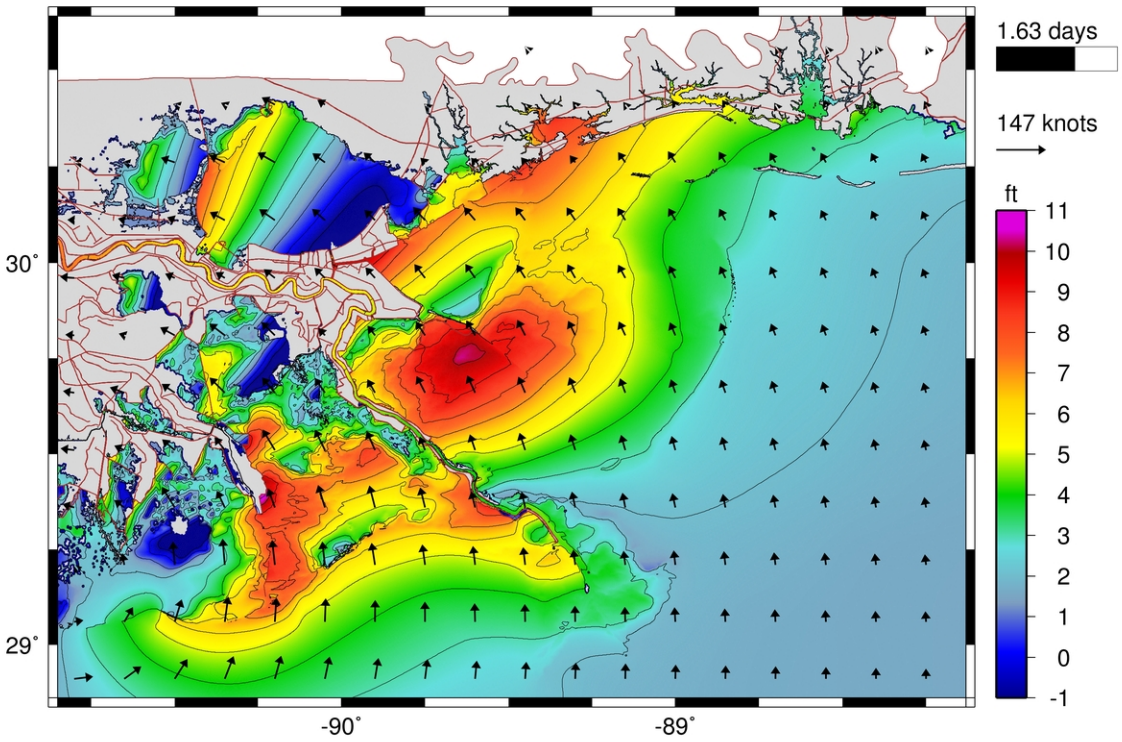


Figure 230: ADCIRC surface elevations (ft) and wind vectors (knots) for a Hurricane Gustav forecast using Advisory 32 at time equals 1.63 days.

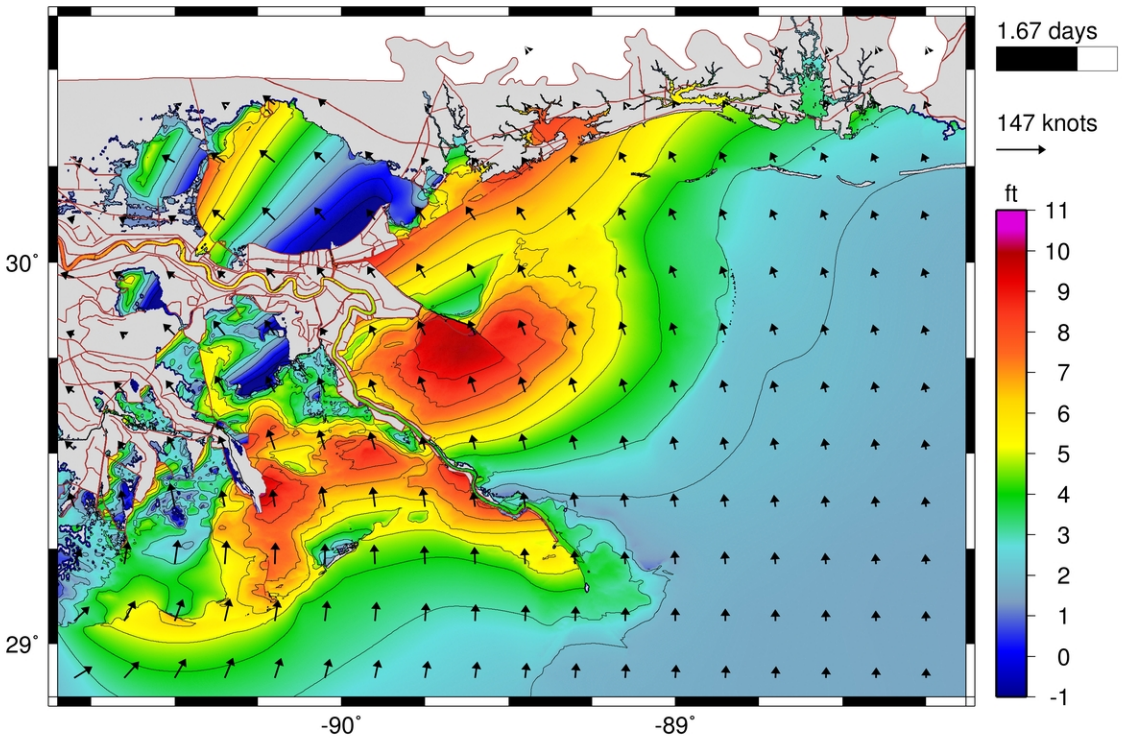


Figure 231: ADCIRC surface elevations (ft) and wind vectors (knots) for a Hurricane Gustav forecast using Advisory 32 at time equals 1.67 days.

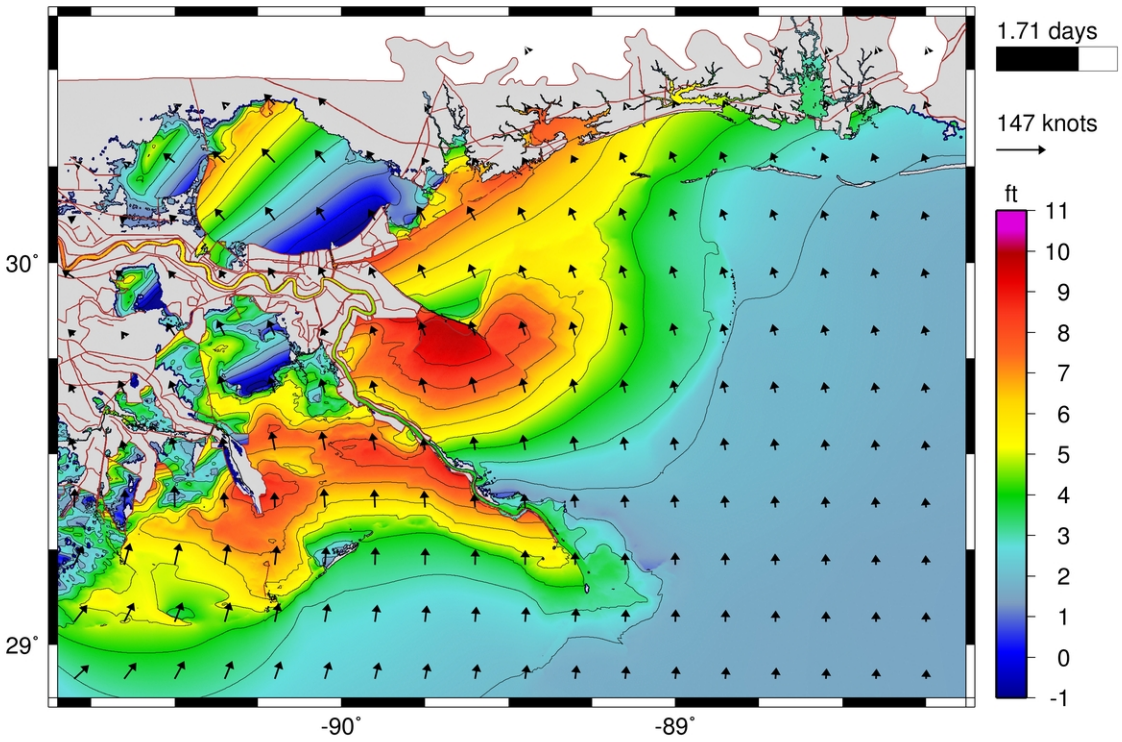


Figure 232: ADCIRC surface elevations (ft) and wind vectors (knots) for a Hurricane Gustav forecast using Advisory 32 at time equals 1.71 days.

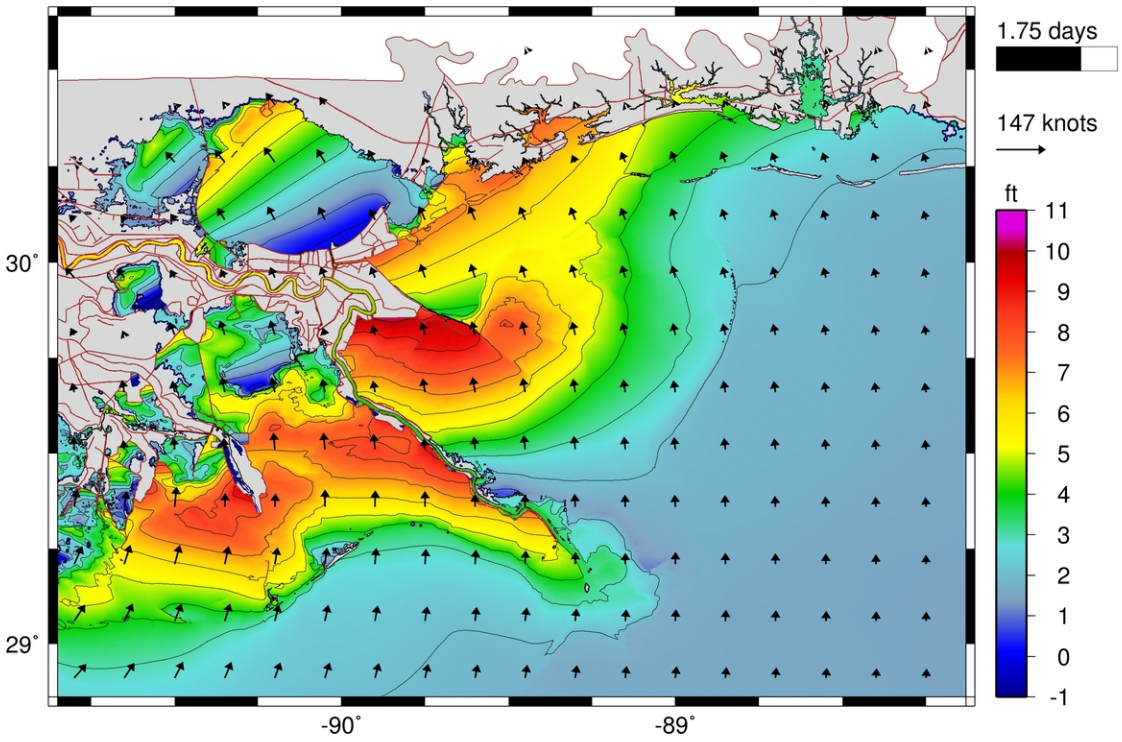


Figure 233: ADCIRC surface elevations (ft) and wind vectors (knots) for a Hurricane Gustav forecast using Advisory 32 at time equals 1.75 days.

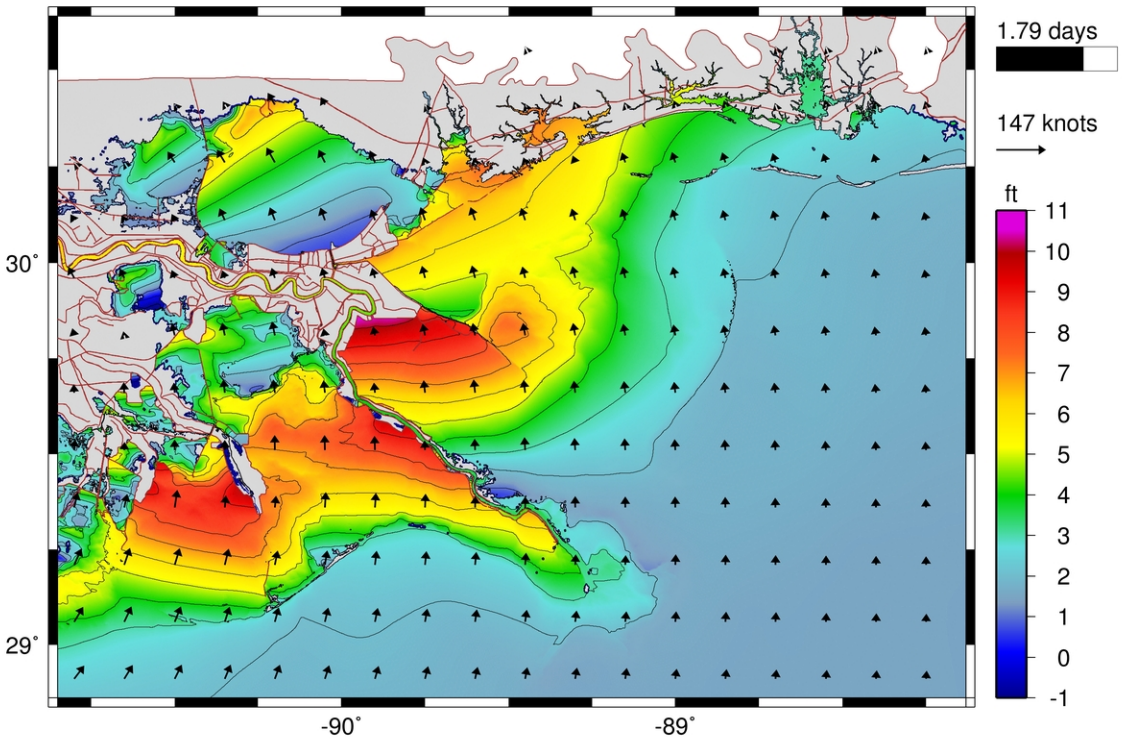


Figure 234: ADCIRC surface elevations (ft) and wind vectors (knots) for a Hurricane Gustav forecast using Advisory 32 at time equals 1.79 days.

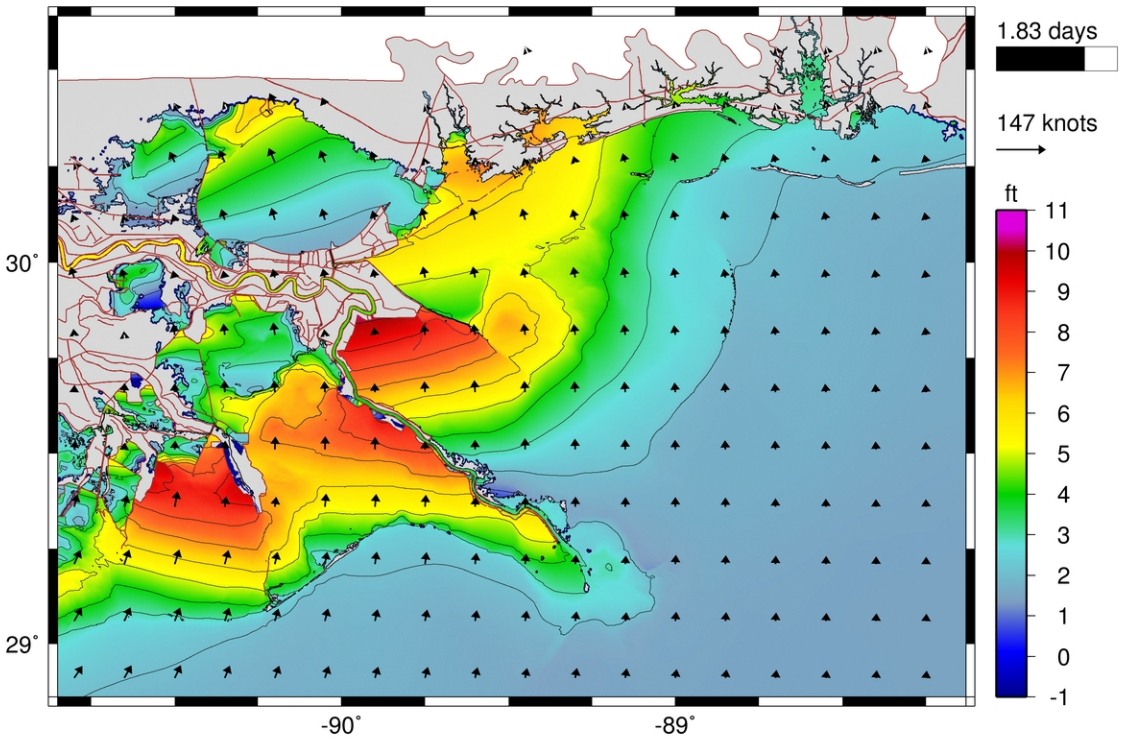


Figure 235: ADCIRC surface elevations (ft) and wind vectors (knots) for a Hurricane Gustav forecast using Advisory 32 at time equals 1.83 days.

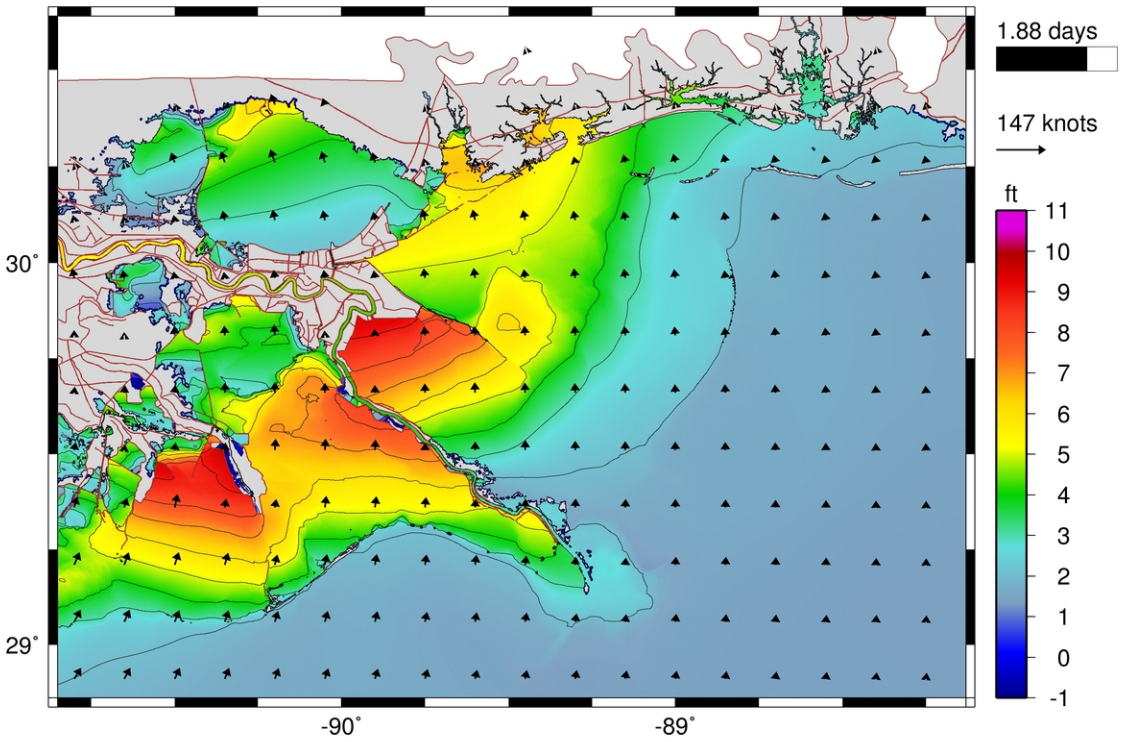


Figure 236: ADCIRC surface elevations (ft) and wind vectors (knots) for a Hurricane Gustav forecast using Advisory 32 at time equals 1.88 days.

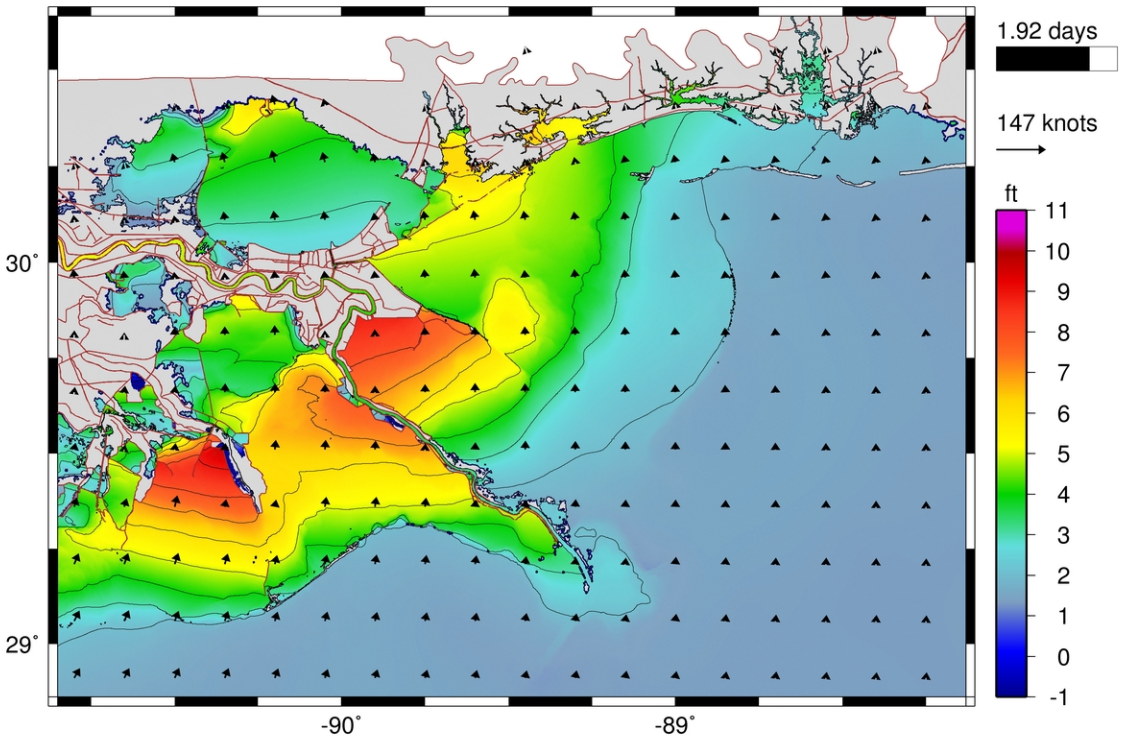


Figure 237: ADCIRC surface elevations (ft) and wind vectors (knots) for a Hurricane Gustav forecast using Advisory 32 at time equals 1.92 days.

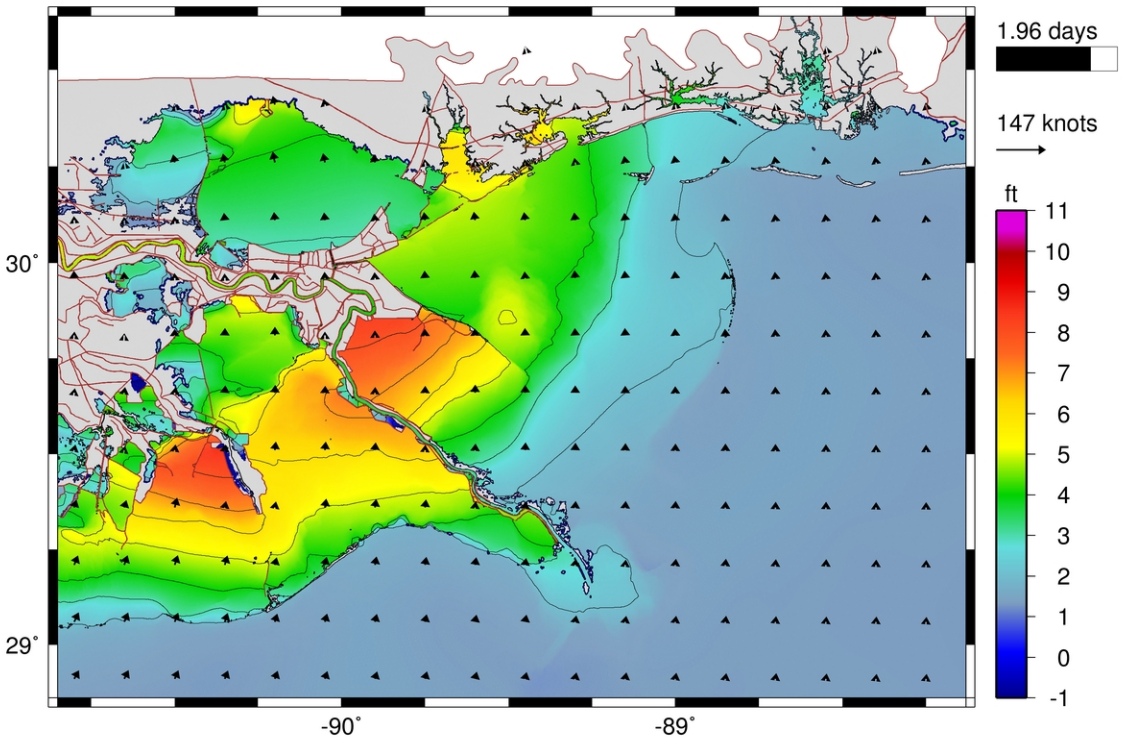


Figure 238: ADCIRC surface elevations (ft) and wind vectors (knots) for a Hurricane Gustav forecast using Advisory 32 at time equals 1.96 days.

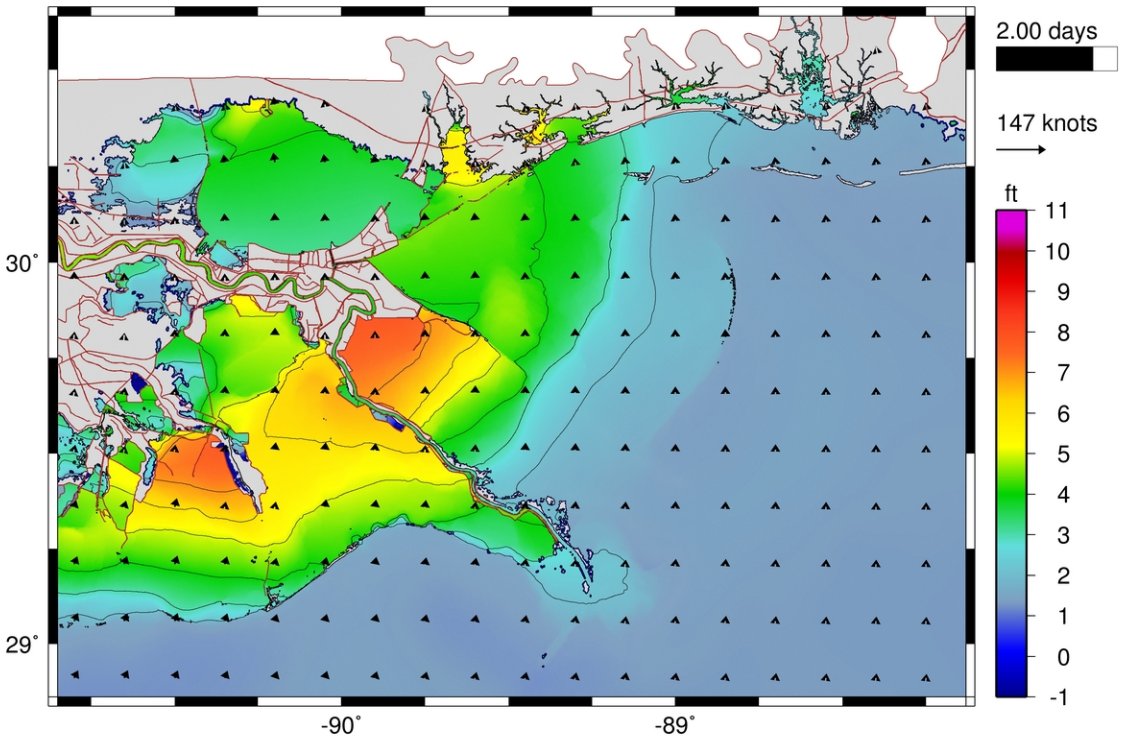


Figure 239: ADCIRC surface elevations (ft) and wind vectors (knots) for a Hurricane Gustav forecast using Advisory 32 at time equals 2.00 days.

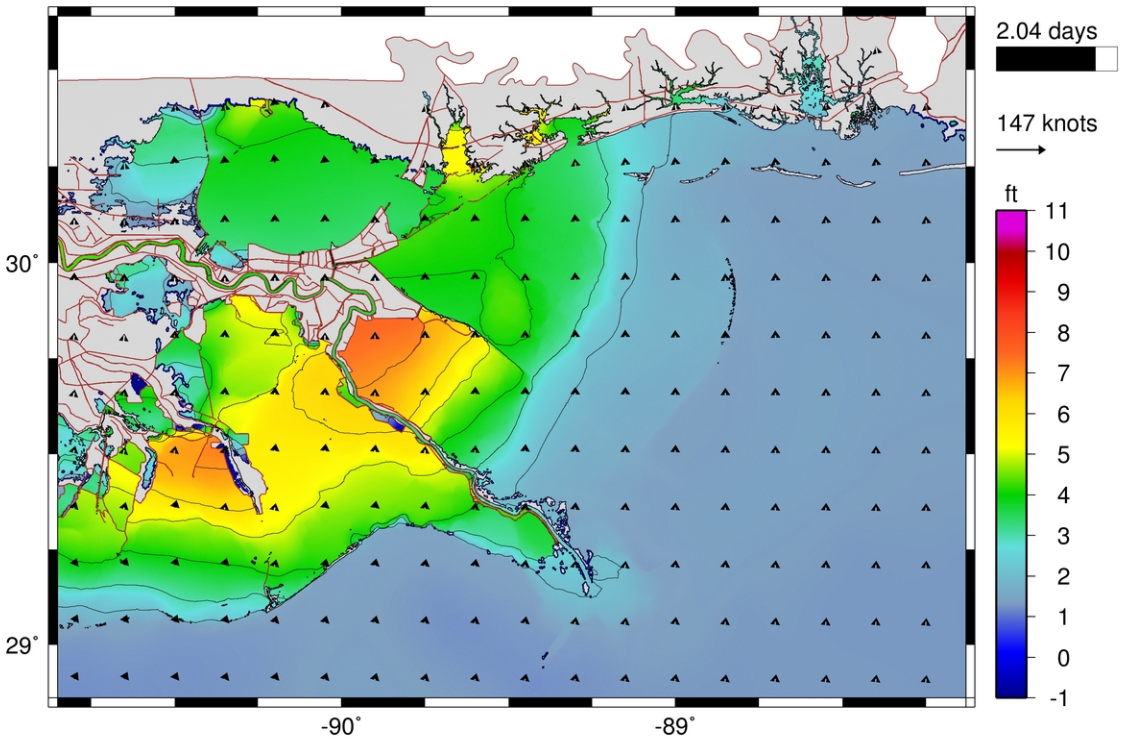


Figure 240: ADCIRC surface elevations (ft) and wind vectors (knots) for a Hurricane Gustav forecast using Advisory 32 at time equals 2.04 days.

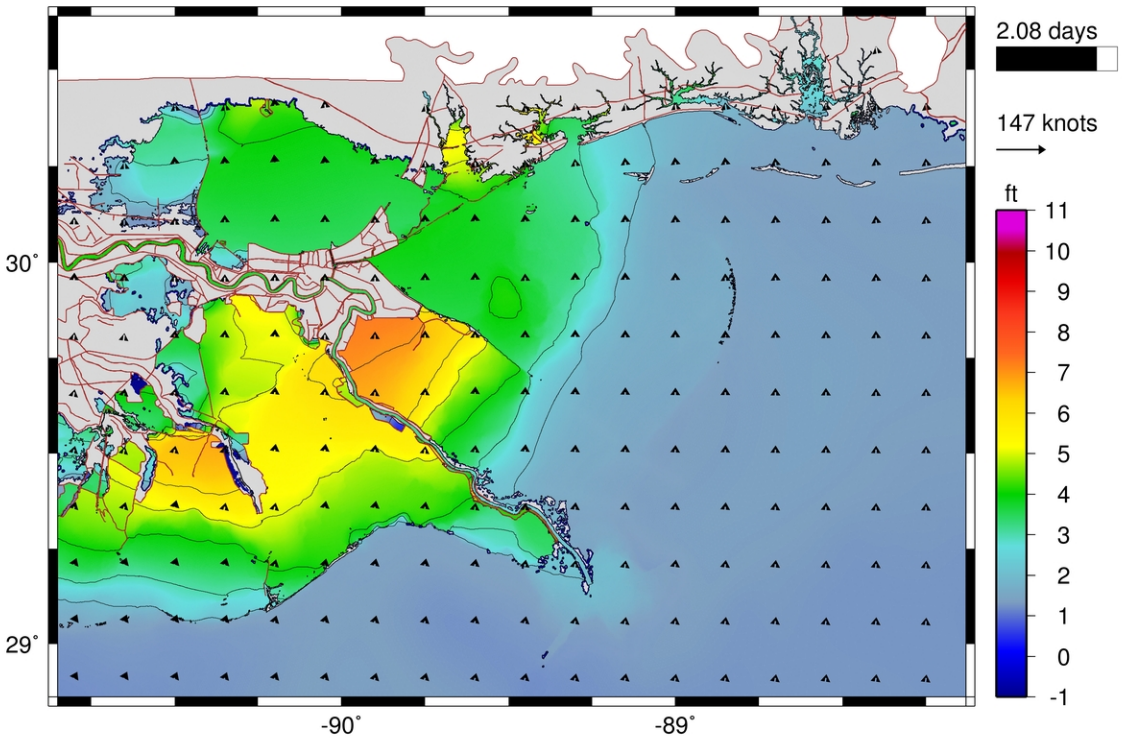


Figure 241: ADCIRC surface elevations (ft) and wind vectors (knots) for a Hurricane Gustav forecast using Advisory 32 at time equals 2.08 days.

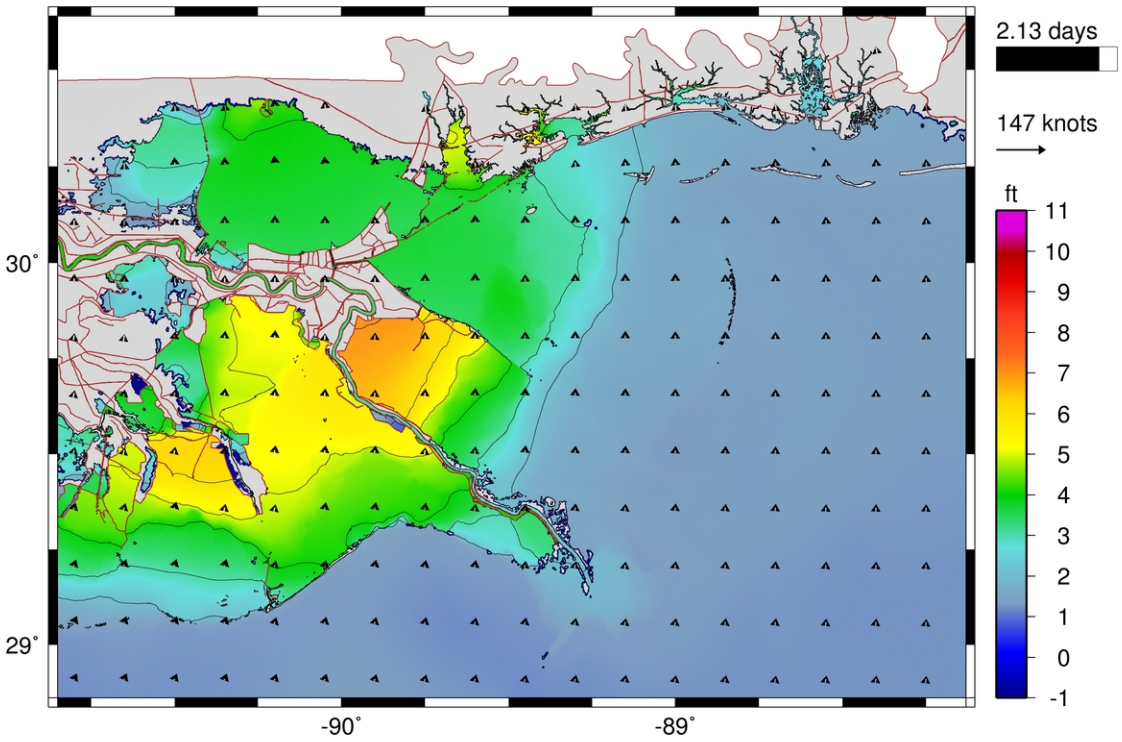


Figure 242: ADCIRC surface elevations (ft) and wind vectors (knots) for a Hurricane Gustav forecast using Advisory 32 at time equals 2.13 days.

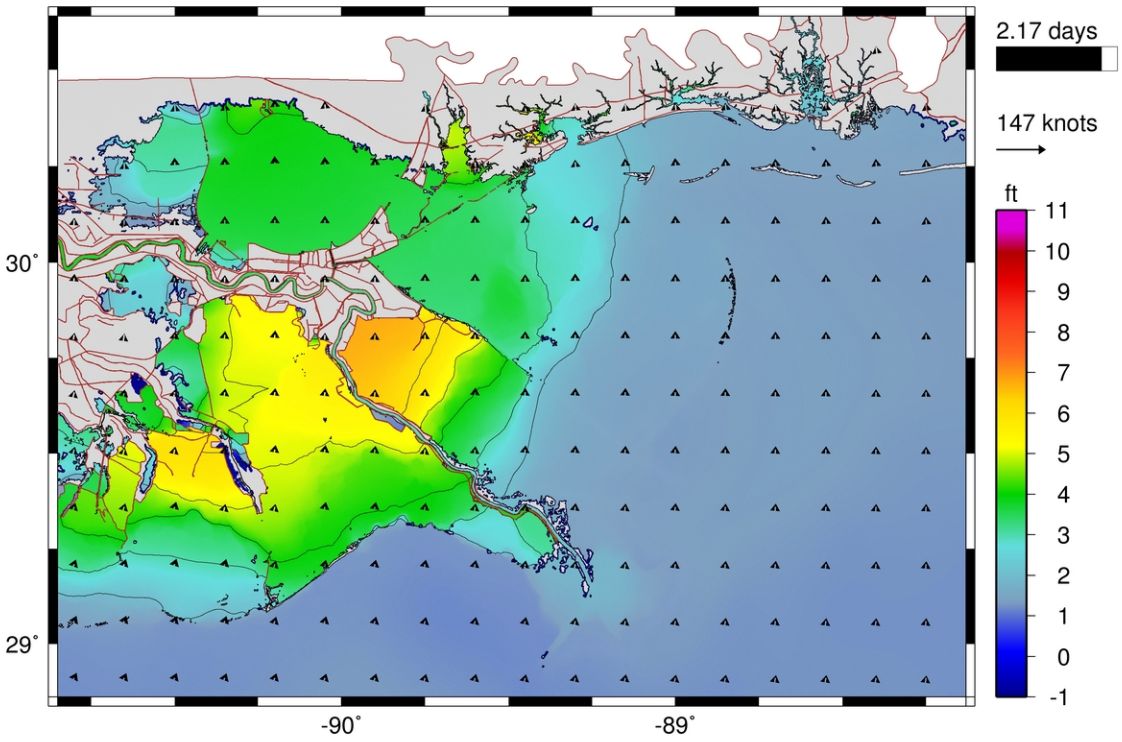


Figure 243: ADCIRC surface elevations (ft) and wind vectors (knots) for a Hurricane Gustav forecast using Advisory 32 at time equals 2.17 days.

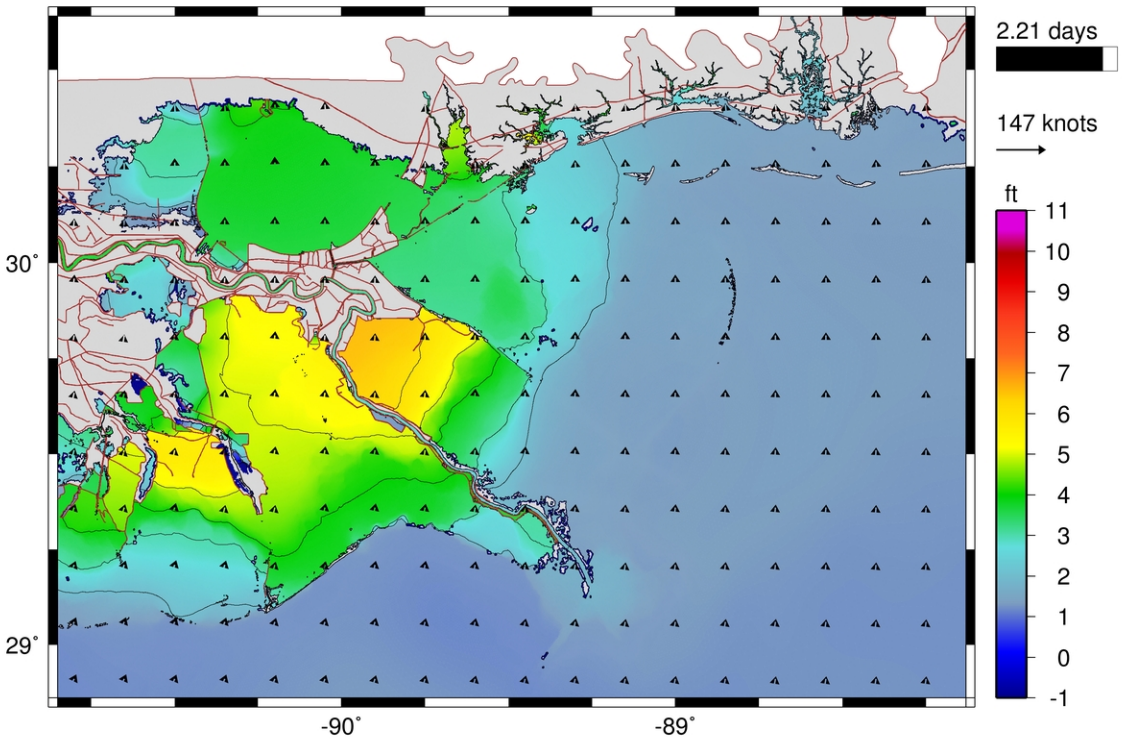


Figure 244: ADCIRC surface elevations (ft) and wind vectors (knots) for a Hurricane Gustav forecast using Advisory 32 at time equals 2.21 days.

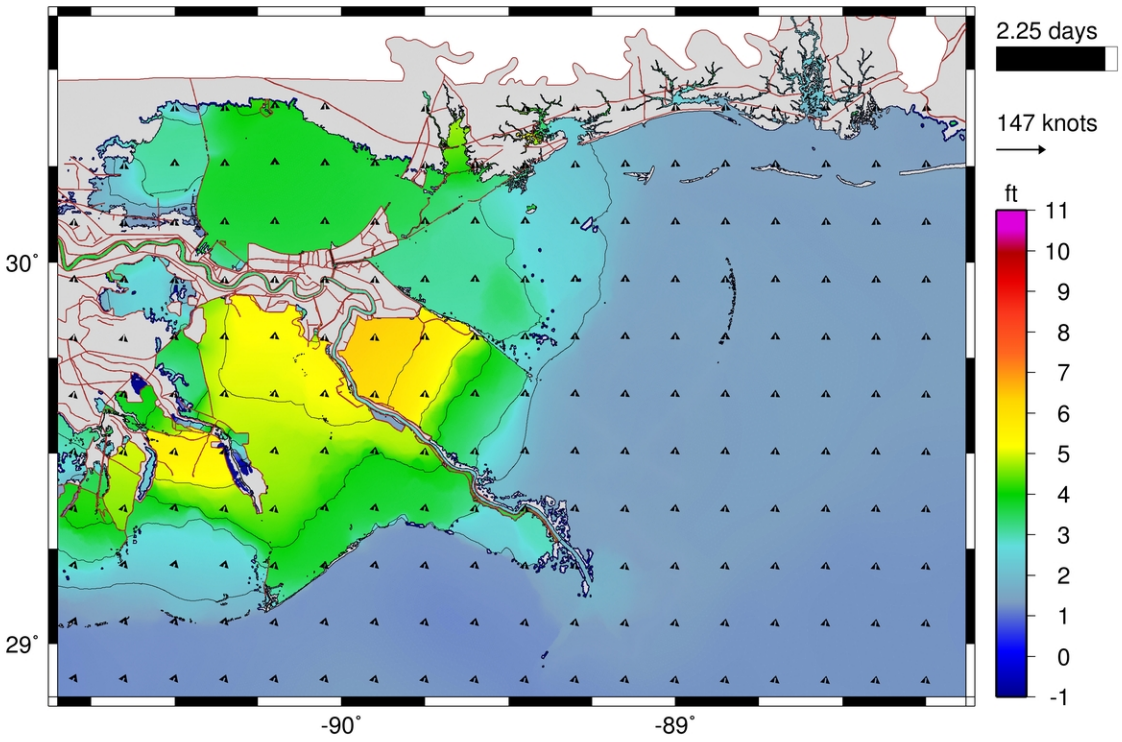


Figure 245: ADCIRC surface elevations (ft) and wind vectors (knots) for a Hurricane Gustav forecast using Advisory 32 at time equals 2.25 days.

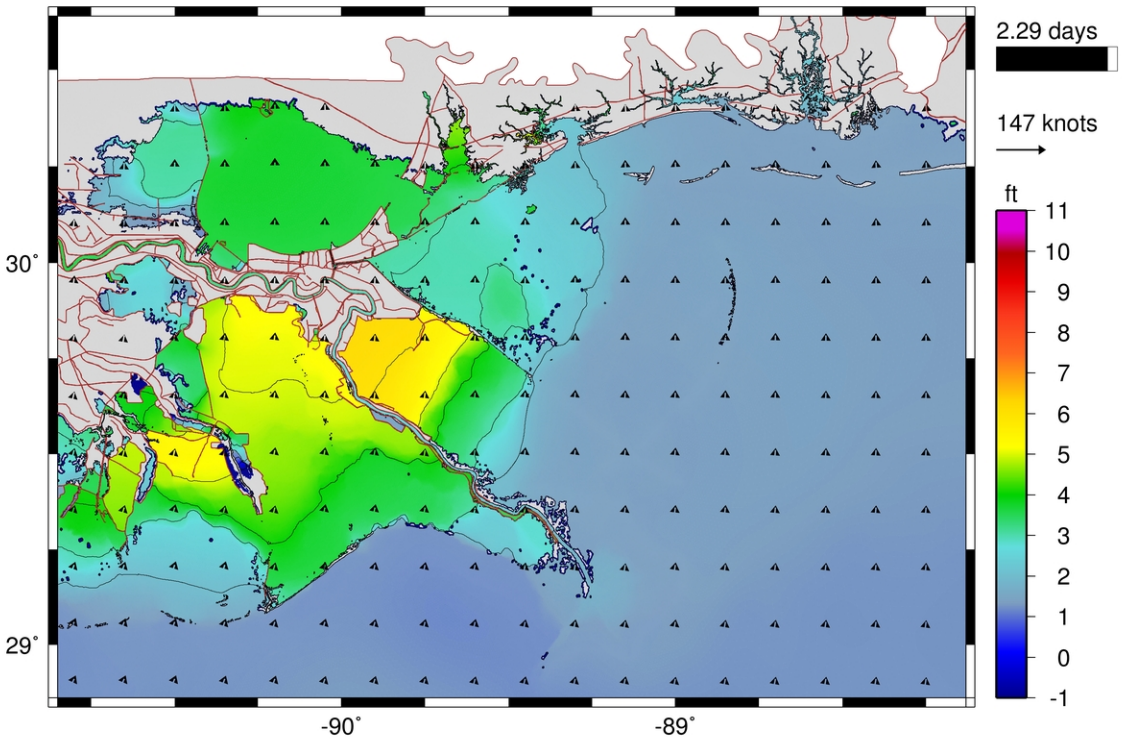


Figure 246: ADCIRC surface elevations (ft) and wind vectors (knots) for a Hurricane Gustav forecast using Advisory 32 at time equals 2.29 days.

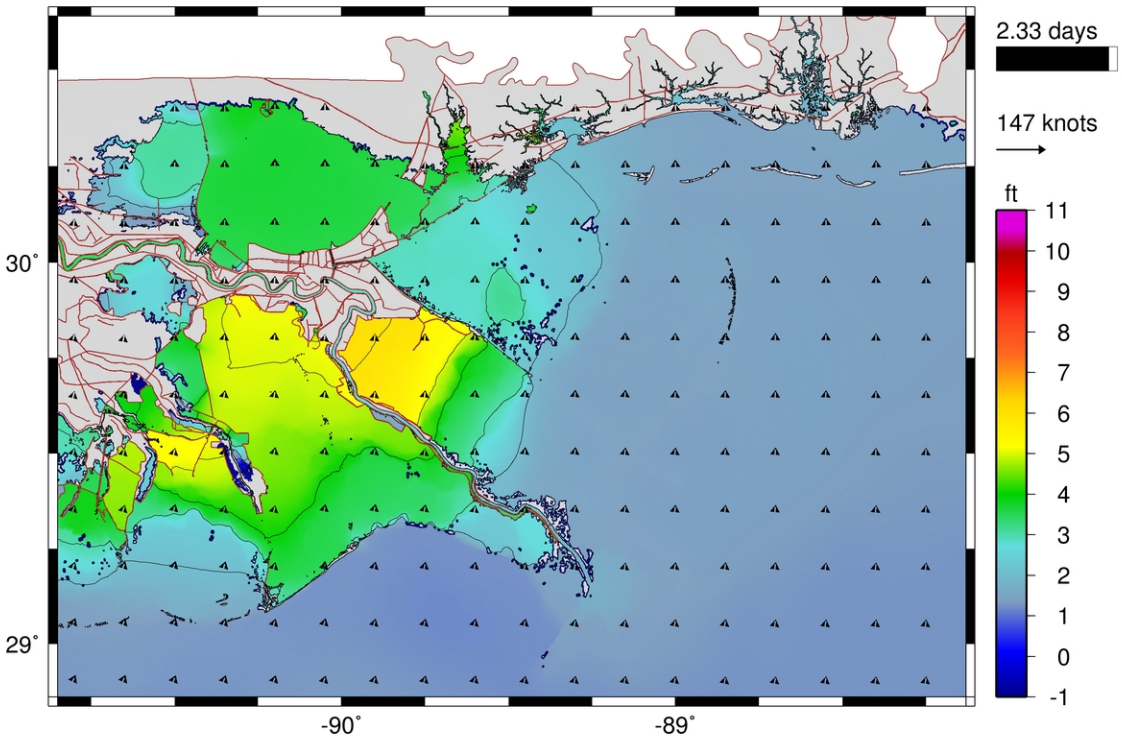


Figure 247: ADCIRC surface elevations (ft) and wind vectors (knots) for a Hurricane Gustav forecast using Advisory 32 at time equals 2.33 days.

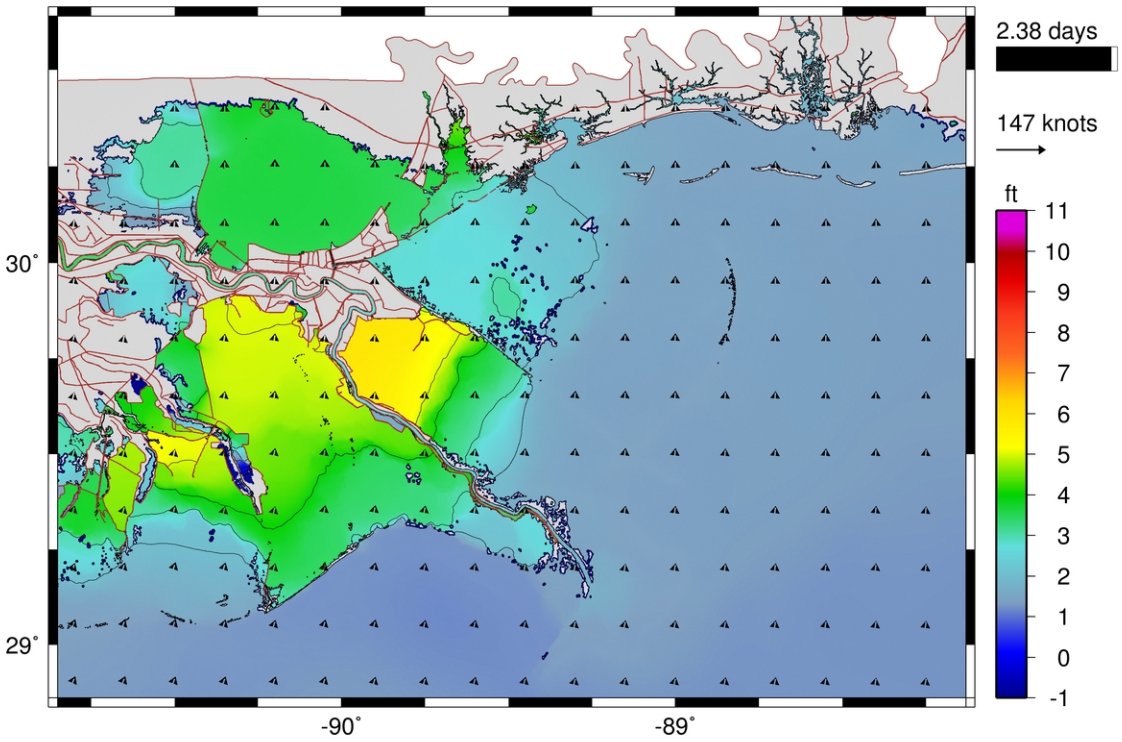


Figure 248: ADCIRC surface elevations (ft) and wind vectors (knots) for a Hurricane Gustav forecast using Advisory 32 at time equals 2.38 days.

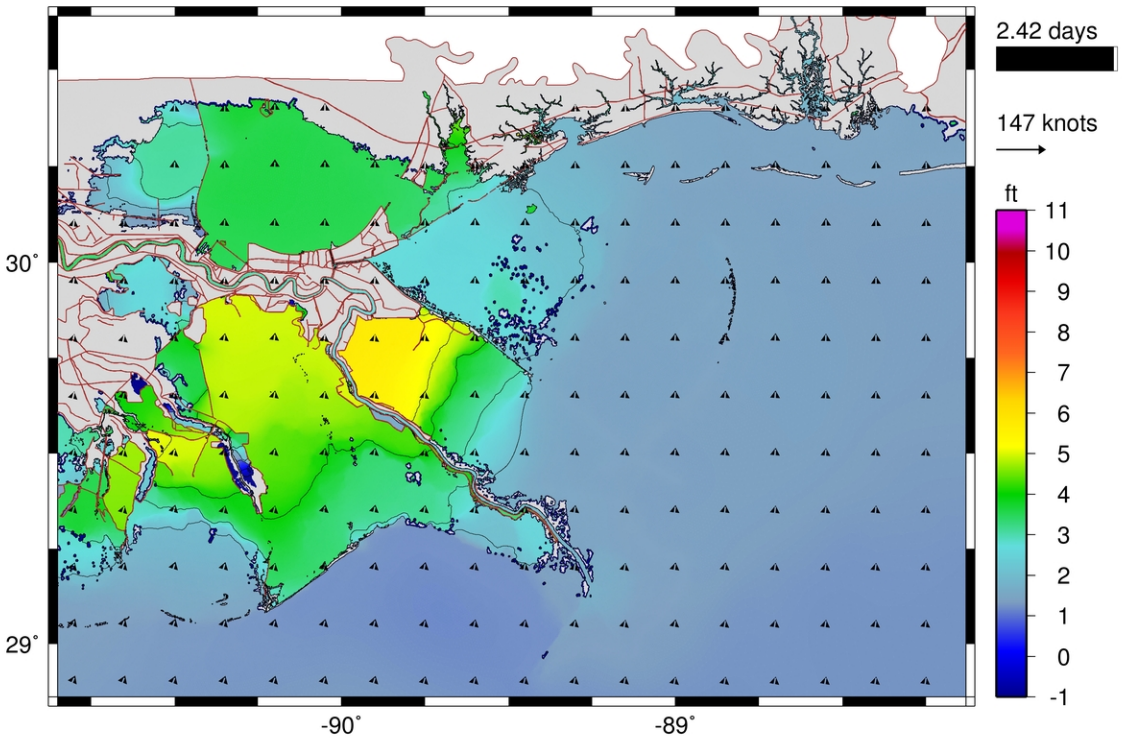


Figure 249: ADCIRC surface elevations (ft) and wind vectors (knots) for a Hurricane Gustav forecast using Advisory 32 at time equals 2.42 days.

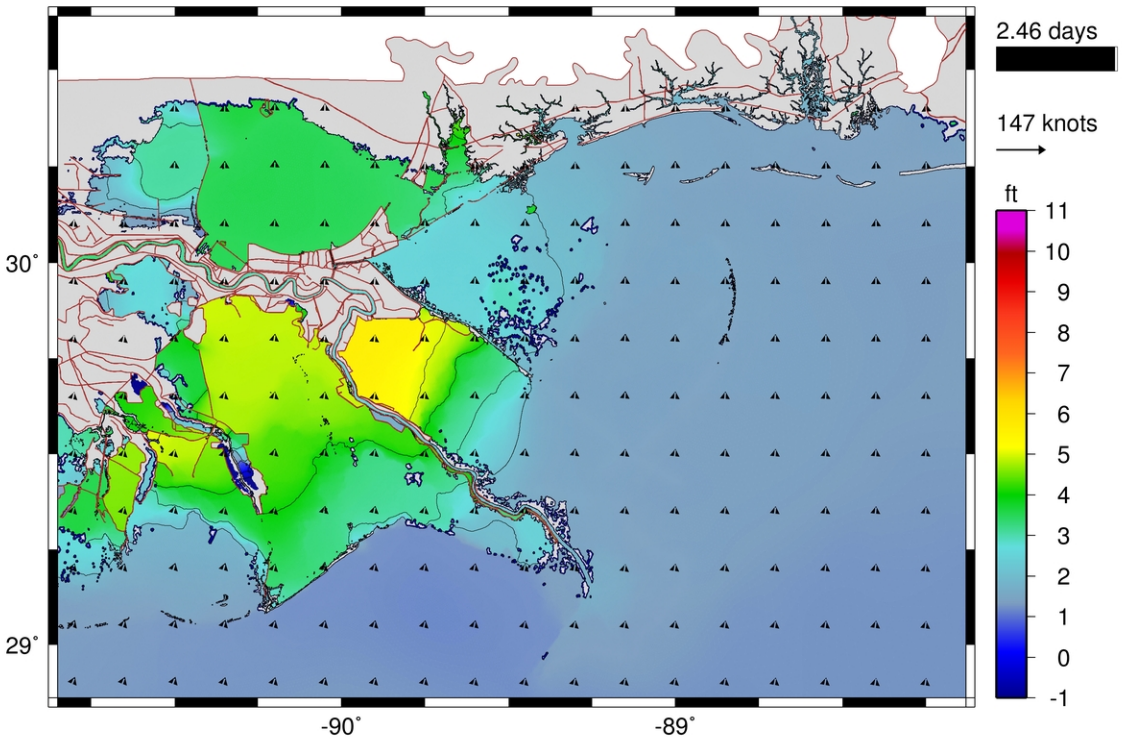


Figure 250: ADCIRC surface elevations (ft) and wind vectors (knots) for a Hurricane Gustav forecast using Advisory 32 at time equals 2.46 days.

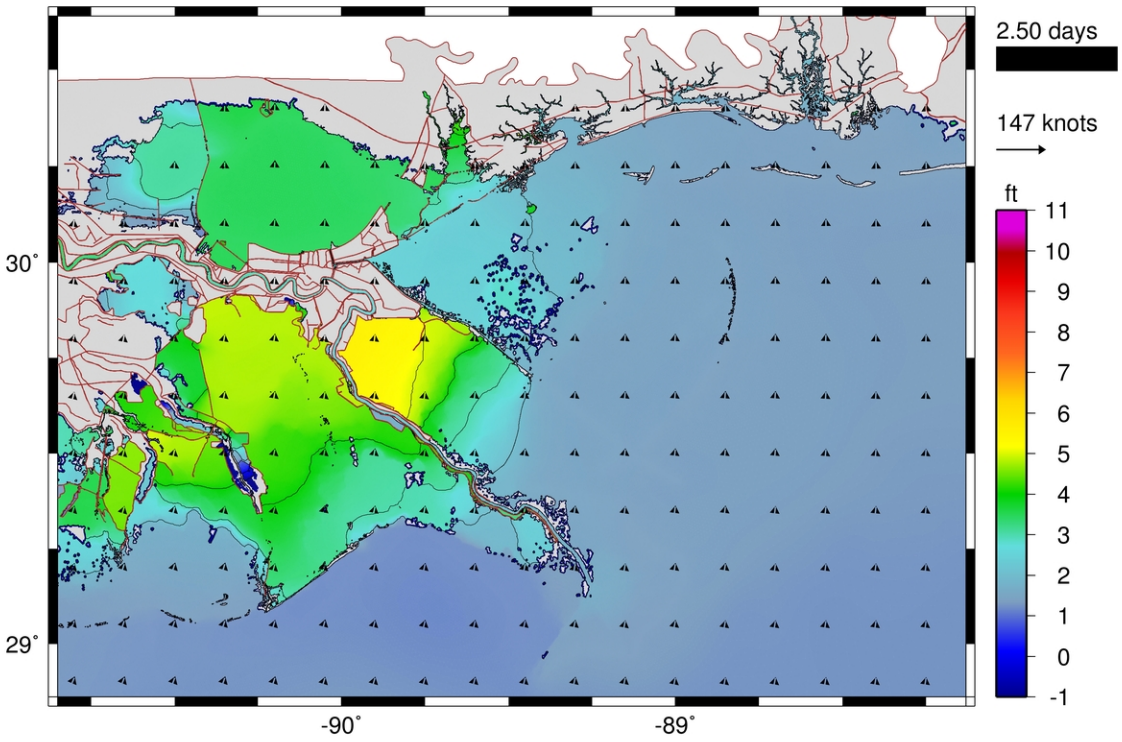


Figure 251: ADCIRC surface elevations (ft) and wind vectors (knots) for a Hurricane Gustav forecast using Advisory 32 at time equals 2.50 days.



Figure 252: View 1 of flooding at Braithwaite, LA. during Hurricane Gustav on September 1, 2008. (U.S. Army Corps of Engineers, New Orleans District, 2008)



Figure 253: View 2 of flooding at Braithwaite, LA. during Hurricane Gustav on September 1, 2008. (U.S. Army Corps of Engineers, New Orleans District, 2008)



Figure 254: View 3 of flooding at Braithwaite, LA. during Hurricane Gustav on September 1, 2008. (U.S. Army Corps of Engineers, New Orleans District, 2008)



Figure 255: View 4 of flooding at Braithwaite, LA. during Hurricane Gustav on September 1, 2008. (U.S. Army Corps of Engineers, New Orleans District, 2008)



Figure 256: View 5 of flooding at Braithwaite, LA. during Hurricane Gustav on September 1, 2008. (U.S. Army Corps of Engineers, New Orleans District, 2008)

APPENDIX A: Curriculum Vita

Joannes Jacobus A. Westerink

Professor, Department of Civil Engineering and Geological Sciences
Concurrent Professor, Department of Mathematics
University of Notre Dame
Notre Dame, IN 46556-0767
Phone: (574) 631-6475 Fax: (575) 631-9236
e-mail: jjw@nd.edu

EDUCATION

1981-1984	Ph.D. Civil Engineering, Massachusetts Institute of Technology
1979-1981	M.S. Civil Engineering, State University of New York at Buffalo
1975-1979	B.S. Civil Engineering, Summa Cum Laude, State University of New York at Buffalo

EMPLOYMENT

2007-present	Concurrent Professor of Mathematics, University of Notre Dame
2006-present	Professor of Civil Engineering, University of Notre Dame
1995-2006	Associate Professor of Civil Engineering, University of Notre Dame
1990-1995	Assistant Professor of Civil Engineering, University of Notre Dame
1987-1990	Assistant Professor of Civil and Ocean Engineering, Texas A&M University
1984-1987	Assistant Professor of Civil Engineering, Princeton University
1981-1984	Research Assistant, Department of Civil Engineering, Massachusetts Institute of Technology
1979-1981	Research Assistant, Department of Civil Engineering, State University of New York at Buffalo

RESEARCH INTERESTS

Computational fluid mechanics
Finite element methods
Modeling of circulation and transport in coastal seas and oceans
Tidal hydrodynamics
Hurricane storm surge prediction
Geophysical turbulence modeling
Numerical modeling of the convection-diffusion and Navier-Stokes equations
Environmental fluid mechanics

AWARDS AND FELLOWSHIPS

R.P. Apmann Memorial Scholarship, State University of New York at Buffalo, 1979
Seagrant Scholar, National Oceanic and Atmospheric Administration, 1979-1981
Kaneb Teaching Award, Department of Civil Engineering and Geological Sciences, University of Notre Dame, 2000
BP Outstanding Teacher of the Year Award, College of Engineering, University of Notre Dame, 2004
Faculty Fellow, John A. Kaneb Center for Teaching and Learning, University of Notre Dame, 2005-2006
U.S. Army Corps of Engineers Interagency Performance Evaluation Task Force Leadership Award, 2007
Department of the Army, Outstanding Civilian Service Medal, 2007

PROFESSIONAL ACTIVITIES

Member American Geophysical Union

Associate Member American Society of Civil Engineers

Editorial board member for *Advances in Water Resources* (1989-1997)

Advisor member of the Computational Hydraulics Committee, ASCE Hydraulics Division (1990-1994)

Affiliate Scientist, Center for Coastal and Land Margin Research, Oregon Graduate Institute (1992-1996)

Control member of the Task Committee on Pre-Standardization of Estuarine Tidal Modeling, ASCE Hydraulics Division (1992-1994)

Control member of the Computational Hydraulics Committee, ASCE Hydraulics Division (1994-1996): Secretary (1994)

Member, International Scientific Advisory Committee, Coastal Engineering 95, Cancun, Mexico (1994-1995)

Member, International Scientific Advisory Committee, Coastal Engineering 97, La Coruna, Spain (1996-1997)

Member, International Scientific Advisory Committee, Coastal Engineering 99, Lemnos, Greece (1998-1999)

Member, Organizing Committee, Fifth SIAM Conference on Mathematical and Computational Issues in the Geosciences, San Antonio, TX, March 24-27, 1999 (1998-1999)

Member, International Organizing Committee, Twelfth International Conference on Finite Element Methods in Flow Problems, Meijo University, Nagoya, Japan, April 2-4, 2003 (2001-2003)

Member, Advisory Committee, Coastal and Environmental Modeling Laboratory, Louisiana State University, Baton Rouge, LA, (2003).

U.S. Congressional Briefing with Clint Dawson entitled, "From Katrina Forward; How Mathematical Modeling Predicts Storm Surges," for the American Mathematical Society, U.S. Congress, Washington D.C., November 3, 2005.

Co-organizer with M. Iskandarani and J. Pietrzak the Fifth International Workshop on Unstructured Mesh Numerical Modeling of Coastal, Shelf and Ocean Flows, Miami FL, November 13-15, 2006.

Numerical Modeling of Hurricane Katrina Surge and Wave Environment Team co-leader for the U.S. Army Corps of Engineers' Interagency Performance Evaluation Task Force (IPET) of New Orleans and Southeastern Louisiana Hurricane Protection Projects (2005-2007).

Commissioner, Southeast Louisiana Flood Protection Authority–West Bank (2007-present).

Storm Surge Model Development Team leader for the U.S. Army Corps of Engineers' (USACE) and Federal Emergency Management Agency's (FEMA) Joint Coastal Surge (JCS) study of Louisiana and Texas in support of the USACE Hurricane Protection Office (USACE-HPO) rebuilding of the Southern Louisiana Federal levee systems, the Congressionally mandated Louisiana Coastal Protection and Restoration (LACPR) study, and the FEMA Digital Flood Insurance Rate Maps (DFIRMS) (2006-present).

REFEREED JOURNAL PUBLICATIONS

1. Westerink, J.J., J.J. Connor and K.D. Stolzenbach, "A Primitive Pseudo Wave Equation Formulation for Solving the Harmonic Shallow Water Equations," *Advances in Water Resources*, **10**, 188-199, 1987.

2. Westerink, J.J., J.J. Connor and K.D. Stolzenbach, "A Frequency-Time Domain Finite Element Model for Tidal Circulation Based on the Least Squares Harmonic Analysis Method," *International Journal for Numerical Methods in Fluids*, **8**, 813-843, 1988.

3. Westerink, J.J. and D. Shea, "Consistent Higher Degree Petrov-Galerkin Methods for the Solution of the Transient Convection-Diffusion Equation," *International Journal for Numerical Methods in Engineering*, **28**, 1077-1101, 1989.

4. Westerink, J.J., K.D. Stolzenbach and J.J. Connor, "General Spectral Computations of the Nonlinear Shallow Water Tidal Interactions Within the Bight of Abaco," *Journal of Physical Oceanography*, **19,** 1350-1373, 1989.

5. Baptista, A.M., J.J. Westerink and P.J. Turner, "Tides in the English Channel and Southern North Sea. A Frequency Domain Analysis Using Model TEA-NL," *Advances in Water Resources*, **12**, 166-183, 1989.

6. Cantekin, M.E. and J.J. Westerink, "Non-Diffusive N+2 Degree Petrov-Galerkin Methods for Two-Dimensional Transient Transport Computations," *International Journal for Numerical Methods in Engineering*, **30**, 397-418, 1990.

7. Luettich, R.A. and J.J. Westerink, "A Solution for the Vertical Variation of Stress, Rather than Velocity, in a Three-Dimensional Circulation Model," *International Journal for Numerical Methods in Fluids*, **12**, 911-928, 1991.

8. Westerink, J.J. and W.G. Gray, "Progress in Surface Water Modeling," *Reviews of Geophysics*, **29**, April Supplement, 210-217, 1991.

9. Westerink, J.J., R.A. Luettich, A.M. Baptista, N.W. Scheffner and P. Farrar, "Tide and Storm Surge Predictions Using a Finite Element Model," *Journal of Hydraulic Engineering*, **118**, 1373-1390, 1992.

10. Cantekin, M.E., J.J. Westerink and R.A. Luettich, "Low and Moderate Reynolds Number Transient Flow Simulations Using Space Filtered Navier Stokes Equations," *Numerical Methods for Partial Differential Equations*, **10**, 491-524, 1994.

11. Kolar, R.L., J.J. Westerink, M.E. Cantekin and C.A. Blain, "Aspects of Nonlinear Simulations Using Shallow Water Models Based on the Wave Continuity Equation," *Computers and Fluids*, **23**, 3, 523-538, 1994.

12. Kolar, R.L., W.G. Gray, J.J. Westerink and R.A. Luettich, "Shallow Water Modeling in Spherical Coordinates: Equation Formulation, Numerical Implementation and Application," *Journal of Hydraulic Research*, **32**, 1, 3-24, 1994.

13. Westerink, J.J., R.A. Luettich and J.C. Muccino, "Modeling Tides in the Western North Atlantic Using Unstructured Graded Grids," *Tellus*, **46A**, 178-199, 1994.

14. Westerink, J.J., R.A. Luettich, J.K. Wu and R.L. Kolar, "The Influence of Normal Flow Boundary Conditions on Spurious Modes in Finite Element Solutions to the Shallow Water Equations," *International Journal for Numerical Methods in Fluids*, **18**, 1021-1060, 1994.

15. Luettich, R.A., S. Hu and J.J. Westerink, "Development of the Direct Stress Solution Technique for Three Dimensional Hydrodynamic Models Using Finite Elements," *International Journal for Numerical Methods in Fluids*, **19**, 295-319, 1994.

16. Blain, C.A., J.J. Westerink and R.A. Luettich, "The Influence of Domain Size on the Response Characteristics of a Hurricane Storm Surge Model," *Journal of Geophysical Research*, **99, C9**, 18467-18479, 1994.

17. Grenier, R.R., R.A. Luettich and J.J. Westerink, "A Comparison of the Nonlinear Frictional Characteristics of Two-Dimensional and Three-Dimensional Models of a Shallow Tidal Embayment," *Journal of Geophysical Research*, **100, C7**, 13719-13735, 1995.

18. Kolar, R.L., W.G. Gray and J.J. Westerink, "Boundary Conditions in Shallow Water Models - An Alternative Implementation for Finite Element Codes," *International Journal for Numerical Methods in Fluids*, **22**, 603-618, 1996.

19. Blain, C.A., J.J. Westerink and R.A. Luettich, "Grid Convergence Studies for the Prediction of Hurricane Storm Surge," *International Journal for Numerical Methods in Fluids*, **26**, 369-401, 1998.

20. Hagen, S.C., J.J. Westerink and R.L. Kolar, "One-Dimensional Finite Element Grids Based on a Localized Truncation Error Analysis," *International Journal for Numerical Methods in Fluids*, **32**, 241-261, 2000.

21. Hagen, S.C., J.J. Westerink, R.L. Kolar and O. Horstmann, "Two Dimensional Unstructured Mesh Generation for Tidal Models," *International Journal for Numerical Methods in Fluids*, **35**, 669-686, 2001.

22. Atkinson, J.H., J.J. Westerink and J.M. Hervouet, "Similarities between the Quasi-Bubble and the Generalized Wave Continuity Equation Solutions to the Shallow Water Equations," *International Journal for Numerical Methods in Fluids*, **45,** 689-714, 2004.

23. Atkinson, J.H., J.J. Westerink and R.A. Luettich, "Two-Dimensional Dispersion Analysis of Finite Element Approximations to the Shallow Water Equations," *International Journal for Numerical Methods in Fluids*, **45,** 715-749, 2004.

24. Bunya, S., J.J. Westerink and S. Yoshimura, "Discontinuous Boundary Implementations for the Shallow Water Equations," *International Journal for Numerical Methods in Fluids*, **47**, 1451-1468, 2005.

25. Bunya, S., S. Yoshimura and J.J. Westerink, "Improvements in the Mass Conservation Using Alternative Boundary Implementations for a Quasi Bubble Finite Element Shallow Water Model," *International Journal for Numerical Methods in Fluids*, **51**, 1277-1296**,** 2006.

26. Dawson, C., J.J. Westerink, J.C. Feyen and D. Pothina, "Continuous, Discontinuous and Coupled Discontinuous-Continuous Galerkin Finite Element Methods for the Shallow Water Equations," *International Journal for Numerical Methods in Fluids*, **52**, 63-88, 2006.

27. Kubatko, E.J., J.J. Westerink and C. Dawson, "An Unstructured Grid Morphodynamic Model with a Discontinuous Galerkin Method for Bed Evolution," *Ocean Modeling*, **15**, 71-89, 2006.

28. Kubatko, E.J., J.J. Westerink and C. Dawson, "*hp* Discontinuous Galerkin Methods for Advection Dominated Problems in Shallow Water Flow," *Computer Methods in Applied Mechanics and Engineering*, **196**, 437-451, 2006.

29. Ebersole, B.A., D. Resio, and J.J. Westerink, "A Community Approach to Improved Prediction and Characterization of Coastal Storm Hazards," *Marine Technology Society Journal*, **40**, 4, 56-68, 2006/2007.

30. Kubatko, E.J and J.J. Westerink, "Exact Discontinuous Solutions of Exner's Bed Evolution Model: Simple Theory for Sediment Bores," *Journal of Hydraulic Engineering*, **133**, 305-311, 2007.

31. Kubatko, E.J., J.J. Westerink and C. Dawson, "Semi-discrete Discontinuous Galerkin Methods and Stage Exceeding Order Strong Stability Preserving Runge-Kutta Time Discretizations," *Journal of Computational Physics*, **222**, 832-848, 2007.

32. Westerink, J.J., R.A. Luettich , J.C. Feyen, J.H. Atkinson, , C. Dawson, H.J. Roberts, M.D. Powell, J.P. Dunion, E.J. Kubatko, H. Pourtaheri, "A Basin to Channel Scale Unstructured Grid Hurricane Storm Surge Model Applied to Southern Louisiana," *Monthly Weather Review*, **136**, 3, 833-864, 2008.

33. Bunya, S., E.J. Kubatko, J.J. Westerink, C. Dawson, "A Wetting and Drying Treatment for the Runge-Kutta Discontinuous Galerkin Solution to the Shallow Water Equations," *Computer Methods in Applied Mechanics and Engineering*, Accepted for Publication, 2008.

34. Kubatko, E.J., S. Bunya, C. Dawson, J.J. Westerink, "Dynamic *p*-adaptive Runge-Kutta Discontinuous Galerkin Methods for the Shallow Water Equations," *Computer Methods in Applied Mechanics and Engineering*, Accepted for Publication, 2008.

35. Kubatko, E.J., C. Dawson, J.J. Westerink, "Time Step Restrictions for Runge-Kutta Discontinuous Galerkin Methods on Triangular Grids," *Journal Computational Physics*, **227**, 9697-9710, 2008.

36. Kubatko, E.J., S. Bunya, C. Dawson, J.J. Westerink, C. Mirabito, "A Comparison of Continuous and Discontinuous Finite Element Shallow Water Models," *Journal of Scientific Computing*, Accepted for Publication, 2008.

37. Bunya S. and J.J. Westerink, "Hurricane Katrina Storm Surge Simulation Using a Coupled Storm Surge, Wind Wave, and Tidal Current Model on an Unstructured Grid," (in Japanese), *Coastal Engineering Journal of the Japan Society of Civil Engineers*, In Press, 2008.

38. Resio, D.T. and J.J. Westerink, "Hurricanes and the Physics of Surges," *Physics Today*, **61**, 9, 33-38, 2008.

39. Bunya, S., J.C. Dietrich, J.J. Westerink, B.A. Ebersole, J.M. Smith, J.H. Atkinson, R. Jensen, D.T. Resio, R.A. Luettich, C. Dawson, V.J. Cardone, A.T. Cox, M.D. Powell, H.J. Westerink, H.J. Roberts, "A High Resolution Coupled Riverine Flow, Tide, Wind, Wind Wave and Storm Surge Model for Southern Louisiana and Mississippi: Part I - Model Development and Validation," *Monthly Weather Review*, In Review, 2008.

40. Dietrich, J.C., S. Bunya, J.J. Westerink, B.A. Ebersole, J.M. Smith, J.H. Atkinson, R. Jensen, D.T. Resio, R.A. Luettich, C. Dawson, V.J. Cardone, A.T. Cox, M.D. Powell, H.J. Westerink, H.J. Roberts, "A High Resolution Coupled Riverine Flow, Tide, Wind, Wind Wave and Storm Surge Model for Southern Louisiana and Mississippi: Part II - Synoptic Description and Analyses of Hurricanes Katrina and Rita ," *Monthly Weather Review*, In Review, 2008.

TRADE JOURNAL PUBLICATIONS

1. Ledden, M. van, W. de Jong, J. Westerink, "New Orleans Wapent Zich met Robuuster Dijkontwerp," (in Dutch). *Land + Water: Magazine voor Civiele- en Milieutechniek*, 19 Oktober , 16-17, 2007

REFEREED BOOK CHAPTERS (I - indicates invited)

1.*I* Luettich, R.A. and J.J. Westerink, "Continental Shelf Scale Convergence Studies with a Barotropic Tidal Model," in Quantitative Skill Assessment for Coastal Ocean Models, D.R. Lynch and A.M. Davies, Editors, Coastal and Estuarine Studies Series, **47**, American Geophysical Union, Washington, D.C., 1995

REFEREED CONFERENCE PROCEEDINGS

1. Westerink, J.J., "The Solution of the Shock Wave Problem Using the Fractional Step Method," Proceedings of the Symposium on Computational Acoustics, Yale University, New Haven, Ct., D. Lee, R. Sternberg and M. Schulz, Eds., 1986.

2. Luettich, R.A., S. Hu, J.J. Westerink and N.W. Scheffner, "Modeling 3-D Circulation Using the DSS Technique," Estuarine and Coastal Modeling, M. Spaulding Ed., ASCE, N.Y., N.Y., 1992.

3. Westerink, J.J., J.C. Muccino and R.A. Luettich, "Tide and Storm Surge Computations for the Western North Atlantic and Gulf of Mexico," Estuarine and Coastal Modeling, M. Spaulding Ed., ASCE, N.Y., N.Y., 1992.

4. Grenier, R.R., R.A. Luettich and J.J. Westerink, "Comparison of 2D and 3D Models for Computing Shallow Water Tides in a Friction Dominated Tidal Embayment," Estuarine and Coastal Modeling III, M. Spaulding et al. Eds., ASCE, New York, NY, 58-70, 1994.

5. Spargo, E., J.J. Westerink, R.A. Luettich and D. Mark, "Developing a Tidal Constituent Database for the Eastern North Pacific Ocean," Estuarine and Coastal Modeling, Proceedings of the Eight International Conference, November 3-5, 2003, Monterey, CA, M. Spaulding et al. Eds., ASCE, New York, NY, 2004.

6. Dietrich, J.C., R.L. Kolar and J.J. Westerink, “Refinements in Continuous Galerkin Wetting and Drying Algorithms,” Estuarine and Coastal Modeling, Proceedings of the Ninth International Conference, October 31- November 2, 2005, Charleston, SC, M. Spaulding et al. Eds., 2006.

7. Atkinson, J., J. Westerink, T. Wamsley, M. Cialone, C. Dietrich, K. Dresback, R. Kolar, D. Resio, C. Bender, B. Blanton, S. Bunya, W. de Jong, B. Ebersole, A. Grzegorzewski, B. Jensen, H. Pourtaheri, J. Ratcliff, H. Roberts, J. Smith, and C. Szpilka, “Hurricane Storm Surge and Wave Modeling in Southern Louisiana: A Brief Overview,” Estuarine and Coastal Modeling, Proceedings of the Tenth International Conference, November 5-7, 2007, Newport, RI, M. Spaulding Ed. ASCE, 2008.

8. Forbes, C., J. Fleming, C. Mattocks, C. Fulcher, R. Luettich, J. Westerink, and S. Bunya, “New Developments in the ADCIRC Community Model,” Estuarine and Coastal Modeling, Proceedings of the Tenth International Conference, November 5-7, 2007, Newport, RI, M. Spaulding Ed. ASCE, 2008.

8. Clint Dawson, Joannes Westerink, Ethan Kubatko, Jennifer Proft and Chris Mirabito, "Parallel Finite Element Models for Hurricane Storm Surges," Proceedings of the Teragrid '08 Conference, Las Vegas, NV, June 9-13, 2008.

REFEREED TECHNICAL REPORTS

1. Luettich, R.A., J.J. Westerink and N.W. Scheffner, “ADCIRC: An Advanced Three-Dimensional Circulation Model for Shelves, Coasts and Estuaries, Report 1: Theory and Methodology of ADCIRC-2DDI and ADCIRC-3DL,” Technical Report DRP-92-6, Department of the Army, US Army Corps of Engineers, Washington D.C., November 1992.

2. Westerink, J.J., R.A. Luettich and N.W. Scheffner, “ADCIRC: An Advanced Three-Dimensional Circulation Model for Shelves, Coasts, and Estuaries, Report 3: Development of a Tidal Constituent Database for the Western North Atlantic and Gulf of Mexico,” Department of the Army, US Army Corps of Engineers, Washington, D.C., June 1993.

3. Blain, C.A., J.J. Westerink, R.A. Luettich and N.W. Scheffner, “Generation of a Storm Surge Data Base from the Hindcast of 153 Historical Hurricane Events,” Department of the Army, US Army Corps of Engineers, Washington, D.C., 1993.

4. Westerink, J.J., R.A. Luettich, C.A. Blain and N.W. Scheffner, “ADCIRC: An Advanced Three-Dimensional Circulation Model for Shelves, Coasts and Estuaries; Report 2: Users Manual for ADCIRC-2DDI,” Department of the Army, US Army Corps of Engineers, Washington D.C., January 1994.

5. Blain, C.A., J.J. Westerink, R.A. Luettich and N.W. Scheffner, “ADCIRC: An Advanced Three-Dimensional Circulation Model for Shelves, Coasts, and Estuaries, Report 4: Hurricane Storm Surge Modeling Using Large Domains,” Department of the Army, US Army Corps of Engineers, Washington, D.C., August 1994.

6. Scheffner, N.W., D.J. Mark, C.A. Blain, J.J. Westerink and R.A. Luettich, “ADCIRC: An Advanced Three-Dimensional Circulation Model for Shelves, Coasts, and Estuaries, Report 5: A Tropical Storm Database for the East and Gulf of Mexico Coasts of the United States,” Department of the Army, US Army Corps of Engineers, Washington, D.C., August 1994.

7. Hench, J.L., R.A. Luettich, J.J. Westerink and N.W. Scheffner, “Development of a Tidal Constituent Database for the Eastern North Pacific,” Department of the Army, U.S. Army Corps of Engineers, Washington, D.C., 1994.

8. Blain, C.A., J.J. Westerink, R.A. Luettich and N.W. Scheffner, “The Influence of Domain Size and Grid Structure on the Response Characteristics of a Hurricane Storm Surge Model,” Department of the Army Waterways Experiment Station, Vicksburg MS, March 1995.

9. Mukai, A., J.J. Westerink and R.A. Luettich, "Guidelines for Using the Eastcoast 2001 Database of Tidal Constituents within the Western North Atlantic Ocean, Gulf of Mexico and Caribbean Sea," Coastal and Hydraulic Engineering Technical Note, U.S. Army Engineer Research and Development Center, Vicksburg MS, September 2001.

10. Mukai, A., J.J. Westerink, R.A. Luettich and D.J. Mark, "A Tidal Constituent Database for the Western North Atlantic Ocean, Gulf of Mexico and Caribbean Sea," Technical Report, U.S. Army Engineer Research and Development Center, Vicksburg MS, Report ERDC/CHL TR-02-24, September 2002.

11. Spargo, E.A., J.J. Westerink, R.A. Luettich and D.J. Mark, "ENPAC 2003: A Tidal Constituent Database for the Eastern North Pacific Ocean," Technical Report, U.S. Army Engineer Research and Development Center, Vicksburg MS, Report ERDC/CHL TR-04-12, September 2004.

12. Ebersole, B.A., J.J. Westerink, D.T. Resio, R.G. Dean, "Performance Evaluation of the New Orleans and Southeast Louisiana Hurricane Protection System," Volume IV – The Storm, Final Report of the Interagency Performance Evaluation Task Force, U.S. Army Corps of Engineers, Washington, D.C., March 2007.

13. Link, L.E., J.J. Jaeger, J. Stevenson, W. Stroupe, R.L. Mosher, D. Martin, J.K. Garster, D.B. Zilkoski, B.A. Ebersole, J.J. Westerink, D.T. Resio, R.G. Dean, M.K. Sharp, R.S. Steedman, J.M. Duncan, B.L. Moentenich, B. Howard, J. Harris, S. Fitzgerald, D. Moser, P. Canning, J. Foster, B. Muller, "Performance Evaluation of the New Orleans and Southeast Louisiana Hurricane Protection System," Volume I – Executive Summary and Overview, Final Report of the Interagency Performance Task Force, U.S. Army Corps of Engineers, Washington, D.C., June 2008.

14. Flood Insurance Study: Southeastern Parishes, Louisiana, Intermediate Submission 2: Offshore Water Levels and Waves, FEMA, US Army Corps of Engineers, New Orleans District, July 24, 2008

BOOK CHAPTERS (I - indicates invited)

1.*I* Westerink, J.J., R.A. Luettich, C.A. Blain and S.C. Hagen, "Surface Elevation and Circulation in Continental Margin Waters," in Finite Element Modeling of Environmental Problems, Surface and Subsurface Flow and Transport, G.F. Carey, Ed., J. Wiley and Sons, Chichester, 1995.

2.*I* Westerink, J.J. and P.J. Roache, "Issues in Convergence Studies in Geophysical Flow Computations," in Next Generation Environmental Models Computational Methods, G. Delic and M.F. Wheeler, Eds., Society for Industrial and Applied Mathematics, Philadelphia, PA, 1997.

CONFERENCE PROCEEDINGS (*I* - indicates invited, P - indicates invited Plenary speaker)

1. Harms, V.W., C.T. Bishop and J.J. Westerink, "Pipe-Tire Floating Breakwater Design Criteria," Floating Breakwater Conference, Seattle, Washington, October 19-21, 1981.

2. Westerink, J.J., J.J. Connor and K.D. Stolzenbach., "Harmonic Finite Element Model of Tidal Circulation for Small Bays," Proceedings of the Conference on Frontiers in Hydraulic Engineering, H.T. Shen, Ed., ASCE, N.Y., 1983.

3. Westerink, J.J., J.J. Connor and K.D. Stolzenbach, "Spectral Computations within the Bight of Abaco Using a Frequency-Time Domain Finite Element Model," Proceedings of the Sixth International Conference on Finite Elements in Water Resources, A. Sa da Costa et al., Eds., Lisbon, Portugal, 1986.

4. Westerink, J.J., D. Shea and M.E. Cantekin, "Non-diffusive N+2 Degree Upwinding Methods for the Finite Element Solution of the Time Dependent Transport Equation," VIIth International Conference on Computational Methods in Water Resources, Cambridge, MA, M. Celia et al. Eds., 1988.

5. Miller, M.C., W.E. Roper, L.E. Borgman and J.J. Westerink, “Development of Water Level and Wave Height Design Data,” Proceedings, 23rd Joint Meeting, United States - Japan Program in Natural Resources, Panel on Wind and Seismic Effects, Tsukuba, Japan, 14-17 May, 1991.

6. Kolar, R.L., W.G. Gray and J.J. Westerink, “An Analysis of the Mass Conserving Properties of the Generalized Wave Continuity Equation,” Proceedings of the IX International Conference on Computational Methods in Water Resources, T. Russell et al. Eds., Denver, CO., June 1992.

7. Luettich, R.A. and J.J. Westerink, “A Three Dimensional Circulation Model Using a Direct Stress Solution over the Vertical,” Proceedings of the IX International Conference on Computational Methods in Water Resources, T. Russell et al. Eds., Denver, CO., June 1992.

8. Westerink, J.J., J.C. Muccino and R.A. Luettich, “Resolution Requirements for a Tidal Model of the Western North Atlantic and Gulf of Mexico,” Proceedings of the IX International Conference on Computational Methods in Water Resources, T. Russell et al. Eds., Denver, CO., June 1992.

9. Kareem, A., J.J. Westerink and L.E. Borgman, “Integrated Risk Assessment for Coastal Regions Subjected to Tropical Storms/Global Climate Change,” Proceedings of the 7th U.S. National Conference on Wind Engineering, UCLA, June 1993.

10. Kolar, R.L., W.G. Gray and J.J. Westerink, “Normal Flow Boundary Conditions in Shallow Water Models - Affect on Mass Conservation and Accuracy,” Proceedings of the X International Conference on Computational Methods in Water Resources, A. Peters et al. Eds, Heidelberg, July, 1994.

11. Blain, C.A., J.J. Westerink and R.A. Luettich, “Domain and Grid Sensitivity Studies for Hurricane Storm Surge Predictions,” Proceedings of the X International Conference on Computational Methods in Water Resources, A. Peters et al. Eds., Heidelberg, July, 1994.

12.*I* Westerink, J.J. and R.A. Luettich, “Meshing Requirements for Large Scale Coastal Ocean Tidal Models,” Proceedings of the X International Conference on Computational Methods in Water Resources, A. Peters et al. Eds., Heidelberg, July, 1994.

13.*I* Hagen, S.C. and J.J. Westerink, “Finite Element Grids Based on Truncation Error Analysis,” Second International Conference on Hydro-science and Engineering, Beijing, China, March, 1995.

14. Hagen, S.C. and J.J. Westerink, “First Element Grid Resolution Based on Second and Fourth Order Truncation Error Analysis,” Coastal Engineering ‘95, C.A. Brebbia et al. Eds., Cancun, Mexico, September, 1995.

15. Blain, C.A., J.J. Westerink and R.A. Luettich, “Application of a Domain Size and Gridding Strategy in the Prediction of Hurricane Storm Surge,” Computer Modeling of Seas and Coastal Regions II, C.A. Brebbia et al. Eds., Computational Mechanics Publications, Southampton, 301-308, 1995.

16. Scheffner, N.W., J.J. Westerink and R.A. Luettich, “Applications of a Longwave Hydrodynamic Model Generated Tropical and Extra-tropical Storm Surge Database,” Computer Modeling of Seas and Coastal Regions II, C.A. Brebbia et al. Eds., Computational Mechanics Publications, Southampton, 327-334, 1995.

17.*I* Westerink, J.J. and P.J. Roache, “Issues in Convergence Studies in Geophysical Flow Computations,” Joint ASME/JSME Fluids Engineering Conference, Hilton Head, SC, August, 1995.

18.*P* Westerink, J.J., R.A. Luettich and R.L Kolar, “Advances in Finite Element Modeling of Coastal Ocean Hydrodynamics,” Computational Methods in Water Resources XI, Volume 2, Computational Methods in Surface Flow and Transport Problems, A. Aldama et al. Eds., Computational Mechanics Publications, Southampton, 313-322, 1996.

19. Kolar, R.L., J.J. Westerink and S.C. Hagen, “Truncation Error Analysis of Shallow Water Models Based on the Generalized Wave Continuity Equation,” Computational Methods in Water Resources XI, Volume 2, Computational Methods in Surface Flow and Transport Problems, A. Aldama et al. Eds., Computational Mechanics Publications, Southampton, 215-222, 1996.

20.*I* Westerink, J.J., R.A. Luettich and R.L Kolar, "ADCIRC, An Advanced Finite Element Model for Coastal Ocean Circulation," The Third Asian Pacific Conference on Computational Mechanics, 16-18 September, Seoul, Korea, 1996.

21. Hagen, S.C. and J.J. Westerink, "Utilization of an Imposed Multiple of Change in Finite Element Grid Generation," The Third Asian Pacific Conference on Computational Mechanics, 16-18 September, Seoul, Korea, 1996.

22. Kolar, R.L., J.P. Looper, J.J. Westerink and W.G. Gray, "An Improved Time Marching Algorithm for GWC Shallow Water Models," Computational Methods in Water Resources XII, Volume 2, Computational Methods in Surface and Ground Water Transport, V.N. Burganos et al. Eds., Computational Mechanics Publications, Southampton, 379-386, 1998.

23. Atkinson, J.H. and J.J. Westerink, "Evaluation of Spatial Discretizations of the Shallow Water Equations," Computational Methods in Water Resources XIII, L. Bentley et al. Eds., Volume 2, Computational Methods, Surface Waters Systems and Hydrology, Balkema Publishers, Rotterdam, 873-880, 2000.

24. Feyen, J.C., J.H. Atkinson and J.J. Westerink, "Issues in Hurricane Surge Computations Using a GWCE Based F.E. Model," Computational Methods in Water Resources XIII, L. Bentley et al. Eds., Volume 2, Computational Methods, Surface Waters Systems and Hydrology, Balkema Publishers, Rotterdam, 865-872, 2000.

25. Aldama, A., A. Aguillar, R. Kolar and J.J. Westerink, "A Mass Conservation Analysis of the GWCE Formulation," Computational Methods in Water Resources XIII, L. Bentley et al. Eds., Volume 2, Computational Methods, Surface Waters Systems and Hydrology, Balkema Publishers, Rotterdam, 907-912, 2000.

26. Kolar, R. and J.J. Westerink, "A Look Back at 20 Years of GWC Based Shallow Water Models," Computational Methods in Water Resources XIII, L. Bentley et al. Eds., Volume 2, Computational Methods, Surface Waters Systems and Hydrology, Balkema Publishers, Rotterdam, 899-906, 2000.

27. Feyen, J.C., J.H. Atkinson and J.J. Westerink, "GWCE-based Shallow Water Equation Simulations of the Lake Pontchartrain - Lake Borgne Tidal System," Computational Methods in Water Resources XIV, S.M. Hassanizadeh et al. Eds., Volume 2, Developments in Water Science, 47, Elsevier, Amsterdam, 1581-1588, 2002.

CONFERENCE ABSTRACTS (*I* - indicates Invited; P - indicates invited Plenary speaker)

1. Westerink, J.J., J.J. Connor and K.D. Stolzenbach., "A Numerical Study of the Tides within the Bight of Abaco," Fall Meeting of the American Geophysical Union, San Francisco, EOS, Vol. 66, No. 46, 1985.

2.*I* Westerink, J.J. and M.E. Cantekin, "Superconvergent Petrov-Galerkin Methods for the Transient Transport Equation," Fall Meeting of the American Geophysical Union, San Francisco, EOS, Vol. 70, No. 43, 1989.

3. Wu, J., J.J. Westerink and R.A. Luettich, "Boundary Condition Control on Spurious Modes in Finite Element Solutions of the Shallow Water Equations," Fall Meeting of the American Geophysical Union, San Francisco, EOS, Vol. 70, No. 43, 1989.

4. Luettich, R.A., S. Hu and J.J. Westerink, "An Efficient Method for Including Boundary Layers in 3-D Hydrodynamic Models: Solving for the Vertical Variation of Shear Stress Rather than Velocity," Fall Meeting of the American Geophysical Union, EOS, Vol. 71, No. 43, 1990.

5.*I* Westerink, J.J., "Non-Diffusive Petrov-Galerkin Methods for the Transient Transport Equation," Workshop on Advances in Computational Methods for Transport Phenomena, University of Kentucky, Lexington KY, January 7-9, 1991.

6. Westerink, J.J., R.A. Luettich, A.M. Baptista and N.W. Scheffner, "Tidal Circulation Computations for the Western Atlantic Shelf and Gulf of Mexico," 25th Annual Congress of the Canadian Meteorological and Oceanographic Society, Winnipeg, Canada, 3-7 June, 1991.

7. Luettich, R.A., S. Hu and J.J. Westerink, "Development and Application of a Three-Dimensional Circulation Model Using a Direct Stress Solution Over the Vertical," 25th Annual Congress of the Canadian Meteorological and Oceanographic Society, Winnipeg, Canada, 3-7 June, 1991.

8.*I* Cantekin, M.E., J.J. Westerink, R.A. Luettich, "Lid Driven Cavity Flow Computations Using Filtered Navier Stokes Equations," First U.S. National Congress on Computational Mechanics, Chicago, July 21-24, 1991.

9.*I* Westerink, J.J. and R.A. Luettich, "Modeling Tides and Hurricane Storm Surge in the Western Atlantic Using the Generalized Wave Continuity Equation Model," JONSMOD '92, P.P. Dyke, Ed., Copenhagen, August 3-6, 1992.

10.*I* Luettich, R.A. and J.J. Westerink, "Assessing the Physics of Coastal Flow Models by Examining the Spectral Distribution of Nonlinear Tides," SIAM Conference on Mathematical and Computational Issues in the Geosciences, Houston, TX, April, 1993.

11.*I* Westerink, J.J. and R.A. Luettich, "Grid Convergence Studies for Coastal Ocean Models," SIAM Conference on Mathematical and Computational Issues in the Geosciences, Houston, TX, April, 1993.

12. Westerink, J.J. and R.A. Luettich, "Sensitivity Studies of Forcing Mechanisms for the Western North Atlantic Tidal Model," 3rd International Conference on Estuarine and Coastal Modeling, Oak Brook, IL, September, 1993.

13.*I* Westerink, J.J. and R.A. Luettich, "Convergence Studies of Tidal and Hurricane Storm Surge Response for Continental Margin Waters," Workshop on Finite Element Modeling of Environmental Problems, G.F. Carey, Ed., Computational Fluid Dynamics Laboratory, University of Texas at Austin, Austin, TX, March 4-5, 1994.

14.*I* Luettich, R.A. and J.J. Westerink, "Tidal Characteristics from a Barotropic Tidal Model of the Western North Atlantic and the Gulf of Mexico," JONSMOD '94, P.P. Dyke, Ed., Brussels, July 25-28, 1994.

15.*I* Westerink, J.J., C.A. Blain and R.A. Luettich, "Convergence Studies of Hurricane Storm Surge Response over a Large Scale Shelf Model," JONSMOD '94, P.P. Dyke, Ed., Brussels, July 25-28, 1994.

16.*P* Westerink, J.J. and R.A. Luettich, "Convergence Studies of Tides and Hurricane Response in Continental Margin Waters," SIAM Conference on Mathematical and Computational Issues in the Geosciences, San Antonio, TX, February 8-11, 1995.

17.*I* Westerink, J.J. and R.A. Luettich, "Unstructured Mesh Design and Error Assessment for Surface Water Flow Models," Workshop on the Next Generation Environmental Models Computational Methods, U.S. Environmental Protection Agency National Environmental Supercomputing Center, Bay City, MI, August 1995.

18.*I* Westerink, J.J. and R.L. Kolar, "Analysis of Boundary Conditions for Shallow Water Equation Models," Coastal Engineering 95, C.A. Brebbia et al. Eds., Cancun, Mexico, September 1995.

19. Hagen, S.C. and J.J. Westerink, "A Practical Approach for Two-Dimensional Finite Element Mesh Generation Based on Localized Truncation Error Analysis," Fourth International Conference on Estuarine and Coastal Modeling, San Diego, CA, October 26-28, 1995.

20. Luettich, R.A. and J.J. Westerink, "Recent Results from a Tidal Model of the Western North Atlantic, Gulf of Mexico and Caribbean Sea," Fourth International Conference on Estuarine and Coastal Modeling, San Diego, CA, October 26-28, 1995.

21. Luettich, R.A., J.J. Westerink and J. Hudgins, "Initial Results from a Combined Tide and Storm Surge Forecast Model of the U.S. East Coast, Gulf of Mexico and Caribbean Sea," 7th Pacific Congress on Marine Science and Technology, Honolulu, HA, June, 1996.

22. Luettich, R.A. and J.J. Westerink, "Sensitivity Studies with a Finite Element Tidal Model of the Western North Atlantic, Gulf of Mexico and Caribbean Sea," Tidal Sciences 1996, London, October, 1996.

23. Atkinson, J.H. and J.J. Westerink, "Convergence Study of Solutions to the Advection-Diffusion Equation," Fourth SIAM Conference on Mathematical and Computational Issues in the Geosciences, Albuquerque, NM, June 16-19, 1997.

24. Kolar, R.L. and J.J. Westerink, "A Look Back at 20 Years of Wave Equation Models," Fifth SIAM Conference on Mathematical and Computational Issues in the Geosciences, San Antonio TX, March 24-27, 1999

25. Westerink, J.J., R.L. Kolar, and R.A. Luettich, "Issues of Mass Conservation Associated with GWCE Based Finite Element Surface Water Models," Fifth SIAM Conference on Mathematical and Computational Issues in the Geosciences, San Antonio TX, March 24-27, 1999

26.***P*** Westerink, J.J., "Modeling Hurricane Storm Surge Using Large Domains and Unstructured Grids," 1999 Gordon Research Conference on Coastal Ocean Modeling, Colby-Sawyer College, New London NH, June 20-24, 1999

27.***I*** Westerink, J.J., "Modeling Hurricane Storm Surge Using Large Domains and Unstructured Grids," Society for Engineering Science, Austin TX, October 25-27, 1999.

28. Atkinson, J.H. and J.J. Westerink, "Similarities between the Quasi-Bubble and the Generalized Wave Continuity Equation Solutions to the Shallow Water Equations," Fifteenth International Symposium on Mathematical Theory of Networks and Systems, University of Notre Dame, August 12-16, 2002.

29. Spargo, E., J.J. Westerink and R.A. Luettich, "A Tidal Constituent Database for the Eastern North Pacific Ocean," Twelfth International Conference on Finite Element Methods in Flow Problems, Meijo University, Nagoya, Japan, April 2-4, 2003.

30. Feyen, J.C., J.J. Westerink and C. Dawson, "A Comparison of the Generalized Wave Continuity Equation and Discontinuous Galerkin Finite Element Methods for the Shallow Water Equations," Twelfth International Conference on Finite Element Methods in Flow Problems, Meijo University, Nagoya, Japan, April 2-4, 2003.

31. Kubatko, E.J. and J.J. Westerink, "Applying the Discontinuous Galerkin Method to the Equation of Sediment Continuity," Twelfth International Conference on Finite Element Methods in Flow Problems, Meijo University, Nagoya, Japan, April 2-4, 2003.

32.***I*** Westerink, J.J., "Hurricane Storm Surge Simulations Using a Large Domain Finite Element Model in Southern Louisiana," The Second International Workshop on Unstructured Grid Numerical Modeling of Coastal, Shelf and Ocean Flows, Delft University of Technology, Delft, Netherlands, 23-25 September, 2003.

33.***I*** Luettich, R.A. and J.J. Westerink, "Hurricane Storm Surge Simulations Using the ADCIRC Coastal Ocean Hydrodynamic Model," 58th Interdepartmental Hurricane Conference, Charleston, SC, March, 2004.

34. van Heerden, I.L. and J.J. Westerink, "The Use of the ADCIRC Hydrodynamic Model for Computing Hurricane Storm Surge in Southern Louisiana," 58th Interdepartmental Hurricane Conference, Charleston, SC, March, 2004.

35. Kubatko, E.J., J.J. Westerink, and C. Dawson, "The *h-p* Discontinuous Galerkin Method Applied to the Shallow Water Equations," The Third International Workshop on Unstructured Grid Numerical

Modeling of Coastal, Shelf and Ocean Flows, Laboratoire d'Etudes en Geodesie et Oceanographie Spatiales, Obsevatoire Midi-Pyrenees, Toulouse, France, 20-22 September, 2004.

36.*I* Westerink, J.J., J.C. Feyen, J.H. Atkinson, R.A. Luettich, C. Dawson, H.J. Roberts, and E.J. Kubatko, "Development of a Large Domain Finite Element Storm Surge Model for Southern Louisiana," International Workshops on Advances in Computational Mechanics, Tokyo, Japan, 3-6 November, 2004.

37.*I* Kubatko, E.J., J.J. Westerink, and C. Dawson, "*h-p* Discontinuous Galerkin Methods for Coastal and Estuarine Circulation and Transport," International Workshops on Advances in Computational Mechanics, Tokyo, Japan, 3-6 November, 2004.

38. Bunya, S., S. Yoshimura, and J.J. Westerink, "Quasi-bubble Finite Element Formulation for the Shallow Water Equations with Discontinuous Boundary Implementation," International Conference on Computational Mechanics 2004, Singapore, 15-17 December 2004.

39. Kolar, R.L., K. Dresback, J.C. Dietrich, J.J. Westerink and R.A. Luettich, "Recent Advances with the ADCIRC Family of Hydrodynamic Models; Part 1 - Development," Eighth U.S. National Congress on Computational Mechanics, Austin, TX, July 24-28, 2005.

40. Kolar, R.L., K. Dresback, J.C. Dietrich, J.J. Westerink and R.A. Luettich, "Recent Advances with the ADCIRC Family of Hydrodynamic Models; Part 2 - Applications," Eighth U.S. National Congress on Computational Mechanics, Austin, TX, July 24-28, 2005.

41. Kubatko, E.J., J.J. Westerink and C. Dawson, "*h-p* Discontinuous Galerkin Methods for Shallow Water Flow and Transport," Eighth U.S. National Congress on Computational Mechanics, Austin, TX, July 24-28, 2005.

42. Bunya, S., S. Yoshimura and J.J. Westerink, "Alternative Formulations of Open Boundary Forcing for Shallow Water Flows," Eighth U.S. National Congress on Computational Mechanics, Austin, TX, July 24-28, 2005.

43.*P* Westerink, J.J., E.J. Kubatko, S. Bunya, C. Dawson and R.A. Luettich, "Coupled Shallow Water Equation - Morphological Computations Using Continuous Galerkin and Discontinuous Galerkin Based Finite Element Solutions," The Fourth International Workshop on Unstructured Grid Numerical Modeling of Coastal, Shelf and Ocean Flows, Bremerhaven Germany, October 10-12, 2005.

44. Kubatko, E.J., S. Bunya, J.J. Westerink and C. Dawson, "Recent Developments and Applications of an *h-p* Discontinuous Galerkin Model for Shallow Water Flow and Transport," The Fourth International Workshop on Unstructured Grid Numerical Modeling of Coastal, Shelf and Ocean Flows, Bremerhaven Germany, October 10-12, 2005

45. Dawson, C., J. Westerink, E. Kubatko, "A DG-Based Hydrodynamic Storm Surge Model," The Seventh World Congress on Computational Mechanics, Los Angeles, CA, July 16-22, 2006.

46. Westerink, J., S. Bunya, J.C. Dietrich, H. Westerink, R. Luettich, C. Dawson, "High Resolution Unstructured Storm Surge Models of the Gulf of Mexico," The Seventh World Congress on Computational Mechanics, Los Angeles, CA, July 16-22, 2006.

47. Bunya, S., J. Westerink, E. Kubatko, C. Dawson, S. Yoshimura, "A New Wetting and Drying Algorithm for Discontinuous Galerkin Solutions to the Shallow Water Equations," The Seventh World Congress on Computational Mechanics, Los Angeles, CA, July 16-22, 2006.

48. Kubatko, E., J. Westerink, C. Dawson, S. Bunya, "High-Order Discontinuous Galerkin Methods for Advection Dominated Shallow Water Hydrodynamics and Transport," The Seventh World Congress on Computational Mechanics, Los Angeles, CA, July 16-22, 2006.

49.*I* Westerink, J., S. Bunya, J.C. Dietrich, R. Luettich, B. Ebersole, J. Atkinson, H. Westerink, J. Smith, B. Jensen, A. Cox, V. Cardonne, M. Powell, "High Resolution Unstructured Grid Storm Surge

Modeling for Southern Louisiana," Rebuilding the New Orleans Region: Infrastructure Systems and Technology Innovation Forum, New Orleans, LA, September 24-26, 2006.

50. Bunya, S., J. Westerink, J.C. Dietrich, "Next-generation Hurricane/Typhoon Storm Surge Modeling Using Unstructured Grids in HPC Environments," The 84th Conference of the Fluids Engineering Division of the Japan Society of Mechanical Engineers, Toyo University, Kawagoe, Japan, October 28-29, 2006.

51.*P* Westerink, J., S. Bunya, J.C. Dietrich, "Hindcasting Hurricane Katrina Using the ADCIRC High Resolution Unstructured Grid Coastal Ocean Model," The 84th Conference of the Fluids Engineering Division of the Japan Society of Mechanical Engineers, Toyo University, Kawagoe, Japan, October 28-29, 2006.

52. Bunya, S., J. Westerink, E. Kubatko, C. Dawson, "Mass Conservative Wetting and Drying Algorithm for Discontinuous Galerkin Solutions to the Shallow Water Equations," The Fifth International Workshop on Unstructured Grid Numerical Modelling of Coastal, Shelf, and Ocean Flows, Miami, FL, November 13-15, 2006.

53. Kubatko, E., C. Dawson, J. Westerink, "hp-adaptive Discontinuous Galerkin Methods for the Shallow Water Equations," The Fifth International Workshop on Unstructured Grid Numerical Modelling of Coastal, Shelf, and Ocean Flows, Miami, FL, November 13-15, 2006.

54. Tromble, E., R. Kolar, J. Westerink, "Optimal Parameter Selection in GWCE-based Shallow Water Models," The Fifth International Workshop on Unstructured Grid Numerical Modelling of Coastal, Shelf, and Ocean Flows, Miami, FL, November 13-15, 2006.

55. Westerink, J., S. Bunya, J.C. Dietrich, R. Luettich, B. Ebersole, J. Atkinson, H. Westerink, J. Smith, B. Jensen, A. Cox, V. Cardonne, M. Powell, "High Resolution Unstructured Grid Storm Surge Modeling for Southern Louisiana," The Fifth International Workshop on Unstructured Grid Numerical Modelling of Coastal, Shelf, and Ocean Flows, Miami, FL, November 13-15, 2006.

56.*I* Westerink, J., "An Overview of Hurricane Science and Modeling," 2007 American Association for the Advancement of Science Annual Meeting, Science and Technology for Sustainable Well-Being, San Francisco, CA, February 15-19, 2007.

57. Westerink, J., "High Resolution Multi-Scale Storm Surge Modeling for Southern Louisiana," 2007 SIAM Conference on Mathematical and Computational Issues in the Geosciences, Santa FE, NM, March 19-22, 2007.

58.*I* Westerink, J., "ADCIRC – Hurricane Katrina Surge Analysis," ASCE's Hurricane Katrina External Review Panel, World Environmental & Water Resources Congress 2007, Tampa, FL, May 15-19, 2007.

59. Kubatko, E., S. Bunya, C. Dawson, J. Westerink, "Verification and Validation of a Discontinuous Galerkin Method for Shallow Water Flow and Transport," Ninth US National Congress on Computational Mechanics, San Francisco, CA, July 22-26, 2007.

60. Westerink, J., J. Atkinson, S. Bunya, C. Dawson, J.C. Dietrich, E. Kubatko, R. Luettich, H. Westerink, "Modeling Hurricane Storm Surge along the Gulf Coast – Toward Petaflop Computations," Ninth US National Congress on Computational Mechanics, San Francisco, CA, July 22-26, 2007.

61. Bunya, S., C. Dawson, E. Kubatko, J. Westerink, S. Yoshimura, "Validation of a Moving Boundary RKDG Method for the Shallow Water Equations," Ninth US National Congress on Computational Mechanics, San Francisco, CA, July 22-26, 2007.

62. Dietrich, J.C. and J. Westerink, "Modeling the Coupled Winds, Waves, and Storm Surge of Hurricane Rita," Ninth US National Congress on Computational Mechanics, San Francisco, CA, July 22-26, 2007.

63.*I* Westerink, J., M. Cialone, B. Ebersole, S. Bunya, J. Atkinson, J. Smith, R. Jensen, V. Cardone, A.

Cox, M. Powell, "High Resolution Multi-Process Hurricane Storm Surge Modeling in Southern Louisiana," JCOMM, Joint World Meteorological Organization – Intergovernmental Oceanographic Commission of UNESCO Technical Commission for Oceanography and Marine Meteorology, Scientific and Technical Symposium on Storm Surges, Seoul, Korea, October 2-6, 2007.

64. Bunya, S., J. Westerink, B. Ebersole, J. Atkinson, J. Smith, R. Jensen, V. Cardone, A. Cox, M. Powell, M. Cialone, H. Westerink, R. Luettich, C. Dawson, "Hindcasting Winds, Waves, and Storm Surge for Hurricane Katrina," 10th International Conference on Estuarine and Coastal Modeling, Newport, RI, November 5-7, 2007.

65. Dietrich, C., J. Westerink, J. Atkinson, S. Bunya, J. Smith, R. Jensen, V. Cardone, A. Cox, H. Westerink, R. Luettich, C. Dawson, "Hindcasting Winds, Waves and Storm Surge for Hurricane Rita," 10th International Conference on Estuarine and Coastal Modeling, Newport, RI, November 5-7, 2007.

66. Resio, D., J. Ratcliff, T. Wamsley, H. Roberts, J. Atkinson, B. Blanton, M. Cialone, A. Grzegorzewski, K. Dresback, R. Kolar, J. Smith, R. Jensen, C. Bender, S. Bunya, J. Westerink, H. Westerink, C. Dawson, "Stochastic Framework for Analyzing Hurricane Storm Surge Probabilities within Southern Louisiana and Mississippi," 10th International Conference on Estuarine and Coastal Modeling, Newport, RI, November 5-7, 2007.

67. Grzegorzewski, A., W. de Jong, H. Roberts, J. Atkinson, T. Wamsley, K. Dresback, R. Kolar, J. Westerink, "The Influence of Barrier Islands on Storm Surge in Southern Louisiana," 10th International Conference on Estuarine and Coastal Modeling, Newport, RI, November 5-7, 2007.

68. Atkinson, J., T. Wamsley, A. Grzegorzewski, M. Cialone, K. Dresback, R. Kolar, J. Westerink, "The Influence of Marshes on Hurricane Wind Waves and Storm Surge in Louisiana and Mississippi," 10th International Conference on Estuarine and Coastal Modeling, Newport, RI, November 5-7, 2007.

69. de Jong, W., D. Resio, J. Westerink, V. Stutts, T. Wamsley, J. Atkinson, K. Dresback, R. Kolar, J. Ratcliff, L. Westerink, "The Influence of Lower Plaquemines Parish Mississippi River Levees on Storm Surge in Southern Louisiana," 10th International Conference on Estuarine and Coastal Modeling, Newport, RI, November 5-7, 2007.

70. Westerink, J., J. Smith, V. Cardone, A. Cox, D. Resio, R. Jensen, T. Wamsley, B. Ebersole, "Hurricane Wave and Surge Computations: Deficiencies & Research Needs," 10th International Workshop on Wave Hindcasting and Forecasting and Coastal Hazard Symposium, Oahu, Hawaii, November 11-16, 2007.

71. Bunya, S., J. Westerink, B. Ebersole, J. Atkinson, J. Smith, R. Jensen, V. Cardone, A. Cox, M. Powell, M. Cialone, H. Westerink, R. Luettich, C. Dawson., "Hindcasting Winds, Waves and Storm Surge for Hurricane Katrina," 10th International Workshop on Wave Hindcasting and Forecasting and Coastal Hazard Symposium, Oahu, Hawaii, November 11-16, 2007.

72. Dietrich, C., J. Smith, J. Westerink, J. Atkinson, S. Bunya, R. Jensen, V. Cardone, A. Cox, H. Westerink, R. Luettich, C. Dawson, "Hindcasting Winds, Waves and Storm Surge for Hurricane Rita," 10th International Workshop on Wave Hindcasting and Forecasting and Coastal Hazard Symposium, Oahu, Hawaii, November 11-16, 2007.

73. Dawson, C., E. Kubatko, J. Westerink, "High Performance Computing to Resolve Propagation and Advection Dominated Multi-Scale Multi-Process Physics," 10th International Workshop on Wave Hindcasting and Forecasting and Coastal Hazard Symposium, Oahu, Hawaii, November 11-16, 2007.

74. Westerink, J., S. Bunya, C. Dietrich, E. Kubatko, C. Dawson, R. Luettich, "Modeling Hurricane Storm Surge along the Gulf Coast in the Wake of Katrina – Towards Petaflop Computations," Third Asian Pacific Congress on Computational Mechanics in conjunction with Eleventh International Conference on Enhancement and Promotion of Computational Methods in Engineering and Science, Kyoto, Japan, December 3-6, 2007.

75. Bunya, S., S. Yoshimura, J. Westerink, "Applications of a Moving Boundary Runge-Kutta Discontinuous Galerkin Method to Large-scale Coastal Flow Problems," Third Asian Pacific Congress on Computational Mechanics in conjunction with Eleventh International Conference on Enhancement and Promotion of Computational Methods in Engineering and Science, Kyoto, Japan, December 3-6, 2007.

76. Wamsley, T., D. V. Stutts, J. Westerink, "Surge and Wave Modeling for the Louisiana Coastal Protection and Restoration Study (LACPR)," 31st International Conference on Coastal Engineering, Hamburg, Germany, August 31 – September 5, 2008.

77. Dawson, C., J. Proft, J. Westerink, S. Tanaka, E. Kubatko, S. Bunya, "A Comparative Study of Continuous and Discontinuous Finite Element Methods for the Shallow Water Equations," Seventh International Workshop on Unstructured Grid Numerical Modelling of Coastal, Shelf, and Ocean Flows, Dartmouth, Nova Scotia, September 17-19, 2008.

78. Westerink, J., C. Dietrich, R. Martyr, J. Atkinson, H. Roberts, C. Dawson, H. Westerink, L. Westerink, "Riverine Flow, Tides and Hurricane Storm Surge in the Lower Mississippi River and Delta," Seventh International Workshop on Unstructured Grid Numerical Modelling of Coastal, Shelf, and Ocean Flows, Dartmouth, Nova Scotia, September 17-19, 2008.

79. Dietrich, C., J. Westerink, M. Zijlema, C. Dawson, R. Luettich, J. Fleming, "Coupled, Unstructured Grid, Wave and Circulation Models: Validation and Resolution Requirements," Seventh International Workshop on Unstructured Grid Numerical Modelling of Coastal, Shelf, and Ocean Flows, Dartmouth, Nova Scotia, September 17-19, 2008.

80. Bunya, S., E. Kubatko, J. Westerink, C. Dawson, S. Serhadlioglu, "Shallow Water Model for Coastal and Riverine Flow Problems Containing Wetting and Drying Zones," Seventh International Workshop on Unstructured Grid Numerical Modelling of Coastal, Shelf, and Ocean Flows, Dartmouth, Nova Scotia, September 17-19, 2008.

81. Roberts, H., J. Atkinson, F.R. Clark, J. Westerink, A. Sleath, "An ADCIRC Analysis of Variance in Marshland Hydroperiod Induced by Flood Protection Barriers," 2008 Annual Water Resources Conference, American Water Resources Association, New Orleans, Louisiana, November 17-20, 2008.

82. Martyr, R., M. Hope, C. Dietrich, J. Westerink, J. Atkinson, H. Roberts, C. Szpilka, "Storm Surge Propagation in the Lower Mississippi River," 2008 Annual Water Resources Conference, American Water Resources Association, New Orleans, Louisiana, November 17-20, 2008.

TECHNICAL REPORTS

1. Harms, V.W., B. Safaie, S.N. Kam, and J.J. Westerink, "Computer Manual for Calculating Wave Height Distributions about Offshore Structures," WREE Report 79-4, Department of Civil Engineering, State University of New York at Buffalo, September 1979.

2. Harms, V.W. and J.J. Westerink, "Wave Transmission and Mooring-Force Characteristics of Pipe-Tire Breakwaters," Lawrence Berkeley Laboratory Report No. 11778, University of California, Berkeley, October 1980.

3. Harms, V.W., J.J. Westerink, R.M. Sorenson and J.E. McTamany, "Wave Transmission and Mooring-Force Characteristics of Pipe-Tire Breakwaters," CERC Technical Paper No. 82-4, U.S. Army Engineer Waterways Experiment Station, Vicksburg, Mississippi, 1982.

4. Bishop, C.T., V.W. Harms and J.J. Westerink, "Pipe-Tire Breakwater Model Tests Data Report," Hydraulics Division Report L7R4A6, National Water Research Institute, Canada Centre for Inland Waters, Environment Canada, March 1982.

5. Westerink, J.J., J.J. Connor, K.D. Stolzenbach, E.E. Adams and A.M. Baptista, "TEA: A Linear Frequency Domain Finite Element Model for Tidal Embayment Analysis," Technical Report, M.I.T. Energy Laboratory, Cambridge, Mass., February 1984.

6. Westerink, J.J., K.D. Stolzenbach and J.J. Connor, "A Frequency Domain Finite Element Model for Tidal Circulation," Report No. MIT-EL 85-006, M.I.T. Energy Laboratory, Cambridge, Mass., 1985.

7. Westerink, J.J., E. Cantekin and D. Shea, "The Development of Higher Order Finite Element Upwinding Schemes for Convection Dominated Turbulent Flow Problems," Report No. COE-303, Ocean Engineering Program, Texas A&M University, 1988.

8. Westerink, J.J. and R.A. Luettich, "Review of Numerical Modeling Strategies for Predicting the Long Term Hydrodynamic Circulation for Estimating the Fate of Disposed Dredged Materials," Report No. COE-304, Ocean Engineering Program, Texas A&M University, 1989.

9. Westerink, J.J. and R.A. Luettich, "Tide and Storm Surge Predictions in the Gulf of Mexico Using Model ADCIRC-2D," Report to the US Army Engineer Waterways Experiment Station, July 1991.

10. Luettich, R.A., R.H. Birkhahn and J.J. Westerink, "Application of ADCIRC-2DDI to Masonboro Inlet, North Carolina: A Brief Numerical Modeling Study," Contractors Report to the US Army Engineer Waterways Experiment Station, August 1991.

11. Westerink, J.J., "Tidal Prediction in the Gulf of Mexico/Galveston Bay Using Model ADCIRC-2DDI," Contractors Report to the US Army Engineer Waterways Experiment Station, January 1993.

12. Blain, C.A., J.J. Westerink, R.A. Luettich and N.W. Scheffner, "Generation of a Storm Surge Time History Data Base From the Hindcast of Extratropical Storm Events from 1977-1992," Contractors report to the U.S. Army Engineer Waterways Experiment Station, December 1994.

13. Westerink, J.J. and R.A. Luettich, "Tidal Predictions for Galveston Bay, Texas Using Model ADCIRC-2DDI," Report to the Texas Water Development Board, State of Texas, Austin TX, December 1997.

14. Westerink, J.J., R.A. Luettich and A. Militello, "Leaky Internal-Barrier Normal-Flow Boundaries in the ADCIRC Coastal Hydrodynamics Code," Coastal and Hydraulic Engineering Technical Note IV-XX, U.S. Army Engineer Research and Development Center, Vicksburg MS, May 2001.

OTHER INVITED LECTURES AND ADDRESSES

1. "A Frequency-Time Domain Finite Element Model for Tidal Circulation," Department of Civil Engineering, University of California at Berkeley, January 1984.

2. "Computations of Nonlinear Shallow Water Tidal Interactions using a General Spectral Finite Element Model," Department of Civil Engineering, The University of Delaware, May 1987.

3. "Numerical Modeling of Coastal Circulation," Naval Oceanographic Research and Development Activity, U.S. Navy, Bay St. Louis, MS, January 1988.

4. "Finite Element Modeling of Shallow Water Tidal Circulation," National Research Council, Ottawa, Canada, March 1989.

5. "Improved Finite Element Methods for Circulation and Transport in Coastal Seas," Texas Institute for Computational Mechanics, The University of Texas at Austin, March 1989.

6. "Advances in Finite Element Modeling of Coastal Ocean Hydrodynamics," Department of Civil Engineering, Chuo University, Tokyo, Japan, September 1996.

7. "Convergence and Grid Issues for Finite Element Solutions to the Shallow Water Equations," Mexican Institute for Water Technology, Jiutepec, Mexico, November 1996.

8. "ADCIRC Overview and Perspective on 20 years of GWCE Based Modeling," 4th Army-Navy ADCIRC Model Workshop, Naval Research Laboratory, Stennis Space Center, MS, February 20-21, 2001.

9. "ADCIRC Developments and Directions," 5th ADCIRC Model Workshop, Naval Research Laboratory, Stennis Space Center, MS, February 2-4, 2001.

10. "ADCIRC Overview and Model Features," "Modeling Strategy and Example Applications," "Grays Harbor Grid Design and Parameter Selection," Coastal Inlets Research Program, SMS Steering Module Workshop, U.S. Army Engineering Research and Development Center, Vicksburg, MS, July 29-August 2, 2002.

11. "Hurricane Hindcasts in Southern Louisiana Using a GWCE-based Finite Element Model," Advisory Board Meeting, Louisiana State University Hurricane Center, Baton Rouge, LA, August 21, 2002.

12. "ADCIRC Progress and Development Report: Implementation of Discontinuous Galerkin Methods for Hydrodynamic and Transport Modeling," Coastal Inlets Research Program Inlet Modeling System Sediment Transport and Morphology Change Team Meeting # 2, Ponte Vedra Beach, Fl, February 11, 2003.

13. "ADCIRC Tidal Data Bases, Implementation of Discontinuous Galerkin Methods for Hydrodynamic and Transport Modeling, ADCIRC Parallel Processing," Coastal Inlets Research Program Inlet Modeling System Sediment Transport and Morphology Change Team Meeting # 2, Ponte Vedra Beach, Fl, February 11, 2003.

14. "Overview of the ADCIRC Model," Florida Coastal Hydraulics Workshop, University of Central Florida, Orlando, FL, June 4-6, 2003.

15. "Louisiana Storm Surge Study," Florida Coastal Hydraulics Workshop, University of Central Florida, Orlando, FL, June 4-6, 2003.

16. "Future Development of ADCIRC," Florida Coastal Hydraulics Workshop, University of Central Florida, Orlando, FL, June 4-6, 2003.

17. "Storm Surge Flooding along the Southern Louisiana Coast," ADCIRC Briefing to U.S. Army Corps of Engineers Management, U.S. Army Engineer Research and Development Center, Vicksburg, MS, June 9, 2003.

18. "Storm Surge Flooding Realities - ADCIRC Modeling," Center for the Study of Public Health Impacts of Hurricanes, Advisory Committee Meeting, Louisiana State University, Baton Rouge, LA, September 15, 2003.

19. "Impact of Advances in High Performance Computing on Storm Surge Modeling," Coastal and Environmental Modeling Laboratory, Advisory Committee Meeting, Louisiana State University, Baton Rouge, LA, September 30, 2003.

20. "Hurricane Storm Surge Calculations in Southern Louisiana Using a Finite Element Based Model," Applied Mathematics Seminar, University of Notre Dame, Notre Dame, IN, October 13, 2003.

21. "Large Scale - Small Scale Applications of the ADCIRC Hydrodynamic Model," Texas Water Development Board, State of Texas, Austin, TX, April 28, 2004.

22. "Storm Surge Modeling in the Gulf of Mexico Using ADCIRC," Chester Jelesnianski Seminar in Ocean Engineering, Department of Civil Engineering, Texas A&M University, College Station, TX, April 29, 2004.

23. "An Overview of ADCIRC-IMS, A System of CG and DG Based Solutions for 2D and 3D Hydrodynamics and Transport," U.S. Army Research and Development Center, Vicksburg, MS, September 8, 2004.

24. "Unstructured Grid Shallow Water Equation Applications and Algorithms," Delft University of Technology, December 17, 2004.

25. "ADCIRC Storm Surge Computations in Southern Louisiana," U.S. Army Corps of Engineers New Orleans District, Federal Emergency Management Agency - ADCIRC Meeting, February 16, 2005.

26. "Hindcasting Hurricane Katrina Using an Unstructured Grid Model for Southern Louisiana," Notre Dame booth at Supercomputing 2005, Seattle WA, November 16, 2005.

27. "The Impact of Hurricane Katrina and Predicting Storm Surges in Southern Louisiana," Scholars in the classroom series, Kaneb Center for Teaching and Learning, University of Notre Dame, Notre Dame, IN, February 23, 2006.

28. "An Overview of Hurricane Inundation Modeling in the Gulf of Mexico and the Need for Statistical Quantification of High Impact Very Low Frequency Events," Workshop on Stochastic Modeling, Center for Applied Mathematics, University of Notre Dame, Notre Dame, IN, March 26, 2006.

29. "The Impact of Hurricane Katrina and Predicting Storm Surges in Southern Louisiana," Interdisciplinary Studies in Tsunami Impacts and Mitigation, Research Experience for Undergraduates, Department of Civil Engineer and Geological Sciences, University of Notre Dame, Notre Dame, IN, June 14, 2006.

30. "Modeling Hurricane Storm Surge along the Gulf Coast in the Wake of Katrina – Towards Petaflop Computations," Workshop on Scientific Computing, Center for Research Computing, University of Notre Dame, Notre Dame, IN, May 15, 2007.

31. "The Impact of Hurricane Katrina and Predicting Storm Surges in Southern Louisiana," Interdisciplinary Studies in Tsunami Impacts and Mitigation, Research Experience for Undergraduates, Department of Civil Engineer and Geological Sciences, University of Notre Dame, Notre Dame, IN, July 11, 2007.

32. "Modeling Hurricane Storm Surge along the Gulf Coast in Southern Louisiana – Towards Petaflop Computations," Department of Civil and Environmental Engineering, University of New Orleans, New Orleans, LA, September 25, 2008.

33. "Modeling Hurricane Storm Surge along the Gulf Coast in Southern Louisiana – Towards Petaflop Computations," School of Marine and Atmospheric Sciences, State University of New York, Stony Brook, NY, October 10, 2008.

34. "Massively Parallel Coastal Ocean Flow and Wind Wave Simulations," Department of Computer Science and Engineering Seminar Series, University of Notre Dame, IN, December 11, 2008.

SPONSORED RESEARCH

1. National Science Foundation: Grant EET-8718436, September 1987 - December 1989, "Improved Computations for Convection Dominated Turbulent Flow Problems Using the Fractional Step Method," Principal Investigator; Award $59,978.

2. Texas A&M Engineering Excellence Award: April 1988 - March 1989, "Development of Filtered Solution Techniques for Turbulent Flow Simulation," Principal Investigator; Award $15,000.

3. U.S. Army Engineers, Waterways Experiment Station, Grant DACW39-86-D-0004/0001, July 1988 - December 1989, "Development of a Two-Dimensional Numerical Model for Estimating the Long Term Fate of Dredged Material," Principal Investigator; Award $116,093.

4. National Science Foundation Offshore Technology Research Center: Grant CDR-8721512-Project 6300A13, October 1988 - September 1989, "Forces on Slender Structures," Co-principal Investigator with Jun Zhang, Texas A&M University; Award $96,630.

5. U.S. Army Engineers, Waterways Experiment Station, Grant DACW39-86-D-0004/0002, August 1989 - September 1990, "New York Bight Model Feasibility Study," Principal Investigator; Award $54,335.

6. National Science Foundation Offshore Technology Research Center: Grant CDR-8721512-Project 6300A13, October 1989 - September 1990, "Forces on Slender Structures," Co-principal Investigator with Jun Zhang, Texas A&M University; Award $81,217.

7. U.S. Army Engineers, Waterways Experiment Station, Grant DACW39-90-M-2965, April 1990 - September 1990, "A Storm Surge Application of the DRP Circulation Model to the Gulf of Mexico," Principal Investigator; Award $21,457.

8. U.S. Army Engineers, Waterways Experiment Station, Grant DACW 39-90-K-0021, May 1990 - September 1994, "Two-Dimensional and Three-Dimensional Tidal and Storm Surge Circulation Computations for the Western Atlantic Shelf and the Gulf of Mexico," Principal Investigator with R.A. Luettich, University of North Carolina at Chapel Hill; Award $375,302

9. National Science Foundation Offshore Technology Center: Grant CDR-8721512; October 1990 - November 1992, "Turbulent Flow Modeling with Space-Time Filtered Solutions to the Navier Stokes Equations," Principle Investigator; Award $30,210.

10. U.S. Army Engineers, Waterways Experiment Station, Grant DACW 39-92-M-0352, December 1991 - June 1992, "Tidal Predictions in Galveston Bay Using the Gulf of Mexico Model," Principal Investigator; Award $9,443.

11. U.S. Army Engineers, Waterways Experiment Station, October 1994 - January 2000, Grant DACW 39-95-K-0011, "Enhancements of the ADCIRC Model for the Analysis of Coastal Inlet Hydrodynamics," Principal Investigator with R.A. Luettich, University of North Carolina at Chapel Hill; Award $343,265.

12. Texas Water Development Board, November 1994 - December 1995, "Computer Simulation of Water Movement and Salinity Transport in Galveston Bay, Texas," Principal Investigator; Award $15,000.

13. U.S. Army Engineers, Waterways Experiment Station, May 1995 - December 1996, "Development of Second Generation Long Wave Hydrodynamic Databases for U.S. Coastal and Continental Margin Waters," Principal Investigator with R.A. Luettich, University of North Carolina at Chapel Hill; Award $114,721.

14. U.S. Naval Research Laboratory, April 1997 - September 1999, "Development and Application of a Prognostic 3 Dimensional Baroclinic Capability in the ADCIRC Hydrodynamic Model," Co-Principal Investigator with R.A. Luettich, University of North Carolina at Chapel Hill; Amount $131,972.

15. Army Research Office, April 1998 - March 1999, Grant DAAG55-98-1-0091, "Scalable Meta-Computing in Computational Sciences and Engineering," Co-Principal Investigator with A. Lumsdaine, N. Chrisochoides, E. Maginn, M. Stadtherr and R. Stevenson, University of Notre Dame; Amount $400,000.

16. Texas Water Development Board, State of Texas, September 1998 - August 1999, "Baroclinic Hydrodynamic Simulations for the Texas Gulf Coast and Gulf of Mexico," Principal Investigator; Award $21,000.

17. Texas Water Development Board, State of Texas, September 1999 - January 2001, "ADCIRC Model for Shelves, Coasts and Estuaries to the Texas Gulf Coast," Principal Investigator; Award $21,000.

18. University of Notre Dame Graduate School, Equipment Restoration Fund, January 2000, "Scalable Meta-Computing for High Performance Computational Science and Engineering," Co-Principal Investigator with A. Lumsdaine, N. Chrisochoides, E. Maginn, M. Stadtherr and R. Stevenson, University of Notre Dame; Amount $200,000.

19. U.S. Army Engineer Research and Development Center, February 2000 - January 2005, Grant DACW 42-00-C-0006, "ADCIRC Hydrodynamic Circulation and Transport Code Development and Applications," Principal Investigator with R.A. Luettich, University of North Carolina at Chapel Hill; Award $674,450.

20. U.S. Army Corps of Engineers, New Orleans District, September 2000 - August 2001, Grant DACW29-00-C-0085, "Modifications of the ADCIRC-NO Hurricane Model to Enhance Robustness, Accuracy and Ease of Implementation," Principal Investigator; Award $247,928.

21. National Science Foundation, September 2001 - August 2004, "Adaptive Multinumeric Finite Element Methods for Shallow Water Flow," Co-Principal Investigator with C. Dawson at University of Texas at Austin; Award to Notre Dame $77,322.

22. Texas Water Development Board, State of Texas, June 2001- May 2002, "ADCIRC Model for Shelves, Coasts and Estuaries to the Texas Gulf Coast," Principal Investigator; Award $21,000.

23. Millennium Trust, Health Excellence Fund, State of Louisiana/ Subcontract through Louisiana State University Hurricane Center, January 2002 - December 2005, "Hydrodynamic Modeling of Flooding Events in Southern Louisiana," Principal Investigator; Award to Notre Dame $209,846.

24. Texas Water Development Board, State of Texas, July 2002- June 2003, "ADCIRC Model for Shelves, Coasts and Estuaries to the Texas Gulf Coast," Principal Investigator; Award $20,000.

25. Sun Microsystems Matching Equipment Grant Program Q4 FY03, July 2003, Principal Investigator; Award $40,896.50.

26. U.S. Army Engineer Research and Development Center, February 2005 - January 2007, Grant W912HZ-05-C-0022, "ADCIRC-CZMS Coastal Zone Modeling System for Circulation, Transport and Morphology: Development and Applications," Principal Investigator; Award $445,506.

27. Offshore and Coastal Technologies Inc., May 2005 - August 2005, "Chesapeake Bay Sediment Hydrodynamic Modeling," Principal Investigator; Award $15,000.

28. U.S. Army Corps of Engineers, New Orleans District, September 2005, Addition to Grant W912HZ-05-C-0022, "Category 5 Hurricane Protection for Louisiana Study," Principal Investigator; Award $77,760.

29. U.S. Army Corps of Engineers, New Orleans District (through Arcadis Inc. as project managers for FEMA and USACE New Orleans District), October 2005 - October 2006, "Development of a Gulf of Mexico Storm Surge Model from Texas to Florida," Principal Investigator, Award $141,000.

30. U.S. Army Corps of Engineers, Mobile District, November 2005 – November 2008, contract W91278-05-D-0018/003 (through Woolpert Inc. as part of a project funded through a direct Congressional appropriation), "Morphos 3D Long Wave Hydrodynamic Modeling," Principal Investigator; Award $175,095.

31. Office of Naval Research, December 2005 – December 2008, "Wave and Circulation Modeling on Unstructured Grids," Principal Investigator with C. Dawson at the University of Texas at Austin and R.A. Luettich at the University of North Carolina at Chapel Hill; Award $452,910.

    (This project is in cooperation with a separately ONR funded parallel project entitled "A Spectral Shallow Water Wave Model with Nonlinear Energy and Phase Evolution" by L.H. Holthuijsen and G.S. Stelling at Delft University of Technology)

32. National Aeronautics and Space Administration, May 2006 - April 2009, "Topographic and Hydrologic Modeling Constraints on Martian Channel Flow and Erosion," Co-Principal Investigator with Principal Investigator S. Sakimoto at the University of Notre Dame and Collaborators L. Keszthelyi of the United States Geological Survey and R. Williams of the Planetary Science Institute; Award $99,239.

33. U.S. Army Corps of Engineers, New Orleans District (through Arcadis Inc. as project managers for FEMA and USACE New Orleans District), November 2006 – November 2007, "USACE/FEMA Storm Surge Modeling Study-Phase I: Eastern Louisiana," Principal Investigator, Award $531,260.

34. U.S. Army Engineer Research and Development Center, October 2006 - March 2007, "Regional Hydrodynamics Task Co-leadership and Storm Surge Analysis and Modeling," Principal Investigator; $299,644.

35. National Science Foundation, September 2006 – August 2009, "CMG Collaborative Research: Adaptive Numerical Methods for Shallow Water Circulation with Applications to Hurricane Storm Surge Modeling," Co-Principal Investigator with C. Dawson at the University of Texas at Austin and R.A. Luettich at the University of North Carolina at Chapel Hill; Project Award $600,000, Award to Notre Dame $207,723.

36. National Science Foundation, October 2007 – September 2011, "Collaborative Research: NSF PetaApps Storm Surge Modeling on Petascale Computers," Co-Principal Investigator with C. Dawson at the University of Texas at Austin and A. Spagnuolo, Oakland University. Award $1,600,000; Award to Notre Dame $503,809.

37. U.S. Army Corps of Engineers, New Orleans District (through Arcadis Inc. as project managers for USACE New Orleans District), January 2008 – December 2008, "IHNC Storm Surge Study for USACE HPO," Principal Investigator, Award: $51,770.

38. U.S. Army Corps of Engineers, New Orleans District (through Arcadis Inc. as project managers for FEMA and USACE New Orleans District), January 2008 - December 2008, "USACE/FEMA Storm Surge Modeling Study of the Texas Coast," Principal Investigator, Award: $186,394.

39. U.S. Army Corps of Engineers, Philadelphia District, April 2008 – December 2008, "USACE - Developing Advanced Hurricane Storm Surge Modeling Capabilities – Research Needs," Principal Investigator, Award: $72,723.

40. U.S. Army Corps of Engineers, New Orleans District (through Arcadis Inc. as project managers for FEMA and USACE New Orleans District), April 2008 – December 2008, "USACE - St. Charles Parish Surge Sensitivity Analysis," Principal Investigator, Award: $8,000.

41. U.S. Army Corps of Engineers, New Orleans District (through Arcadis Inc. as project managers for FEMA and USACE New Orleans District), April 2008 – December 2008, "USACE – Mississippi River Surge Propagation," Principal Investigator, Award: $14,700.

42. U.S. Army Corps of Engineers, New Orleans District (through Arcadis Inc. as project managers for FEMA and USACE New Orleans District), May 2008 – December 2008, "USACE – IHNC Hydroperiod Analysis," Principal Investigator, Award: $5,000.

RESEARCH SUPERVISED

Undergraduate Research

D. Shea, Topic: Petrov-Galerkin Solutions to the Convection-Diffusion Equation, senior thesis, August 1986 - July 1987.

S. Liu, Topic: Petrov-Galerkin Solutions to the Convection-Diffusion Equation, senior thesis, August 1986 - May 1987.

H. Zhao, Topic: New York Bight Circulation Studies, January - July 1990.

L. O'Brien, Topic: Finite Element Grid Development for Coastal Circulation Models, NSF Research Experience for Undergraduates, June - July 1991.

S. Hagen, Topic: Truncation Error Analysis for Shallow Water Equations, NSF Research Experience for Undergraduates, June - July 1992.

R. Li, Topic: Finite Element Grid Studies for Coastal Circulation Models, NSF Research Experience for Undergraduates, June - July 1994.

K. Adu-Sarkodie, Topic: Influence of Grid Valence on the Generation of Spurious Modes in Solutions to the Shallow Water Equations, independent study, January - May 2000.

M. Altman, Topic: Hurricane Storm Surge Calculations in Southern Louisiana, January 2001 - May 2002.

P. Drummey, Topic: Tidal Computations in Texas Coastal Inlets, January - December 2001, August 2002 - May 2003.

A. Henisey, Topic: Tidal Computations in Texas Coastal Inlets, January - May 2002.

P.J. Craig, Topic: Resonant Modes of the Gulf of Mexico, September 2004 - May 2005.

J. Breckler, Topic: The Influence of South Western Levees on Storm Surge Propagating Up the Mississippi River Under High River Stage Conditions, September – December 2005.

T. Roy, Topic: Grid Resolution Effects on the Mississippi River, January 2007 – May 2008.

J. Jeray, Topic: Grid Resolution Effects on the Mississippi River, September 2007 – May 2008.

M. Shubert, Topic: Grid Resolution Effects on the Mississippi River, January 2008 – May 2008.

C. Harris, Topic: Grid Resolution Effects on the Mississippi River, January 2008 – May 2008.

Master's Theses Directed

J.C. Muccino, "Grid Resolution Studies of the Western North Atlantic Ocean, Gulf of Mexico and Caribbean Sea," Department of Civil Engineering and Geological Sciences, University of Notre Dame, M.S., completed November 1992.

M.J. Roe, "Achieving a Dynamic Steady State in the Western North Atlantic/Gulf of Mexico/Caribbean Using Graded Finite Element Grids," Department of Civil Engineering and Geological Sciences, University of Notre Dame, M.S., completed August 1998.

A. Mukai, "Tidal Computations within the Western North Atlantic Using a High Resolution Unstructured Finite Element Mesh," Department of Civil Engineering and Geological Sciences, University of Notre Dame, M.S., completed September 2001.

E. Spargo, "Using a Finite Element Model of the Shallow Water Equations to Model Tides in the Eastern North Pacific Ocean," Department of Civil Engineering and Geological Sciences, University of Notre Dame, M.S., completed September 2003.

H.J. Roberts, "Grid Generation Methods for High Resolution Finite Element Models Used for Hurricane Storm Surge Prediction," Department of Civil Engineering and Geological Sciences, University of Notre Dame, M.S., completed December 2004.

P. Miller, "Grid Resolution and Parameter Study for Coupled Hydrodynamic Sediment Wave Models over an Idealization of the Shinnecock Inlet, New York," Department of Civil Engineering and Geological Sciences, University of Notre Dame, M.S., completed April 2005.

Visiting Graduate Students

A.A. Chavez, Instituto Mexicano de Technologia del Agua, Topic: Simulation of Flushing of Inlets in Cancun, Mexico, February - May 1997.

S. Bunya, University of Tokyo, Topic: Boundary Condition Implementations for Quasi-Bubble Solutions to Shallow Water Equations, July 2003 - June 2004.

Doctoral Dissertations Directed

M.E. Cantekin, "Numerical Simulation with Gaussian Low Pass Filtered Navier Stokes Equations," Department of Civil Engineering, Texas A&M University, Ph.D., completed July 1991.

C.A. Blain, "The Influence of Domain Size and Grid Structure on the Response Characteristics of a Hurricane Storm Surge Model," Department of Civil Engineering and Geological Sciences, University of Notre Dame, Ph.D., completed June 1994.

S.C. Hagen, "Truncation Error Analysis and Grid Design for Long Wave Propagation in Continental Margin Waters," Department of Civil Engineering and Geological Sciences, University of Notre Dame, Ph.D., completed July 1997.

J. H. Atkinson, "Two-dimensional Analysis of Spatial Discretizations of the Shallow Water Equations," Department of Civil Engineering and Geological Sciences, University of Notre Dame, Ph.D., completed October 2002.

J. C. Feyen, "Predictive Hurricane Storm Surge Modeling through Use of a Large Scale Locally Refined Finite Element Model," Department of Civil Engineering and Geological Sciences, University of Notre Dame, Ph.D., completed April 2005.

E.J. Kubatko, "Development, Implementation, and Verification of *hp* Discontinuous Galerkin Models for Shallow Water Hydrodynamics and Transport," Department of Civil Engineering and Geological Sciences, University of Notre Dame, Ph.D., completed December 2005.

D.J. Mark, Ph.D. candidate.

J.C. Dietrich, Ph.D. program.

R. Martyr, Ph.D. program

M. Hope, Ph.D. program

Post Doctoral Associates

J.K. Wu, Topic: Finite Element Based Solutions to the Shallow Water Equations, August 1988 - August 1990

M.E. Cantekin, Topic: Analysis of Finite Element Based Solutions to the Shallow Water Equations, August 1991 - July 1992

R.L. Kolar, Topic: Mass Conservation Issues for Finite Element Solutions to the Shallow Water Equations, July - August 1992.

S. Bunya (visiting assistant professor), Topic: Discontinuous Galerkin Implementations for Coupled Shallow Water Equations, June 2005 – May 2007

E.J. Kubatko, Topic: Discontinuous Galerkin Solutions to the Shallow Water Equations," January – August 2006.

S. Tanaka (assistant research professor), Topic: High Performance Computational Models of the Coastal Ocean, April 2008 – present

D. Wirasaet, (assistant research professor), Topic: High Performance Computational Models of the Coastal Ocean, August 2008 – present

COURSES TAUGHT

Princeton University

CE 276	Introduction to Water Resources
CE 306	Applied Engineering Hydraulics
CE 508	Numerical Methods in Engineering
CE 581	Advanced Hydraulics

Texas A&M University

ENGR 102	Engineering Analysis II
CVEN 311	Fluid Dynamics
OCEN 678	Hydromechanics
CVEN 688	Computational Fluid Dynamics

University of Notre Dame *(with Teacher Course Evaluation scores out of 4.0)*

CE 242	Introduction to Civil Engineering
CE 341	Computational Methods (3.60)
CE 344	Hydraulic Engineering (3.73)
CE 441	Numerical Methods in Engineering (3.83, 3.89, 3.83, 3.55)
CE 539	Advanced Hydraulics (4.00, 4.00)
CE 563	Finite Elements in Engineering (3.63, 3.84, 3.80, 3.86)
CE 598	Modeling Surface Water Flow and Transport
CE30125	Computational Methods (3.73, 3.78, 3.88)
CE60450	Advanced Hydraulics (4.00)

CONFERENCE SESSIONS ORGANIZED

Co-organized with W.G. Gray a mini-symposium at the Third SIAM Conference on Mathematical and Computational Issues in the Geosciences, San Antonio, TX, February 8-10, 1995, entitled "Finite Element Methods for Surface Water Flow and Transport" (1994-1995)

Co-organized with R. Kolar a mini-symposium at the Fifth SIAM Conference on Mathematical and Computational Issues in the Geosciences, San Antonio, TX, March 24-27, 1999, entitled "Solution Strategies to the Shallow Water Equations" (1998-1999)

Co-organized with C. Dawson, S. Yoshimura and K. Kashiyama a mini-symposium at the Eighth U.S. National Congress on Computational Mechanics, Austin, TX, July 24-28, 2005, entitled "Finite Element Methods in Environmental Fluid Mechanics" (2005)

Co-organized with K. Kashiyama three technical sessions at the Seventh World Congress on Computational Mechanics, Los Angeles, CA, July 16-22, 2006, entitled "Finite Element Methods in Environmental Fluid Mechanics" (2006)

Co-organized with K. Kashiyama a mini-symposium at the Ninth US National Congress on Computational Mechanics, San Francisco, CA, July 22-26, 2007, entitled "Finite Element Methods in Environmental Fluid Mechanics" (2007)

Co-organized with T. Wamsley and J. Atkinson two technical sessions at the 10th International Conference on Estuarine and Coastal Modeling, Newport, RI, November 5-7, 2007, entitled "Hurricane Storm Surge Modeling in Southern Louisiana" (2007)

Co-organized with T. Wamsley a technical session at the 10th International Workshop on Wave Hindcasting and Forecasting and Coastal Hazard Symposium, Oahu, Hawaii, November 11-16, 2007, entitled "Estimation of Coastal Hazards" (2007)

TECHNICAL REVIEWER

Journals

Advances in Water Resources
Communications in Applied Numerical Methods
International Journal for Numerical Methods in Fluids
International Journal for Numerical Methods for Heat and Fluid Flow
Journal of Continental Shelf Research
Journal of Engineering Mechanics
Journal of Geophysical Research
Journal of Hydraulic Engineering
Journal of Physical Oceanography
Journal of Waterway, Port, Coastal and Ocean Engineering
Nature
Numerical Methods for Partial Differential Equations
Water Resources Research

COMMITTEES/SERVICE ACTIVITIES

Princeton University

Fall 1985-Spring 1987	ASCE Student Chapter Advisor
Fall 1985-Spring 1987	Departmental Library Liaison

Texas A&M University

Fall 1989-Spring 1990	Member Departmental Computer Committee

University of Notre Dame

Fall 1991-Summer 1992	Member Departmental Computing Committee
Fall 1991-Summer 1994	Member of the College Library Committee
Fall 1992-Summer 1994	Chair of the Departmental Computing Committee
Fall 1992-Spring 1993	Member of the Departmental Undergraduate Curriculum

	Committee
Fall 1992-Summer 2007	Member of the College Computing Committee
Spring 1993-Fall 1993	Member of the University Subcommittee on Large Scale Technical Computing
Fall 1993	Member of the Departmental Catholic Character Committee
Fall 1993-Summer 1994	Member of the Departmental Honesty Committee
Spring 1994-Summer 1994	Member of the Office of University Computing UNIX Search Committee
Spring 1994-Spring 1995	Member of the University Off-Campus Computer Access Committee
Spring 1994-Summer 1994	Member of the University Subcommittee on Resource Allocation for the IBM SP1 Computing Facility
Summer 1994-Summer 1996	Member of the University Committee on Technical Computing
Fall 1994	Member of the College Computing UNIX Search Committee
Summer 1995-Summer 1996	Member of the University Committee on Computing and Information Services
Fall 1995-Summer 1996	Chair of the College Computing Committee
Fall 1995-present	Member of Departmental Committee on Appointments and Promotions
Fall 1997	Moran Search Committee
Fall 2000-Spring 2003	Executive Committee Center for Applied Mathematics
Spring 2000	Member of the University Committee on Technical Computing
Fall 2001-Summer 2002	Member of the Ad Hoc Committee on Computing in the College of Engineering
Fall 2001-present	Civil Engineering Program Class Co-advisor
Spring 2007	Computing Strategic Plan Task Force
Fall 2007 – present	Chair, CE/GEOS Massman Chair Search Committee
Spring 2008 – present	CE/GEOS Graduate Studies Committee
Spring 2008 – present	Organizer, Undergraduate Lecture Series, “Challenges and Innovation in Civil and Environmental Engineering”

APPENDIX B: Litigation Involvement and Compensation

I have been involved in one other litigation case in the past four years. I served as an expert witness for Northrop Grumman Corporation in the litigation of Northrop Grumman Corporation v. Factory Mut. Ins. Co. et al., Case No. CV05-8444 DDP PLAx (C.D. CA). I was deposed on February 22, 2007.

My consulting rates are $250 per hour for consulting services and $500 per hour for depositions and testimony.